Methods in
Molecular Biology 2601

Springer Protocols

Peter Sass *Editor*

Antibiotics

Methods and Protocols

Second Edition

Humana Press

METHODS IN MOLECULAR BIOLOGY

Series Editor
John M. Walker
School of Life and Medical Sciences
University of Hertfordshire
Hatfield, Hertfordshire, UK

For further volumes:
http://www.springer.com/series/7651

For over 35 years, biological scientists have come to rely on the research protocols and methodologies in the critically acclaimed *Methods in Molecular Biology* series. The series was the first to introduce the step-by-step protocols approach that has become the standard in all biomedical protocol publishing. Each protocol is provided in readily-reproducible step-by-step fashion, opening with an introductory overview, a list of the materials and reagents needed to complete the experiment, and followed by a detailed procedure that is supported with a helpful notes section offering tips and tricks of the trade as well as troubleshooting advice. These hallmark features were introduced by series editor Dr. John Walker and constitute the key ingredient in each and every volume of the *Methods in Molecular Biology* series. Tested and trusted, comprehensive and reliable, all protocols from the series are indexed in PubMed.

Antibiotics

Methods and Protocols

Second Edition

Edited by

Peter Sass

Interfaculty Institute for Microbiology and Infection Medicine, University of Tübingen, Tübingen, Germany

Humana Press

Editor
Peter Sass
Interfaculty Institute for Microbiology
and Infection Medicine
University of Tübingen
Tübingen, Germany

ISSN 1064-3745 ISSN 1940-6029 (electronic)
Methods in Molecular Biology
ISBN 978-1-0716-2854-6 ISBN 978-1-0716-2855-3 (eBook)
https://doi.org/10.1007/978-1-0716-2855-3

This Humana imprint is published by the registered company Springer Science+Business Media, LLC, part of Springer Nature.
The registered company address is: 1 New York Plaza, New York, NY 10004, U.S.A.

Preface

Antibiotics are among the most important discoveries in medical history, saving millions of lives, since they allow the effective treatment of even complicated, life-threatening bacterial infections. Also, antibiotics revolutionized our possibilities of medical intervention, thereby significantly increasing the quality of human life. Today, the benefits of antibiotic intervention are at elevated risk, and an increasing prevalence of antibiotic-resistant microbes challenges modern medicine, posing serious threats to human and animal health. A post-antibiotic era has already begun, and more than ever, we need new antibiotics with novel mechanisms of action and resistance-breaking properties.

The second edition of *Antibiotics: Methods and Protocols* in the Springer series Methods in Molecular Biology continues to provide state-of-the-art and novel methods on antibiotic isolation and purification, identification of antimicrobial killing mechanisms, and methods for the analysis and detection of microbial responses and adaptation strategies. Accordingly, the chapters are organized under two major themes: (i) production and design, and (ii) mode of action and resistance. Following an overview on common antibiotics and examples for novel antibiotic modes of action (Chap. 1), the first part, on antibiotic production and design, includes methods to detect antibacterial activities in culture supernatants of actinomycetes (Chap. 2), to sample human microbiomes and screen them for antibiotic-producing commensals (Chap. 3), and to produce and isolate such compounds (Chaps. 4 and 5). With a new compound in hand, structure elucidation is important for compound characterization (Chap. 6) and provides the basis for further optimization, that is, by structure- and ligand-based drug design (Chap. 7) to improve compound-target interactions. To be considered as a promising new therapeutic, the selected compound should have no or only low cytotoxic activity on eukaryotic cells. This can be monitored by methods provided in Chap. 8 and should be assessed before further steps are taken.

In the second part, the chapters lead the reader through methods to further explore antibiotic mechanisms of action as well as related bacterial responses and resistance mechanisms. With a special focus on advanced microscopy techniques, which has greatly contributed to the elucidation of antibiotic modes of action in the past, Chaps. 9 to 12 describe an assay to characterize bacterial phenotypes upon antibiotic treatment via a microscopy-based multiwell assay (Chap. 9), explain a method for expansion microscopy to enable super-resolved visualization of specimen without the need of highly sophisticated and expensive optical instruments (Chap. 10), and show how to track the global and local changes in membrane fluidity through fluorescence spectroscopy and microscopy (Chap. 11). In addition, bioinformatic tools are presented to analyze microscopy image data qualitatively and quantitatively (Chap. 12). In the following chapters, further cell-based and *in vitro* assays are presented that help to characterize antibiotic modes of action and their impact on certain biosynthesis pathways or cellular structures. Here, for example, the bacterial cell envelope represents a validated target for antibiotics. To detect antibiotics that interfere with cell wall integrity and synthesis, their ability to induce specific cell wall stress-responsive promoter fusions can be measured (Chap. 13). An impairment of the bacterial membrane can be determined by measuring the effect of antibiotics on membrane potential and potassium release from whole cells (Chap. 14). Also, antibiotics are frequently found to interfere with DNA replication and translation. Here, Chap. 15 provides a robust

colorimetric assay that enables the identification and the validation of inhibitors of bacterial primases, such as DnaG, which play essential roles in DNA replication, while Chap. 16 reports on the screening for inhibitors of the translation initiation pathway. A different target area is covered by Chap. 17, which describes *in vitro* and *in vivo* inhibitor screens to search for modulators of bacterial histidine kinases, some of which either are essential for survival or were found to be involved in the development of antibiotic resistance. Understanding bacterial responses to antibiotics as well as the established resistance mechanisms to clinically used drugs is mandatory to evaluate alternatives to commonly applied treatment strategies.

To address these aspects, global profiling methods to study the proteome or metal ion homeostasis (Chaps. 18 and 19) of susceptible versus resistant strains (or untreated versus antibiotic-treated strains) have the potential to uncover the underlying antibiotic modes of action as well as resistance mechanisms. Chapter 20 goes further into this direction and characterizes alterations in the stoichiometry and composition of ribosomal and ribosome-associated proteins during antibiotic stress, which impact on protein expression profiles or hibernating ribosomes. Heading further towards antibacterial resistance, functional metagenomics emerged as a highly useful way to identify novel resistance genes from environmental samples (Chap. 21), which do not necessarily rely on the culturability of a specific strain in the laboratory, thus allowing to study antibiotic resistance in very diverse microbial communities such as soil-, marine-, human-, wastewater-, or animal- and agriculture-associated communities.

I would like to thank all contributing authors of the first and second edition of *Antibiotics: Methods and Protocols* for sharing their expertise and protocols, thereby essentially contributing to the success of this book. Antibiotic research is a multidisciplinary approach, and thus *Antibiotics: Methods and Protocols* addresses scientists from diverse fields involving microbiologists, cell biologists, molecular geneticists, pharmacists, immunologists, infectiologists, biochemists, biophysicists, bioinformaticians, and many others. We hope that the book will inspire your scientific work in the exciting field of antibiotic research, and we would be pleased to see the book more often in your lab than in the library.

Tübingen, Germany ***Peter Sass***

Contents

Contributors

Ireny Abdelmesseh Nekhala • *Division of Chemical Biology, Department of Biology and Biological Engineering, Chalmers University of Technology, Gothenburg, Sweden*

Emilio Alvarez-Ruiz • *GlaxoSmithKline Platform Technologies and Science, Parque Tecnologico de Madrid, Madrid, Spain*

Minia Antelo-Varela • *Department of Microbial Proteomics, University of Greifswald, Institute of Microbiology, Greifswald, Germany; University of Basel, Biozentrum, Focal Area Infection Biology, Basel, Switzerland*

Julia E. Bandow • *Applied Microbiology, Ruhr-Universität Bochum, Bochum, Germany; Ruhr-Universität Bochum, Applied Microbiology, Bochum, Germany*

Dörte Becher • *Department of Microbial Proteomics, University of Greifswald, Institute of Microbiology, Greifswald, Germany*

Gabriele Bierbaum • *Institute of Medical Microbiology, Immunology and Parasitology, University of Bonn, Bonn, Germany*

Florian Bonn • *Department of Microbial Proteomics, University of Greifswald, Institute of Microbiology, Greifswald, Germany; Immundiagnostik AG, Bensheim, Germany*

Manish Boolchandani • *The Edison Family Center for Genome Sciences & Systems Biology, Washington University School of Medicine, St. Louis, MO, USA*

Dominik Brajtenbach • *Institute of Physical and Theoretical Chemistry, University of Bonn, Bonn, Germany*

Federica Briani • *Dipartimento di Bioscienze, Università degli Studi di Milano, Milan, Italy*

Jessica A. Buttress • *Centre for Bacterial Cell Biology, Biosciences Institute, Newcastle University, Newcastle upon Tyne, UK*

Laura Camus • *Interfaculty Institute of Microbiology and Infection Medicine, Institute for Medical Microbiology and Hygiene, Tübingen, Germany; (DFG) Cluster of Excellence EXC 2124 Controlling Microbes to Fight Infections, Tübingen, Germany; German Centre for Infection Research (DZIF), Partner Site Tübingen, Tübingen, Germany*

Georgios Daletos • *Institute of Pharmaceutical Biology and Biotechnology, Heinrich-Heine-University, Düsseldorf, Germany*

Gautam Dantas • *The Edison Family Center for Genome Sciences & Systems Biology, Washington University School of Medicine, St. Louis, MO, USA; Department of Pathology and Immunology, Washington University School of Medicine, St. Louis, MO, USA; Department of Biomedical Engineering, Washington University in St. Louis, St. Louis, MO, USA; Department of Molecular Microbiology, Washington University School of Medicine, St. Louis, MO, USA; Department of Pediatrics, Washington University School of Medicine, St. Louis, MO, USA*

Alina Dietrich • *Institute of Medical Microbiology, Immunology and Parasitology, University of Bonn, Bonn, Germany*

Pascal Dietze • *Ruhr-Universität Bochum, Applied Microbiology, Bochum, Germany*

Miriam Fuerst-Wilmes • *Institute of Medical Microbiology, Immunology and Parasitology, University of Bonn, Bonn, Germany*

Mike Gajdiss • *Institute of Medical Microbiology, Immunology and Parasitology, University of Bonn, Bonn, Germany*

Susanne Gebhard • *Life Sciences Department, Milner Centre for Evolution, University of Bath, Bath, UK*

Fabian Grein • *Institute for Pharmaceutical Microbiology, University Hospital Bonn, University of Bonn, Bonn, Germany; German Center for Infection Research (DZIF), Partner Site Bonn-Cologne, Bonn, Germany*

Simon Heilbronner • *Interfaculty Institute of Microbiology and Infection Medicine, Institute for Medical Microbiology and Hygiene, Tübingen, Germany; (DFG) Cluster of Excellence EXC 2124 Controlling Microbes to Fight Infections, Tübingen, Germany; German Centre for Infection Research (DZIF), Partner Site Tübingen, Tübingen, Germany*

Chambers C. Hughes • *Department of Microbial Bioactive Compounds, Interfaculty Institute of Microbiology and Infection Medicine, University of Tübingen, Tübingen, Germany*

Madeleine Humphrey • *Centre for Bacterial Cell Biology, Biosciences Institute, Newcastle University, Newcastle upon Tyne, UK*

Carolin Martina Kobras • *Life Sciences Department, Milner Centre for Evolution, University of Bath, Bath, UK; The Florey Institute for Host-Pathogen Interactions, School of Biosciences, University of Sheffield, Sheffield, UK*

I. Dewa M. Kresna • *Institute for Insect Biotechnology, Justus-Liebig-University Giessen, Giessen, Germany*

Dorothee Kretschmer • *Infection Biology, Interfaculty Institute for Microbiology and Infection Medicine Tübingen (IMIT), University of Tübingen, Tübingen, Germany*

Oxana Krylova • *Department of Chemical Biology, Leibniz-Institut für Molekulare Pharmakologie (FMP), Berlin, Germany*

Ulrich Kubitscheck • *Institute of Physical and Theoretical Chemistry, University of Bonn, Bonn, Germany*

Andreas Kulik • *Microbial Bioactive Compounds, Interfaculty Institute of Microbiology and Infection Medicine Tübingen, Eberhard Karls University Tübingen, Tübingen, Germany*

Anna Lange • *Interfaculty Institute of Microbiology and Infection Medicine, Institute for Medical Microbiology and Hygiene, Tübingen, Germany; (DFG) Cluster of Excellence EXC 2124 Controlling Microbes to Fight Infections, Tübingen, Germany; German Centre for Infection Research (DZIF), Partner Site Tübingen, Tübingen, Germany*

Sandra Maaß • *Department of Microbial Proteomics, University of Greifswald, Institute of Microbiology, Greifswald, Germany*

Alexander D. MacKerell Jr • *Department of Pharmaceutical Sciences, Computer-Aided Drug Design Center, School of Pharmacy, University of Maryland, Baltimore, MD, USA; Institute for Bioscience and Biotechnology Research (IBBR), Rockville, MD, USA; Center for Biomolecular Therapeutics (CBT), School of Medicine, University of Maryland, Baltimore, MD, USA*

Bejan Mahmud • *The Edison Family Center for Genome Sciences & Systems Biology, Washington University School of Medicine, St. Louis, MO, USA*

Thorsten Mascher • *Institut für Mikrobiologie, Technische Universität Dresden, Dresden, Germany*

Cruz L. Matos de Opitz • *Interfaculty Institute of Microbiology and Infection Medicine, Microbial Bioactive Compounds, University of Tübingen, Tübingen, Germany*

Viola Middelhauve • *Institute of Physical and Theoretical Chemistry, University of Bonn, Bonn, Germany*

Lena Mitousis • *Interfaculty Institute of Microbiology and Infection Medicine (IMIT), Microbiology/Biotechnology, University of Tübingen, Tübingen, Germany; Cluster of Excellence 'Controlling Microbes to Fight Infections' (CMFI), University of Tübingen, Tübingen, Germany*

Ian Monk • *Institute of Medical Microbiology, Immunology and Parasitology, University of Bonn, Bonn, Germany; Doherty Institute for Infection and Immunity, Department of Microbiology and Immunology, University of Melbourne, Melbourne, Australia*

Sali May Morris • *Life Sciences Department, Milner Centre for Evolution, University of Bath, Bath, UK*

Julia Moschny • *Department of Microbial Bioactive Compounds, Interfaculty Institute of Microbiology and Infection Medicine, University of Tübingen, Tübingen, Germany*

Danuta Mossakovska • *GlaxoSmithKline, Stevenage, Hertfordshire, UK; Malopolska Centre of Biotechnology, Jagiellonian University, Kraków, Poland*

Ewa Maria Musiol-Kroll • *Interfaculty Institute of Microbiology and Infection Medicine (IMIT), Microbiology/Biotechnology, University of Tübingen, Tübingen, Germany; Cluster of Excellence 'Controlling Microbes to Fight Infections' (CMFI), University of Tübingen, Tübingen, Germany*

Allan H. Pang • *Department of Pharmaceutical Sciences, College of Pharmacy, University of Kentucky, Lexington, KY, USA*

Sanket Patel • *The Edison Family Center for Genome Sciences & Systems Biology, Washington University School of Medicine, St. Louis, MO, USA; Department of Pathology and Immunology, Washington University School of Medicine, St. Louis, MO, USA*

Peter Proksch • *Institute of Pharmaceutical Biology and Biotechnology, Heinrich-Heine-University, Düsseldorf, Germany*

Jan-Samuel Puls • *Institute for Pharmaceutical Microbiology, University Hospital Bonn, University of Bonn, Bonn, Germany*

Matteo Raneri • *Dipartimento di Bioscienze, Università degli Studi di Milano, Milan, Italy; Sacco S.r.l., Cadorago, Italy*

Anika Rütten • *Interfaculty Institute of Microbiology and Infection Medicine (IMIT), Microbiology/Biotechnology, University of Tübingen, Tübingen, Germany; Cluster of Excellence 'Controlling Microbes to Fight Infections' (CMFI), University of Tübingen, Tübingen, Germany*

Hans-Georg Sahl • *Institute of Medical Microbiology, Immunology and Parasitology, University of Bonn, Bonn, Germany*

Peter Sass • *Interfaculty Institute for Microbiology and Infection Medicine, Microbial Bioactive Compounds, University of Tübingen, Tübingen, Germany*

Till F. Schäberle • *Institute for Insect Biotechnology, Justus-Liebig-University Giessen, Giessen, Germany; Fraunhofer Institute for Molecular Biology and Applied Ecology (IME), Branch for Bioresources, Giessen, Germany; German Center of Infection Research (DZIF), Partner Site Giessen-Marburg-Langen, Giessen, Germany*

Ann-Britt Schäfer • *Division of Chemical Biology, Department of Biology and Biological Engineering, Chalmers University of Technology, Gothenburg, Sweden*

Thomas Schafhauser • *Microbiology and Biotechnology, Interfaculty Institute of Microbiology and Infection Medicine Tübingen, Eberhard Karls University Tübingen, Tübingen, Germany*

Sina Schäkermann • *Ruhr-Universität Bochum, Applied Microbiology, Bochum, Germany*

Kathi Scheinpflug • *Department of Chemical Biology, Leibniz-Institut für Molekulare Pharmakologie (FMP), Berlin, Germany*

Jasmin Scheurer • *Department of Dermatology, Division of Dermatooncology, University of Tübingen, Tübingen, Germany*
Christoph H. R. Senges • *Applied Microbiology, Ruhr-Universität Bochum, Bochum, Germany*
Jan Peter Siebrasse • *Institute of Physical and Theoretical Chemistry, University of Bonn, Bonn, Germany*
Henrik Strahl • *Centre for Bacterial Cell Biology, Biosciences Institute, Newcastle University, Newcastle upon Tyne, UK*
Benjamin Torres Salazar • *Interfaculty Institute of Microbiology and Infection Medicine, Institute for Medical Microbiology and Hygiene, Tübingen, Germany; (DFG) Cluster of Excellence EXC 2124 Controlling Microbes to Fight Infections, Tübingen, Germany*
Oleg V. Tsodikov • *Department of Pharmaceutical Sciences, College of Pharmacy, University of Kentucky, Lexington, KY, USA*
Michael Türck • *Institute of Medical Microbiology, Immunology and Parasitology, University of Bonn, Bonn, Germany*
David J. Weber • *Institute for Bioscience and Biotechnology Research (IBBR), Rockville, MD, USA; Center for Biomolecular Therapeutics (CBT), School of Medicine, University of Maryland, Baltimore, MD, USA*
Michaela Wenzel • *Division of Chemical Biology, Department of Biology and Biological Engineering, Chalmers University of Technology, Gothenburg, Sweden*
Wolfgang Wohlleben • *Interfaculty Institute of Microbiology and Infection Medicine (IMIT), Microbiology/Biotechnology, University of Tübingen, Tübingen, Germany; Cluster of Excellence 'Controlling Microbes to Fight Infections' (CMFI), University of Tübingen, Tübingen, Germany*
Zerlina G. Wuisan • *Institute for Insect Biotechnology, Justus-Liebig-University Giessen, Giessen, Germany; German Center of Infection Research (DZIF), Partner Site Giessen-Marburg-Langen, Giessen, Germany*
Wenbo Yu • *Department of Pharmaceutical Sciences, Computer-Aided Drug Design Center, School of Pharmacy, University of Maryland, Baltimore, MD, USA; Institute for Bioscience and Biotechnology Research (IBBR), Rockville, MD, USA; Center for Biomolecular Therapeutics (CBT), School of Medicine, University of Maryland, Baltimore, MD, USA*
Alexander Zipperer • *Infection Biology, Interfaculty Institute for Microbiology and Infection Medicine Tübingen (IMIT), University of Tübingen, Tübingen, Germany*

Part I

Production and Design

Chapter 1

Antibiotics: Precious Goods in Changing Times

Peter Sass

Abstract

Antibiotics represent a first line of defense of diverse microorganisms, which produce and use antibiotics to counteract natural enemies or competitors for nutritional resources in their nearby environment. For antimicrobial activity, nature has invented a great variety of antibiotic modes of action that involve the perturbation of essential bacterial structures or biosynthesis pathways of macromolecules such as the bacterial cell wall, DNA, RNA, or proteins, thereby threatening the specific microbial lifestyle and eventually even survival. However, along with highly inventive modes of antibiotic action, nature also developed a comparable set of resistance mechanisms that help the bacteria to circumvent antibiotic action. Microorganisms have evolved specific adaptive responses that allow to appropriately react to the presence of antimicrobial agents, thereby ensuring survival during antimicrobial stress. In times of rapid development and spread of antibiotic (multi-)resistance, new resistance-breaking strategies to counteract bacterial infections are desperately needed. This chapter is an update to Chapter 1 of the first edition of this book and intends to give an overview of common antibiotics and their target pathways. It will also present examples for new antibiotics with novel modes of action, illustrating that nature's repertoire of innovative new antimicrobial agents has not been fully exploited yet, and we still might find new drugs that help to evade established antimicrobial resistance strategies.

Key words Antimicrobial agents, Drug discovery, Mode of action, Antibiotic resistance, MRSA

1 The Times They Are Still Changing

Antibiotics represent one of the most important discoveries in medical history. Although the term antibiotics literally means "against life", their use as therapeutic agents starting in the first half of the twentieth century for the first time allowed an effective treatment of even complicated, life-threatening bacterial infections (e.g., tuberculosis and septicemia), thereby saving millions of lives. In addition, antibiotics represent important tools in modern medicine to enable, for example, cancer chemotherapy, orthopedic surgery, and transplantation. Thus, antibiotics have not just decreased mortality and morbidity caused by bacterial infections, they further

Peter Sass (ed.), *Antibiotics: Methods and Protocols*,
Methods in Molecular Biology, vol. 2601, https://doi.org/10.1007/978-1-0716-2855-3_1,

revolutionized the possibilities concerning medical intervention to help increase the quality of human life.

Today, the situation has changed dramatically which is primarily due to the overuse and/or misuse of antibiotics in the clinics and to an even more serious extent in agriculture. We are now experiencing an increasing prevalence of microbes that are resistant to one, several, or almost all clinically used antibiotics. Bacterial infections that could once easily be cured are becoming harder to treat or are even untreatable, challenging modern medicine and posing one of the most serious threats to human and animal health as recognized by the World Health Organization [1]. As many pathogens (resistant and susceptible) are often characterized to sensitively respond to antibiotic stress and regulate their metabolism to survive antibacterial treatment, it can be assumed that the resistance situation will not substantially relax in the future [2].

In the light of this alarming development and spread of antibiotic (multi-)resistance, and since too few new antibiotics with resistance breaking properties enter the clinics (the "golden age of antibiotic discovery" has long since passed), we need fast and coordinated actions to avoid the risk of heading toward a post-antibiotic era. Such necessary actions need to be supported by physicians, pharmacists, agriculturists, scientists, politicians, and, of course, people in the community. Efficient means for infection monitoring, control, and prevention are needed, accompanied by improved hygiene standards (in the community as well as in the clinic) and a far more responsible handling of antibiotic prescription and usage (in humans and livestock). In the community, we need a better awareness of resistance prevalence, how to avoid spread of pathogens, and when antibiotics are necessary and how they should be used. As stated by the Centers for Disease Control and Prevention (CDC) in April 2011, a huge economic burden comes along with antimicrobial resistance with costs of approx. 55 billion USD a year only in the United States [3]. And according to the Review on Antimicrobial Resistance of March 2016 [4], which was commissioned by the UK Prime Minister and is hosted by the Wellcome Trust, without a coordinated global response to counter drug resistance we could be facing a threat claiming 10 million lives a year by 2050, at an accumulated cost of 100 trillion USD. Whatever costs (human or economic) drive an initiative for assessing solutions to counteract antimicrobial resistance and antibiotic run out, it is an important step forward that this issue is increasingly discussed worldwide including the UN General Assemblies and the G7 and G20 group meetings during the last 6 years. Indeed, the disastrous consequences of the SARS-CoV-2 coronavirus outbreak on human lives and our economy during the last 2 years should have finally made clear which severe consequences can be expected from an enduring antibiotic crisis [2]. Hence, in 2022, it is still important to reinforce that "we have reached a critical point and

must act now on a global scale to slow down antimicrobial resistance" (citation by Professor Dame Sally Davies, UK Chief Medical Officer) [5].

However, decelerating development and spread of antimicrobial resistance will not be sufficient to avert the scenario described above, as we also need new antibiotics with extended or novel mechanisms of action that have resistance-breaking properties, that is, improved antibiotics of established classes and/or new compounds with novel targets. But although desperately needed, during the last decades antibiotic research suffered from questioning its economic viability, and the interest of the private sector in developing new antibacterial drugs constantly decreased, which among other reasons resulted in a misguided trend that also reduced basic research on the development of new antibiotic drugs [2]. Despite an increasing public and political awareness about rising AMR, the number of new and innovative antibiotics entering the market is declining (only 12 new antibiotics (or antibiotic combinations) have been approved since 2000), and most big pharmaceutical companies stopped their antibiotic research programs [6]. During the last 6 years, the pharma giants AstraZeneca (2016), Novartis, Sanofi (both in 2018), and Johnson & Johnson (2019) quit their antibiotic research and development programs, although they had previously announced to further invest in antibiotic research to fight AMR ("AMR Industry Alliance") in early 2016, thereby risking that the antibiotic pipeline is about to dry up [7].

During the last years, however, several new initiatives started to oppose this trend. For example, the Innovative Medicines Initiative (IMI), a public-private partnership that is co-financed by the EU and the EFPIA (European Federation of Pharmaceutical Industries and Associations), was launched in 2008 to foster (pre-)clinical development and to address the regulatory and business challenges of antibiotic R&D programs [8]. Later, the EU set up an action plan against the rising threats from AMR in 2011 [9], which developed into the EU's *One Health Action Plan against AMR* in 2017, with the overarching goal to preserve the possibility of effective treatment of infections in humans and animals [10]. Here, EU initiatives included the New Drugs for Bad Bugs (ND4BB) program starting in 2011, the world's biggest public-private AMR research partnership between industry, academia, and biotech organizations to combat antimicrobial resistance in Europe [11], as well as the Joint Programming Initiative on AMR (JPIAMR) [12], which aims to better coordinate and align worldwide AMR research efforts. Similarly, in the United States, the "10 by 20" program from 2010 [13], run by the Infectious Disease Society, and CARB-X [8], a nonprofit public-private partnership initiated in 2016 by the US Department of Health and Human Services' Biomedical Advanced Research and Development

Authority (BARDA) and the National Institute of Allergy and Infectious Diseases (NIAID/NIH), support innovative antimicrobial research and the development of new antibiotics worldwide. Further, the nonprofit Global Antibiotic Research and Development Partnership (GARDP) was initiated by the WHO and the Drugs for Neglected Diseases Initiative (DNDi) to promote antibiotic R&D with the goal of sustainable and worldwide access [14]. In Germany, for example, the themed collaborative research unit of the German Research Foundation (DFG) designated "Post-Genomic Strategies for New Antibiotic Drugs and Targets" (FOR854) started as early as in 2009 with the goal to study promising new antibiotic compounds, molecular mechanisms, and targets using post-genome era strategies [15]. In 2010, the German Federal Ministry of Education and Research initiated the German Center for Infection Research (DZIF) that runs several task force units on infection research, one unit with a special focus on *Novel Antibiotics*, which aims to bring basic research and current anti-infective development activities back together [16]. More recently, the Transregional Collaborative Research Center TRR261 *Antibiotic CellMAP* [17] as well as the Cluster of Excellence *Controlling Microbes to Fight Infections* [18] were launched. Both initiatives are funded by the German Research Foundation (DFG, Deutsche Forschungsgemeinschaft) with the goal to explore antibiotic modes of action and to assess an effective use of antibiotics to counter infections while protecting the microbial communities that populate the human body. In addition to these initiatives, the Gordon Research Conference on New Antibacterial Discovery and Development was launched as an excellent platform to discuss and to share ideas between academia, industry, and government agencies on target discovery and validation, hit identification and chemical optimization, as well as clinical trial design and execution, thereby supporting the efforts of the abovementioned research initiatives [19]. However, to attract *Big Pharma* back to the antibacterial drug discovery field, it seems that such initiatives need to be accompanied by a new rising commercial value of antibiotics, for example, based on their value for our society and medicine.

2 Antibiotic Modes of Action

Microorganisms produce antibiotics for several reasons; the most obvious role is the direct counteraction of competitive or invading bacteria by inhibiting their growth. This chapter is an update to Chapter 1 of the first edition of this book [20] and intends to summarize the more common antibiotics and their cellular targets, and it will highlight examples for new antibiotics with novel modes of action that have been identified by antibiotic researchers in

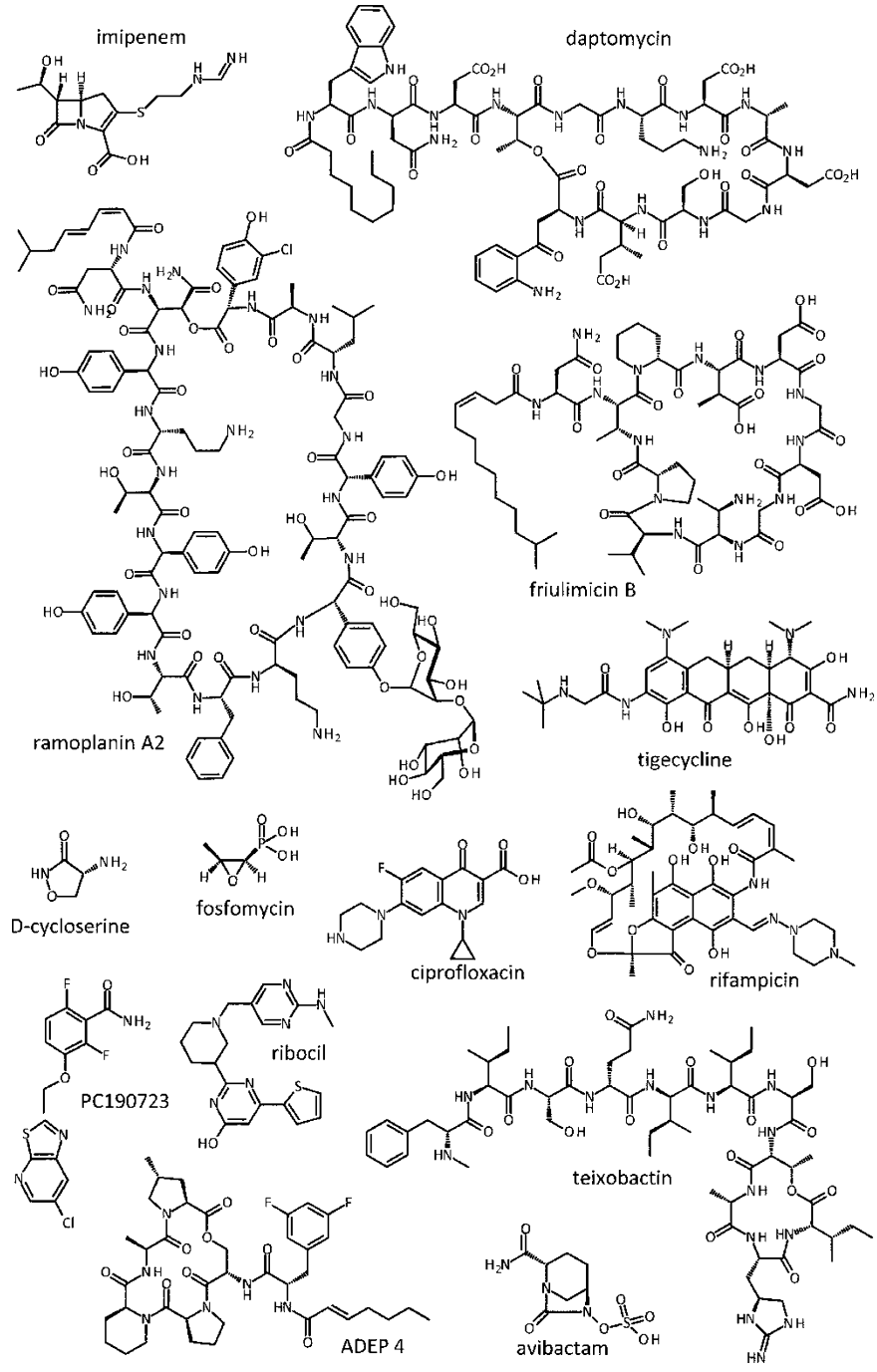

Fig. 1 Structures of exemplary antibiotics discussed in this chapter. (Figure reprinted from Ref. [20])

recent years (Fig. 1). Many different antimicrobial agents are known which can be characterized and differentiated by their individual modes of action and cellular targets. The bacterial cell envelope represents one such prominent target pathway that is unique

to bacteria and fulfills many important physiological functions. Further validated target pathways for antibiotic attack include protein biosynthesis as well as DNA and RNA metabolism, where the target sites sufficiently vary from their eukaryotic counterparts to allow selective inhibition of the bacteria. Depending on the compound and its target site, some antibiotics have a broad spectrum or a narrow spectrum of activity targeting multiple bacterial species or only a small, selected group of species, respectively. Some antimicrobial agents are multi-targeted compounds that act against a broad range of microorganisms in a concentration-dependent manner. Such sanitizers possess rather unspecific modes of action, for example, by penetrating and disturbing the integrity of the bacterial cell membrane, by producing DNA cross linkage, or by abrogating spore outgrowth [21].

However, antibacterial activity is not the only function of antibiotics as their name would suggest, and it is increasingly recognized that some members of antibiotic classes have evolved as bacterial tools for intra- and inter-domain communication [22]. For instance, antimicrobial peptides act as modulators of the innate immune response in higher organisms [23–25]. In streptomycetes, some lanthionine-containing antibiotics (*lantibiotics*) have morphogenic effects by modulating the formation of aerial hyphae [26]. Other lantibiotics induce their own production in a quorum-dependent manner thereby showing similarities to peptide pheromones [27, 28]. Despite these exciting new functions of antibiotics, which certainly deserve and would easily fill a review on their own, the next sections will focus on the mechanisms how antibiotics exert their growth inhibitory effects or even kill bacteria.

2.1 The Bacterial Cell Envelope as Antibiotic Target

Many vital cellular functions are attributed to the bacterial cell envelope, including its role as a diffusion barrier, a shape-giving structure, and an essential communication interface between different cells in a community as well as their surrounding environment. Structurally, the cell envelope of bacteria is built up of one or two lipid membranes and the glycopeptide scaffold of the cell wall (peptidoglycan). In general, there are two different types of cell envelope in bacteria, a Gram-positive and a Gram-negative type. The cell envelope of Gram-positive bacteria consists of a thick cell wall layer that is located outside the bacterial plasma membrane and completely covers the cell. Here, the cell wall forms a multilayered heteropolymer, which is largely composed of the sugar-peptide polymer peptidoglycan to which diverse accessory molecules like proteins, teichoic acids, teichuronic acids, carbohydrates, and polyphosphates are attached to. The peptidoglycan mainly consists of linear glycan chains with the two alternating amino sugars N-acetylglucosamine (GlcNAc) and N-acetylmuramic acid (MurNAc). These glycan chains are further cross-linked by short peptides that are bound to the MurNAc moieties and which can vary between

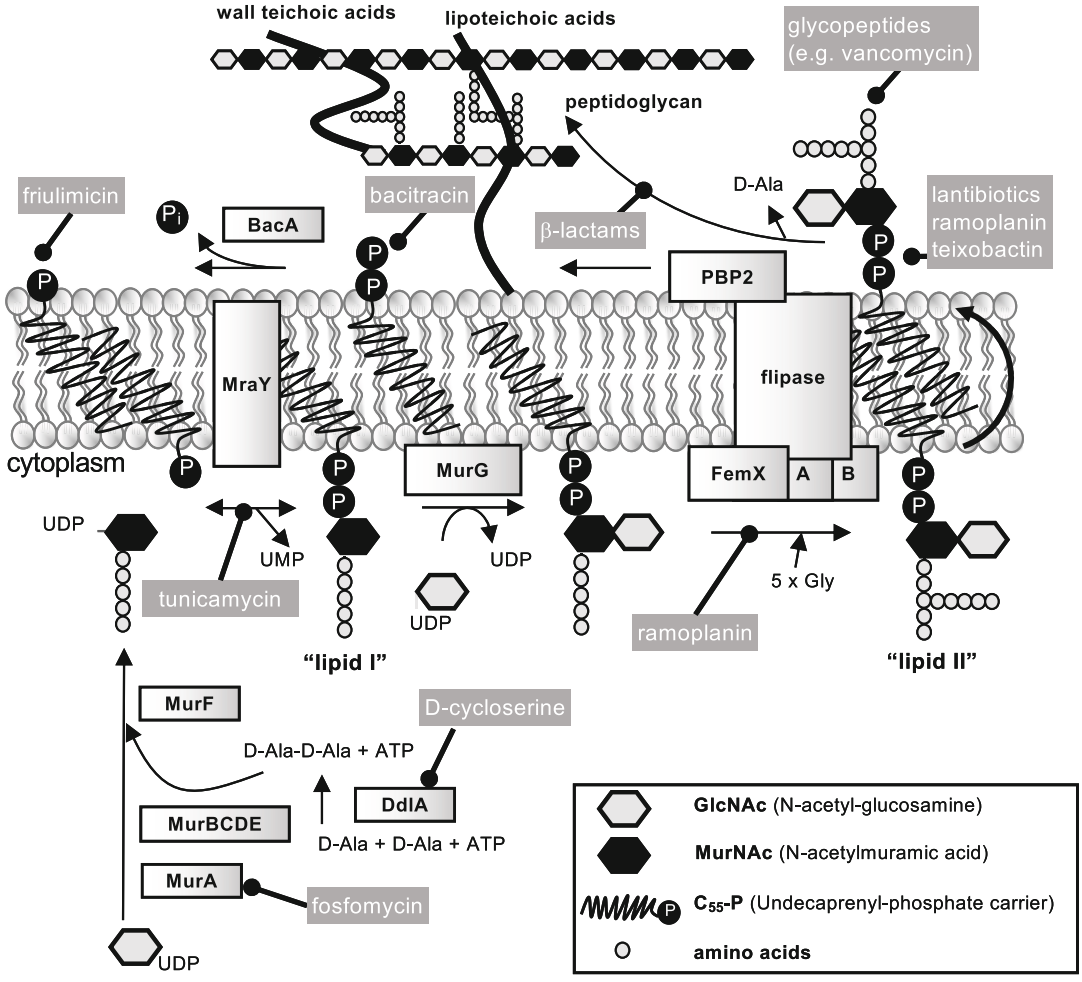

Fig. 2 Inhibition of cell wall biosynthesis of *Staphylococcus aureus* by antibiotic action. (Figure modified from Ref. [20])

different bacteria (Fig. 2). Depending on the bacterial species, the peptide side chains are either directly cross-linked to the peptide side chains of neighboring glycan strands, or they may be connected via interpeptide bridges of characteristic additional amino acids. By that, an elastic, three-dimensional network is produced which is intimately involved in vital bacterial processes such as cell division and autolysis, and it essentially contributes to maintain bacterial cell shape and integrity by withstanding the internal osmotic pressure [29, 30]. Gram-negative bacteria possess a significantly different cell envelope architecture, as they have an additional outer lipid membrane and a much thinner peptidoglycan layer, which, however, structurally resembles the peptidoglycan of Gram-positive species. With regard to antibiotic research, the outer lipid membrane represents an intrinsic antibiotic resistance factor

that acts as a diffusion barrier for a multitude of compounds including antimicrobial agents and thus protects the bacteria from the potentially lethal effects of many antibiotics. The space between inner and outer membrane, the periplasm, harbors various enzymes that play roles in distinct physiological pathways like peptidoglycan biosynthesis, nutrient uptake, electron transfer systems, as well as detoxification [31].

The cell wall is essential for and unique to bacteria and thus is a favored target site for antibiotics (Fig. 2). Antibiotics interfere with almost every step of peptidoglycan synthesis by either sequestering an essential substrate of the synthesis reaction or by directly inhibiting a specific enzymatic reaction, which both prevent the production of new cell wall material and finally lead to cell death of the growing bacteria [32, 33]. Penicillin G, probably the most prominent antibiotic to date, and other β-lactams interfere with enzyme reactions during peptidoglycan synthesis. To do so, β-lactams imitate the D-alanyl-D-alanine motif of the peptidoglycan precursor lipid II and bind to the active sites of transpeptidases and carboxypeptidases, which are therefore called penicillin-binding proteins (PBPs). Thereby, β-lactam binding inhibits the function of PBPs and thus prevents the cross-linking reactions of the glycan strands making the cell vulnerable to lysis during growth [34, 35]. D-Cycloserine, an oxazolidinone antibiotic, inhibits both D-alanine racemase and D-alanine-D-alanine ligase and blocks the conversion of L-alanine to D-alanine and the subsequent production of D-alanyl-D-alanine dipeptide [36, 37]. Fosfomycin is a structural analog of phosphoenol pyruvate and therefore interferes with the activity of MurA, an enzyme that converts UDP-GlcNAc into UDP-MurNAc, representing the first committed step of peptidoglycan biosynthesis [38]. The enzymatic activity of MraY is inhibited by the antibiotics tunicamycin, mureidomycin, amphomycin, muraymycin, and liposidomycin, thereby preventing the transfer of the UDP-MurNAc-pentapeptide motif onto the undecaprenyl phosphate carrier, which is the first membrane-bound step of peptidoglycan synthesis yielding lipid I [39].

Some antibiotics act by sequestering an essential substrate of cell wall biosynthesis, which leads to a significantly decreased availability of central building blocks for the synthesis of peptidoglycan. Bacitracin, a cyclic dodecylpeptide antibiotic, sequesters the lipid carriers of the essential peptidoglycan precursor molecule lipid II in its undecaprenyl-pyrophosphate state (C_{55}-PP), thereby preventing the recycling of the lipid carrier by dephosphorylation [40, 41]. The lipopeptide antibiotic friulimicin B interferes with C_{55}-P to decrease the availability of the lipid carrier and leads to an effective inhibition of the MraY reaction [42]. Antibiotics like vancomycin, teicoplanin, and ramoplanin or some lantibiotics directly bind and sequester the precursor molecule lipid II. The

glycopeptide vancomycin, which is an antibiotic of last resort for the treatment of serious infections caused by methicillin-resistant *Staphylococcus aureus* (MRSA), complexes the D-alanyl-D-alanine terminus of lipid II to inhibit peptidoglycan synthesis [43]. Ramoplanin, a strongly amphipathic glycolipodepsipeptide antibiotic with a short acyl side chain, prevents bacterial cell wall biosynthesis by interacting with the sugar phosphate head group of lipid II instead of binding to its D-alanyl-D-alanine terminus. Ramoplanin even seems to be translocated across the membrane to inhibit intracellular lipid I- and lipid II-consuming reactions, for example, catalyzed by MurG and FemXAB [44]. Lantibiotics are antimicrobial peptide antibiotics that undergo posttranslational modification resulting in the formation of the cyclic thioether amino acids lanthionine and 3-methyllanthionine [45, 46]. Some lantibiotics such as mersacidin, which belongs to a rather globular type of lantibiotics, also bind to the pyrophosphate group of lipid II thereby inhibiting transglycosylation reactions and finally the incorporation of the precursor into the nascent peptidoglycan during cell wall biosynthesis [47]. Nisin, another type of lantibiotic with rather elongated structure, is commonly used as a food preservative [48]. Nisin exhibits a dual mode of action: one mode is its specific binding to the sugar-pyrophosphate moiety of lipid II to cause inhibition of cell wall biosynthesis. In addition, nisin uses lipid II as a docking molecule to insert into the bacterial membrane, which results in pore formation, ion efflux, and finally bacterial cell death [49, 50].

In contrast to lantibiotics, the mode of action of cationic antimicrobial peptides (CAMPs) appears to be mostly based on their cationic and amphiphilic nature which allows such peptides to interact with negatively charged bacterial surfaces and membranes [51]. However, mere membrane perturbation does not fully explain their antimicrobial activity. Most probably, CAMPs do not just impair the membrane but also exert unspecific, disturbing effects on multi-component biosynthetic machineries like the peptidoglycan synthesis complex, thus acting like "sand in a gearbox" [52].

Such a "sand in a gearbox" mechanism was also suggested for the antimicrobial activity of the lipodepsipeptide daptomycin, one of few antibiotics that was approved for clinical use in the last two decades and is now successfully being applied to treat infections by vancomycin-resistant enterococci (VRE) and MRSA. Despite the successful use of daptomycin in the clinical setting, its mode of action was incompletely understood for years and subject to controversial discussions hypothesizing on either a more targeted mode of action, that is, inhibition of cell wall biosynthesis or lipoteichoic acid biosynthesis pathways, or a rather generalized killing mechanism by inducing membrane depolarization. It has been further discussed that Ca^{2+}-daptomycin may have a CAMP-

like behavior in that it forms oligomeric structures and attaches to anionic membrane surfaces to perturb vital barrier functions of the bilayer [33]. However, the better potency of daptomycin compared to CAMPs and the fact that daptomycin specifically induces the so-called cell wall stress response in bacteria [53–55], which is commonly induced by cell wall synthesis-perturbing agents including β-lactams, glycopeptides, and mersacidin [56–58], points at a more clearly defined target in cell wall synthesis. Recent breakthrough studies shed light on the mode of daptomycin activity. It emerged that daptomycin affects overall membrane fluidity by inducing a severe rearrangement of fluid lipid domains, which then caused a rapid detachment of the membrane-associated lipid II synthase MurG and the phospholipid synthase PlsX that both preferentially colocalize with fluid membrane microdomains [59]. Moreover, a specific molecular target for Ca^{2+}-daptomycin could be discovered, that is, undecaprenyl-coupled cell envelope precursors in the presence of the anionic phospholipid phosphatidylglycerol, leading to the formation of a tripartite complex with undecaprenyl-coupled intermediates and membrane lipids [60]. Here, binding mainly occurred at the septum area and abrogated cell wall biosynthesis, which led to a delocalization of cell wall synthesis proteins and massive membrane rearrangements. Such mechanism may well result in the pleiotropic cellular effects that have been previously reported for daptomycin and explains the specificity of daptomycin for bacterial cells, thereby providing a concise model for the mode of action of daptomycin [60].

2.2 Inhibitors of RNA and Protein Synthesis

Bacterial transcription/translation is a further essential biosynthesis pathway that is targeted by various antimicrobial agents. Three different groups of antibiotics can be categorized that target different stages of the protein biosynthesis machinery (Fig. 3). One group of inhibitors interferes with DNA-dependent RNA polymerase (RNAP) to block transcription. Another group binds to the 30S or 50S ribosomal subunits to inhibit translation initiation and elongation or affect translational accuracy. Some antibiotics interfere with tRNA synthases and elongation factors to perturb the cellular concentration of charged tRNA molecules or the delivery and release of tRNA molecules to and from the ribosome.

Bacterial DNA-dependent RNAP is an attractive antimicrobial target, since RNA synthesis is essential for bacterial growth. The semisynthetic antibiotic rifampicin (also known as rifampin) is probably the best-known representative of RNAP inhibitors, which binds to RNAP at a site adjacent to the RNAP active center and inhibits the initiation of RNA synthesis by physically blocking the formation of the phosphodiester bond in the RNA backbone by a “steric occlusion” mechanism [61]. Other protein synthesis inhibitors directly interfere with the ribosomal complex. Aminoglycosides like streptomycin and gentamicin bind to a conserved rRNA

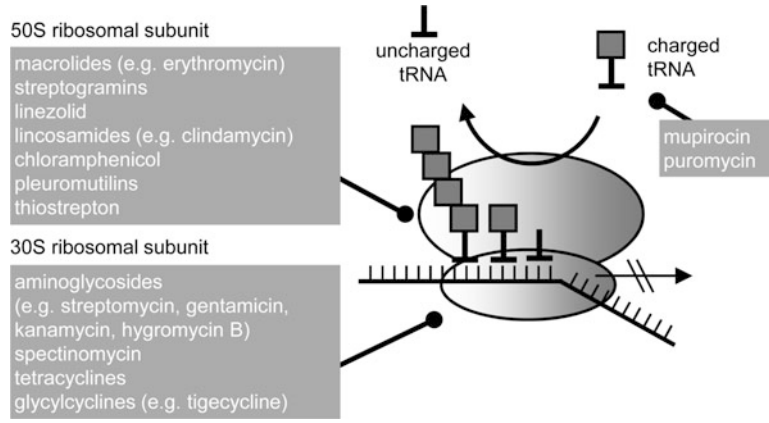

Fig. 3 Target sites of protein biosynthesis inhibitors. (Figure reprinted from Ref. [20])

sequence that is near the A-site of the 30S ribosomal subunit and affect the accuracy of translation. The interaction of aminoglycosides with the A-site disturbs the proofreading steps of the ribosome that are important to ensure translational fidelity and finally results in misreading of the mRNA code and the synthesis of erroneous proteins [62, 63]. Tetracyclines and glycylcyclines such as tigecycline also bind to the 30S ribosomal subunit in a region that is close to the codon-anticodon recognition site (A-site), thereby preventing the productive binding of charged aminoacyl-tRNAs to the ribosomal A-site [64]. Erythromycin and chloramphenicol both target the 50S ribosomal subunit and inhibit translation elongation. Erythromycin, a macrolide antibiotic, prevents the movement and release of the nascent peptide by blocking the tunnel that channels the nascent peptides away from the peptidyl transferase center [65]. Chloramphenicol prevents peptide bond formation by directly binding to the peptidyl transferase center [65–67].

Some antibiotics interfere with components in the periphery of the ribosome. For example, mupirocin, a mixture of several pseudomonic acids, blocks the activity of isoleucyl-tRNA synthetase, which prevents the charging of tRNA-Ile with the corresponding amino acid isoleucine [68, 69]. Noteworthy, the activities of aminoacyl-tRNA synthetase inhibitors like mupirocin were shown to ultimately induce the stringent response of bacteria [70, 71]. Puromycin is an aminoacyl-tRNA analog and thus incorporates into the nascent peptide chain causing premature termination and release [65]. Fusidic acid is a steroidal antibiotic that prevents the turnover of elongation factor G (EF-G) and arrests it at the ribosome after GTP hydrolysis. Although this does not lead to an inhibition of the EF-G-catalyzed translocation step of the ribosome, it will block the subsequent productive binding of new

aminoacyl-tRNA to the A-site. This is because functional aminoacyl-tRNA binding requires the elongation factor Tu (EF-Tu), but EF-G and EF-Tu mutually exclude themselves regarding their presence on the same ribosome [72, 73].

2.3 Inhibitors of DNA Synthesis

Antibiotics further successfully target essential bacterial processes involved in DNA replication and turnover. Here, quinolones are probably the most famous class of DNA synthesis inhibitors, which include the antibiotics ciprofloxacin and nalidixic acid. Quinolones perturb gyrase (topoisomerase II) and topoisomerase IV activities, enzymes that play important roles in chromosome function by coiling and uncoiling of DNA. Gyrase, for example, removes knots from DNA, assists for the bending and folding of DNA, activates the chromosome for all processes involving strand separation, and even responds to environmental changes by facilitating the movement of replication and transcription complexes through DNA by adding negative supercoils in front of the complex [74]. Gyrase forms a tetramer to bind DNA in which two A and two B subunits wrap the DNA into a negative supercoil. In a next step, gyrase breaks and rejoins DNA strands in an ATP-dependent manner to pass one region of duplex DNA through another [75]. By introducing such negative supercoils into DNA, gyrase relieves the topological stress that occurs during the translocation of transcription and replication complexes along the DNA strand. Topoisomerase IV is a decatenating enzyme and resolves interlinked daughter chromosomes upon DNA replication. Similar to gyrase, topoisomerase IV cleaves the phosphodiester bonds in a DNA double strand and stabilizes the break by covalent and non-covalent interactions. Subsequently, a second double strand is passed through the open gap followed by religation of the passage [76]. Here, the principles of gyrase and topoisomerase IV activities differ concerning their mechanism of DNA wrapping. While gyrase wraps DNA around itself, topoisomerase IV does not [74, 77]. Gyrase and topoisomerases play vital roles in DNA replication, transcription, repair, and recombination by ensuring an optimal level of global DNA supercoiling and removing local topological barriers, which make them essential enzymes for cell growth and division. This central role of gyrase and topoisomerase IV in DNA metabolism is one reason for the effectivity of quinolone antibiotics. However, quinolones do not simply inhibit the enzymatic functions of these enzymes. Quinolones rather lock the enzyme complexes after cleavage of the DNA strands but before they are rejoined. By this, quinolones produce double-strand breaks that are not resealed. Thus, quinolones stall gyrase and topoisomerase IV complexes on replicative DNA strands, which eventually leads to the deleterious release of double-strand DNA breaks and fragmentation of DNA finally causing bacterial cell death.

Mitomycin C, a natural product produced by *Streptomyces caespitosus*, is another antibiotic that efficiently interferes with DNA synthesis. Instead of inhibiting an enzyme function, mitomycin C has potent DNA cross-linking activity and catalyzes the intra- and interstrand cross-linkage of DNA strands as well as monofunctional alkyl lesions. Such cross-linking reactions inevitably lead to an arrest of DNA replication and subsequently bacterial cell death [78, 79]. However, due to its mechanism of action, which is not selectively acting against bacteria, mitomycin C is also used as an antitumor drug for the treatment of stomach, bladder, and pancreas cancer. Aside from mutations in gyrase or topoisomerase enzymes that are a common cause of quinolone resistance, bacteria have elicited a highly effective response cascade to evade the deleterious action of DNA damaging agents including quinolones and mitomycin C, the so-called SOS response. This DNA damage-induced stress response allows the bacterial cell to minimize the lethal and mutagenic consequences of the exposure to these antibiotics and helps the cells to cope with such agents at low concentrations [74, 80–83].

2.4 Antibiotics with Extended or Novel Modes of Action

In times of an increasing spread of bacterial resistance to clinically used antibiotics, we face an urgent need to find and develop novel antibiotics with new modes of action and resistance breaking properties. This section intends to highlight some of the recent advances from academia and industry to satisfy this need, covering antibiotics that inhibit or activate novel targets to cause lethal effects, drugs that efficiently interfere with known resistance factors or even compounds that show no detectable resistance at all.

Teixobactin is a member of a new class of antibiotics that is produced by the hitherto undescribed Gram-negative soil bacterium *Eleftheria terrae* [84]. Teixobactin is antibacterially active against many pathogenic Gram-positive bacteria as well as mycobacteria including *Mycobacterium tuberculosis* but lacks activity against Gram-negatives, most probably due to ineffective penetration of the outer membrane and/or efflux. Teixobactin was also effective in reducing the bacterial load in experimental infections of MRSA and *Streptococcus pneumoniae* in mice. Teixobactin uses a dual mechanism of action that is currently not used by any clinically applied antibiotic. To kill the bacteria, teixobactin interferes with cell wall synthesis reactions at several stages by sequestering the essential precursors of peptidoglycan synthesis (lipid II) as well as of teichoic acid synthesis (lipid III). Noteworthy, it seems difficult for unrelated strains to gain resistance to teixobactin. In vitro, no teixobactin-resistant mutants of *S. aureus* or *M. tuberculosis* were isolated at four times the MIC, which may be attributed to the dual mode of action of teixobactin by targeting more than one essential bacterial macromolecule. However, bacteria have eventually always found ways to adapt to antibiotic action, and it may be just a matter of time that a resistance mechanism to teixobactin will be identified.

β-Lactams are probably the most frequently used antibiotics to date and have a successful history in curing patients from infectious diseases, which is also due to their relatively small size as well as their good tolerability by the patients. However, the effectivity of β-lactam antibiotics is severely hampered by the action of β-lactamases, which can break down nearly every β-lactam by deacylation. Currently, more than thousand different β-lactamases from various structural classes and a wide range of substrate promiscuities and catalytic efficiencies are known, constantly evolving and disseminating with new β-lactam antibiotics that are introduced into clinical use. One strategy to overcome this problem is the constant derivatization and optimization of β-lactams to achieve species specificities and/or reduced susceptibility to β-lactamases. The direct inhibition of β-lactamases by β-lactamase inhibitors is another effective means to recover activity of β-lactam antibiotics. However, one disadvantage of β-lactamase inhibitors, which are also compounds with a β-lactam ring structure, is that they are also consumed by the β-lactamases, although at a much slower rate. Avibactam is a novel non-β-lactam β-lactamase inhibitor in clinical development combined with β-lactam antibiotic partners to treat infections with Gram-negative bacteria [85–87]. In contrast to other known β-lactamase inhibitors, avibactam covalently and slowly reversibly binds to various types of β-lactamases including TEM-1. Hence, deacylation of avibactam proceeds through regeneration of intact avibactam and not hydrolysis, which is a new and unique mechanism of inhibition among β-lactamase inhibitors.

Ribocil interferes with bacterial non-coding RNA (ncRNA), a new target molecule that is currently not used by any other clinically used antibiotic [88]. The researchers identified ribocil during a phenotypical screen for inhibitors of a metabolic pathway leading to the synthesis of riboflavin, also called vitamin B2, which is a crucial precursor of essential cofactors required for various enzyme reactions. One such cofactor is flavin mononucleotide (FMN) that functions as prosthetic group of several oxidoreductases including NADH dehydrogenase. Inside the human host, riboflavin is a rather rare metabolite that has to be produced by the bacteria to ensure their growth and vitality, rendering this pathway essential under such conditions. Ribocil-resistant mutants carry mutations in a non-coding DNA region of the bacterial genome, indicating that ribocil rather acts on the level of gene regulation than direct interaction with a riboflavin biosynthesis enzyme. The involved ncRNA domain is located upstream of the translational start site of a key synthase enzyme in the riboflavin biosynthesis pathway and constitutes a so-called riboswitch. Riboswitches are RNA regions that can change their structure upon binding to a corresponding ligand (here FMN ligand) in order to modulate the access of the transcription and translation machinery to the gene locus and thus prevent

expression of this gene. This mechanism allows the bacteria to shut down the riboflavin biosynthesis pathway when sufficient riboflavin is available. Like FMN ligands, ribocil also binds to this riboswitch and shuts down riboflavin synthesis, thereby killing the bacteria by depriving them of the essential precursor metabolite. Noteworthy, ribocil is not a close structural analog of a metabolite ligand, reducing the possibility of off-target effects on other pathways that involve riboflavin and FMN in the human host, which is underlined by the observation that even high doses of the compound were not toxic in mice.

Darobactin is a new, silent operon-derived and ribosomally synthesized antibiotic that emerged from a screen of *Photorhabdus* isolates. Darobactin acts against important Gram-negative pathogens both in vitro and in animal models of infection. Darobactin unfolds its new mode of action by targeting the bacterial insertase BamA, the central unit of the essential BAM complex that folds and inserts outer membrane proteins [89]. To this end, darobactin adopts a rigid β-strand conformation, mimicking the recognition signal of native BamA substrates to bind to the lateral gate of BamA. Upon binding to BamA, darobactin uses the membrane environment as an extended binding pocket by replacing a lipid molecule from the lateral gate of BamA, thereby mainly establishing backbone contacts which provides some potential robustness against resistance mutations [90].

Optimized arylomycins are a new class of Gram-negative antibiotics [91]. Arylomycins usually lack activity against Gram-negative pathogens, which is in part due to a naturally occurring mutation in the essential bacterial type I signal peptidase LepB of Gram-negative bacteria that reduces the binding affinity of arylomycin. The synthetic arylomycin derivative G0775 emerged from a systematic optimization program to yield arylomycin derivatives with increased target affinity and improved outer membrane penetration characteristics. By these means, G0775 exerts potent in vitro and in vivo activity against MDR Gram-negative bacteria and bypasses existing resistance mechanisms, for example, the deletion of the AcrB or TolC efflux pump subunits in wild-type *E. coli* did not affect the potency of G0775, indicating that the native *E. coli* efflux systems do not considerably confer resistance to G0775 [91].

PC190723, a benzamide derivative, is a potent and selective inhibitor of the essential cell division pacemaker protein FtsZ. PC190723 shows specific antibacterial activity against staphylococci including MRSA with minimal inhibitory concentrations (MICs) in the range of 1.4–2.8 μM. Further, it is the first FtsZ inhibitor with reported in vivo efficacy as it is effective in a murine septicemia model of staphylococcal infection [92, 93]. Bacterial cell division is achieved by the divisome, a multi-protein complex that is characterized by the time-dependent assembly of specific cell

division proteins [94]. At the onset of cell division, the tubulin homolog FtsZ localizes at mid cell to form the so-called FtsZ-ring or Z-ring in a GTP-dependent manner. The Z-ring functions as a scaffold for the assembly of the bacterial cytokinetic machinery. PC190723-treated rods like *Bacillus subtilis* show an elongated phenotype, while staphylococci show enlarged spherical cells. Localization of FtsZ revealed the formation of multiple rings and arcs in *S. aureus* and abnormal discrete foci throughout *B. subtilis* cells, indicating an interference of PC190723 with Z-ring formation [92, 95, 96]. There are discussions about the effect of PC190723 on the GTPase activity of FtsZ. While some studies could show a concentration-dependent inhibition of the GTPase activity of *S. aureus* and *B. subtilis* FtsZ [92, 96, 97], some more recent studies did not come to the same results but observed an increased GTPase activity of *S. aureus* FtsZ or no effect on *B. subtilis* FtsZ [98, 99]. The binding site of PC190723 maps to a cleft formed by the H7 helix, the T7-loop, and the C-terminal four-stranded β-sheet of *S. aureus* FtsZ [95, 98, 100]. Thus, the binding site is rather away from the GTP binding pocket, indicating that there seems to be at least no direct interference of PC190723 with the catalytic site of the GTPase domain. PC190723 further shows synergy with β-lactam antibiotics to kill MRSA [95]. Importantly, PC190723 re-sensitized MRSA to β-lactam antibiotics in vitro as well as in a mouse model of MRSA infection. This synergy is most probably achieved by the concomitant delocalization of their respective drug targets FtsZ and PBP2, since PBP2 depends on FtsZ for correct localization at the septum, where it is needed for transglycosylation of peptidoglycan in MRSA. Besides the synergistic effects, combination of imipenem with PC190723 significantly reduced the spontaneous frequency of PC190723-resistant mutants, which also showed an attenuated virulence. Thus, PC190723 represents an interesting new antibiotic that modulates the assembly/disassembly dynamics of FtsZ with promising antibacterial activity against an important human pathogen.

ADEP antibiotics belong to a new class of antibiotic acyldepsipeptides that exert prominent antibacterial activity against Gram-positive bacteria including MRSA in vitro and in vivo [101]. ADEP1, a natural product of *Streptomyces hawaiiensis* NRRL 15010, was first described in the 1980s [102]. Later, several new synthetic derivatives of ADEP1 with improved chemical and metabolic stability were obtained when researchers established a route for total ADEP synthesis and initiated a chemistry program. One of these derivatives, ADEP4, showed impressive MICs in the sub-μg/ml range against MRSA. ADEPs demonstrate an unprecedented mode of action by targeting ClpP, the proteolytic core unit of the bacterial Clp protease complex (Fig. 4) [101, 103–106]. Clp proteases are important for protein turnover and homeostasis in

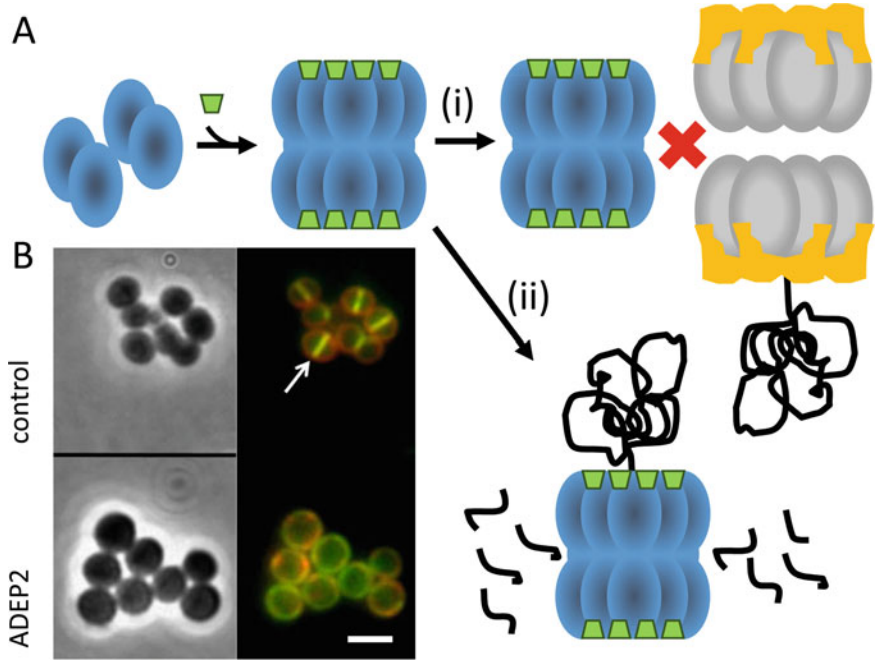

Fig. 4 ADEPs deregulate the proteolytic activity of ClpP. (**A**) Model on the ADEP mechanism of action. ADEPs (green) perturb the activity of ClpP in a multilayered fashion: ADEPs induce the oligomerization of ClpP monomers (blue) into the tetradecameric complex. ADEPs and Clp-ATPases (gray) share the same binding sites on ClpP. By binding to ClpP, ADEPs abrogate the interaction of ClpP with corresponding Clp-ATPase, which leads to the inhibition of the natural functions of Clp in protein turnover (i). ADEPs bind to the outer rim of the apical and distal surfaces of ClpP in a 1:1 stoichiometry. Upon binding, ADEP induces a conformational shift in the N-terminal region of ClpP that results in the enlargement of the entrance pore to the proteolytic chamber of ClpP. Now, also non-native protein substrates gain access to the proteolytic chamber of ClpP, releasing the degradative capacity of ClpP from strict regulation by Clp-ATPases, which leads to an untimely degradation of specific proteins or nascent polypeptides at the ribosome (ii). (**B**) ADEP treatment of *S. aureus* leads to cell division inhibition and finally bacterial death. Fluorescence images show the bacterial membrane (red) and the divisome protein PBP2 (green). PBP2 usually localizes at mid cell of dividing bacteria (upper panel, arrow). Upon ADEP treatment, PBP2 delocalizes from the division site (lower panel), which is representative for the delocalization of several important cell division proteins under these conditions. This delocalization is a result of the degradation of the essential FtsZ protein by ADEP-activated ClpP. Scale bar, 2.5 μm. (Figure reprinted from Ref. [20])

bacteria to maintain vital cellular functions particularly under stress conditions. Apart from their crucial role in general protein quality control by degrading abnormally folded or otherwise aberrant or malfunctioning proteins, their temporally and spatially precise proteolysis of key regulatory proteins additionally directs developmental processes like cell motility, genetic competence, cell differentiation, sporulation, as well as important aspects of virulence. Due to their apparent relevance for many physiological processes and their conservation among diverse bacterial species including human pathogens, the bacterial Clp protease emerged

as a new target for antibiotic intervention and virulence inhibition [107, 108]. Usually, ClpP is tightly regulated by Clp-ATPases and is unable to degrade proteins on its own. Biochemical studies demonstrated that ADEPs induce ClpP oligomerization and activate ClpP to degrade unfolded polypeptides as well as flexible proteins independently [103]. In addition, ADEPs abrogate the interaction of ClpP with cooperating Clp-ATPases thereby preventing all natural functions of ClpP in general and regulatory proteolysis. Crystal structures and EM images of ClpP in its free form and in complex with ADEPs provided a rational for these biochemical observations. ADEPs compete with the Clp-ATPases for the same binding site and finally trigger a closed- to open-gate structural transition of the ClpP N-terminal segments that opens the substrate entrance pore of ClpP, which is otherwise tightly closed [104, 109]. In the cellular context, interestingly, high-resolution microscopy revealed a significant swelling of coccoid *S. aureus* and *S. pneumoniae* cells as well as an impressive filamentation of rod-shaped *B. subtilis* cells in the presence of low inhibitory ADEP concentrations, clearly indicating stalled bacterial cell division [110]. Following the localization of fluorescently labelled cell division proteins by fluorescence microscopy revealed a mislocalization of essential members of the divisome including FtsZ [110–113]. Immunodetection of FtsZ in ADEP-treated cells showed a significant reduction of the concentration of FtsZ protein in a time-dependent manner, and indeed, ADEP-activated ClpP rapidly degraded purified FtsZ protein in vitro [110, 114]. Thus, ADEPs prevent bacterial cell division by a different, yet unprecedented mechanism that is by activating a bacterial enzyme rather than inhibition of an enzymatic reaction, which destines the bacteria to death in a suicidal manner. Noteworthy, ADEPs were also shown to kill mycobacteria by inhibiting the natural functions of the Clp system instead of over-activating ClpP [115], thereby revealing that ADEPs employ different killing mechanisms depending on the target microorganism.

Antibiotics play an important role in our everyday life, since they are essential weapons in our fight against bacterial infections and additionally provide powerful tools, for example, in the food industry or in microbiology research. The examples in this chapter show how inventive nature is in establishing new antibiotic mechanisms of action and that there may be still more, yet unknown ways to interfere with the bacterial lifestyle. By studying such modes of action along with the coevolving resistance mechanisms, we will gain deeper insights into the bacterial way of life, which is an essential step toward the goal of developing new strategies to treat life-threatening bacterial infections while minimizing their impact on human health.

Acknowledgment

I appreciate funding by the Deutsche Forschungsgemeinschaft (DFG, German Research Foundation): Project-ID 398967434 (TRR 261-A02), the German Center for Infection Research (DZIF; TTU 09.815), as well as support by infrastructural funding from the Cluster of Excellence EXC 2124 Controlling Microbes to Fight Infections. I deeply thank Anne Berscheid for her continuous support, helpful discussions, and endless patience.

References

1. WHO (2015) http://www.who.int/mediacentre/factsheets/fs194/en/. Accessed 29 June 2022
2. Matos C, Sass P (2020) Tackling antimicrobial resistance by exploring new mechanisms of antibiotic action. Future Microbiol 15: 703–708
3. CDC (2011) Antimicrobial Resistance Posing Growing Health Threat. Centers for Disease Control and Prevention. http://www.cdc.gov/media/releases/2011/p0407_antimicrobialresistance.html. Accessed 29 June 2022
4. AMR-review (2016) 22nd March 2016-Infection Prevention Control and Surveillance: limiting the development and spread of drug resistance. http://amr-review.org/. Accessed 29 June 2022
5. Resistance RoA (2016) Tackling drug-resistant infections globally: final report and recommendations. https://amr-review.org. Accessed 29 June 2022
6. Nature E (2018) Wanted: a reward for antibiotic development. Nat Biotechnol 36:555
7. Cooper MA, Shlaes D (2011) Fix the antibiotics pipeline. Nature 472(7341):32
8. EU-Commission (2008) Innovative Medicines Initiative (IMI). https://www.imi.europa.eu. Accessed 29 June 2022
9. EU-Commission (2011) Action plan against the rising threats from Antimicrobial Resistance. https://health.ec.europa.eu/system/files/2020-01/communication_amr_2011_748_en_0.pdf. Accessed 29 June 2022
10. EU-Commission (2017) A European One Health Action Plan against Antimicrobial Resistance (AMR). https://health.ec.europa.eu/system/files/2020-01/amr_2017_action-plan_0.pdf. Accessed 29 June 2022
11. EU-Commission (2011) New Drugs for Bad Bugs (ND4BB). https://www.imi.europa.eu/projects-results/project-factsheets/nd4bb. Accessed 29 June 2022
12. EU-Commission (2011) Joint Programming Initiative on AMR (JPIAMR). https://www.jpiamr.eu. Accessed 29 June 2022
13. America IDSo (2010) The 10 × '20 Initiative: pursuing a global commitment to develop 10 new antibacterial drugs by 2020. Clin Infect Dis 50 (8):1081-1083
14. Partnership GGARD GARDP. Global Antibiotic Research & Development Partnership. https://www.gardp.org. Accessed 29 June 2022
15. FOR854 (2008) https://gepris.dfg.de/gepris/projekt/33421847. Accessed 29 June 2022
16. DZIF (2010) http://www.dzif.de/en/research/novel_antiinfectives/. Accessed 29 June 2022
17. CMFI CoE controlling microbes to fight infections. https://uni-tuebingen.de/en/research/core-research/cluster-of-excellence-cmfi/. Accessed 29 June 2022
18. Transregional Collaborative Research Center TRR261. https://trr261.de. Accessed 29 June 2022
19. GRC (2016) Gordon Research Conference: new antibacterial discovery & development. https://www.grc.org/new-antibacterial-discovery-and-development-conference/default.aspx. Accessed 29 June 2022
20. Sass P (2017) Antibiotics: precious goods in changing times. Methods Mol Biol 1520:3–22
21. Russell AD (2003) Similarities and differences in the responses of microorganisms to biocides. J Antimicrob Chemother 52(5): 750–763
22. Aminov RI (2009) The role of antibiotics and antibiotic resistance in nature. Environ Microbiol 11(12):2970–2988

23. Yang D, Biragyn A, Kwak LW, Oppenheim JJ (2002) Mammalian defensins in immunity: more than just microbicidal. Trends Immunol 23(6):291–296
24. Yang D, Biragyn A, Hoover DM, Lubkowski J, Oppenheim JJ (2004) Multiple roles of antimicrobial defensins, cathelicidins, and eosinophil-derived neurotoxin in host defense. Annu Rev Immunol 22:181–215
25. Bowdish DM, Davidson DJ, Hancock RE (2005) A re-evaluation of the role of host defence peptides in mammalian immunity. Curr Protein Pept Sci 6(1):35–51
26. Kodani S, Hudson ME, Durrant MC, Buttner MJ, Nodwell JR, Willey JM (2004) The SapB morphogen is a lantibiotic-like peptide derived from the product of the developmental gene *ramS* in *Streptomyces coelicolor*. Proc Natl Acad Sci U S A 101(31):11448–11453
27. Kleerebezem M (2004) Quorum sensing control of lantibiotic production; nisin and subtilin autoregulate their own biosynthesis. Peptides 25(9):1405–1414
28. Schmitz S, Hoffmann A, Szekat C, Rudd B, Bierbaum G (2006) The lantibiotic mersacidin is an autoinducing peptide. Appl Environ Microbiol 72(11):7270–7277
29. Navarre WW, Schneewind O (1999) Surface proteins of gram-positive bacteria and mechanisms of their targeting to the cell wall envelope. Microbiol Mol Biol Rev 63(1): 174–229
30. van Heijenoort J (2001) Formation of the glycan chains in the synthesis of bacterial peptidoglycan. Glycobiology 11(3):25–36
31. Pages JM, James CE, Winterhalter M (2008) The porin and the permeating antibiotic: a selective diffusion barrier in Gram-negative bacteria. Nat Rev Microbiol 6(12):893–903
32. Coyette J, van der Ende A (2008) Peptidoglycan: the bacterial Achilles heel. FEMS Microbiol Rev 32(2):147–148
33. Schneider T, Sahl HG (2010) An oldie but a goodie – cell wall biosynthesis as antibiotic target pathway. Int J Med Microbiol 300(2-3):161–169
34. Yocum RR, Rasmussen JR, Strominger JL (1980) The mechanism of action of penicillin. Penicillin acylates the active site of *Bacillus stearothermophilus* D-alanine carboxypeptidase. J Biol Chem 255(9):3977–3986
35. Yocum RR, Waxman DJ, Rasmussen JR, Strominger JL (1979) Mechanism of penicillin action: penicillin and substrate bind covalently to the same active site serine in two bacterial D-alanine carboxypeptidases. Proc Natl Acad Sci U S A 76(6):2730–2734
36. Neuhaus FC, Lynch JL (1964) The enzymatic synthesis of D-alanyl-D-alanine. 3. On the inhibition of D-alanyl-D-alanine synthetase by the antibiotic D-cycloserine. Biochemistry 3:471–480
37. Lambert MP, Neuhaus FC (1972) Mechanism of D-cycloserine action: alanine racemase from *Escherichia coli* W. J Bacteriol 110(3):978–987
38. Kahan FM, Kahan JS, Cassidy PJ, Kropp H (1974) The mechanism of action of fosfomycin (phosphonomycin). Ann N Y Acad Sci 235 (0):364-386
39. Bouhss A, Crouvoisier M, Blanot D, Mengin-Lecreulx D (2004) Purification and characterization of the bacterial MraY translocase catalyzing the first membrane step of peptidoglycan biosynthesis. J Biol Chem 279(29):29974–29980
40. Stone KJ, Strominger JL (1971) Mechanism of action of bacitracin: complexation with metal ion and C 55 -isoprenyl pyrophosphate. Proc Natl Acad Sci U S A 68(12):3223–3227
41. Storm DR, Strominger JL (1973) Complex formation between bacitracin peptides and isoprenyl pyrophosphates. The specificity of lipid-peptide interactions. J Biol Chem 248(11):3940–3945
42. Schneider T, Gries K, Josten M, Wiedemann I, Pelzer S, Labischinski H, Sahl HG (2009) The lipopeptide antibiotic Friulimicin B inhibits cell wall biosynthesis through complex formation with bactoprenol phosphate. Antimicrob Agents Chemother 53(4): 1610–1618
43. Hiramatsu K (2001) Vancomycin-resistant *Staphylococcus aureus*: a new model of antibiotic resistance. Lancet Infect Dis 1(3): 147–155
44. Cudic P, Kranz JK, Behenna DC, Kruger RG, Tadesse H, Wand AJ, Veklich YI, Weisel JW, McCafferty DG (2002) Complexation of peptidoglycan intermediates by the lipoglycodepsipeptide antibiotic ramoplanin: minimal structural requirements for intermolecular complexation and fibril formation. Proc Natl Acad Sci U S A 99(11):7384–7389
45. Bierbaum G, Sahl HG (2009) Lantibiotics: mode of action, biosynthesis and bioengineering. Curr Pharm Biotechnol 10:2–18
46. Sahl HG, Bierbaum G (1998) Lantibiotics: biosynthesis and biological activities of uniquely modified peptides from gram-positive bacteria. Annu Rev Microbiol 52: 41–79
47. Brötz H, Bierbaum G, Leopold K, Reynolds PE, Sahl HG (1998) The lantibiotic mersacidin inhibits peptidoglycan synthesis by

targeting lipid II. Antimicrob Agents Chemother 42(1):154–160

48. Galvez A, Abriouel H, Lopez RL, Ben Omar N (2007) Bacteriocin-based strategies for food biopreservation. Int J Food Microbiol 120(1-2):51–70
49. Brötz H, Josten M, Wiedemann I, Schneider U, Gotz F, Bierbaum G, Sahl HG (1998) Role of lipid-bound peptidoglycan precursors in the formation of pores by nisin, epidermin and other lantibiotics. Mol Microbiol 30(2):317–327
50. Wiedemann I, Breukink E, van Kraaij C, Kuipers OP, Bierbaum G, de Kruijff B, Sahl HG (2001) Specific binding of nisin to the peptidoglycan precursor lipid II combines pore formation and inhibition of cell wall biosynthesis for potent antibiotic activity. J Biol Chem 276(3):1772–1779
51. Peschel A, Sahl HG (2006) The co-evolution of host cationic antimicrobial peptides and microbial resistance. Nat Rev Microbiol 4(7):529–536
52. Sass V, Pag U, Tossi A, Bierbaum G, Sahl HG (2008) Mode of action of human beta-defensin 3 (hBD3) against *Staphylococcus aureus* and transcriptional analysis of responses to defensin challenge. Int J Med Microbiol 298:619–633
53. Muthaiyan A, Silverman JA, Jayaswal RK, Wilkinson BJ (2008) Transcriptional profiling reveals that daptomycin induces the *Staphylococcus aureus* cell wall stress stimulon and genes responsive to membrane depolarization. Antimicrob Agents Chemother 52: 980–990
54. Wecke T, Zuhlke D, Mader U, Jordan S, Voigt B, Pelzer S, Labischinski H, Homuth G, Hecker M, Mascher T (2009) Daptomycin versus Friulimicin B: in-depth profiling of *Bacillus subtilis* cell envelope stress responses. Antimicrob Agents Chemother 53(4):1619–1623
55. Camargo IL, Neoh HM, Cui L, Hiramatsu K (2008) Serial daptomycin selection generates daptomycin-nonsusceptible Staphylococcus aureus strains with a heterogeneous vancomycin-intermediate phenotype. Antimicrob Agents Chemother 52(12):4289–4299
56. Kuroda M, Kuroda H, Oshima T, Takeuchi F, Mori H, Hiramatsu K (2003) Two-component system VraSR positively modulates the regulation of cell-wall biosynthesis pathway in *Staphylococcus aureus*. Mol Microbiol 49(3):807–821
57. Utaida S, Dunman PM, Macapagal D, Murphy E, Projan SJ, Singh VK, Jayaswal RK, Wilkinson BJ (2003) Genome-wide transcriptional profiling of the response of *Staphylococcus aureus* to cell-wall-active antibiotics reveals a cell-wall-stress stimulon. Microbiology 149(Pt 10):2719–2732
58. Sass P, Jansen A, Szekat C, Sass V, Sahl HG, Bierbaum G (2008) The lantibiotic mersacidin is a strong inducer of the cell wall stress response of *Staphylococcus aureus*. BMC Microbiol 8:186
59. Müller A, Wenzel M, Strahl H, Grein F, Saaki TNV, Kohl B, Siersma T, Bandow JE, Sahl HG, Schneider T, Hamoen LW (2016) Daptomycin inhibits cell envelope synthesis by interfering with fluid membrane microdomains. Proc Natl Acad Sci U S A 113(45): E7077–e7086
60. Grein F, Müller A, Scherer KM, Liu X, Ludwig KC, Klöckner A, Strach M, Sahl HG, Kubitscheck U, Schneider T (2020) Ca(2+)-Daptomycin targets cell wall biosynthesis by forming a tripartite complex with undecaprenyl-coupled intermediates and membrane lipids. Nat Commun 11(1):1455
61. Cavalleri B, Turconi M, Tamborini G, Occelli E, Cietto G, Pallanza R, Scotti R, Berti M, Romano G, Parenti F (1990) Synthesis and biological activity of some derivatives of rifamycin P. J Med Chem 33(5): 1470–1476
62. Yoshizawa S, Fourmy D, Puglisi JD (1998) Structural origins of gentamicin antibiotic action. EMBO J 17(22):6437–6448
63. Carter AP, Clemons WM, Brodersen DE, Morgan-Warren RJ, Wimberly BT, Ramakrishnan V (2000) Functional insights from the structure of the 30S ribosomal subunit and its interactions with antibiotics. Nature 407(6802):340–348
64. Pioletti M, Schlünzen F, Harms J, Zarivach R, Gluhmann M, Avila H, Bashan A, Bartels H, Auerbach T, Jacobi C, Hartsch T, Yonath A, Franceschi F (2001) Crystal structures of complexes of the small ribosomal subunit with tetracycline, edeine and IF3. EMBO J 20(8):1829–1839
65. Schlünzen F, Zarivach R, Harms J, Bashan A, Tocilj A, Albrecht R, Yonath A, Franceschi F (2001) Structural basis for the interaction of antibiotics with the peptidyl transferase centre in eubacteria. Nature 413(6858):814–821
66. Long KS, Porse BT (2003) A conserved chloramphenicol binding site at the entrance to the ribosomal peptide exit tunnel. Nucleic Acids Res 31(24):7208–7215
67. Moazed D, Noller HF (1987) Chloramphenicol, erythromycin, carbomycin and

vernamycin B protect overlapping sites in the peptidyl transferase region of 23S ribosomal RNA. Biochimie 69(8):879–884

68. Cassels R, Oliva B, Knowles D (1995) Occurrence of the regulatory nucleotides ppGpp and pppGpp following induction of the stringent response in staphylococci. J Bacteriol 177(17):5161–5165
69. Crosse AM, Greenway DL, England RR (2000) Accumulation of ppGpp and ppGp in *Staphylococcus aureus* 8325-4 following nutrient starvation. Lett Appl Microbiol 31(4): 332–337
70. Abranches J, Martinez AR, Kajfasz JK, Chavez V, Garsin DA, Lemos JA (2009) The molecular alarmone (p)ppGpp mediates stress responses, vancomycin tolerance, and virulence in *Enterococcus faecalis*. J Bacteriol 191(7):2248–2256
71. Reiss S, Pane-Farre J, Fuchs S, Francois P, Liebeke M, Schrenzel J, Lindequist U, Lalk M, Wolz C, Hecker M, Engelmann S (2012) Global analysis of the *Staphylococcus aureus* response to mupirocin. Antimicrob Agents Chemother 56(2):787–804
72. Otaka T, Kaji A (1973) Evidence that fusidic acid inhibits the binding of aminoacyl-tRNA to the donor as well as the acceptor site of the ribosomes. Eur J Biochem 38(1):46–53
73. Gao YG, Selmer M, Dunham CM, Weixlbaumer A, Kelley AC, Ramakrishnan V (2009) The structure of the ribosome with elongation factor G trapped in the posttranslocational state. Science 326(5953):694–699
74. Drlica K, Zhao X (1997) DNA gyrase, topoisomerase IV, and the 4-quinolones. Microbiol Mol Biol Rev 61(3):377–392
75. Reece RJ, Maxwell A (1991) DNA gyrase: structure and function. Crit Rev Biochem Mol Biol 26(3-4):335–375
76. Roca J (1995) The mechanisms of DNA topoisomerases. Trends Biochem Sci 20(4): 156–160
77. Peng H, Marians KJ (1995) The interaction of *Escherichia coli* topoisomerase IV with DNA. J Biol Chem 270(42):25286–25290
78. Danshiitsoodol N, de Pinho CA, Matoba Y, Kumagai T, Sugiyama M (2006) The mitomycin C (MMC)-binding protein from MMC-producing microorganisms protects from the lethal effect of bleomycin: crystallographic analysis to elucidate the binding mode of the antibiotic to the protein. J Mol Biol 360(2):398–408
79. Claverys JP, Prudhomme M, Martin B (2006) Induction of competence regulons as a general response to stress in gram-positive bacteria. Annu Rev Microbiol 60:451–475
80. Au N, Kuester-Schoeck E, Mandava V, Bothwell LE, Canny SP, Chachu K, Colavito SA, Fuller SN, Groban ES, Hensley LA, O'Brien TC, Shah A, Tierney JT, Tomm LL, O'Gara TM, Goranov AI, Grossman AD, Lovett CM (2005) Genetic composition of the *Bacillus subtilis* SOS system. J Bacteriol 187(22):7655–7666
81. Friedman N, Vardi S, Ronen M, Alon U, Stavans J (2005) Precise temporal modulation in the response of the SOS DNA repair network in individual bacteria. PLoS Biol 3(7):e238
82. Kelley WL (2006) Lex marks the spot: the virulent side of SOS and a closer look at the LexA regulon. Mol Microbiol 62(5): 1228–1238
83. Michel B (2005) After 30 years of study, the bacterial SOS response still surprises us. PLoS Biol 3(7):e255
84. Ling LL, Schneider T, Peoples AJ, Spoering AL, Engels I, Conlon BP, Mueller A, Schaberle TF, Hughes DE, Epstein S, Jones M, Lazarides L, Steadman VA, Cohen DR, Felix CR, Fetterman KA, Millett WP, Nitti AG, Zullo AM, Chen C, Lewis K (2015) A new antibiotic kills pathogens without detectable resistance. Nature 517(7535):455–459
85. Ehmann DE, Jahic H, Ross PL, Gu RF, Hu J, Kern G, Walkup GK, Fisher SL (2012) Avibactam is a covalent, reversible, non-beta-lactam beta-lactamase inhibitor. Proc Natl Acad Sci U S A 109(29):11663–11668
86. Ehmann DE, Jahic H, Ross PL, Gu RF, Hu J, Durand-Reville TF, Lahiri S, Thresher J, Livchak S, Gao N, Palmer T, Walkup GK, Fisher SL (2013) Kinetics of avibactam inhibition against Class A, C, and D beta-lactamases. J Biol Chem 288(39): 27960–27971
87. Lahiri SD, Mangani S, Jahic H, Benvenuti M, Durand-Reville TF, De Luca F, Ehmann DE, Rossolini GM, Alm RA, Docquier JD (2015) Molecular basis of selective inhibition and slow reversibility of avibactam against class D carbapenemases: a structure-guided study of OXA-24 and OXA-48. ACS Chem Biol 10(2):591–600
88. Howe JA, Wang H, Fischmann TO, Balibar CJ, Xiao L, Galgoci AM, Malinverni JC, Mayhood T, Villafania A, Nahvi A, Murgolo N, Barbieri CM, Mann PA, Carr D, Xia E, Zuck P, Riley D, Painter RE, Walker SS, Sherborne B, de Jesus R, Pan W, Plotkin MA, Wu J, Rindgen D, Cummings J, Garlisi CG, Zhang R, Sheth PR, Gill CJ, Tang H, Roemer T (2015) Selective small-molecule

inhibition of an RNA structural element. Nature 526(7575):672–677

89. Imai Y, Meyer KJ, Iinishi A, Favre-Godal Q, Green R, Manuse S, Caboni M, Mori M, Niles S, Ghiglieri M, Honrao C, Ma X, Guo JJ, Makriyannis A, Linares-Otoya L, Böhringer N, Wuisan ZG, Kaur H, Wu R, Mateus A, Typas A, Savitski MM, Espinoza JL, O'Rourke A, Nelson KE, Hiller S, Noinaj N, Schäberle TF, D'Onofrio A, Lewis K (2019) A new antibiotic selectively kills Gram-negative pathogens. Nature 576(7787):459–464
90. Kaur H, Jakob RP, Marzinek JK, Green R, Imai Y, Bolla JR, Agustoni E, Robinson CV, Bond PJ, Lewis K, Maier T, Hiller S (2021) The antibiotic darobactin mimics a β-strand to inhibit outer membrane insertase. Nature 593(7857):125–129
91. Smith PA, Koehler MFT, Girgis HS, Yan D, Chen Y, Chen Y, Crawford JJ, Durk MR, Higuchi RI, Kang J, Murray J, Paraselli P, Park S, Phung W, Quinn JG, Roberts TC, Rougé L, Schwarz JB, Skippington E, Wai J, Xu M, Yu Z, Zhang H, Tan MW, Heise CE (2018) Optimized arylomycins are a new class of Gram-negative antibiotics. Nature 561(7722):189–194
92. Haydon DJ, Stokes NR, Ure R, Galbraith G, Bennett JM, Brown DR, Baker PJ, Barynin VV, Rice DW, Sedelnikova SE, Heal JR, Sheridan JM, Aiwale ST, Chauhan PK, Srivastava A, Taneja A, Collins I, Errington J, Czaplewski LG (2008) An inhibitor of FtsZ with potent and selective anti-staphylococcal activity. Science 321(5896): 1673–1675
93. Haydon DJ, Bennett JM, Brown D, Collins I, Galbraith G, Lancett P, Macdonald R, Stokes NR, Chauhan PK, Sutariya JK, Nayal N, Srivastava A, Beanland J, Hall R, Henstock V, Noula C, Rockley C, Czaplewski L (2010) Creating an antibacterial with in vivo efficacy: synthesis and characterization of potent inhibitors of the bacterial cell division protein FtsZ with improved pharmaceutical properties. J Med Chem 53(10): 3927–3936
94. Adams DW, Errington J (2009) Bacterial cell division: assembly, maintenance and disassembly of the Z ring. Nat Rev Microbiol 7(9): 642–653
95. Tan CM, Therien AG, Lu J, Lee SH, Caron A, Gill CJ, Lebeau-Jacob C, Benton-Perdomo L, Monteiro JM, Pereira PM, Elsen NL, Wu J, Deschamps K, Petcu M, Wong S, Daigneault E, Kramer S, Liang L, Maxwell E, Claveau D, Vaillancourt J, Skorey K, Tam J, Wang H, Meredith TC, Sillaots S, Wang-Jarantow L, Ramtohul Y, Langlois E, Landry F, Reid JC, Parthasarathy G, Sharma S, Baryshnikova A, Lumb KJ, Pinho MG, Soisson SM, Roemer T (2012) Restoring methicillin-resistant *Staphylococcus aureus* susceptibility to beta-lactam antibiotics. Sci Transl Med 4(126):126ra135
96. Adams DW, Wu LJ, Czaplewski LG, Errington J (2011) Multiple effects of benzamide antibiotics on FtsZ function. Mol Microbiol 80(1):68–84
97. Andreu JM, Schaffner-Barbero C, Huecas S, Alonso D, Lopez-Rodriguez ML, Ruiz-Avila LB, Nunez-Ramirez R, Llorca O, Martin-Galiano AJ (2010) The antibacterial cell division inhibitor PC190723 is an FtsZ polymer-stabilizing agent that induces filament assembly and condensation. J Biol Chem 285(19): 14239–14246
98. Elsen NL, Lu J, Parthasarathy G, Reid JC, Sharma S, Soisson SM, Lumb KJ (2012) Mechanism of action of the cell-division inhibitor PC190723: modulation of FtsZ assembly cooperativity. J Am Chem Soc 134(30):12342–12345
99. Anderson DE, Kim MB, Moore JT, O'Brien TE, Sorto NA, Grove CI, Lackner LL, Ames JB, Shaw JT (2012) Comparison of small molecule inhibitors of the bacterial cell division protein FtsZ and identification of a reliable cross-species inhibitor. ACS Chem Biol 7(11):1918–1928
100. Matsui T, Yamane J, Mogi N, Yamaguchi H, Takemoto H, Yao M, Tanaka I (2012) Structural reorganization of the bacterial cell-division protein FtsZ from *Staphylococcus aureus*. Acta Crystallogr Sect D Biol Crystallogr 68(Pt 9):1175–1188
101. Brötz-Oesterhelt H, Beyer D, Kroll HP, Endermann R, Ladel C, Schroeder W, Hinzen B, Raddatz S, Paulsen H, Henninger K, Bandow JE, Sahl HG, Labischinski H (2005) Dysregulation of bacterial proteolytic machinery by a new class of antibiotics. Nat Med 11(10):1082–1087
102. Michel KH, Kastner RE (1985) A54556 antibiotics and process for production thereof. US patent 4,492,650, 1985
103. Kirstein J, Hoffmann A, Lilie H, Schmidt R, Rübsamen-Waigmann H, Brötz-Oesterhelt H, Mogk A, Turgay K (2009) The antibiotic ADEP reprogrammes ClpP, switching it from a regulated to an uncontrolled protease. EMBO Mol Med 1(1): 37–49
104. Lee BG, Park EY, Jeon H, Sung KH, Paulsen H, Rübsamen-Schaeff H, Brötz-

Oesterhelt H, Song HK (2010) Structures of ClpP in complex with a novel class of antibiotics reveal its activation mechanism. Nat Struct Mol Biol 17(4):471–478

105. Gersch M, Famulla K, Dahmen M, Gobl C, Malik I, Richter K, Korotkov VS, Sass P, Rubsamen-Schaeff H, Madl T, Brotz-Oesterhelt H, Sieber SA (2015) AAA+ chaperones and acyldepsipeptides activate the ClpP protease via conformational control. Nat Commun 6:6320
106. Pan S, Malik IT, Thomy D, Henrichfreise B, Sass P (2019) The functional ClpXP protease of *Chlamydia trachomatis* requires distinct *clpP* genes from separate genetic loci. Sci Rep 9(1):14129
107. Sass P, Brötz-Oesterhelt H (2013) Bacterial caseinolytic proteases as novel targets for antibacterial treatment. Int J Med Microbiol 304: 23
108. Baker TA, Sauer RT (2012) ClpXP, an ATP-powered unfolding and protein-degradation machine. Biochim Biophys Acta 1823(1):15–28
109. Li DH, Chung YS, Gloyd M, Joseph E, Ghirlando R, Wright GD, Cheng YQ, Maurizi MR, Guarne A, Ortega J (2010) Acyldepsipeptide antibiotics induce the formation of a structured axial channel in ClpP: a model for the ClpX/ClpA-bound state of ClpP. Chem Biol 17(9):959–969
110. Sass P, Josten M, Famulla K, Schiffer G, Sahl HG, Hamoen L, Brötz-Oesterhelt H (2011) Antibiotic acyldepsipeptides activate ClpP peptidase to degrade the cell division protein FtsZ. Proc Natl Acad Sci USA 108(42): 17474–17479
111. Silber N, Mayer C, Matos C, Sass P (2021) Progression of the late-stage divisome is unaffected by the depletion of the cytoplasmic FtsZ pool. Commun Biol 4(1):270
112. Mayer C, Sass P, Brötz-Oesterhelt H (2019) Consequences of dosing and timing on the antibacterial effects of ADEP antibiotics. Int J Med Microbiol 309(7):151329
113. Silber N, Matos C, Mayer C, Sass P (2020) Cell division protein FtsZ: from structure and mechanism to antibiotic target. Future Microbiol 15:801–831
114. Silber N, Pan S, Schäkermann S, Mayer C, Brötz-Oesterhelt H, Sass P (2020) Cell division protein FtsZ is unfolded for N-terminal degradation by antibiotic-activated ClpP. MBio 11(3):e01006–e01020
115. Famulla K, Sass P, Malik I, Akopian T, Kandror O, Alber M, Hinzen B, Ruebsamen-Schaeff H, Kalscheuer R, Goldberg AL, Brotz-Oesterhelt H (2016) Acyldepsipeptide antibiotics kill mycobacteria by preventing the physiological functions of the ClpP1P2 protease. Mol Microbiol. 101(2): 194-209

Chapter 2

A Whole-Cell Assay for Detection of Antibacterial Activity in Actinomycete Culture Supernatants

Anika Rütten, Wolfgang Wohlleben, Lena Mitousis, and Ewa Maria Musiol-Kroll

Abstract

Whole-cell antibacterial assays are particularly suitable for fast detection and semi-quantification of bioactivities in extracts or other solutions such as microbial culture supernatants. As *Actinomycetales*, including the members of the genus *Streptomyces*, are one of the most potent "suppliers" of antibiotics and other bioactive compounds, there is a strong interest in the development of useful assays enabling early identification of such valuable producers. Furthermore, such assays facilitate the screening of a large collection of clones for the detection of engineered "super-producers" that are essential for industrial manufacturing of the respective product.

In this protocol, we describe a whole-cell assay for a fast detection of antimicrobial agents in culture supernatants. As model, *Streptomyces fradiae* DSM 41546, the producer of the antibiotic tylosin, and the test strain *Bacillus subtilis* ATCC 6051 are used. Culture supernatants of *S. fradiae* DSM 41546 and controls are diluted, and their antibiotic activity is tested against *B. subtilis* ATCC 6051. For the dilutions of tylosin-containing culture supernatant, a clear concentration-dependent growth inhibition effect on *B. subtilis* ATCC 6051 is demonstrated. In contrast, dilutions of the culture supernatant lacking tylosin do not inhibit the growth of *B. subtilis*. Moreover, including defined concentrations of tylosin facilitates the semi-quantification of tylosin in the culture supernatants.

Our results confirm the applicability of the assay in fast screenings for antimicrobial products in culture supernatants. The protocol can be used as positive control within screening campaigns in the drug discovery field.

Key words Antimicrobial whole-cell assay, Screening, Actinomycetes, Antibiotics, Growth inhibition, *Bacillus subtilis*

1 Introduction

Actinomycetes are prolific producers of bioactive compounds, in particular antibiotics [1–3]. As the number of multidrug-resistant bacterial pathogens is constantly increasing [4], actinomycetes became even more important in screenings for new antimicrobial

Peter Sass (ed.), *Antibiotics: Methods and Protocols*,
Methods in Molecular Biology, vol. 2601, https://doi.org/10.1007/978-1-0716-2855-3_2,

agents. Once a promising drug candidate showing the desired properties was identified, the production must be improved for compound purification, further testing, and finally, manufacturing. In both cases, classical screening approaches including cultivation of the producer strains in different media, extraction of the products, disc diffusion assays, and/or HPLC/MS analysis can be applied to examine the quality and quantity of the products in the sample. Although the combination of these methods provides us with additional data (e.g., details about the composition of the sample), this procedure is laborious and time-consuming. Whole-cell assays are therefore of great importance as they serve as useful and fast pre-screening methods for the identification of bioactive compounds that were derived from newly found producers as well as for screening of engineered strains, in which the production of the respective agent might be improved. In most of the described examples [5–8], the material (e.g., environmental samples, microbial liquid culture) is subjected to extraction with a solvent and the obtained extracts are applied in the screening. On the one hand, this strategy leads to the enrichment of the bioactive compounds whenever the extracts are concentrated by using evaporation systems (e.g., rotary evaporator), and on the other hand, the bioactivity might be lost when wrong solvents are used for the extraction. Here, we present a simple whole-cell assay that enables the testing of antibiotic activity in actinomycete culture directly from the supernatants, without the need of prior extraction of the antimicrobial compound(s).

To demonstrate the applicability of this assay, the tylosin producer *Streptomyces fradiae* DSM 41546 and the test strain *Bacillus subtilis* ATCC 6051 are used as model. Tylosin is a 16-membered macrolide. The antibiotic targets the 50S ribosomal subunit and inhibits protein biosynthesis [9–11]. Tylosin and its derivatives are primary active against Gram-positive bacteria [12, 13] and mycoplasma [14]. Thus, the compound is applied in veterinary medicine to treat infections caused by these pathogens.

For the verification of the whole-cell assay, *S. fradiae* DSM 41546 is cultivated in tylosin production medium, and the obtained culture supernatants are diluted 1:5, 1:10, 1:50, 1:100, 1:500, 1:1000, and 1:5000. The dilutions of the culture supernatants and defined concentration of tylosin (reference (positive control), 1000 μg/mL, 500 μg/mL, 100 μg/mL, 50 μg/mL, 10 μg/mL, 5 μg/mL, 1 μg/mL) as well as the tylosin production medium (negative control) are then added to a *B. subtilis* ATCC 6051 suspension (OD_{600}~0.6) that was prepared in a microtiter plate for testing of the antibacterial activity (Fig. 1). To monitor the growth in presence of the added solution, the absorbance is measured using a microplate reader (Table 1).

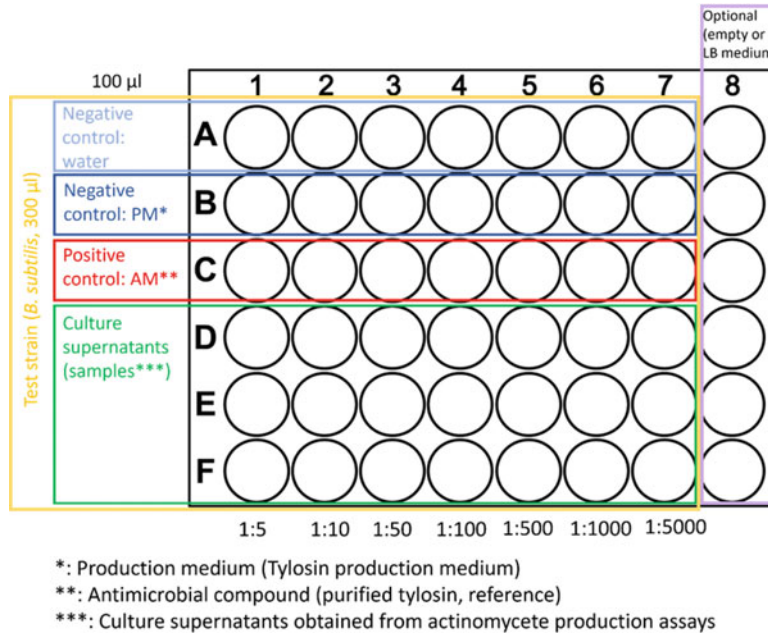

Fig. 1 Scheme for pipetting the whole-cell assay

A concentration-dependent inhibition of the growth of *B. subtilis* ATCC 6051 is detected for the culture supernatants containing tylosin and the tylosin reference (Fig. 2). In contrast, no inhibitory effects are observed for the negative controls (production medium and/or water). Furthermore, the serial dilution (1:5, 1:10, 1:50, 1:100, 1:500, 1:1000, 1:5000) of a culture supernatant obtained from a *S. fradiae* DSM 41546 cultivation, in which no or only traces of tylosin are present, is analyzed in the whole-cell assay. In those samples, the growth of *B. subtilis* ATCC 6051 is not affected. The moderate inhibitory effect in the well containing the 1:5 dilution (Fig. 2) might be caused by traces of tylosin or other less-active antimicrobial compounds present in the culture supernatant. The results should be validated in three independent experiments (three biological replicates). To confirm that the concentration-dependent inhibition in the culture supernatant containing tylosin is indeed triggered by this compound, the samples, including the tylosin reference, are analyzed by HPLC. The HPLC data confirm the presence of tylosin in those samples (Table 2). Furthermore, the concentration of the antibiotic correlates with the inhibitory effect on the growth of *B. subtilis* in the whole-cell assay (the higher the tylosin concentration, the stronger the growth inhibition). Taken together, these results demonstrate that the herein described whole-cell assay is a useful tool for the detection of antimicrobial activity in actinomycete cultures.

Table 1
The method and parameters used here for the measurement of the whole-cell assay employing a microplate reader (Tecan Infinite® M200 PRO)

Plate	**Greiner 48 flat bottom transparent polystyrene Cat. No.: 677180/677102**	
Wait (plate)	On	Target temperature: 37 °C
Wait (plate temperature)	Valid range: 36.5–37.5 °C	
List of actions in this measurement script:		
Kinetic		
Shaking (orbital) duration	10 s	
Shaking (orbital) amplitude	3 mm	
Absorbance		
Incubation time	00:28:00 (hh:mm:ss) includes two shaking and zero waiting times	
	Shaking 500 s Amplitude: 3 mm Mode: Orbital	
	Shaking 500 s Amplitude: 3 mm Mode: Orbital	
	Remaining wait time	
Incubation time	00:28:00 (hh:mm:ss) includes two shaking and zero waiting times	
	Shaking 500 s Amplitude: 1 mm Mode: Linear	
	Shaking 500 s Amplitude: 3 mm Mode: Orbital	
	Remaining wait time	
Label: label1		
Kinetic measurement		
Kinetic duration	6–23 h (*see* **Note 9**)	
Interval time	01:00:00	
Mode	Absorbance	
Wavelength	600 nm	
Bandwidth	600 nm	
Number of flashes	9 nm	
Settle time	25	
Settle time	100 ms	

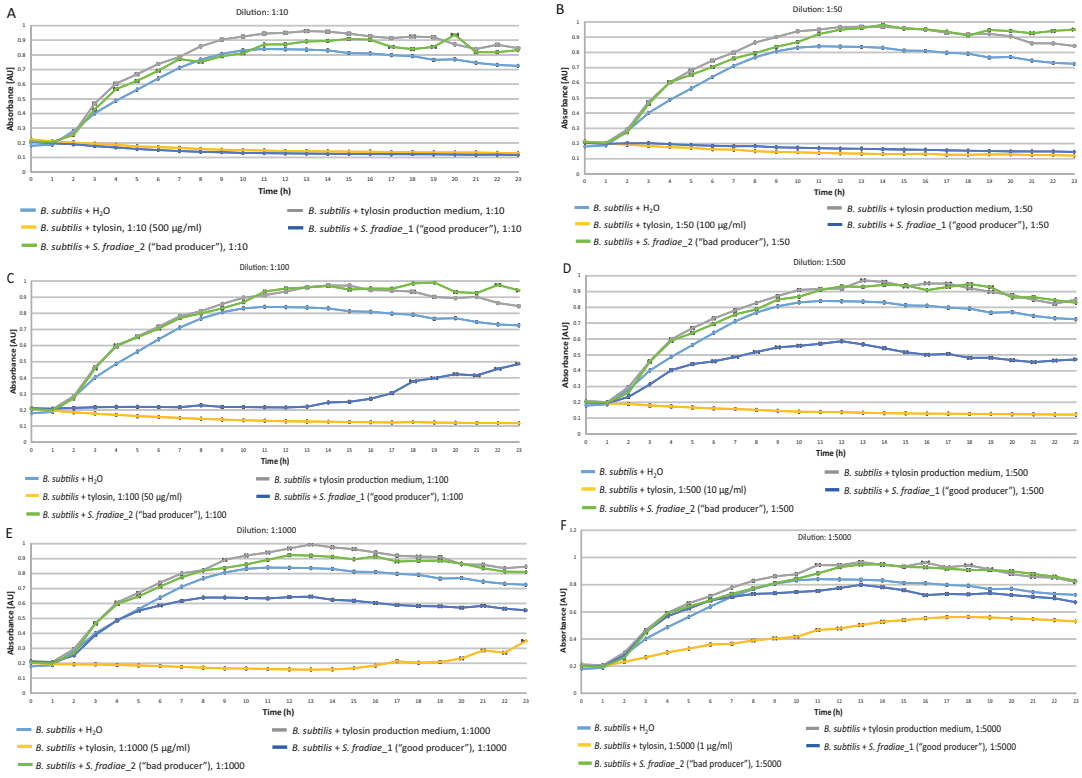

Fig. 2 Examples for the whole-cell assay. *B. subtilis* growth curves for the 1:10 dilution (**a**), 1:50 dilution (**b**), 1:100 dilution (**c**), 1:500 dilution (**d**), 1:1000 dilution (**e**), 1:5000 dilution (**f**). Water and tylosin production medium were used as negative controls; tylosin (reference compound) was used as positive control; *S. fradiae*_1: culture supernatant containing tylosin; *S. fradiae*_2: culture supernatant containing traces or no tylosin (*see* **Note 10**)

Table 2
Determination of the tylosin concentration in the reference and culture supernatant samples

	Tylosin concentration		
Dilution	**Reference (Tylosin) (µg/mL)**	**Culture supernatant 1 (*S. fradiae*_1) (µg/mL)**	**Culture supernatant 2 (*S. fradiae*_2) (µg/mL)**
1:5	1000	80	0.06
1:10	500	40	0.03
1:50	100	8	0.006
1:100	50	4	0.003
1:500	10	0.8	0.0006
1:1000	5	0.4	0.0003
1:5000	1	0.08	0.00006

2 Materials

2.1 Equipment

1. Autoclave.
2. Gloves (nitrile gloves, 24 cm).
3. Laboratory bottles (volume: 500 mL, 1000 mL).
4. Sterile Erlenmeyer flasks (volume of 500 mL, without baffles) for the cultivation of *B. subtilis* ATCC 6051.
5. Sterile Erlenmeyer baffled flasks (volume of 250 mL, with one baffle and a metal spiral (*see* **Note 1**)) for the cultivation of *S. fradiae* DSM 41546.
6. Pipettes (single-channel pipettes, volume 20 μL, 1000 μL; eight-channel pipette, volume 20–300 μL).
7. Sterile tips (volume: 10 μL, 200 μL, and 1000 μL).
8. Sterile glass pipettes (volume: 2 mL, 5 mL, 10 mL, and 20 mL).
9. Pipette controller.
10. Class II laminar flow hood.
11. Temperature-controlled shaking incubators.
12. Centrifuge for 1.5 mL and 2.0 mL reaction tubes.
13. Centrifuge for 15 mL and 50 mL centrifuge tubes.
14. Microbiological incubators (29 °C and 37 °C).
15. Reaction tubes (polypropylene, volume 1.5 mL).
16. Sterile petri dishes (92 × 16 mm with ventilation cams).
17. Sterile polypropylene centrifuge tubes (volume: 15 mL and 50 mL).
18. Suspension culture multi-well plates (48-well PS clear, with lid).
19. Cuvettes (polystyrene, 10 × 4 × 45 mm).
20. Ultrospec™ 10-cell density meter (Amersham Biosciences Europe GmbH).
21. Microplate reader (Tecan Infinite® M200 PRO).
22. Microplate reader software (Tecan i-control™ 1.11).
23. Computer or other electronic devices with Microsoft® Excel.
24. Optional: Agilent Technologies HPLC-LC/MSD Ultra Trap System XCT 6330 instrument and the respective software (Agilent Online LC Monitoring Software; Agilent ChemStation Instrument 1 (offline) software).

2.2 Media, Solvents, Culture Supernatants, and Reference Compound

All solutions should be prepared in ultrapure or distilled water (dH_2O).

1. Sterile distilled water (dH_2O).
2. Glycerol solution (50% glycerol in H_2O).
3. Methanol ≥99%.
4. Lysogeny broth (LB): 20 g LB powder (ready-to-use) dissolved in 1 L dH_2O.
5. LB agar: 20 g LB powder (ready-to-use) and 16 g agar dissolved in 1 L dH_2O.
6. Tryptic Soy Broth (TSB) medium: 30 g BD™ TSB powder (ready-to-use) dissolved in 1L dH_2O.
7. TSB agar: 30 g BD™ TSB powder (ready-to-use) and 16 g agar dissolved in 1L dH_2O.
8. Tylosin production (TP) medium: 16.5 g wheat meal, 10.6 g fish meal, 9.6 g corn gluten, 1.1 g potassium chloride (KCl), 0.55 g betaine, and 0.44 g diammonium phosphate $(NH_4)2HPO_4$ dissolve in 900 mL dH_2O and adjust the pH to 7.0–7.2. After the pH adjustment, add 45 mL soybean oil, 2.2 g calcium carbonate ($CaCO_3$), 1 mL of 0.44% $NiSO_4 \cdot 6H_2O$, and 1 mL of 0.33% $CoCl_2 \cdot 6H_2O$. Adjust the volume to 1 L dH_2O.
9. Culture supernatants (in this protocol, the culture supernatants were obtained from the cultivation of *S. fradiae* DSM 41546 in tylosin production medium (Subheading 3.2)).
10. Tylosin (reference antimicrobial compound).

2.3 Strains

1. Actinomycete: *Streptomyces fradiae* DSM 41546.
2. Test strain: *Bacillus subtilis* (Ehrenberg) Cohn ATCC 6051.

3 Methods

3.1 Cultivation and Storage of B. subtilis ATCC 6051

1. Sterilize a 500 mL Erlenmeyer flask and 500 mL LB medium.
2. Transfer 100 mL LB medium into the sterile flask and add 1 mL of a glycerol stock of the test strain (in this protocol, *B. subtilis* ATCC 6051 was used) or some cell material scratched from a previously prepared plate (LB agar plate with the strain grown overnight at 37 °C) to the medium.
3. Incubate the culture at 37 °C in a shaking incubator (180 rpm, overnight 16–24 h).
4. Take a sample of the overnight culture and use it for the whole-cell assay (Subheading 3.3, **steps 1** and **7**).

5. For long-time storage, take 5 mL of the overnight culture and mix it with 5 mL of 50% glycerol (final concentration of the glycerol: 25%). Store the glycerol stock at −20 °C or −80 °C (*see* **Note 2**).

3.2 Cultivation of Streptomyces fradiae DSM 41546 (Tylosin Production Assay)

1. Prepare a glycerol stock of an actinomycete (in this protocol, the *S. fradiae* DSM 41546 was used as model). Alternatively streak the strain on agar plate containing the suitable medium (e.g., *S. fradiae* DSM 41546 was cultivated on TSB agar at 29 °C).
2. Prepare and sterilize the required number of flasks (e.g., 250 mL Erlenmeyer flasks with one baffle and a metal spiral) and the required amount of medium for the pre-culture (e.g., production of biomass in TSB medium) and the planned production assay (e.g., tylosin production medium).
3. Inoculate the actinomycete in a suitable medium to produce biomass (pre-culture). In this protocol, *S. fradiae* DSM 41546 was used (e.g., 5 mL of a glycerol stock or a piece (approx. 1 cm^2) of the TSB agar with actinomycete mycelium was transferred into a flask with 45 mL TSB medium in a 250 mL Erlenmeyer flask with one baffle and a metal spiral).
4. Incubate the actinomycete culture at suitable conditions (e.g., *S. fradiae* DSM 41546: 29 °C, 180 rpm, 3–4 days).
5. Use 5 mL of the actinomycete pre-culture and add it to 45 mL of production medium (for *S. fradiae* DSM 41546, tylosin production medium was applied) in a sterile 250 mL Erlenmeyer flask with one baffle and a metal spiral. Run the production culture for 7–10 days (for *S. fradiae* DSM 41546, the culture was incubated for 10 days) in a shaking incubator (29 °C, 180 rpm) (*see* **Note 3**).
6. Take a sample (10 mL) of the production culture and transfer it into a 15 mL tube. Centrifuge the sample (20 °C, 6441 × *g*, 10 min). Transfer the supernatant (*see* **Note 4**) into fresh 15 mL tube. Discard the pellet (*see* **Note 5**). Store the sample at −20 °C or use a portion of the culture supernatant directly for the whole-cell assay (Subheading 3.3) and/or HPLC analysis (Subheading 3.4).

3.3 Whole-Cell Assay for Detection of Antibacterial Activity

1. Prepare the test strain culture: Inoculate the test strain (in this protocol, *B. subtilis* (Ehrenberg) Cohn ATCC 6051 was used) in LB medium, and cultivate the culture at 37 °C for 16–24 h (Subheading 3.1). The overnight culture is used in **step 7** (Subheading 3.3).
2. Prepare the solvent for serial dilution: Prepare and autoclave 500–1000 mL production medium (in this protocol, the tylosin production medium was used). Centrifuge 40 mL of the

sterile medium in a 50 mL tube (20 °C, 6441 × *g*, 10 min), and transfer the supernatant into a fresh 50 mL tube (*see* **Note 6**). This solution is used for the serial dilution of the negative control (production medium), the positive control (reference compound, tylosin), and the culture supernatants of *S. fradiae* DSM 41546.

3. Prepare water for use as the negative control: Autoclave distilled water (e.g., 500 mL).
4. Prepare the production medium (negative control): Consider the potential antimicrobial activity of solvents (e.g., methanol) that are used to prepare a solution of the reference compound (*see* **Note 7**). Normalize the content of methanol (25%) in all tested samples.
5. Prepare the reference compound (tylosin, positive control): Prepare a stock solution of 5 mg/mL tylosin (reference compound). Then, use a mixture of 25% methanol (methanol in water or production medium) as solvent. Pipette a serial dilution of the reference compound (5 mg/mL tylosin resolved in a mixture of tylosin production medium and methanol (25%)). Use the supernatant of the production medium obtained in **step 2** (Subheading 3.3) as solvent for the following serial dilution: 1:5 dilution (1000 μg/mL tylosin; example: add 1 volume tylosin (5 mg/mL) to 4 volumes solvent), 1:10 dilution (500 μg/mL tylosin), 1:50 dilution (100 μg/mL tylosin), 1:100 dilution (50 μg/mL tylosin), 1:500 dilution (10 μg/mL tylosin), 1:1000 (5 μg/mL tylosin), 1:5000 (1 μg/mL tylosin).
6. Prepare the actinomycete culture supernatant: Use a portion (e.g., 1 mL) of the actinomycete culture supernatant that was obtained from production assays (in this protocol, the culture supernatants of *S. fradiae* DSM 415465 were applied) (Subheading 3.2). Mix three volumes (e.g., 750 μL) of the culture supernatant with one volume of methanol (e.g., 250 μL) to normalize the content of methanol (25%) in the culture supernatant (*see* **Note 8**). Use this solution for the preparation of a serial dilution (1:5, 1:10, 1:50, 1:100, 1:500, 1:1000, 1:5000) of the culture supernatant. Use the tylosin production medium without methanol as solvent (supernatant of the tylosin production medium obtained in **step 2** (Subheading 3.3)).
7. Prepare the test strain suspension: Dilute the overnight culture (**step 1**, Subheading 3.3) of the test strain with sterile LB medium to obtain a suspension with an optical density of 0.6 (OD_{600} = 0.6 measured with the Ultrospec™ 10-cell density meter). Pipette 300 μL of this test strain suspension into each well of the 48-well plate, except the blank (e.g., LB medium).

8. Prepare a scheme for pipetting the whole-cell assay (an example was presented in Fig. 1). Transfer 300 µL of the test strain suspension to the respective wells as suggested in **step 7** (Subheading 3.3). Add 100 µL of the dilutions from **steps 3–6** (negative controls, positive control, or culture supernatant).
9. Measure the absorbance using a microplate reader: Prepare a microplate reader, and design a method (e.g., Table 1) using the respective software for measurement of the absorbance in samples that were mixed in the 48-well plate (**step 8**, Subheading 3.3).

3.4 Data Evaluation Using an Example of a Whole-Cell Assay

Collect and save the data from the measurements. Use Microsoft® Excel or another suitable software for the evaluation of the data. Plot the absorbance versus time and draw the curves for each sample (e.g., as presented in Fig. 2).

3.5 Optional: HPLC Analysis of the Culture Supernatants of S. fradiae *DSM 41546 (Tylosin Analytic)*

1. Centrifuge 1.5 mL sample for the whole-cell assay (e.g., culture supernatants of the tylosin production assays (Subheading 3.2)) in a 2 mL microcentrifuge tube (22 °C, 9391 × *g*, 5 min).
2. In addition, resolve 1 mg of the reference compound (e.g., tylosin) in 1 mL tylosin production medium, and centrifuge the sample as suggested in **step 1** (Subheading 3.5).
3. Transfer 0.5–1 mL of the sample supernatant (**steps 1** and **2**, Subheading 3.5) into a HPLC glass vial.
4. Prepare the HPLC system, the Phenomenex Luna C18 column (150 mm × 3 mm ID, 5 µm) (stationary phase), and the buffers (mobile phase) for the HPLC analysis.
5. Program the HPLC system for the analysis (the method described below was applied for tylosin analytic): Separation of the analyte by gradient elution; gradient elution: 30% acetonitrile to 36.5% acetonitrile in 10 min, t12 = t15 = 100% B, post-time: 8 min; flow rate: 0.5 mL/min; injection volume: 5 µL; using 0.1% trifluoroacetic acid in acetonitrile as mobile phase; UV detection at 280 nm.
6. Place the samples into the sampler and run the HPLC system.
7. Collect and save the data. Use the software "Agilent ChemStation (offline)" and evaluate the tylosin amount based on the characteristic retention time (for tylosin: absorption maxima λ = 280 nm) and the peak area (mAU) of the included reference sample (1 mg/mL).

4 Notes

1. Many actinomycetes form clumps of mycelium in liquid medium. Use flasks containing a metal spiral to avoid the clump formation and promote a more dispersed growth.
2. The purity of the glycerol stock and liquid culture can be tested by taking a sample of 50 μL and plating the material onto LB agar plates using the dilution streaking method. For *B. subtilis*, incubate the plates for 16–24 h at 37 °C. Examine the purity by visual assessment of the morphological characteristics of the strain [15].
3. The purity of the glycerol stock and liquid culture can be tested by taking a sample of 100 μL and plating the material onto TSB agar plates using the dilution streaking method. For *S. fradiae* DSM 41546, incubate the plates for 2–4 days at 29 °C. Examine the purity by visual assessment of the morphological characteristics of the strain [16].
4. As the tylosin production medium (including other actinomycete production media) contains oil, the supernatant might be coated with an oil layer. Try to remove this layer and use the phase between the layer and the pellet for the whole-cell assay and/or the HPLC analysis.
5. The tylosin production medium (including many other actinomycete production media) contains insoluble components. Thus, the pellet may contain two or more phases.
6. This step is optional for clear production media. For complex media containing insoluble components, the centrifugation facilitates the separation of those particles.
7. As in this protocol, the reference compound (5 mg tylosin) was resolved in a mixture of production medium and methanol (25%), and the content of methanol had to be normalized in all samples. Therefore, a mixture of the production medium and methanol (25%) was used as initial solution for the negative control. This solution was subjected to the serial dilution (1:5, 1:10, 1:50, 1:100, 1:500, 1:1000, 1:5000) in the negative control (tylosin production medium).
8. This step is optional for assays in which the reference was resolved in water or production medium without additional solvents such as methanol. In this protocol, the actinomycete culture supernatants were normalized (final concentration: 25% methanol) to make them comparable with the reference.
9. The time of the measurement depends on the mode of action of the tested active compound and can be shortened (e.g., for tylosin, the effects are visible already after approx. 6 h) to save time and make the procedure more sustainable.

10. The negative controls (*B. subtilis* with water or production medium) should show identical or very similar growth behavior (no growth inhibition). In case, the production medium contains compound(s) that influence the growth (e.g., inhibition of the growth), and the curves will not overlap. Consider this effect when evaluating the data. The positive control (reference compound) should result in a partial/full inhibition of the growth or killing of the cells ("bacteriostatic" or "bactericidal" effect). This depends on the used concentration and mode of action of the compound.

References

1. Robertsen HL, Musiol-Kroll EM (2019) Actinomycete-derived polyketides as a source of antibiotics and lead structures for the development of new antimicrobial drugs. J Antibiot 8(4):157
2. Ravishankar VR, Jamuna AB (eds) (2022) Natural products from Actinomycetes: diversity, ecology and drug discovery. Springer, Singapore
3. Atanasov AG, Zotchev SB, Dirsch VM, Supuran CT (2021) Natural products in drug discovery: advances and opportunities. Nat Rev Drug Discov 20(3):200–216
4. World Health Organization. https://www.who.int/news-room/fact-sheets/detail/antimicrobial-resistance. Accessed 05 Jan 2022
5. Liao J, Xu G, Mevers EE, Clardy J, Watnick PI (2018) A high-throughput, whole cell assay to identify compounds active against carbapenem-resistant *Klebsiella pneumoniae*. PLoS One 13(12):e0209389
6. Balouiri M, Sadiki M, Ibnsouda SK (2016) Methods for in vitro evaluating antimicrobial activity: a review. J Pharm Anal 6(2):71–79
7. Nybond S, Karp M, Yrjönen T, Tammela P (2015) Bioluminescent whole-cell reporter gene assays as screening tools in the identification of antimicrobial natural product extracts. J Microbiol Methods 114:54–56
8. Vinuesa MA, Fernandez A (2021) A simple antifungal assay for testing actinomycetes and other microbial extracts. Methods Mol Biol 2296:217–225
9. McGuire JM, Boniece WS, Higgens CE, Hoehn MM, Stark WM, Westhead J, Wolfe RN (1961) Tylosin, a new antibiotic: I. Microbiological studies. Antibiot Chemother 11(5):320–327
10. Hamill RL, Haney ME Jr, Stamper M, Wlley PF (1961) Tylosin, a new antibiotic: II. Isolation, properties, and preparation of pesmycosin, a microbiologically active degradation product. Antibiot Chemother 11 (5): 328-334
11. Omura S, Inokoshi J, Matsubara H, Tanaka H (1983) Ribosome-binding activities and antimicrobial activities of tylosin and its related compounds. J Antibiot 36(12):1709–1712
12. Gingerich DA, Baggot JD, Kowalski JJ (1977) Tylosin antimicrobial activity and pharmacokinetics in cows. Can Vet J 18(4):96
13. Tsuchiya M, Hamada M, Takeuchi T, Umezawa H, Yamamoto K, Tanaka H, Kiyoshima K, Mori S, Okamoto R (1982) Studies of tylosin derivatives effective against macrolide-resistant strains: synthesis and structure-activity relationships. J Antibiot 35(6):661–672
14. Ose EE, Tonkinson LV (1985) Comparison of the antimycoplasma activity of two commercially available tylosin premixes. Poult Sci J 64(2):287–293
15. American Type Culture Collection (ATCC). https://www.atcc.org/products/6051. Accessed 27 Jan 2022
16. Bacterial Diversity (BacDive), Deutsche Sammlung von Mikroorganismen und Zellkulturen (DSMZ). https://bacdive.dsmz.de/strain/15193. Accessed 27 Jan 2022

Chapter 3

Sampling of Human Microbiomes to Screen for Antibiotic-Producing Commensals

Benjamin Torres Salazar, Anna Lange, Laura Camus, and Simon Heilbronner

Abstract

Soil-derived microorganisms have been sampled intensively throughout the last decades in order to discover bacterial strains that produce new antibiotics. The increasing emergence of multidrug-resistant bacteria and the constant high demand for new antibiotic classes are leading to the sampling and investigation of new microbiomes that contain antimicrobial producers. Human-associated microbiomes are therefore gaining more and more attention. This chapter presents a detailed description of how human microbiomes can be sampled and how microbiota members from skin and nasal samples can be isolated. Different methods for antimicrobial compound screening are presented.

Key words Microbiome sampling, Nose, Skin, Isolation of bacterial strains, Antimicrobial compound, ESKAPE pathogens, *Staphylococcus*

1 Introduction

Multidrug-resistant (MDR) bacterial pathogens such as methicillin-resistant *Staphylococcus aureus* (MRSA), vancomycin-resistant enterococci (VRE), or Gram-negative bacteria producing "extended-spectrum β-lactamases (ESBL)" are a worldwide problem which will intensify in the coming decades. Infections caused by MDRs are estimated to cause 1.3 million deaths per year [1] with an estimated increase to 10 million deaths by 2050 [2]. The increasing occurrence of MDR pathogens in combination with draining pipelines for the development of novel antibiotic molecules demands a change in bioprospecting strategies to identify novel antimicrobial agents [2, 3].

Authors Benjamin Torres Salazar and Anna Lange have equally contributed to this chapter

Peter Sass (ed.), *Antibiotics: Methods and Protocols*,
Methods in Molecular Biology, vol. 2601, https://doi.org/10.1007/978-1-0716-2855-3_3,

One reason for the stagnating discovery of new compounds is that the same environments are repetitively sampled (e.g., soil from different geographic locations), entailing the redundant discovery of known compounds [4]. Accordingly, a shift in screening approaches is needed. Besides extreme environmental habitats such as marine microbiomes from the Arctic sea [5, 6], human-associated bacterial communities are increasingly recognized as a potential source of novel antibacterial compounds [7, 8].

Human microbiomes are a huge reservoir of microorganisms of various species and genera with strikingly different anabolic and catabolic abilities. Especially the human skin and nasal cavity represent highly competitive environments since nutrients and physical space for expanding bacterial populations are limited. Antimicrobial compounds are effective measures providing competitive fitness, and species colonizing these body sites are reported to produce a plethora of antimicrobial compounds [9, 10]. This has been demonstrated in particular for staphylococcal species that typically colonize the human skin and nose [9]. Commonly produced bacteriocins such as epidermin show antibiotic activity against MRSA and VRE [11], aureocin is active against MRSA [12], and even entirely new antibiotic molecules were identified that are produced via nonribosomal peptide synthetases (NRPS) and possess activity against various Gram-positive bacteria [13].

Of note, gene clusters responsible for antibiotic biosynthesis within human microbiomes are frequently associated with mobile genetic elements and do frequently represent strain- rather than species-specific traits [14]. This finding, together with the fact that attempts to isolate antibiotic producers for human microbiomes have been limited, strongly suggests that further sampling of human microbiomes has the potential to uncover further novel compounds.

The human body offers a multitude of different niches that are characterized by distinct environmental conditions and are, therefore, inhabited by microbiomes of varying compositions. For example, the skin and the nasal cavity represent nutrient-poor environments as opposed to nutrient-rich environments such as the gut or the mouth. Hence, it is likely that in each specific body site the colonizing bacteria will produce specialized antimicrobial molecules with different ranges of activity. Accordingly, there is plentiful opportunity for research to screen human-associated microbes for the production of novel antibacterial molecules.

Several human microbiomes can be conveniently sampled using noninvasive swabbing of the appropriate body parts. This chapter provides a guide to the general procedures associated with the sampling of host-associated microbiomes with a special focus on the skin and nasal microbiomes. We will provide insights into the ethical and legal requirements and describe the sampling processes. Further, we will describe how bacterial strains are isolated and

screened for antimicrobial activity. Finally, we will also discuss the initial steps of characterization of compound producers allowing a rapid assessment of the novelty of the produced compound.

2 Materials

2.1 Consumables

1. Reaction tubes 1.5/2.0 mL.
2. Cryotubes 2 mL.
3. Culture tubes 5 mL.
4. 90 mm polystyrene petri dishes.
5. Glass petri dish.
6. Syringe (2 mL).
7. Inoculation loops.
8. Sterile filter (0.22 μm).
9. 24 well plates (flat bottom).
10. Plate sealing film.
11. Cotton swabs.
12. eSwab containing 1 mL Amies medium (Copan).
13. AnaeroGen (Thermo Scientific).
14. CO_2Gen (Thermo Scientific).
15. Cork borer (e.g., ø 5 mm).

2.2 Chemicals and Buffers

1. 80% ethanol.
2. 30% hydrogen peroxide stock (H_2O_2).
3. 20 mM 2,2′-bipyridine stock (iron chelator).
4. 1 × phosphate-buffered saline (PBS): 8.0 g/L NaCl, 0.2 g/L KCl, 1.15 g/L Na_2HPO_4, 0.2 g/L KH_2PO_4, pH 7.3, autoclaved.
5. 80% glycerol, autoclaved.
6. Chloroform.
7. Mass spectrometry (MS) matrix solution.
8. 70% formic acid.
9. Y-PER lysis buffer (Thermo Scientific).
10. Taq polymerase.

2.3 Media and Agar

1. Brain Heart Infusion medium (BHI).
2. Tryptic Soy Broth (TSB).
3. Basic medium (BM): 5 g yeast extract, 10 g soy peptone, 5 g NaCl, 1 g glucose, 1 g $K_2HPO_4 \times 3\ H_2O$. Add dH_2O to a volume of 1 L and autoclave. Adjust to pH 7.2, if necessary, using 1 M NaOH.

4. Nutrient agar: For BM, TSB, or BHI agar, add 1.5% (w/v) (15 g/L) agar and a magnetic stir bar prior autoclaving. Alternatively, equal volumes of 50 °C 2× nutrient media and 50 °C 2× agar can be mixed to generate 1× agar. Cool down agar to ~50 °C while stirring and pour approx. 20 mL into 90 mm sterile petri dishes.
5. Blood agar: For blood agar, add sheep blood to a final concentration of 5% (v/v) to cooled (40–50 °C), autoclaved BM or TSB agar.
6. Soft agar: For BM, TSB, or BHI soft agar, add 0.3% (w/v) (3 g/L) agar and a magnetic stir bar prior autoclaving. Alternatively, equal volumes of 50 °C 2× nutrient media and 50 °C 0.6% agar can be mixed to generate 1× soft agar. Before inoculating, let the soft agar cool down to 40–45 °C while stirring.
7. Columbia agar with 5% sheep blood (COL).
8. Schaedler agar with 5% sheep blood (SSB).
9. Chocolate agar with 10% sheep blood (CHO).
10. Schaedler agar with 5% horse blood and kanamycin/vancomycin (SHB).

2.4 Instruments and Equipment

1. Incubators (30–37 °C, 0–10% CO_2).
2. Shaker(s) (30–37 °C).
3. MALDI Biotyper (Bruker).
4. Vortex.
5. Bunsen burner (and a lighter, if needed).
6. Benchtop centrifuge with rotor for 1.5/2.0 mL reaction tubes.
7. Spectrophotometer.
8. Magnetic stirrer and magnetic stir bar.
9. Autoclave.
10. PCR thermocycler.
11. Replica stamp (self-made or commercial).
12. MS plate.

2.5 Test Bacteria

ESKAPE bacteria: *Enterococcus faecium*, *Staphylococcus aureus*, *Klebsiella pneumoniae*, *Acinetobacter baumannii*, *Pseudomonas aeruginosa*, and *Enterobacter* spp. (*see* **Note 1**).

2.6 Ethical Considerations

Research involving human subjects is in general subject to ethical evaluation, and the study and procedures need to be approved by the responsible legal authority.

In general, "Informed Written Consent" is necessary when research involves healthy human volunteers and if biological

samples and/or personal data are collected. The informed consent contains the information about the research topic and the proposed treatment or sampling; it includes the discussion of possible risks and benefits of the treatment or sampling; it assesses that the patient or volunteers has understood all information [15, 16].

However, the sampling strategy described herein is noninvasive and harbors minimal risks for the participating volunteers.

3 Methods

In general, work under sterile conditions and use a clean bench with lamina flow. It is important to carry out any work associated with human samples in laboratories of biosafety levels S2 since the isolated bacterial species (e.g., *Staphylococcus aureus*) might be subject to S2 safety regulation. If hazardous chemicals are used, they should be handled under a fume hood, and gloves, safety goggles, and a lab coat should be used when necessary.

This section will provide a detailed guide on how nasal and skin samples can be obtained and residing bacteria can be isolated. An overview on the workflow is given in Fig. 1. After bacterial isolation different screening procedures for antimicrobial compounds are described. An antimicrobial producer can then be identified *via* MALDI-TOF MS and/or 16s rDNA analysis.

3.1 Collection of Microbiome Samples from the Nasal Cavities and Skin

1. Use eSwabs and the provided Amies medium which allows cultivation of anaerobic, aerobic, and fastidious bacteria. Unpack each directly before use.
   (a) For nasal samples: Place the head of the swab into nasal vestibule. Do not place it into the middle or the rear parts of the nose. Rotate swab with light pressure six times along the nasal vestibule (the swab should be slightly bended) [17]. Repeat procedure in the second nostril (use one swab for both nostrils).
   (b) For skin samples: Guide the swab carefully along the skin with slight pressure and swipe two to three times back and forth (*see* **Note 2**).
2. Place the swab into the swab tube containing the Amies medium and break it at the colored breakpoint mark.
3. Close tube tightly and mix thoroughly by vortexing.

3.2 Isolation of Potential Antimicrobial Producers (PAPs)

After the collection step the specimen should be processed as soon as possible. If inevitable, specimen can be stored at 4–8 °C for up to 24 h.

1. Transfer 500 μL of the bacterial suspension from the swab tube into a cryotube and mix with 500 μL 80% glycerol for storage at

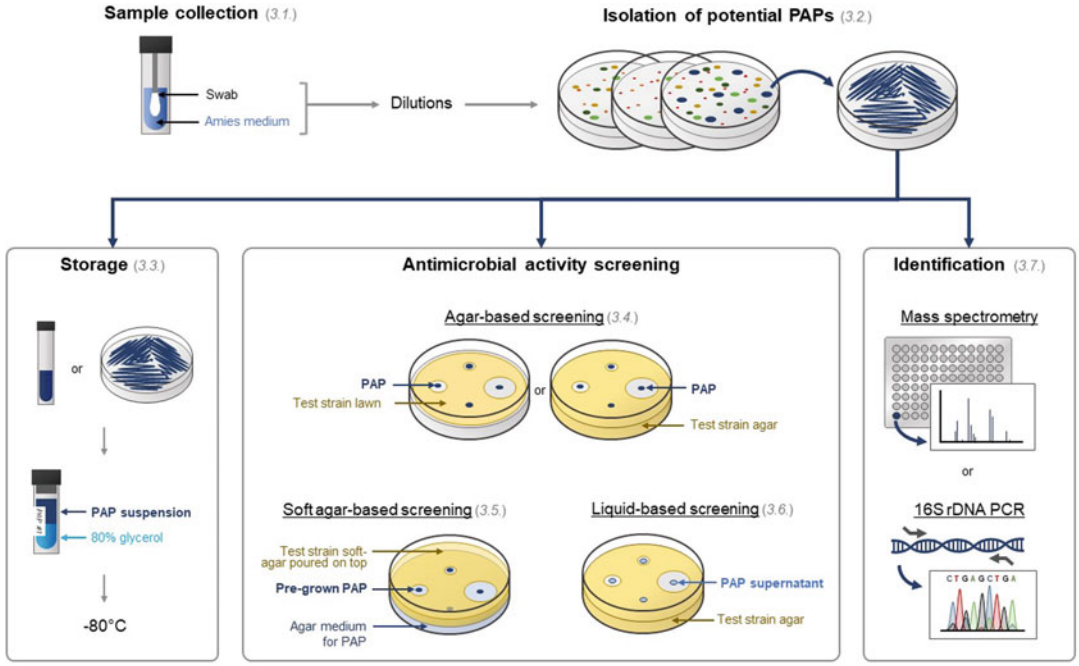

Fig. 1 Methodical approach for screening of potential antimicrobial producers isolated from human microbiomes. Sampling from nasal or skin microbiomes is followed by isolation and storage of the resident potential antimicrobial producer strains. Potential antimicrobial activity can be investigated by the use of agar-based, soft agar-based, or liquid-based screening techniques. If a bacterial strain produces antimicrobial compounds, the strain can be identified by MALDI-TOF MS and/or analysis of the 16s rDNA gene

−80 °C. If any problem occurs during strain isolation, this stored sample can be used for recultivation of the microbiome-derived bacteria. Shock freezing, e.g., in liquid nitrogen, is not needed.

2. Use the remaining bacterial suspension to isolate PAPs by plating the suspension onto different types of nutrient agar (*see* **Note 3**).
3. Prepare 1:10 serial dilutions (to 10^{-4}) of the initial sample in PBS.
4. Plate 50 µL of 10^{-1} to 10^{-4} dilutions on different nutrient agar plates (we normally recover single colonies that can be picked conveniently on 10^{-2} and 10^{-3} dilutions) (*see* **Note 4**). Prepare a set of agar plates (COL, CHO, SSB SHB) for each dilution and each growth condition (aerobic, CO_2, anaerobic incubation) at 37 °C. Allow incubation of agar plates under aerobic conditions and with 5–10% CO_2 for 7 days. If available, use a cell culture incubator or alternatively use an anaerobic jar with CO_2 generator sachets. For growth of anaerobic bacteria, incubate plates under anaerobic conditions for at least 7 days. Prepare an additional COL agar plate for each dilution and growth

condition (aerobic, CO_2, anaerobic incubation) to be incubated at 30 °C.

5. After the incubation of the agar plates, document the different colony morphotypes according to their color, size, texture, mucoidy, and hemolytic activity (*see* **Note 5**). Choose at least one or two colonies of each morphotype, and isolate them on a fresh plate and incubate according to the defined cultivation conditions. Assign all necessary information to each colony (volunteer number, colony number, growth conditions, agar and dilution, morphotype description).

3.3 Storage of PAPs

1. Cultivate the chosen strains in 5 mL liquid broth (e.g., BHI or BHI containing 0.2–1% Tween 80 for cultivation of *Corynebacteria* spp.) for 24 h to 72 h depending on the expected species until sufficient turbidity of the culture can be observed (*see* **Note 6**).
2. Mix 500 µL of bacterial suspension with 500 µL of 80% glycerol in a cryotube.
3. Store bacterial stocks at −80 °C.

3.4 Agar-Based Screening for Antimicrobial Activity

Bacteria frequently release antimicrobial compounds into the environment to inhibit close-by competitors. Production of antimicrobials can be detected conveniently using agar-based assays. The potential antimicrobial producer is spotted on agar containing either (a) lawns of test strains that were streaked onto the agar or (b) bacteria that were inoculated into the agar. After incubation, a zone of inhibition appears in case of antibiotic compound production (Fig. 2).

1. Prepare suitable nutrient agar for bacteria cultivation. We recommend using the same agar that allowed the isolation of the PAP of interest. The ESKAPE test strains are in general undemanding and will grow on all media suggested herein. If other

Fig. 2 Inhibitory activity of different PAPs against *S. aureus* USA300 on TSA agar. Yellow colonies = *S. aureus* strains; white colonies = *S. epidermidis* strains

test bacteria are used, it needs to be confirmed that the strains can grow under the used conditions (*see* **Note 7**).

2. Prepare agar plates with lawns of test bacteria for antibiotic compound screening (*see* **Note 8**):
   (a) Use an inoculation loop to pick test bacteria that were freshly grown on nutrient agar plate (*see* **Note 9**).
   (b) Resuspend test bacteria in 1× PBS and adjust the optical density (OD_{600}) to 0.01–0.5 (*see* **Note 10**).
   (c) Use a sterile cotton swab to streak out the test bacteria onto a fresh nutrient agar plate.
   (d) Rotate the plate several times to homogenously cover the agar with a bacterial lawn. The resulting plates can be stored for 1–2 weeks at 4 °C.
3. Prepare agar plates with inoculated agar for antibiotic compound screening:
   (a) Use an inoculation loop to pick up test bacteria that were freshly grown on nutrient agar (*see* **Note 9**).
   (b) Resuspend test bacteria in nutrient medium by pipetting and/or vortexing and inoculate a cooled nutrient agar (~40–45 °C) to a final OD_{600} of 0.001 to 0.1 (*see* **Note 10**).
   (c) Generate a homogenous bacteria-agar solution using a sterile magnetic stirrer and pour petri dishes (20 mL of agar). Solidified plates can be stored for 1–2 weeks at 4 °C.
4. Pick the isolated PAPs (*see* **Note 9**) resuspend them in 1× PBS and adjust the OD_{600} to 1–10.
5. Spot 10 μL of bacterial suspension onto the agar plates containing the test bacteria as prepared according to either the above instructions in (2) or (3). If many PAPs are to be tested simultaneously, generate a master plate first. Spot 10 μL of the bacterial suspension on a nutrient agar plate in a certain pattern (Fig. 3). After incubation, a replica stamp can be used to pick up all bacteria from the master plate simultaneously and to transfer them onto (different) agar plates containing the test bacteria (*see* **Note 11**).
6. Invert the agar plates and incubate for 24–48 h at 30–37 °C (*see* **Note 7**). Antibiotic compound production can be detected by a zone of inhibition surrounding the PAP colony.

3.5 Soft Agar-Based Screening for Antimicrobial Activity

Occasionally, PAPs and the test bacteria do not grow on the same nutrient agar, or the PAP is producing an antibiotic compound only under special nutritional conditions that do not support the growth of test strains. These problems can be circumvented by spotting the PAPs onto a suitable nutrient agar plate and allowing them to grow

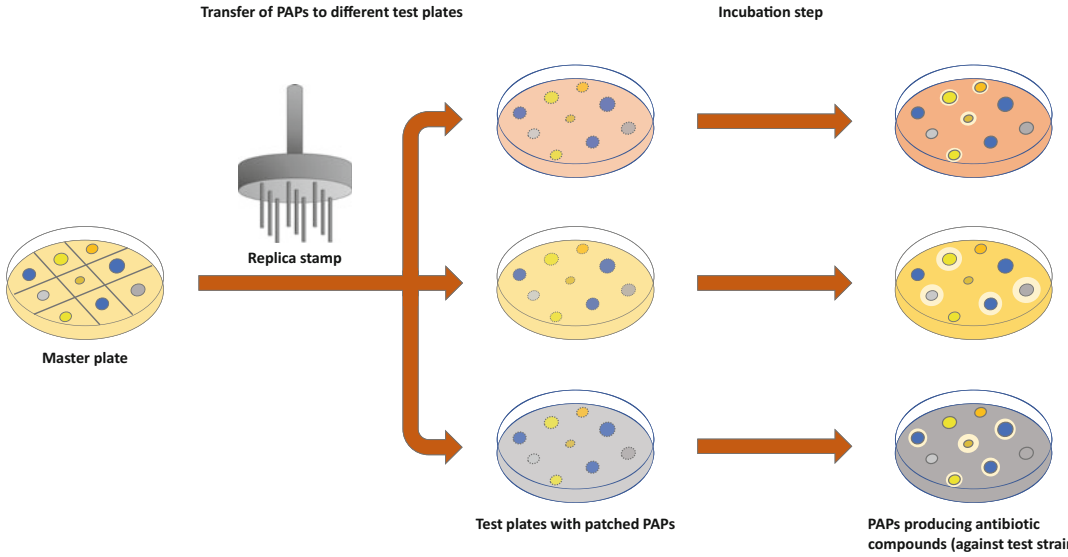

Fig. 3 Screening of potential antibiotic producers (PAPs). (**a**) PAPs are transferred to a nutrient agar plate in a specific pattern to generate a master plate. (**b**) A replica stamp is used to transfer/patch PAPs from the master plate to different nutrient agar plates, which are either inoculated with or contain lawns of test bacteria. (**c**) Following an incubation step, zones of inhibition appear around the PAPs in case of antibiotic production

and produce antimicrobials. Soft agar containing the test bacteria is then poured onto the agar plate containing the PAPs. After solidification of the soft agar and a further incubation step, inhibition zones can be observed in the soft agar layer.

1. Cultivation of PAPs and preparation of nutrient agar plates are analogous to 3.4.
2. If many PAPs are to be tested simultaneously, generate a master plate as described in 3.4. Transfer PAPs onto (different) nutrient agar plates using a replica stamp, and incubate the PAPs for 24–72 h at 30–37 °C (*see* **Note 12**).
3. Use an inoculation loop to pick test bacteria that were freshly grown on nutrient agar (*see* **Note 9**), and resuspend them in nutrient medium by pipetting and/or vortexing and inoculate cooled soft agar (~40–45 °C) to a final OD_{600} of 0.001 to 0.1 (*see* **Note 10**).
4. Stir to generate a homogenous bacteria-soft agar solution and pour 5 mL of the soft agar on top of producer strain-containing agar plates.
5. Optional: Kill the PAPs before applying the soft agar (*see* **Note 13**). For this, pour chloroform (use an extra set of gloves and safety goggles, as chloroform is toxic) into a container (e.g., the lid of glass petri dish), invert the agar plate containing the PAPs, place it on top of the container, and incubate the plate

for 30–60 s under a laboratory hood. Invert the agar plate to allow chloroform residues to evaporate (~1 min).

6. Let the soft agar solidify, invert the agar plates, and incubate for 24–48 h at 30–37 °C (*see* **Note 7**). Antibiotic compound production can be detected by a zone of inhibition in the soft agar.

3.6 Liquid-Based Screening for Antimicrobial Activities

Co-cultivation of the isolated PAPs and the test bacterium on the same nutrient agar may occasionally result in (blurry) zones of inhibition that cannot unequivocally be attributed to antibiotic compound production. For instance, the PAP may have a faster metabolism/growth than the test strain, which can result in starvation of the close-by test strain. Further, bacteria such as *Streptococcus pneumoniae* can release H_2O_2 upon contact with *S. aureus*, which induces prophage activation in *S. aureus* and therefore subsequent phage-mediated rather than antimicrobial-mediated killing [18, 19]. In these cases, antibiotic compound production can be validated using supernatants of PAP cultures that were grown in the absence of other bacterial species.

1. For antibiotic compound production, prepare a 24 well plate with 1 mL nutrient medium in each well.
2. Inoculate each well with a PAP and seal the plate with an adhesive sealing film that allows gas exchange.
3. Incubate the plate for 24–72 h at 30–37 °C with agitation (*see* **Note 14**).
4. Transfer the 1 mL PAP cultures into 1.5 mL reaction tubes, and centrifuge the cultures for 5 min at 8000 × *g* in a benchtop centrifuge.
5. Collect the supernatants of the PAP cultures and sterile filter the supernatants using a 0.22 μm filter.
6. Use a sterile cork borer (e.g., ø 5 mm) to punch holes into the agar plates containing the test strains (preparation described in Subheading 3.4). When punching holes into various agar plates, each with a different test bacterial species, sterilize the cork borer by flaming (use 80% ethanol) in-between plates.
7. Fill the holes with up to 60 μL cell-free supernatant spent media of the PAPs.
8. Let the supernatant diffuse into the agar and incubate for 24–48 h at 30–37 °C (*see* **Note 7**).
9. Antibiotic compound production can be detected by an inhibition zone surrounding the holes.

3.7 Species Identification of PAPs by MALDI-TOF MS

Some human commensal species such as *Staphylococcus lugdunensis* are known to produce core genome-encoded antibacterial compounds [13]. To avoid re-identification of known compounds, it is therefore advisable to identify antibiotic producers to the species level prior to extensive further characterization. In clinical bacteriology, matrix-assisted laser desorption/ionization-time-of-flight mass spectrometry (MALDI-TOF MS) is frequently used for the rapid identification of human-associated microbes. Researchers with connections to Medical Microbiology Laboratories should consider request access to this technique as it is high throughput, cheap, quick, and perfectly suited for the identification of human-associated bacteria. Alternatively, 16s rDNA analysis can be performed for species identification (*see* Subheading 3.8).

1. Transfer a little bit of colony material with a pipette tip to a well of the MS plate. Scratch the colony on the whole surface of the well until a very light smear is visible. Remove any excess of colony (less is more!).
2. Add 1 μL of 70% formic acid to each MS well and let it dry (this will improve the lysis and thus the identification of some species).
3. Add 1 μL of the matrix solution to each well and let it dry.
4. Analyze the MS plate without delay in the MALDI-TOF MS according to manufacturer's instructions.
5. Bacterial species will be identified by comparing the spectra of the analyzed bacteria and the microorganism spectra database using the Biotyper software (*see* **Note 15**).

3.8 16s rDNA PCR-Based Species Identification

1. To amplify the 16s rRNA DNA, pick colony material from the plate and mix the material with 20 μL of Y-PER lysis buffer in a 1.5 mL reaction tube.
2. Vortex the reaction for 10 s and incubate it at 98 °C for 5 min.
3. Centrifuge for 5 min at 4000 × *g*.
4. Collect lysate supernatant and dilute with molecular grade H_2O at a 1:5–1:20 ratio. This will serve as template for the PCR reaction.
5. Prepare PCR in a 50 μL reaction mix using Taq polymerase buffer, 2 pmol of the primers 338F-M13 (5′GTA AAC GAC GGC CAG TGC TCC TAC GGG WGG CAG CAG T′3) and 1044R-M13 (5′GGA AAC AGC TAT GAC CAT GAC TAC GAG CTG AGC ACA RCC ATG′3) [20], 4 μmol of each dNTP, 1 μL of template, and 1 unit of Taq polymerase. Amplify 16s rDNA fragment by PCR (35 cycles with an initial denaturation of 3 min at 95 °C. Each cycle consists of the following steps: 95 °C for 30 s, 56 °C for 30 s, and 72 °C for 60 s and a final extension of 7 min.)
6. Check size of PCR fragment on a 1% agarose gel (~750 bp).

7. Purify PCR fragment using a PCR clean up system according to user manual.
8. Analyze the fragment using commercial Sanger sequencing.
9. Analyze resulting nucleotide sequence with BLASTx and identify bacterial species.

3.9 First Steps of Compound Identification

If microbes are identified that show interesting capacity to inhibit one or several target strains, quick insights into the putative nature of the compound will be needed. Whole genome sequencing (WGS) of the strain has proven to be a quick and effective method to achieve this. Short-read sequencing using Illumina technology (MiSeq, HiSeq, NextSeq) is sufficient for this purpose. The reads can be assembled de novo, and biosynthetic gene clusters (BGCs) can be identified as described elsewhere [21]. If BGCs are identified that show little similarity to those of already known compounds, the isolate represents a candidate for further investigation.

The next step of the experimental analysis is generally the creation of deletion mutants lacking the identified BGCs to validate their involvement in the observed antimicrobial activities.

These approaches are followed by attempts to purify the antimicrobial molecule and by chemical structure elucidation. Further details for bulk production of antimicrobial compound producers by fermentation are summarized in [22]. How natural products can be recovered is described in chapter topic "Isolation and purification of natural products from microbial cultures" by Schafhauser and Kulik in this edition [23].

4 Notes

1. We propose a selection of test bacteria that are clinically relevant. According to different scientific questions, further or different sets of test bacteria can be included in a study.
2. Sampling of "unusual" skin sites might be more interesting. More promising PAPs might be recovered from sites that are not regularly washed. For example, sampling of the area under the foot nails, knee pits, or similar might be of interest.
3. A variety of nutrient agar types can be used for isolation of bacterial strains from microbiome samples. We recommend using a wide range of different agars for isolation of the bacteria, such as COL, CHO, SSB, and SHB (especially for anaerobic bacteria). Further TSB, BHI, or BM agar can be used. Our media recommendations are based on Kaspar et al. [24] and Timm et al. [25]. The use of different media will lead to redundant growth of certain bacterial species on different plates, but at the same time this will increase the chances to

cultivate low abundant species that have particular metabolic requirements.

4. If a volunteer harbors only low abundance of bacteria, spread the pure swab medium which was frozen initially at −80 °C on the different agar plates, and incubate plates under the different conditions (aerobic/anaerobic, 30–37 °C).
5. It might be helpful to take photographs to keep morphotype information.
6. Sufficient turbidity should be observable in the liquid culture. If necessary, prolong incubation time or centrifuge the culture, remove a part of the supernatant, and concentrate the pellet in the remaining medium. In case of a very long incubation time (anaerobic bacteria occasionally need a full week), preserve the strain by taking colony material from an agar plate. For this, streak out the colony on a fresh plate followed by incubation. Use a sterile inoculation loop and suspend bacteria in BHI medium. Mix 1:2 with 80% of glycerol in a cryotube and store at −80 °C.
7. Incubation time, incubation temperature, oxygen/carbon dioxide levels, and the nutrient agar can vary and depend on the bacterial species. More information on bacterial cultivation is available on the following websites: https://www.dsmz.de/ and https://www.atcc.org/. Choosing the correct nutrient medium/agar and growth conditions are particularly crucial prerequisites for the success of the method Subheading 3.4. Ensure that PAPs and the test strains are both able to grow under the chosen conditions. Otherwise, the test bacterium/a should not be included in this assay.
8. It is recommended to use different nutrient agars and mild cellular stresses for antibiotic compound screening. This will enhance the chances/probability to identify producers, as antibiotic compounds may only be produced under certain environmental conditions and stresses. For example, production of lugdunin from *S. lugdunensis* could only be observed on BM agar, and the zone of inhibition increased when the bacteria were grown under iron limitation [9]. For this, sterile 0.01% (v/v) H_2O_2 or 200 μM 2,2′-bipyridine can be added to the (40–50 °C) nutrient agar to generate oxidative or iron limitation stress, respectively.
9. Alternatively, an overnight culture of the test bacteria and/or PAPs can be used. Therefore, centrifuge 1–5 mL bacterial culture (5 min, 8000 × *g*), discard the supernatant, and add 1 mL of 1× PBS (for the generation of test bacterial lawns or PAPs stocks) or 1 mL of nutrient medium (for (soft) agar inoculation) to resuspend the bacterial pellet.

10. The OD_{600} used for inoculation of agar is dependent on the bacterial strain. Some bacteria, such as *Staphylococcu*s spp., only require a low OD_{600} of 0.001 to generate a turbid agar with a high bacterial density after incubation, whereas, e.g., *Micrococcus* spp. require an OD_{600} of 0.01 to achieve a comparable density.
11. When many PAPs are to be tested simultaneously, a metallic, self-made replica stamp may be used (Fig. 3). The stamp should be sterilized by flaming after each transfer of bacteria. After cooling, the metallic stamp can be reused for other plates. Alternatively, a commercially available replica stamp, such as replicator stamp from Carl Roth (https://www.carlroth.com/com/en/accessories-for-petri-dishes/replicator-stamp-blue/p/4708.1), can be used. If PAPs are transferred onto a plate already containing test bacteria, do not use the same tissue for more than one plate; otherwise, test bacteria may be also transferred to the next plate(s), leading to cross-contamination. If they are transferred onto nutrient agar, the same tissue can be reused.
12. In many cases, antibiotic compound production can be observed in late stationary growth phase. Thus, incubation span may be extended even beyond 72 h.
13. Pouring the soft agar on top of bacteriocin producers may wash off a producer from its original position, thereby "contaminating" other areas of the nutrient agar, which complicates the readout of the plate. Thus, to prevent the producer from further bacteriocin production, killing off the producers before soft agar topping may be helpful/useful.
14. Place the closed 24 well plate into a box, which is bedded with water-soaked paper that keeps the box humid, thereby preventing the well plate from drying.
15. If the initial MS analysis is not conclusive, repeat the analysis adding *less* colony material. If the analysis fails repeatedly, use an alternative method for strain identification.

Acknowledgments

We thank Libera Lo Presti for critically reading and editing the manuscript. The work of the authors is financed by grants of the "Deutsche Forschungsgemeinschaft (DFG)" TRR261 (project ID 398967434) to S.H and by the Cluster of Excellence EXC 2124 Controlling Microbes to Fight Infections to LC (EXC-2124/1-09.031). Further we acknowledge funding by "Deutsches Zentrum für Infektionsforschung (DZIF) TTU HAARBI," grant number TTU 08.708 to SH.

References

1. Antimicrobial Resistance C (2022) Global burden of bacterial antimicrobial resistance in 2019: a systematic analysis. Lancet 399(10325):629–655. https://doi.org/10.1016/S0140-6736(21)02724-0
2. Huemer M, Mairpady Shambat S, Brugger SD, Zinkernagel AS (2020) Antibiotic resistance and persistence-implications for human health and treatment perspectives. EMBO Rep 21(12):e51034. https://doi.org/10.15252/embr.202051034
3. De Oliveira DMP, Forde BM, Kidd TJ, Harris PNA, Schembri MA, Beatson SA et al (2020) Antimicrobial resistance in ESKAPE pathogens. Clin Microbiol Rev 33(3). https://doi.org/10.1128/CMR.00181-19
4. Molloy EM, Hertweck C (2017) Antimicrobial discovery inspired by ecological interactions. Curr Opin Microbiol 39:121–127. https://doi.org/10.1016/j.mib.2017.09.006
5. Wietz M, Mansson M, Bowman JS, Blom N, Ng Y, Gram L (2012) Wide distribution of closely related, antibiotic-producing Arthrobacter strains throughout the Arctic Ocean. Appl Environ Microbiol 78(6):2039–2042. https://doi.org/10.1128/AEM.07096-11
6. Busetti A, Maggs CA, Gilmore BF (2017) Marine macroalgae and their associated microbiomes as a source of antimicrobial chemical diversity. Eur J Phycol 52(4):452–465. https://doi.org/10.1080/09670262.2017.1376709
7. Donia MS, Cimermancic P, Schulze CJ, Wieland Brown LC, Martin J, Mitreva M et al (2014) A systematic analysis of biosynthetic gene clusters in the human microbiome reveals a common family of antibiotics. Cell 158(6):1402–1414. https://doi.org/10.1016/j.cell.2014.08.032
8. Boutin S, Dalpke AH (2020) The microbiome: a reservoir to discover new antimicrobials agents. Curr Top Med Chem 20(14):1291–1299. https://doi.org/10.2174/1568026620666200320112731
9. Janek D, Zipperer A, Kulik A, Krismer B, Peschel A (2016) High frequency and diversity of antimicrobial activities produced by Nasal Staphylococcus Strains against bacterial competitors. PLoS Pathog 12(8):e1005812. https://doi.org/10.1371/journal.ppat.1005812
10. Liu Y, Liu Y, Du Z, Zhang L, Chen J, Shen Z et al (2020) Skin microbiota analysis-inspired development of novel anti-infectives. Microbiome 8(1):85. https://doi.org/10.1186/s40168-020-00866-1
11. Kalsbeek H, Verrips GH, Frencken JE, van Eck AA (1990) Dental fluorosis in relation to the use of fluoride tablets. Ned Tijdschr Tandheelkd 97(6):269–273
12. Nascimento Jdos S, Coelho ML, Ceotto H, Potter A, Fleming LR, Salehian Z et al (2012) Genes involved in immunity to and secretion of aureocin A53, an atypical class II bacteriocin produced by Staphylococcus aureus A53. J Bacteriol 194(4):875–883. https://doi.org/10.1128/JB.06203-11
13. Zipperer A, Konnerth MC, Laux C, Berscheid A, Janek D, Weidenmaier C et al (2016) Human commensals producing a novel antibiotic impair pathogen colonization. Nature 535(7613):511–516. https://doi.org/10.1038/nature18634
14. Heilbronner S, Krismer B, Brotz-Oesterhelt H, Peschel A (2021) The microbiome-shaping roles of bacteriocins. Nat Rev Microbiol 19(11):726–739. https://doi.org/10.1038/s41579-021-00569-w
15. Rossfeld KK, Cloyd JM, Palmer E, Pawlik TM (2020) Ethics (Informed consent and conflicts of interest). In: Pawlik TM, Sosa JA (eds) Clinical trials. Springer, Cham, pp 17–31
16. Jefford M, Moore R (2008) Improvement of informed consent and the quality of consent documents. Lancet Oncol 9(5):485–493. https://doi.org/10.1016/S1470-2045(08)70128-1
17. Warnke P, Harnack T, Ottl P, Kundt G, Podbielski A. Nasal screening for Staphylococcus aureus–daily routine with improvement potentials. PLoS One 2014;9(2):e89667. doi: https://doi.org/10.1371/journal.pone.0089667.
18. Uehara Y, Kikuchi K, Nakamura T, Nakama H, Agematsu K, Kawakami Y et al (2001) H(2)O(2) produced by viridans group streptococci may contribute to inhibition of methicillin-resistant Staphylococcus aureus colonization of oral cavities in newborns. Clin Infect Dis 32(10):1408–1413. https://doi.org/10.1086/320179
19. Selva L, Viana D, Regev-Yochay G, Trzcinski K, Corpa JM, Lasa I et al (2009) Killing niche competitors by remote-control bacteriophage induction. Proc Natl Acad Sci U S A 106(4):1234–1238. https://doi.org/10.1073/pnas.0809600106

20. Gronbach K, Flade I, Holst O, Lindner B, Ruscheweyh HJ, Wittmann A et al (2014) Endotoxicity of lipopolysaccharide as a determinant of T-cell-mediated colitis induction in mice. Gastroenterology 146(3):765–775. https://doi.org/10.1053/j.gastro.2013.11.033
21. Adamek M, Spohn M, Stegmann E, Ziemert N (2017) Mining bacterial genomes for secondary metabolite gene clusters. In Sass P (ed) Antibiotics: methods and protocols. 2017. Methods Mol Biol 1520:23–47
22. Harms H, König GM, Schäberle TF (2017) Production of antimicrobial compounds by fermentation. In Sass P (ed) Antibiotics: methods and protocols. 2017. Methods Mol Biol 1520: 49–61
23. Schafhauser T, Kulik A (2022) Isolation and purification of natural products from microbial cultures. In Sass P (ed) Antibiotics: methods and protocols. 2022. Methods Mol Biol
24. Kaspar U, Kriegeskorte A, Schubert T, Peters G, Rudack C, Pieper DH et al (2016) The culturome of the human nose habitats reveals individual bacterial fingerprint patterns. Environ Microbiol 18(7):2130–2142. https://doi.org/10.1111/1462-2920.12891
25. Timm CM, Loomis K, Stone W, Mehoke T, Brensinger B, Pellicore M et al (2020) Isolation and characterization of diverse microbial representatives from the human skin microbiome. Microbiome 8(1):58. https://doi.org/10.1186/s40168-020-00831-y

Chapter 4

Production of Antimicrobial Compounds by Homologous and Heterologous Expression

I. Dewa M. Kresna, Zerlina G. Wuisan, and Till F. Schäberle

Abstract

Natural product discovery campaigns aim to identify compounds with the desired bioactivity, for example, metabolites with antibiotic activity. The major driver of many projects is still the finding of bioactive extracts, which will be followed up to isolate the activity-causing agent as pure compound. However, nowadays also additional strategies can be used to increase the probability of success. Metabolomic approaches indicate chemical novelty, and genomics allow identification of putative biosynthetic gene clusters (BGCs) of interest, even though the corresponding metabolite is unknown. Whatever the entry to the campaign is, at one point the scientists need to have the desired compound in hand to analyze it in detail. Hence, expression must be achieved to yield the compound of interest, either to link it to the corresponding putative BGC or to overcome the bottleneck of sparse compound supply. Therefore, homologous and heterologous expression approaches are feasible ways forward to increase production yield, shorten fermentation time, or to get BGCs expressed at all for which no suitable fermentation condition was identified.

In this chapter, expression approaches in bacteria are described to biosynthesize compounds of interest. Homologous expression, by genetic manipulation of the original *Streptomyces* producer strain, and heterologous expression in the microbial workhorse *Escherichia coli* are exemplified.

Key words Heterologous expression, Homologous expression, *E. coli*, *Streptomyces*

1 Introduction

The initial production of antimicrobial compounds is a prerequisite for research and development projects, starting with first bioactivity screening and advancing to identification, purification, and structure elucidation of hits, to enable rational-based decisions about if an active compound should be moved on to the next development steps. Considering natural products, the producer organism has to biosynthesize the compound of interest in sufficient amounts, and therefore, suitable conditions must exist. This can be achieved by fermentation of the original producer using different conditions, as described in the first edition of this book [1]. However, if no

Peter Sass (ed.), *Antibiotics: Methods and Protocols*,
Methods in Molecular Biology, vol. 2601, https://doi.org/10.1007/978-1-0716-2855-3_4,

suitable condition is identifiable, there are still further options. The expression of the biosynthetic gene cluster (BGC) within the producer strain could be switched on, for example, by the insertion of a, or several, promoter(s) upstream of the genes of interest. Increasing the expression yield of a gene, or a complete BGC, in a system from where it originates (i.e., the natural producer) is called homologous expression. However, to do so, first knowledge about the producer strain must be available, for example, which promoter regions will increase expression. Second, genetic manipulation of the strain must be possible. Another option would be to transfer the genetic information to biosynthesize the compound of interest into a heterologous host to reach heterologous expression therein. Several bacterial strains optimized for expression of single genes and BGCs are available. In addition, other types of host organisms beside bacteria exist and are established, for example, fungal strains and cell lines of mammalian or plant origin. A close phylogenetic relationship between original and heterologous host is often productive. However, the more exotic a natural producer is, the less is known about which hosts might be suitable. Due to the fact that the degenerated genetic code comprises more than one triplet codon for one specific amino acid to be added to the growing peptide chain during translation, different bacteria have their own preferences. Therefore, it might be useful to not work with the original DNA sequence for heterologous expression. Instead, a codon-optimized version of the gene(s) can be synthesized, adapted to the envisaged heterologous host. Several commercial suppliers offer to synthesize the DNA sequence of interest and directly provide the option to optimize the codon usage for the chosen host. Once, the expression is reached, this will open new possibilities to further tune the expression yield or to even modify the compound by biotechnological approaches.

In this chapter, a workflow is presented that can be easily adapted to your lab. It is exemplified by (i) the homologous expression of a modular non-ribosomal peptide synthetase (NRPS) and polyketide synthase (PKS) hybrid BGC in a *Streptomyces* strain [2]. The latter strain was isolated from an environmental sample [3] and by (ii) the heterologous expression of a ribosomally and posttranslational modified peptide (RiPP) BGC in *Escherichia coli* cells [4].

2 Materials

2.1 Cloning Procedure

2.1.1 Instrumentation

1. PCR machine.
2. Centrifuge for 1.5–2 mL tubes.
3. Centrifuge for 15–50 mL tubes.
4. Safety cabinet.

5. Vortex.
6. Shaking device with temperature control.
7. Incubator.
8. Ice generator machine.
9. Nanodrop or any instrument to measure DNA concentration and OD_{600}.
10. MicroPulser (including 0.2 cm cuvettes) for electroporation.
11. Complete module for agarose gel electrophoresis including gel documentation instrument.
12. Autoclave.
13. −80 °C freezer for long-time storage of microorganisms.
14. −20 °C freezer for short-time storage.
15. 4 °C fridge.
16. Temperature controllable shaker or water bath.
17. Hot plate with magnetic stirrer.
18. pH meter.
19. Micropipette 100–1000 μL.
20. Micropipette 10–100 μL.
21. Micropipette 1–10 μL.
22. 60 °C incubator.
23. Rotary evaporator.

2.1.2 Kits

1. Agarose purification for large fragment kit.
2. Bacterial DNA isolation kit.
3. Plasmid purification kit.

2.1.3 Strains, Plasmids, and Primers

1. Plasmid pCAP03-acc(3)IV (kanamycin and apramycin resistance) [5].
2. *E. coli* ET12567/pUB307 (chloramphenicol and kanamycin resistance) [6].
3. *E. coli* ET12567 (chloramphenicol resistance) [6].
4. Apramycin resistance cassette with *oriT* and *ermE** promoter. The cassette could be purchased, and the DNA sequence is shown in Sequence S1 (*see* Appendix).
5. Primers for the experiment as described in Subheadings 3.2 and 3.3.
6. Target *Streptomyces* strain which is genetically accessible.
7. *E. coli* host strain for heterologous expression.
8. pRSFduet™-1.

2.1.4 Chemicals

1. Tryptone.
2. Yeast extract.
3. NaCl.
4. Agar.
5. Mannitol.
6. Soya flour.
7. Soytone.
8. Glucose.
9. K_2HPO_4.
10. Isopropyl β-D-1-thiogalactopyranoside (IPTG): store at −20 °C freezer.
11. Kanamycin: store at 4 °C fridge.
12. Apramycin: store at 4 °C fridge.
13. Chloramphenicol: store at 4 °C fridge.
14. Nalidixid acid: store at 4 °C fridge.
15. ddH_2O.
16. Glycerol.
17. Tris Base.
18. HCl.
19. $MgCl_2$.
20. dNTPs: store at −20 °C.
21. Dithiothreitol (DTT): store at −20 °C freezer.
22. Polyethylene glycol (PEG) 8000.
23. Nicotinamide adenine dinucleotide (NAD): store at −20 °C freezer.
24. T5 exonuclease: store at −20 °C freezer.
25. DNA polymerase for PCR (Phusion): store at −20 °C freezer.
26. Taq ligase: store at −20 °C freezer.
27. TE buffer: 10 mM Tris-HCl pH 8, 1 mM EDTA; store at room temperature.
28. Lysozyme: 10 mg/mL stock solution in TE buffer; store at −20 °C in 1 mL aliquots.
29. High-Fidelity DNA Polymerase for PCR (Hot Start): store at −20 °C.
30. Restriction enzymes: store at −20 °C.
31. Agarose: 1% stock solution (w/v) in TAE buffer; store at 60 °C.
32. TAE buffer, 50× stock solution: 242.2 g Tris base, 18.612 g EDTA disodium salt dihydrate, 57.1 mL acetic acid, dissolved

in 1 L ddH_2O. Working solution is prepared by diluting 40 mL of 50× stock solution into 2 L ddH_2O; store at room temperature.

33. Midori Green DNA stain: store at 4 °C.
34. Methanol (HPLC grade).

2.1.5 Others

1. Mixed cellulose ester (MCE) membrane, hydrophilic, 0.025 μm pore size.
2. 15 mL conical centrifuge tubes.
3. 50 mL conical centrifuge tubes.
4. Syringes.
5. Sterile filters (0.2 μm pore size).
6. Petri dishes.
7. Schott bottles with cap (as media and buffer containers).
8. 0.2 mL PCR tubes.
9. 1.5–2 mL tubes.
10. 2 mL cryo-tubes.
11. Cotton.
12. Scalpel.
13. 100 mL round-bottom flasks.

2.2 Medium

Before use, medium has to be sterilized by using an autoclave and cooled to room temperature (RT). Initially, weight all the necessary materials and pour them into a 1 L Schott bottle. Thereafter, add ddH_2O up to the required volume and homogenize the solution by shaking or stirring. Then, autoclave the solution and let it cool to RT (*see* **Note 1**). In the following, the recipes of the media used in this experiment are described.

1. Lysogeny broth (LB): 10 g/L tryptone, 5 g/L yeast extract, 10 g/L NaCl, and 15 g/L agar (agar is only added for solid medium).
2. 2× WT broth: 16 g/L tryptone, 10 g/L yeast extract, 5 g/L NaCl.
3. MS medium: 20 g/L mannitol, 20 g/L soya flour, 20 g/L agar.
4. TSB medium: 17 g/L tryptone, 3 g/L soytone, 2.5 g/L glucose, 5 g/L NaCl, 2.5 g/L K_2HPO_4.
5. Med-3: 10 g/L glucose (500 g/L stock solution; autoclaved separately and mixed prior to use), 5 g/L NaCl, 3 g/L $CaCO_3$, 20 g/L soybean powder.

2.3 Antibiotic and IPTG Stock Solutions

The antibiotic stock solutions are prepared in a 1000× concentration (in relation to the final working concentration). Concentration of the IPTG stock solution is 1 M. Filters with a pore size of 0.2 μm are used to sterilize the solution, to prevent degradation of the antibiotic and IPTG by autoclaving. Thereafter, store the solutions at −20 °C in a freezer (*see* **Note 2**).

1. Kanamycin (Kan): 50 mg/mL in ddH_2O.
2. Apramycin (Apra): 50 mg/mL in ddH_2O.
3. Chloramphenicol (Cm): 25 mg/mL in EtOH.
4. Nalidixic acid (NA): 20 mg/mL in ddH_2O (*see* **Note 3**).
5. IPTG: 1 M in ddH_2O.

3 Methods

3.1 Cloning Procedure

3.1.1 Generating Electro-Competent Cells

1. Grow the pre-culture of the desired *E. coli* strain in 5 mL LB with necessary antibiotics in 15 mL conical centrifuge tubes or other sterile containers. Incubate at 37 °C in a shaker (180 rpm) overnight.
2. Transfer an inoculum of the pre-culture to a sterilized vessel containing 50 mL LB medium (this will be the main culture) with necessary antibiotics. Of the pre-culture 1% is used to inoculate the main culture.
3. Incubate the main culture in a shaker (180 rpm) at 37 °C until it reaches an OD_{600} of 0.4–0.6.
4. Transfer the main culture to a 50 mL conical centrifuge tube, and pellet the cells by centrifugation at 15,000 g, 2 min, at 4 °C.
5. Discard the supernatant. All following steps should be performed on ice.
6. Add 30 mL of ice-cold sterile ddH_2O and redissolve the pellet by shaking and vortex vigorously.
7. Centrifuge the suspension at 15,000 g, 2 min, at 4 °C.
8. Discard the supernatant.
9. Repeat steps 6–8 to rewash the cell.
10. Add 30 mL of ice-cold sterile 10% (w/v) glycerol and redissolve the pellet by shaking and vortex vigorously.
11. Repeat steps 7–8.
12. Add 400 μL of ice-cold sterile 10% (w/v) glycerol and resuspend cells until the solution is homogenous. After this step, the cells have become electro-competent and can be directly used or stored at −80 °C.

13. Prepare aliquots of 50 µL of the competent cells in 1.5 mL or 2 mL sterile tubes until all the competent cells are consumed.
14. Store the ready-to-use electro-competent cells in a − 80 °C freezer.

3.1.2 Preparing the Ready-to-Use Gibson Assembly (GA) Master Mix [7]

1. Add the following ingredients to a 1.5 mL tube: 250 µL 1 M Tris–HCl pH 7.5, 25 µL 1 M $MgCl_2$, 50 µL 10 mM dNTP, 25 µL 1 M DTT, 125 mg PEG-8000, and 1.7 mg NAD.
2. Dissolve the ingredients completely by pipetting up and down (*see* **Note 4**).
3. Add ddH_2O to the final volume of 500 µL and resuspend. This solution represents the 5× isothermal buffer.
4. Transfer 320 µL of the isothermal buffer solution from the previous step to a new 1.5 mL or 2 mL tube.
5. From now on, each step has to be performed on ice. To the 320 µL 5× isothermal buffer solution, add 1.2 µL of T5 exonuclease, 20 µL Phusion polymerase (not Hot Start), 160 µL Taq ligase, and 700 µL ddH_2O.
6. Homogenize the solution by pipetting up and down and vortexing.
7. Prepare 15 µL aliquots of the solution in PCR tubes until all the solution is consumed. Each of the tubes contains now the ready-to-use Gibson Assembly (GA) master mix solution needed for one experiment.
8. Store the aliquots at −20 °C in a freezer.

3.1.3 Transformation of E. coli by Electroporation [8]

1. All steps should be performed on ice-cold temperature.
2. Prepare the ice-cold ready-to-use electro-competent cells (*see* Subheading 3.**1 step 1**), ice-cold LB, the salt-free-DNA to be transferred, and ice-cold 0.2 cm cuvette(s).
3. Turn on the MicroPulser for electroporation.
4. Set the pre-programmed setting to Ec2 (2.5 kV).
5. Add 2–4 µL of the salt-free-DNA (*see* **Note 5**) to a ready-to-use 50 µL of electro-competent cells (*see* Subheading 3.**1 step 1**).
6. Transfer the electro-competent cell-DNA mix to the 0.2 cm cuvette (make sure the solution is touching both electrodes).
7. Place the cuvette in the chamber slide.
8. Release the pulse once and thereafter directly resuspend the mix by adding 1 mL of ice-cold LB to the cuvette and mix by pipetting until homogeny (*see* **Note 6**).
9. Transfer the solution to a 1.5 mL or 2 mL tube, and incubate at 37 °C and shaking (180 rpm) for 45–60 min.

10. Centrifuge the culture at 15,000 × g, 1 min, and discard the supernatant until only around 100 μL of supernatant are remaining.
11. Resuspend the solution by pipetting and spread it to LB agar plates containing the corresponding antibiotics for selection.
12. Incubate the plate at 37 °C overnight.

3.1.4 Generation of E. coli Cryo-Cultures for Storage

1. Prepare a sufficient amount of sterile 50% glycerol (w/v) in ddH_2O by autoclaving.
2. Grow the *E. coli* strain in 3–5 mL of LB medium with corresponding antibiotic(s) for selection overnight at 37 °C in a shaker (180 rpm) as pre-culture.
3. Transfer 1 mL of the pre-culture to a sterile cryo-tube and add an equal amount of 50% sterile glycerol (w/v).
4. Vortex the cryo-culture and store at −80 °C in a freezer.

3.1.5 Generation of Streptomycete Spore Suspension for Storage [9]

1. Spread a desired *Streptomyces* strain on MS agar medium with corresponding antibiotics at its optimal growth temperature (usually 28–30 °C are used) for several days until sporulation can be observed. Sporulation can be recognized by a grayish coloration, since the spores are pigmented.
2. Add 4 mL of sterile ddH_2O on top of the agar plate and gently scrape off the spores using sterile cotton.
3. Take a sterile syringe and suck the spore-containing water through the cotton (which will serve as a filter for bigger particles), and collect the ddH_2O containing the spores in a sterile 15 mL conical centrifuge tube.
4. Centrifuge the spore suspension at 15,000 × g for 5 min and thereafter discard the supernatant.
5. Add 1–2 mL of sterile 20% glycerol (w/v) to the spore pellet and resuspend the spores therein.
6. Transfer the spore suspension to a sterile cryo-tube and store it at −80 °C.

3.1.6 Restriction Analysis of Plasmid DNA

1. Inoculate the clone tested positive by colony PCR in 5 mL LB medium containing necessary antibiotics (*see* **Note 7**).
2. Incubate the culture at 37 °C, on a shaker (180 rpm), overnight.
3. Isolate the plasmid from the culture using a plasmid isolation kit.
4. For restriction analysis take an aliquot of the plasmid DNA, and add the selected restriction enzymes and their respective buffer according to the restriction enzyme manufacturer's protocol. Total volume of the restriction mix should be 20–50 μL.

5. Incubate the restriction mix overnight at the recommended temperature optimum of the restriction enzymes (usually 37 °C).
6. For analysis, add loading dye and run the mix over a 1% agarose gel.
7. Analyze and document the DNA restriction pattern.

3.2 Construction of the Plasmid to Be Used for Conjugation and Homologous Recombination into the Genome of the Streptomyces Homologous Host

The DNA manipulation explained herein relies on a double crossover recombination event. The homologous regions necessary for the recombination event to take place are introduced into the bacterium as part of a designed plasmid. This plasmid has several features: (i) Two DNA regions homologous to the sequences flanking the desired site of modification, (ii) resistance genes to enable selection in *E. coli* cells during vector construction and in *Streptomyces* cells after the recombination event took place, (iii) an origin of transcription (*ori*) for propagation of the plasmid in *E. coli*, (iv) an origin of transfer (*oriT*) to enable transfer of the DNA by conjugating from the donor *E. coli* to the recipient *Streptomyces* cell, and (v) if necessary a promoter (*ermE** in our example) (Fig. 1). The plasmid can replicate in *E. coli*, which enables construction of the plasmid in this host. However, the plasmid is used to transfer the desired DNA sequence, but cannot be propagated by the recipient *Streptomyces* strain. The initial (single) crossover could happen in either homologous region 1 or 2. Regardless in which region the recombination took place, the whole plasmid would be integrated, resulting in a strain that possesses the genes for kanamycin and apramycin resistance. When the second crossover takes place, it could happen at each of the homologous region, either 1 or 2. If the second crossover happens in the same region as the initial crossover, then the chromosome is reverted back to the original wild-type status, which does not have any antibiotic resistance gene—and thus will die during antibiotic selection pressure. If the second crossover happens in the region different from the initial crossover event, the resulting strain will carry only the apramycin and not the kanamycin-resistant cassette. To identify the latter case, the clones are screened using two replica plates with supplemented with a different antibiotic.

3.2.1 DNA Fragment of Homologous Regions 1 and 2

1. Determine the objective of the experiment. Is an overexpression or a knockout desired?
2. Decide which manipulation should be performed, for example, deletion, insertion (introducing *ermE**), or both (replacement).
3. Determine the homologous regions (HR) 1 and 2 (each ±1000 bps in length, example in Fig. 1).

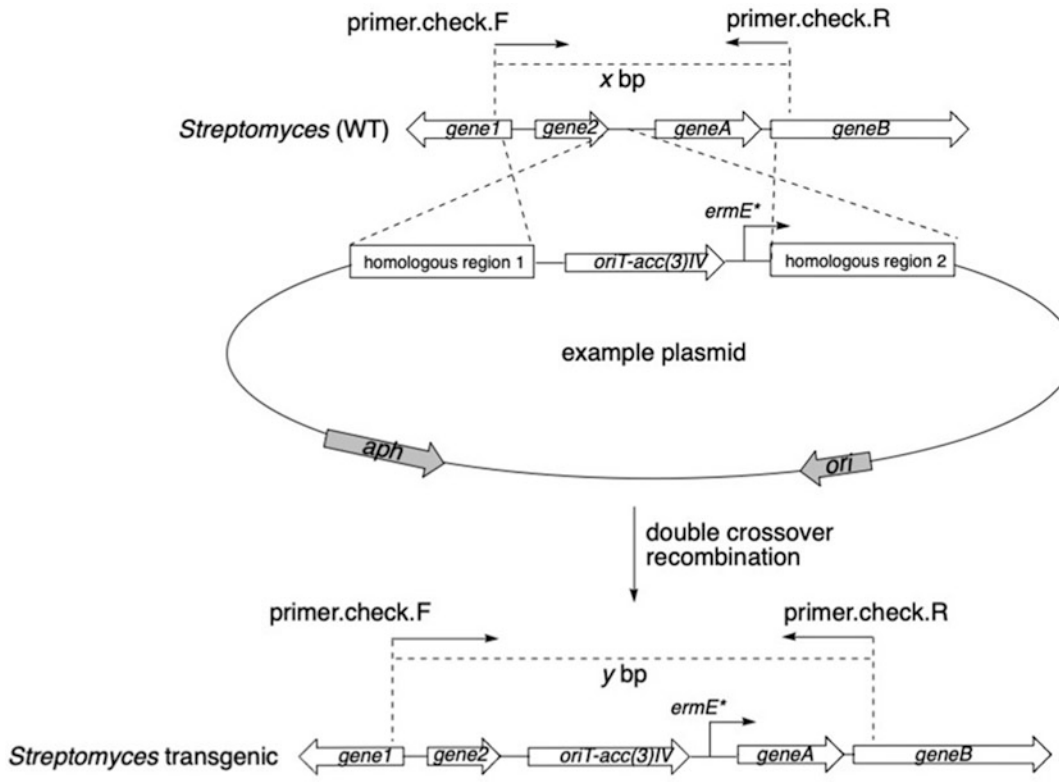

Fig. 1 Scheme of the introduction of the constitutive ermE* promoter by double crossover. To introduce the promoter upstream of the target gene A, a plasmid is designed that carries two sequence regions, which are homologous to the genome of the *Streptomyces* wild-type (WT) host. Here, the example plasmid carries the antibiotic resistance cassettes for apramycin (encoded by the gene *acc*(3)IV) and kanamycin (encoded by the *aph* gene). The genetic organizations of the WT and the mutant strain after successful integration of the apramycin resistance cassette in combination with the ermE* promoter are given. The location of a primer pair to analyze if the targeted integration took place is indicated

4. Design a primer that can amplify the HRs 1 and 2 with annealing temperature (Tm) of 65–66 °C (to determine the Tm, use the online tool provided by the company from which the DNA polymerase is purchased). Next, add additional extension nucleotides 5′-cctgaactcaccgcgacgta-3′ to the 5′-forward primer of HR1, 5′-ggtcgacggatccccggaat-3′ to the 5′-reverse primer of HR1, 5′-aggatccagcgggtaggagg-3′ to the 5′-forward primer of HR2, and 5′-cactcaaccctatctcggtc-3′ to the 5′ of the reverse primer of HR2 (*see* **Note 8**).
5. Using the designed primers and genomic DNA of your *Streptomyces* WT strain as a template, amplify the homologous regions 1 and 2 by PCR. The annealing temperature is chosen according to the primers (in our example 65 °C).

6. Isolate the desired PCR products by agarose gel and subsequent large fragment purification kit.
7. Determine the DNA concentration of HR1 and HR2 in pmol/μL (*see* **Note 9**).

3.2.2 DNA Fragment of the Vector

1. Digest the vector pCAP03-acc(3)IV with the restriction enzymes *Xho*I and *Nde*I by overnight incubation at 37 °C.
2. Purify the 10,551 bps linear DNA fragment by agarose gel and subsequent large fragment purification kit.
3. Used the pure DNA fragment as a template for PCR using primers pCAP03.part.F (gaccgagatagggttgagtg) and pCAP03.part.R (tacgtcgcggtgagttcagg). The annealing temperature for the PCR program is 55 °C. The desired PCR amplificate (fragment length is 3877 bps) carries a kanamycin resistance gene (*aph*) and an *ori*.
4. Purify the desired PCR product by agarose gel and subsequent large fragment purification kit.
5. Determine the DNA concentration in pmol/μL (*see* **Note 9**).

*3.2.3 DNA Fragment of the Apramycin Resistance Gene (*Acc*(3)IV) and* oriT

1. Amplify the apramycin resistance cassette containing *oriT* using primer cassette.F (attccggggatccgtcgacc) and cassette.R (tgtaggctggagctgcttcgaa) for a knockout experiment or using primer cassette.F and ermE*.R (cctcctacccgctggatcct) for an overexpression experiment (the latter primer pair will result in an amplicon that includes the *ermE** promoter). The annealing temperature is 65 °C.
2. Purify the resulting 1369–1499 bps desired PCR product by agarose gel and subsequent large fragment purification kit.
3. Determine the DNA concentration in pmol/μL (*see* **Note 9**).

3.2.4 Fusion of the Four DNA Fragments Using Gibson Assembly

1. Calculate how many μL of each DNA fragment (from Subheading 3.2 **steps 1–3**) should be used to reach a molar ratio of vector:HR1:HR2:cassette of 1:1:1:1. The final volume should be 5 μL.
2. Add the 5 μL mix of the DNA fragments to the ready-to-use 15 μL Gibson Assembly (GA) master mix (*see* Subheading 3.1 **step 2**).
3. Incubate the GA reaction at 50 °C for 2 h (use PCR machine if possible).
4. During waiting for step 3, pour 20 mL of ddH_2O into a petri dish, and place a 0.025 μm pore size MCE membrane on the water.

5. After the isothermal incubation (**step 3**), transfer the complete 20 μL of the GA reaction carefully using a micropipette onto the prepared 0.025 μm pore size MCE membrane (**step 4**).
6. Dialyze the GA reaction for 15–30 minutes.
7. Transfer the desalted GA mix to *E. coli* ET12567 cells by electroporation (*see* Subheading 3.1 **step 3**), and thereafter spread it on LB agar supplemented with the three antibiotics Cm/Kan/Apra.
8. Verify colonies growing on the LB $agar_{Cm/Kan/Apra}$ selection plates by colony PCR. Replicate the colony to a new LB $agar_{Cm/Kan/Apra}$ plate for maintaining the colony, and incubate it at 37 °C overnight.
9. Isolate the plasmid DNA from the clones tested positive by colony PCR to analyze the DNA restriction pattern (*see* Subheading 3.1 **step 6**).
10. As a final verification, you can submit the plasmid DNA tested positive by colony PCR and by DNA restriction analysis for Sanger sequencing (plasmid DNA is obtained by Subheading 3.1 **step 6**).
11. Pick one validated colony carrying the correct construct from the agar plate, and prepare a cryo-culture for storage (*see* Subheading 3.1 **step 4**).

3.2.5 Transfer of the Generated Plasmid to the Streptomyces *Strain by Tri-Parental Conjugation [9]*

1. Inoculate *E. coli* ET12567/pUB307 (carrying the helper plasmid necessary for tri-parental conjugation) and *E. coli* ET12567 (carrying the plasmid generated before, *see* Method 3.2.4) each separately into 10 mL LB medium supplemented with Kan and Cm for *E. coli* ET12567/pUB307 and additional Apra for the strain carrying the generated plasmid for transfer (*see* Subheading 3.2 **step 4**).
2. Grow them overnight at 37 °C in a shaker (180 rpm).
3. Take an inoculum of 100 μL of each of the overnight cultures into separate 10 mL of fresh LB medium with the corresponding antibiotics. Incubate at 37 °C in a shaker (180 rpm) until an OD_{600} of 0.4–0.6 is reached (*see* **Note 10**).
4. Wash the cells twice with 10 mL of LB medium to remove the antibiotics that might inhibit the *Streptomyces* strain.
5. Resuspend the cell pellet of strain *E. coli* ET12567/pUB307 in 0.5–1 mL of LB medium and the pellet of *E. coli* ET12567 carrying the plasmid to be transferred in 0.2–0.4 mL of LB medium. Now, the *E. coli* cells are ready for conjugation.
6. For the *Streptomyces* cells, add 10–20 μL of the *Streptomyces* wild-type spore suspension (previously generated in the way explained in Subheading 3.1 **step 5**) to 200 μL of 2× YT broth.

For each conjugation reaction, a separate tube should be prepared. Heat shock the spore suspension at 50 °C for 10 min, and then allow it to cool down to room temperature (RT).

7. Mix 0.1 mL of each of the two *E. coli* cell suspensions and 0.2 mL of the heat-shocked spores by pipetting up and down.
8. Plate out 50 μL and 350 μL of the mixture on two MS agar plates containing 10 mM $MgCl_2$ (without antibiotics), and incubate at 30 °C for 16–20 h.
9. Overlay the plates with 1.5 mL of sterile ddH_2O containing 0.5 mg of NA (equivalent to 20 μL of NA stock solution) and 2–4 mg Kan (40 μL of Kan stock solution). Use a spreader to lightly distribute the antibiotic solution evenly.
10. Continue incubation at the optimum growth temperature of the used *Streptomyces* strain until sporulation can be observed.
11. Pick up several single colonies and streak them as separated colonies on an MS agar plate supplemented with NA and Apra. By this plating, single colonies should be obtained, and you should get rid of remaining *E. coli* cells.
12. Incubate the plates at the optimum growth temperature of the *Streptomyces* strain until sporulation can be observed.
13. To verify the positive double crossover recombination event, pick and replica streak several single colonies on MS agar supplemented with Kan and onto MS agar supplemented with Apra to maintain the colonies. The inability of the picked colonies to grow under Kan selection confirms the double cross recombination event (*see* **Note 11**).
14. To verify if the recombination took place at the desired location, do a PCR test using two primers that bind outside of the recombination event border (primer.check.F and primer.check.R in Fig. 1). The length of the PCR product should be different (in case there is a deletion or insertion of nucleotides) in comparison to the WT strain (*see* **Note 12**).
15. Once a transgenic colony has been verified, prepare a spore suspension for storage (*see* Subheading 3.1 **step 5**).
16. The transgenic strain is ready to be used for cultivation.

3.2.6 Cultivation of the Homologous Expression Host

1. Take 5 μL of the spore suspension prepared in 3.2.5, **step 15** to inoculate 20 mL of Med-3 in a 100 mL Erlenmeyer flask.
2. Incubate the culture at 30 °C with 180 rpm shaking.
3. Harvest the culture for LC-MS analysis to detect/follow compound production after at least 3-day cultivation (*see* **Notes 20** and **22**).

3.3 Heterologous Expression of a BGC in Escherichia coli

In contrast to the homologous expression approach, the heterologous expression system described here is plasmid-based, which means that the target BGC is cloned into an expression vector and then introduced into the heterologous expression host, in which it is propagated. The plasmid pRSFDuet™-1 was chosen as the heterologous expression vector due to several reasons: (i) the presence of two multiple cloning sites, (ii) the presence of T7-*lac* operon that facilitates high gene expression upon IPTG induction, (iii) high plasmid copy number, and (iv) kanamycin resistance cassette that does not interfere with the resistance gene of the selected heterologous expression host *E. coli* Rosetta™(DE3) that has chloramphenicol resistance. *E. coli* Rosetta™ (DE3) was chosen as the heterologous host because it carries the pRARE plasmid that provides tRNAs for rare codons in *E. coli* (i.e., AGG, AGA, AUA, CUA, CCC, GGA). The cloning of the target BGC into the heterologous expression vector is done by Gibson Assembly. Therefore, 20–40 bp overlaps at each end of the fragments are needed (Fig. 2). pRSFDuet™-1 as the heterologous expression vector is linearized by *Nde*I and *Avr*II to remove the S-tag in the second multiple cloning site. The digestion using both restriction enzymes will

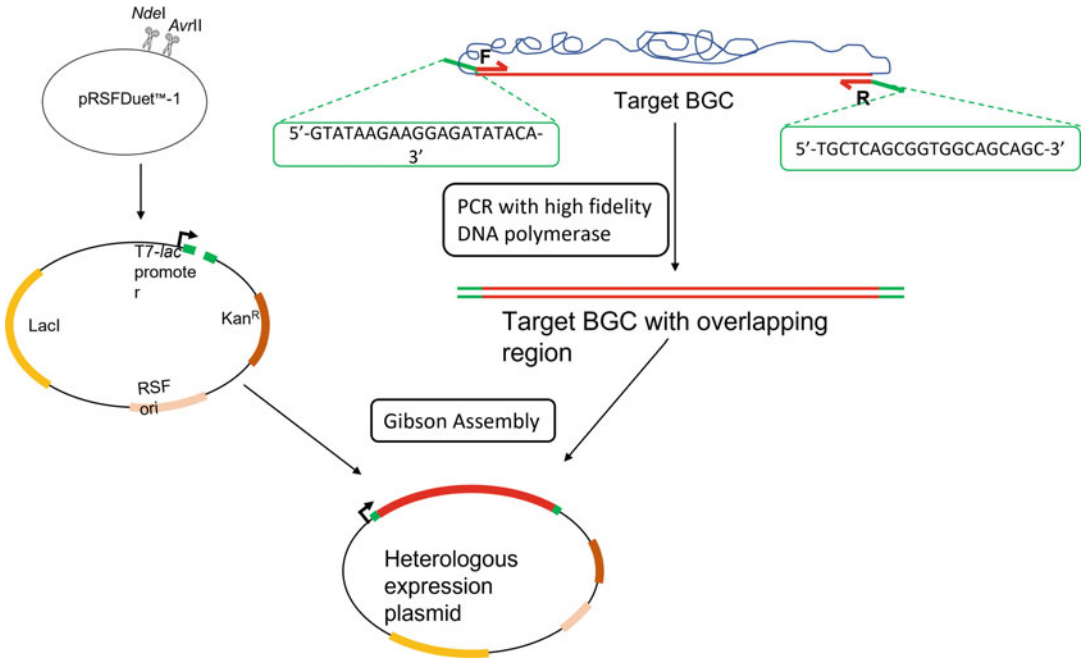

Fig. 2 Scheme for cloning the target BGC into the heterologous expression vector. *Nde*I and *Avr*II are used to linearize pRSFDuet™-1. The forward (**F**) and reverse (**R**) primers that are used for amplification of the target BGC from the genomic DNA of the original strain should have at least a 20 bp region that is homologous to the ends of the linearized plasmid (highlighted in green). The target BGC is inserted into the heterologous expression vector by Gibson Assembly (therefore, the homologous regions between the DNA fragments are needed)

result in sticky ends. However, during the Gibson Assembly reaction, the T5 exonuclease will chew the 5′ ends of the fragments. Therefore, the overlapping regions that should be introduced to the fragments by using PCR are as follows: (i) in the forward primer: 5′- GTATAAGAAGGAGATATACA -3′ and (ii) in the reverse primer: 5′- TGCTCAGCGGTGGCAGCAGC -3′.

3.3.1 Preparation of Gibson Assembly Fragments

1. Design a PCR primer pair for amplification of the target BGC. Each primer should have a minimum length of 40 bp. 20 nt of the 5′ end of the primers should contain overlapping regions with the heterologous expression vector, and 20 nt of the 3′ end of the primers should bind to target BGC (*see* **Notes 13** and **14**).
2. Amplify target BGC using High-Fidelity DNA Polymerase according to manufacturer's protocol.
3. Linearize pRSFDuet™-1 as the heterologous expression vector using the following reaction at 37 °C, overnight (*see* **Note 15**): 16 μL pRSFDuet™-1*, 1 μL *Nde*I (20 U/μL), 1 μL *Avr*II (20 U/μL), 2 μL 10× restriction enzyme buffer.

   *Plasmid was isolated from its maintenance host using plasmid isolation kit. The optimal plasmid concentration should be around 100 ng/μL (*see* **Note 16**).
4. Run a 1% agarose gel for visualization of the Gibson Assembly fragments (amplified target BGC and linearized heterologous expression vector). To prevent DNA damage from UV, use Midori Green instead of ethidium bromide.
5. Cut the DNA fragments with correct size using a scalpel, and collect the fragments in different 2 mL tubes.
6. Purify DNA from agarose gel using "Agarose purification for large fragment kit." Elute the pure DNA using ≤10 μL autoclaved ddH_2O, pre-warmed in a 60 °C oven.

3.3.2 Plasmid Construction by Gibson Assembly [7] and Transferring the Heterologous Expression Construct into a Heterologous Host

1. Take 1 aliquot (15 μL) of the ready-to-use GA master mix *(see* Subheading 3.1 **step 2**), and add a total volume of 5 μL of the purified DNA fragments in equimolar amounts (*see* **Note 17**).
2. Incubate at 50 °C for 1 h (*see* **Note 18**).
3. Pour 20 mL ddH_2O into a petri dish and place a 0.025 μm nitrocellulose membrane on the water.
4. After the isothermal incubation (**step 2**), take all 20 μL of the GA reaction carefully using a micropipette, and place it on the 0.025 μm nitrocellulose membrane.
5. Dialyze the GA reaction for 15–30 min.
6. Transfer 5 μL of the GA reaction into a ready-to-use electrocompetent cell of *E. coli* previously prepared (*see* Subheading 3.1 **step 1**) and do transformation as described in Subheading 3.1 **step 3**.

7. Plate transformed cells on LB agar medium supplemented with 50 μg/mL kanamycin (for selection of resistant cells harboring the desired plasmid), and incubate at 37 °C overnight (*see* **Note 19**).
8. Take a single colony carrying the constructed plasmid that was proven to be assembled correctly by PCR test and restriction enzyme analysis (*see* Subheading 3.1 **step 6**). This colony should be preserved as cryo-culture (*see* Subheading 3.1 **step 4**).

3.3.3 Cultivation of Heterologous Expression Host

1. Inoculate single colony (from Subheading 3.3.2 **step 8**) into 5 mL LB supplemented with kanamycin (50 μg/mL) and chloramphenicol (25 μg/mL), and incubate at 37 °C with 180 rpm shaking overnight.
2. On the next day, take 500 μL of the overnight culture to inoculate 50 mL LB supplemented with kanamycin (50 μg/mL) and chloramphenicol (25 μg/mL), and incubate at 37 °C with 180 rpm shaking until an OD_{600} of 0.4–0.6 is reached.
3. Induce with 25 μL of 1 M IPTG (final concentration of 0.5 mM). Incubate at 37 °C with 180 rpm shaking.
4. Take 1 mL samples for LC-MS analysis to detect/follow compound production after at least 1-day cultivation (*see* **Notes 20**, **21**, and **22**).

4 Notes

1. Hot medium in glassware can be cooled faster using normal tap water. Put the hot bottle into a vessel containing room temperature tap water for several minutes. Do not completely sink the bottle to prevent contamination at the bottleneck and lid area.
2. It might be useful to divide the antibiotic stock solution into aliquots of smaller volume 1–1.5 mL in sterile 1.5–2 mL tubes. This will reduce the time needed for thawing the frozen solution before use.
3. Nalidixic acid is not easily soluble in water. To increase the solubility, you could add several drops of 1 M NaOH.
4. If necessary, heat the solution to 60 °C to increase the solubility.
5. Pipetting DNA has to be done slow and carefully to prevent breaking due to shearing forces.
6. If a short circuit occurs, repeat **step 4** in Subheading 3.1.3 with less volume of DNA solution. There might be remaining impurities like salts.

7. For picking the colony from the agar plate, you can use a sterile pipette tip or tooth pick. Take only half of the colony so that you still have another half left for further steps. If most of the colony is used up, you can also just re-incubate the plate at 37 °C overnight. Then, the remaining cells will multiply again and can be used for the next steps.
8. The additional nucleotides in the primer sequences are meant to be the homologous regions for Gibson Assembly.
9. If a nanodrop instrument is used, the DNA concentration will be given μL/mL. To adjust the concentration for GA, you must convert it to pmol/mL. You could use online tools like the Promega biomath calculator (https://www.promega.de/en/resources/tools/biomath/) to do so. Subsequently, you can calculate that the fragments are used in the same molarity.
10. Normally, *E. coli* ET12567/pUB307 will grow faster than *E. coli* ET12567 carrying the designed plasmid.
11. It might happen that only a single crossover event took place from all the picked colonies, which would result in clones that carry apramycin and kanamycin resistance genes. If necessary, you can verify this by PCR using primer.check.F and primer.check.R (remember that in case of only single crossover event, whole plasmid is integrated meaning that you need to recalculate the extension time for PCR). As a solution, you can grow these single crossover clones in TSB medium for several days; thereafter, take 100 μL of the culture and spread it on MS agar supplemented with Apra to get single clones. Then, continue with **step 12** in Subheading 3.2.5.
12. Keep in mind that the length of the PCR amplificate is only an indication, and small changes in the DNA length (between mutant and WT) might not be observable in the agarose gel after PCR. In this case, further verification by Sanger sequencing might be necessary.
13. Overlapping regions between the DNA fragments can be extended up to 40 bp to increase the efficiency of Gibson Assembly.
14. If the target BGC is larger than 10 kb, it can be amplified as two fragments. The overlapping region of 20–40 bp between the fragments needs to be taken into account during primer design. Increasing amount of fragments could decrease Gibson Assembly efficiency. It is advised to have not more than five fragments.
15. Linearized plasmid can also be generated by amplification using a High-Fidelity DNA Polymerase according to manufacturer's protocol. After the final elongation step of the PCR, 1 μL of *Dpn*I is added into the PCR reaction tube and incubated at 37 °C for 1 h. This step reduces false positives.

16. Lower plasmid concentration could lead to a lower number of colonies after Gibson Assembly.
17. The concentration of the fragments to be assembled should be between 0.05 and 0.5 pmols for a GA using two to three fragments. If any fragments are smaller than 200 bp, use a fivefold excess of these fragments.
18. During the isothermal incubation for Gibson Assembly, prepare electro-competent cells to be transformed with the Gibson Assembly result.
19. Corroborate the correct assemblies by doing PCR tests and checking the restriction pattern using suitable restriction enzyme(s).
20. Samples can be taken at certain time points to find the optimum cultivation period for compound production.
21. Samples taken before 1-day cultivation after IPTG induction might produce too low amount of the target compound to be unambiguously detected by LC-MS analysis.
22. As negative control, prepare a clone of the expression host carrying the empty expression vector, and cultivate it using the exactly same conditions as for the expression culture.

Appendix

Sequence S1

ATTCCGGGGATCCGTCGACCTGCAGTTCGAAGTTCC-
TATTCTCTAGAAAGTATAGGAACTTCGAAGTTCCCGC-
CAGCCTCGCAGAGCAGGATTCCCGTTGAGCACCGC-
CAGGTGCGAATAAGGGACAGTGAAGAAGGAA-
CACCCGCTCGCGGGTGGGCCTACTTCACC-
TATCCTGCCCGGCTGACGCCGTTGGATACACCAAG-
GAAAGTCTACACGAACCCTTTGGCAAAATCCTGTA-
TATCGTGCGAAAAAGGATGGATATACCGAAAAAATCGC-
TATAATGACCCCGAAGCAGGGTTATGCAGCGGAAAATG-
CAGCTCACGGTAACTGATGCCGTATTTGCAGTAC-
CAGCGTACGGCCCACAGAATGATGTCACGCT-
GAAAATGCCGGCCTTTGAATGGGTTCATGTGCAGCTC-
CATCAGCAAAAGGGGATGATAAGTTTATCACCACCGAC-
TATTTGCAACAGTGCCGTTGATCGTGCTATGATCGACT-
GATGTCATCAGCGGTGGAGTGCAATGTCGTGCAATAC-
GAATGGCGAAAAGCCGAGCTCATCGGTCAGCTTCT-
CAACCTTGGGGTTACCCCCGGCGGTGTGCTGCTGGTC-
CACAGCTCCTTCCGTAGCGTCCGGCCCCTCGAA-
GATGGGCCACTTGGACTGATC-
GAGGCCCTGCGTGCTGCGCTGGGTCCGGGAGG-
GACGCTCGTCATGCCCTCGTGGTCAGGTCTGGACGAC-
GAGCCGTTCGATCCTGCCACGTCGCCCGTTACACCG-

GACCTTGGAGTTGTCTCTGACACATTCTGGCGCCTGC-
CAAATGTAAAGCGCAGCGCCCATCCATTTGCCTTTGCGG-
CAGCGGGGCCACAGGCAGAGCAGATCATCTCTGATC-
CATTGCCCCTGCCACCTCACTCGCCTG-
CAAGCCCGGTCGCCCGTGTCCATGAACTCGATGGG-
CAGGTACTTCTCCTCGGCGTGGGACACGATGCCAACAC-
GACGCTGCATCTTGCCGAGTTGATGGCAAAGGTTCCC-
TATGGGGTGCCGAGACACTGCACCATTCTTCAGGATGG-
CAAGTTGGTACGCGTCGATTATCTCGAGAATGAC-
CACTGCTGTGAGCGCTTTGCCTTGGCGGACAGGTGGCT-
CAAGGAGAAGAGCCTTCAGAAGGAAGGTCCAGTCGGT-
CATGCCTTTGCTCGGTTGATCCGCTCCCGCGA-
CATTGTGGCGACAGCCCTGGGTCAACTGGGCCGA-
GATCCGTTGATCTTCCTGCATCCGCCAGAGGCGG-
GATGCGAAGAATGCGATGCCGCTCGCCAGTC-
GATTGGCTGAGCTCATAAGTTCCTATTCCGAAGTTCC-
TATTCTCTAGAAAGTATAGGAACTTCGAAGCAGCTC-
CAGCCTACAGCTAGCCGCGGTCGATCTTGACGGCTGGC-
GAGAGGTGCGGGGAGGATCTGACCGACGCGGTCCA-
CACGTGGCACCGCGATGCTGTTGTGGGCA-
CAATCGTGCCGGTTGGTAGGATCCAGCGGGTAGGAGG.

References

1. Harms H, König GM, Schäberle TF (2017) Production of antimicrobial compounds by fermentation. In: Sass P (ed) Antibiotics. Methods in molecular biology, vol 1520. Humana Press, New York, pp 49–61. https://doi.org/10.1007/978-1-4939-6634-9_3
2. Kresna IDM, Wuisan ZG, Pohl J-M, Mettal U, Otoya VL, Gand M, Marner M, Otoya LL, Böhringer N, Vilcinskas A, Schäberle TF (2022) Genome mining-guided discovery and characterization of the PKS-NRPS-hybrid polyoxyperuin produced by a marine streptomycete. Under revision
3. Linares-Otoya L, Linares-Otoya V, Armas-Mantilla L, Blanco-Olano C, Crüsemann M, Ganoza-Yupanqui ML, Campos-Florian J, König GM, Schäberle TF (2017) Diversity and antimicrobial potential of predatory bacteria from the Peruvian coastline. Mar Drugs 15(10) 308:1–14. https://doi.org/10.3390/md15100308
4. Wuisan ZG, Kresna IDM, Böhringer N, Lewis K, Schäberle TF (2021) Optimization of heterologous Darobactin a expression and identification of the minimal biosynthetic gene cluster. Metab Eng 66:123–136. https://doi.org/10.1016/j.ymben.2021.04.007
5. Tang X, Li J, Millán-Aguiñaga N, Zhang JJ, O'Neill EC, Ugalde JA, Jensen PR, Mantovani SM, Moore BS (2015) Identification of thiotetronic acid antibiotic biosynthetic pathways by target-directed genome mining. ACS Chem Biol 10(12):2841–2849. https://doi.org/10.1021/acschembio.5b00658
6. Flett F, Mersinias V, Smith CP (1997) High efficiency intergeneric conjugal transfer of plasmid DNA from Escherichia coli to methyl DNA-restricting streptomycetes. FEMS Microbiol Lett 155:223–229. https://doi.org/10.1111/j.1574-6968.1997.tb13882.x
7. Gibson DG, Young L, Chuan R-Y et al (2009) Enzymatic assembly of DNA molecules up to several hundred kilobases. Nat Methods 6:343–345. https://doi.org/10.1038/nmeth.1318
8. BIO-RAD (−) MicroPulser™ Electroporation Apparatus Operating Instruction and Application Guide. BIO-RAD. Available vio DIALOG. https://www.bio-rad.com/webroot/web/pdf/lsr/literature/4006174B.pdf. Accessed 24 Dec 2021
9. Tang X (−) direct cloning and heterologous expression of biosynthetic gene cluster. The Moore Lab Available via DIALOG https://media.addgene.org/data/plasmids/69/69862/69862-attachment_sMTMGzzwy5aw.pdf. Accessed 24 Dec 2021

Chapter 5

Isolation and Purification of Natural Products from Microbial Cultures

Thomas Schafhauser and Andreas Kulik

Abstract

Antibiotic natural products from microbes are characterized by diverse and mostly complex chemical structures, which challenge their total chemical synthesis and make biotechnological production to the predominant production route. In order to reach these valuable compounds in the fermentation broth, sophisticated recovery methods are required, and a high degree of purity is essential for a thorough exploration of their beneficial properties in subsequent assays. The isolation and purification of natural products from microbial cultures is mainly based on the repeated application of extraction and chromatographic separation methods.

This chapter describes the general strategy of natural product recovery from microbial cultures, gives theoretical and practical insights to underlying methods—essentially compound extraction and preparative chromatography—and describes a specific methodical approach to isolate and purify the natural product fusarubin from the culture of the fungus *Fusarium* sp.

Key words Natural product, Compound isolation, Purification, Extraction, Downstream processing, Chromatography, Silica gel, Size-exclusion chromatography, Preparative HPLC, Fusarubin

1 Introduction

Microorganisms such as bacteria and fungi still display a promising source of novel natural products with antibiotic activity [1–3]. When a candidate compound has been detected in a microbial culture—for example, by means of activity assays—important next steps involve structure elucidation and extensive biological testing using in vitro assays and animal models in order to characterize the compound as precisely as possible [4]. Several milligrams of very pure compound are required to perform these tasks adequately [5]. Unless the molecular structure is simple and enables chemical synthesis, the desired compound has to be produced biotechnologically—that is, cultivation of the producing organism followed by compound recovery.

Peter Sass (ed.), *Antibiotics: Methods and Protocols*,
Methods in Molecular Biology, vol. 2601, https://doi.org/10.1007/978-1-0716-2855-3_5,

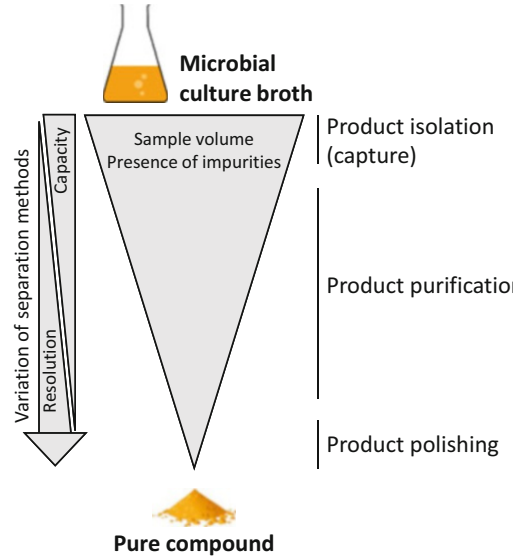

Fig. 1 General process of compound recovery

Unfortunately, microorganisms tend to produce only minor amounts of the desired compound, which thus represent only a very small proportion of the cultivation broth [6]. The broth itself is a complex mixture of a plethora of molecules, including those with similar structural and chemical features to the target molecule. In order to eventually bring the target molecule from its natural state as a component of a fermentation broth in purity and concentration, sophisticated separation processes have to be applied. These processes make use of physicochemical differences between the numerous molecules present. Solubility, hydrophilicity, acid-base properties, charge, stability (chemical, thermal, oxidative), and molecular weight are key factors to be considered during the recovery process [7]. Consequently, principle physicochemical separation techniques essentially include filtration, solvation, and adsorption (in the broadest sense). The entire operation is referred to as downstream processing. The procedure usually is divided into the stages product isolation (capture), product purification, and product polishing (*see* Fig. 1).

1.1 Product Isolation (Capture)

Downstream processing starts with the isolation of the target molecule from its original environment. This means—depending on whether it is secreted into the medium or not—the compound has to be removed from the cell or from the aqueous surrounding in order to capture it as a solute in a particulate-free liquid. To achieve this, the biomass usually first is separated from the culture medium with appropriate techniques such as filtration (using vacuum or pressure if required) or centrifugation. This is then followed by extraction, which is defined as a process of dissolving, washing, or

leaching of substances of a solid or a liquid by the aid of a solvent. The extracting solvent, the extractant, usually is a liquid but can also be a solid. The removed soluble fraction is called solute and the resulting solution that is enriched in solutes is called extract. The distribution of a solute between the (original) matrix and the extractant occurs until a state of equilibrium is reached. Consequently, an exhaustive extraction can only be achieved when the saturated extract is repeatedly replaced with fresh solvent.

The main purpose of compound isolation is to remove those components whose properties vary considerably. At this stage of downstream processing, the sample volume is usually at its largest, and capacity and recovery are more important than the purification process per se or the resolution of the method (*see* Fig. 1). Depending on the compound's location (biomass or culture filtrate), different capture methods have to be considered.

1.1.1 Capture from Biomass

The process of dissolving a desired compound out from a solid matrix such as cellular material is termed solid-liquid extraction or leaching. The chosen solvent needs to dissolve both the target molecule and the lipid bilayer of the membrane in order to destroy the cell envelope (*see* Fig. 2, left part). The latter usually is achieved with nonpolar organic solvents, and a mixture of acetone and methanol (1:1) works well for the extraction of (moderate) lipophilic compounds [8]. For more hydrophilic compounds, polar solvents in combination with a mechanical or enzymatic cell disruption can be applied.

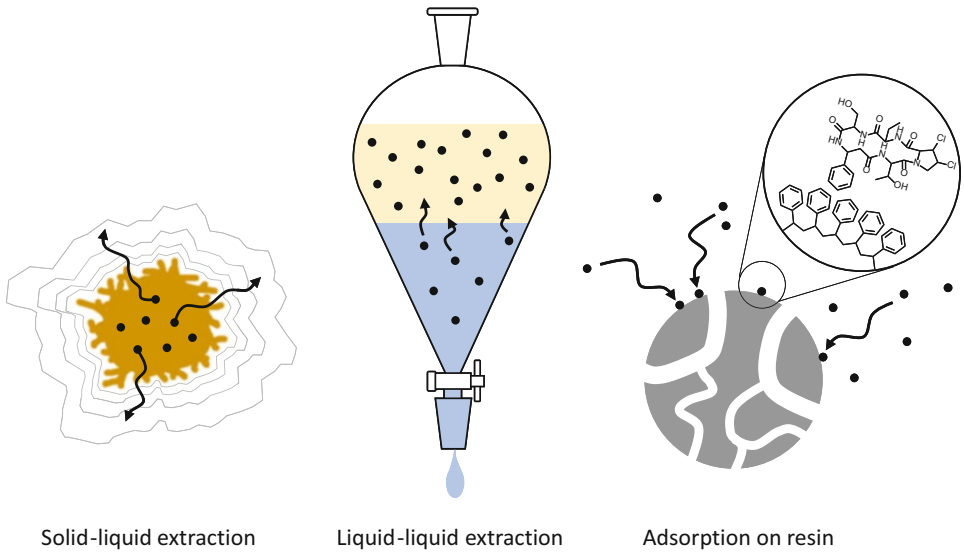

Fig. 2 Compound capture. The target compound (black circle) is extracted by means of organic solvents or adsorbent resins from biomass pellets (left) or culture filtrate (middle and right)

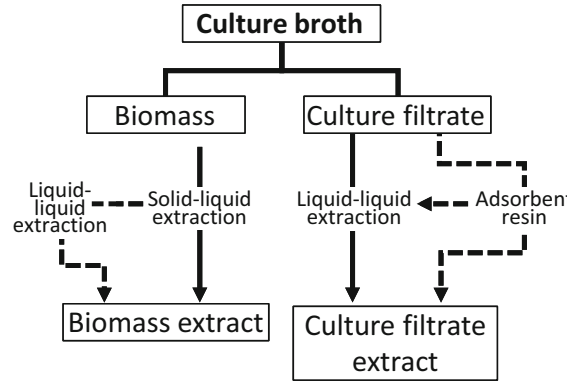

Fig. 3 Overview of the extraction process. Dotted arrows show optional routes

Agitation, heat, or pressure accelerates the adjustment of equilibrium and hence speeds up the extraction process. This principle—in parts combined with continuous solvent recharge—is exploited in several extraction methods (such as digestion, infusion, percolation, the so-called Soxhlet extraction, supercritical fluid extraction, microwave-assisted, and ultrasound-assisted extraction). Obviously, the target molecule has to remain intact during these processes.

When extraction is performed on larger amounts of biomass, the extract comprises significant quantities of water from the cytoplasm of the cells. In this case, the biomass extract usually is partly evaporated to remove the organic solvents, and then the aqueous remnant is subjected to a subsequent liquid-liquid extraction [9] (*see* Fig. 3 and also next paragraph).

1.1.2 Capture from Culture Filtrate

(a) *Liquid-Liquid Extraction (Partition)*

If the desired product is present in the aqueous culture filtrate (or in the aqueous remnants of the biomass extract), immiscible solvents that dissolve the target compound have to be used as extractants, for example, 1-butanol, ethyl acetate, dichloromethane, or petroleum benzine. Compounds will dissolve in the two phases in accordance to their partition coefficient in a process referred to as liquid-liquid extraction or partition (*see* Fig. 2, middle part). Equilibrium conditions usually are reached within seconds when the liquids are agitated vigorously, and therefore the rate-limiting steps are settling and phase separation (*see* **Note 1**). Multiple consecutive extractions using small amounts of extractant (e.g., 5 × 20 mL) are much more effective than using one large volume (e.g., 100 mL). Extraction conveniently is performed in separation funnels.

The solvent choice for extraction essentially depends on the polarity of the target molecule. When functional groups such as amines, carboxylic acids, or alcohols are present in the target

compound, changes of pH of the aqueous phase can alter the state of charge which in turn affects polarity and solubility. This can dramatically facilitate the extraction process.

Moreover, liquid-liquid extraction can be applied to wash out unwanted impurities (e.g., defatting with hexane), and also here, variation of the pH can expose or hide the charge of molecules that are to be disposed.

(b) *Adsorption on Resins*

Besides liquid-liquid extraction, the desired compound can alternatively be captured from the culture filtrate by means of adsorbent resins, which have a strong affinity for organic molecules (the process is sometimes called liquid-solid extraction). The adsorbent resins consist of highly porous, spherical particles, which are characterized by large surface areas (*see* Fig. 2, right part). Structurally, the particle matrices are varieties of synthetic polymers, such as the cross-linked, hydrophobic polystyrene (also known as aromatic resin). Resins of the AmberLite XAD series are commonly used in the field of (microbial) natural product recovery [10, 11], though there are many others.

The resin is either added directly to the culture filtrate (followed by gentle stirring and another filtration), or it is packed in a column before the culture filtrate is poured over. Moderately lipophilic and lipophilic solutes adsorb at the resin via hydrophobic interactions. Basically, nonpolar parts of the solute are rejected by the solvent—the aqueous culture filtrate—and are attracted by the resin matrix (the underlying principles are the same as in reversed-phase chromatography, *see* below). The adsorbed molecules are subsequently eluted by adding increasing amounts of an organic solvent that is less polar and miscible with water (mostly methanol). Furthermore, after removal of the organic solvents of the elution fractions, the aqueous remnant containing the desired compound can be subjected to liquid-liquid extraction (*see* Fig. 3). The adsorbent resins can easily be regenerated for reuse.

Due to the combination of porosity and large surface of the resin particles, very high recovery rates of solutes from the culture filtrate are obtained. The possibility to use small elution volumes leads to a high concentration of solutes. However, this method does not provide great selectivity.

1.2 Product Purification

The intermediate stage "product purification" refers to the processing and purification of the captured compounds. The main purpose is to separate the desired compound from most of the bulk impurities. This stage contributes the most significant part of the entire downstream processing effort, and it requires sensitive and sophisticated techniques to resolve similar components since contaminants might have similar physical and chemical properties to the target compound.

The biomass extract can be combined with the extract of the culture filtrate at this point, if required. To promote product purification, the extract is gradually subjected to varying separation procedures resulting in fractions, of which some may contain the enriched compound of interest. After each purification step, solvents need to be removed in order to narrow down the fraction volume for the subsequent separation step. Solvent removal is routinely achieved using rotary evaporators (for organic solvents) or by lyophilization (freeze-drying, when solvent is water).

The method chromatography is central at this stage. Furthermore, other methods such as crystallization can also be applied, provided that a certain concentration of the desired compound has already been reached [12, 13] (*see* **Note 2**).

1.2.1 Principles of Chromatography

Chromatography is a technique for the separation of a mixture of solutes by means of interaction with two phases. The so-called mobile phase carries the solutes along an immobile material, the stationary phase. The system in which the two phases are localized is termed chromatographic bed. It is either flat (as in thin layer chromatography, TLC) or a column. Moreover, liquid chromatography (LC) and gas chromatography (GC) are distinguished according to the physical state of the mobile phase, though GC can only be applied for volatile compounds and those that evaporate at higher temperatures without decomposition.

Mobile and stationary phases are in close contact and separation of the compound mixture occurs because the different solutes tend to have different affinities for the stationary phase and thus some remain longer in or at the stationary phase than others—that is, they have different retention times (*see* Fig. 4). Eventually, the separated solutes elute at different time points (in column chromatography) or appear as different spots (in TLC). Whenever the separated compounds are intended for later use, the process is called preparative [14].

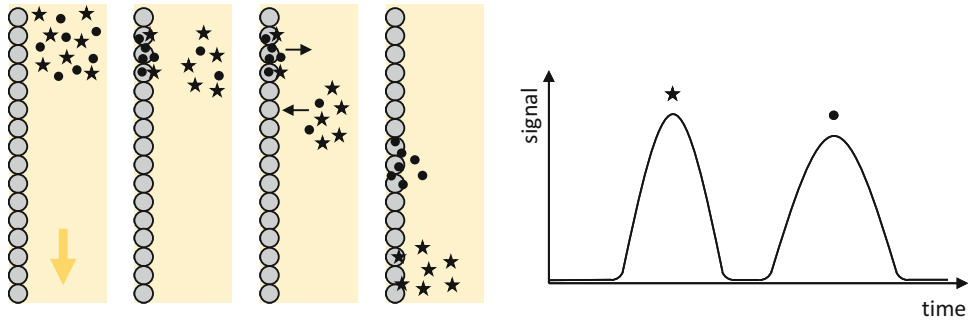

Fig. 4 Chromatographic separation of two compounds. A mixture of A (asterisk) and B (black circle) is applied to the chromatographic system. B interacts stronger with the stationary phase (gray circles) than A, while the mobile-phase solvent (yellow background) flows through the stationary phase. The constant alternation of interactions with both phases leads to a gradual separation of the compounds, and finally, A elutes earlier than B, which is visualized on a chromatogram (right)

A general preparative column chromatography procedure comprises (i) sample loading on top of the column, (ii) sample separation by applying the mobile phase flow, (iii) elution and fraction collection, and (iv) analyzing the fractions in order to detect the desired compound—which in chromatography is named analyte. The usage of an online ultraviolet-visible (UV-vis) spectroscopic detector is common for LC systems. Alternatively, if no online measurement is available, the individual fractions need to be analyzed either using appropriate detection systems (e.g., LC coupled to spectroscopic detectors or mass spectrometers, TLC, etc.), or they are assayed for their biological activity.

In most common chromatographic applications, the stationary phase consists of spherical, highly porous particles with a large surface area (similar to adsorption resins). The particle matrix provides a support for the surface material, on which solute interaction takes place. The smaller the particles are, the larger is the surface area and thus more interactions are possible leading to increased separation of structurally similar compounds—that is, a higher resolution of the analytes is achieved (*see* **Note 3**). On the other side, however, small particles cause increased back pressure on the mobile phase, and hence, pressure is required to guarantee a constant flow rate. Accordingly, a distinction is made between "gravity flow" chromatography (no pressure), flash chromatography (air pressure), solid-phase extraction (vacuum), low-pressure LC (LPLC, 40–200 μm particle size), medium-pressure LC (MPLC, 25–40 μm), and high-pressure LC (HPLC, 3–12 μm).

While different chromatographic techniques function by the same general principle, the physicochemical interactions between the solute and the stationary phase—which finally causes separation—strongly depend on the nature of the particle's surface. Basically, one (or sometimes several at once) of the following processes between solutes and stationary phase occurs: polar interaction, nonpolar interaction, ion exchange, affinity, solvation, or steric hindrance/filtering (*see* Fig. 5). A large variety of chromatographic techniques have been developed on these principles, and some of the frequently used ones in natural product recovery are briefly presented in the next paragraphs.

1.2.2 Chromatographic Techniques in Natural Product Recovery

(a) *Normal-Phase Chromatography*

In normal-phase chromatography (also known as adsorption chromatography), the stationary phase consists of a polar material. The probably most common is silica gel made of amorphic silicon dioxide with end-standing polar silanol groups (other material includes diol-modified silica, aluminum oxide, etc.). Silica gel forms highly porous particles with a large surface area.

Solutes of the mobile phase adsorb at the silanol groups by polar and electrostatic interactions (*see* Fig. 5, polar). When a

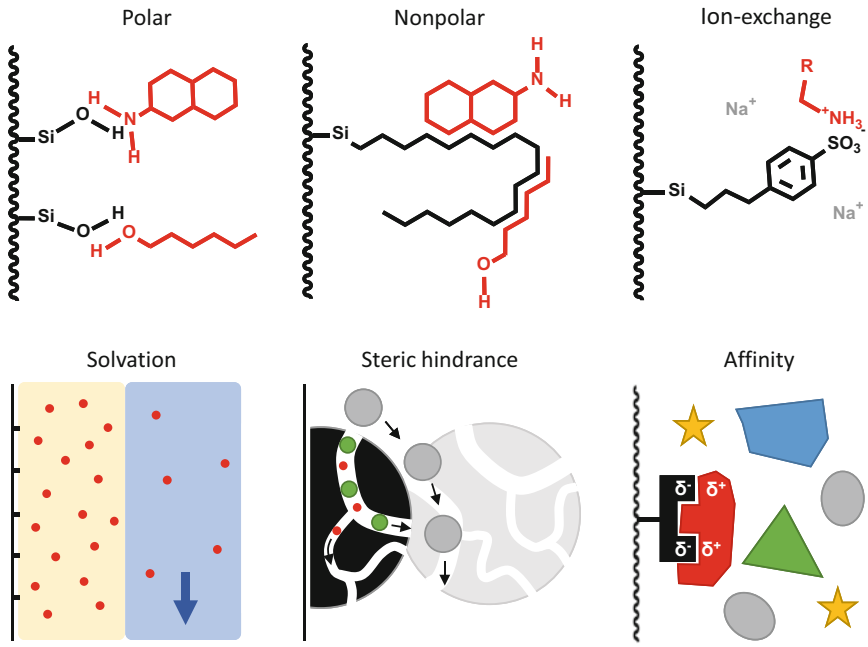

Fig. 5 Principles of interaction in chromatography. The desired compounds are illustrated in red

compound contains several functional groups, retention is determined by the most polar one. Consequently, hydrophilic compounds are strongly retained by the stationary phase and hydrophobic compounds elute first.

Typically, the elution strength of the mobile phase is increased during the chromatographic run: starting with a weak, nonpolar solvent such as hexene or dichloromethane, a miscible solvent that is more polar (such as methanol or ethyl acetate) is increasingly added. Alternatively, isocratic separation systems are applied in which the mobile-phase composition remains constant throughout the procedure.

(b) *Reversed-Phase Chromatography*

In reversed-phase chromatography, the polarity conditions of the whole system are reversed to normal-phase chromatography. The nonpolar stationary phase is composed of modified silica gel, which means that silicon dioxide still displays the support matrix but the end-standing silanol groups are covalently linked to nonpolar groups, most commonly to carbon hydrates (e.g., C8, C18). Besides, ligands with intermediate polarity exist (e.g., the so-called phenyl, diol, or cyano phases).

Solutes present in the mobile phase that obtain nonpolar structural parts are retained due to hydrophobic interactions with the carbon hydrate ligands (*see* Fig. 5, nonpolar). The underlying mechanism of retention involves both, adsorption and partition

[15]. As the bonded ligands are somewhat flexible, the stationary phase can be regarded as an immobilized solvent able to dissolve hydrophobic molecules (or parts thereof) that essentially are rejected by the polar solvent (partition principle). In addition, the hydrophobic analytes might adhere to the hydrophobic ligand tips at the interface of both phases (adsorption principle).

During a usual reversed-phase chromatographic run, the elution strength of the mobile phase is enhanced, similar to normal-phase chromatography; however, polarities are opposite: typically, a weak, polar solvent (usually water) is gradually mixed with increasing amounts of a strong, less polar (miscible) solvent such as methanol or acetonitrile (*see* **Note 4**). As opposite to normal-phase chromatography, hydrophilic compounds elute first.

(c) *Size-Exclusion Chromatography*

Size-exclusion chromatography fundamentally differs from the aforementioned chromatographic techniques, since the surface is (supposed to be) inert. As a consequence, only steric interactions take place and, counterintuitively, those compounds that are retained by steric hindrance elute earlier. This is because only smaller solutes can enter the stationary-phase particles. The particles are filled with solvent and provide room for diffusion, which is why smaller molecules need more time to travel through the column (*see* Fig. 5, steric hindrance). In reality, however, also adsorptive effects play a role to some extent, especially in the separation of low-molecular-weight compound mixtures such as microbial natural product extracts.

Frequently used stationary phases include Sephadex LH-20 (modified dextran), Bio-Gel P2 (polyacrylamide), and Toyopearl HW-40 (polymer of ethylene glycol and methacrylate). The choice of the mobile phase arises from the analyte's solubility and the stability of the stationary phase (predominantly water and methanol are used).

(d) *Others*

Other chromatographic techniques applied in microbial natural product recovery are countercurrent chromatography, affinity chromatography, and ion-exchange chromatography to name a few.

Countercurrent chromatography uses a liquid stationary phase and operates exclusively by partition principles. It is inherently the mildest form of chromatography. Even very similar compounds can have surprisingly different partition coefficients and can be separated [16].

Affinity chromatography is based on strong and specific binding between two components of which at least one usually is a larger biomolecule, such as the pairs protein/antibody, enzyme/substrate, or enzyme/inhibitor.

Ion-exchange chromatography relies on bonded polyelectrolytes that exchange their counter ions against those dissolved in the (normally aqueous) mobile phase. The ion-exchange process is influenced by the type of counter ion, the ion strength, and the pH. Many different stationary phases are available.

1.3 Product Polishing

The final processes in the preparation of a pure product refer to as product polishing. This includes operations to remove contaminants and impurities, which at this stage usually only occur in minor amounts. However, those final impurities often are derivatives of the target compound with similar physicochemical properties, and therefore, sophisticated separation techniques with great resolution are essential. The method of choice is preparative HPLC. Alternatively, crystallization might also be an option to conveniently increase the product purity (*see* **Note 2**). It should be noted here that an absolute purification is never possible, each purification step simply causes an enrichment of the target compound, and no substance has been found to be 100% pure [17].

Product polishing also includes removal of the solvent (which at this stage often is water) by desiccation, spray-drying, or lyophilization. Finally, the purified compound should be in a form suitable for storage, transport, or its intended subsequent use.

1.4 Practical Concerns in Natural Product Recovery

Due to the versatile chemistry of natural products, no universal recovery procedure can be described, and depending on the target molecule, an individual downstream process has to be developed each time. When the structure of the target molecule is not known, the recovery process usually is characterized by a stepwise approach of testing different separation strategies at which more and more insights into structural properties of the target molecule are gained. Evidently, the entire recovery process becomes faster and simpler when the compound concentration in the starting material is as high as possible (*see* **Note 5**). In order to successfully remove the unwanted molecules while simultaneously enriching the desired compound, it is essential to vary between as many different separation methods as possible. Therefore, a reasonable advice during the course of downstream processing is to alter the chromatographic principles, the nature of the stationary phases, the mobile phases, or at least the gradient of the mobile-phase solvents. Only this ensures separation of compounds with similar chemical and physical properties. Even if a method turns out to be nonselective for the target compound, it still might be very helpful since dominant impurities could easily be removed—that is, for example, the impurities retain during chromatography or dissolve in the chosen extractant instead of the target molecules.

Obviously, it is necessary to keep the stability of the target molecule in view during downstream processing, and harsh pH, heat, and reactions with the solvent should be avoided. Finally, the

chosen recovery process also depends on the laboratory equipment and the available budget. There is usually more than one strategy that yields a pure compound.

2 Materials

1. Plastic tubes (only for method described in Sect. 3.1): 2 mL, 15 mL, and 50 mL. Standard glassware (*see* **Note 6**): flasks (baffled, 100 mL and 1 L), beakers (of various sizes, 100 mL–1 L), separation funnels (e.g., 200 mL, 1 L), tubes for fraction collector (e.g., 30 mL), bottles (100 mL, 0.5 L, 1 L, 2 L, and 5 L), columns of different sizes (if possible, with frit and stopcock, *see* Fig. 6a), Pasteur pipettes.
2. Solvents: methanol, acetone, 1-butanol, ethyl acetate, dichloromethane, dimethyl sulfoxide (DMSO), dimethylformamide, acetonitrile (*see* **Note 7**).
3. Devices: incubator shaker, benchtop centrifuge (for 2 mL, 15 mL, and 50 mL tubes), ultrasonic bath, vacuum pump, preparative HPLC system (*see* Fig. 6b), equipment for concentration of extracts such as rotary evaporator, centrifugal vacuum concentrator, and lyophilizer.
4. Stationary phases: adsorbent resin AmberLite XAD-16 (optionally Sepabeads SP-207, Diaion HP20), normal-phase silica gel 60, size-exclusion phase Sephadex LH-20, suitable prepacked preparative (reversed-phase) HPLC columns.

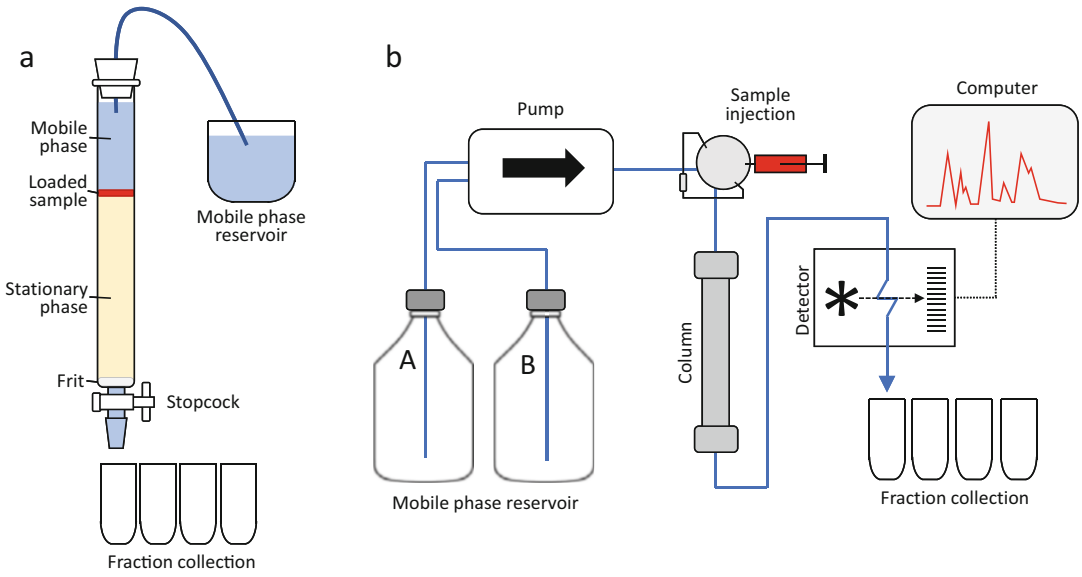

Fig. 6 Schematic setup of chromatographic systems in natural product recovery. (**a**) Column chromatography, (**b**) preparative HPLC system

5. Other material: cheesecloth, diverse tubing (preferably made of Teflon), potato dextrose broth (PDB).
6. Suitable screening assay to test the biological activity of extracts and fractions (e. g., inhibition zone test [18]).

3 Methods

In this section we describe (i) pretests that help to develop a recovery strategy of an unknown biological active compound from a microbial culture and (ii) a protocol for the recovery of fusarubin from the fungus *Fusarium* sp.

3.1 Development of a Recovery Strategy

If the structure of the active compound in a microbial culture is unknown, we carry out the following standard protocols to obtain first ideas about the nature of the molecule. For this purpose, only a small fraction of the culture broth is needed. Of course, this pretest protocol does not yield pure compound, but it should help to isolate and concentrate the desired compound from a larger production scale to a purity suitable to apply high-resolution separation techniques such as preparative HPLC. Note that highly polar compounds might not be captured with this approach [11].

3.1.1 Locate the Active Compound

1. Pellet 10 mL of the culture, decant, and collect the supernatant.
2. Add 10 mL of methanol/acetone (1 + 1) on the pellet, vortex vigorously, centrifuge, and collect organic phase (pellet extract) in a fresh tube.
3. Perform activity test with unaffected supernatant and with the pellet extract in order to assign the activity.

3.1.2 Capture Active Compound from Biomass

1. Centrifuge 100 mL of the culture, and use the pellet.
2. Add 10 mL methanol/acetone (1 + 1), vortex vigorously, and centrifuge. Take off the organic phase, evaporate to the aqueous remnant, and fill up to 10 mL with water.
3. Transfer three times 3 mL of the aqueous solution to fresh tubes and adjust the pH to 4, 7, and 10.
4. Perform liquid-liquid extraction: for each pH adjusted extract, transfer 1 mL in a fresh tube, and add 1 mL of 1-butanol, ethyl acetate, or dichloromethane, respectively. Vortex vigorously, centrifuge, carefully take off the organic phase with a glass Pasteur pipette (note that dichloromethane has higher density than water), and evaporate to dryness. Resuspend in 500 μL methanol (if applicable, DMSO can be used instead).
5. Perform activity test with the biomass extracts.

3.1.3 Capture Active Compound from Culture Supernatant

Centrifuge 100 mL of the culture, and use the supernatant for liquid-liquid extraction and for the adsorption test on resins.

(a) Liquid-Liquid Extraction

1. Transfer three times 3 mL of the supernatant to fresh tubes and adjust the pH to 4, 7, and 10.
2. For each pH adjusted supernatant, transfer 1 mL in a fresh tube, and add 1 mL of 1-butanol, ethyl acetate, or dichloromethane, respectively. Vortex vigorously, centrifuge, carefully take off the organic phase, and evaporate to dryness. Resuspend in 50 µL methanol or DMSO.
3. Perform activity test with the extracts.

(b) Adsorption Test on Resins

1. Prepare a small glass column (volume ca. 15 mL) for each polystyrene adsorbent resin to be tested (*see* **Note 8**).
2. Fill in approx. 5 mL of one of the adsorbent resins, and add sufficient water to generously wet the resins. If necessary, stir with a glass rod or similar to remove air. Add more water and adjust the flow rate to approx. 10 bed volumes per hour (*see* **Note 9**).
3. Add 20 mL of the culture supernatant. Whenever the applied liquid changes, wait until the previous liquid has flowed completely into the resin.
4. Consecutively wash/elute with 20 mL of 0%, 20%, 40%, 60%, 80%, and 100% methanol in water, and collect elution fractions separately in a tube or beaker (*see* **Notes 10** and **11**).
5. Take 2 mL of each fraction, evaporate to dryness, resuspend in 100 µL MeOH, and perform activity test (*see* **Note 12**).

3.1.4 Normal-Phase Chromatography in Pretest

1. Depending on the location of the active compound (*see* **steps 3.1.1**), use either 50 mL of culture supernatant or 50 mL of the aqueous remnant obtained from a 50 mL methanol/acetone pellet extract that in turn has been prepared from 50 mL culture broth.
2. Depending on the best liquid-liquid extraction result in the pretest, adjust the pH accordingly, and extract with 50 mL of the appropriate organic solvent using a separating funnel.
3. Take off the organic phase, evaporate to dryness, and resolve in 10 mL (or more) dichloromethane (*see* **Note 13**).
4. Prepare the silica column: pour 25 mL of silica gel 60 (*see* **Note 14**) in a beaker, add sufficient dichloromethane, stir the slurry by swirling, and pour the slurry in a 50 mL glass column (smaller columns increase the risk of air bubbles and are not

recommended). Adjust the dichloromethane solvent flow rate to approx. 2 bed volumes per hour. Whenever the applied liquid changes, wait until the previous liquid has flowed completely into the gel.

5. Load the sample directly on the gel (*see* **Note 15**), consecutively wash/elute with 2 bed volumes of 0%, 2%, 5%, 10%, and 20% methanol in dichloromethane (*see* **Note 10**). Collect each fraction separately in an appropriate container (*see* **Note 16**).
6. Take 2 mL of each fraction, evaporate to dryness, resuspend in 100 μL methanol, and perform activity test (*see* **Note 12**).

3.2 Recovery of Fusarubin as an Example

This section provides a protocol for the recovery of fusarubin and structural derivatives from the cultivation broth of the fungus *Fusarium* sp. The fungus has been isolated as an endophyte from the plant *Aster tataricus* [19].

3.2.1 Fungus Cultivation and Compound Capture

1. Cultivate the pre-culture: add 50 mL PDB and some fungal cell material from a cryo- or permanent culture (*see* **Note 17**) to a 100 mL baffled Erlenmeyer flask. Incubate for 3 days at 25 °C while shaking (180 rpm).
2. Cultivate the main culture: add 1.6 L PDB and 5 mL of the pre-culture (*see* **Note 17**), mix and split on four baffled Erlenmeyer flasks (size 1 L), and incubate for 10 days at 25 °C and 180 rpm.
3. Separate biomass from the aqueous culture using a funnel covered with cheesecloth (or a similar filtering material). Wring out the cheesecloth and discard the retained biomass.
4. Adjust the pH of the filtrate to approx. 4 using concentrated hydrochloric acid. Consecutively extract five times with 1 L 1-butanol using a separation funnel, and collect and combine the butanol phases. Evaporate to dryness. Yield of the crude extract: 1.6 g.

3.2.2 Fungal Extract Purification on Silica Column

1. Prepare the sample (for dry loading): dissolve the crude extract in generous amounts of methanol in a round-bottom flask, add 10 mL (or more) silica gel, and evaporate to dryness (*see* **Note 13**).
2. Prepare the silica column: pour 150 mL of dry silica gel 60 (*see* **Note 14**) in a beaker, add sufficient dichloromethane, stir the slurry by swirling, and pour the slurry in a 200 mL glass column (dimensions for instance: 40 cm length x 2.5 cm inner diameter [i.d.]) (*see* **Note 18**). Adjust the dichloromethane solvent flow rate to approx. 2 bed volumes per hour (*see* **Note 10**). Whenever the applied liquid changes, wait until the previous liquid has flowed completely into the gel.

3. Load the sample (*see* **Note 15**): fill the dry silica gel loaded with extract on top of the column bed, wet the loaded sample with dichloromethane, and restart the flow.
4. Consecutively wash/elute with 2.5 bed volumes of 0%, 2%, 5%, 5%, 5%, and 10% methanol in dichloromethane (*see* **Note 19**). Collect each of the six fractions separately in an appropriate glass container (*see* **Note 16**).
5. Combine the fusarubin-containing (bioactive) fractions 2–5 and evaporate to dryness. This yields up to 370 mg.

3.2.3 Purification Fusarium-Containing Fractions on Size-Exclusion Column

1. Prepare a Sephadex LH-20 column: pour 200 mL of dry Sephadex LH-20 in a Büchner flask, add the solvent methanol/dichloromethane (1 + 1) until the material becomes a slurry gel, and swell the gel for at least 3 h at room temperature. Briefly degas by applying vacuum and then pour the slurry into a glass column with appropriate dimensions (e.g., length 90 cm × 2.5 cm i.d.; *see* **Note 20**), and open the column outlet. Remove any air bubbles with a glass rod. Attach a reservoir filled with solvent (*see* **Note 10**). Adjust the flow rate to approx. 30 mL/h (*see* **Note 21**). Equilibrate the column with at least 2 bed volumes of solvent.
2. Sample preparation: dissolve the sample obtained from the last purification step in as little solvent as possible (solvent: methanol/dichloromethane (1 + 1)) (*see* **Note 22**).
3. Sample loading: disconnect the column from the reservoir, let the solvent sink in (*see* **Note 23**), and carefully load the sample onto the surface of the gel (optimally 1 mL, max. 2.5 mL per run, use a glass Pasteur pipette). Make sure not to whirl up the gel. The column must never get dry. Immediately after sample loading, carefully fill up with solvent and then reconnect the tube to the reservoir.
4. Constantly collect fractions (e.g., every 15 minutes) (*see* **Note 24**), and screen the fractions, for example, by analytical HPLC-UV/vis or by activity testing for the presence of fusarubin (*see* **Note 25**).
5. Combine all relevant fractions and evaporate to dryness. This yields up to 280 mg.

3.2.4 Polishing Fusarubin on Preparative Reversed-Phase HPLC

1. Prepare the preparative HPLC system: install a purchased, prepacked column (stationary phase: C18 [e.g., ReproSil-Pur Basic-C18, Dr. Maisch], dimensions: 250 mm length x 20 mm i.d., particle size 10 μm), attach the degassed mobile-phase solvents water and acetonitrile in separate bottles (*see* **Note 26**), launch the system according to manufacturer's specifications, and program an appropriate gradient (e.g., 40% to 100% acetonitrile in water in 20 min, *see* **Notes 4** and **27**).

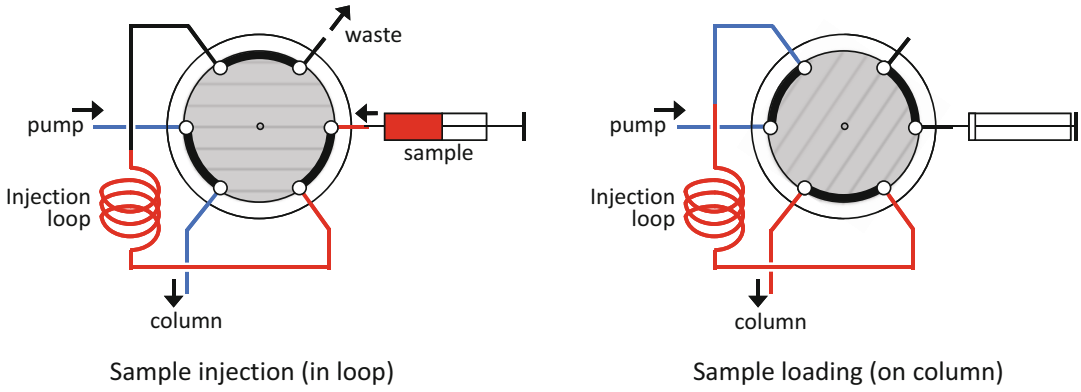

Fig. 7 Schematic diagram of the manual injection valve

2. Apply flow rate (24 ml/h) for 15 min to equilibrate the column under starting conditions (40% acetonitrile).
3. Sample preparation and loading: dissolve the sample obtained from the last purification step in as little dimethylformamide as possible (*see* **Note 22**). Load max. 4 mL on the column when using a 5 mL injection loop (*see* Fig. 7, *see* **Note 28**), apply flow rate, and start the programmed solvent gradient.
4. Manually collect six different compound fractions in round-bottom flasks (*see* **Note 29**) while observing the detector (230 nm, *see* **Note 30**).
5. Repeat steps 2–4 with remaining sample (e.g., we need 13 runs in total).
6. Combine the respective fractions and completely remove solvent (by evaporation and freeze-drying, *see* **Note 31**). This yields up to100 mg of compound 1 (cmp1 = fusarubin), 7 mg of cmp2, 24 mg of cmp3, 22 mg of cmp4, 5 mg of cmp5, and 17 mg of cmp6.
7. Prepare all six samples for the final chromatographic separation step: dissolve each compound in as little dimethylformamide as possible (*see* **Note 22**).
8. Change the HPLC column (use a column with same dimensions but different phases [e.g., ReproSil-Pur 120 ODS-3, Dr. Maisch]), equilibrate the column for 15 min, consecutively load the samples, apply flow, and start the individual solvent gradient (35–60% for cmp1, 45–70% for cmp2, 50–80% for cmp3, 55–85% for cmp4, 62–90% for cmp5, 65–100% for cmp6, acetonitrile in water for 15 min, respectively).
9. Manually collect six different compound fractions while observing the detector (230 nm) in round-bottom flasks, combine the respective fractions, and remove the solvent by evaporation and freeze-drying (*see* **Note 31**).

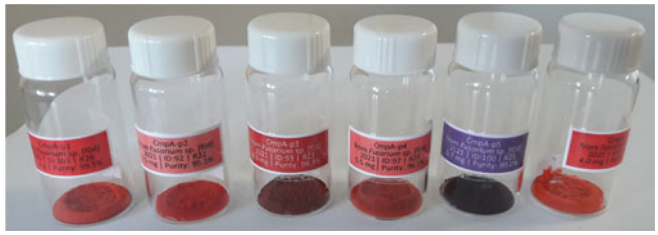

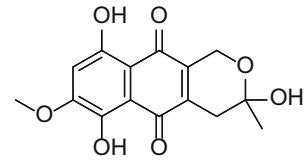

fusarubin

Fig. 8 Natural products recovered from *Fusarium* sp. About 5 mg of each—fusarubin and five additional compounds, likely structural derivatives—are stored in pure form (purity approx. 95–99%, according to analytical HPLC-UV/vis and HPLC-mass spectrometric measurements). The molecular structure of fusarubin is shown; the structure of the other compounds is still unknown

10. This yields pure compounds of approx. 82 mg of fusarubin (cmp1), 5 mg of cmp2, 20 mg of cmp3, 16 mg of cmp4, 16 mg of cmp5, and 4 mg of cmp6 (*see* Fig. 8).

4 Notes

1. Phase separation is accelerated by centrifugation or by adding salt (usually sodium sulfate) to the liquids.
2. Crystallization occurs when the solubility of the solutes is somehow reduced. This can be achieved by (i) cooling, (ii) addition of an anti-solvent, (iii) solvent removal, or (iv) upon chemical reaction (precipitation).
3. There are more factors that influence resolution of compounds besides the size of stationary-phase particles; in particular, these include particle size distribution and mobile-phase flow rate.
4. It might be crucial to add some acid or base to the mobile-phase solvents in order to hide charges of analytes by neutralizing their functional groups. This increases potential nonpolar interactions. In preparative HPLC, volatility of the additives (i.e., a low boiling point) is more important than UV compatibility with the sensor. Using trifluoroacetic acid—a common additive in analytical HPLC—in a preparative approach can problematically reduce the pH when the fraction is evaporated after the HPLC run and potentially destroys the compound. More suitable additives (since more volatile) are formic acid or ammonia, usually in concentrations of 0.1%.
5. A high concentration of the desired compound in the starting material (i.e., the cultivation broth) is essential and dramatically facilitates the whole downstream process. The usage of complex production media with many ingredients might lead to higher production titers than defined media; however, it must be considered that this simultaneously introduces a whole host of further potential contaminants.

6. Use consequently glassware (or steel columns) when working preparatively, as softening agents hard to get rid of might dissolve from plastic material when organic solvents are used.
7. Always consider safety and purity of solvents. Take precautions when solvents are toxic (to humans or to the nature) and/or flammable and explosive. In the first steps of compound recovery (e.g., during compound capture), purity is not so important, and the use of technical-grade solvent can save much money. Toward the later stages, however, purity is extremely crucial, since non-ultrapure solvents can be a considerable source of impurities, which remain and are even concentrated during solvent removal. This also applies to water.
8. Polystyrene resins are characterized by a large surface area (300–750 m^2/g), relatively large particles (100–1000 μm, no pressure needed), and a great chemical stability (pH ranges from 1 to 14 and numerous organic solvents are tolerated).
9. A flow rate of 10 bed volumes per hour for pretests and 5 bed volumes per hour in the actual application are common practices for adsorbent resins. The sample volume is no issue and can be very high. As a rule of thumb, the amount of resin is often 10% of the volume of the culture filtrate.
10. Solvents are added manually, or they are supplied in a reservoir, from which they are transported either with a peristaltic pump or by hydrostatic pressure. For the latter, the reservoir has to be positioned slightly elevated regarding the column outlet, and the connecting tube (use Teflon for dichloromethane instead of silicone) has to be attached airtight to column head (principle of communicating vessels).
11. Regenerate polystyrene resins by applying each 4 bed volumes of (i) a 9 + 1 mixture of methanol and 1 M hydrochloric acid followed by (ii) acetone and (iii) 1 M sodium hydroxide (use lab coat, protective gloves, and goggles!). Then wash the column extensively with water until neutrality (check with pH indicator paper).
12. There are several possible reasons if no activity is detected in the fractions [7]: (i) the active compound is still on the column, (ii) the compound is unstable under chosen conditions, (iii) the compound is spread on too many fractions causing undetectable concentrations, or (iv) the activity may have arisen of a synergy effect of two or more compounds, which now are separated from each other.
13. When the sample is insoluble in the nonpolar mobile phase—which frequently occurs—simply dissolve the sample in an appropriate (volatile) solvent such as methanol, transfer it into a round-bottom flask, add generous amounts of silica gel, and evaporate the mixture to dryness. The sample will

now stick to the dry silica particles and can directly be loaded on top of the column material. Once on the column, quickly add some mobile-phase solvent.

14. The number "60" indicates that the mean pore diameter of the silica particles is 60 Å, which is the most commonly used material. Typical distribution of the particle size is 70–230 μm. The particle surface area is large (200–800 m^2/g). As an alternative for silica gel, diol-modified silica gel can be used (e.g., LiChroprep Diol, standard gradient for elution: 0%, 1%, 2%, 3%, 4%, 5% methanol in dichloromethane).
15. Capacities of normal-phase material are high. Silica gel can be loaded with roughly up to 20 g of sample per L bed volume, LiChroprep Diol with approx. 4–10 g per L bed volume. The sample volume is not an issue.
16. Silica gel is cheap and thus usually is discarded after usage. Expensive materials such as LiChroprep Diol, however, can be regenerated—that is, removed from bound substances—using methanol (add 1% acetic acid in methanol, if necessary, then wash again with pure methanol). Then store dry.
17. Filamentous fungi tend to produce pellets in liquid culture, especially when the inoculum material is clumpy. To obtain a dispersed culture, homogenize the inoculum material with a sterile glass homogenizer.
18. Silica gel chromatography can be performed in columns that do not have a frit. However, precautions need to be taken to avoid leakage of the gel: add some solvent and close the tap, then push some glass wool on the outlet using a glass rod or similar, and add sea sand (~ 2 cm layer). Now, pour in the silica gel.
19. If the eluate is colored during stepwise gradient elution, always apply as much elution solvent of the current solvent mixture until the colored compound has eluted entirely. Otherwise use approx. 2.5 bed volumes.
20. In contrast to other column chromatographic techniques where a column length of ~30 cm is sufficient, size-exclusion chromatography requires much longer columns (1 m is optimal) to enable adequate separation of compounds of different sizes (the diffusion processes take time). Moreover, install the column exactly vertically.
21. In size-exclusion chromatography, only a small sample volume can be applied to the column bed since no concentration effects occur during the chromatographic run. Likewise, the flow rate has to be slow to allow good resolution of the different analytes. As a general rule for 2.5 cm columns (diameter), follow these guidelines: optimal flow rate 30 mL/h, optimal

sample volume 1 mL, and optimal sample amount 200 mg. Note that these values change in proportion to the square of the column diameter. A reasonable way to adjust the flow rate is to use adequately small capillary tubes at the column outlet.

22. Always centrifuge the sample before loading to avoid precipitates at the top of the stationary-phase material, which will gradually dissolve with the solvent stream and ruin the separation. Resolve any pellets in the sample tube with fresh solvent for a subsequent run.
23. The surface at the top of the stationary phase in size-exclusion chromatography has to be exactly plain before the sample is loaded to obtain an optimal resolution of the analytes. If this is not the case, simply whirl up some gel material and let it settle again while applying a constant solvent flow. For sample application, better use a short Pasteur pipette since long ones easily brake and fall onto the gel material.
24. Any compounds that stick to the Sephadex LH-20 or Toyopearl HW-40 gel material can be eluted with a 9 + 1 mixture of methanol and 1 M ammonium acetate (alternatively, 1% acetic acid in methanol can be used). Afterward, wash thoroughly.
25. If a large number of fractions has been collected, the compound screening process can be facilitated by analyzing only every third, fourth, or fifth position, since the active compound usually is spread over several fractions. Only when an active fraction has been identified, the neighboring intermediate fractions are analyzed in a further screening.
26. Degas all solvents before usage in preparative HPLC by means of a vacuum pump and an ultrasonic bath to avoid that dissolved air interferes with the detector (degassing water takes at least 30 min, for organic solvents ~1 min is sufficient). Helium sparging during the chromatographic run is not necessary.
27. Before running a preparative HPLC, the optimal separation conditions need to be established in a pilot run using a smaller column (same length, smaller diameter) with identical stationary phase. Use only few amounts of the sample. Reduce the flow rate accordingly: if the column diameter is reduced by half, then the flow rate must be reduced to one quarter to maintain the original linear flow [20].
28. Sample amounts of approx. 20–100 mg can be considered as a rough guide in terms of loading capacity for columns with ~20 mm i.d., but it finally depends on the separation properties and the purity of the content. With regard to the solvent, the sample is ideally dissolved in the mobile-phase solvent (starting condition). If this is not possible, dissolve the sample in a small volume of a completely miscible solvent, and mix with the mobile phase in the injection syringe [21].

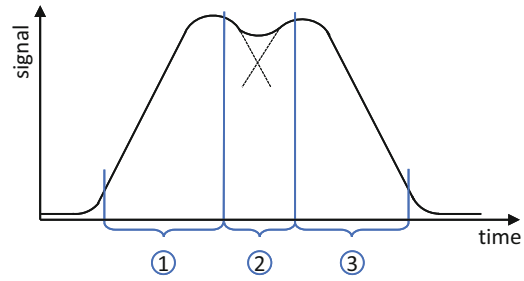

Fig. 9 Chromatogram with overlapping compound peaks. Fractionation is illustrated by numbers

29. When compounds are not completely separated (i.e., when the compound peaks are partly overlapping), collect an intermediate fraction containing the compound mixture (*see* Fig. 9), then evaporate, resolve, and reapply it in a new run.
30. According to experience, UV detection at 210 nm is too sensitive in preparative chromatography as compound density in the eluate is much higher than in analytical chromatography.
31. Ideally for lyophilization, the sample/compound is dissolved in pure water. Another solvent appropriate for lyophilization is 50% tert-butyl alcohol.

References

1. Atanasov AG, Zotchev SB, Dirsch VM, International Natural Product Sciences T, Supuran CT (2021) Natural products in drug discovery: advances and opportunities. Nat Rev Drug Discov 20(3):200–216
2. Cragg GM, Newman DJ (2013) Natural products: a continuing source of novel drug leads. Biochim Biophys Acta 1830(6):3670–3695
3. Li JW, Vederas JC (2009) Drug discovery and natural products: end of an era or an endless frontier? Science 325(5937):161–165
4. Miethke M, Pieroni M, Weber T, Brönstrup M, Hammann P, Halby L, Arimondo PB, Glaser P, Aigle B, Bode HB, Moreira R, Li Y, Luzhetskyy A, Medema MH, Pernodet JL, Stadler M, Tormo JR, Genilloud O, Truman AW, Weissman KJ, Takano E, Sabatini S, Stegmann E, Brötz-Oesterhelt H, Wohlleben W, Seemann M, Empting M, Hirsch AKH, Loretz B, Lehr CM, Titz A, Herrmann J, Jaeger T, Alt S, Hesterkamp T, Winterhalter M, Schiefer A, Pfarr K, Hoerauf A, Graz H, Graz M, Lindvall M, Ramurthy S, Karlén A, van Dongen M, Petkovic H, Keller A, Peyrane F, Donadio S, Fraisse L, Piddock LJV, Gilbert IH, Moser HE, Müller R (2021) Towards the sustainable discovery and development of new antibiotics. Nat Rev Chem 5:726–749
5. Wilson BAP, Thornburg CC, Henrich CJ, Grkovic T, O'Keefe BR (2020) Creating and screening natural product libraries. Nat Prod Rep 37(7):893–918
6. Cannell RJP (1998) How to approach the isolation of a natural product. In: Cannell RJP (ed) Natural products isolation. Humana Press, Totowa, NJ, pp 1–51
7. Sarker SD, Nahar L (2012) An introduction to natural products isolation. In: Sarker SD, Nahar L (eds) Natural products isolation. Humana Press, Totowa, NJ, pp 1–25
8. Helaly SE, Kulik A, Zinecker H, Ramachandaran K, Tan GY, Imhoff JF, Süssmuth RD, Fiedler HP, Sabaratnam V (2012) Langkolide, a 32-membered macrolactone antibiotic produced by *Streptomyces* sp. Acta 3062. J Nat Prod 75(6):1018–1024
9. Nachtigall J, Kulik A, Helaly S, Bull AT, Goodfellow M, Asenjo JA, Maier A, Wiese J, Imhoff JF, Süssmuth RD, Fiedler HP (2011) Atacamycins A-C, 22-membered antitumor macrolactones produced by *Streptomyces* sp. C38. J Antibiot (Tokyo) 64(12):775–780

10. Fiedler H-P (1977) Isolierung von mikrobiellen Stoffwechselprodukten mit Hilfe von Adsorberharzen. Chemische Rundschau 30:2–3
11. Berlinck RGS, Crnkovic CM, Gubiani JR, Bernardi DI, Ióca LP, Quintana-Bulla JI (2021) The isolation of water-soluble natural products – challenges, strategies and perspectives. Nat Prod Rep
12. Arslanian RL, Parker CD, Wang PK, McIntire JR, Lau J, Starks C, Licari PJ (2002) Large-scale isolation and crystallization of epothilone D from *Myxococcus xanthus* cultures. J Nat Prod 65(4):570–572
13. Horosanskaia E, Triemer S, Seidel-Morgenstern A, Lorenz H (2019) Purification of artemisinin from the product solution of a semisynthetic reaction within a single crystallization step. Org Process Res Dev 23(9): 2074–2079
14. Meyer V (2004) Präparative HPLC. In: Praxis der Hochleistungs-Flüssigchromatographie. Wiley GmbH & Co. KGaA, Weinheim, pp 285–296
15. Vailaya A, Horvath C (1998) Retention in reversed-phase chromatography: partition or adsorption? J Chromatogr A 829(1–2):1–27
16. Yoon KD, Chin YW, Kim J (2010) Centrifugal partition chromatography: application to natural products in 1994–2009. J Liq Chromatogr R T 33(9–12):1208–1254
17. Abdin AY, Yeboah P, Jacob C (2020) Chemical impurities: an epistemological riddle with serious side effects. Int J Environ Res Public Health 17(3)
18. CLSI (2019) Performance standards for antimicrobial susceptibility testing. CLSI guidline M100, 29th edn. Clinical and Laboratory Standards Institute, Wayne
19. Schafhauser T, Jahn L, Kirchner N, Kulik A, Flor L, Lang A, Caradec T, Fewer DP, Sivonen K, van Berkel WJH, Jacques P, Weber T, Gross H, van Pee KH, Wohlleben W, Ludwig-Müller J (2019) Antitumor astins originate from the fungal endophyte *Cyanodermella asteris* living within the medicinal plant *Aster tataricus*. Proc Natl Acad Sci U S A 116(52):26909–26917
20. Golay MJE (1958) Theory of chromatography in open and open tubular columns with round and rectangular cross sections. In: Desty DH (ed) Gas chromatography. Butterworths, London, pp 36–55
21. Kulik A, Fiedler H-P (1998) Some aspects of the purification of anthraquinone antibiotics by preparative reversed-phase liquid chromatography. J Chromatogr A 812:117–121

Chapter 6

Structure Elucidation of Antibiotics

Julia Moschny, Georgios Daletos, Peter Proksch, and Chambers C. Hughes

Abstract

To date, there are hundreds of characterized natural products with antibacterial activity against pathogenic bacteria, and several have become bonafide antibiotic drugs. The development of antibacterial natural products into antibiotic drugs, both in the past and in the future, hinges upon an accurate description of the exact chemical structure of the compound. Bolstered by some form of mass spectrometry (MS), nuclear magnetic resonance (NMR) spectroscopy is the primary technique for elucidating the chemical structure of organic molecules including natural products. By combining various one-dimensional (1D) and two-dimensional (2D) experiments, the connectivity between atoms is established and a complete "picture" of the molecule is thereby revealed.

Key words NMR, HPLC-MS, Structure elucidation, Antibiotics, Natural products, Tylosin A

1 Introduction

The vast majority of antibiotics are categorized as natural products, semisynthetic natural product derivatives, and natural product-inspired compounds [1]. Thus, most antibiotic structures were taken from nature either directly or indirectly; all come from microorganisms and most come from bacteria. Remarkably, the most prolific source of bacterial derived antibiotics is one specific group of filamentous, soil-dwelling bacteria known as the actinomycetes, which includes the renowned genus *Streptomyces*. Some antibiotics, such as ciprofloxacin and linezolid, are purely synthetic. Their structures bear little to no resemblance to those of naturally occurring compounds.

The discovery of penicillin in 1928 heralded the "Golden Age of Antibiotic Discovery," a period from about 1940 to 1960, when the majority of antibiotics used today were first discovered [2, 3]. Detailed analysis of bacterial cultures during that time led to the discovery of entirely new classes of antibiotics, such as

Peter Sass (ed.), *Antibiotics: Methods and Protocols*,
Methods in Molecular Biology, vol. 2601, https://doi.org/10.1007/978-1-0716-2855-3_6,

aminoglycosides (e.g., kanamycin), tetracyclines (e.g., doxycycline), amphenicols (e.g., chloramphenicol), cephalosporins (e.g., cephalexin), macrolides (e.g., erythromycin), glycopeptides (e.g., vancomycin), and ansamycins (e.g., rifamycin). After this period, the pace of discovering new antibiotic classes greatly diminished. Today, new antibiotics have reached and continue to reach the market, but their core structures are borrowed from the older classes of antibiotics. In other words, except for a few exceptions (e.g., the lipopeptide daptomycin, the lipiarmycin fidaxomicin, the pleuromutilin retapamulin), new antibiotic classes are not being developed. Instead, old antibiotics are continuously being "tweaked" to extend their efficacy in the face of widespread antibiotic resistance. Although this strategy has been successful—a triumph of modern medicinal chemistry—it is not likely to succeed indefinitely. For this reason, the discovery and development of new antibiotics, especially those belonging to entirely new antibiotic classes, is critical to avoid a return to the pre-antibiotic era.

The good news is that microorganisms still possess enormous potential to provide new antibiotics in the future. Bioinformatic analysis of bacterial and fungal genomes shows an enormous number of "orphan" biosynthetic gene clusters, the genetic blueprint of potential lifesaving antibiotics, for which no characterized compounds exist [4]. Accessing the natural products from these "silent" biosynthetic gene clusters is not necessarily an easy task, but new methods are continuously being developed to do just this.

The bad news is that natural products chemistry is expensive and time-consuming. Generally speaking, purifying antibacterial compounds from complex mixtures of bacterial metabolites is laborious. Obtaining sufficient quantities of these compounds for full biological characterization is often arduous. Defining the chemical structure of a potential antibiotic is also fraught with difficulty. On the one hand, natural products can be large, complex chemical entities with multiple carbon stereogenic centers that must be properly defined. On the other hand, thousands of antibacterial compounds have already been isolated, characterized, and tested. The ability to rapidly elucidate the molecular structure of an antibacterial "hit" and thereby distinguish a known chemical scaffold from a new drug lead is vitally important. Devoting limited resources to a compound from the past is highly undesirable, while focusing efforts on a new drug lead can have an immense impact on human health.

High-performance liquid chromatography-mass spectrometry (HPLC-MS) is a magnificent method for defining the components of a complex mixture like a bacterial extract. The basics of liquid chromatography are covered in the Chap. 5 on "Isolation and purification of natural products from microbial cultures" by Schafhauser and Kulik in this edition. Coupling an HPLC system to a mass spectrometer provides, in the case of high-resolution

instruments, a putative molecular formula for each chemical constituent without the need to actually isolate the compound. "Guiding" the isolation and discovery of antibacterial compounds using a combination of HPLC-MS and antibacterial bioassays can be extremely effective.

Once an antibacterial compound in a bacterial extract is deemed worthy of the time and effort required to purify and characterize it, a decision which usually has something to do with its perceived structural novelty or unique mechanism of action [5, 6], nuclear magnetic resonance (NMR) spectroscopy becomes indispensable [7]. The NMR section of this chapter is an update to a previously published chapter in the first edition of this book [8]. NMR spectroscopy is central to natural product structure elucidation because it is finely tuned to the detection of hydrogen (H) and carbon (C) atoms, which are the most common atoms in organic molecules including natural products. Depending on the size, position, and appearance of proton or carbon signals in an NMR spectrum, the immediate environment of the atoms can be discerned. ^{1}H NMR spectroscopy is highly sensitive because 100% of proton atoms exist as the NMR active ^{1}H isotope; ^{13}C NMR spectroscopy is inherently less sensitive since only 1.1% of carbon atoms exist as the NMR active ^{13}C isotope. Two-dimensional (2D) NMR experiments, the most useful of which relate protons to other protons or protons to carbons, provide a map that can directly reveal chemical structure when deciphered by a seasoned spectroscopist.

2 Materials

2.1 Extract Analysis and Structure Dereplication by HPLC-(HR)MS

1. HPLC-(HR)MS system with a binary or quaternary pump, autosampler, and (high-resolution) mass spectrometer.
2. Analytical RP-C18 HPLC column.
3. Acetonitrile (MS grade).
4. Water (MS grade).
5. Formic acid (MS grade).
6. Glass vial with dried extract.
7. Methanol (HPLC grade or better) (*see* **Note 1**).
8. High-speed benchtop centrifuge (*see* **Note 2**).
9. Glass Pasteur pipettes, rubber bulb, centrifuge tubes, glass vials for HPLC with septum caps (*see* **Note 3**).
10. Access to a natural product database, e.g., COCONUT, The Natural Products Atlas, Dictionary of Natural Products (*see* **Note 4**).

2.2 Structure Elucidation by NMR

1. Glass vial with purified compound (*see* **Note 5**).
2. Deuterated solvents, such as DMSO-d_6, $CDCl_3$, acetonitrile-d_3, methanol-d_4 (*see* **Notes 6** and **7**).
3. NMR tubes (*see* **Notes 8** and **9**).
4. Glass Pasteur pipettes, rubber bulb, glass wool, and Teflon tape (*see* **Note 10**).

3 Methods

3.1 Extract Analysis and Structure Dereplication by HPLC-(HR)MS

1. Dissolve the extract in methanol at a concentration of 1 mg/mL (*see* **Notes 1** and **11**).
2. If insoluble material is observed, transfer the solution into a centrifuge tube and spin down the insoluble material at maximum speed (min. 13,000 g) for 5 min at room temperature (*see* **Note 2**).
3. Transfer the supernatant into a glass vial for HPLC and close it with a septum cap (*see* **Note 3**).
4. Select an HPLC screening method for reversed-phase chromatography with gradient elution from a low to high proportion of acetonitrile. Adjust all parameters to your column dimensions and instrumental setup (*see* **Note 12**).
5. Select two MS signal traces for monitoring and set one to full mass scan in positive mode and one to full mass scan in negative mode (*see* **Note 13**).
6. Analyze the extract on the HPLC-(HR)MS by injecting 1–5 μL of the sample solution (*see* **Note 11**).
7. Extract the mass spectrum of your peak of interest from the MS chromatograms and determine the exact mass of the compound (*see* **Notes 13** and **14**). The MS chromatogram obtained via HPLC-MS analysis of a microbial extract is shown in Fig. 1. The MS spectrum of the natural product with a retention time (t_R) = 6 min is depicted. The HRMS spectrum of the same natural product, obtained via HPLC-HRMS analysis, is shown in Fig. 2.
8. Enter the exact mass (or calculated molecular formula) of your compound of interest into the query of your NP database and examine putative matches (*see* **Notes 15**–**17**).

3.2 Sample Preparation for NMR Analysis

1. Dry the purified compound (*see* **Note 5**).
2. Use a glass Pasteur pipette for adding a suitable deuterated solvent to the sample (*see* **Note 18**).
3. If necessary, filter your sample using glass wool (*see* **Note 19**).
4. Pipette the sample into an NMR tube (*see* **Notes 20** and **21**).

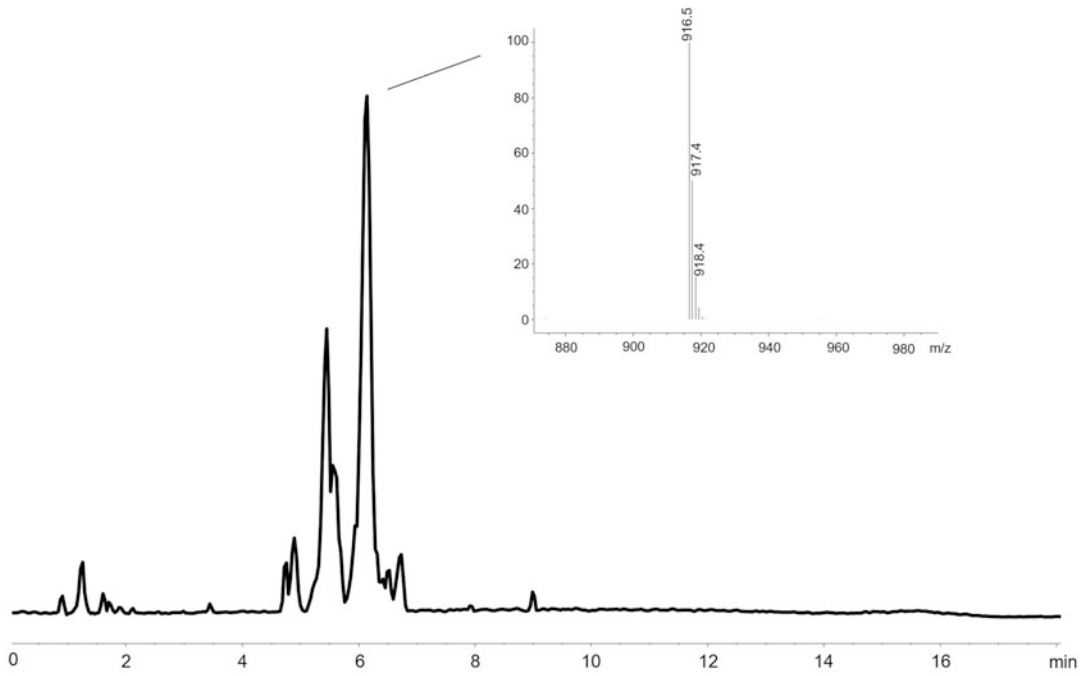

Fig. 1 MS chromatogram (BPC) of a microbial extract obtained using an HPLC-MS in positive mode. The MS spectrum of a natural product with a pseudomolecular ion *m/z* $[M+H]^+ = 916.5$ is depicted. The exact mass, therefore, is 915.5. In practice, structure dereplication using low-resolution exact mass data is difficult because many matching molecular formulae exist and so too many compounds will "fit" the data

5. Wrap a piece of Teflon tape around the cap of the NMR tube (*see* **Note 22**).
6. Label your sample at the top of NMR tube.

3.3 Useful Information from NMR Measurements

At this point, it is important to emphasize the most useful information that can be extracted from NMR spectra, including the chemical shift, coupling constant, and integration.

3.3.1 Chemical Shift

1. The chemical shift (δ) is a measure of the resonant frequency of an NMR-active nucleus (e.g., ^{1}H, ^{13}C, or ^{15}N) and is reported in parts per million (ppm) (*see* **Note 23**).
2. The chemical shift denotes the positions of the NMR peaks relative to a reference compound (usually residual solvent or TMS) (*see* **Note 6**).
3. By convention the shielded signals of TMS are set to 0 ppm, situated on the right side of the chemical shift scale in the NMR spectrum. The resonances of common functional groups are less shielded, that is, they have higher shifts, and appear left of the TMS signal.

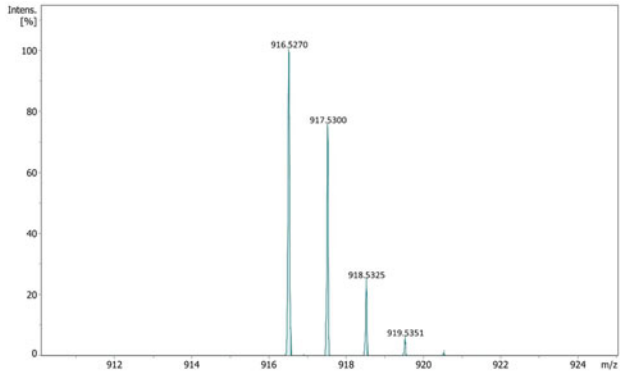

Meas. m/z	#	Ion Formula	m/z	err [ppm]
916.5270	1	$C_{60}H_{66}N_7O_2$	916.5273	0.3
916.5270	2	$C_{59}H_{70}N_3O_6$	916.5259	-1.2
916.5270	3	$C_{45}H_{62}N_{19}O_3$	916.5278	0.8
916.5270	4	$C_{46}H_{78}NO_{17}$	916.5264	-0.6
916.5270	5	$C_{47}H_{74}N_5O_{13}$	916.5278	0.8
916.5270	6	$C_{44}H_{66}N_{15}O_7$	916.5264	-0.6

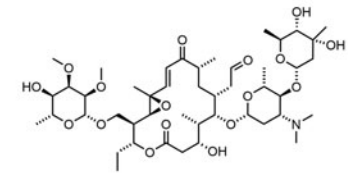
angolamycin

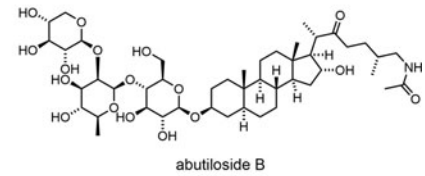
abutiloside B

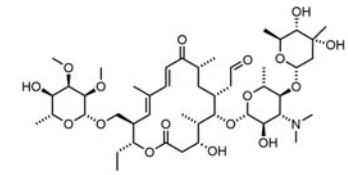
tylosin A

Fig. 2 HRMS spectrum of a natural product with a pseudomolecular ion *m/z* $[M+H]^+ = 916.5270$, which matches $C_{46}H_{78}NO_{17}^+$ (calculated mass = 916.5264) with an error of only 0.6 ppm. The molecular formula of the natural product, therefore, is $C_{46}H_{77}NO_{17}$. The COCONUT database shows three hits for this molecular formula: angolamycin, abutiloside B, and tylosin A. The possibility that the compound has a previously undescribed structure with the molecular formula $C_{46}H_{77}NO_{17}$, i.e., that the compound is "new," cannot be ruled out. Notice that, in a strictly mathematical sense, other molecular formulae match the measured *m/z* within an acceptable error range. In a chemical sense, however, compounds with certain molecular formulae (e.g., $C_{45}H_{61}N_{19}O_3$) are not likely to exist. In practice, once a compound is purified, ^1H and ^{13}C NMR data are taken into consideration when proposing molecular formula from mass data, and this practice further reduces the number of matching molecular formulae (*see* Subheadings 3.3.3 and 3.4)

3.3.2 Coupling Constant

1. Coupling constant is the absolute separation between two and more peaks (splitting) of each NMR signal, arising from coupling between nuclei, such as proton-proton or proton-carbon coupling.
2. This intramolecular communication, caused by through-bond interactions of nuclei, is the phenomenon known as spin-spin, scalar, or *J*-coupling (*see* **Note 24**).
3. *J*-couplings are measured in cycles per second (Hz), and their magnitude depends on the distance between nuclei, their relative configuration, and their chemical environment.
4. The observation of *J*-couplings is important, as useful structural information can be derived, including bond linkage (*see* **Note 25**) and molecular conformation (*see* **Note 26**).

3.3.3 Integration

1. In the ^1H NMR spectrum, integral values of peak areas underneath the NMR signals are proportional to the number of

equivalent hydrogen atoms producing the signal in the molecule (*see* **Note 27**).

2. In sample mixtures, the quantitative relationship between the individual components can be determined by the different ratio of the integrals in the spectrum.

3.4 1D NMR Methods

The 1D NMR spectrum is a plot showing amplitude along a frequency axis, which is typically the chemical shift axis. To obtain this spectrum, the nuclei are irradiated and generate signals that are detected in the time domain and then converted mathematically into the frequency domain by employing a mathematical procedure known as Fourier transformation.

3.4.1 ^{1}H NMR

1. By measuring a ^{1}H NMR spectrum, we observe frequency ranges of ^{1}H resonances with common chemical shifts from 0 to 12 ppm. Thus, a typical spectral window for ^{1}H NMR is at least 12 ppm wide. The ^{1}H NMR spectrum of tylosin A at 700 MHz in acetonitrile-d_3 is shown in Fig. 3 (*see* **Note 28**).
2. Reference signal(s) in the ^{1}H NMR spectrum to the residual solvent peak.
3. Integrate the ^{1}H NMR spectrum to obtain a total hydrogen count (*see* **Note 29**).
4. List all ^{1}H NMR chemical shifts to two decimal places (*see* **Note 30**).
5. List the multiplicities and coupling constants (J in Hz) for all ^{1}H NMR signals (*see* **Note 31**).
6. Inspect the spectrum and identify obvious functional groups, such as aldehydes (~9.0–10.0 ppm), aromatics (~7.0–8.0 ppm), alkenes (~5.0–7.0 ppm), methoxy (~3.5–4.0 ppm), and methyl (~1.0–2.0 ppm) groups, from their characteristic shifts, multiplicities, and integrations (*see* **Note 32**).

3.4.2 ^{13}C NMR

1. The ^{13}C NMR spectrum shows the chemical shifts of carbon resonances and thus the total carbon number of a molecule. The frequency range for common ^{13}C shifts is from 0 to 220 ppm. Due to the low isotopic abundance (1.1%) of ^{13}C, as well as its inherent low sensitivity (~1/64 to that of ^{1}H), the signals are weaker than those of ^{1}H, and thus more time for spectra recording is required (*see* **Notes 33** and **34**). The ^{13}C NMR spectrum of tylosin A at 175 MHz in acetonitrile-d_3 is shown in Fig. 4.
2. Reference the ^{13}C NMR spectrum to the deuterated solvent peak.

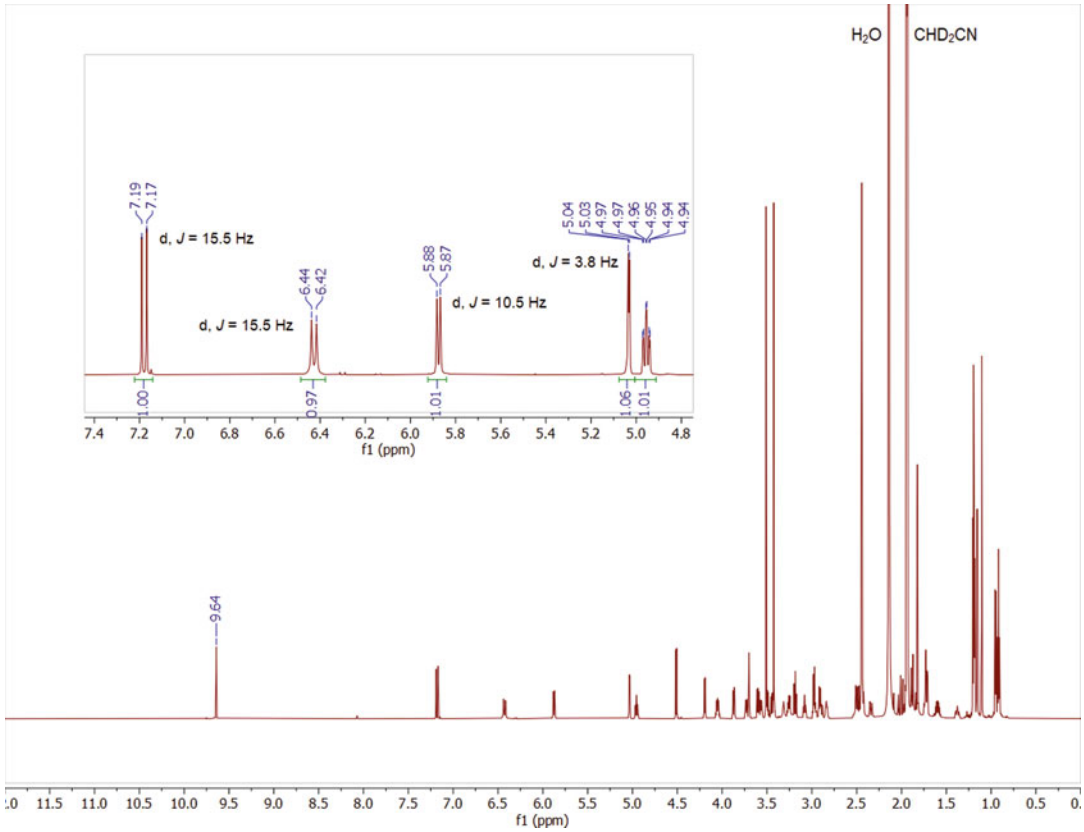

Fig. 3 ^{1}H NMR spectrum (700 MHz) of tylosin A in acetonitrile-d_3 (CD_3CN). The spectrum was referenced to residual solvent (CHD_2CN), which gives a reliable signal at 1.94 ppm. Water (H_2O) is responsible for the other large signal at 2.13 ppm. Given that there are 77 individual protons in the structure of tylosin A, the ^{1}H NMR spectrum is rather complex. The insert shows the less crowded region between 7.4 and 4.8 ppm, with signals that all integrate to 1H

3. List all ^{13}C NMR chemical shifts to one decimal place (*see* **Note 35**).
4. As in the case of the ^{1}H spectrum, inspect the ^{13}C spectrum for obvious functional groups, such as carbonyls (~170–220 ppm), aromatics (~100–155 ppm), alkenes (~110–150 ppm), and methoxy (~50–60 ppm), and methyl (~10–30 ppm) groups.

3.5 2D NMR Methods

A 2D NMR spectrum is obtained using multipulse experiments that correlate signals from two frequency domains ($f1$ and $f2$). Contour plots show cross peaks that associate information on one axis with information on the second axis. These methods are valuable tools for structure determination of complex compounds, since either through-bond or through-space interactions are revealed between nuclei of the same (homonuclear, typically proton) or different (heteronuclear, typically proton and carbon)

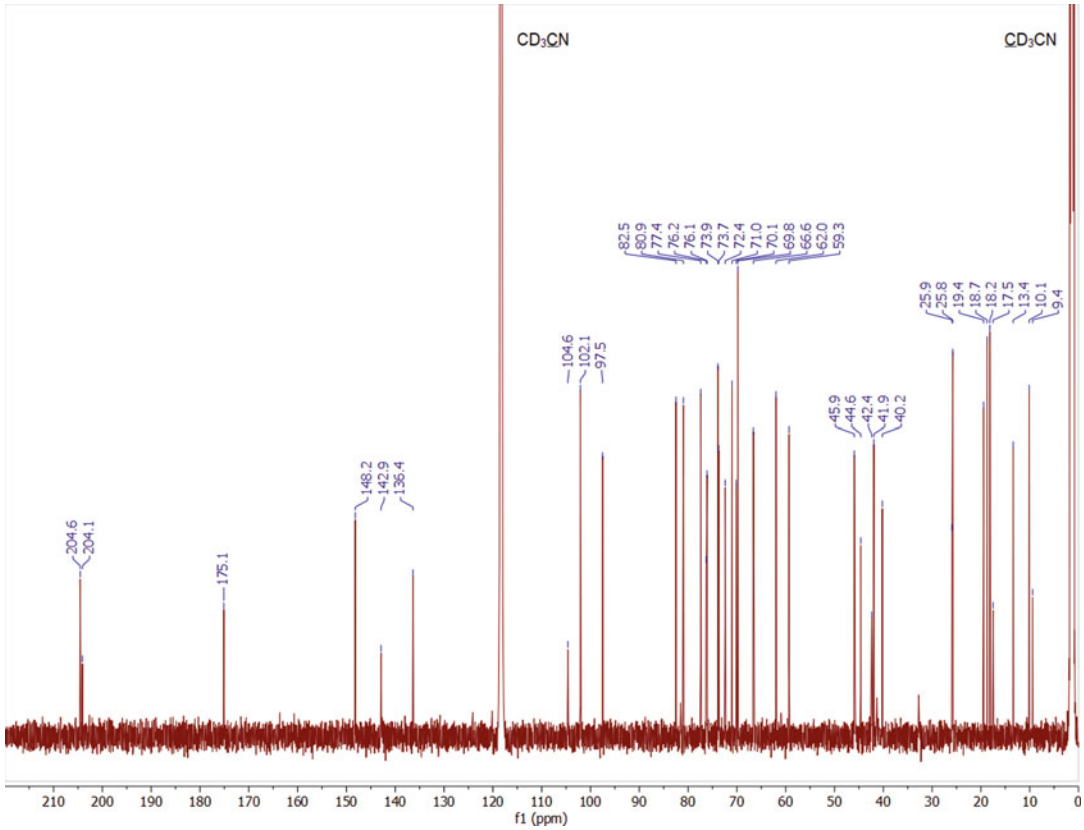

Fig. 4 ^{13}C NMR spectrum (175 MHz) of tylosin A in acetonitrile-d_3 (CD_3CN). The spectrum was referenced to the fully deuterated solvent, which gives reliable signals at 118.3 ppm and 1.3 ppm

elements (*see* **Note 36**). In addition, cross peaks observed in 2D spectra allow the assessment of accurate chemical shift values and *J*-couplings that cannot be assigned directly from the 1D spectrum due to signal overlap.

3.5.1 COSY

1. The homonuclear shift *co*rrelation *s*pectroscop*y* (^{1}H, ^{1}H-COSY, or COSY) spectrum shows the through-bond coupling connectivities between groups containing hydrogen atoms, based on geminal (^2J) and vicinal (^3J) proton couplings (*see* **Notes 37** and **38**). The COSY spectrum of tylosin A in acetonitrile-d_3 is shown in Fig. 5.
2. The ^{1}H spectrum of the sample is set on both horizontal (f_2) and vertical (f_1) axes. Autocorrelated peaks appear on the diagonal ($\delta 1 = \delta 2$), which is the symmetrical axis of the COSY spectrum.
3. A signal situated off the diagonal is called a cross peak and appears whenever protons with resonances at $\delta 1$ and $\delta 2$ ($\delta 1 \neq \delta 2$) are coupled to one another.

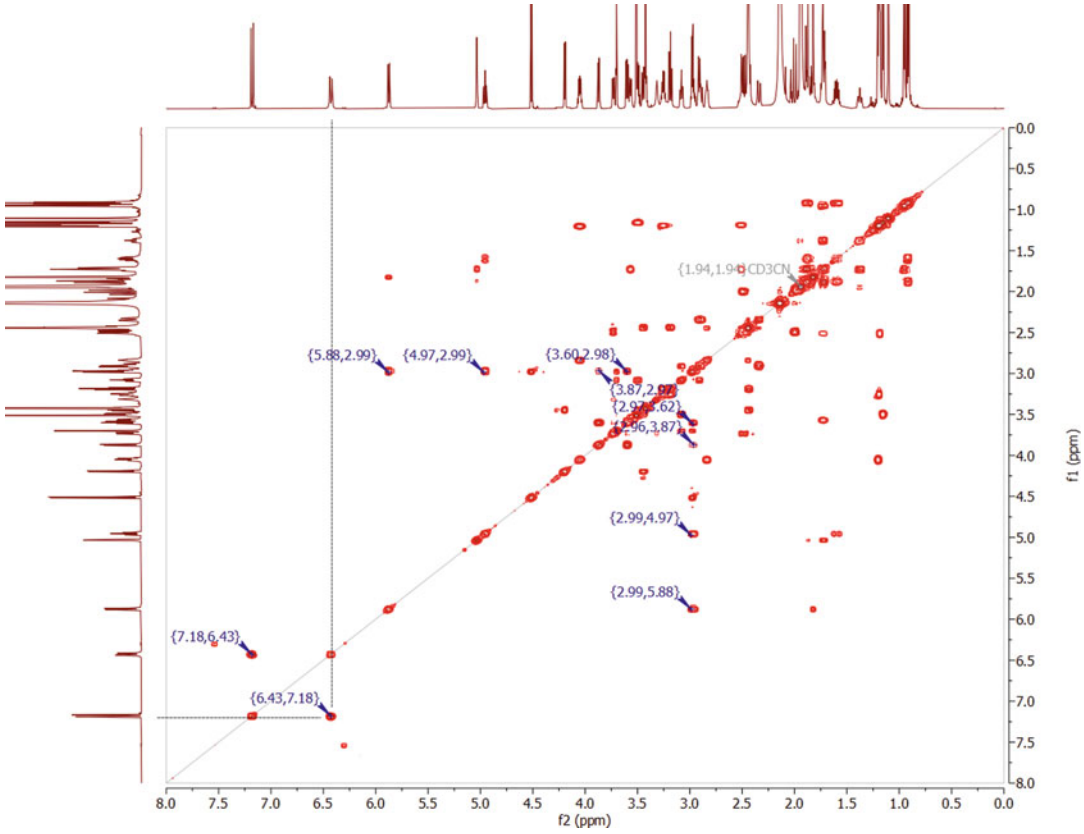

Fig. 5 COSY spectrum of tylosin A in acetonitrile-d_3 (CD_3CN). The spectrum was referenced to residual solvent (CHD_2CN). The COSY correlation between the proton signals at 7.18 ppm and 6.43 ppm is indicated with dashed lines

4. A pair of coupled protons can be identified by lines through the cross peak, which is symmetrical with respect to the diagonal (*see* **Note 39**). Analysis of the COSY spectrum is performed as follows.
5. Draw a vertical line from a known diagonal peak (H_A) until you connect with a cross peak (H_A, H_B). The horizontal line from this cross peak to the diagonal identifies the shift of the coupled proton (H_B).
6. In a similar manner, projecting from the last diagonal peak to the next cross peak and then back to the diagonal allows the assignment of the whole coupling network ("spin system") in the molecule.
7. Check the ^{1}H NMR spectrum to confirm that *J*-couplings and integrals are in agreement with the assignments made by COSY.

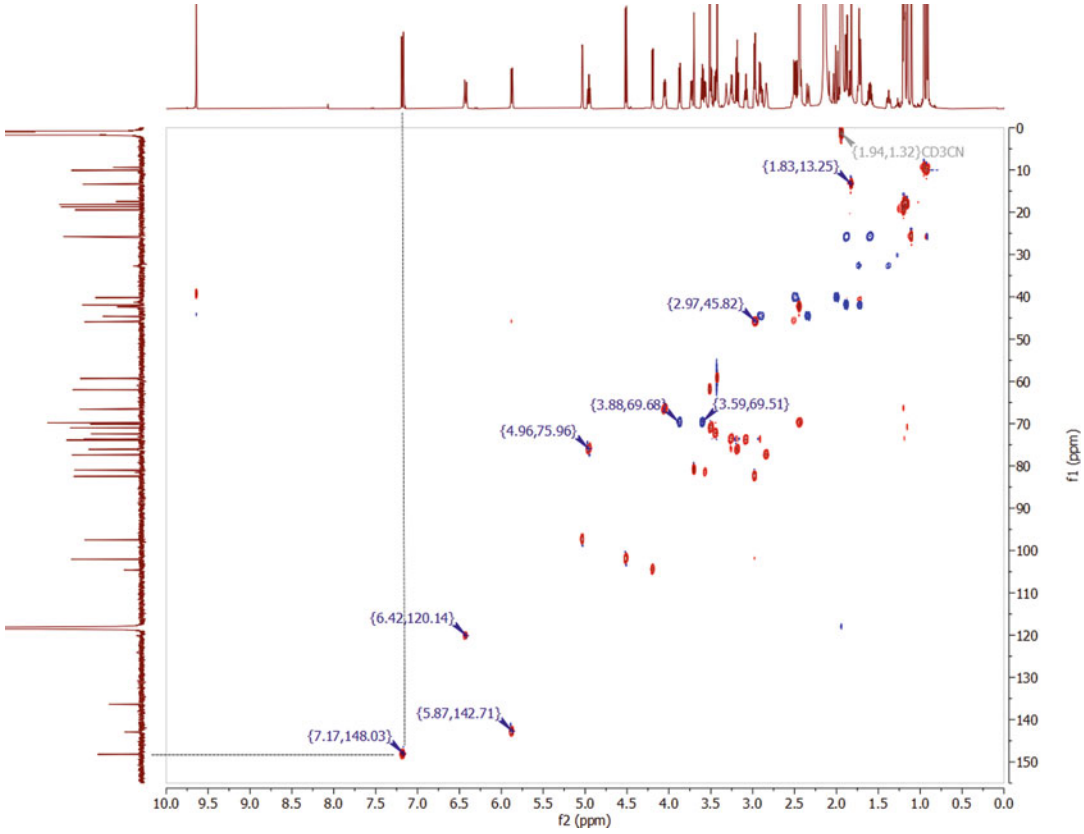

Fig. 6 HSQC spectrum of tylosin A in acetonitrile-d_3 (CD_3CN). The spectrum was referenced to residual solvent (1.94 ppm) along the f_2 axis and deuterated solvent (1.32 ppm) along the f_1 axis. The HSQC correlation between the proton signal at 7.18 ppm and the carbon signal at 148.2 ppm is indicated with dashed lines

3.5.2 ^{1}H-^{13}C- HMQC/ HSQC

1. ^{1}H–^{13}C HMQC (or HMQC) is an abbreviation for ^{1}H detected *h*eteronuclear *m*ultiple *q*uantum *c*oherence and ^{1}H–^{13}C HSQC (or HSQC) for ^{1}H detected *h*eteronuclear *s*ingle *q*uantum *c*oherence. The HMQC/HSQC spectra detect one-bond couplings (ca. 140 Hz) between the protons of a molecule and the carbons to which they are directly attached (*see* **Note 40**). The HSQC spectrum of tylosin A in acetonitrile-d_3 is shown in Fig. 6.
2. The ^{1}H spectrum of the sample is commonly set along the horizontal (f_2) axis, whereas the ^{13}C spectrum is set along the vertical (f_1) axis. HMQC/HSQC interpretation is performed as follows.
3. Draw vertical and horizontal lines through a selected cross peak in the HSQC/HMQC spectrum. The lines will pass through a peak in the ^{1}H NMR spectrum and a peak in the ^{13}C NMR spectrum that indicates direct attachment of the respective nuclei (*see* **Notes 41** and **42**).

4. Assign all correlations between the ^{13}C spectrum and the ^{1}H spectrum.
5. Identify diastereotopic (nonequivalent) protons of methylene groups (*see* **Note 43**).
6. Determine the connections of carbons and assemble substructures using a combination of the HMQC/HSQC and COSY data.

3.5.3 ^{1}H-^{13}C HMBC

1. The ^{1}H detected *h*eteronuclear *m*ultiple *b*ond *c*orrelation (^{1}H–^{13}C HMBC or HMBC) experiment shows long-range correlations between hydrogen and carbon (couplings of ca. 2–8 Hz), typically separated by two or three bonds (*see* **Note 44**). The HMBC spectrum of tylosin A in acetonitrile-d_3 is shown in Fig. 7.

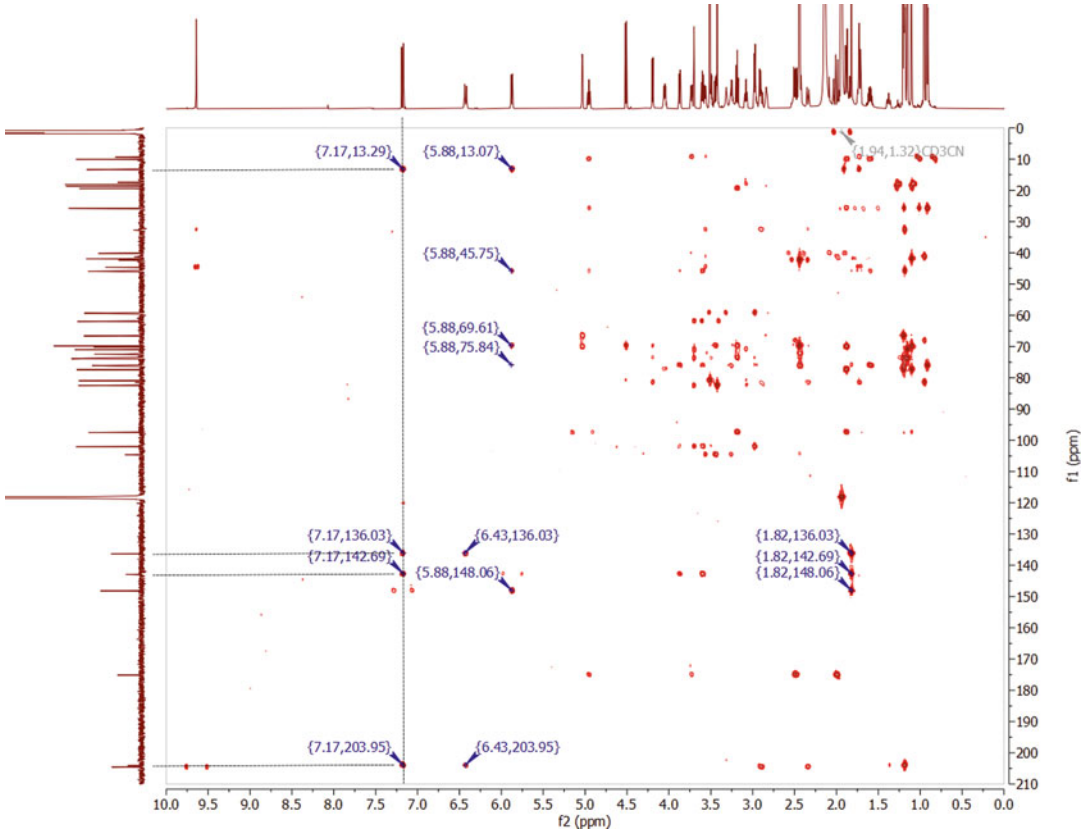

Fig. 7 HMBC spectrum of tylosin A in acetonitrile-d_3 (CD_3CN). The spectrum was referenced to residual solvent (1.94 ppm) along the f_2 axis and deuterated solvent (1.32 ppm) along the f_1 axis. The HMBC correlations between the proton signal at 7.18 ppm and the carbon signals at 204.1, 142.9, 136.1, and 13.4 ppm are indicated with dashed lines

2. As with the HSQC/HMQC spectra, the HMBC spectrum contains cross peaks corresponding to proton peaks along the horizontal (f_2) axis and sets of carbon peaks along the vertical (f_1) axis (*see* **Notes 45** and **46**). HMBC spectrum analysis is performed as follows.
3. Draw a vertical line through a selected peak in the ^{1}H NMR spectrum (f_2 axis). This line will pass through one or more related cross peaks.
4. From the respective cross-peaks project horizontal lines to the ^{13}C spectrum (f_1 axis). The lines allow the assignment of all ^{13}C peaks that are coupled through long-range couplings to the selected hydrogen atom (*see* **Note 47**).
5. Combine substructures into all feasible structures through long-range couplings, and check consistency with the previous 1D and 2D NMR data (*see* **Note 48**).

3.6 Partial Structure Elucidation of Tylosin A

1. Several functional groups can be quickly identified via inspection of the ^{1}H NMR spectrum of tylosin A, and this information can immediately be used to exclude abutiloside B and angolamycin, which have the same molecular formula as tylosin A, from further consideration as possible structures (Fig. 2). The signal at δ_H 9.64 (s, 1H) corresponds to an aldehyde proton (Fig. 3). The signals at δ_H 7.18 (d, 1H), 6.43 (d, 1H), and 5.88 (d, 1H) can be attributed to aromatic or alkene protons; the large coupling constant associated with the first two signals (15.5 Hz) supports their assignment as alkene protons (*see* **Note 26**). The signals at δ_H 3.51 (s, 3H) and 3.42 (s, 3H) can be assigned to methoxy groups, while the 3H singlets, doublets, and triplets between 0.85 and 1.25 ppm (e.g., δ_H 1.16, 1.10, 0.95, 0.92) can be assigned to methyl groups (Fig. 8). The signals between δ_H 5.10 and 2.80 belong to protons that are attached to electron-deficient oxygenated or nitrogenated carbons. Since abutiloside B lacks an aldehyde group and angolamycin has only two alkene protons, these structures are not consistent with the ^{1}H NMR data, despite having an exact mass and molecular formula that is consistent with the HRMS data.
2. Inspection of the ^{13}C NMR spectrum of tylosin A also indicates the presence of several functional groups (Fig. 4). The signals at δ_C 204.6, 204.1, and 175.1 can be assigned to carbonyl carbons. Of the two signals at δ_C 204.6 and 204.1, one corresponds to the aldehyde mentioned above, and one must correspond to a ketone functional group. The chemical shift of the signal at δ_C 175.1 points toward a carboxylic acid or derivative (e.g., an amide or ester). The signals at δ_C 148.2, 142.9, and 136.4 are indicative of aromatic and alkene carbons.

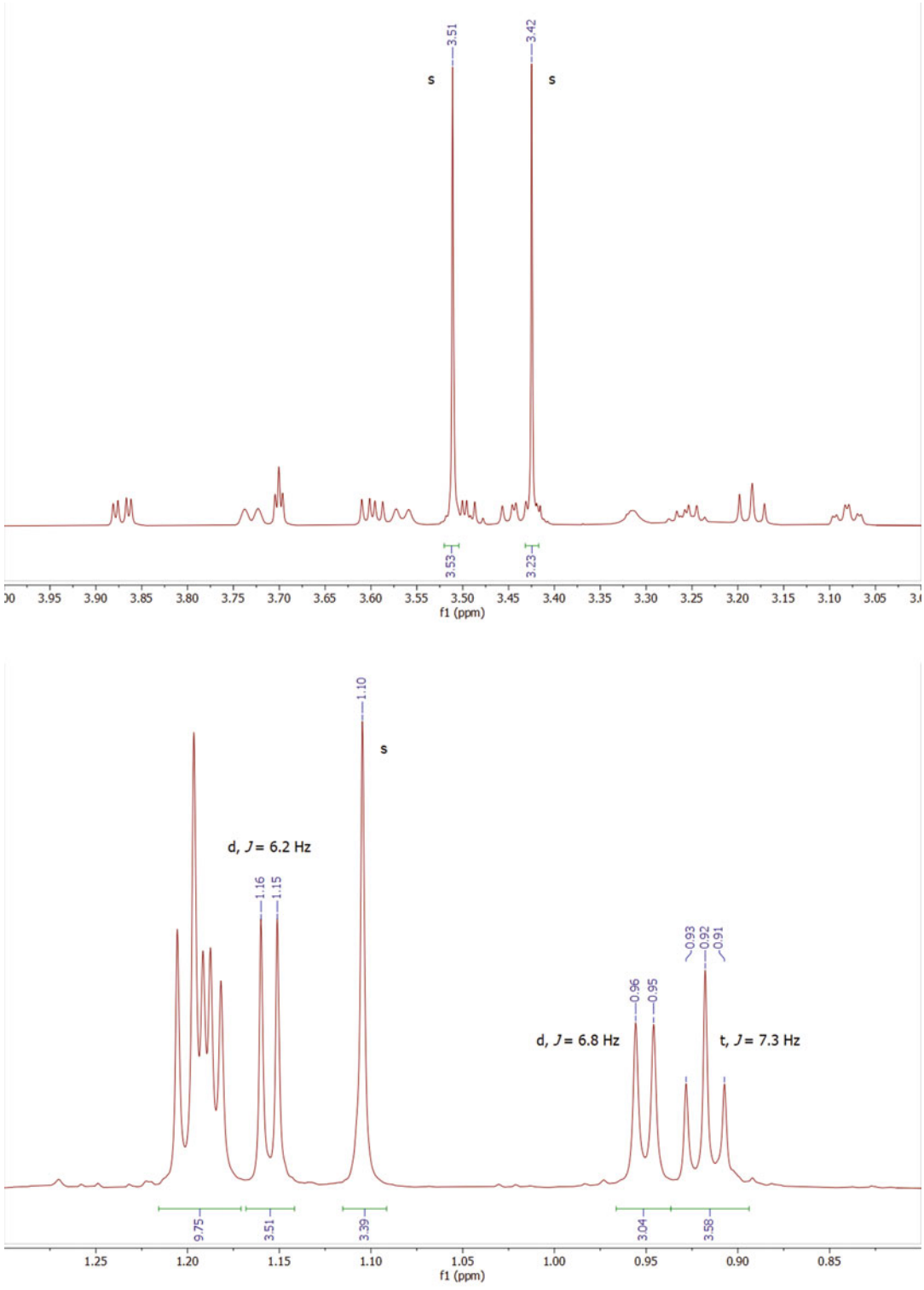

Fig. 8 ^{1}H NMR spectrum of tylosin A in acetonitrile-d_3 (4.00–3.00 ppm and 1.30–0.80 ppm)

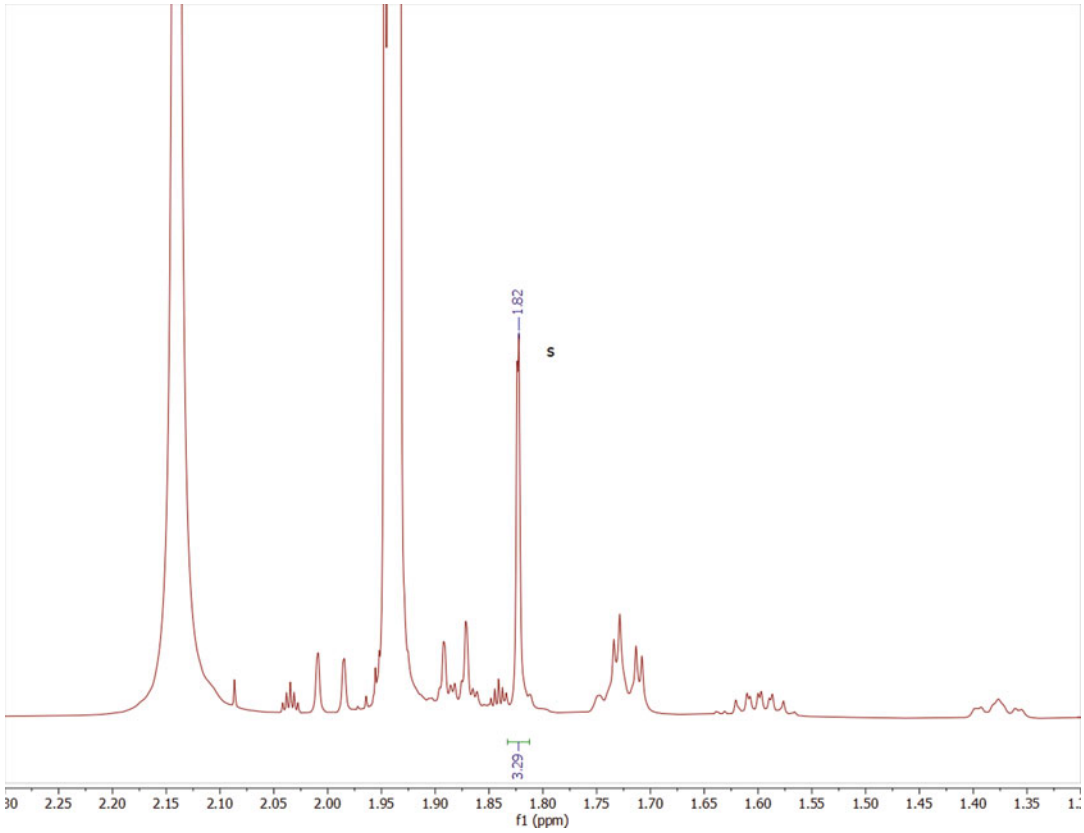

Fig. 9 ^{1}H NMR spectrum of tylosin A in acetonitrile-d_3 (2.30–1.30 ppm, 5.50–4.50 ppm, 4.20–3.20 ppm, and 3.50–2.50 ppm)

Given the distinctly alkene protons observed in the ^{1}H NMR spectrum, these signals in the ^{13}C NMR spectrum likely correspond to alkene carbons.

3. As an "entry point," we begin with the well-resolved doublet at δ_H 6.43. A COSY correlation to δ_H 7.18 and their mutually large coupling constant of 15.5 Hz establishes the *E*-configured alkene shown in Figs. 9 and 5. HSQC data allows these proton signals to be connected to their respective carbon signals (δ_H 6.43/δ_C 120.1 and δ_H 7.18/δ_C 148.2) (Fig. 6).
4. Since no additional COSY correlations for δ_H 6.43 and δ_H 7.18 are present, we rely on HMBC data to continue the structure assignment. The proton at δ_H 6.43 shows HMBC correlations to the carbons at δ_C 204.1 and 136.1 (Fig. 7). According to the HSQC spectrum, both carbons are quaternary, i.e., no one-bond proton-carbon correlations are apparent. The proton at δ_H 7.18 shows HMBC correlations to the carbons at δ_C 204.1, 142.9, 136.1, and 13.4. Since HMBC spectra favor two- and three-bond correlations, it stands to reason that the

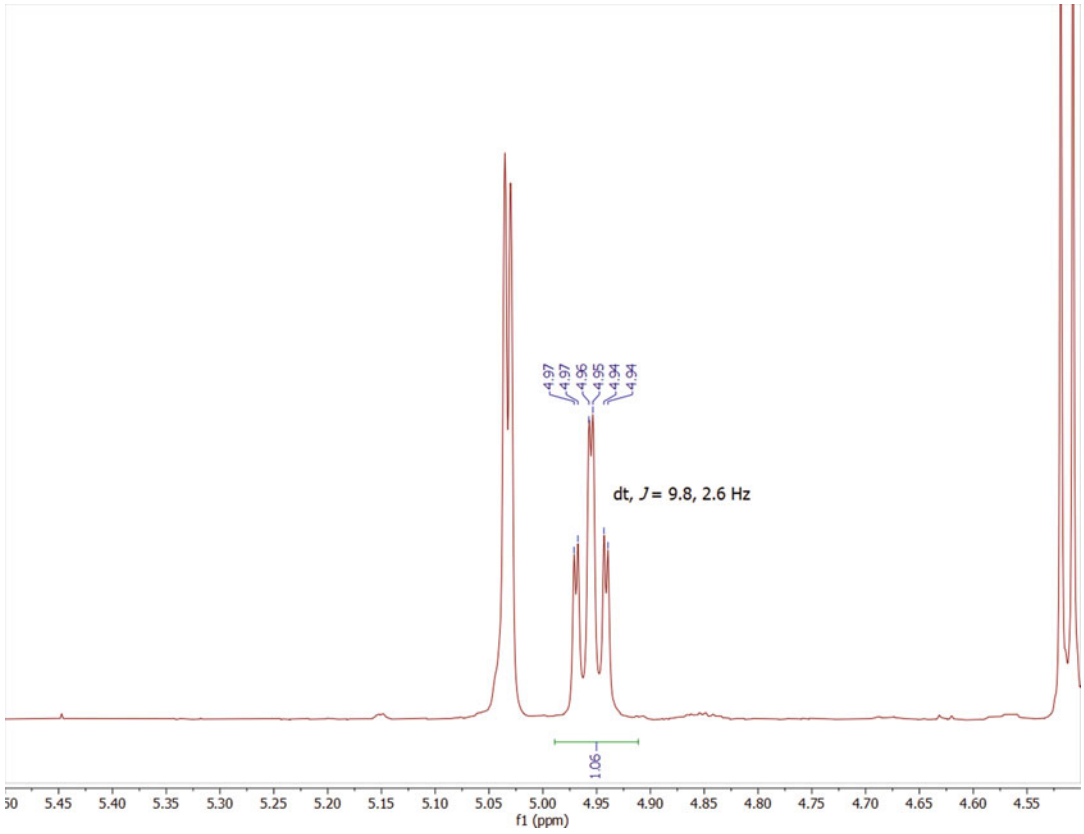

Fig. 9 (continued)

carbons at δ_C 204.1 and 136.1 must be within three bonds of both alkene protons. In other words, the carbon at δ_C 204.1 is two bonds away from the proton at δ_H 6.43 and three bonds away from the proton at δ_H 7.18 or vice versa. Likewise, the carbon at δ_C 136.1 is two bonds away from the proton at δ_H 7.18 and three bonds away from the proton at δ_H 6.43 or vice versa. Considering that the *beta* carbon of an alkene conjugated to a ketone functional group (δ_C 204.1) is typically electron-deficient, the ketone is placed adjacent to the proton/carbon at δ_H 6.43/δ_C 120.1.

5. As the proton at δ_H 7.18 shows additional HMBC correlations, we continue the structure assignment in that direction. Although the carbon at δ_C 136.1 is quaternary, HSQC data allows the carbons at δ_C 142.9 and 13.4 to be connected to their respective proton signals (δ_H 5.88/δ_C 142.9 and δ_H 1.82/δ_C 13.4). The 3H integration of the proton at δ_H 1.82 indicates a methyl group (Fig. 9). In order to satisfy the proton multiplicity and HMBC correlations from the proton at δ_H 1.82 (s) to the carbons at δ_C 148.2, 142.9, and 136.1 and the proton multiplicity and HMBC correlations from the

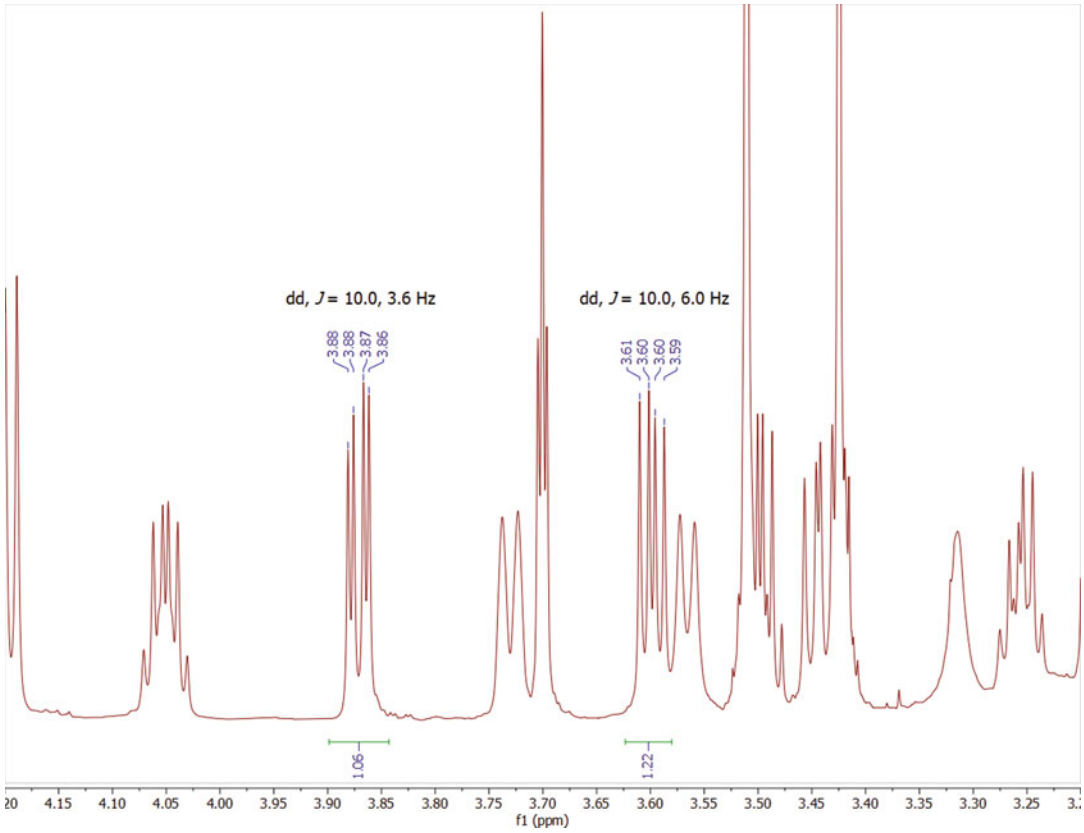

Fig. 9 (continued)

proton at δ_H 5.88 (d, $J = 10.5$ Hz) to the carbons at δ_C 148.2 and 13.4, the 4-methyl dienone system show in Fig. 10 is constructed.

6. From the proton at δ_H 5.88, both COSY and HMBC correlations can be used to extend the structure assignment beyond this substructure. In addition to the carbons at δ_C 148.2 and 13.4 discussed previously, the proton at δ_H 5.88 also shows HMBC correlations to carbons at δ_C 75.9, 69.7, and 45.8. HSQC data allows these carbons to be connected to their respective proton signals (δ_H 4.95/δ_C 75.9, δ_H 3.87,3.60/δ_C 69.7, and δ_H 2.98/δ_C 45.8). While the signals at δ_H 4.95 (dt, $J = 9.8$, 2.6 Hz) and δ_H 2.98 (overlapped) correspond to methine protons integrating to 1H, the pair of signals at δ_H 3.87 (dd, $J = 10.0$, 3.6 Hz) and 3.60 (dd, $J = 10.0$, 6.0 Hz) must correspond to diastereotopic methylene protons since they correlate to the same carbon (*see* **Note 42**). COSY correlations reveal that the proton at δ_H 5.88 is adjacent to the proton at δ_H 2.98 and that the proton at δ_H 2.98 is adjacent to the protons at δ_H 4.95 and the pair of protons at δ_H

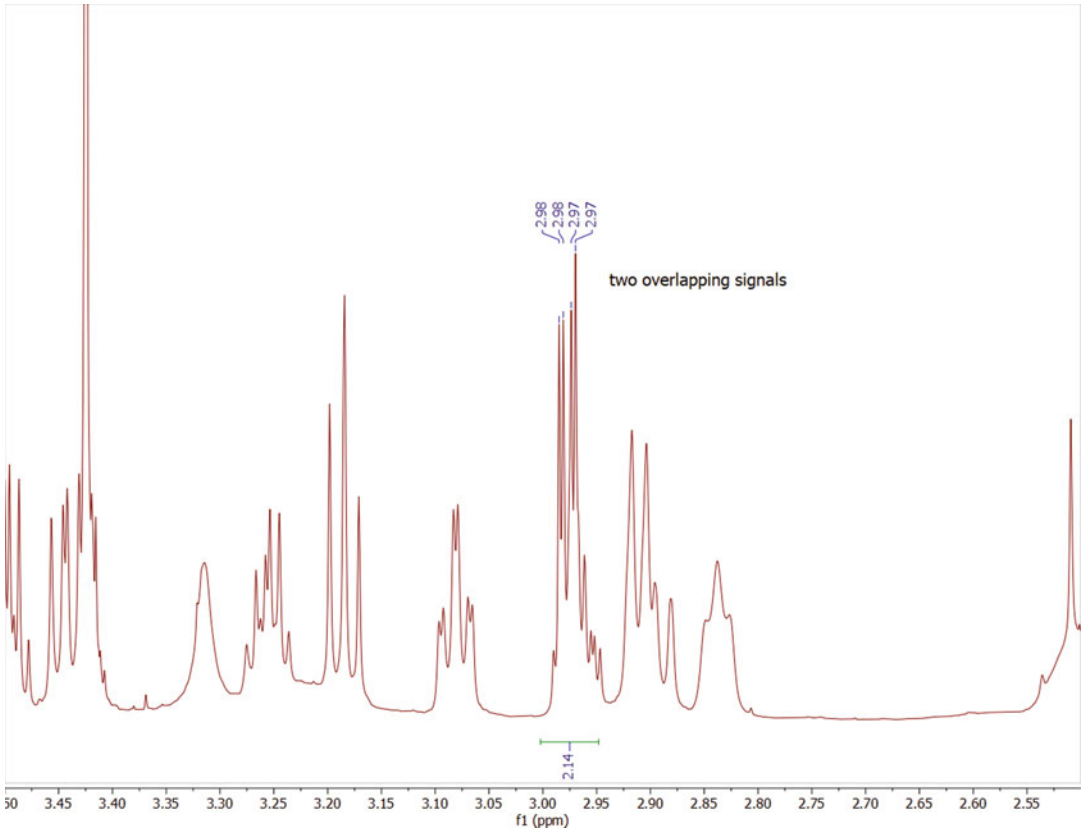

Fig. 9 (continued)

3.87,3.60. Furthermore, the carbon chemical shifts of δ_C 75.9 and δ_C 69.7 suggest that these carbons are oxygenated.

7. The remainder of the structure elucidation proceeds in a similar manner (not depicted in Fig. 10). The HMBC correlation from the proton at δ_H 4.95 to the ester carbonyl at δ_C 175.1 provides entry to the eastern half of the macrolide. The protons that correlate via HMBC to this carbonyl must be two and three bonds away. Likewise, the protons that correlate via HMBC to the ketone carbonyl at δ_C 204.1 must also be two and three bonds away. The HMBC correlation from the protons at δ_H 3.87,3.60 to the anomeric carbon at δ_C 102.1 provides entry to the western sugar moiety.

4 Notes

1. Dissolving an extract in methanol usually leaves little to no insoluble material. However, if a significant portion of the extract does not dissolve, the use of acetonitrile or water, either as the primary solvent or as a co-solvent, may be more suitable.

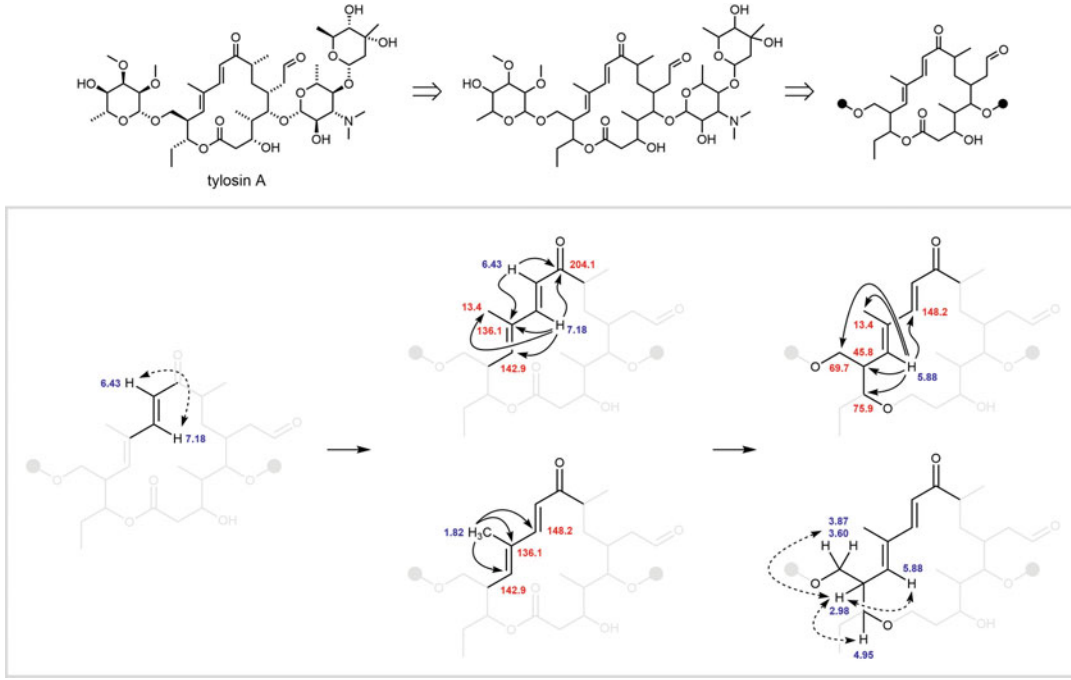

Fig. 10 Partial NMR-based structure elucidation of tylosin A. Note that only the planar structure of tylosin A is considered here and the sugar moieties are disregarded. ^{1}H-^{1}H COSY correlations are indicated by a double-headed dotted arrow; ^{1}H-^{13}C HMBC correlations are indicated by a solid arrow drawn from the proton to the carbon

2. Removing any insoluble material from the solution is crucial prior to HPLC-(HR)MS analysis because small particles can clog the injection needle, needle seat, and thin capillaries of the system as well as the HPLC column itself. In lieu of centrifugation, filtration with a syringe filter having a 0.2 μm pore size is also acceptable.
3. The level of the sample solution needs to be high enough so that the injector needle is fully submerged upon sampling the solution. Glass inserts for HPLC vials can be used for small sample volumes.
4. The COCONUT database can be found at https://coconut.naturalproducts.net/. The Natural Products Atlas database can be found at https://www.npatlas.org/. The Dictionary of Natural Products can be found at https://dnp.chemnetbase.com/faces/chemical/ChemicalSearch.xhtml. Many natural product databases exist, each with somewhat different coverage of natural product space [9, 10]. Some, like COCONUT and NP Atlas, are open access; others, like the Dictionary of Natural Products, require a paid subscription.

5. The sample to be measured must be as dry as possible to prevent the residual water peak from obscuring signals derived from the compound. High vacuum desiccation is the method of choice for this purpose because elevated temperatures, which can degrade thermolabile compounds, should be avoided.
6. Deuteration is required in order to mask signals from the solvent. However, the deuterium enrichment for each of these solvents is less than 100%, and thus they give noticeable peaks, either singlets or multiplets, in the ^{1}H NMR spectrum. The signals associated with this "residual" solvent are used directly as internal chemical shift references. In some cases, NMR solvents spiked with 0.03–1% tetramethylsilane (TMS) are used in order to provide an internal standard.
7. For natural products in very limited quantity, it is preferable to use deuterated solvent from an individual ampule, rather than a bottle, as the latter likely contains oxygen and water. Also note that an opened bottle of deuterated chloroform ($CDCl_3$) may become sufficiently acidic to cause chemical modifications of acid-labile compounds.
8. Probes for NMR spectroscopy are typically designed to accommodate NMR tubes with outside diameters of 1.7, 3, and 5 mm, with 5 mm tubes being the most common.
9. The NMR tubes should be thoroughly cleaned before use, preferably with spectroscopic grade solvents. For this purpose, the use of nonvolatile solvents, such as dimethylsulfoxide (DMSO) or dimethylformamide (DMF), which are difficult to remove completely, should be avoided.
10. Care should be taken to avoid contamination of the purified compound. Two common examples of impurities are the phthalates from plastic tubing and grease used to lubricate ground glass joints. Paramagnetic impurities, often originating from a spatula, should be also avoided, since these cause extensive line broadening.
11. HPLC-(HR)MS analysis is a very sensitive method and only requires tiny amounts of sample. Injecting too much sample and, thus, overloading the system can lead to a severe contamination of the mass spectrometer, leading to signal "carryover," and can only be eliminated by intensive cleaning, maintenance, and service.
12. Refer to Chap. 5 "Isolation and purification of natural products from microbial cultures" by Schafhauser and Kulik in this edition for the principles of liquid chromatography and method setup.

13. Depending on the type of mass spectrometer, the acquisition of data in positive and negative mode is performed in either one analysis or in two separate ones. Time-of-flight (TOF) mass spectrometers cannot switch between polarities and maintain a stable electric field required to obtain accurate *m/z* values. Therefore, the mass spectra in negative and positive mode should be recorded in separate analyses in instrumental setups with TOF-MS.
14. There are two different types of MS chromatograms for extracting MS spectra: the total ion chromatogram (TIC) and the base peak chromatogram (BPC). The TIC depicts the intensity of the total ion current at a point in time and, depending on background noise, often shows unresolved peaks with little to no baseline separation. In this case, it is recommended to extract the MS spectra from the BPC, which only displays the intensity of the most abundant *m/z* at a point in time and is more likely to show a well-resolved peak corresponding to the compound of interest.
15. The exact mass of the compound of interest cannot be directly observed from the MS spectrum because it appears in a charged state (ions) with a respective *m/z*. In positive mode, this can be the protonated molecular ion $[M+H]^+$, a sodium $[M+Na]^+$ adduct, a potassium $[M+K]^+$ adduct, or an ammonium $[M+NH_4]^+$ adduct, with M referring to the exact mass of the compound of interest. In negative mode, the most commonly observed ions are the deprotonated molecular ion $[M-H]^-$, the formate $[M+HCOO]^-$ adduct, or the chloride $[M+Cl]^-$ adduct. If several *m/z* values occur in a single MS spectrum, care must be taken to calculate the exact mass correctly because the molecular ion and adducts can be present simultaneously in differing abundances.
16. HRMS analysis offers the possibility to calculate the molecular formula for the compound of interest. Still, the proposed molecular formulae are associated with a certain error, and more than one option is possible, especially for large compounds. By picking one molecular formula for database research, the query will be biased and can lead to false-negative or false-positive hits. Thus, it is recommended to use the exact mass instead of the molecular formula, whenever possible.
17. When entering the exact mass into the query, it is recommended to include the error of the mass spectrometer and use the range instead of the absolute value. For most mass spectrometers, the error is ± 5 ppm.
18. The solvent should completely dissolve the sample. Common deuterated NMR solvents are DMSO-d_6, $CDCl_3$, acetonitrile-d_3, and methanol-d_4.

19. The solution should be clear as particles cause line broadening. These particles can be removed via filtration using a Pasteur pipette packed with a small amount of glass wool. Addition of a small amount of solvent to a saturated solution may also minimize the line broadening caused by microscopic nucleation of particles.
20. Signal resolution results are optimal when there is an approx. 3 cm liquid height in the NMR tube (i.e., a volume between 0.5 and 0.7 mL in a 5 mm diameter NMR tube). Lower than optimal solution volumes cause poor line shape in the spectrum.
21. For natural products, where only a milligram of sample may be available, a minimum solvent volume is generally preferred, as this will maximize concentration and thus the intensity of the signal. However, care should be taken so that the high sample concentration does not cause broadening of the NMR signals due to high viscosity or turbidity.
22. Teflon tape will limit evaporation of volatile solvents.
23. The chemical shift is characteristic of the different types of chemical groups and their chemical environment. For instance, protons next to electronegative atoms, such as oxygen or nitrogen, will have less electron density and as a result will be deshielded from the full effect of the applied field resonating at a higher frequency for a given field strength.
24. *J*-coupling is independent of the strength of the magnetic field. However, higher applied magnetic field is preferable for the analysis of structurally complex molecules with highly overlapped signals because the latter will proportionally occupy less space on the ppm scale than they do with a lower magnetic field.
25. *J*-coupling is a reciprocal process and the same coupling constant is found between interacting NMR nuclei. Therefore, according to the splitting pattern and the magnitude of the coupling constants, the connection between interacting groups can be determined.
26. The dihedral angle between coupled nuclei separated by three bonds provides important information about local molecular conformation. For instance, in cyclohexane rings, the coupling constant of two (vicinal) protons with an axial-axial relationship ($\Phi = 180°$, $J = 8$–15 Hz) is greater than that from two (vicinal) protons with an axial-equatorial relationship ($\Phi = 60°$, $J = 2$–5 Hz). Likewise, in alkenes the *Z* or *E* configuration can be differentiated according to the observed *J* value of the respective protons (8–12 or 15–18 Hz, respectively).

27. This implies that the protons of a methyl group (CH_3) produce three times the signal of a methine proton (CH). Keep in mind that the integration provides only relative intensity data, so that the experimentalist must select a resonance with a known or suspected number of protons and normalize the other integrals accordingly.
28. A software program to process and analyze NMR data is required. Here, we use Mnova 14.1.2 (Mestrelab Research). Other programs include TopSpin (Bruker), Delta (Jeol), and iNMR (Nucleomatica).
29. Impurities in the sample can affect the measured integrals, especially if the signal to noise ratio of the spectrum is low. The presence of paramagnetic species, such as metal ions, or changes in the temperature and pH may also affect the intensity of the various resonances in the spectrum.
30. It is a good approach to tabulate the chemical shifts, multiplicities, and integrations of the observed resonances, so that vital information will not be overlooked. Please keep in mind that the ^{1}H chemical shifts are dependent on the identity of the deuterated solvent. When reporting ^{1}H chemical shifts, therefore, the solvent used should always be stated.
31. In the ^{1}H NMR spectrum the multiplicity of the peaks is determined by the $n + 1$ rule, where n is the number of the protons that participate in coupling (first-order spectra). Thus, the methyl group in ethanol is split from the methylene group (CH_2) into $2 + 1 = 3$ lines (triplet). In addition, the relative intensities of the peaks follow the properties of Pascal's triangle, which explains the 1:2:1 intensity of the aforementioned methyl group in the ^{1}H NMR spectrum. However, if we suppose that the two hydrogen atoms of the methylene group were not magnetically equivalent, that is, they have different coupling constants to the methyl group due to restricted rotation or close proximity to a stereogenic center, then the $n + 1$ rule should be considered twice. As a result, the methyl group would show a peak pattern of $(1 + 1)(1 + 1)$, that is, 2×2 or doublet of doublet (dd). At this point, please keep in mind that in cases when the chemical differences between the interacting protons ($\Delta\nu$) are not large enough compared to their coupling constants (J), i.e., $\Delta\nu/J < 5$, the lines and intensities of the peaks do not follow the aforementioned rules and their splitting pattern is more complicated (second-order spectra).
32. The chemical shifts and signal dispersion are influenced by various physical conditions. Thus, when peaks coincide in the NMR spectrum, you can improve resolution by changing the solvent, the temperature, the pH, or even the magnetic field strength. The latter option produces more predictable results.

33. Keep in mind that the major isotope ^{12}C has no magnetic properties. On the other hand, ^{13}C has an odd mass and is NMR active. Other common NMR active nuclei are ^{1}H, ^{15}N, and ^{31}P.
34. The ^{13}C resonances display multiplicity due to the carbon-proton couplings, and thus signals from methyl groups (CH_3) are split into four lines (quartet), signals from methylene groups (CH_2) are split into three lines (triplet), signals from methine groups (CH) are split into two lines (doublet), and signals from quaternary carbons (C) appear as singlets. In practice, during acquisition of a ^{13}C NMR spectrum, the carbon-proton couplings are usually eliminated by irradiating of ^{1}H across a broad range of frequencies (broadband ^{1}H decoupling). This technique simplifies the ^{13}C spectrum, since one singlet arises for each distinct type of carbon. However, the integration is less reliable, because the decoupling field perturbs the intensities of the peaks. Please also keep in mind that due to the low natural abundance of ^{13}C, the probability of having two adjacent ^{13}C nuclei in a single molecule is highly unlikely (0.01%), which removes complications from ^{13}C–^{13}C couplings.
35. When you attempt to measure ^{13}C chemical shifts, you may encounter a poor signal to noise ratio in the ^{13}C NMR spectrum. Moreover, quaternary carbons often exhibit low signal intensity, and it is difficult to assign them. In this case, you may resort to the use of indirect detection methods, such as HSQC or HMBC, to obtain the missing chemical shifts.
36. Keep in mind that these techniques can also be applied to other common nuclei in organic molecules, such as nitrogen. Unfortunately, the very low intrinsic sensitivity and natural abundance of the NMR-active isotope ^{15}N (0.37%) has precluded the routine acquisition of ^{15}N spectra. Nevertheless, it can provide valuable structural information, especially in the case of highly substituted heterocyclic ring structures.
37. The intensity of COSY cross peaks varies in direct proportion to the magnitude of the *J*-coupling(s) between the correlated peaks. Please note that a coupling of zero obscures the passage of magnetization resulting in no cross peaks. Therefore, according to the Karplus diagram, in aliphatic systems when the dihedral angle is 90°, the vicinal correlation (^{3}J) may not be observed.
38. Exceptions, however, can be expected for some aromatic, olefinic, and special configuration systems, since long-range couplings (^{4}J or even ^{5}J) with observable coupling constants can be found in a COSY spectrum.

39. This duplication can be useful as it enables us to distinguish true correlations from artifacts, since the latter are rarely symmetrical.
40. The interpretation methods for HMQC and HSQC are the same. However, the spectrum of HSQC enjoys the benefits of fewer artifacts and slightly better resolution in the ^{13}C domain.
41. If the chemical shift of a specific proton is known, the chemical shift of the coupled carbon can be determined and vice versa, which is important for postulating the chemical environment of the functional group.
42. The lack of a ^{1}J CH correlation indicates that the carbon is quaternary.
43. The COSY spectrum cannot differentiate between geminal and vicinal proton connectivities. However, in the HSQC spectrum, if two nonequivalent protons (diastereotopic) are attached to a common carbon, they will both correlate to the same ^{13}C peak. This information is very useful to identify diastereotopic methylene protons and is particularly noticeable in a multiplicity-edited HSQC, where the amplitude of the methylene (CH_2) protons is negative compared to methine (CH) and methyl (CH_3) protons. In addition, as the resolution of the HMQC (or HSQC) spectrum is higher than that of the ^{1}H NMR spectrum, interpretation of the HMQC/HSQC can help to resolve the overlapped correlated peaks in the ^{1}H and COSY spectra.
44. In practice, the HMBC sequence is optimized for three-bond correlations, even though it is not obvious by inspection which ones are two- and which ones are three-bond correlations. In addition, carbons separated by more than three bonds can be detected, especially in the case of aromatic and olefinic (allylic) systems, but the intensity of the signals will not be as strong.
45. In some cases, one-bond correlations can also be observed in the HMBC spectrum. They are characterized by a pair of signals/contours that are situated on a horizontal line that passes through the correlated peak in the ^{13}C spectrum. The signals are symmetrically displayed on either side of the proton peak that they relate to. Pay particular attention when these signals line up exactly with peaks in the ^{1}H NMR spectrum along the horizontal (f_2) axis, giving rise to artifacts that appear as potential cross peaks. Therefore, it is always very useful to identify the single-bond correlations before you begin interpreting the HMBC spectrum.
46. Keep in mind that the correlation peaks of broad proton resonances are usually weak or even unobservable.

47. In an analogous manner, a horizontal line through a selected peak in the ^{13}C NMR spectrum (f_1 axis) allows the assignment of all ^{1}H peaks that are coupled through long-range couplings to the selected carbon.
48. Note that connectivities can occur between protons and carbons separated by heteroatoms (e.g., oxygen, nitrogen, or sulfur) or by quaternary carbons. Therefore, the HMBC experiment is a powerful tool for the connection of structural units within a molecule.

Acknowledgments

C.H. thanks DZIF TTU 09.716 for financial support. The authors acknowledge infrastructural support by the Cluster of Excellence EXC 2124: Controlling Microbes to Fight Infection (CMFI).

References

1. Newman DJ, Cragg GM (2016) Natural Products as Sources of New Drugs from 1981 to 2014. J Nat Prod 79:629–661
2. Hutchings M, Truman A, Wilkinson B (2019) Antibiotics: past, present and future. Curr Opin Microbiol 51:72–80
3. Brown ED, Wright GD (2016) Antibacterial drug discovery in the resistance era. Nature 529:336–343
4. Gavriilidou A, Kautsar SA, Zaburannyi N, Krug D, Müller R, Medema MH, Ziemert N (2022) Compendium of specialized metabolite biosynthetic diversity encoded in bacterial genomes. Nat Microbiol 7:726–735
5. Gualerzi CA, Brandi L, Fabbretti A, Pon CN (eds) (2014) Antibiotics: targets, mechanisms and resistancee. Wiley, Weinheim
6. Wex KW, Saur JS, Handel F, Ortlieb N, Mokeev V, Kulik A, Niedermeyer THJ, Mast Y, Grond S, Berscheid A, Brötz-Oesterhelt H (2020) Bioreporters for direct mode of action-guided screening of antibiotic producer strains. SSRN Electron J 28:1242
7. Silverstein RM, Webster FX, Kiemle DJ (2005) Spectrometric identification of organic compounds, 7th edn. Wiley, Hoboken
8. Daletos G, Ancheeva E, Orfali R, Wray V, Proksch P (2017) Antibiotics: methods and protocols. *Methods Mol. Biol.* (Sass P, ed). Springer, Cham
9. Sorokina M, Steinbeck C (2020) Review on natural products databases: where to find data in 2020. J Cheminform *12*:1–51
10. Van Santen JA, Kautsar SA, Medema MH, Linington RG (2021) Microbial natural product databases: moving forward in the multi-omics era. Nat Prod Rep *38*:264–278

Chapter 7

Computer-Aided Drug Design: An Update

Wenbo Yu, David J. Weber, and Alexander D. MacKerell Jr

Abstract

Computer-aided drug design (CADD) approaches are playing an increasingly important role in understanding the fundamentals of ligand-receptor interactions and helping medicinal chemists design therapeutics. About 5 years ago, we presented a chapter devoted to an overview of CADD methods and covered typical CADD protocols including structure-based drug design (SBDD) and ligand-based drug design (LBDD) approaches that were frequently used in the antibiotic drug design process. Advances in computational hardware and algorithms and emerging CADD methods are enhancing the accuracy and ability of CADD in drug design and development. In this chapter, an update to our previous chapter is provided with a focus on new CADD approaches from our laboratory and other peers that can be employed to facilitate the development of antibiotic therapeutics.

Key words Computer-aided drug design, Machine learning, Drude polarizable force field, Molecular dynamics, Site identification by ligand competitive saturation, SILCS, Binding site prediction, Protein-protein interaction, Membrane permeation, Biologics

1 Introduction

Following the significant milestone that penicillin represents in human medical history, the battle between humans and bacteria has never settled down and becomes even more vigorous caused by the steady rise of drug resistance. This problem persists despite the availability of large number of antibiotic drugs, indicating the need for more novel antibiotic drug classes to overcome the resistance problem [1, 2]. Toward this need, computer-aided drug design (CADD) methods are very helpful tools and have been regularly to study the structure and function relationships of antibiotic targets that contribute to drug resistance and to search for new antibiotics, at a relatively cheaper cost compared to using only experimental wet lab methods owing to the powerful modern computational resources [3, 4].

Previously, we published a chapter in the first edition of this book that was dedicated to an overview of CADD and included

Peter Sass (ed.), *Antibiotics: Methods and Protocols*,
Methods in Molecular Biology, vol. 2601, https://doi.org/10.1007/978-1-0716-2855-3_7,

information on routinely utilized protocols, especially tools used in our laboratory, toward the design of antibiotic therapeutics [4]. Applications of these CADD methods in real-life studies were also presented. Since then, CADD methods have been employed extensively to facilitate the development of novel antibiotics by the computational chemistry community and us for the past 5 years. This included studies on the mechanism behind antibiotic resistance that may help to guide the design of new antibiotic drugs to overcome such resistance. For example, Stote et al. studied the mechanism of an S222T mutation-induced resistance of 1-deoxy-d-xylulose-5-phosphate reductoisomerase (DXR) to fosmidomycin using molecular dynamics (MD) simulations [5]. The MD simulations revealed the structural and energetic basis of the single mutation that induced resistance shedding light on the development of a new antibiotic compound targeting DXR. Verma et al. recently explored the molecular mechanism of polymyxin E (colistin) resistance in mobile colistin-resistant (*mcr*-1) bacteria [6]. Colistin is the only FDA-approved membrane-active drug to tackle Gram-negative bacteria despite its high toxicity. However, the appearance of *mcr*-1 bacteria identified in 2015 has worsened the situation [7]. MD simulations revealed the mechanism of interruption to the outer membrane of normal Gram-negative bacteria caused by colistin and dissected the mechanism of resistance in *mcr*-1 bacteria to the action of colistin and other cationic peptides due to the covalently attached phosphoethanolamine group modification in lipids. The simulation results provide clues for the design of new membrane disruptors to treat *mcr*-1 infections.

Identification and developing drug candidates against novel antibiotic targets for specific bacteria still serves as an important alternative to overcome the antibiotic resistance issue. Heme oxygenase (HemO) is a novel antibiotic target involved in the metabolism of heme by bacteria as required to access iron. Previous bioassay data supported that *Pseudomonas aeruginosa* HemO (*pa*-HemO) inhibitors, by blocking a key mechanism of the iron acquisition system, represent a promising therapeutic target for *pa* infections [8, 9]. Collaborating with the Wilks laboratory, our group has continued to apply CADD methods to optimize *pa*-HemO small molecule inhibitors. In a recent study, a series of inhibitors based on a previously established scaffold were designed and tested to develop a structure-activity relationship (SAR) [10]. Binding orientations and affinities were predicted and used to interpret SAR. Good correlation between predicted affinities and bioassay potency data was observed and validated the utility of the computational model in the further refinement of the current scaffold targeting *pa*-HemO. In another recent study, the structure of the *Clostridioides difficile* (*C. diff*) binary toxin (CDTa and CDTb), which is associated with the most serious outbreaks of drug-resistant *C. diff* infection in the twenty-first century, was solved [11]. Using normal

mode analysis, we explored the possible mechanism behind the translocation of CDTa, which is the enzymatic component, helped by the CDTb that serves as the pore-forming or delivery subunit. Such analysis helps to elucidate the *C. diff* binary toxin infection mechanism and shape potential therapeutic strategies in the future [11].

Searching for new antibiotics against established targets is still continuing where CADD methods are playing important roles. Our laboratory together with de Leeuw and coworkers is continuing the design of novel agents against bacteria cell wall biosynthesis [12, 13]. In a recent study, SAR for a series of compounds that have benzothiazole indolene scaffold was pursued targeting the essential bacterial cell wall precursor molecule Lipid II [14]. Using MD simulations, we predicted binding free energies and binding modes of Lipid II binders and gained atomic details on the interactions between designed molecules with Lipid II, information that will be useful for further development of antibacterial therapeutics.

β-Lactamase was used as a target in combination therapy against multidrug-resistant *Enterobacteriaceae* [15]. β-Lactamase inhibitors may help to inactivate the β-lactamase enzyme of the pathogen and restore the function of β-lactam antibiotics to overcome the enzyme-mediated resistance. Using the full Site Identification by Ligand Competitive Saturation (SILCS) [16–18] technology developed in our laboratory (Fig. 1), we identified β-lactamase CMY-10 inhibitors with our experimental collaborators [19]. The SILCS-based CADD method was fully described in the first edition of our chapter [4] as well as another chapter previously published in this same book series [20]. The de novo drug design started from running SILCS simulations, which conduct all-atom explicit-solvent combined Grand Canonical Monte Carlo/MD (GCMC/MD) simulations that include small organic solutes such as propane, benzene, methanol, and others, to identify 3D functional-group binding patterns (FragMaps) on the CMY-10 protein target. Then SILCS-Pharm [21, 22] was conducted to extract important binding patterns from FragMaps and turn them into pharmacophore features at the R1 and R2 subsites of CMY-10. Pharmacophore models were then constructed and used to initiate virtual screenings (VS) against over 750,000 commercially available compounds. Top 10,000 hit compounds from the initial pharmacophore screen were selected for SILCS-Monte Carlo (SILCS-MC) sampling for further binding pose refinement and estimation of the binding affinity based on the ligand grid free energy (LGFE) evaluation. Fingerprint-based similarity clustering was then conducted to maximize the chemical diversity of the ranked compounds to be selected for bioassay testing. Several compounds leading to decreased β-lactamase activity were confirmed by bioassay tests. The best hit compound was then subject to a similarity search for

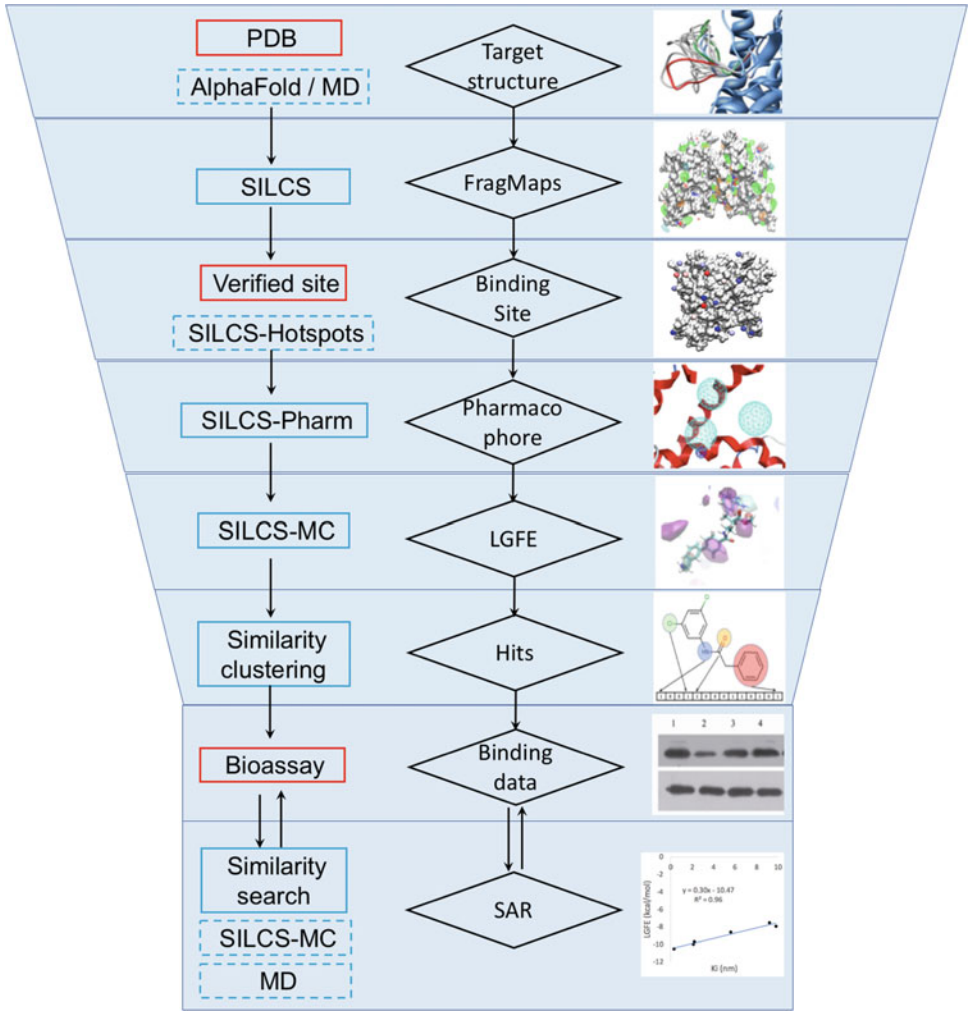

Fig. 1 SILCS oriented CADD workflow developed in our laboratory and used in the CMY-10 project [19]. Wet-lab and CADD techniques are colored in red and blue, respectively. Boxes with solid lines indicate methods used in the CMY-10 study, while boxes with dashed lines mark methods not used in the CMY-10 study but in other studies. Double arrows indicate the two techniques can be used interactively in several iterative drug design rounds

chemically similar analogs and more inhibitory compounds were identified. Such identified non-β-lactam-based β-lactamase inhibitors have the potential to be used in combination therapy with lactam-based antibiotics against multidrug-resistant clinical isolates.

With the fast development of more powerful computing hardware, expensive algorithms such as free energy perturbation methods [23], which can only be used to finely tune the drug candidates at the lead optimization stage, become much more affordable and have been routinely used in a range of applications [24–

26]. Alternative CADD methods based on precomputed ensembles represent novel solutions that interrogate the interactions between low molecular weight solutes and targets are also seeing wider use. Of these cosolvent simulation methods, our laboratory put forward the SILCS methodology, as described previously, and information from SILCS can be utilized in many different ways in various aspects of drug discovery [16–18]. Significant advancements are developments in machine learning (ML), especially deep learning (DL)-based CADD algorithms [27] owing, in part, to the development of artificial intelligence (AI) methods in other areas [28].

ML algorithms are not new to the CADD area, but the increasing need for AI in areas such as image recognition and text processing promotes powerful novel ML algorithms that can handle a vast amount of data [29, 30]. The refined graphic processing unit (GPU) architecture [31] and its growing computing power further accelerate the applications of ML, and its adaptations in CADD have erupted in recent years. This includes quite a lot of antibiotic drug development studies employing ML [32, 33]. For example, Palsson et al. developed an ML workflow for identifying genetic features driving antibiotic resistance [34]. ML models were trained against the resistance profiles of 14 antibiotics across three urgent pathogens using genome sequences as inputs. The ML workflow was verified to be able to generate models not only capable of predicting resistance profiles but also identifying the responsible genes. In another study [35], Collins et al. conducted an antibiotic activity assay screen of near 2300 chemically diverse FDA-approved and natural product compounds targeting *E. coli*. Deep neural network-based DL models were then trained to predict the inhibition probabilities from the chemical structures and properties of tested compounds alone. The resulting DL model was used to screen the Drug Repurposing Hub database [36], and a known c-Jun N-terminal kinase inhibitor SU3327 was predicted to be an antibiotic targeting *E. coli*. This molecule is structurally divergent from conventional antibiotics and was confirmed to display bactericidal activity against a wide phylogenetic spectrum of pathogens, demonstrating how ML can guide antibiotics discovery.

In the rest of this chapter which serves as an update to our first edition, recent progresses in our laboratory toward the development of novel SILCS-based CADD methods will be overviewed. Typical ML method will also be covered. Readers are highly recommended to refer to the first edition of this chapter [4] for basic CADD concepts and classical protocols to gain a fundamental understanding about CADD methods toward antibiotics development.

2 Materials

Similar to other computational sciences, the two basic materials in CADD are the specific hardware and software that are suitable for the current study of interest. The hardware, which refers to the computational resources, can be established locally, for example, computer clusters being purchased and equipped in the working place, or obtained on-the-fly, e.g., computing times applied from public supercomputer resources such as XSEDE [37] or purchased from private companies such as popularized cloud computing on the Amazon Web Services (AWS) or Microsoft Azure cloud platforms [38]. On the other side, software requirements are varied depending on the specific study goals. In the first edition of this book, we introduced fundamental tools for CADD. Here, an update is provided with an emphasis on the common CADD tools used in our laboratory.

1. MD simulation packages such as CHARMM [39], GROMACS [40], NAMD [41], and OpenMM [42], among others, are continually being optimized. Better computational performance is reached through algorithm refinement and software engineering as well as optimized computing using GPUs [41–44]. New MD programs developed in the GPU era are also emerging and get more attentions. For example, ACEMD [45] which was optimized for use on Nvidia GPUs maximizes its performance by running the full computation on GPUs rather than dividing the job between CPUs and GPUs.
2. Target structures are required for the SBDD method and can be downloaded from the Protein Data Bank (PDB) [46] if it has been solved by X-ray crystallography, nuclear magnetic resonance (NMR), or recently matured cryogenic electron microscopy (cryo-EM) techniques [47]. For unsolved protein targets, 3D structures can be predicted using the recently released RoseTTA fold from Baker's group [48] and AlphaFold ML model from the Google DeepMind team, which was verified to have the best accuracy among other protein structure prediction methods [49]. For most proteins, predicted structures using the AlphaFold ML model are available to be downloaded from the server hosted by the European Bioinformatics Institute (https://alphafold.ebi.ac.uk/) [50, 51].
3. Force fields, which are used to estimate the energies and forces within and between molecules, continue to be refined. This includes the CHARMM [52–55] or AMBER [56, 57] families among others to describe both macromolecules, such as the CHARMM36 protein force field [52, 53], and small molecules such as the CHARMM General Force Field (CGenFF) [54, 55]. To automate the creation of the topologies and

parameters for new molecules, program like CGenFF program (see https://cgenff.paramchem.org) [58, 59] can be used. And for experts who want to further optimize force field parameters, a standalone package named FFParam is available for CHARMM force field parametrization [60]. In addition to the additive force fields that have a long history, emerging polarizable force fields such as the CHARMM Drude force field [61, 62] and AMOEBA [63] are now available that treat electronic polarization effects explicitly thereby describing the interactions between molecules more realistically. The increased computational cost introduced by polarization terms (~fourfold over the additive model with the Drude FF) is gradually being overcome by better computing algorithms and growing GPU ability [64, 65]. Accordingly, it may be anticipated that polarizable FFs will see routine use in the near future to describe interactions between antibiotics and bacteria targets in CADD. As a further note, new types of force field based on different perspectives, such as Open Force Field [66, 67] that is coded by direct chemical perception instead of predefined atom types for atoms or driven by ML such as PhysNet [68, 69], which is based on deep neural networks, are also emerging, even though their capabilities need to be thoroughly tested before their broader use in CADD applications.

4. Virtual database screening (VS) is used to screen large chemical libraries to search for potential small molecule binders for a given macromolecule target. CADD methods such as docking [70] or pharmacophore modeling [71] can be adapted for this purpose. For docking, both free software, such as AutoDock Vina [72], and commercial ones such as GOLD [73] are available among others [74]. Open-source toolkits with interface to existing docking software are also available to facilitate a more integrated docking-based CADD cycle. For example, the open drug discovery toolkit (OOTD) [75], which is currently interfaced with AutoDock Vina, offers researcher the ease of conducting the full docking workflow including in silico compound library preparation, library filtering, docking pose rescoring, docking performance evaluation, and SAR model training. Another example is VirtualFlow [76], which has similar functions as OOTD but offers an interface to additional docking programs and is built on an optimized architecture to enable efficient parallelization and balanced workload for a better docking job performance against huge chemical libraries. Web-based docking platforms are also available for a convenient use even for non-experts. For example, Webina [77] offers users the ease of using AutoDock Vina on the web without installation. Another web-based docking interface,

SeamDock [78], allows users to select from four docking codes for their docking needs and also provides the ability to share visualization of docking results with other researchers. For structure-based pharmacophore modeling, the open-source program Pharmer [79] can perform pharmacophore searching efficiently on large databases. It also provides a web interface ZINCPharmer [80] for interactive environment for the virtual screening of the ZINC or Molport databases using pharmacophores, and later the same research group launched another web service called Pharmit [81] for online pharmacophore VS using user-tailored or a variety of pre-loaded databases. It should be noted that, for pharmacophore searching, multiple conformations of each molecule in the database are required as well as assignment of the correct protonation and tautomeric states, with the latter requirement true for all in silico databases used for either docking or pharmacophore screening.

5. VS uses chemical libraries to identify small molecules to be tested in biological assays for ligand discovery. While researchers can resort to in-house compounds based on their own chemical synthesis work, purchasing compounds from commercial chemical vendors is a convenient way to assist the discovery at the early stage. ZINC [82] as well as MolPort [83] provide such platforms for chemical compound sourcing from various vendors. For de novo drug design, exploration of larger chemical space holds the promise for higher success rates in general. The ultra-large REadily AccessibLe (REAL) [84] compound library from Enamine represents the largest purchasable chemical collection currently available. Its REAL database currently contains 4.1 billion enumerated compounds and can be extended to over 20 billion compounds in the Enamine synthetically accessible database called REAL Space, for which compound synthesis time is ~8 weeks from order to delivery with an average of over 80% of the requested compounds actually being synthesized and delivered. As an alternative to de novo drug development, drug repurposing is a lower-cost method which explores existing therapeutics for a new disease indication [85, 86]. For this purpose, the library of FDA-approved drugs can be downloaded from various sources, e.g., as a subset from ZINC [82]. Another comprehensive library of clinical compounds, called Drug Repurposing Hub [36], provides a hand-curated collection of thousands of approved and in-clinic compounds with annotated identities also available.
6. Integrated commercial software such as Discovery Studio [87] and MOE [88], among others, incorporates a broad range of CADD capabilities. On the open-source side, even though quite a lot of choices are available for specific CADD needs,

integrated code is rare. However, commercial packages such as OpenEye [89] offer no cost license for pure noncommercial research, while others provide discounted licensing for academic use. Similarly, the software suite from SilcsBio LLC [90], which offers end-to-end drug design capabilities in the context of the SILCS technology is available at no cost to noncommercial research groups. Online platforms that offer integrated CADD capabilities without the hassle of installing on your local machine and do not require advanced computer knowledge are also emerging. One example is PlayMolecule [91] from Acellera, which offers CADD workflows and covers target preparation, binding site identification, force field parametrization, MD simulation, docking, as well as ML model generation on the cloud. Most of these services are free to the public with some limitations, and full service is also available for purchase. Traditional CADD software companies are also in the transition to offer cloud services, such as OpenEye [89] launched the Orion platform to offer a web-based environment for their software.

3 Methods

In addition to the common methods introduced in the first edition of this chapter [4], additional CADD methods developed recently in our laboratory as well as from other laboratories will be described below.

3.1 Protein Structure Prediction Using AlphaFold

For SBDD, protein 3D structure is required to explore atomic-level details of the ligand-protein interactions. When no protein structure is available from the PDB, structure prediction methods such as homology modeling [92] were used traditionally to generate 3D models. With the surging of AI and related DL techniques, DL-driven structure prediction methods such as RoseTTA fold [48] and AlphaFold [49] can now predict most protein 3D structures to a level of approaching experimental accuracy. In the recent challenging 14th Critical Assessment of protein Structure Prediction (CASP14), AlphaFold was demonstrated to greatly outperform other methods, and its predictions are competitive with experimental structures in a majority of cases. This promising progress makes the initiation of SBDD methods much more feasible. Below are general steps to prepare a protein structure using AlphaFold:

1. Go to the AlphaFold database hosted by the European Molecular Biology Laboratory-European Bioinformatics Institute (EMBL-EBI) at https://alphafold.ebi.ac.uk and input the protein name, gene name, or UniProt accession name in the search

bar. The DeepMind team has already predicted the structures of most known human proteins as well as those of 20 model organisms [50, 51], including bacteria such as *Escherichia coli* and *Staphylococcus aureus*, and deposited them to the EMBL-EBI server.

2. Click on the most relevant entry from the search hit list from the results page if the search is conducted using text other than the UniProt accession ID. On the next page, the predicted 3D structure is displayed with residues colored according to the predicted local distance difference test (pLDDT) metric, and the predicted aligned error (PAE) matrix is also shown.
3. Check the prediction quality by looking at both the pLDDT metric, which is per-residue confidence metric that reflects the local confidence in the structure, and the PAE metric which can be used to assess the confidence in the relative orientation of different parts, e.g., domains, of the model.
4. The predicted structure can then be downloaded in PDB or mmCIF format to users' machine for further analysis. For example, in some cases, the predicted structure covers the full length of the sequence, but the user may want to only focus on a specific domain of the protein for drug design purposes. In such cases, the downloaded structure can be trimmed for subsequent use. For regions with lower pLDDT values, MD simulation can further be conducted to equilibrate and refine the structure.
5. For proteins not yet deposited in the AlphaFold database, the 3D structure can be predicted using the AlphaFold code that may be downloaded from AlphaFold GitHub deposit at https://github.com/deepmind/alphafold/. Follow the README file there to install required environment and load AlphaFold program. Prepare a FASTA file of the sequence of the protein to be predicted and input into the Python script to run the prediction. Following completion of the prediction, the output structures are saved in a subdirectory provided by user via the "--output_dir" flag of using the Python script. It should be noted limitations in the true resolution of the structures from AI prediction methods exist and that these methods do not account for the presence of alternate conformations of the protein (e.g., allosteric states) which need to be considered when using 3D structures generated from these methods [93].

3.2 MD Simulations with Polarizable Force Field

MD simulations model how atoms in a protein or other molecular systems will move over time based on force field description [94] through the integration of Newton's equations of motion. These simulations can capture a wide range of important biomolecular processes such as conformational change and drug binding, where

the dynamics of the systems allows for the inclusion of the entropic contributions to ligand binding to be taken into account as required for calculating free energies. Accordingly, the rich information from MD simulation acts as the foundation for other CADD techniques such as FEP and SILCS developed in our laboratory. Big improvements in simulation speed, accuracy, and accessibility of MD simulation software and environment have increased the utility of MD in CADD. Beyond the classic additive force fields [52–57] currently used in the majority of MD simulations, polarizable force fields that explicitly account for induced electronic polarization represent the next generation of physical models for MD simulations [95–101]. Our laboratory studied the impact of electronic polarizability on protein-fragment interactions using the in-house developed classical Drude oscillator model, showing that the polarizable force field helps to improve the prediction of protein-ligand interactions indicating the utility of a polarizable force field in CADD [102]. The Drude oscillator FF models electronic polarization by attaching a charged particle to the nucleus of each non-hydrogen atom via a harmonic spring and allowing those particles to relax in the surrounding electric field with the nuclear position fixed, as previously described. While the additional terms introduced in the force field associated with the treatment of polarization increase the computational cost, improved algorithms and computational power make this class of simulations accessible [64, 65]. For example, the computational overhead of the Drude FF over the additive CHARMM FF is approximately fourfold [64, 65]. Thus, the Drude as well as other polarizable FFs represent new tools to study molecular systems that will make significant contributions to CADD.

In the first edition of this chapter, we introduced a standard MD simulation protocol. Here we present MD simulation protocol using the Drude polarizable force field:

1. Obtain the protein structure from PDB or predict the protein structure as described above in Subheading 3.1. Prepare the protein structure for MD simulations by adding missing hydrogens, assigning appropriate protonation state of residues, etc. These steps can be performed by a number of the publicly available and commercial modeling packages as discussed above. Generate CHARMM protein structure file (PSF) file for the simulation system based on CHARMM additive force fields using the web tool CHARMM-GUI (http://www.charmm-gui.org) [103] or locally by running the CHARMM code. The CHARMM-GUI may be used for initial protein preparation as well as for the preparation of the PSF and is available to noncommercial users.
2. Go to the CHARMM-GUI at http://www.charmm-gui.org and select Drude Prepper [104], and upload the additive PSF

and coordinate files to construct the Drude force field-based PSF and PDB files with added Drude particles and lone pairs. Also provided are the CHARMM input files for subsequent calculations listed below and the needed topology and parameter files. In addition, the user may request input files compatible with MD programs such as OpenMM and NAMD that support the Drude FF.

3. Similar to the protocol previously described for the additive FF [4], the system will go through minimization, equilibration, and production steps. During minimization, Drude particles will be minimized first and then the entire system using the adopted-basis Newton-Raphson (ABNR) minimizer.
4. For equilibration and production runs, a hard wall restraint of 0.2 Å between the parent atom and the Drude particle is applied to prevent instability and large displacements of Drude particles. The hard wall is designed to avoid polarization catastrophe that may occur due to low-frequency close interactions between atoms during the MD simulation leading to over polarization [105]. During Drude simulations, the extended Lagrangian dynamics scheme [106] for integration of Newton's equations of motion is used where the real atoms and the Drude particles are coupled to a dual thermostat responsible for uniting their dynamics. The physical and Drude thermostats are maintained at different temperatures of 298 K and 1 K with friction coefficients of 5 ps^{-1} and 20 ps^{-1}, respectively. Drude simulations are typically propagated with a 1 fs time step.
5. Analysis of Drude simulations, beyond that used for all MD simulations, can include variations in the dipole moments of various groups in the systems being studied. This allows for an understanding of how variations in the electronic structure of the system associated with the explicit inclusion of polarizability are impacting the properties of the system. When calculating dipole moments, care must be taken as the dipole is not spatially invariant when the sum of the charges is not zero. To account for this and facilitate dipole analysis with the Drude FF, the sum of the charges on all particles are integers (e.g., on protein side chains and nucleic acid bases) though the spatial orientations of charged groups must still be considered.

3.3 Docking Using SILCS-MC and ML-Based Reweighting for SAR

Docking is a useful CADD tool to predict binding orientation of a ligand molecule within target binding site as well as to evaluate its binding strength [70]. Traditional docking methods only consider rigid or limited protein flexibility and ignore or treat the contribution of desolvation to binding in an empirical way. While FEP and molecular mechanics (MM) with Poisson-Boltzmann (PB) and surface area solvation (MM/PBSA) as well as MM/generalized-Born

SA (GBSA) methods [107] do account desolvation, these are computational demanding approaches that limit their utility in CADD. A novel method designed to overcome this drawback is the SILCS-MC [19] docking method put forward by our laboratory. SILCS-MC conducts ligand sampling within the GFE FragMap free energy grids from SILCS. This takes advantage of the use of GCMC/MD simulations of the protein in an aqueous solution with selected organic solutes to precompute the GFE FragMaps that are free energy functional group affinity patterns that encompass the entire protein and account for protein flexibility and desolvation contributions [108–110]. SILCS-MC then involves simply assigning the GFE value for the appropriate FragMap type to each atom in the molecule and summing those values to get the LGFE score. MC conformational sampling is then performed to allow the orientation and conformation of the ligands to relax in the field of the GFE FragMaps. This allows for SILCS-MC docking to be performed in a highly computationally efficient fashion while achieving a level of accuracy similar to highly expensive FEP methods [109]. The SILCS method was fully described in the first edition of this chapter [4]. Below we present the SILCS-MC docking protocol assuming the user has already run the SILCS simulations and obtained the GFE FragMaps. A Bayesian ML-based reweighting protocol is also described for improving the predictability of the SILCS method that can be applied when experimental data on a small set of ligands (ten or more) is available [108]:

1. Prepare molecule coordinate files for ligands to be docked in either mol2 or sdf format. For mol2 format, each mol2 file contains a single molecule, while for sdf format, multiple molecule entries are allowed in a single sdf file by the current SILCS-MC code.
2. Select an atom classification scheme (ACS) for the SILCS-MC run. When performing SILCS-MC, GFE is evaluated for each atom in the molecule with an assigned type that overlapped with SILCS FragMaps of the same type. ACS controls the assignment of FragMap types to each atom in a molecule based on their CGenFF atom type and chemical connectivity during the initiation of a SILCS-MC run. Typical ACS includes generic and specific types. Generic ACS has more general FragMap types, e.g., both aromatic and aliphatic carbon atoms in a molecule will be assigned with generic nonpolar GENN FragMap type, while specific ACS has specific FragMap types being assigned to specific atoms, e.g., aromatic carbon atom has BENC (benzene carbons) FragMap type, while aliphatic carbon gets PRPC (propane carbons) type. The generic ACS is the default method.

3. Choose a MC sampling protocol for the SILCS-MC run. Ligand binding poses are sampled using Metropolis MC sampling and followed by simulated annealing (SA) during a SILCS-MC run. Thus, MC/SA parameters such as simulation cycles (n_{CY}) and steps (n_{MC}/n_{SA}) as well as range of global rotational ($d\theta$), translational (dX), and intramolecular dihedral ($d\varphi$) degrees of freedom can be adjusted depending on the specific system. Typical protocols include local and exhaustive types even though users can customize their own protocol by changing corresponding parameters in the SILCS-MC input file. Local MC is designed for pose refinement and the sampling starts from the user supplied pose with limited conformational sampling with $n_{CY} = 10$, $n_{MC} = 100$, dX = 0.5 Å, $d\theta = 15°$, $d\varphi = 45°$, and $n_{SA} = 1000$. An exhaustive protocol is designed for full docking of the ligand orientation and conformation in a given pocket to determine its most favorable orientation when no initial binding information is available from experiment. It starts with a randomized orientation for the ligand within a sphere with user-defined center and radius. MC sampling is performed to allow for larger conformational changes with $n_{CY} = 250$, $n_{MC} = 10{,}000$, dX = 1 Å, $d\theta = 180°$, $d\varphi = 180°$, and $n_{SA} = 40{,}000$. For both local and exhaustive sampling, SA steps following MC in each cycle adapt parameters as dX = 0.2 Å, $d\theta = 9°$, and $d\varphi = 9°$.
4. Run SILCS-MC simulations using the SILCS-MC code with the ACS file, the CGenFF rules and parameter files, the GFE FragMap files, exclusion map file, and user-defined parameters. CGenFF parameters are initially assigned to the ligand powered by the CGenFF engine to allow for energy minimization of the ligand during initiation of SILCS-MC simulation and used to calculate intramolecular energy during the MC calculation. The exclusion map represents the forbidden region of the protein not sampled by the solutes or water non-hydrogen atoms during the SILCS simulation and used as a penalty score to guide the sampling. Usually, five independent SILCS-MC runs are conducted in parallel to expediate the convergence of the docking results. In each run, after a minimum of 50 MC/SA cycles, if the lowest three LGFE scores are within 0.5 kcal/mol, the run will be considered converged and terminated. Otherwise, cycles will continue either until the convergence criterion is met or until the user-defined maximum MC/SA cycles, 250 by default, have been reached.
5. After the SILCS-MC simulations are finished, the docking pose with the lowest LGFE score can be extracted and used as the predicted binding orientation for the ligand. The docking pose can be visualized together with the protein structure and FragMaps and analyzed. One advantage of SILCS-MC over

traditional docking methods is the ease of decomposition of total docking score into atomic contributions which are especially useful during the ligand optimization step [111, 112]. Atomic GFE values can be visually checked for a ligand to determine beneficial and unsatisfactory functional groups. For example, when modifying a ligand, favorable gains associated with the modification may be offset by a loss of favorable contributions in another part of the molecule, information that is not readily accessible to other CADD docking methods [109]. In addition, visualization of FragMaps around the docking pose of a ligand can also offer ideas about additional functional groups that may be introduced to the current scaffold to further improve affinity.

6. SILCS Bayesian ML reweighting: When experimental binding data is available, LGFE scores can be trained using ML for a refined prediction yielding a more accurate SAR model. The LGFE is a simple summation over all atomic GFE contributions from different FragMap types, assuming the contribution from each FragMap type is well balanced when fragments form a full molecule. In practice, this represents an approximation since the sum of binding affinities of individual fragments in a molecule does not formally equal the binding affinity of the full molecule due to the energy adjustment through linking fragments into a molecule. Accordingly, the GFE FragMap contributions in LGFE can be reweighted based on experimental binding data to improve the predictability of SILCS-MC. This is done by using a Bayesian Markov-Chain Monte Carlo-based ML (BML) method [108].
7. To start the reweighting BML process, experimental data and SILCS-MC docking poses in PDB format are required. The ML training can be conducted by optimizing the root-mean-square deviation (RMSD), Pearson correlation, or percent correct (true positives and true negatives) metrics between the LGFE and experimental binding free energies. The user can also select from three restraint types such as flat-bottom, hard wall, and harmonic to prevent over-fitting problem. Running the BML code will yield trained weighting factors for each FragMap type and estimated prediction improvement based on the current docking poses. The optimized weighting factors of the FragMaps are then used to redo the SILCS-MC run to verify the real improvement. The new LGFE score formula with trained reweighting factors can then be used for new ligand designs for the current protein target. In cases where overfitting of the weighting factors occurs, the resulting docking poses and LGFE scores from the second SILCS-MC run get highly perturbed and in poorer agreement with experiment, respectively, allowing for a check on the applied BML fitting parameters.

3.4 Binding Site Identification Using SILCS-Hotspots

Computational binding site identification methods can be used to exploit novel, druggable sites on new protein targets for potential therapeutic development [113]. For antibiotics development, such methods can be employed to search for putative allosteric sites as alternatives to the active or orthosteric sites on bacterial proteins to overcome drug resistance issues [114]. A binding site identification method under the SILCS framework, named SILCS-Hotspots, was developed recently by our laboratory [115]. SILCS-Hotspots is designed to identify fragment binding hotspots that are spatially distributed across the global protein structure including both surface and interior binding sites. The general protocol using SILCS-Hotspots to identify putative binding sites on a protein is described as the following. The protocol requires that the SILCS FragMaps are already available:

1. Select a collection of representative molecular fragments to be used for the hotspots search. The Astex MiniFrag set [116] and the collection of ~90 mono- and bicyclic rings present in drug molecules [117] are both good fragment libraries to be used.
2. Partition the protein system into a set of overlapping 14.14 $Å^3$ subspaces that encompass the entire protein. For each individual sampling box, exhaustive SILCS-MC as described in Subheading 3.3 is conducted for every fragment in the library. All SILCS-MC docking poses that are sampled over the full space are collected for each fragment. Fragment docking poses with LGFE scores of −2 kcal/mol or more favorable and within 6 Å of any protein Cα atoms are selected as relevant binding poses and subjected to the following clustering steps.
3. For each fragment, a center-of-mass (COM)-based clustering with 3 Å cluster radius is performed. Clustering determines the number of neighbors within a 3 Å radius of COM of each docking pose and then identifies the pose with the largest number of neighbors. The remaining cluster members are then removed from the pool of docking poses with the process continued until no additional poses remain. This step selects presentative docking poses for each fragment.
4. A second round of clustering is conducted over docking poses of all fragments obtained from the first round of clustering. The same clustering algorithm is used but with a radius of 4 Å, from which clusters that contain representative docking poses for one or more fragments are identified. These cluster centers are defined as Hotspots. Information on the hotspots include the number and types of fragments in the site, the LGFE scores of all fragments, and their spatial relationships. Hotspot ranking may then be performed based on the average LGFE scores or the number of fragments in a site.

5. As previously discussed, top ranking sites based on quantitative criteria do not always correspond to known binding sites of drug-like molecules including allosteric modulators [115]. Rather, visual inspection of the hotspots is undertaken to identify those in which two or more hotspots are adjacent to each other as required to covalently link fragments occupying each site to create drug-like molecules. This qualitative selection of sites is facilitated by analysis of the SILCS FragMaps to identify sites with apolar characteristics indicative of hydrophobic forces driving binding, along with FragMaps representative of polar groups. In addition, analysis of the SILCS exclusion map allows the for identification of regions of the protein that open between Hotspots, allowing for chemically linking fragments in those sites that is not evident from analysis of the solvent accessible surface.

   Figure 2 shows an example of representative sites from this qualitative selection process for the bacterial enzyme TEM-1 beta-lactamase [118, 119]. Evident is that the sites contain favorable hotspots including the presence of apolar FragMaps (green), as such interactions are important to drive ligand affinity, along with multiple polar FragMaps such as H-bond donor and acceptor types that can contribute to specificity (e.g., sites 1–3 in Fig. 2). All the qualitatively selected sites can be further evaluated quantitatively.

6. Quantitative evaluation may be performed through exhaustive SILCS-MC docking on each selected site using a library of drug molecules, for example, FDA-approved drugs. In house, ~380 chemically diverse FDA-approved compounds were constructed for this purpose. Exhaustive SILCS-MC docking is performed with the center of each site defined based on the central hotspot along with a 5 Å radius; the process may be repeated with each hotspot within an interesting site as the center of the docking region. For each site, the average LGFE scores of the top-ranked 25 FDA compounds based on the LGFE scores are obtained along with the percent relative solvent accessible surface area (rSASA%) [120]. The rSASA% is calculated using the solvent accessibility of each ligand in the presence and absence of the protein. Free software such as FreeSASA can be used for such a calculation [121]. The combination of these metrics is then used to quantify the binding sites with ideal sites giving highly favorable LGFE scores (<-10 kcal/mol) and small rSASA% ($<40\%$) which indicate they are suitable for binding drug-like molecules. For example, Fig. 2 shows that sites 1 and 2 have more favorable LGFEs than site 3 and both those sites have reasonable rSASA% around 30% compared to site 3 (~50%). Thus sites 1 and 2 are predicted to be putative binding sites over site 3. Experimental

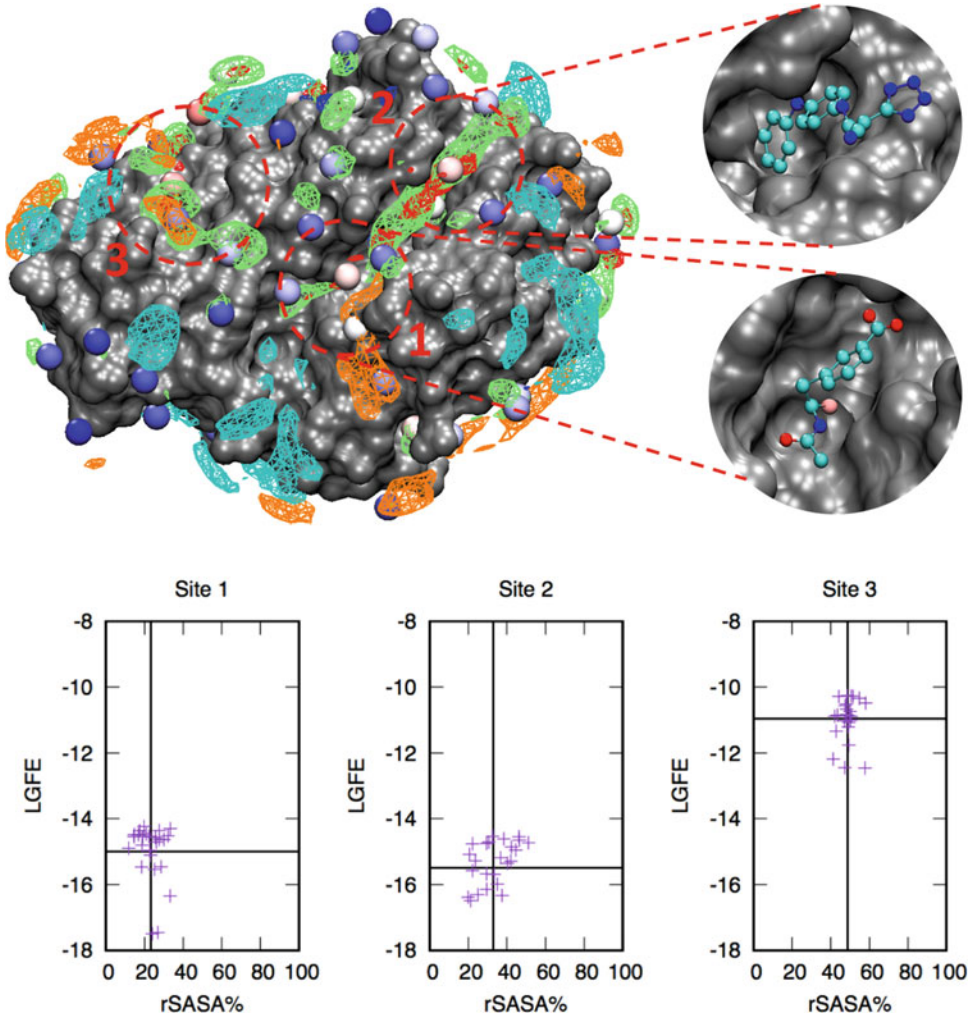

Fig. 2 SILCS-Hotspots analysis for the bacterial enzyme TEM-1 beta-lactamase using the Astex MiniFrag set. SILCS apolar (green), H-bond donor (blue), and H-bond acceptor (red). FragMaps are rendered at −1.0 kcal/mol, while positively charged (cyan) and negatively charged (orange) FragMaps are rendered at −1.2 kcal/mol. Hotspots are shown as spheres with average LGFE colored in red-white-blue (more to less favorable) scale. Putative binding sites selected based on adjacent hotspots, FragMaps, and exclusion maps are shown in red dashed circles. Crystal binding modes of an active site (PDB:1ERM) [118] and an allosteric site (PDB:1PZP) [119] binder are shown. rSASA% vs LGFE plots are shown in the lower panel for top 25 LGFE-ranked FDA compounds for all three sites with average values indicated as vertical and horizon lines

crystal complex structures confirmed this with site 1 being the active site and site 2 serving as an allosteric site for TEM-1 beta-lactamase.

3.5 Membrane Permeation Prediction Using SILCS

Most antibiotics were designed to target proteins involved in intracellular processes; thus the outer membrane of bacteria needs to be penetrated for antibiotics to function. Drug resistance involving

modifications of macromolecules in the outer membrane is a common issue that needs to be considered when searching for new antibiotics [122, 123]. While bacterial membranes are complex environments with multiple transport and pore proteins, it is of utility to estimate the pure membrane permeability of drug candidates during drug discovery as this may contribute to drug bioavailability. Traditionally, potential of mean force (PMF) free energy profiles for a compound across membrane lipid bilayers are derived using MD simulations [124]. The PMF may then be used together with position-specific diffusion coefficient in the inhomogeneous solubility-diffusion equation [125] to derive effective resistivity, which may be inverted into permeability. Under the SILCS framework, we recently put forward a protocol to calculate the permeation-related resistant coefficient of a molecule to cross membranes [126] using LGFE energy profile and is described in the following:

1. Set up the membrane lipid bilayer system. This can be a bilayer system with lipopolysaccharide composition that is specific for the bacteria outer membrane of interest [127] or just a bilayer model. Examples include pure 1,2-dipalmitoyl-*sn*-glycero-3-phosphocholine (DPPC), a (0.9:0.1) 1-palmitoyl-2-oleoyl-*sn*-glycero-3-phosphocholine (POPC)/cholesterol mixture or a (0.52:0.18:0.3) 1,2-dioleoyl-*sn*-glycero-3-phosphocholine (DOPC)/1,2-dioleoyl-*sn*-glycero-3-phospho-l-serine (DOPS)/cholesterol composition that mimics the lipid mixture used in a parallel artificial membrane permeability assay (PAMPA) experimental study [128]. The membrane builder functionality [129] in CHARMM-GUI is a very convenient tool to set up such lipid bilayer systems. Minimization and short MD simulation can be conducted to further stabilize the lipid bilayer model using protocol and inputs supplied by the CHARMM-GUI.
2. Perform the standard SILCS simulation on the lipid bilayer system and generate the GFE FragMaps.
3. Calculate the LGFE profile for drug-like ligands across the lipid bilayer. Run SILCS-MC for the ligand along the normal Z to the bilayer with 1 Å increments covering the full bilayer system including both the lipid and water phases. At each Z position, SILCS-MC is performed under exhaustive mode as described in Subheading 3.3 except for that the ligand COM is only allowed to vary by 1 Å maximum from the assigned Z value during MC sampling. SILCS-MC simulation can be conducted at multiple different (X,Y) positions along the plane of the bilayer to ensure proper samplings. LGFE profile is constructed at each (X,Y) position along Z, and multiple energy profiles are averaged over different (X,Y) positions to get the final LGFE profile with standard deviation being evaluated.

4. Use the LGFE energy profile G(z) along Z axis to calculate permeation-related resistant factor R. The effective membrane permeability P_{eff} can be calculated from the effective resistivity R_{eff} through equation: $1/P_{eff} = R_{eff} = \int_h R(z)dz.$, where h is the bilayer thickness, and resistivity R(z) at position z is defined as: $R(z) = e^{\beta(\Delta G(z))}/D(z)$, where D(z) is the position-specific diffusion coefficient at position z and $\Delta G(z) = G(z)\text{-}G_{ref}$. Here, G(z) is the LGFE profile as a function of z, and G_{ref} is the reference-free energy in the water phase that can be calculated from the average LGFE over the water phase. $\beta = 1/k_BT$, where k_B is the Boltzmann constant and T is the absolute temperature. In the current protocol, D(z) is not calculated and is assumed to be a constant D so that $1/P_{eff} = R/D$ where $R = \int_h e^{\beta(\Delta G(z))}dz$ will be calculated as the resistant coefficient.

3.6 Protein-Protein Interaction Prediction Using SILCS-PPI

Protein-protein interactions (PPIs) are involved in a tremendous amount of vital cellular processes in bacteria and can serve as novel antibiotic targets [130, 131]. Efforts toward the inhibition of PPIs related to division and replication, transcription, outer membrane protein complexes, as well as toxin-antitoxin systems in bacteria are ongoing [132]. Thus, PPI prediction is of utility to identify novel druggable PPI interfaces in bacterial proteins and pave the way toward novel antibiotic therapeutics. Traditional PPI prediction methods are mostly based on rigid protein structures with limited flexibility considerations [133]. Using the GFE FragMap and protein residue occupancy distributions, or protein probability grids (PPG), calculated from SILCS, a PPI prediction method named SILCS-PPI was put forward in our laboratory [134]. It uses SILCS FragMaps and PPG from both proteins involved in a PPI which have flexibility considerations intrinsically embedded in them together with fast Fourier transforms (FFT)-enhanced sampling to sample a comprehensive set of PPI interaction orientations that are then ranked based on the overlap of the FragMaps and PPG of the protein partners. The general SILCS-PPI protocol is described as the following and requires that the SILCS FragMaps and PPG for both proteins are already available:

1. Run SILCS-PPI prediction using both FragMaps and PPGs as well as exclusion maps from both proteins. During the run, FragMaps from the ligand protein will be spatially operated to match PPGs from the receptor protein and vice visa. To expedite the process, unique rigid body rotations [135] are considered for the ligand protein, and for each rotation, FFT is used to calculate PPI scores for all global translations in one go. The final SILCS-PPI score is obtained by summing overall ligand FragMap-receptor PPG scores and receptor FragMap-ligand

PPG scores of all types as well as an exclusion score calculated from the correlation of exclusion maps from the two proteins which serve as an alternative shape complementary score.

2. Save top-ranked solutions (global translation and rotation parameters) and construct PPI complex coordinates. Then two-pass clustering is used to cluster all complex models. In the first step, COM-based clustering is conducted to put all models whose COM distances are within 6 Å into the same cluster. Next, a second orientation-based clustering is performed using an angular distance metric that preserves periodicity [136]. The distance cutoff is set to 0.5, which corresponds to about 30° in an angle. After the two-pass clustering, the best scoring pose from each cluster is saved for further evaluation.
3. COM of top-ranked solutions can be visualized on the surfaces of both ligand and receptor proteins and colored by SILCS-PPI scores to help interpret the predicted PPI interfaces. The populations of COMs on the protein surface can be used to predict alternative PPI sites. In addition, the PDB coordinates of the PPI complexes may be accessed, though they are based on the rigid crystal structures used to initiate the SILCS-PPI calculation such that there will typically be steric overlap between the two proteins that require careful relaxation of the structures prior to MD simulations.

3.7 Biologic Formulation Using SILCS

Besides efforts to develop small molecule antibiotics to counteract the evolving drug resistance of bacteria, researchers are also applying biologic-based drugs such as monoclonal antibodies (mAbs) in the battle [137–140]. Biomacromolecular therapeutics, or so-called biologics, need to be carefully formulated to maximize protein stability and minimize viscosity, so as to ensure both efficacy and safety for highly concentrated formulations [141]. Toward maximizing stability, biologics can be formulated with excipients to help minimize aggregation and denaturation of the biologic in a solution formulation [142]. To assist the rational selection of excipients for biologics, we developed the SILCS-Biologics protocol [143, 144] which combines SILCS-PPI and SILCS-Hotspots as described above to predict both PPIs that can contribute to protein aggregation and increased viscosity and binding sites of excipients. This information is then combined to build a model for protein stability, aggregation, and viscosity prediction. Basic protocol is shown in the following:

1. Run SILCS simulation on the biologic protein and generate both FragMaps and PPGs as described in Subheading 3.6.
2. Predict PPI sites using SILCS-PPI as described in Subheading 3.6. Instead of two proteins, here the SILCS-PPI calculation is conducted against the same set of FragMaps and PPGs from

the single protein. After the two-pass clustering in SILCS-PPI, all selected poses are used to calculate a per-residue PPI preference value (PPIP) by counting the number of contacts between the receptor and ligand (the same protein) atoms within a 5 Å cutoff over all poses and normalized by the maximum PPIP value to get the final PPIP score for all residues that contribute PPI. Such PPIP score suggests the likelihood of a residue being involved in a PPI that may lead to aggregation or increase viscosity.

3. Run SILCS-Hotspots to map excipient binding sites on the biologic protein. The user can choose a collection of excipient molecules desired for the formulation. In our in-house tests [143], amino acid and sugar excipient molecules used include alanine, arginine, aspartate, citrate, glucose, glutamate, glycine, histidine, lactate, lysine, malate, mannitol, phosphate, proline, sorbitol, succinate, sucrose, threonine, trehalose, and valine. This list may be easily altered or extended as needed.
4. Combine the calculated PPIP from step 2 and excipient binding site profiles from step 3 to investigate the potential effect of excipient molecules on biologic protein aggregation. For example, the number of excipient binding sites that satisfy a range of PPIP and energy criteria may be selected. These may then be partitioned into the number of sites involving individual excipients. In addition to LGFE, ligand efficiency (LE), which is defined as LGFE divided by number of non-hydrogen atoms in a molecule, is also employed to rank excipients since it is independent of the size of the excipient molecules. In a study on the NIST mAb, it was found that a criterion defined as number of excipient binding sites that have average LE < -0.25 kcal/mol and PPIP >0.1, correlates well with experimental viscosity profile in general [143]. Such criterion has the ability to indicate the strength of excipient to prevent aggregation since it incorporates information about favorable excipient binding (more negative LE) against more likely aggregation-involved regions (higher PPIP). In practice, user can try different criteria using PPIP, LGFE, and LE metrics for biologic protein of interest and even build a regression model using these metrics if there is experimental aggregation-related data available. We note that given the challenges associated with biologic formulations, it is likely that different criteria will be required for different proteins, even with different mAb molecules of the same class.

4 Notes

1. For protein structure prediction using AlphaFold, regions with low pLDDT values are often intrinsically disordered regions [50], which are generally not suitable for drug targeting purposes. The intrinsically disordered regions are often presented as extended polypeptide regions in the predicted 3D structures. If a well-structured region in your model has low pLDDT values, this then might indicate that the quality of the model is questionable and needs to be examined.
2. Docking pose of a ligand from a SILCS-MC run can have clashes with the protein structure that is used to initialize the SILCS simulation. This is because SILCS-MC docking uses SILCS FragMaps that incorporate the protein flexibility during the MD simulation. An alternative is to visualize the docking pose with the SILCS exclusion map which can serve as a flexibility accounting alternative to the protein surface representation based on a single rigid protein structure. To present the SILCS-MC docking pose in a classic protein-ligand interaction representation fashion, it is also practical to extract protein structures from the SILCS simulation that have no clashes with the pose to present the result. Finally, when combining the SILCS-MC predicted ligand orientation with the protein structure used to initiate the simulation or one extracted from the SILCS simulations, it is important to perform careful relaxation of the protein around the ligand prior to the production of MD simulations.
3. In the current version of SILCS-PPI, only protein structures that used to initialize SILCS simulations are used to construct PPI complex coordinates. In practice, representative protein structures from SILCS simulations can be extracted for model construction purposes, and minimization with short-time MD simulation is also desired to further refine the complex model for a better PPI representation.

Acknowledgments

This work was supported by NIH grants R35GM131710 (AM), GM129327 (DW), AI152397 (DW), the University of Maryland Center for Biomolecular Therapeutics (CBT), the Samuel Waxman Cancer Research Foundation, and the Computer-Aided Drug Design (CADD) Center at the University of Maryland, Baltimore.

Conflict of Interest A.D.M. is co-founder and CSO of SilcsBio LLC.

References

1. Blaskovich MAT (2020) Antibiotics special issue: challenges and opportunities in antibiotic discovery and development. ACS Infect Dis 6:1286–1288
2. Ribeiro da Cunha B, Fonseca LP, Calado CRC (2019) Antibiotic discovery: where have we come from, where do we go? Antibiotics 8:45
3. Yu W, Guvench O, MacKerell AD (2013) Computational approaches for the design of protein–protein interaction inhibitors. In: Zinzalla G (ed) Understanding and exploiting protein–protein interactions as drug targets. Future Science Ltd., London, pp 99–102
4. Yu W, MacKerell AD (2017) Computer-aided drug design method. In: Sass P (ed) Antibiotics methods and protocols. Methods in Molecular Biology. Springer Science+Business Media, New York, pp 85–106
5. Krebs FS, Esque J, Stote RH (2019) A computational study of the molecular basis of antibiotic resistance in a DXR mutant. J Comput Aided Mol Des 33:927–940
6. Li J, Beuerman R, Verma CS (2020) Dissecting the molecular mechanism of colistin resistance in *mcr*-1 bacteria. J Chem Inf Model 60: 4975–4984
7. Liu Y, Wang Y, Walsh TR, Yi L, Zhang R, Spencer J, Doi Y, Tian G, Dong B, Huang X, Yu L, Gu D, Ren H, Chen X, Lv L, He D, Zhou H, Liang Z, Liu J, Shen J (2016) Emergence of plasmid-mediated colistin resistance mechanism MCR-1 in animals and human beings in China: a microbiological and molecular biological study. Lancet Infect Dis 16:161–168
8. O'Neill MJ, Wilks A (2013) The P. aeruginosa Heme binding protein PhuS is a Heme oxygenase titratable regulator of Heme uptake. ACS Chem Biol 8:1794–1802
9. Nguyen AT, O'Neill MJ, Watts AM, Robson CL, Lamont IL, Wilks A, Oglesby-Sherrouse AG (2014) Adaptation of iron homeostasis pathways by a Pseudomonas aeruginosa Pyoverdine mutant in the cystic fibrosis lung. J Bacteriol 196:2265–2276
10. Liang D, Robinson E, Hom K, Yu W, Nguyen N, Li Y, Zong Q, Wilks A, Xue F (2018) Structure-based design and biological evaluation of inhibitors of the pseudomonas aeruginosa heme oxygenase (pa-HemO). Bioorg Med Chem Lett 28:1024–1029
11. Xu X, Godoy-Ruiz R, Adipietro KA, Peralta C, Ben-Hail D, Varney KM, Cook ME, Roth BM, Wilder PT, Cleveland T, Grishaev A, Neu HM, Michel SL, Yu W, Beckett D, Rustandi RR, Lancaster C, Loughney JW, Kristopeit A, Christanti S, Olson JW, MacKerell AD, Des Georges A, Pozharski E, Weber DJ (2020) Structure of the cell-binding component of the *Clostridium difficile* binary toxin reveals a di-heptamer macromolecular assembly. Proc Natl Acad Sci U S A 117:1049–1058
12. Varney KM, Bonvin AMJJ, Pazgier M, Malin J, Yu W, Ateh E, Oashi T, Lu W, Huang J, Diepeveen-de Buin M, Bryant J, Breukink E, MacKerell AD, de Leeuw EPH (2013) Turning defense into offense: Defensin mimetics as novel antibiotics targeting lipid II. PLoS Pathog 9:e1003732
13. Fletcher S, Yu W, Huang J, Kwasny SM, Chauhan J, Opperman TJ, MacKerell AD, de Leeuw EPH (2015) Structure-activity exploration of a small-molecule lipid II inhibitor. Drug Des Devel Ther 9:2383–2394
14. Chauhan J, Yu W, Cardinale S, Opperman TJ, MacKerell AD, Fletcher S, de Leeuw EPH (2020) Optimization of a Benzothiazole Indolene scaffold targeting bacterial cell wall assembly. Drug Des Devel Ther 14:567–574
15. Tooke CL, Hinchliffe P, Bragginton EC, Colenso CK, Hirvonen VHA, Takebayashi Y, Spencer J (2019) β-Lactamases and β-lactamase inhibitors in the 21st century. J Mol Biol 431:3472–3500
16. Guvench O, MacKerell AD (2009) Computational fragment-based binding site identification by ligand competitive saturation. PLoS Comput Biol 5:e1000435
17. Raman EP, Yu W, Guvench O, MacKerell AD (2011) Reproducing crystal binding modes of ligand functional groups using site-identification by ligand competitive saturation (SILCS) simulations. J Chem Inf Model 51: 877–896
18. Raman EP, Yu W, Lakkaraju SK, MacKerell AD (2013) Inclusion of multiple fragment types in the site identification by ligand competitive saturation (SILCS) approach. J Chem Inf Model 53:3384–3398
19. Parvaiz N, Ahmad F, Yu W, MacKerell AD, Azam SS (2021) Discovery of beta-lactamase CMY-10 inhibitors for combination therapy against multi-drug resistant Enterobacteriaceae. PLoS One 16:e0244967
20. Faller C, Raman EP, MacKerell AD, Guvench O (2015) Site identification by ligand competitive saturation (SILCS) simulations for fragment-based drug design. In: Klon AE

(ed) Fragment-based methods in drug discovery. Springer, New York, pp 75–87

21. Yu W, Lakkaraju S, Raman EP, MacKerell AD (2014) Site-identification by ligand competitive saturation (SILCS) assisted pharmacophore modeling. J Comput Aided Mol Des 28:491–507
22. Yu W, Lakkaraju SK, Raman EP, Fang L, MacKerell AD (2015) Pharmacophore modeling using site-identification by ligand competitive saturation (SILCS) with multiple probe molecules. J Chem Inf Model 55:407–420
23. Abel R, Wang L, Harder ED, Berne BJ, Friesner RA (2017) Advancing drug discovery through enhanced free energy calculations. Acc Chem Res 50:1625–1632
24. King E, Aitchison E, Li H, Luo R (2021) Recent developments in free energy calculations for drug discovery. Front Mol Biosci 8: 712085
25. Chen J, Wang X, Pang L, Zhang JZH, Zhu T (2019) Effect of mutations on binding of ligands to guanine riboswitch probed by free energy perturbation and molecular dynamics simulations. Nucleic Acids Res 47:6618–6631
26. Fowler PW (2020) How quickly can we predict trimethoprim resistance using alchemical free energy methods? Interface Focus 10: 20190141
27. Vamathevan J, Clark D, Czodrowski P, Dunham I, Ferran E, Lee G, Li B, Madabhushi A, Shah P, Spitzer M, Zhao S (2019) Applications of machine learning in drug discovery and development. Nat Rev Drug Discov 18:463–477
28. Jackson PC (2019) Introduction to artificial intelligence: third edition. Dover Publications Inc, Mineola, New York
29. Hosny A, Parmar C, Quackenbush J, Schwartz LH, Aerts HJWL (2018) Artificial intelligence in radiology. Nat Rev Cancer 18: 500–510
30. Manning CD (2015) Computational linguistics and deep learning. Comput Linguist 41: 701–707
31. Owens JD, Houston M, Luebke D, Green S, Stone JE, Phillips JC (2008) GPU computing. Proc IEEE 96:879–899
32. Melo MCR, Maasch JRMA, de la Fuente-Nunez C (2021) Accelerating antibiotic discovery through artificial intelligence. Commun Biol 4:1050
33. Anahtar MN, Yang JH, Kanjilal S (2021) Applications of machine learning to the problem of antimicrobial resistance: an emerging model for translational research. J Clin Microbiol 59:e01260–e01220
34. Hyun JC, Kavvas ES, Monk JM, Palsson BO (2020) Machine learning with random subspace ensembles identifies antimicrobial resistance determinants from pan-genomes of three pathogens. PLoS Comput Biol 16: e1007608
35. Stokes JM, Yang K, Swanson K, Jin W, Cubillos-Ruiz A, Donghia NM, MacNair CR, French S, Carfrae LA, Bloom-Ackerman-Z, Tran VM, Chiappino-Pepe A, Badran AH, Andrews IW, Chory EJ, Church GM, Brown ED, Jaakkola TS, Barzilay R, Collins JJ (2020) A deep learning approach to antibiotic discovery. Cell 180:688–702
36. Corsello SM, Bittker JA, Liu Z, Gould J, McCarren P, Hirschman JE, Johnston SE, Vrcic A, Wong B, Khan M, Asiedu J, Narayan R, Mader CC, Subramanian A, Golub TR (2017) The drug repurposing hub: a next-generation drug library and information resource. Nat Med 23:405–408
37. Towns J, Cockerill T, Dahan M, Foster I, Gaither K, Grimshaw A, Hazlewood V, Lathrop S, Lifka D, Peterson GD, Roskies R, Scott JR, Wilkins-Diehr N (2014) XSEDE: accelerating scientific discovery. Comput Sci Eng 16:62–74
38. Kotas C, Naughton T, Imam N (2018) A comparison of Amazon Web Services and Microsoft Azure cloud platforms for high performance computing. 2018 IEEE International Conference on Consumer Electronics (ICCE), pp 1–4
39. Brooks BR, Brooks CL, Mackerell AD, Nilsson L, Petrella RJ, Roux B, Won Y, Archontis G, Bartels C, Boresch S, Caflisch A, Caves L, Cui Q, Dinner AR, Feig M, Fischer S, Gao J, Hodoscek M, Im W, Kuczera K, Lazaridis T, Ma J, Ovchinnikov V, Paci E, Pastor RW, Post CB, Pu JZ, Schaefer M, Tidor B, Venable RM, Woodcock HL, Wu X, Yang W, York DM, Karplus M (2009) CHARMM: the biomolecular simulation program. J Comput Chem 30: 1545–1614
40. Van Der Spoel D, Lindahl E, Hess B, Groenhof G, Mark AE, Berendsen HJC (2005) GROMACS: fast flexible and free. J Comput Chem 26:1701–1718
41. Phillips JC, Hardy DJ, Maia JD, Stone JE, Ribeiro JV, Bernardi RC, Buch R, Fiorin G, Hénin J, Jiang W, McGreevy R (2020) Scalable molecular dynamics on CPU and GPU architectures with NAMD. J Chem Phys 153: 044130

42. Eastman P, Swails J, Chodera JD, McGibbon RT, Zhao Y, Beauchamp KA, Wang L, Simmonett AC, Harrigan MP, Stern CD, Wiewiora RP, Brooks BR, Pande VS (2017) OpenMM 7: rapid development of high performance algorithms for molecular dynamics. PLoS Comput Biol 13:e1005659
43. Hynninen A, Crowley MF (2014) New faster CHARMM molecular dynamics engine. J Comput Chem 35:406–413
44. Kohnke B, Kutzner C, Grubmuller H (2020) A GPU-accelerated fast multipole method for GROMACS: performance and accuracy. J Chem Theory Comput 16:6938–6949
45. Harvey MJ, Giupponi G, De Fabritiis G (2009) ACEMD: accelerating biomolecular dynamics in the microsecond time scale. J Chem Theory Comput 5:1632–1639
46. Bernstein FC, Koetzle TF, Williams GJB, Meyer EF Jr, Brice MD, Rodgers JR, Kennard O, Shimanouchi T, Tasumi M (1977) The protein data bank: a computer-based archival file for macromolecular structures. J Mol Biol 112:535–542
47. Renaud JP, Chari A, Ciferri C, Liu W, Remigy H, Stark H, Wiesmann C (2018) Cryo-EM in drug discovery: achievements limitations and prospects. Nat Rev Drug Discov 17:471–492
48. Baek M, DiMaio F, Anishchenko I, Dauparas J, Ovchinnikov S, Lee GR, Wang J, Cong Q, Kinch LN, Schaeffer RD, Millán C, Park H, Adams C, Glassman CR, DeGiovanni A, Pereira JH, Rodrigues AV, van Dijk AA, Ebrecht AC, Opperman DJ, Sagmeister T, Buhlheller C, Pavkov-Keller T, Rathinaswamy MK, Dalwadi U, Yip CK, Burke JE, Garcia KC, Grishin NV, Adams PD, Read RJ, Baker D (2021) Accurate prediction of protein structures and interactions using a three-track neural network. Science 373:871–876
49. Jumper J, Evans R, Pritzel A, Green T, Figurnov M, Ronneberger O, Tunyasuvunakool K, Bates R, Žídek A, Potapenko A, Bridgland A, Meyer C, Kohl SAA, Ballard AJ, Cowie A, Romera-Paredes B, Nikolov S, Jain R, Adler J, Back T, Petersen S, Reiman D, Clancy E, Zielinski M, Steinegger M, Pacholska M, Berghammer T, Bodenstein S, Silver D, Vinyals O, Senior AW, Kavukcuoglu K, Kohli P, Hassabis D (2021) Highly accurate protein structure prediction with AlphaFold. Nature 596:583–589
50. Tunyasuvunakool K, Adler J, Wu Z, Green T, Zielinski M, Žídek A, Bridgland A, Cowie A, Meyer C, Laydon A, Velankar S, Kleywegt GJ, Bateman A, Evans R, Pritzel A, Figurnov M, Ronneberger O, Bates R, Kohl SAA, Potapenko A, Ballard AJ, Romera-Paredes B, Nikolov S, Jain R, Clancy E, Reiman D, Petersen S, Senior AW, Kavukcuoglu K, Birney E, Kohli P, Jumper J, Hassabis D (2021) Highly accurate protein structure prediction for the human proteome. Nature 596:590–596
51. Varadi M, Anyango S, Deshpande M, Nair S, Natassia C, Yordanova G, Yuan D, Stroe O, Wood G, Laydon A, Žídek A, Green T, Tunyasuvunakool K, Petersen S, Jumper J, Clancy E, Green R, Vora A, Lutfi M, Figurnov M, Cowie A, Hobbs N, Kohli P, Kleywegt G, Birney E, Hassabis D, Velankar S (2022) AlphaFold protein structure database: massively expanding the structural coverage of protein-sequence space with high-accuracy models. Nucleic Acids Res 50:D439–D444
52. MacKerell AD, Bashford D, Bellott M, Dunbrack RL, Evanseck JD, Field MJ, Fischer S, Gao J, Guo H, Ha S, Joseph-McCarthy D, Kuchnir L, Kuczera K, Lau FTK, Mattos C, Michnick S, Ngo T, Nguyen DT, Prodhom B, Reiher WE, Roux B, Schlenkrich M, Smith JC, Stote R, Straub J, Watanabe M, Wiórkiewicz-Kuczera J, Yin D, Karplus M (1998) All-atom empirical potential for molecular modeling and dynamics studies of proteins. J Phys Chem B 102:3586–3616
53. Best RB, Zhu X, Shim J, Lopes PEM, Mittal J, Feig M, MacKerell AD (2012) Optimization of the additive CHARMM all-atom protein force field targeting improved sampling of the backbone ϕ ψ and side-chain $\chi 1$ and $\chi 2$ dihedral angles. J Chem Theory Comput 8:3257–3273
54. Vanommeslaeghe K, Hatcher E, Acharya C, Kundu S, Zhong S, Shim J, Darian E, Guvench O, Lopes P, Vorobyov I, Mackerell AD (2010) CHARMM general force field: a force field for drug-like molecules compatible with the CHARMM all-atom additive biological force fields. J Comput Chem 31:671–690
55. Yu W, He X, Vanommeslaeghe K, MacKerell AD (2012) Extension of the CHARMM general force field to sulfonyl-containing compounds and its utility in biomolecular simulations. J Comput Chem 33:2451–2468
56. Cornell WD, Cieplak P, Bayly CI, Gould IR, Merz KM, Ferguson DM, Spellmeyer DC, Fox T, Caldwell JW, Kollman PA (1995) A second generation force field for the simulation of proteins, nucleic acids and organic molecules. J Am Chem Soc 117:5179–5197

57. Wang J, Wolf RM, Caldwell JW, Kollman PA, Case DA (2004) Development and testing of a general amber force field. J Comput Chem 25:1157–1174
58. Vanommeslaeghe K, MacKerell AD (2012) Automation of the CHARMM General Force field (CGenFF) I: bond perception and atom typing. J Chem Infor Model 52: 3144–3154
59. Vanommeslaeghe K, Raman EP, MacKerell AD (2012) Automation of the CHARMM General Force field (CGenFF) II: assignment of bonded parameters and partial atomic charges. J Chem Infor Model 52:3155–3168
60. Kumar A, Yoluk O, MacKerell AD (2019) FFParam: standalone package for CHARMM additive and Drude polarizable force field parametrization of small molecules. J Comput Chem 41:958–970
61. Lopes PEM, Huang J, Shim J, Luo Y, Li H, Roux B, MacKerell AD (2013) Polarizable force field for peptides and proteins based on the classical Drude oscillator. J Chem Theory Comput 9:5430–5449
62. Lemkul JA, Huang J, Roux B, MacKerell AD (2016) An empirical polarizable force field based on the classical Drude oscillator model: development history and recent applications. Chem Rev 116:4983–5013
63. Ponder JW, Wu C, Ren P, Pande VS, Chodera JD, Schnieders MJ, Haque I, Mobley DL, Lambrecht DS, DiStasio RA, Head-Gordon-M, Clark GNI, Johnson ME, Head-Gordon T (2010) Current status of the amoeba polarizable force field. J Phys Chem B 114:2549–2564
64. Huang J, Lopes PEM, Roux B, MacKerell AD (2014) Recent advances in polarizable force fields for macromolecules: microsecond simulations of proteins using the classical Drude oscillator model. J Phys Chem Lett 5:3144–3150
65. Huang J, Lemkul JA, Eastman PK, MacKerell AD (2018) Molecular dynamics simulations using the drude polarizable force field on GPUs with OpenMM: implementation validation and benchmarks. J Comput Chem 39: 1682–1689
66. Mobley DL, Bannan CC, Rizzi A, Bayly CI, Chodera JD, Lim VT, Lim NM, Beauchamp KA, Slochower DR, Shirts MR, Gilson MK, Eastman PK (2018) Escaping atom types in force fields using direct chemical perception. J Chem Theory Comput 14:6076–6092
67. Qiu Y, Smith DGA, Boothroyd S, Jang H, Hahn DF, Wagner J, Bannan CC, Gokey T, Lim VT, Stern CD, Rizzi A, Tjanaka B, Tresadern G, Lucas X, Shirts MR, Gilson MK, Chodera JD, Bayly CI, Mobley DL, Wang LP (2021) Development and benchmarking of open force Field v1.0.0-the parsley small-molecule force field. J Chem Theory Comput 17:6262–6280
68. Unke OT, Meuwly M (2019) PhysNet: a neural network for predicting energies, forces, dipole moments and partial charges. J Chem Theory Comput 15:3678–3693
69. Poltavsky I, Tkatchenko A (2021) Machine learning force fields: recent advances and remaining challenges. J Phys Chem Lett 12: 6551–6564
70. Bender BJ, Gahbauer S, Luttens A, Lyu J, Webb CM, Stein RM, Fink EA, Balius TE, Carlsson J, Irwin JJ, Shoichet BK (2021) A practical guide to large-scale docking. Nat Protoc 16:4799–4832
71. Schaller D, Šribar D, Noonan T, Deng L, Nguyen TN, Pach S, Machalz D, Bermudez M, Wolber G (2020) Next generation 3D pharmacophore modeling. Wiley Interdiscip Rev Comput Mol Sci 10:e1468
72. Trott O, Olson AJ (2010) AutoDock Vina: improving the speed and accuracy of docking with a new scoring function efficient optimization and multithreading. J Comput Chem 31:455–461
73. Verdonk ML, Cole JC, Hartshorn MJ, Murray CW, Taylor RD (2003) Improved protein-ligand docking using GOLD. Proteins: Struct Funct Bioinf 52:609–623
74. Pagadala NS, Syed K, Tuszynski J (2017) Software for molecular docking: a review. Biophys Rev 9:91–102
75. Wójcikowski M, Zielenkiewicz P, Siedlecki P (2015) Open Drug Discovery Toolkit (ODDT): a new open-source player in the drug discovery field. J Cheminform 7:26
76. Gorgulla C, Boeszoermenyi A, Wang ZF, Fischer PD, Coote PW, Padmanabha Das KM, Malets YS, Radchenko DS, Moroz YS, Scott DA, Fackeldey K, Hoffmann M, Iavniuk I, Wagner G, Arthanari H (2020) An open-source drug discovery platform enables ultra-large virtual screens. Nature 580:663–668
77. Kochnev Y, Hellemann E, Cassidy KC, Durrant JD (2020) Webina: an open-source library and web app that runs AutoDock Vina entirely in the web browser. Bioinformatics 36:4513–4515
78. Murail S, de Vries SJ, Rey J, Moroy G, Tufféry P (2021) SeamDock: an interactive and collaborative online docking resource to assist

small compound molecular docking. Front Mol Biosci 8:716466
79. Koes DR, Camacho CJ (2011) Pharmer: efficient and exact pharmacophore search. J Chem Inf Model 51:1307–1314
80. Koes DR, Camacho CJ (2012) ZINCPharmer: pharmacophore search of the ZINC database. Nucleic Acids Res 40:W409–W414
81. Sunseri J, Koes DR (2016) Pharmit: interactive exploration of chemical space. Nucleic Acids Res 44:W442–W448
82. Irwin JJ, Tang KG, Young J, Dandarchuluun C, Wong BR, Khurelbaatar M, Moroz YS, Mayfield J, Sayle RA (2020) ZINC20-a free ultralarge-scale chemical database for ligand discovery. J Chem Inf Model 60:6065–6073
83. https://www.molport.com
84. Grygorenko OO, Radchenko DS, Dziuba I, Chuprina A, Gubina KE, Moroz YS (2020) Generating multibillion chemical space of readily accessible screening compounds. iScience 23:101681
85. Boyd NK, Teng C, Frei CR (2021) Brief overview of approaches and challenges in new antibiotic development: a focus on drug repurposing. Front Cell Infect Microbiol 11: 684515
86. Konreddy AK, Rani GU, Lee K, Choi Y (2019) Recent drug-repurposing-driven advances in the discovery of novel antibiotics. Curr Med Chem 26:5363–5388
87. Discovery Studio Modeling Environment, Dassault Systèmes BIOVIA., https://www.3ds.com/products-services/biovia/: San Diego
88. Molecular Operating Environment (MOE), Chemical Computing Group Inc., https://www.chemcomp.com: Montreal
89. OEChem, OpenEye Scientific Software, Inc. https://www.eyesopen.com: Santa Fe
90. SILCS, SilcsBio, LLC. https://www.silcsbio.com: Baltimore
91. PlayMolecule, Acellera Inc., https://www.acellera.com: Barcelona
92. Muhammed MT, Aki-Yalcin E (2019) Homology modeling in drug discovery: overview current applications and future perspectives. Chem Biol Drug Des 93:12–20
93. Moore PB, Hendrickson WA, Henderson R, Brunger AT (2022) The protein-folding problem: not yet solved. Science 375:507
94. Hollingsworth SA, Dror RO (2018) Molecular dynamics simulation for all. Neuron 99: 1129–1143
95. Lamoureux G, Harder E, Vorobyov IV, Roux B, MacKerell AD (2006) A polarizable model of water for molecular dynamics simulations of biomolecules. Chem Phys Lett 418: 245–249
96. Yu W, Lopes PEM, Roux B, MacKerell AD (2013) Six-site polarizable model of water based on the classical Drude oscillator. J Chem Phys 138:034508
97. Lin F, Huang J, Pandey P, Rupakheti C, Li J, Roux BT, MacKerell AD (2020) Further optimization and validation of the classical Drude polarizable protein force field. J Chem Theory Comput 16:3221–3239
98. Shi Y, Xia Z, Zhang J, Best R, Wu C, Ponder JW, Ren P (2013) The polarizable atomic multipole-based AMOEBA force field for proteins. J Chem Theory Comput 9:4046–4063
99. Kunz AP, van Gunsteren WF (2009) Development of a nonlinear classical polarization model for liquid water and aqueous solutions: COS/D. J Phys Chem A 113:11570–11579
100. Visscher KM, Geerke DP (2020) Deriving a polarizable force field for biomolecular building blocks with minimal empirical calibration. J Phys Chem B 124:1628–1636
101. Donchev AG, Ozrin VD, Subbotin MV, Tarasov OV, Tarasov VI (2005) A quantum mechanical polarizable force field for biomolecular interactions. Proc Natl Acad Sci U S A 102:7829–7834
102. Goel H, Yu W, Ustach VD, Aytenfisu AH, Sun D, MacKerell AD (2020) Impact of electronic polarizability on protein-functional group interactions. Phys Chem Chem Phys 22:6848–6860
103. Jo S, Cheng X, Lee J, Kim S, Park SJ, Patel DS, Beaven AH, Lee KI, Rui H, Park S, Lee HS, Roux B, MacKerell AD, Klauda JB, Qi Y, Im W (2017) CHARMM-GUI 10 years for biomolecular modeling and simulation. J Comput Chem 38:1114–1124
104. Kognole A, Lee J, Park SJ, Jo S, Chatterjee P, Lemkul JA, Huang J, MacKerell AD, Im W (2022) CHARMM-GUI Drude prepper for molecular dynamics simulation using the classical Drude polarizable force field. J Comput Chem 43:359–375
105. Chowdhary J, Harder E, Lopes PE, Huang L, MacKerell AD, Roux B (2013) A polarizable force field of dipalmitoylphosphatidylcholine based on the classical Drude model for molecular dynamics simulations of lipids. J Phys Chem B 117:9142–9160
106. Lamoureux G, MacKerell AD, Roux B (2003) A simple polarizable model of water based on

classical Drude oscillators. J Chem Phys 119: 5185–5197

107. Genheden S, Ryde U (2015) The MM/PBSA and MM/GBSA methods to estimate ligand-binding affinities. Expert Opin Drug Discov 10:449–461
108. Ustach VD, Lakkaraju SK, Jo S, Yu W, Jiang W, MacKerell AD (2019) Optimization and evaluation of site-identification by ligand competitive saturation (SILCS) as a tool for target-based ligand optimization. J Chem Inf Model 59:3018–3035
109. Goel H, Hazel A, Ustach VD, Jo S, Yu W, MacKerell AD (2021) Rapid and accurate estimation of protein-ligand relative binding affinities using site-identification by ligand competitive saturation. Chem Sci 12:8844–8858
110. Goel H, Hazel A, Yu W, Jo S, MacKerell AD (2022) Application of site-identification by ligand competitive saturation in computer-aided drug design. New J Chem 46:919–932
111. Lanning ME, Yu W, Yap JL, Chauhan J, Chen L, Whiting E, Pidugu LS, Atkinson T, Bailey H, Li W, Roth BM, Hynicka L, Chesko K, Toth EA, Shapiro P, MacKerell AD, Wilder PT, Fletcher S (2016) Structure-based design of N-substituted 1-hydroxy-4-sulfamoyl-2-naphthoates as selective inhibitors of the Mcl-1 oncoprotein. Eur J Med Chem 113:273–292
112. Young BD, Yu W, Rodríguez DJV, Varney KM, MacKerell AD, Weber DJ (2021) Specificity of molecular fragments binding to S100B versus S100A1 as identified by NMR and site identification by ligand competitive saturation (SILCS). Molecules 26:381
113. Broomhead NK, Soliman ME (2017) Can we rely on computational predictions to correctly identify ligand binding sites on novel protein drug targets? Assessment of binding site prediction methods and a protocol for validation of predicted binding sites. Cell Biochem Biophys 75:15–23
114. Shanina E, Kuhaudomlarp S, Lal K, Seeberger PH, Imberty A, Rademacher C (2022) Druggable allosteric sites in β-propeller lectins. Angew Chem Int Ed 61:e202109339
115. MacKerell AD, Jo S, Lakkaraju SK, Lind C, Yu W (2020) Identification and characterization of fragment binding sites for allosteric ligand design using the site identification by ligand competitive saturation hotspots approach (SILCS-hotspots). Biochim Biophys Acta Gen Subj 1864:129519
116. O'Reilly M, Cleasby A, Davies TG, Hall RJ, Ludlow RF, Murray CW, Tisi D, Jhoti H (2019) Crystallographic screening using ultra-low-molecular-weight ligands to guide drug design. Drug Discov Today 24:1081–1086
117. Taylor RD, MacCoss M, Lawson AD (2014) Rings in drugs. J Med Chem 57:5845–5859
118. Ness S, Martin R, Kindler AM, Paetzel M, Gold M, Jensen SE, Jones JB, Strynadka NC (2000) Structure-based design guides the improved efficacy of deacylation transition state analogue inhibitors of TEM-1 beta-lactamase. Biochemistry 39:5312–5321
119. Horn JR, Shoichet BK (2004) Allosteric inhibition through core disruption. J Mol Biol 336:1283–1291
120. Trisciuzzi D, Nicolotti O, Miteva MA, Villoutreix BO (2019) Analysis of solvent-exposed and buried co-crystallized ligands: a case study to support the design of novel protein-protein interaction inhibitors. Drug Discov Today 24:551–559
121. Mitternacht S (2016) FreeSASA: an open source C library for solvent accessible surface area calculations. F1000Res 5:189
122. Delcour AH (2009) Outer membrane permeability and antibiotic resistance. Biochim Biophys Acta 1794:808–816
123. May KL, Grabowicz M (2018) The bacterial outer membrane is an evolving antibiotic barrier. Proc Natl Acad Sci U S A 115:8852–8854
124. Bennion BJ, Be NA, McNerney MW, Lao V, Carlson EM, Valdez CA, Malfatti MA, Enright HA, Nguyen TH, Lightstone FC, Carpenter TS (2017) Predicting a drug's membrane permeability: a computational model validated with *in vitro* permeability assay data. J Phys Chem B 121:5228–5237
125. Marrink S, Berendsen HJC (1994) Simulation of water transport through a lipid membrane. J Phys Chem 98:4155–4168
126. Lind C, Pandey P, Pastor RW, MacKerell AD (2021) Functional group distributions partition coefficients and resistance factors in lipid bilayers using site identification by ligand competitive saturation. J Chem Theory Comput 17:3188–3202
127. Gao Y, Lee J, Widmalm G, Im W (2020) Modeling and simulation of bacterial outer membranes with lipopolysaccharides and enterobacterial common antigen. J Phys Chem B 124:5948–5956
128. Kansy M, Senner F, Gubernator K (1998) Physicochemical high throughput screening: parallel artificial membrane permeation assay in the description of passive absorption processes. J Med Chem 41:1007–1010

129. Lee J, Patel DS, Ståhle J, Park SJ, Kern NR, Kim S, Lee J, Cheng X, Valvano MA, Holst O, Knirel YA, Qi Y, Jo S, Klauda JB, Widmalm G, Im W (2019) CHARMM-GUI membrane builder for complex biological membrane simulations with glycolipids and lipoglycans. J Chem Theory Comput 15:775–786
130. Carro L (2018) Protein-protein interactions in bacteria: a promising and challenging avenue towards the discovery of new antibiotics. Beilstein J Org Chem 14:2881–2896
131. Cossar PJ, Lewis PJ, McCluskey A (2020) Protein-protein interactions as antibiotic targets: a medicinal chemistry perspective. Med Res Rev 40:469–494
132. Kahan R, Worm DJ, de Castro GV, Ng S, Barnard A (2021) Modulators of protein-protein interactions as antimicrobial agents. RSC Chem Biol 2:387–409
133. Huang S (2014) Search strategies and evaluation in protein–protein docking: principles advances and challenges. Drug Discov Today 19:1081–1096
134. Yu W, Jo S, Lakkaraju SK, Weber DJ, MacKerell AD (2019) Exploring protein-protein interactions using the site-identification by ligand competitive saturation methodology. Proteins: Struct Funct Bioinf 87:289–301
135. Solernou A, Fernandez-Recio J (2010) Protein docking by rotation-based uniform sampling (RotBUS) with fast computing of intermolecular contact distance and residue desolvation. BMC Bioinformatics 11:352
136. Gaile GL, Burt JE (1980) Directional statistics. Concepts and techniques in modern geography, 25th edn. Geo Books, Norwich
137. Challener C (2018) Fighting bacterial resistance with biologics. Pharm Technol 42:36–37
138. Kollef MH, Betthauser KD (2021) Monoclonal antibodies as antibacterial therapies: thinking outside of the box. Lancet Infect Dis 21:1201–1202
139. Zurawski DV, McLendon MK (2020) Monoclonal antibodies as an antibacterial approach against bacterial pathogens. Antibiotics (Basel) 9:155
140. Watson A, Li H, Ma B, Weiss R, Bendayan D, Abramovitz L, Ben-Shalom N, Mor M, Pinko E, Bar Oz M, Wang Z, Du F, Lu Y, Rybniker J, Dahan R, Huang H, Barkan D, Xiang Y, Javid B, Freund NT (2021) Human antibodies targeting a mycobacterium transporter protein mediate protection against tuberculosis. Nat Commun 12:602
141. Shire SJ (2009) Formulation and manufacturability of biologics. Curr Opin Biotechnol 20: 708–714
142. Kamerzell TJ, Esfandiary R, Joshi SB, Middaugh CR, Volkin DB (2011) Protein-excipient interactions: mechanisms and biophysical characterization applied to protein formulation development. Adv Drug Deliv Rev 63:1118–1159
143. Jo S, Xu A, Curtis JE, Somani S, MacKerell AD (2020) Computational characterization of antibody-excipient interactions for rational excipient selection using the site identification by ligand competitive saturation-biologics approach. Mol Pharm 17:4323–4333
144. Somani S, Jo S, Thirumangalathu R, Rodrigues D, Tanenbaum LM, Amin K, MacKerell AD, Thakkar SV (2021) Toward biotherapeutics formulation composition engineering using site-identification by ligand competitive saturation (SILCS). J Pharm Sci 110:1103–1110

Chapter 8

Cytotoxicity Assays as Predictors of the Safety and Efficacy of Antimicrobial Agents

Alexander Zipperer, Jasmin Scheurer, and Dorothee Kretschmer

Abstract

The development of safe antimicrobial agents is important for the effective treatment of pathogens. From a multitude of discovered inhibitory compounds, only a few antimicrobial agents are able to enter the market. Many antimicrobials are, on the one hand, quite effective in killing pathogens but, on the other hand, cytotoxic to eukaryotic cells. Cell health can be monitored by various methods. Plasma membrane integrity, DNA synthesis, enzyme activity, and reducing conditions within the cell are known indicators of cell viability and cell death. For a comprehensive overview, methods to analyze cytotoxic and hemolytic effects, e.g., lactate dehydrogenase release, cell proliferation analysis, cell viability analysis based on the activity of different intracellular enzymes, and hemolysis assay of antimicrobial compounds on human cells, are described in this updated chapter.

Key words Cytotoxicity assay, Lactate dehydrogenase release, Resazurin-based cell viability assay, Cell proliferation reagent WST-1, Hemolysis assay

1 Introduction

The emergence of multidrug-resistant organisms (MDRO) makes it essential to have access to adequate techniques to analyze drugs not only in relation to their antimicrobial effects but also regarding their cytotoxic potential. Although MDROs have evolved over decades, there are only very few antibiotics on the market, which can be used to treat such infections. The example of vancomycin shows how important it is to develop novel antibiotics. Vancomycin is an antibiotic of last resort and of high clinical importance since it is applied to treat persistent infections. However, it also possesses nephrotoxic and ototoxic properties and can cause renal failure when injected intravenously [1]. The identification of treatment alternatives with fewer side effects is therefore essential to ensure patients' well-being. Cytotoxicity can be analyzed by various methods, for example, via measuring the cell membrane integrity

Peter Sass (ed.), *Antibiotics: Methods and Protocols*,
Methods in Molecular Biology, vol. 2601, https://doi.org/10.1007/978-1-0716-2855-3_8,

through membrane leakage assays. One example (to measure the toxicity of substances) is the labeling of cells with Trypan Blue, a vital stain (diazo dye) that crosses only damaged membranes and will therefore stain only damaged/dead cells. The activity of the enzyme lactate dehydrogenase (LDH) is another indicator that is used very frequently to measure the integrity of cell membranes after treatment with cytotoxic compounds. LDH is present in nearly all cells and cell lines and catalyzes the conversion of lactate into pyruvate. Damage of the plasma membrane leads to rapid release of LDH into the cell culture supernatant where its activity can be determined via an enzymatic test [2–5].

Further assays that can be used to analyze cytotoxicity are based on the activity measurement of mitochondrial enzymes of healthy cells [6–14]. Resazurin functions as an indicator for cell health by using the reducing power of living cells to quantitatively measure the proliferation of various cell lines. Thereby the relative cytotoxicity of agents can be measured. Living cells maintain a reducing environment within the cytosol of the cell. Resazurin is a nontoxic, cell-permeable compound that is blue in color and nonfluorescent. Upon entering the cells, resazurin is reduced to resorufin, a compound that is red in color and highly fluorescent. Viable cells continuously convert resazurin into resorufin, increasing the overall fluorescence and the color of the growth medium. Like resazurin WST-1 can be used for the analysis of cytotoxic compounds based on the investigation of cell proliferation. This test is based on the cleavage of tetrazolium salts to formazan by cellular enzymes. The proliferation of cells results in an increase in the overall activity of mitochondrial dehydrogenases in the sample. This augmentation in enzyme activity leads to an increase in the amount of formazan dye and correlates directly to the number of metabolically active cells in the culture [15, 16]. In contrast to resazurin WST-1 is a red substrate. The color of WST-1 changes into yellow if the cells are alive. To investigate cytotoxicity, e.g., in keratinocytes, the 4-methylumbelliferyl heptanoate (MUH) assay can be used. In this assay, intracellular esterases of viable cells hydrolyze the MUH fluorochrome into a highly fluorescent dye [17–19]. A further method to analyze the toxicity of antimicrobials is to use non-membrane-permeable fluorescent dyes like 7-amino-actinomycin-D (7-AAD), which can intercalate in the DNA if cell membranes are damaged and undergoes a spectral shift upon association with DNA. Therefore, 7-AAD can be used as a marker for necrotic cells. The advantage of this method is that analyzing can occur via fluorescence-activated cell sorting (FACS) by a FACS analyzer.

A further method to analyze the toxicity of compounds is to determine the capacity of the antimicrobials to induce the lysis of red blood cells. In the case of red blood cells, this process is called hemolysis. This compound, an iron-containing oxygen-transport metalloprotein, is able to transport four oxygen molecules from the

lung to distant tissues and organs where it is released to facilitate aerobic respiration. Simultaneously hemoglobin returns carbon dioxide back to the lungs where the cycle is refreshed with the exchange of carbon dioxide to oxygen. Hemolysis can be easily measured via analyzing the amount of hemoglobin in the supernatant of erythrocytes [20–22].

The dissemination of more and more MDROs results in the urgent need for potent antimicrobial compounds. In order to develop not only effective but also safe drugs, it is necessary to ascertain if compounds are cytotoxic or induce hemolysis of erythrocytes. To determine the potential cytotoxicity of compounds, leukocytes, which are quite sensitive cells, are commonly used. In this updated chapter [23], we describe some basic, easy-to-perform methods that are frequently applied to analyze the cytotoxicity of various antimicrobial compounds.

2 Materials

2.1 Isolation of Human Neutrophils and Erythrocytes

1. Sodium heparin-containing tubes.
2. Pyrogen-free PBS.
3. Histopaque (density 1.119 g/mL).
4. Ficoll (density 1.007 g/mL).
5. Dulbecco's phosphate-buffered saline (DPBS).
6. Assay medium: RPMI 1640 w/o L-glutamine.
7. 4% Trypan Blue solution.
8. Erythrocyte lysis buffer: to 500 mL bidest. H_2O add 4.145 g NH_4Cl, 0.5006 g $KHCO_3$, 0.0146 g EDTA.
9. Cell culture microscope.
10. Neubauer chamber for cell counting.

2.2 LDH Activity

1. Incubator (37 °C, 5% CO_2, 95% humidity).
2. Centrifuge with rotor for microtiter plates (MTP).
3. Microtiter plate reader with 490–492 nm filter (if a reference wavelength should be subtracted, a filter over 600 nm is recommended).
4. Cell culture microscope.
5. 96-well microplates with U-bottom for suspension cells and flat bottom for adherent cells. For color development in all assays: optically clear flat-bottomed MTPs.
6. Assay medium: RPMI 1640 without phenol red containing 1% serum or 0.05% HSA.

7. Triton X-100 solution: 2% Triton X-100 in assay medium. The maximum amount of releasable LDH enzyme activity is determined by lysing the cells with Triton X-100 (final concentration: 1% Triton X-100). At this concentration Triton X-100 does not affect the LDH activity.
8. Reaction mixture: consists usually of two compounds which have to be mixed shortly before use (depending on manufacturer's instructions).
9. Optional: 1 N HCl stop solution. The enzyme reaction can be stopped by the addition of 50 μL/well 1 N HCl (final concentration: 0.2 N HCl).
10. Optional: LDH standard preparation. If the released LDH activity has to be calculated in U/mL instead of relative cytotoxicity in percent of absorbance, it is recommended to use an appropriate LDH preparation as standard.

2.3 Cell Viability Assay Based on Resazurin

1. Human leukemic monocytes (THP-1 cells).
2. Incubator (37 °C, 5% CO_2, 95% humidity).
3. Centrifuge with rotor for microtiter plates.
4. Microtiter plate reader to determine excitation at 560 nm and emission at 600 nm, optically clear flat-bottomed 96-well microtiter plates.
5. Assay medium: RPMI-1640 with 2 g $NaHCO_3$, 10% heat-inactivated fetal calf serum (FCS), 1% L-glutamine, and 1% penicillin-streptomycin, all components have to be sterile and suitable for cell culture.
6. 2% Triton X-100 as a positive control for strong cytotoxic activity.
7. Alamar Blue (Invitrogen, AbD Serotec®, G-Biosciences, Sigma-Aldrich).

2.4 Cell Proliferation Assay Using WST-1

1. Incubator (37 °C, 5% CO_2, 95% humidity).
2. Centrifuge (with rotor for MTP).
3. ELISA reader with a filter for a wavelength between 420 and 480 nm (if a reference wavelength is to be subtracted, a filter above 600 nm is recommended).
4. Cell culture microscope.
5. Hemocytometer.
6. 96-well microplates (flat bottom for adherent cells, tissue culture grade).

7. Assay medium: RPMI 1640 containing 10% heat-inactivated FCS, 2 mM L-glutamine, optionally add penicillin/streptomycin.
8. Cell Proliferation Reagent WST-1.

2.5 Cell Death Analysis with 7-Aminoactinomycin D (7-AAD)

1. 7-Aminoactinomycin-D (7-AAD).
2. Assay medium: RPMI 1640.
3. FACS tubes (5 mL).
4. Flow cytometer with a 488 nm laser.
5. Incubator for heating cells up to 75 °C (e.g., thermomixer).
6. Flow cytometer software (FlowJo or other) to analyze the FACS data.

2.6 Isolation and Cell Culture of Primary Human Keratinocytes

11. Dispase® II (neutral protease, grade II) (Roche).
12. Epidermal keratinocyte base medium with supplements (CnT-07 Epithelial Proliferation Medium, CELLnTEC).
13. Dulbecco's phosphate-buffered saline (PBS).
14. Assay medium: RPMI 1640 w/o L-glutamine.
15. Fetal bovine serum.
16. 0.05% trypsin-EDTA.
17. Gentamycin.
18. Amphotericin B.
19. 100 μM pore size cell strainer.
20. Collagen-coated tissue flasks (e.g., Corning or BioCoat™).

2.7 Cell Viability Assay Using 4-Methylumbelliferyl Heptanoate (MUH)

8. Human primary keratinocytes.
9. Optically clear flat-bottomed 96-well microtiter plates.
10. Incubator (37 °C, 5% CO_2, 95% humidity).
11. Microplate fluorimeter to determine excitation at 355 nm and emission at 460 nm.
12. Collagen type I (e.g., rat tail; Corning).
13. 0.05% trypsin-EDTA.
14. Trypan Blue.
15. Dulbecco's phosphate-buffered saline (PBS).
16. Epidermal keratinocyte base medium with supplements (CnT-07 Epithelial Proliferation Medium, CELLnTEC).
17. 2% Triton X-100 as a positive control for strong cytotoxic activity.
18. 4-Methylumbelliferyl heptanoate.

2.8 Hemolysis Assay

1. Histopaque, Ficoll, heparinized tubes (*see* Subheading 2.1: isolation of leukocytes).
2. Incubator (37 °C, 5% CO_2, 95% humidity).
3. Centrifuge for reaction tubes (1.5 mL, 2 mL, 15 mL, 50 mL).
4. Spectral photometer with 540 nm absorbance measurement.
5. Centrifuge with rotor for MTP.
6. Assay medium: 1 × phosphate-buffered saline (PBS).
7. 2% Triton X-100 in 1 × PBS as positive control.

3 Methods

3.1 Isolation of Human Neutrophils and Erythrocytes

1. Collect blood obtained from healthy human volunteers into sodium heparin-containing tubes for neutrophil isolation.
2. Dilute the heparinized blood 1:2 (v/v) with pyrogen-free PBS, and layer it carefully onto a gradient of 12 mL Histopaque (density 1.119 g/mL) and 10 mL Ficoll (density 1.007 g/mL) in a 50 mL conical centrifuge tubes. A maximum of 25 mL of the diluted blood can be used per tube.
3. Centrifuge the tube at 380 × g for 20 min at room temperature (RT) with a maximum of acceleration and without brake.
4. After centrifugation isolate the neutrophils from the Histopaque phase, transfer the cells to a new 50 mL conical centrifuge tube, and wash them with RPMI and added 0.05% HSA (RPMI/HSA) at 250 × g for 10 min at RT with a maximum of acceleration and with brake (Fig. 1).
5. Discard the supernatant carefully.

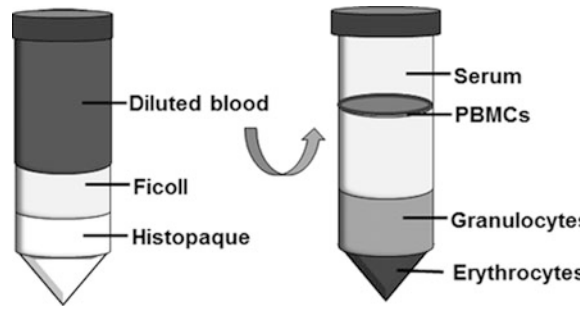

Fig. 1 Isolation of neutrophils and erythrocytes by density gradient centrifugation. Gradient before (left side) and after (right side) centrifugation. (Figure reprinted from [23])

6. Incubate the cell pellet, which contains the neutrophils and residual erythrocytes, for 3 min at 37 °C and 5% CO_2 with 5 mL erythrocyte lysis buffer.
7. After incubation, wash neutrophils again with RPMI/HSA at 250 × g for 10 min at RT and discard the supernatant. Solve the remaining cell pellet in 1–3 mL RPMI/HSA and determine the cell number (next step).
8. To analyze the cell number, mix 90 µL Trypan Blue with 10 µL of the cell suspension. Add 10 µL of this mixture to a Neubauer chamber. To calculate the number of cells in the chamber, 4 big squares containing 16 small squares have to be enumerated, respectively. The cell number per mL can be determined with this formula:

$$\text{cell number per mL} = \frac{\text{counted cells}}{4} * 10\ (\text{Dilution factor}) + 10^{4}\ (\text{Chamber factor})$$

3.2 Isolation and Cultivation of Primary Human Keratinocytes

1. Collect skin punches, e.g., from juvenile foreskin after routine circumcision or from surgical discard skin.
2. Remove fat and vascular tissue and cut skin into small 1 cm^2 pieces.
3. Incubate skin overnight at 4 °C in epidermal keratinocyte base medium supplemented with 10 µg/mL gentamycin and 0.25 µg/mL amphotericin B. Add 10 mg/mL Dispase® II to digest the basal lamina. The skin pieces should only float with the underside in the media and the epidermis should remain dry.
4. The next day, carefully separate epidermis from dermis and cut epidermis in small pieces.
5. Incubate epidermis slices in 0.05% trypsin-EDTA for 10 min at 37 °C and 5% CO_2.
6. Stop digestion using RPMI containing 10% fetal bovine serum.
7. Prepare a single cell suspension by pipetting slices up and down, and transfer the cells to a cell strainer with 100 µM pore size. Collect the cells in a 50 mL conical centrifuge tubes.
8. Centrifuge cells at 290 × g for 4 min at RT.
9. Culture keratinocytes in collagen-coated tissue flasks in epidermal keratinocyte base medium with supplements at 37 °C and 5% CO_2.

3.3 LDH Activity Assay

Colorimetric assay for the quantification of cell death and cell lysis. The assay is based on the measurement of lactate dehydrogenase (LDH) activity in cell supernatants. This allows indirect assessment of membrane integrity since LDH is released from the cytosol only if cell membranes are damaged. NAD+ is reduced to NADH/H+

by the LDH catalyzed conversion of lactate to pyruvate. In a second step, the catalyst transfers H/H+ from NADH/H+ to the tetrazolium salt which is reduced to formazan resulting in a change of color:

1. Adjust cell number to 3×10^6 cells/mL (for neutrophils; for HL60 cells: 1×10^6 cells/mL) in RPMI without phenol red. For other cells first determine the optimal cell number for this assay (*see* **Notes 1** and **2**).
2. Use a 96-well microtiter plate (round bottom for cells grown in suspension), and set up the following reactions: (a) 200 μL medium, (b) 100 μL medium +100 μL cells, (c) 100 μL 2% Triton X-100 + 100 μL cells, and (d) 100 μL of diluted compound (dilute in RPMI 1640 without phenol red) + 100 μl cells. Test all reactions in triplicates (*see* **Note 3**).
3. Incubate the microtiter plate with the samples at 37 °C, 5% CO_2, 95% humidity in the incubator (stimulation time depends on your sample; it is recommended to test the optimal incubation time in a first experiment, e.g., after 1 h, 3 h, 6 h, 12 h, and 24 h).
4. After incubation time centrifuge the microplate at 250 × g for 10 min.
5. Carefully take 100 μL/well of the supernatants (without cells), and transfer to the correspondent wells of a second flat-bottom microtiter plate.
6. Add 100 μL/well of freshly prepared reaction mixture to the second microtiter plate (calculate the appropriate amount for your experiment: mix compound one with compound 2, *see* **Note 4**).
7. Incubate the microtiter plate with the samples up to 30 min protected from light at RT.
8. Measure absorbance at 490 nm (reference wavelength should be more than 600 nm) in an ELISA reader.

3.4 Cell Viability Assay Based on Resazurin

The major component of the cell viability indicator Alamar Blue® is resazurin, a nontoxic and cell-permeable compound. Viable cells convert resazurin into the red-fluorescent resorufin. The amount of fluorescence measured is proportional to the number of living cells:

1. Culture THP-1 cells in RPMI-1640 *with* penicillin-streptomycin in a cell culture flask (*see* **Note 5**).
2. Count cell numbers by Trypan Blue staining (*see* **Note 6**).
3. If your culture contains sufficient cell numbers, centrifuge (10 min, 250 × g) and resuspend the pellet in RPMI-1640 *without* penicillin-streptomycin and *without* phenol red.

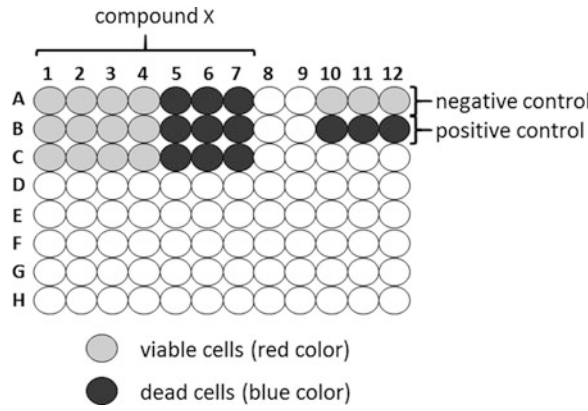

Fig. 2 Analysis of cell proliferation and cytotoxicity with resazurin. Defined cell numbers were incubated with various concentrations of compound X. After the subsequent addition of Alamar Blue®, wells are stained depending on the cell condition. (Figure reprinted from [23])

4. Prepare a 96-well microtiter plate with your test compounds, 2% Triton X-100 as positive control (final concentration per well) and corresponding solvent(s) in which the test compounds were diluted as negative control(s).
5. Add 1×10^4 THP-1 cells in 188 µL medium into each well and to your test compound (2 µL per well).
6. Incubate your samples for 48 h at 37 °C and 5% CO_2.
7. Add 10 µL Alamar Blue® to each well and incubate the samples for 24 h at 37 °C and 5% CO_2 protected from direct light (*see* **Note 7**).
8. Determine the relative fluorescent units (excitation 560 nm and emission 600 nm, *see* **Note 8**) in your microtiter plate reader with a peak emission at 585 nm (Fig. 2).
9. Results are analyzed by plotting fluorescence intensity (or absorbance) versus compound concentration.

3.5 Cell Viability Assay Based on Cell Proliferation Reagent WST-1

Analysis of cytotoxic compounds such as antimicrobials or other potential toxic compounds. This assay can be used, if the number of dead cells in the negative control without compound is quite high:

1. Seed cells at a concentration of 5×10^4 cells/well (depending on the cell type, *see* **Notes 9** and **10**) in 100 µL assay medium (RPMI +10% heat-inactivated FCS) and different concentrations of the test compound (depending on the compound) into 96-well microplates.
2. Incubate cell cultures for 24 h in a humidified atmosphere at 37 °C, 5% CO_2, 95% H_2O.

3. Add 10 μL Cell Proliferation Reagent WST-1 (*see* **Note 11**) to each well, and incubate for up to 4 h (*see* **Note 12**) at 37 °C and 5% CO_2.
4. Shake cells thoroughly for 1 min (300 rpm) on a shaker or in the microplate reader (*see* **Note 13**).
5. Measure absorbance of the samples against a medium control as blank using an ELISA reader according to the filters available for the ELISA reader. The wavelength for measuring the absorbance of the formazan product is between 420 and 480 nm (max. Absorption 440 nm).

3.6 Cell Death Analysis with 7-Aminoactinomycin-D (7-AAD)

If the cell membrane is disrupted by toxic substances, 7-AAD can bind selectively to the GC regions of the DNA. Consequently, necrotic cells are stained with 7-AAD, while living cells with intact membranes are not stained. After incubation of the samples with 7-AAD, the fluorescence of the samples can be measured with a flow cytometer.

1. Transfer 250 μL cells in medium (e.g., RPMI 1640) into 5 mL FACS tubes, with a final concentration of 2.5×10^5 cells/tube. Add 250 μL of the test compound in various concentrations or controls (for the positive control heat cells up to 75 °C for 45 min, thereby cells undergo necrosis; for the negative control, use medium).
2. Incubate cells with antimicrobials or controls for up to 24 h (depending on the substance and the cells) at 37 °C, 5% CO_2 in an incubator.
3. Minutes before measurement of the samples, add 7-AAD at a concentration of 5 μL/tube (0.25 μg/tube) and incubate the cells in the incubator.
4. Stop the reaction by transferring the tubes on ice and measure fluorescence by using a flow cytometer.

3.7 Keratinocyte Cell Viability Analysis Using 4-Methylumbelliferyl Heptanoate (MUH)

Keratinocytes are the most abundant cell type in the epidermis, the outermost layer of the skin, which makes them attractive to study especially the cytotoxic effects of topical antimicrobial agents. The MUH assay can be used to detect cell cytotoxicity. Intracellular esterases of viable cells hydrolyze 4-methylumbelliferyl heptanoate to highly fluorescent 4-methylumbelliferone that can be measured in a microplate fluorimeter. The amount of fluorescence measured is proportional to the number of living cells:

1. If your culture contains sufficient cell numbers, harvest keratinocytes using 0.05% trypsin-EDTA and by incubating the flask at 37 °C for 2–5 min (*see* **Notes 14, 15**, and **16**).
2. Once cells appear detached, add 2 volumes of pre-warmed RPMI containing 10% fetal bovine serum to inactivate trypsin.

3. Centrifuge the cells for 4 min at 290 × g at RT, and resuspend the pellet in epidermal keratinocyte base medium with supplements.
4. Count cell numbers by Trypan Blue staining (*see* **Note 17**).
5. Precoat wells of a 96-well microtiter plate with 25 μg/mL collagen type I and incubate for 2 h at 37 °C.
6. Wash 96-well microtiter plate twice with PBS.
7. Seed 1.5×10^6 cells per 96-well microtiter plate (125 μL/well), and culture for 1 day at 37 °C and 5% CO_2 that cells attach to the bottom of the wells.
8. The next day, when the cells are >90% confluent (*see* **Note 18**), the cells can be treated with test compounds of interest, 2% Triton X-100 as positive control (final concentration per well), and corresponding solvent(s) in which the test compounds were diluted as negative control(s).
9. Wash the cells twice with PBS.
10. Incubate cells with 100 μg/mL MUH in PBS for 1 h at 37 °C and 5% CO_2.
11. Determine absolute fluorescent intensity (excitation 355 nm and emission 460 nm) using a microplate fluorimeter.
12. The amount of fluorescence measured is proportional to the number of living cells. Normalize results to the untreated controls.

3.8 Hemolysis Assay

Lysis of erythrocytes leads to a release of hemoglobin into the supernatant, which can be measured spectrophotometrically [5, 24, 25]. Isolate the red blood cells from healthy human volunteers (*see* **Notes 19** and **20**) by standard Histopaque/Ficoll centrifugation:

1. Wash the red blood cells with 1 × PBS in 50 mL, 15 mL, or 2 mL reaction tubes depending on the volume of blood you use.
2. Dilute the red blood cells 1:50 with 1 × PBS to prepare a 2% suspension.
3. Add your compounds to the 2% suspension of red blood cells, and incubate them at 37 °C for 60 min (incubate red blood cells with Triton X-100 at a final concentration of 2% as positive control and red blood cells in 1 × PBS as negative control).
4. Centrifuge samples for 10 min at 100 × g. Transfer the supernatant into a new tube and dilute it 1:10 with 1 × PBS (Fig. 3).
5. Determine the hemolytic activity by measuring the optical density (hemoglobin absorbance at 540 nm) of the cell-free supernatant with a spectrophotometer.

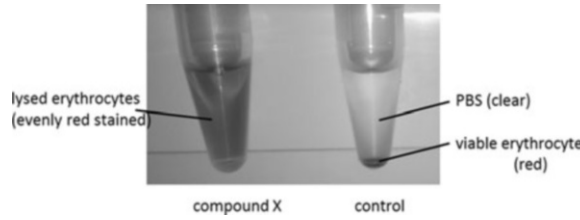

Fig. 3 Analysis of compound-dependent erythrocyte lysis. Erythrocytes were incubated with compound X. The lysis of red blood cells was subsequently monitored by OD measurement of the supernatant. (Figure reprinted from [23])

4 Notes

1. Before you start with your experiment, determine the optimal cell concentration for the assay since different cell types contain different amounts of LDH. Therefore, the optimum cell concentration for a specific cell type should be determined in a preliminary experiment. In general, the cell concentration, in which the difference between the negative and positive control is at a maximum, should be used for the subsequent assay. The optimal concentration for most cell lines is between 0.5 and 2×10^4 cells/well in 200 µL. To this you have to adjust the cell suspensions to a concentration of 2×10^6 cell/mL, and titrate the cells by twofold serial dilutions across the plates. For each concentration you need a negative control (= culture medium, spontaneous LDH release) and a positive control (100 µL per well 2% Triton X-100 solution). The best cell concentration shows the highest difference between positive and negative control.
2. Add 100 µL cell suspension per well to a sterile 96-well tissue culture plate (flat bottom), and incubate the cells overnight (or longer, depending on the cell type) in an incubator to allow the cells to adhere tightly. Remove the assay medium from the adherent cells, and add 100 µL fresh medium to each well. Then add your test substance to the adherent cells, and incubate them (2–24 h dependent on your assay). For example, seed A549 lung epithelial cells 1.14×10^4 cells/well in 1 mL in a 24-well plate and after 4 days stimulate cells for 24 h.
3. Use always media without phenol red, since phenol red can influence the absorbance.
4. The freshly prepared reaction mixture should not be stored, due to its sensitivity to light. When the two compounds for the reaction mixture are thawed, they can be stored at 4 °C for up to 6 weeks. In general, all substances have to be regarded as unstable.

5. Cultivation of leukemic monocytes to obtain sufficient cell numbers: use RMPI-1640 with 1% penicillin-streptomycin and phenol red. Renew the medium every 3–4 days by centrifugation, removal of the supernatant, and resuspension into fresh RPMI-1640.
6. Counting cells numbers: centrifuge the cell culture (10 min, 250 × g), remove the supernatant, and resuspend the pellet in 1 mL RPMI-1640 *without* phenol red. Mix an aliquot of this suspension in a ratio of 1:1 with Trypan Blue, and count the cells (e.g., with an automated cell counter).
7. 5% Alamar Blue (10 μL) is less than stated in the manufacturer's protocol but sufficient. Optional: Add 50 μL 3% SDS directly to 100 μL of cells in Alamar Blue® reagent to stop the reaction.
8. If a microplate reader is not available, you can also measure your samples in a spectral photometer at an absorbance of 540–570 nm (peak excitation is 570 nm). Please note that this measurement is less sensitive! Assay plates or tubes can be wrapped in foil, stored at 4 °C, and read within 1–3 days without affecting the fluorescence or absorbance values.
9. For each cell type you should determine the optimal cell number and incubation time with WST-1, because a high cell number and proliferation leads to a detection limitation of the negative control (high absorbance).
10. After choosing a certain cell line, use only cells with low passage; otherwise the results strongly vary.
11. The substrate is light and temperature sensitive. It is recommended to prepare aliquots of the substrate and to freeze it in adequate amounts.
12. For samples with higher cell numbers, you can use shorter incubation times of 4 h or less. In general, the sensitivity of detection increases with longer incubation times.
13. Before you measure absorbance, always remove bubbles, since they can falsify the result. To distribute the color equally in the well, you should always shake the microtiter plate for 1 min before measuring the absorbance.
14. Primary human keratinocytes can be isolated from the skin of various locations, including foreskin, face, breast, abdomen, or thighs (ethical approvement). As an alternative to isolating human keratinocytes from the skin, primary keratinocytes or keratinocyte cell lines can be ordered, e.g., from ATCC. Here, observe the culture conditions recommended by the companies.
15. Before freshly isolated keratinocytes are used for analyses, they should be passaged. Use only cells with low passage (passage 1–4) for experiments; otherwise, the results strongly vary.

16. If less than 90% of cells are detached, incubate for another 2 min at 37 °C and observe the cells for every 30 s with the microscope.
17. Mix an aliquot of cell suspension in a ratio of 1:1 with Trypan Blue and count the cells (e.g., by using a Neubauer chamber and microscope).
18. For analysis cells should be >90% confluent. If not, culture cells for another day at 37 °C and 5% CO_2.
19. In case that human red blood cells are not available, the assay can be performed with rabbit or sheep red blood cells as well.
20. Blood samples can be stored at 4 °C overnight after the addition of Histopaque/Ficoll as the included heparin acts as an anticoagulant.

Acknowledgments

This work was supported by grants from the German Research Council (TRR156, TRR34 to DK) and the Fortüne Program of the Medical Faculty, University of Tübingen (to D.K.).

References

1. Bruniera FR, Ferreira FM, Saviolli LR, Bacci MR, Feder D, da Luz Goncalves Pedreira M, Sorgini Peterlini MA, Azzalis LA, Campos Junqueira VB, Fonseca FL (2015) The use of vancomycin with its therapeutic and adverse effects: a review. Eur Rev Med Pharmacol Sci 19(4):694–700
2. Decker T, Lohmann-Matthes ML (1988) A quick and simple method for the quantitation of lactate dehydrogenase release in measurements of cellular cytotoxicity and tumor necrosis factor (TNF) activity. J Immunol Methods 115(1):61–69
3. Korzeniewski C, Callewaert DM (1983) An enzyme-release assay for natural cytotoxicity. J Immunol Methods 64(3):313–320
4. Naal FD, Salzmann GM, von Knoch F, Tuebel J, Diehl P, Gradinger R, Schauwecker J (2008) The effects of clindamycin on human osteoblasts in vitro. Arch Orthop Trauma Surg 128(3):317–323
5. Wang R, Braughton KR, Kretschmer D, Bach TH, Queck SY, Li M, Kennedy AD, Dorward DW, Klebanoff SJ, Peschel A, DeLeo FR, Otto M (2007) Identification of novel cytolytic peptides as key virulence determinants for community-associated MRSA. Nat Med 13(12):1510–1514
6. Bara R, Zerfass I, Aly AH, Goldbach-Gecke H, Raghavan V, Sass P, Mandi A, Wray V, Polavarapu PL, Pretsch A, Lin W, Kurtan T, Debbab A, Brotz-Oesterhelt H, Proksch P (2013) Atropisomeric dihydroanthracenones as inhibitors of multiresistant *Staphylococcus aureus*. J Med Chem 56(8):3257–3272
7. Antczak C, Shum D, Escobar S, Bassit B, Kim E, Seshan VE, Wu N, Yang G, Ouerfelli O, Li YM, Scheinberg DA, Djaballah H (2007) High-throughput identification of inhibitors of human mitochondrial peptide deformylase. J Biomol Screen 12(4):521–535
8. Al-Nasiry S, Geusens N, Hanssens M, Luyten C, Pijnenborg R (2007) The use of Alamar Blue assay for quantitative analysis of viability, migration and invasion of choriocarcinoma cells. Hum Reprod 22(5):1304–1309
9. Gartlon J, Kinsner A, Bal-Price A, Coecke S, Clothier RH (2006) Evaluation of a proposed in vitro test strategy using neuronal and non-neuronal cell systems for detecting neurotoxicity. Toxicol In Vitro 20(8):1569–1581
10. Ovcharenko D, Jarvis R, Hunicke-Smith S, Kelnar K, Brown D (2005) High-throughput RNAi screening in vitro: from cell lines to primary cells. RNA 11(6):985–993

11. Hamid R, Rotshteyn Y, Rabadi L, Parikh R, Bullock P (2004) Comparison of alamar blue and MTT assays for high through-put screening. Toxicol In Vitro 18(5):703–710
12. Gloeckner H, Jonuleit T, Lemke HD (2001) Monitoring of cell viability and cell growth in a hollow-fiber bioreactor by use of the dye Alamar Blue. J Immunol Methods 252(1–2): 131–138
13. Nociari MM, Shalev A, Benias P, Russo C (1998) A novel one-step, highly sensitive fluorometric assay to evaluate cell-mediated cytotoxicity. J Immunol Methods 213(2):157–167
14. Nakayama GR, Caton MC, Nova MP, Parandoosh Z (1997) Assessment of the Alamar Blue assay for cellular growth and viability in vitro. J Immunol Methods 204(2):205–208
15. Roehm NW, Rodgers GH, Hatfield SM, Glasebrook AL (1991) An improved colorimetric assay for cell proliferation and viability utilizing the tetrazolium salt XTT. J Immunol Methods 142(2):257–265
16. Ishiyama M, Tominaga H, Shiga M, Sasamoto K, Ohkura Y, Ueno K (1996) A combined assay of cell viability and in vitro cytotoxicity with a highly water-soluble tetrazolium salt, neutral red and crystal violet. Biol Pharm Bull 19(11):1518–1520
17. Whiteley L, Meffert T, Haug M, Weidenmaier C, Hopf V, Bitschar K, Schittek B, Kohler C, Steinmetz I, West TE, Schwarz S (2017) Entry, intracellular survival, and multinucleated-giant-cell-forming activity of Burkholderia pseudomallei in human primary phagocytic and nonphagocytic cells. Infect Immun 85(10):1–12
18. Bitschar K, Sauer B, Focken J, Dehmer H, Moos S, Konnerth M, Schilling NA, Grond S, Kalbacher H, Kurschus FC, Götz F, Krismer B, Peschel A, Schittek B (2019) Lugdunin amplifies innate immune responses in the skin in synergy with host- and microbiota-derived factors. Nat Commun 10(1):2730
19. Bitschar K, Staudenmaier L, Klink L, Focken J, Sauer B, Fehrenbacher B, Herster F, Bittner Z, Bleul L, Schaller M, Wolz C, Weber ANR, Peschel A, Schittek B (2020) *Staphylococcus aureus* skin colonization is enhanced by the interaction of neutrophil extracellular traps with keratinocytes. J Invest Dermatol 140(5): 1054–1065 e1054
20. Gallagher P (2011) Hemolytic anemias: red cell membrane and metabolic defects. In: Goldman L, Schafer A (eds) Cecil medicine, vol 24. Saunders Elsevier, Philadelphia
21. Powers ASL (2008) Autoimmune hemolytic anemia. In: Hoffman RBE, Shattil SS (eds) Hematology: basic principles and practice, 5th edn. Elsevier Churchill Livingstone, Philadelphia
22. Schrier SPE (2008) Extrinsic nonimmune hemolytic anemias. In: Hoffman RBE, Shattil SS (eds) Hematology: basic principles and practice, 5th edn. Elsevier Churchill Livingstone, Philadelphia
23. Zipperer A, Kretschmer D (2017) Cytotoxicity assays as predictors of the safety and efficacy of antimicrobial agents. Methods Mol Biol 1520: 107–118
24. Torres VJ, Attia AS, Mason WJ, Hood MI, Corbin BD, Beasley FC, Anderson KL, Stauff DL, McDonald WH, Zimmerman LJ, Friedman DB, Heinrichs DE, Dunman PM, Skaar EP (2010) *Staphylococcus aureus* fur regulates the expression of virulence factors that contribute to the pathogenesis of pneumonia. Infect Immun 78(4):1618–1628
25. Blevins JS, Beenken KE, Elasri MO, Hurlburt BK, Smeltzer MS (2002) Strain-dependent differences in the regulatory roles of sarA and agr in *Staphylococcus aureus.* Infect Immun 70(2): 470–480

Part II

Mode of Action and Resistance

Chapter 9

Microscopy-Based Multiwell Assay to Characterize Disturbed Bacterial Morphogenesis Upon Antibiotic Action

Cruz L. Matos de Opitz and Peter Sass

Abstract

The urgent need of new antimicrobial agents to combat life-threatening bacterial infections demands the identification and characterization of novel compounds that interfere with new and unprecedented target pathways or structures in multiresistant bacteria. Here, bacterial cell division has emerged as a new and promising target pathway for antibiotic intervention. Compounds, which inhibit division, commonly induce a characteristic filamentation phenotype of rod-shaped bacteria, such as *Bacillus subtilis*. Hence, this filamentation phenotype can be used to identify and characterize novel compounds that primarily target bacterial cell division. Since novel compounds of both synthetic and natural product origin are often available in small amounts only, thereby limiting the number of assays during mode of action studies, we here describe a semiautomated, microscopy-based approach that requires only small volumes of compounds to allow for the real-time observation of their effects on living bacteria, such as filamentation or cell lysis, in high-throughput 96-well-based formats. We provide a detailed workflow for the initial characterization of multiple compounds at once and further tools for the initial, microscopy-based characterization of their antibacterial mode of action.

Key words *Bacillus subtilis*, *Staphylococcus aureus*, *Escherichia coli*, Bacterial phenotyping, Antibiotic compound libraries, Antibiotic modes of action, Bacteria cell division, Automated microscopy, Fluorescence labeling, Microscopy image analysis

1 Introduction

There is no doubt we are heading toward a global antimicrobial crisis, since new antibiotics with desired modes of action are becoming scarce goods. The ever-increasing abundance of multidrug-resistant bacteria puts harsh pressure on our healthcare system, and the future looks uncertain, as it is expected that by 2050 the number of deaths per year attributed to antimicrobial resistance will reach over ten million if this problem is not adequately addressed [1, 2]. Advances in molecular and biochemical methods have simplified antimicrobial discovery and susceptibility

Peter Sass (ed.), *Antibiotics: Methods and Protocols*,
Methods in Molecular Biology, vol. 2601, https://doi.org/10.1007/978-1-0716-2855-3_9,

testing, for instance, outer membrane vesicles are envisioned as future platforms for testing of membrane active compounds in clinically relevant Gram-negative bacteria [3]. Other studies are specific for cellular targets or molecular structures [4–6] or are based in the development of tools for microscaling susceptibility testing, using chips for analyzing the effect of antimicrobials on biofilms [7]. In principle, simultaneous and systematic analysis (preferably of large compound collections), nanotechnologies, and automation become more and more indispensable for pursuing antibiotic discovery. Microscopy techniques have always been central in microbiology and antibiotic drug discovery, since phenotypic changes of a living organism, i.e., in response to antibiotic action, can be directly evaluated in real time. Moreover, compared to other analytical techniques, microscopy adds another level of information because it allows the evaluation of heterogeneity between a population of cells [8]. Recently, bacterial cytological profiling [9, 10] proved useful for the future evaluation of candidate drugs in tuberculosis treatment [11] or to identify the molecular targets of compounds targeting diverse cellular pathways [4]. In this regard, bacterial cell division has attracted considerable attention as a new target pathway for antibiotic intervention [12–16]. Here, we made use of the characteristic filamentation phenotype of rod-shaped bacteria, such as the bacterial model organism *Bacillus subtilis*, that is observed when the bacterial cells are treated with cell division-interfering compounds. We describe a semiautomated, microscopy-based protocol to identify and characterize antibiotic-induced bacterial phenotypes, including filamentation phenotypes, which is validated by known antibiotics with established modes of action. This method is easily reproducible and can be implemented in future mode of action studies for novel antimicrobial compounds or lead molecules. Moreover, we provide protocols for bacterial cytological profiling of Gram-positive bacteria, e.g., *B. subtilis* and *Staphylococcus aureus*, as an additional tool for initial antibiotic mode of action analyses. Both approaches only require small amounts of compound, which is a crucial benefit since antibiotic mode of action studies are often hampered by an insufficient availability of the novel compounds.

2 Materials

All solutions should be prepared in ultrapure or double distilled water (ddH2O). Depending on the strains, solutions, and antibiotics you use, we recommend to carefully follow general good laboratory practice (GLP) rules [17].

2.1 Semiautomated, 96-Well-Based Microscopy Assay for Bacterial Phenotyping

2.1.1 Growth Media, Reagents/Materials, and Bacterial Strains

1. Lysogeny broth (LB): 10 g peptone, 5 g yeast extract, 10 g NaCl, pH 7.3. Add 900 mL water, and adjust to pH 7.3 with 1 M NaOH. Complete to 1 L with ultrapure water. Store at room temperature or 4 °C.
2. Bacterial strains: Gram-positive *B. subtilis* 168 or any similar *B. subtilis* wild-type laboratory strain; Gram-negative *Escherichia coli* ATCC 25922 or similar *E. coli* reference strain.
3. Agarose 500 g, CAS Number-9012-36-6, low electroendosmosis (EEO)/multipurpose/molecular biology grade, EEO 0.09 to 0.13, DNase-free, gelation temperature 34.5–37.5 °C, gel strength approx. 1200 g/cm^2. Use this to prepare a 1% agarose solution: weigh 1 g of molecular grade agarose and transfer to a 250 mL flask. Add 100 mL water and use a microwave to dissolve (*see* **Note 1**).
4. Antibiotics to test (e.g., ciprofloxacin, actinomycin D, chloramphenicol, rifampicin, ampicillin, kanamycin, trimethoprim) and solvents used in the preparation of the antibiotic stocks and dilutions (e.g., dimethyl sulfoxide (DMSO), ethanol, methanol). A list of antibiotics with their corresponding solvents for antibiotic stock preparation is displayed in Table 1.
5. 96-well microplates, flat base, material: polystyrene, transparent, medium binding, free from DNase/RNase/DNA, pyrogens and endotoxins, non-cytotoxic (e.g., Sarstedt 82.1581001).
6. 96-well microplate shaker or incubator shaker with adhesive mats or sticky pads.

Table 1
Antibiotics with their corresponding solvents for antibiotic stock preparation

Antibiotic	Stock concentration (mg/mL)	Concentration in first well (μg/mL)	Solvent
Ciprofloxacin	3.2	16	0.1 N HCl
Actinomycin D	0.4	2	DMSO
Chloramphenicol	0.8	4	DMSO
Rifampicin	0.4	2	DMSO
ADEP2	0.4	2	DMSO
Ampicillin	0.4	2	H_2O
Kanamycin	3.2	16	H_2O
Trimethoprim	3.2	16	DMSO

7. 96-channel handheld electronic pipette (e.g., VIAFLO 96, Integra Biosciences), 0.5–12.5 µL pipette head. Alternative 8- or 12-channel pipette (maximum volume 10 µL) or a 96-pin microplate replicator.
8. Pipette tips, volume 12.5 µL, or similar.
9. 96-well plate lid: polystyrene, single packed, high profile (9 mm), transparent, sterile (e.g., Greiner, Item No.: 656161).
10. Custom coverslips: 75 × 115 mm, No. 1.5 (e.g., Marienfeld, F000828, 50 pieces). As many as 96-well plates and time points to evaluate.
11. Spirit level (optional).
12. Disposable, electrostatic dust cleaning wipes (optional).

2.1.2 Hardware and Software

1. Inverted motorized microscope, equipped with a scientific camera (CCD or sCMOS). We used a Nikon Eclipse Ti automated microscope equipped with a Perfect Focus system, a long-distance CFI S Plan-Fluor ELWD ADL 60×/0.70 Air Ph2 objective (Nikon Instruments Europe BV, Netherlands), and an Orca Flash 4.0 camera (Hamamatsu, Photonics, Japan).
2. Focus stabilization, e.g., Perfect Focus System (PFS, Nikon), and motorized stage (x, y, z).
3. Hardware controllable bright field illumination (ideally a LED illumination).
4. OKO okolab H201-K-frame with multi-well plate holder (H201-MW-holder).
5. Image acquisition and automated microscopy software. We used the software package NIS-Elements AR 5.21.03 64-bit (Nikon).
6. Analysis software and plugins: Fiji [18] or ImageJ [19], Oufti (http://www.oufti.org/) [20], MicrobeJ (https://www.microbej.com/) [21], Morphometrics [22] (https://simtk.org/projects/morphometrics), or equivalent.

2.2 Phenotypic Profiling Using Fluorescence Microscopy

2.2.1 Growth Media, Reagents/Materials, and Bacterial Strains

1. LB broth, same as Subheading 2.1.1.
2. Antibiotics of choice for treatment or plasmid selection (e.g., spectinomycin) (*see* **Note 2**).
3. Fluorescent dyes: membrane dyes (e.g., FM4–64, FM5–95, Nile red), DNA dyes (e.g., 4′,6-diamidino-2-phenylindole (DAPI), Hoechst), other dyes (e.g., Vancomycin-BODIPY FL to label free D-alanine-D-alanine residues in the cell wall, for example, at the septum area).
4. Bacterial strains of interest, e.g., *B. subtilis* 168, *Staphylococcus aureus* NCTC 8325, or *B. subtilis* strains carrying fluorescently tagged proteins, e.g., *B. subtilis* FtsZ-GFP, *B. subtilis* and MinD-GFP, among others.

5. 1% agarose, prepare as described in Subheading 2.1.1.
6. 96-well plates, flat base or round base, material: polystyrene, transparent, medium binding, free from DNase/RNase/DNA, pyrogens and endotoxins, non-cytotoxic (e.g., Sarstedt 82.1581001 or 82.1582.001) (*see* **Note 3**).
7. Microscope slides (ISO 8037-1): prepare and clean as many microscope glass slides as necessary (26 mm × 76 mm) using 70% ethanol (*see* **Note 4**).
8. Microscope coverslips, optimally precision cover glasses thickness No. 1.5H (ISO 8255).
9. Glass-suitable, lens cleaning wipes.

2.2.2 Hardware and Software

1. Inverted motorized microscope, equipped with scientific camera (CCD or sCMOS). We used a Nikon Eclipse Ti automated microscope equipped with a Perfect Focus system, CFI Plan-Apo DM 100×/1.45 Oil Ph3 objective (Nikon Instruments Europe BV, Netherlands), and an Orca Flash 4.0 camera (Hamamatsu, Photonics, Japan).
2. Focus stabilization, e.g., Perfect Focus System (PFS, Nikon), and motorized stage (x, y, z).
3. Hardware controllable bright field illumination (ideally a LED illumination).
4. SOLA Light Engine, white light output for excitation of DAPI, GFP/FITC, YFP, Cy3, mCherry, Cy5, and spectrally similar fluorophores (Lumencor, USA).
5. Microscopy slide holder.
6. HC Filter sets (IDEX/Semrock, USA): EGFP excitation 472 nm, emission 520 nm; Texas Red excitation 555 nm, emission 617 nm; and DAPI excitation 377 nm, emission 447 nm.
7. Image acquisition software. We used the software package NIS-Elements AR 5.21.03 64 bit (Nikon).
8. Analysis software and plugins: Fiji [3] or ImageJ [4], Oufti (http://www.oufti.org/) [5], MicrobeJ (https://www.microbej.com/) [6], Morphometrics [7] (https://simtk.org/projects/morphometrics), or equivalent.

3 Methods

1. Inoculate cells from *B. subtilis* 168, *E. coli* ATCC 25922, or any other bacterial strain you want to test. Cells are grown from stocks stored at −80 °C in 100 mL flasks containing 20 mL LB medium, supplement with antibiotics if necessary. Grow the cells overnight at 37 °C under shaking conditions (220 rpm).

3.1 Semiautomated, 96-Well-Based Microscopy Assay for Bacterial Phenotyping

3.1.1 Preparation of Bacterial Cultures

2. The following day dilute the cells 1:250 in a 100 mL flask containing 20 mL prewarmed LB medium (*see* **Note 5**), this time without antibiotics. Incubate cells at 37 °C under shaking conditions (220 rpm).
3. Let cells grow to early exponential phase (optical density at 600 nm (OD_{600}) of 0.1–0.2). Usually, *B. subtilis* 168 cells need 1.5–2 h to reach this optical density (*see* **Note 6**).

3.1.2 Preparation of 96-Well Plates for the Antibiotic Treatment of Bacteria

1. Assign an individual condition per well in the 96-well plate. Depending on the purpose of your experiment, either prepare serial dilutions of different antibiotics, or use each well for different compounds, e.g., natural or synthetic compound libraries. In Table 2, we exemplify the distribution of a 96-well plate with serial dilutions of known compounds per row. We recommend 100 µL end volume per well. For instance, let us exemplify a common workflow for a serial dilution using the antibiotic ciprofloxacin:
   (a) Start with 16 µg/mL ciprofloxacin in well A1: add 1 µL of a 3.2 mg/mL ciprofloxacin stock in well A1 and add on top 99 µL prewarmed LB broth.
   (b) Pipette up and down several times to assure proper mixing of the antibiotic with the medium.
   (c) On the wells A2–A12, add 50 µL of prewarmed LB medium.
   (d) Transfer 50 µL of well A1 onto well A2, pipette up and down several times, take 50 µL of well A2 into well A3, mix as previously, and continue dilution series until well A11.
   (e) Discard the last 50 µL from well A11. Well A12 will serve as solvent control (*see* **Note 7**).
2. Incubate the plate with the serial dilutions at 37 °C until the cells are grown to early exponential phase (*see* Subheading 3.1.1), and then transfer 50 µL cells onto each well. Incubate further at 37 °C under shaking conditions and protected from light (*see* **Note 8**).
3. After 3 h incubation (or any other desired incubation time), with a multichannel pipette, collect aliquots for observation under the microscope as described in the next sections.

3.1.3 Preparation of Microplate-Sized Agarose Pads

1. On a flat surface, carefully transfer 45 mL of 1% agarose onto a 96-well lid. Here, it is recommended to use a spirit level to ensure evenness of the agarose pad (*see* **Note 9**).
2. Let the agarose pad cool at room temperature until polymerization occurs. The process might take approx. 20–30 min, depending on the local ambient conditions. During this time

Table 2
Representative 96-well plate, depicting a dilution scheme of antibiotics used for the semiautomated microscopy assay

	Antibiotic (μg/mL)	1	2	3	4	5	6	7	8	9	10	11	12
A	Ciprofloxacin	8	4	2	1	0.5	0.25	0.125	0.0625	0.0313	0.0156	0.0078	DMSO
B	Actinomycin D	1	0.5	0.25	0.125	0.0625	0.0313	0.0156	0.0078	0.0039	0.0020	0.0010	DMSO
C	Chloramphenicol	2	1	0.5	0.25	0.125	0.0625	0.0313	0.0156	0.0078	0.0039	0.0020	DMSO
D	Rifampicin	1	0.5	0.25	0.125	0.0625	0.0313	0.0156	0.0078	0.0039	0.0020	0.0010	DMSO
E	ADEP2	1	0.5	0.25	0.125	0.0625	0.0313	0.0156	0.0078	0.0039	0.0020	0.0010	DMSO
F	Ampicillin	1	0.5	0.25	0.125	0.0625	0.0313	0.0156	0.0078	0.0039	0.0020	0.0010	DMSO
G	Kanamycin	8	4	2	1	0.5	0.25	0.125	0.0625	0.0313	0.0156	0.0078	DMSO
H	Trimethoprim	8	4	2	1	0.5	0.25	0.125	0.0625	0.0313	0.0156	0.0078	DMSO

prevent any movement or vibrations around the surface where the agarose is drying, e.g., vigorously vortexing or centrifugation near the agarose pads (*see* **Note 10**).

3.1.4 Collection of Aliquots and Transfer onto Agarose Pads

1. Remove the 96-well plate from the incubator (Subheading 3.1.2, **step 3**) and proceed with the next steps as quickly as possible. Protect compounds from light whenever possible, and dim or turn off the light of the working area.
2. With the 96-channel electronic pipette dispenser, collect 2–4 μL aliquots of the samples and transfer them onto the surface of the agarose pad as described in Fig. 1. As an alternative to the electronic dispenser, a multichannel pipette or a 96-pin microplate replicator may be used (*see* **Note 11**).
3. Optional: Return the plate to the incubator if you analyze further time points (*see* **Note 12**).
4. Let the droplets dry for a few minutes under the clean bench or any other working area free of air currents.
5. Using gloves and leaving approx. 5 mm space from each side of the top left corner of the lid containing the agarose pad, let the large coverslip (75 × 115 mm) adhere to the left side of the agarose pad. As depicted in Fig. 1, using an approx. 45° angle, let the coverslip slowly attach to the surface of the pad, until the entire area containing the droplets is covered (*see* **Note 13**). Transfer the samples to the microscope in a sealed container.

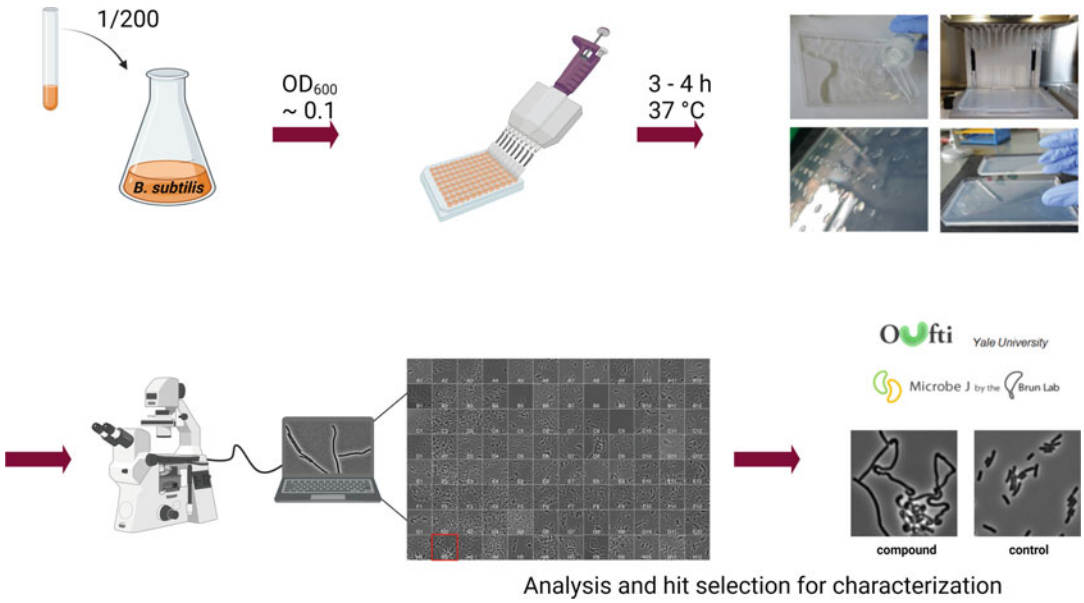

Fig. 1 Workflow of the semiautomated, 96-well-based microscopy assay for bacterial phenotyping. (Image was created with BioRender.com)

3.1.5 Semiautomated Microscopy Workflow for Samples in a 96-Well Format

1. Start the microscope and computer hardware with required peripheral components.
2. Open the NIS-Elements AR software. In the menu bar, select the option JOBS and on the secondary menu select under "JOBS" the option "Create New JOB…", this will display a new window with the name "Job definition". The JOBS module works as a drag and drop program with several options for automated workflows.
3. On the left side of the "Job definition" window, you will see a menu list with different categories. Here, focus first on the category "Well plates". Drag the option "Define plate" and drop it on the empty right side of the "Job definition" window. A task will be displayed under the name "Use Plate with 96 wells". On this task bar under "Well plate name", you can give a custom label to the well plate (microplate) format you are analyzing. More options here include "Select from DB…", where you can choose from different commercially available well plates already stored with the software, or "Custom Well Plate…", which allows to manually enter the properties of your well plate of choice. We selected, for example, the model 655,090 from the database list.
4. Next, it is important that you calibrate the well plate position before every experiment (*see* **Note 14**). For doing so, you may select the option "Re-Align Well plate…" inside the "Define Plate" task or as an independent action by drag and drop of the task "Align Plate" under the category "Well Plates" in the "Job definition" menu. Calibration of the well plate can be also carried out outside the JOBS platform, in the main menu bar of NIS-Elements AR, under this path: "JOBS – Well Plate – Re-Align Well Plate". Once the Re-Align Well plate is activated, a pop-out window will display a 96-well plate scheme. On the thumbnail "Align Wells", you have two methods for calibrating: "Center Point" or "3 Edge points". Regardless of which method you select, the software recommends for calibrating the wells A1, A12, H1, and H12. To do so, move the motorized stage to the named wells and confirm their position by clicking on the button "Add" on the right upper side of the window. A calibrated well is shown as a filled well in green color. To confirm the calibration is successful, select the thumbnail "Test", and here you can click on different wells and confirm the motorized stage is moving to the desired positions (*see* **Note 15**).
5. Add the next task "Select Wells". This time, the displayable menu for this task is called "WellSelection". By holding down the "Ctrl" key in the keyboard and holding down the mouse across the wells, you can select the entire well plate or defined

positions. From the several options available in this task, the most relevant is "Well ordering", which allows you to decide the direction followed by the motorized stage throughout the multiwell plate. Here you can decide between "Meander", "Left to Right", and "Top to bottom". From these alternatives, the "Meander" option is the most time efficient.

6. Next, drag and drop the task "Loop over Wells", which will be shown as "WELL LOOP". In the drop-down menu from this task, it is noted "Wells: for each well in WellSelection.Selection". This action means that every subsequent task added underneath will be repeated for every selected well.
7. Add inside the "WELL LOOP" the task named "GeneratedPoints: generate points in Wells.CurrentWell". This will be found in the menu list on the left side of the "Job definition", under the menu "Stage XY Points – Generate Points". In this task do the following: working area, whole well; mark the option "Customize Preview Field Size"; objective, CFI S Plan-Fluor ELWD ADL 60×/0.70 Air Ph2; area restriction, whole area; point placement, random; count, 10 (number of points to be imaged); distribution, uniform in radius; scan direction, optimal path; and frames on border, frame inside. Alternatively you can tick the option "Always Create New Points" to add another level of randomization to image acquisition.
8. Now, inside the "GeneratedPoints", drag and drop the task "Loop over Points", which will be shown as "POINT LOOP", in the drop-down menu, and it is noted "Points: for each point in Generated.Points.Position". This action means that every subsequent task added underneath will be repeated for every point inside the well.
9. Next, add inside "POINT LOOP" the task "CaptureDefinition" which is located under the same name on the "Job Definition" menu, under the category "Acquisition". In "Capture Definition", select in the optical configuration panel the settings for microscopy with the 60× magnification using the phase-contrast ring 2. In this panel, you may also adjust the focus offset and activate the option "Close Active Shutter", for the LED lamp to be turned off when the motorized stage is moving between points.
10. Also, inside "POINT LOOP", located in the category PFS, drag and drop the task "PFS On and Focus", which will be shown as "PFSON". Mark the option "On fail, do the following:" and choose either "Autofocus" or "Move Z: up and down" to retry the activation of the PFS. This ensures a quick regain of focus by changes in Z during microscopy (*see* **Note 16**).

11. Finally, inside the loop, add the task "Capture", found in the "Acquisition" category. This task will display the information "Capture using CaptureDefinition.Definition". The option allows capturing images that by default will be saved in the computer's hard drive. You may incorporate other tasks, e.g., alternative storage place, change the name of the file, perform few analyses, etc. Using the floppy disk icon on the upper menu, save the JOB program.
12. Take the agarose pad containing the samples as prepared in the previous section, and place it in the inverted plate holder. Using the "Well plate and Slide Navigation" window or manually, move the stage to the position A1. Then, turn on the PFS button, select the optical configuration corresponding to the phase contrast, 60× magnification, activate the live modus on the microscope, and adjust the focus. After localizing the cells and finding the optimal focus, stop the live modus. Start the automatic microscopy image acquisition by clicking on the green "play" icon located on the right side of the lower corner of the JOB definition window.
13. On the JOBS Explorer window, under the name given to the Job Definition, there is an activity log, where all information regarding the time and date of the run experiments is displayed. By selecting and doing a right-click on individual runs, you can access the data-containing folder. The individual micrographs are stored, named with the well ID in the original file extension for the microscope software (.nd2). The files can also be exported into TIFF format or be opened in their original extension in the latest version of Fiji [18] or ImageJ [19] containing the Bio-Formats plugin [23] (*see* **Notes 17** and **18**). The generated data can be analyzed with several bioinformatic tools; a typical outcome of the semiautomated workflow is depicted in Fig. 2.

3.2 Phenotypic Profiling Using Fluorescence Microscopy

3.2.1 Preparation of Bacterial Cultures

1. Inoculate bacterial cells, e.g., *B. subtilis*, from stocks stored at −80 °C in 50 mL flasks containing 10 mL LB medium, supplement with antibiotics if necessary. Grow the cells overnight at 37 °C under shaking conditions (220 rpm).
2. The following day dilute the cells 1:250 in a 50 mL flask containing 10 mL prewarmed LB medium (*see* **Note 5**), this time without antibiotics. Depending on the strain, add appropriate inducers, e.g., xylose or IPTG (isopropylthio-β-galactoside), for the expression of a (fluorophore-fused) protein of interest. Incubate cells at 37 °C under shaking conditions (220 rpm).
3. Let the cells grow to early exponential phase (optical density at 600 nm (OD_{600}) of 0.1–0.2). For example, *B. subtilis* cells usually need 1.5–2 h to reach this optical density (*see* **Note 6**).

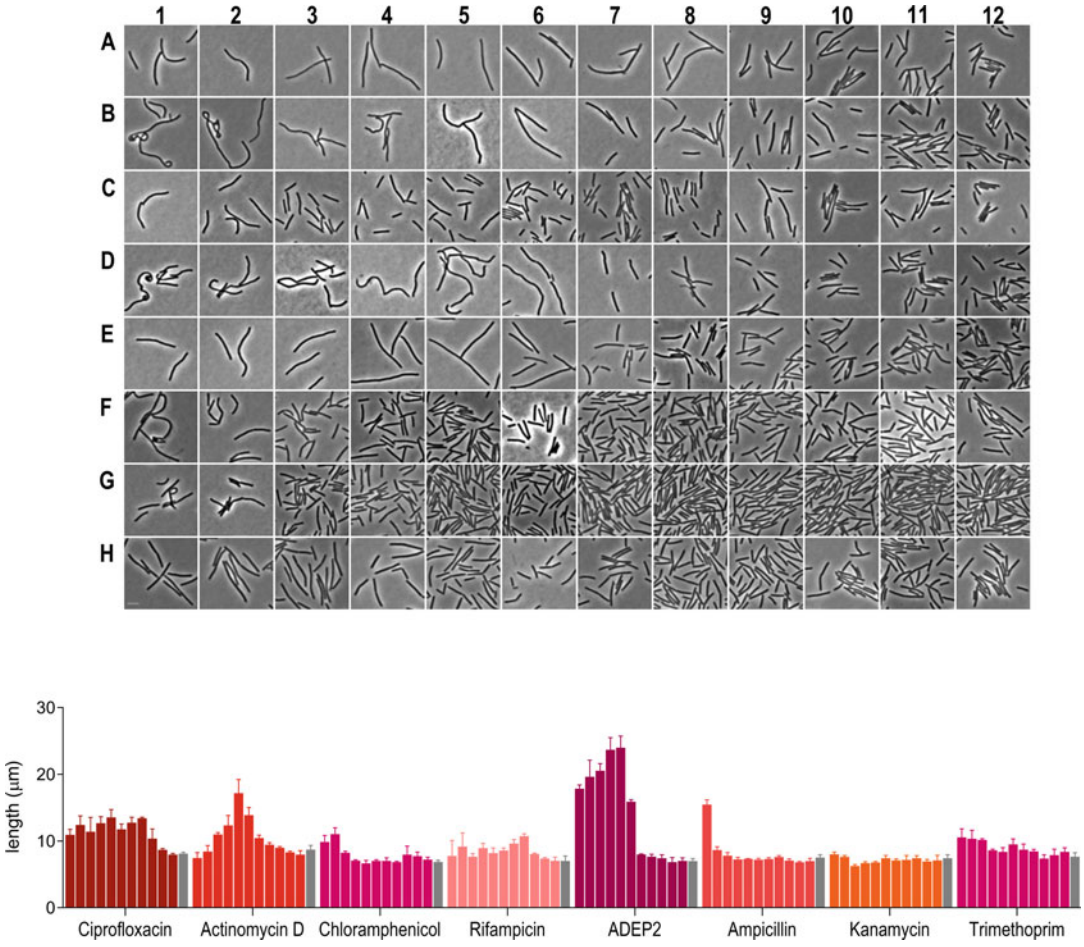

Fig. 2 Outcome of an exemplary semiautomated, 96-well-based microscopy assay phenotyping *B. subtilis* cells treated with different antibiotics. The microplate setup with antibiotic concentrations is detailed in Table 2. Gray bars represent solvent/DMSO controls

3.2.2 Preparation of Agarose-Coated Microscopy Slides

1. Transfer 500 µL agarose in the middle of a previously cleaned glass slide, as described in Subheading 2.2.1, **step 7**. Pipette gradually to contain the volume in a small area, and wait a few seconds until the borders of the agarose bed become more defined.
2. At this point, take an additional, cleaned microscopy slide, and place it on top of the agarose-containing slide, so that the agarose is placed flat between both glass slides (*see* **Note 19**).
3. Let the agarose polymerize before use. The agarose will be completely polymerized when the initially transparent agarose becomes slightly opaque. The process is summarized in Fig. 3.

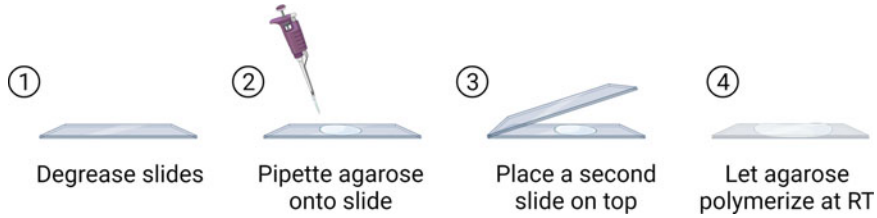

Fig. 3 Schematic representation of the preparation of agarose-coated slides for microscopy. (Image was created with BioRender.com)

3.2.3 Antibiotic Treatment of Bacterial Cells

1. Dilute the cells (Subheading 3.2.1, **step 3**) in prewarmed LB medium containing the desired antibiotic concentration, so that cells are further diluted to a final OD_{600} of 0.05–0.1 (*see* **Notes 6** and **20**).
2. Prepare corresponding control cultures, i.e., untreated cells and solvent control, if the antibiotic is dissolved in DMSO, ethanol, or similar (*see* **Note 7**).

3.2.4 Labeling of Samples with Fluorescent Dyes

1. Take an aliquot of each sample and dye the bacterial cells. For staining the membrane, add Nile Red (1 μg/mL), FM4–64, FM5–95 (10–20 μg/mL), or equivalent, and for the chromosome add DAPI (1 μg/mL). The same sample can be labeled with Vancomycin-BODIPY FL (1 μg/mL) to visualize ongoing peptidoglycan synthesis (*see* **Note 21**).
2. Stain samples for 5 min, protected from light, and evaluate immediately under the microscope (*see* **Note 22**). Typically, labeled *B. subtilis* cells should be observed as in Fig. 4.

3.2.5 Sample Preparation for Microscopy

1. Take a microscopy slide prepared as described in Subheading 3.2.2. Carefully, but with a steady hand, slide off the upper glass slide. If formed, remove any residual agarose from the sides of the slide.
2. Load 0.3 μL of labeled cells onto the agarose bed without touching it with the pipette tip (*see* **Note 23**).
3. Allow the liquid to dry (*see* **Note 24**). The sample will be ready for microscopy when no liquid is visible on the surface (*see* **Note 25**).
4. Place a clean coverslip (22 × 22 mm or similar) on top of the sample. To do so, let one side of the coverslip touch the agarose, and then gently let loose so it adheres completely to the agarose.

3.2.6 Fluorescence Microscopy

1. Start the microscope and computer hardware with all required peripheral components.
2. Select the appropriate objective and filters according to your experimental setup (*see* **Note 26**).

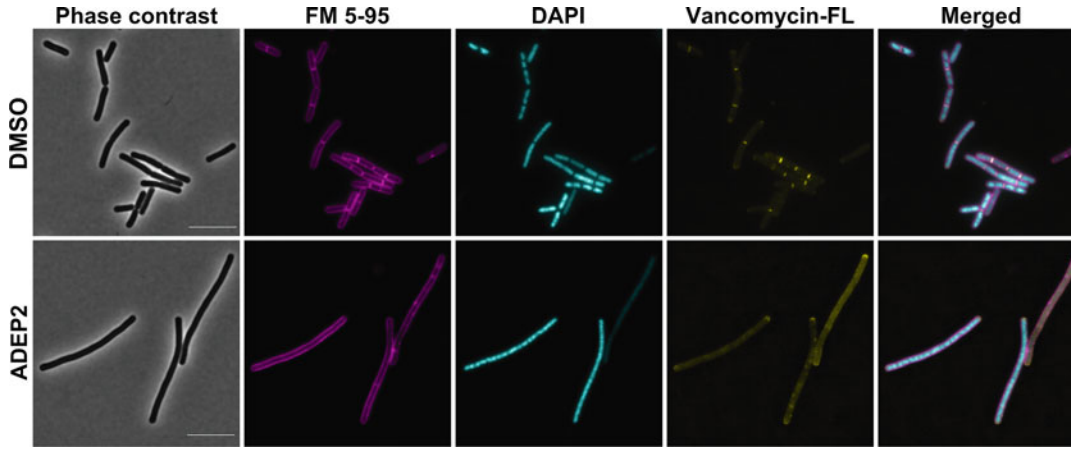

Fig. 4 Phenotypic profiling of *B. subtilis* 168 cells treated with ADEP2. The cells are labeled with FM5–95 (membrane, in magenta), DAPI (chromosome, in cyan), and Vancomycin-BODIPY FL (free D-ala-D-ala residues in the septum area, in yellow)

3. Adjust in advance the program considering the channels/fluorophores to analyze.
4. Set the diascopic LED light iris intensity to 10% and 100 ms exposure, 100× objective, and turret condenser position "Ph3" for phase-contrast images. Next, set the SOLA light intensity to 15%, 100× objective, turret condenser position "bright field", and adjust the exposure to 400 ms for each of the HC filter sets described in Subheading 2.2.2, corresponding to the dyes FM5-95 (Texas Red), Vancomycin-BODIPY FL (eGFP), and DAPI.
5. Place the slide and with help of the PFS locate the cells using phase contrast, finalize to adjust the focus, and search for a position where enough cells are present and distributed in a monolayer.
6. Create enough snaps of different regions of each sample as well as of different conditions tested, e.g., treated and untreated cells, to allow unbiased and comprehensive evaluation of phenotypes. Exemplary images are shown in Fig. 4. We recommend no less than four randomly selected representative regions for each condition for analysis (*see* **Notes 17** and **18**). If you capture more than one image channel, you may combine each micrograph into a stacked file or save individual channels into single files for the analysis; this will depend on the program used for analysis.

4 Notes

1. While melting the agarose, caution is needed as the solution might continue to boil after removing it from the microwave. Ensure that the agarose is completely dissolved and there are no aggregates present, as this may interfere with the quality of the final microscopy images and can cause an increase in background fluorescence. Agarose can be prepared a day before the experiment, and it must be stored at 60 °C to avoid polymerization.
2. When possible always work with fresh antibiotic stocks, and preparing small aliquots to use once per experiment significantly improves reproducibility and avoids antibiotic degradation related to cycles of freezing and thawing.
3. In our experience, *B. subtilis* cells grow better in flat-bottom multiwell plates, whereas *S. aureus* grow preferably in round-bottom plates.
4. Microscopy slides should be thoroughly cleaned and degreased, and using gloves can help to avoid imprinting fingertips on the microscope slides.
5. Using prewarmed medium favors the continuous growth and better adaptation of *B. subtilis* into a new medium.
6. Antibiotic effects on bacterial cells are better observed in cells growing in early exponential phase (OD_{600} 0.1–0.2). Moreover, this OD guarantees an adequate cell number and sufficient spacing between cells per microscopy field.
7. The final solvent concentration is important, as it may affect the growth and phenotype of the bacteria. Before experiments are conducted with antibiotics of interest, you should be acquainted with the bacteria you are working with, evaluate their phenotype under normal growth conditions, and analyze the effect of solvents on their phenotype. We recommend a maximum final concentration of 1–2% DMSO per well [24].
8. Light might interfere with the activity of some antibiotics or compounds that are light sensitive. Protecting from light will avoid degradation of the compounds or changes in their physicochemical properties and activity span.
9. Ensuring an even surface of the agarose pad confers an equal distribution of the spots on the gel surface, which will translate in an unproblematic microscopy of cells. Also, synchronize the preparation of the agarose pad with the last hour of incubation of the cells treated with antibiotics, e.g., if you want to evaluate the antibiotic effect on the cells after 3 h of incubation, start preparing the agarose pad 2 h after the coincubation was initiated. This step is critical for avoiding excessive drying of the agarose pad.

10. Keeping a steady surface, free of vibrations, provides flat gels. We recommend cleaning the surface with an electrostatic dust-cleaning wipe and preventing any air currents to assure that any fibers or dust elements reach the gel surface.
11. Regardless of which material you employ for the collection and dispensing of the aliquots, be careful to place the droplets in the middle of each well without poking on the agarose. These two criteria are of utmost importance for the success of the method. If the droplets are not properly positioned, you may record images in areas of the agarose pad where no sample has been spotted. On the other hand, if you poke holes on the agarose, you will alter the surface of the agarose, which in turn will lower adherence of the coverslip onto the pad or will reduce the area of the droplet available for microscopy.
12. At later time points, you may consider diluting the samples 10- or 20-fold in 0.9% NaCl depending on their turbidity. By doing so, you assure an even distribution of the bacteria in the droplet avoiding overcrowding the sample, which may cause difficulties during the analysis of the micrographs using bioinformatic tools.
13. This step is critical to avoid formation of bubbles, especially inside or in proximity to the droplet area. We recommend practicing placing of the coverslip onto the agarose pad even without sample, until you achieve an optimal adhesion of the coverslip to the agarose pad.
14. Of note, once the program is closed, you will lose the calibration; therefore, it is mandatory that you perform this task before every experiment, especially between working days.
15. It is of interest to evaluate the movement of the motorized stage across the 96-well plate and inside selected points within individual wells. For doing so activate the window "Well plate and Slide Navigation", in the main menu of the NIS-Elements AR, and follow the path: "View – Acquisition Controls – Well plate and Slide Navigation".
16. When setting up the method, you may consider controlling additional parameters to assure the best outcome and stabilization of the PFS, e.g., adjust the speed and acceleration of the motorized stage. Alternatively, once the focus is lost, you may pause the JOB program and manually refocus and continue with image acquisition.
17. Each microscope is equipped with its on software, and generally, raw images are saved into a file extension that is not compatible with every program. Lately, ImageJ and Fiji support images derived from most microscopes; however, it is recommended to export micrographs in a compatible format. The best format to save images for analysis and post-processing

is TIFF (16 bit), and avoid other formats like JPEG and PNG because important information will be lost and the overall quality of the images will reduce.

18. Cell length measurements of *B. subtilis* using phase-contrast microscopy require special attention. In several bacteria including *E. coli*, *Salmonella typhimurium*, and *Caulobacter crescentus*, cell separation is clearly visible, and individual cells are distinguishable even during exponential growth, allowing for a correct measurement of cell length in dividing, but not fully separated daughter cells [8, 25]. On the contrary, during exponential growth, *B. subtilis* cells are characterized by the formation of filamentous cell chains where septal cross walls are only clearly visible when a membrane stain is used or short before autolysis of daughter cells [8, 25, 26]. For further information on quantitative image data analysis, see chapter "Quantitative analysis of microscopy data to evaluate bacterial responses to antibiotic treatment" by Brajtenbach, Puls, Matos de Opitz, et al. in this edition [27].
19. Once the second slide is placed on top of the agarose-containing slide, the agarose should automatically distribute evenly between the two sandwich-forming slides. There is no need to add pressure to flatten the agarose; if this is the case, it is better to start over. Ideally, agarose-coated slides should be no more than 2 mm in thickness and prepared on a flat surface, and this may be ensured using a spirit level. An uneven surface translates to difficulty to focus and areas on the microscopy field that are blurry. Also, avoid unnecessary formation of bubbles by careful pipetting.
20. For this protocol, we collected aliquots of treated cells after 3 h. However, this method allows obtaining samples for microscopic analysis during different time points, letting the user follow antibiotic action over time and defining a correct time point for the identification of the phenotype of interest.
21. Initial experiments using untreated cells are helpful to define the best conditions for follow-up experiments, especially considering that some antibiotics and fluorescent dyes are either expensive or available in limited amounts. Moreover, the concentrations for staining are only a recommendation, and every laboratory/investigator should adjust the best working concentrations to get optimal results.
22. We recommend staining a small sample number at a time. Most used dyes are toxic for the cells; for that reason, the time between preparation of the sample and microscopy should be minimized. Control cells should be imaged last. If the control cells look unperturbed, this is a good indication to trust your results. In addition, protecting the samples from the light is crucial to avoid fluorescence decay.

23. This is a small volume to pipette. If you are not careful enough, a hole will be poked into the agarose, perturbing the integrity of the surface, which will minimize the area that can be analyzed for microscopy, affect the correct pass of light, and it will cause a "movement" of cells around the hole.
24. It is helpful to limit the area under the glass by means of a marker where the droplet will be pipetted; this will simplify locating the cells under the microscope.
25. The droplet transferred into the agarose slide must be completely dry before adding the cover slips; otherwise not properly immobilized bacteria will be moving on the slide which prevents correct focusing.
26. It is very important to keep the same optical configurations in all experiments, especially those selected for quantification and statistical analysis purposes. Always use the diascopic light to initial adjustments and to focus the cells. Before the experiment and if possible, consider setting short exposure times and reduce the intensity of the excitation light to the minimum required; this will help in avoiding bleaching and phototoxicity. Cells and positions should be quickly selected by using the bright field or phase contrast.

Acknowledgments

We gratefully thank all team members for their support and critical discussions. The authors appreciate funding by the Deutsche Forschungsgemeinschaft (DFG, German Research Foundation): Project-ID 398967434 (TRR 261-A02), the German Center for Infection Research (DZIF; TTU 09.815), as well as support by infrastructural funding from the Cluster of Excellence EXC 2124 Controlling Microbes to Fight Infections. The authors declare no competing interests.

References

1. Church NA, McKillip JL (2021) Antibiotic resistance crisis: challenges and imperatives. Biologia 76(5):1535–1550. https://doi.org/10.1007/s11756-021-00697-x
2. Matos de Opitz CL, Sass P (2020) Tackling antimicrobial resistance by exploring new mechanisms of antibiotic action. Future Microbiol 15:703–708. https://doi.org/10.2217/fmb-2020-0048
3. Mohamed Z, Shin J-H, Ghosh S, Sharma AK, Pinnock F, Naser BE, Farnush S, Dörr T, Daniel S (2021) Clinically relevant bacterial outer membrane models for antibiotic screening applications. ACS Infect Dis 7(9):2707–2722. https://doi.org/10.1021/acsinfecdis.1c00217
4. Montaño ET, Nideffer JF, Sugie J, Enustun E, Shapiro AB, Tsunemoto H, Derman AI, Pogliano K, Pogliano J, Metcalf WW (2021) Bacterial cytological profiling identifies rhodanine-containing PAINS analogs as specific inhibitors of *Escherichia coli* Thymidylate kinase *in vivo*. J Bacteriol 203(19):e00105–e00121. https://doi.org/10.1128/JB.00105-21

5. Zhang L, He J, Bai L, Ruan S, Yang T, Luo Y (2021) Ribosome-targeting antibacterial agents: advances, challenges, and opportunities. Med Res Rev 41(4):1855–1889. https://doi.org/10.1002/med.21780
6. Paradis-Bleau C, Kritikos G, Orlova K, Typas A, Bernhardt TG (2014) A genome-wide screen for bacterial envelope biogenesis mutants identifies a novel factor involved in cell wall precursor metabolism. PLoS Genet 10(1):e1004056. https://doi.org/10.1371/journal.pgen.1004056
7. Blanco-Cabra N, López-Martínez MJ, Arévalo-Jaimes BV, Martin-Gómez MT, Samitier J, Torrents E (2021) A new BiofilmChip device for testing biofilm formation and antibiotic susceptibility. npj Biofilms Microbiomes 7(1):62. https://doi.org/10.1038/s41522-021-00236-1
8. Syvertsson S, Vischer NOE, Gao Y, Hamoen LW (2016) When phase contrast fails: ChainTracer and NucTracer, two ImageJ methods for semi-automated single cell analysis using membrane or DNA staining. PLoS One 11(3):e0151267. https://doi.org/10.1371/journal.pone.0151267
9. Nonejuie P, Burkart M, Pogliano K, Pogliano J (2013) Bacterial cytological profiling rapidly identifies the cellular pathways targeted by antibacterial molecules. Proc Natl Acad Sci U S A 110(40):16169–16174. https://doi.org/10.1073/pnas.1311066110
10. Nonejuie P, Trial RM, Newton GL, Lamsa A, Ranmali Perera V, Aguilar J, Liu WT, Dorrestein PC, Pogliano J, Pogliano K (2016) Application of bacterial cytological profiling to crude natural product extracts reveals the antibacterial arsenal of *Bacillus subtilis*. J Antibiot (Tokyo) 69(5):353–361. https://doi.org/10.1038/ja.2015.116
11. Kalsum S, Andersson B, Das J, Schön T, Lerm M (2021) A high-throughput screening assay based on automated microscopy for monitoring antibiotic susceptibility of *Mycobacterium tuberculosis* phenotypes. BMC Microbiol 21(1):167. https://doi.org/10.1186/s12866-021-02212-3
12. Silber N, Matos de Opitz CL, Mayer C, Sass P (2020) Cell division protein FtsZ: from structure and mechanism to antibiotic target. Future Microbiol 15:801–831. https://doi.org/10.2217/fmb-2019-0348
13. Haydon DJ, Stokes NR, Ure R, Galbraith G, Bennett JM, Brown DR, Baker PJ, Barynin VV, Rice DW, Sedelnikova SE, Heal JR, Sheridan JM, Aiwale ST, Chauhan PK, Srivastava A, Taneja A, Collins I, Errington J, Czaplewski LG (2008) An inhibitor of FtsZ with potent and selective anti-staphylococcal activity. Science 321(5896):1673–1675. https://doi.org/10.1126/science.1159961
14. Silber N, Pan S, Schäkermann S, Mayer C, Brötz-Oesterhelt H, Sass P (2020) Cell division protein FtsZ is unfolded for N-terminal degradation by antibiotic-activated ClpP. MBio 11(3). https://doi.org/10.1128/mBio.01006-20
15. Mayer C, Sass P, Brötz-Oesterhelt H (2019) Consequences of dosing and timing on the antibacterial effects of ADEP antibiotics. Int J Med Microbiol 309(7):151329. https://doi.org/10.1016/j.ijmm.2019.151329
16. Silber N, Mayer C, Matos de Opitz CL, Sass P (2021) Progression of the late-stage divisome is unaffected by the depletion of the cytoplasmic FtsZ pool. Commun Biol 4(1):270. https://doi.org/10.1038/s42003-021-01789-9
17. Chidambaram SB, Essa M, Qoronfleh MW (2022) Good laboratory practice. In: Introduction to toxicological screening methods and good laboratory practice. Springer Singapore, Singapore, pp 175–189. https://doi.org/10.1007/978-981-16-6092-4_6
18. Schindelin J, Arganda-Carreras I, Frise E, Kaynig V, Longair M, Pietzsch T, Preibisch S, Rueden C, Saalfeld S, Schmid B, Tinevez J-Y, White DJ, Hartenstein V, Eliceiri K, Tomancak P, Cardona A (2012) Fiji: an open-source platform for biological-image analysis. Nat Methods 9(7):676–682. https://doi.org/10.1038/nmeth.2019
19. Schneider CA, Rasband WS, Eliceiri KW (2012) NIH image to ImageJ: 25 years of image analysis. Nat Methods 9(7):671–675. https://doi.org/10.1038/nmeth.2089
20. Paintdakhi A, Parry B, Campos M, Irnov I, Elf J, Surovtsev I, Jacobs-Wagner C (2016) Oufti: an integrated software package for high-accuracy, high-throughput quantitative microscopy analysis. Mol Microbiol 99(4):767–777. https://doi.org/10.1111/mmi.13264
21. Ducret A, Quardokus EM, Brun YV (2016) MicrobeJ, a tool for high throughput bacterial cell detection and quantitative analysis. Nat Microbiol 1(7):16077. https://doi.org/10.1038/nmicrobiol.2016.77
22. Ursell T, Lee TK, Shiomi D, Shi H, Tropini C, Monds RD, Colavin A, Billings G, Bhaya-Grossman I, Broxton M, Huang BE, Niki H, Huang KC (2017) Rapid, precise quantification of bacterial cellular dimensions across a genomic-scale knockout library. BMC Biol 15(1):17. https://doi.org/10.1186/s12915-017-0348-8

23. Linkert M, Rueden CT, Allan C, Burel J-M, Moore W, Patterson A, Loranger B, Moore J, Neves C, MacDonald D, Tarkowska A, Sticco C, Hill E, Rossner M, Eliceiri KW, Swedlow JR (2010) Metadata matters: access to image data in the real world. J Cell Biol 189(5):777–782. https://doi.org/10.1083/jcb.201004104
24. Dyrda G, Boniewska-Bernacka E, Man D, Barchiewicz K, Słota R (2019) The effect of organic solvents on selected microorganisms and model liposome membrane. Mol Biol Rep 46(3):3225–3232. https://doi.org/10.1007/s11033-019-04782-y
25. Barák I, Wilkinson AJ (2007) Division site recognition in *Escherichia coli* and *Bacillus subtilis*. FEMS Microbiol Rev 31(3):311–326. https://doi.org/10.1111/j.1574-6976.2007.00067.x
26. Errington J, Wu LJ (2017) Cell cycle machinery in *Bacillus subtilis*. In: Löwe J, Amos LA (eds) Prokaryotic cytoskeletons: filamentous protein polymers active in the cytoplasm of bacterial and archaeal cells. Springer, Cham, pp 67–101. https://doi.org/10.1007/978-3-319-53047-5_3
27. Brajtenbach D, Puls JS, Matos de Opitz CL, Sass P, Kubitscheck U, Grein F (this volume) Quantitative analysis of microscopy data to evaluate bacterial responses to antibiotic treatment. In: Sass P (ed) Antibiotics: methods and protocols, Methods in molecular biology. Springer, New York

Chapter 10

Expansion Microscopy of *Bacillus subtilis*

Viola Middelhauve, Jan Peter Siebrasse, and Ulrich Kubitscheck

Abstract

Expansion microscopy enables super-resolved visualization of specimen without the need of highly sophisticated and expensive optical instruments. Instead, the method is executed with conventional chemicals and lab equipment. Imaging of bacteria is performed using standard fluorescence microscopy. This chapter describes a protocol for the expansion microscopy of *Bacillus subtilis* expressing DivIVA-GFP. In addition, the cell wall was labeled by wheat germ agglutinin. Here, we place emphasis on the challenges of selecting the protein and organism of interest.

Key words Expansion microscopy, super resolution, cell wall, fluorescence labeling, mutanolysin

1 Introduction

Fluorescence microscopy is a standard tool to investigate microbiological questions by labeling of specific cellular target structures. Features of the technique are multicolor staining and high image contrast. However, the optical diffraction limit restricts resolution to about 200–300 nm. Especially in the case of microorganisms, this limits the amount of obtainable information. The situation has been improved by the introduction of super-resolution microscopy [1]. Instead of using optical microscopy techniques [2–5], the biological sample itself can physically be enlarged in order to achieve a virtual super resolution. This approach was recently introduced by Chen et al. [6] and is referred to as *expansion microscopy* (ExM). ExM allows the physical expansion of fixed samples via a swellable polyelectrolyte hydrogel by a factor of about 4.5. The method comprises five key steps (Fig. 1). First, the biological sample is chemically fixed. During linking, biomolecules are equipped with chemical anchors, which enable incorporation of the proteins into the polyelectrolyte gel during gel polymerization, that is, the gelation process. Next, the gelled sample is homogenized by an enzymatic digestion to finally enable its subsequent

Peter Sass (ed.), *Antibiotics: Methods and Protocols*,
Methods in Molecular Biology, vol. 2601, https://doi.org/10.1007/978-1-0716-2855-3_10,

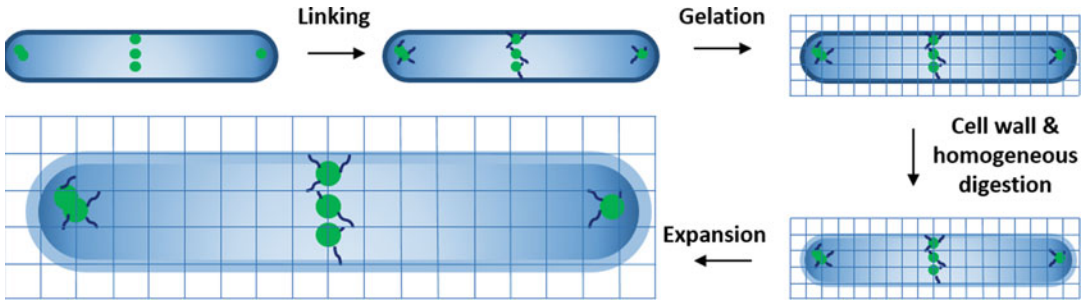

Fig. 1 Schematic workflow for expansion microscopy of bacterial cells. A bacterial cell (blue rod) containing the protein of interest (green) is fixed and is applied with chemical linkers (dark blue). The gel (grid) is formed by polymerization. Subsequently the sample is digested and expanded. Bacterial cells containing a cell wall require an additional step for cell wall digestion

isotropic expansion. The protocol is oftentimes extended by immunofluorescence staining after fixation or digestion.

Up to now, only few studies have successfully applied expansion microscopy to bacteria [7–12], which pose a particular challenge due to their rigid cell wall. Hence, an additional step needs to be added to the protocol: cell wall digestion. Furthermore, low protein copy numbers and non-standardized fixation and immunofluorescence protocols complicate successful ExM. We provide this protocol to enable more researchers to analyze specific bacterial proteins via ExM and to facilitate further protocol optimization and adaptation. We demonstrate ExM of *Bacillus subtilis* expressing DivIVA-GFP in addition to cell wall staining by wheat germ agglutinin (WGA).

2 Materials

Prepare all solutions using double distilled water (ddH_2O).

2.1 Cultivation

1. *B. subtilis* expressing DivIVA-GFP (*see* **Notes 1–3**).
2. Culture medium: Lysogeny Broth (LB, *see* **Note 4**).
3. Selection antibiotic: Chloramphenicol.
4. Cultivation flasks: 50 mL centrifugation tube and baffled Erlenmeyer flask 0.1–1 L.
5. Inoculation loop.
6. Heated shaking incubator.
7. Spectrophotometer measuring at 600 nm.

2.2 Fixation and Staining

1. Phosphate buffered saline (1× PBS): 136.89 mM NaCl, 10 mM $Na_2HPO_4{\cdot}2H_2O$, 1.98 mM KH_2PO_4, 2.68 mM KCl.
2. 15 mL centrifugation tube, 1.5 mL reaction tubes.

3. Centrifuges (15 mL/50 mL tubes, 1.5 mL tubes).
4. 4% Paraformaldehyde (PFA), methanol free in 1× PBS (*see* **Notes 5** and **6**).
5. 0.15 M NaCl.
6. Wheat germ agglutinin-CF633 (WGA-CF633): Create stock solution of 100 μg/mL WGA-CF633 in 0.15 M NaCl in a final volume of 1 mL. Store aliquots of 50 μL (*see* **Notes 6**–**8**).

2.3 Expansion Microscopy

1. Permeabilization buffer: Prepare 1× PBS containing 0.3% Triton-X-100 (PBST).
2. Linker: 1 M methacrylic acid N-hydroxy-succinimide ester (MA-NHS) in DMSO (*see* **Notes 6** and **9**).
3. Monomer solution: Mix 2.25 mL of 19 g/50 mL sodium acrylate, 0.5 mL of 25 g/50 mL acrylamide, 0.75 mL of 1 g/50 mL N,N′-methylenebisacrylamide, 4 mL of 14.6 g/50 mL NaCl with 1 mL of 10× PBS and 0.9 mL of ddH_2O (*see* **Notes 6, 10,** and **11**).
4. 0.5% (w/v) 4-hydroxy-TEMPO.
5. 10% (w/v) ammonium persulfate (APS).
6. Tetramethylethylenediamine (TEMED).
7. Coverslips 22 × 22 mm^2 (bottom coverslip), 15 mm, round, H1.5 (sample coverslip), 18 × 18 mm^2 (top coverslip), and double-sided tape of 100 μm thickness for the gelation chamber.
8. Coverslip (25 mm, round).
9. Soft brush.
10. Coverslip tweezers.
11. Cell wall digestion buffer: Add 160 U/mL mutanolysin to 1× PBS.
12. Proteinase K digestion buffer: Add 50 mM Tris, 1 mM EDTA, 0.5% Triton-X100, 0.8 M guanidine HCl, and 8 U/mL of proteinase K at pH 8.0 (*see* **Notes 6** and **12**).
13. Expansion water: Add 5 mM HEPES to ddH_2O. Adjust to pH 7 (*see* **Note 13**).

2.4 Sample Chamber, Image Acquisition, and Analysis

1. 0.1% (w/v) poly-L-lysine.
2. Sharp, planar cutting tool, for example, razor blade.
3. Imaging chamber with a coverslip (specified H1.5, 170 μm thickness), for example, Ibidi μ-dish.
4. Inverted microscope, for example, Nikon Eclipse Ti.
5. Scientific camera, for example, Photometrics Prime BSI sCMOS camera.

6. High magnification objective with high numerical aperture (NA), for example, 100×, oil immersion, NA 1.49, TIRF.
7. Low fluorescence immersion oil corrected for use at RT.
8. Laser box with emission lines at 488 nm and 638 nm.
9. Highly inclined and laminated optical (HiLo) illumination system [13].
10. Motorized z-stage.
11. Software to automatically control the microscope, for example, MicroManager [14].
12. Computer hardware, for example, Microsoft Windows 10 pro, Intel® Core™ i7-9700 (8cores), 16 MB RAM memory, and integrated graphic card.
13. Software for image processing, for example, Fiji [15].

3 Methods

3.1 Cultivation

1. For a starter culture mix 6 mL LB with 5 μg/mL chloramphenicol in a 50 mL centrifugation tube and inoculate with *B. subtilis* DivIVA-GFP. Incubate overnight (ON) at 37 °C, 180 rpm (*see* **Note 14**).
2. For a main culture, mix 5 mL LB per gel sample with 5 μg/mL chloramphenicol and inoculate with 1% of the starter culture. Incubate at 37 °C, 180 rpm and grow to an optical density at 600 nm (OD_{600}) of 0.5 (*see* **Note 15**).

3.2 Fixation and Staining

1. Spin down the culture at 3000× *g* for 5 min at room temperature (RT) (*see* **Note 16**).
2. Fix immediately with 5 mL 4% PFA in 1× PBS for 15 min at RT, shaking. Afterward wash thrice with 1 mL 1× PBS. Starting here, all centrifugation steps are carried out at 4000× *g* for 1 min (*see* **Notes 17**–**19**).
3. For envelope staining, mix 50 μL of the WGA-CF633 stock in 0.15 M NaCl to a final volume of 1 mL. Mix with the sample pellet and incubate for 2 h at RT, shaking (*see* **Notes 20** and **21**).
4. For fixation of the dye, fix WGA-stained cells with 1 mL 4% PFA for 15 min at RT, shaking. Wash twice with 1× PBS (*see* **Note 22**).

3.3 Expansion Microscopy

1. Permeabilize with 1 mL PBST for 30 min at RT, shaking (*see* **Note 23**). Wash thrice with 1× PBS.
2. Link with 1 mL 2 mM MA-NHS in 1× PBS for 1 h at RT, shaking. Wash thrice with 1× PBS.

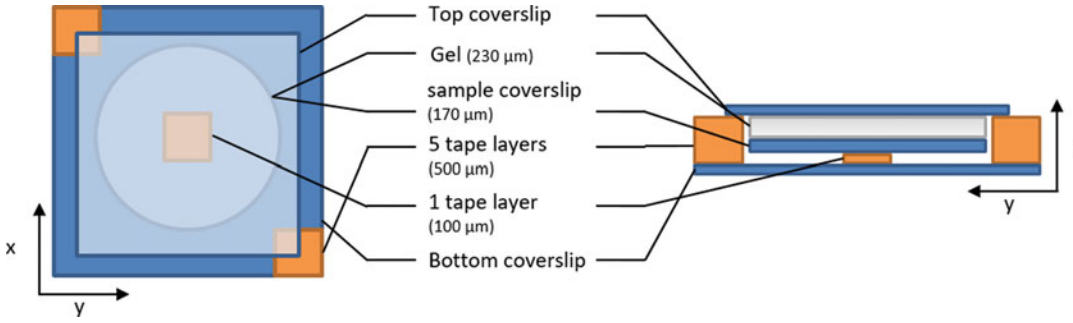

Fig. 2 Gelation chamber to create a 230 µm thick gel. The gel is positioned between the sample and the top coverslip. Coverslips are depicted in blue, tape in orange, the sample gel in gray

3. Prepare gelation chamber. To this end apply five 3 × 3 mm^2 double-sided tape layers (with a total thickness of 500 µm) to the diagonal corners of a 22 × 22 mm^2 coverslip and one double-sided tape layer to the center. Apply a clean 15 mm round coverslip (sample coverslip) with 170 µm thickness to the center tape layer. The top coverslip of 18 × 18 mm^2 will be added later. This will create a gel of 230 µm thickness after gelation (Fig. 2, *see* **Notes 24** and **25**).
4. Gelate. For one sample, 32.9 µL of monomer solution, and 0.7 µL each of 0.5% 4-hydroxy-TEMPO, TEMED, and 10% APS are required. First, add monomer solution to the cell pellet and resuspend. Quickly add 4-hydroxy-TEMPO and resuspend to avoid premature polymerization. Add TEMED and APS and resuspend well. Apply 35 µL of the sample to the gelation chamber. Rapidly add the top coverslip of 18 × 18 mm^2 size with tweezers. Incubate in a humid chamber 2 h at 37 °C (*see* **Note 26**).
5. Disassemble the gelation chamber by removing the upper coverslip and the sample coverslip including the sample gel from the bottom coverslip (*see* **Note 27**).
6. For cell wall digestion, place one 25 mm coverslip to the bottom of a 6-well plate. Add 2.5 mL of 160 U/mL mutanolysin in 1× PBS and add the gelated sample. Incubate ON at 37 °C (*see* **Notes 28**–**30**).
7. Remove mutanolysin reaction mixture.
8. Digest the sample homogeneously with Proteinase K. Mix 2.475 mL digestion buffer with 25 µL of 800 U/mL Proteinase K to create a reaction mixture of 8 U/mL Proteinase K. Incubate 4 h at 37 °C. Wash thrice with 1× PBS for 20 min at 4 °C, shaking.
9. Transfer to a 5 cm petri dish and expand in 5 mL expansion water ON at 4 °C (*see* **Notes 31** and **32**).

3.4 Image Acquisition

1. For sample mounting, coat the coverslip of the imaging chamber with 0.1% poly-l-lysine for 5 min (*see* **Note 33**).
2. Prepare the sample for imaging. Remove the expansion water from the gel and cut out a small piece for imaging with a scalpel. Remove the gel piece on a coverslip and slowly let it slide onto the coated imaging chamber. Apply expansion water to the imaging chamber to prevent drying of the gel (*see* **Notes 34** and **35**).
3. Apply immersion oil onto the objective.
4. Place the sample chamber onto the microscope.
5. Focus on the bacterial cells by utilizing the 638 nm laser line (*see* **Note 36**).
6. Acquire a z-stack using HiLo illumination (Fig. 3, *see* **Note 37**).

4 Notes

1. ExM works best with proteins, which are structurally anchored, such as fluorescently labeled membrane-binding or integral membrane proteins. Here, we show the preparation process for the example of DivIVA-GFP. As a membrane-binding protein, its position is retained after fixation with paraformaldehyde, whereas cytosolic proteins delocalize [18]. Moreover, the high expression level of DivIVA-GFP is well suited for the ExM protocol as it can be visualized even after "spatial dilution" of molecules and concomitant reduction of fluorescence intensity due to the volumetric expansion. Keep in mind that most bacterial proteins are expressed in low copy numbers when compared to eukaryotic systems.
2. A protein of interest (POI) fused to a fluorescent protein (FP) enables the observation of the protein localization at all protocol steps. This is helpful, since many steps can introduce delocalization. Additionally, utilizing a fused FP for localization has the advantage to circumvent the introduction of false-positive fluorescence signal, for example, via immunofluorescence. Prior attempts of signal amplification of GFP in *B. subtilis* and *Staphylococcus aureus* led to false-positive signals due to unspecific binding of the primary or secondary antibody. This is especially the case in *S. aureus*, which expresses immunoglobulin binding proteins SpA and Sbi, which lead to strong false-positive envelope signals.
3. GFP is a commonly used fluorescent reporter protein in ExM and well suited for several reasons. First, it is an FP emitting in the green range of the spectrum and therefore allows to achieve a high resolution. Second, it is an FP with relatively high fluorescence intensity. Third, GFP-like proteins have been

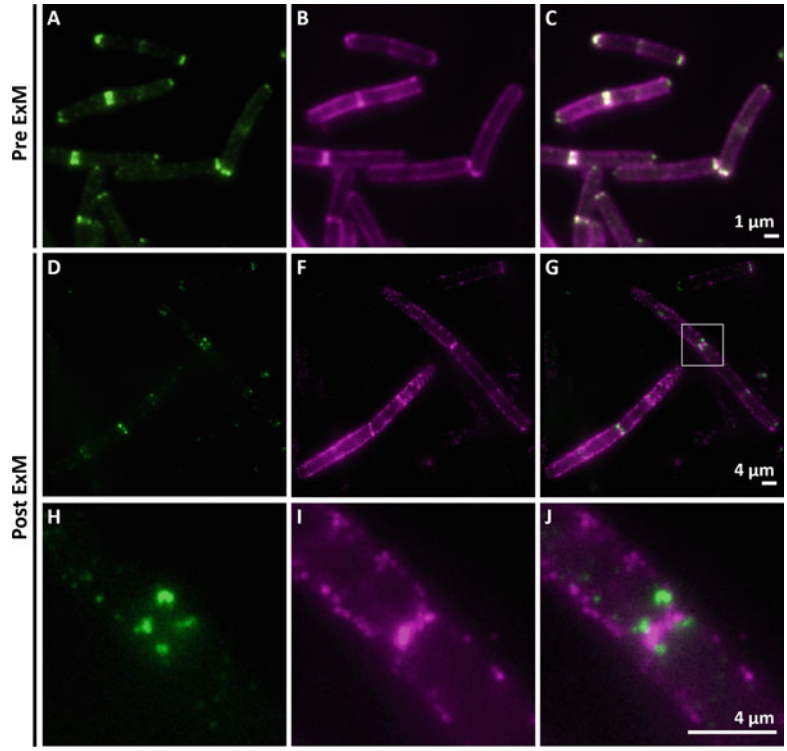

Fig. 3 ExM of *B. subtilis* expressing DivIVA-GFP (green) stained with WGA-CF633 (magenta). (**a**–**c**) Epifluorescence images of one z-slice of the stained and post-fixated sample before expansion. DivIVA-GFP is localized at the division septum and cell poles. (**d**–**j**) Maximum intensity projection of nine planes of the expanded sample acquired with HiLo illumination. (**h**–**j**) Magnified view of the region outlined by the white box in (**g**). The two adjacent DivIVA-rings on either side of the division septum can be resolved and visualized, similar to super-resolved three-dimensional structured illumination microscopy (3D-SIM) in live cells [16]. Images were acquired using a Nikon Eclipse Ti inverted microscope equipped with a Photometrics Prime BSI sCMOS camera and an electronically operated laser box C-FLEX from Hübner Photonics. A 100× oil immersion TIRF objective (NA 1.49) from Nikon was used. For images (**d**, **f**) HiLo illumination was achieved by a custom-built setup [17]. Expanded samples were excited with 488-nm and 638-nm laser lines with 50-mW nominal output and 500 ms integration time. Channels were averaged twice. The z-stack of the cell was taken in 0.25 µm steps. (**c**), (**g**), and (**j**) show overlaid fluorescence images of (**a**, **b**), (**d**, **f**), and (**h**, **i**), respectively

shown to withstand the relatively harsh chemical ExM protocol (retention of fluorescence intensity of >50% [19]). If other FPs are chosen, the preservation of the fluorescence must be checked, as every FP is degraded during the protocol to a different amount [19]. The same applies to other fluorophores, for example, fluorophores conjugated to antibodies for immunofluorescence.

4. As shown by [8], the cultivation medium might reduce the typically 4.5× expansion. Tryptic soy broth (TSB) leads to only ~2× expansion, whereas brain heart infusion broth (BHI) medium leads to typical expansion factors.
5. Prepare 4% PFA working stocks for storage.
6. Prepare aliquots, store at −20 °C. Thaw shortly before use. Avoid freeze-thawing. Discard residual solution after use.
7. WGA-CF633 stains the cell envelope by binding to N-acetylglucosamine of the cell wall. It fulfills two functions: first, it later enables the identification of the focus plane for image acquisition. As the target is present in a high concentration, this staining is stronger than the DivIVA-GFP and easily detectable under the microscope. Second, it prevents bleaching of the POI, DivIVA-GFP, by eliminating the need to identify the focal plane using the GFP signal. Finally, it enables the analysis of the relative position of the POI with regard to the cell wall.
8. The fluorophore CF633 was chosen due to the following reasons. First, its absorption and emission maxima are far from those of GFP enabling visualization without cross talk. The use of additional emission filters is not recommended, as they cut off the already low fluorescence intensity of the labeled POI after expansion (*see* **Note 1**). A long-wavelength fluorophore with lower resolution was used for visualizing the cell outline to allow the use of higher resolution fluorophores for the POI. Finally, CF633 survives the ExM protocol well [19].
9. Prepare 1 M stock solutions in DMSO.
10. Acrylamide, bisacrylamide, NaCl, and 10× PBS stock solutions can be stored at 4 °C. Sodium acrylate solution must be freshly prepared. Use a high purity sodium acrylate. Prepare stock solution with cooled water and mix in a cold water bath. If the solution has a yellow tint, do not use it, as it can negatively affect the experimental outcome. After opening, store the sodium acrylate bottle at low humidity in a desiccator.
11. Prepare monomer solution in an ice bath.
12. Proteinase K activity is heavily pH- and temperature-dependent. Adjust the pH to 8.0. Stock solutions can be prepared without proteinase K.
13. pH-adjusted water stabilizes the fluorescent proteins. Expansion water can be stored up to 3 months at 4 °C.
14. Use large cultivation flasks, filled to a maximum of 10%, and shake at high rpm, because *B. subtilis* is very sensitive to oxygen depletion.
15. When working with another target organism, the volume of culture per sample and the number of washing steps might need to be adjusted. Consider that in each washing step cells will be lost.

16. Avoid exceedingly high centrifugation speeds in all protocol steps as it may mechanically impair the cells.
17. The optimal fixation method might be a different one for your organism and POI. Protocol optimization can be executed by changing incubation times, temperatures, and fixatives. PFA yields good results when fixing membrane proteins in bacteria, whereas cytosolic proteins delocalize.
18. To avoid lysis of cells and concomitant protein delocalization, avoid storage ON and directly continue with the protocol until the sample is anchored in the expansion gel.
19. Starting at this protocol step, always protect the sample from light to avoid bleaching of the fluorophores.
20. The unusually long incubation duration is required in order to achieve a sufficiently high fluorescence intensity for visualization after volumetric expansion. Extension of incubation times with a potentially toxic compound is avoided by staining the cell after fixation.
21. This step needs to be executed before permeabilization to avoid staining of intracellular components.
22. This fixation step is required, because WGA interaction is not covalent and further washing steps are executed until sample gelation.
23. Permeabilization is required for a homogeneous distribution of the ExM chemicals within the sample.
24. A 230 μm thick gel is good to handle, whereas thinner gels break easily.
25. Ensure that all coverslips are dry to avoid dilution of the reaction mixture. In addition, a greater volume of solution leads to spillover, and the gelling solution is drawn under the coverslip by surface tension.
26. A volume of 35 μL is perfect for this setup. If any changes are made, first optimize the volume with gelation solution without sample. Generally, practicing the gelation process and the disassembly of the gel chamber after gel polymerization is strongly advised. In these steps, samples can easily be lost. Therefore, prepare several replicates.
27. For gelation chamber disassembly, first loosen the adhesive tape from the top coverslip by applying a drop of 1× PBS to the tape layers on the corners, for example, with a brush. Next, hold the bottom coverslip, insert a scalpel between the edge of the gel and the upper coverslip, and carefully press up. Remove the top coverslip without the gel. Then, carefully remove the sample coverslip with the gel from the bottom coverslip. Practice these steps and find the best technique. Coverslips do easily break, and the gel sometimes sticks to the top instead of the

sample coverslip. Avoid holding the upper top coverslip in this step but instead hold the bottom coverslip. Proceed with the protocol immediately to prevent the gel from drying out.

28. 6-well plates have been found useful for incubating gels with a diameter of up to 15 mm. To avoid drying out, seal the well plate with laboratory wrapping film in all incubation steps. 25 mm coverslips are added to enable gel transfer, as gel size increases due to swelling in aqueous solution during the digestion steps.
29. Mutanolysin treatment leads to a typical expansion factor of 4× in several tested organisms [8, 9]. The optimal enzyme for cell wall digestion depends on the cell wall architecture of the organism of interest. For example, *S. aureus* can isotropically be expanded after digestion with either mutanolysin or lysostaphin. Lysozyme often results in a non-isotropic expansion [9]. When expanding a bacterium lacking a cell wall, for example, Chlamydia species, this step may be omitted [10].
30. As the gel is transparent, use a dark background in all following pipetting steps for a better recognition of the gel. Additionally, adapt the light settings and viewing angles to the well plate in order to better localize the gel. Pipette very slowly. During these pipetting steps, take care not to suck up the gel into the pipette. Again, optimize the best conditions and practice with a dummy gel.
31. Alternatively, the sample can be expanded in 2 h at 4 °C by replacing the expansion water every 30 min.
32. If the gel shall be stored, keep in 1× PBS containing 0.02% sodium azide to stabilize the fluorophores and prevent microbial growth.
33. Poly-l-lysine coating allows attachment of the gel and prevents movement, which is essential for image acquisition.
34. Treat the expanded sample very gently. Exerted forces will lead to distorted samples, for example, cells stretched in one direction. While cutting, do not draw the razor blade across the gel, but instead press it down. Applying a drop of expansion water to the top of the gel might ease the sliding process.
35. Bacterial cells sink down to the bottom of the gel. Therefore, the bottom of the gel must face the coverslip for the cells to be within the working distance of the objective. Since the gel may rotate its position during preceding pipetting steps, preparation of two gel pieces facing up and down can be helpful to quickly identify the correctly oriented gel.
36. The WGA-CF633 envelope stain should be used for adjusting the focus plane. Exciting the POI, here DivIVA- GFP, bleaches the POI unnecessarily.

37. Due to low signal intensity, it is recommended to perform image acquisition using widefield or HiLo illumination and a sensitive camera. HiLo enhances the contrast, as less out-of-focus light is detected. If using confocal microscopy image acquisition parameters should carefully be optimized.

Acknowledgments

The authors appreciate funding by the Deutsche Forschungsgemeinschaft (DFG, German Research Foundation): Project-ID 398967434 -TRR261 (TRR 261 project Z02).

References

1. Schermelleh L, Ferrand A, Huser T et al (2019) Super-resolution microscopy demystified. Nat Cell Biol 21:72–84. https://doi.org/10.1038/s41556-018-0251-8
2. Hell SW, Wichmann J (1994) Breaking the diffraction resolution limit by stimulated emission: stimulated-emission-depletion fluorescence microscopy. Opt Lett 19:780–782. https://doi.org/10.1364/ol.19.000780
3. Betzig E, Patterson GH, Sougrat R et al (2006) Imaging intracellular fluorescent proteins at nanometer resolution. Science 313:1642–1645. https://doi.org/10.1126/science.1127344
4. Hess ST, Girirajan TPK, Mason MD (2006) Ultra-high resolution imaging by fluorescence photoactivation localization microscopy. Biophys J 91:4258–4272. https://doi.org/10.1529/biophysj.106.091116
5. Rust MJ, Bates M, Zhuang X (2006) Sub-diffraction-limit imaging by stochastic optical reconstruction microscopy (STORM). Nat Methods 3:793–795. https://doi.org/10.1038/nmeth929
6. Chen F, Tillberg PW, Boyden ES (2015) Optical imaging. Expansion microscopy. Science 347:543–548. https://doi.org/10.1126/science.1260088
7. Zhang YS, Chang J-B, Alvarez MM et al (2016) Hybrid microscopy: enabling inexpensive high-performance imaging through combined physical and optical magnifications. Sci Rep 6:22691. https://doi.org/10.1038/srep22691
8. Kunz TC, Rühling M, Moldovan A et al (2021) The expandables: cracking the staphylococcal cell wall for expansion microscopy. Front Cell Infect Microbiol 11:644750. https://doi.org/10.3389/fcimb.2021.644750
9. Lim Y, Shiver AL, Khariton M et al (2019) Mechanically resolved imaging of bacteria using expansion microscopy. PLoS Biol 17:e3000268. https://doi.org/10.1371/journal.pbio.3000268
10. Kunz TC, Götz R, Sauer M et al (2019) Detection of chlamydia developmental forms and secreted effectors by expansion microscopy. Front Cell Infect Microbiol 9:276. https://doi.org/10.3389/fcimb.2019.00276
11. Götz R, Kunz TC, Fink J et al (2020) Nanoscale imaging of bacterial infections by sphingolipid expansion microscopy. Nat Commun 11:6173. https://doi.org/10.1038/s41467-020-19897-1
12. Fan Y, Lim Y, Wyss LS et al (2021) Mechanical expansion microscopy. Methods Cell Biol 161:125–146. https://doi.org/10.1016/bs.mcb.2020.04.013
13. Tokunaga M, Imamoto N, Sakata-Sogawa K (2008) Highly inclined thin illumination enables clear single-molecule imaging in cells. Nat Methods 5:159–161. https://doi.org/10.1038/nmeth1171
14. Edelstein AD, Tsuchida MA, Amodaj N et al (2014) Advanced methods of microscope control using μManager software. J Biol Methods 1:10.14440/jbm.2014.36
15. Schindelin J, Arganda-Carreras I, Frise E et al (2012) Fiji: an open-source platform for biological-image analysis. Nat Methods 9:676–682. https://doi.org/10.1038/nmeth.2019
16. Eswaramoorthy P, Erb ML, Gregory JA et al (2011) Cellular architecture mediates DivIVA ultrastructure and regulates min activity in

Bacillus subtilis. MBio:2. https://doi.org/10.1128/mBio.00257-11

17. Landvogt L, Ruland JA, Montellese C et al (2019) Observing and tracking single small ribosomal subunits in vivo. Methods 153:63–70. https://doi.org/10.1016/j.ymeth.2018.09.001
18. Zhu L, Rajendram M, Huang KC (2021) Effects of fixation on bacterial cellular dimensions and integrity. iScience 24:102348. https://doi.org/10.1016/j.isci.2021.102348
19. Tillberg PW, Chen F, Piatkevich KD et al (2016) Protein-retention expansion microscopy of cells and tissues labeled using standard fluorescent proteins and antibodies. Nat Biotechnol 34:987–992. https://doi.org/10.1038/nbt.3625

Chapter 11

Tracking Global and Local Changes in Membrane Fluidity Through Fluorescence Spectroscopy and Microscopy

Madeleine Humphrey, Ireny Abdelmesseh Nekhala, Kathi Scheinpflug, Oxana Krylova, Ann-Britt Schäfer, Jessica A. Buttress, Michaela Wenzel, and Henrik Strahl

Abstract

Membrane fluidity is a critical parameter of cellular membranes, which cells continuously strive to maintain within a viable range. Interference with the correct membrane fluidity state can strongly inhibit cell function. Triggered changes in membrane fluidity and associated impacts on lipid domains have been postulated to contribute to the mechanism of action of membrane targeting antimicrobials, but the corresponding analyses have been hampered by the absence of readily available analytical tools. Here, we expand upon the protocols outlined in the first edition of this book, providing further and alternative protocols that can be used to measure changes in membrane fluidity. We provide detailed protocols, which allow straightforward in vivo and in vitro measurement of antibiotic compound-triggered changes in membrane fluidity and fluid membrane microdomains. Furthermore, we summarize useful strains constructed by us and others to characterize and confirm lipid specificity of membrane antimicrobials directly in vivo.

Key words Membrane fluidity, Lipid domains, Membrane microdomains, Lipid packing, Fatty acid disorder, Laurdan, Nile Red, $DiIC_{12}$, RIFs, Lipid mutants, Membrane targeting antimicrobials

1 Introduction

Numerous antimicrobial compounds target bacterial cytoplasmic membranes and disrupt the normal function of this essential cellular structure. Membrane-targeting compounds frequently unfold their antimicrobial properties by interfering with the diffusion barrier function of the cytoplasmic membrane [1]. As a consequence, a comprehensive set of tools has been developed to analyze cellular parameters related to membrane permeability, such as ion

Authors Madeleine Humphrey, Ireny Abdelmesseh Nekhala, Kathi Scheinpflug, and Oxana Krylova have equally contributed to this chapter.

Peter Sass (ed.), *Antibiotics: Methods and Protocols*,
Methods in Molecular Biology, vol. 2601, https://doi.org/10.1007/978-1-0716-2855-3_11,

leakage and membrane potential. However, not all membrane-targeting antimicrobials trigger permeabilization of cellular membranes, and the mechanisms of action of this category of antimicrobials are considerably less understood [1].

In addition to its permeability barrier function, a correct fluidity state of the membrane is equally important in order to support the multitude of membrane associated cellular processes [2, 3]. Interference with the fluidity state of the membrane by an antimicrobial compound either by causing changes in the overall membrane fluidity, or by triggering formation of abnormal lipid domains, has high potential to inhibit cell growth [4–7]. The analysis of these important cellular parameters has been greatly hampered by the relative absence of suitable, easy to adapt analytical tools. Here, we provide detailed protocols for the analysis of membrane fluidity of bacterial cell membranes both on a global scale and on a single cell level with spatial resolution. These protocols build and extend upon assays described in a previous edition of this book [8]. The provided measurements can be carried out with widely available standard laboratory equipment such as a fluorescence microplate reader and widefield epifluorescence microscope.

The first set of protocols provided in this chapter make use of a fluorescent, fluidity-sensitive, and non-inhibitory membrane dye Laurdan [9, 10]. The fluorescence emission spectrum of Laurdan is sensitive to the presence of H_2O close to its chromophore. The ability of H_2O to penetrate the hydrophobic membrane interior is dominated by lipid head group packing density and fatty acid disorder of lipid bilayers. As a consequence, the fluorescence emission spectrum of membrane-embedded Laurdan is sensitive to membrane fluidity and disorder in its surroundings (*see* Fig. 1) [9–13]. A protocol for the use of an alternative dye Nile Red to visualize local changes in membrane fluidity is also provided. Such an alternative is important when Laurdan cannot be used, for example, due to spectral overlaps or unfavorable dye-antimicrobial interactions. Nile Red is a lipophilic dye that fluoresces in nonpolar environments such as bacterial membranes and can be used to analyze lipid domains with standard fluorescent microscopes [12, 14]. It also has the valuable property of being neutral, meaning it does not exhibit charge-based preferential interactions with the different phospholipid head groups present in the membrane.

Complementary to Laurdan and Nile Red, the fluid membrane domain reporter $DiIC_{12}$(1,1′-didodecyl-3,3,3′,3-′-tetramethylindocarbocyanine perchlorate) can be used in microscopic analyses. This fluorescent dye binds to cell membranes, where it preferentially inserts into more fluid membrane regions. This selectivity is promoted by its short hydrocarbon tail, which is better accommodated in thinner and more disordered membrane domains (Fig. 2). $DiIC_{12}$ can be used to visualize the distribution

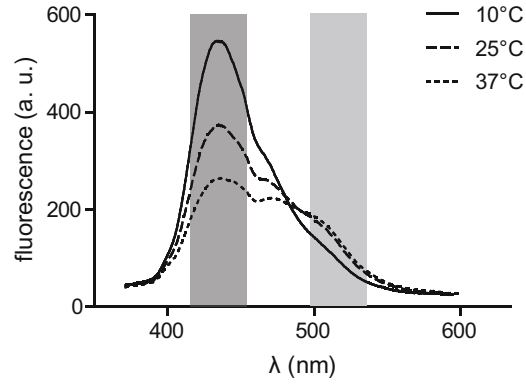

Fig. 1 Fluorescence emission spectrum of Laurdan incorporated in small unilamellar vesicles (SUVs) formed of *E. coli* polar lipid extract. Note the spectral shift towards higher wavelength in higher temperatures (indicating increased membrane fluidity). The wavelength ranges used for the ratiometric measurement of Laurdan fluorescence (Laurdan GP) are highlighted in light and dark grey, respectively. (Figure reprinted from Ref. [8])

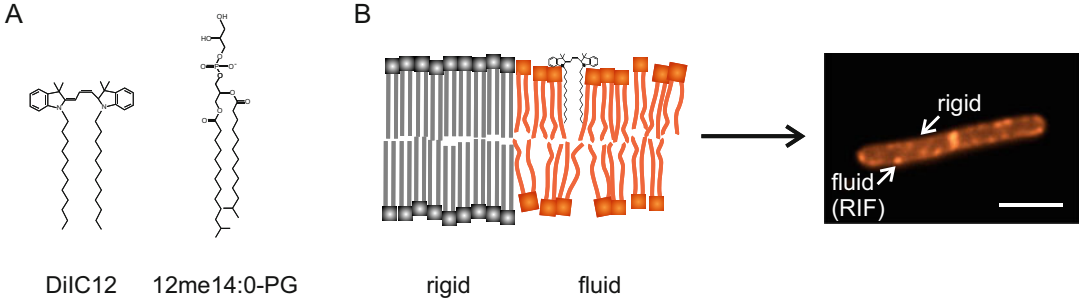

Fig. 2 $DiIC_{12}$ structure and preference for fluid membrane microdomains. (**a**) Structure of $DiIC_{12}$ in comparison with 12-methyltridecanoyl-phosphatidylglycerol (12me14:0-PG). PG is the most abundant head group and 12me14:0 one of the most common fatty acids in *B. subtilis* 168. (**b**) $DiIC_{12}$ prefers thin and disorganised membrane domains (regions of increased fluidity, RIF) over thick and rigid membrane areas (left), resulting in a spotty staining pattern in exponentially growing *B. subtilis* (right). Scale bar 2 μm. Figure adapted from Wenzel et al. [19]

of naturally occurring fluid membrane domains, coined "regions of increased fluidity" (RIFs). These microdomains have been observed both in the gram-positive model *Bacillus subtilis* and in gram-negative *Escherichia coli* and appear to be intimately linked to lateral cell wall synthesis [12, 15]. Several antibiotics have been reported to disturb RIFs, most commonly by clustering them into larger aberrant domains [5, 7, 12, 16–18]. RIFs are growth phase-dependent and only occur in exponential growth phase [17, 19]. The protocol described here is designed to observe naturally occurring RIFs under optimal growth conditions. However, under conditions where RIFs are not natively detectable, $DiIC_{12}$ still stains cell membranes and accumulates in antibiotic induced fluid membrane domains.

The provided protocols not only are optimized for the gram-positive model organism *B. subtilis* but also offer a good starting point for measurements in other gram-positive microorganisms such as *Staphylococcus aureus*. We provide example measurements of how these methods can be applied to gain insight into the mechanism of action of membrane-targeting antimicrobials. At last, we provide a summary of lipid-modified *B. subtilis* strains developed by us and others. These strains enable testing and confirming of the contribution of specific lipid-antimicrobial interactions to the antimicrobial activity directly in vivo.

2 Materials

2.1 Laurdan Fluorescence Spectroscopy In Vivo

1. Laurdan (6-Dodecanoyl-2-Dimethylaminonaphthalene) either from Molecular Probes or Sigma-Aldrich. Prepare a 1 mL stock solution of 1 mM in 100% dimethylformamide (DMF), store in −20 °C, and keep always in the dark.
2. Benzyl alcohol. Prepare a 5 M stock by dilution with dimethyl sulfoxide (DMSO), store in −20 °C, cover stored aliquots with argon or N_2 to prevent oxidation (we recommend 10 μL aliquots, do not reuse once open).
3. Fluorescence microplate reader. Both monochromator-based plate readers and filter-based readers equipped with 350 nm excitation filter and appropriate emission filters (ranges spanning 420–460 nm and 490–520 nm) are suitable.
4. Black, flat bottom 96-well microplates, if reusable microplates are used ensure proper cleaning after use.

2.2 Laurdan Fluorescence Spectroscopy In Vitro

1. Phospholipids of choice. Either natural lipid extracts or mixtures of synthetic or purified lipids can be used. We recommend either *E. coli* polar lipid extract, or a mixture mimicking bacterial cytoplasmic membrane composed of a zwitterionic 1-palmitoyl-2-oleoyl-*sn*-glycero-3-phosphoethanolamine (POPE) combined either with anionic cardiolipin or 1-palmitoyl-2-oleoyl-*sn*-glycero-3[phosphor-*rac*-(1-glycerol)] (POPG). All lipids mentioned above can be purchased from Avanti Polar Lipids.
2. Laurdan (6-Dodecanoyl-2-Dimethylaminonaphthalene, Molecular Probes or Sigma-Aldrich). Prepare a 0.2 mg/mL Laurdan solution in chloroform, store in −20 °C, and keep dark.
3. Buffer of choice. We routinely use 10 mM sodium phosphate (NaH_2PO_4/Na_2HPO_4) buffer containing 154 mM NaCl and 0.1 mM EDTA, pH 7.4.
4. Chloroform and methanol of highest available purity.

5. Nitrogen or argon gas.
6. 1.5 mL or 2 mL microcentrifuge tubes and pipette tips siliconized if necessary (*see* **Note 1**).
7. Round-bottomed glass vials (~5 mL) with tightly sealed caps. Flat-bottomed glass vials (~2 mL) with caps.
8. Graduated glass pipettes (2 mL); Hamilton gastight syringe (100–200 μL).
9. High-vacuum pump (10^{-2}–10^{-4} mbar).
10. Mini-extruder and polycarbonate membranes with defined pore size (*see* **Note 2**). Can be purchased from Avestin Inc. or Avanti Polar Lipids.
11. Dry ice, ultrasound bath with thermoregulation.
12. Fluorescence spectrometer (monochromator-based).
13. Disposable macro UV/VIS cuvettes (3 mL, 1 × 1 cm).
14. Magnetic stir bar (<10 mm in length).

2.3 Laurdan Fluorescence Microscopy

1. Laurdan (6-Dodecanoyl-2-Dimethylaminonaphthalene) either from Molecular Probes or Sigma-Aldrich. Prepare a stock solution of 10 mM in 100% dimethylformamide (DMF).
2. Phosphate-buffered saline (PBS): 8.0 g/L NaCl, 0.2 g/L KCl, 1.15 g/L Na_2HPO_4, 0.2 g/L KH_2PO_4, pH 7.3, supplemented with 0.1% D-glucose.
3. Agarose (electrophoresis grade).
4. High-quality microscope slides, coverslips, and immersion oil.
5. Fluorescence microscope equipped with:
   (a) A high-quality 100× objective with good chromatic correction such as Nikon Plan Apo series, Zeiss Plan Apochromat series or equivalent.
   (b) Appropriate filter sets (excitation at approximately 350 nm, emission at 430–460 and 500–530 nm) (*see* **Note 3**).
   (c) Widefield illumination with strong light output at approximately 350 nm. We prefer an LED light source with 365 nm output for this application, but Hg-vapor or metal halide light sources are good alternatives.
   (d) Temperature control.
   (e) High-sensitivity CCD, EM-CCD or sCMOS camera with maximally 8 × 8 μm pixel size.

2.4 Nile Red Fluorescence Microscopy

1. Nile Red (Sigma-Aldrich). Prepare a stock solution of 50 μg/mL in 100% DMSO, store in −20 °C, and keep always in the dark.
2. Agarose (electrophoresis grade).
3. High-quality microscope slides, coverslips, and immersion oil.
4. Fluorescence microscope equipped with:
   (a) A high-quality 100× objective. Due to the single wavelength imaging, good chromatic correction is not as critical as with Laurdan microscopy.
   (b) Appropriate filter sets (filters for TRITC or red fluorescence proteins are suitable).
   (c) Widefield illumination with strong light output at 540–560 nm. We prefer an LED light source for this application.
   (d) Temperature control.
   (e) High-sensitivity CCD, EM-CCD or sCMOS camera with maximally 8 × 8 μm pixel size.

2.5 $DiIC_{12}$ Fluorescence Microscopy

1. $DiIC_{12}$ (Anaspec). Prepare a 100 μg/mL stock solution in sterile-filtered DMSO. When the dye has dissolved, centrifuge for 5 min (16,000× *g*, room temperature) to spin down any precipitated dye. Take the supernatant to prepare suitable aliquots, for example, 20 μL for 2 mL culture. Store one-time-use aliquots at −20 °C in the dark.
2. *B. subtilis* 168 or other gram-positive organism of choice. Preparing glycerol stocks in the same medium used for $DiIC_{12}$ experiments gives best results (*see* **Notes 4–6)**.
3. Lysogeny broth (LB): 10 g/L tryptone, 5 g/L yeast extract, 10 g/L NaCl (or other medium of choice). For washing steps, prepare medium supplemented with 1% DMSO. Pre-warm medium to growth temperature before use (*see* **Notes 7–9**).
4. Plastic culture tubes. *B. subtilis* is extremely sensitive to oxygen depletion and sub-optimal aeration results in severe disturbance of membrane domains. We found that growing 2 mL of culture in 50 mL conical centrifuge (falcon) tubes, tilted at 45° in a rotary shaker, provides optimal aeration (*see* also **Notes 9–11**).
5. 2 ml microcentrifuge tubes. To ensure optimal aeration, no more than 200 μL of culture should be used in a 2 ml microcentrifuge tube (*see* also **Notes 9** and **11**–**12**).
6. 1.2% agarose in water, kept liquid at 60 °C.
7. High-quality microscope slides, coverslips, and immersion oil.
8. Temperature-controlled microcentrifuge.

9. Thermomixer holding 2 mL microcentrifuge tubes.
10. Carbonyl cyanide m-chlorophenyl hydrazone (CCCP). Prepare a stock solution of 15 mM in 100% DMSO, store in −20 °C.
11. Shaking incubator. In our hands, orbital motion water baths have been proven optimal for growing *B. subtilis* cultures at constant temperature and aeration and provide best $DiIC_{12}$ results (*see* **Note 13**).
12. Fluorescence microscope equipped with environmental control chamber and Cy3 filter (*see* **Note 14–16**).

3 Methods

3.1 Laurdan Fluorescence Spectroscopy In Vivo

3.1.1 Sample Preparation and Data Acquisition

1. Grow cells to an optical density at 600 nm (OD_{600}) of approximately 0.5 in suitable growth medium supplemented with 0.1% glucose at the desired temperature (*see* **Notes 17–19**).
2. Transfer the cell suspension to a 2 mL microcentrifuge tube and add Laurdan to a final concentration of 10 μM (from a 1 mM Laurdan stock solution, *see* **Note 20**).
3. Incubate cells with Laurdan for 5 min at the desired growth temperature in a thermomixer. Cover tubes with aluminum foil to avoid light exposure.
4. Wash cells 4× in 2 mL pre-warmed PBS/glucose (centrifuge for 1 min at 17,000× *g* in a tabletop centrifuge, carefully remove the supernatant by pipetting, resuspend in fresh PBS/glucose, repeat four times). After the last wash, resuspend to obtain an OD_{600} of approximately 0.5 (*see* **Notes 21** and **22**).
5. Remove 500 μL of the cell suspension, transfer to a new microcentrifuge tube, and centrifuge as described above. Carefully harvest ~450 μL of the supernatant, which serves as Laurdan background fluorescence in subsequent measurement (background of buffer + dye not associated with cells).
6. Immediately proceed with fluorimetric measurement by transferring the stained cell suspensions, and the background sample to a pre-warmed black, flat bottom black 96-well microtiter plate (150 μL/well).
7. Depending on the antimicrobial compound of interest and the specific research question, three measurement options are possible:
   (i) Pre-incubation of the cell culture with the antibiotic of choice, followed by staining and measurement. This measurement mode is suitable for slow acting but tightly bound antimicrobials, or for an analysis of potential adaptation to

subinhibitory concentrations. In this case, we recommend a brief (2 min) shaking interval in the microplate reader before the fluorescence measurement.

(ii) Incubation of stained cell suspension with the antibiotic of choice for a given incubation time. In this case, incubate the stained cell suspension with the compound directly in the microtiter plate for a required time under shaking, followed by fluorescence measurement. In well-energized untreated cells (PBS/glucose + shaking), Laurdan GP-values were found to be stable for up to 45 min.

(iii) For a kinetic measurement, Laurdan fluorescence can be measured before and as a time series after addition of the antibiotic of interest. In order to ensure sufficient energization of the cells, we recommend either continuous shaking or a relatively low number of parallel samples. Measurement intervals of 0.5–1 min are a good starting point (*see* **Note 23**).

8. As a positive control, incubate cells with 50 mM membrane fluidizer benzyl alcohol (*see* **Note 24**)
9. Measure Laurdan fluorescence intensities upon excitation at 350 nm at two emission wavelengths. In a monochromator-based fluorimeter, the optimal wavelengths (435 and 500 nm) should be used. In a filter-based fluorimeter, filters with wavelengths centered at 430–460 nm and 490–520 nm are acceptable.

3.1.2 Data Analysis

1. Subtract values obtained from the background sample (fluorescence of unbound dye) from the cell suspension values for each wavelength. The same background values are subtracted from both treated and untreated samples (this assumes that the compound of choice does not have fluorescent properties itself).
2. Calculate Laurdan generalized polarization (GP) as follows:

$$GP = \frac{I_{435} - I_{500}}{I_{435} + I_{500}}$$

On a scale ranging from −1 to +1, high GP values correspond to low membrane fluidity and vice versa [8, 9]. Depending on the exact filters used, the absolute values vary and should be regarded as arbitrary values. Commonly, however, GP values of 0.1–0.6 are measured, *see* Figs. 3 and 4 for examples, where *B. subtilis* has been incubated with benzyl alcohol and the membrane rigidifying antimicrobial peptide cWFW [6].

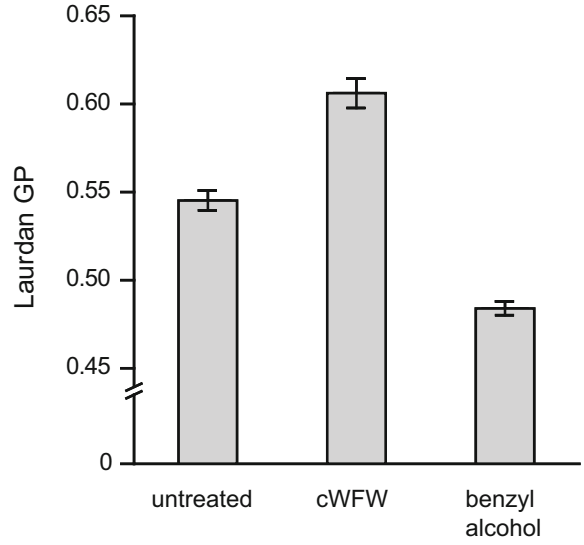

Fig. 3 Laurdan GP values measured for untreated live *B. subtilis* cells, and for cells incubated with membrane fluidizer benzyl alcohol (50 mM) and cWFW (6 μM), respectively. Note the reduced Laurdan GP (increased fluidity) in the presence of benzyl alcohol, and the opposite effect in the presence of cWFW. (Figure reprinted from Ref. [8])

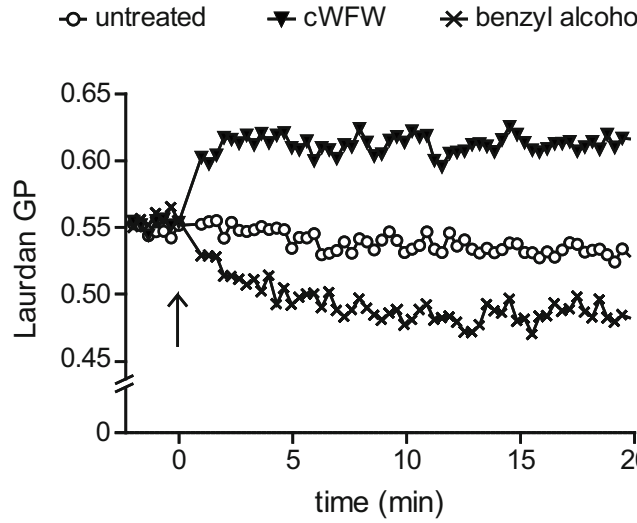

Fig. 4 Continuous measurement of Laurdan GP for untreated wild type *B. subtilis* cells, and for cells incubated with membrane fluidizer benzyl alcohol (50 mM) and cWFW (6 μM). The time point of benzyl alcohol and cWFW addition is indicated with an arrow. (Figure reprinted from Ref. [8])

3.2 Laurdan Fluorescence Spectroscopy In Vitro

3.2.1 Lipid Handling

1. Prepare three round-bottomed glass vials with tightly sealed lids, label the vials (lipid composition, data, etc.). Determine the weights of the vials (with lids on) on a microbalance taking at least five significant digits (*see* **Note 25**).
2. Pipette ~40 mg of lipid in organic solvent into one vial and add an appropriate volume of 0.2 mg/mL Laurdan solution in chloroform (150 μL for 40 mg of *E. coli* polar lipid extract, *see* **Note 26**) resulting in a Laurdan to lipid molar ratio of 1.5: 1000. Use a graduated glass pipette for lipid stock solution and Hamilton gastight syringe for the Laurdan stock solution. If the lipid was purchased in powder form, first dissolve it in chloroform or chloroform/methanol mixture of 3:1 to yield a concentration of 20 mg/mL and then proceed as above. At last, divide the lipid-Laurdan mixture into two other vials to obtain identical samples for replicate experiments.
3. Evaporate the organic solvent with dry nitrogen or argon by passing a gentle gas stream over the lipid-containing solution (*see* **Note 27**). During the procedure, slowly rotate the vial such that a thin lipid film is deposited on the walls and bottom of the vial while the solvent evaporates. Continue the procedure until the solvent has visually disappeared, followed by additional 3–4 min.
4. Use a high-vacuum pump (10^{-3}–10^{-4} mbar) for at least 3 h to remove traces of organic solvent. Seal the vials tightly in order to prevent water absorption from the air (use parafilm sealing over the tube caps after weighing the tubes (*see* **Step 5**)).
5. Weigh closed vials and subtract the weights of empty vials to calculate the net weight of the lipid films. Covered with argon or nitrogen, lipid-Laurdan films can be stored at −20 °C for 2–3 months (*see* **Note 28**).

3.2.2 Vesicle Preparation

1. Hydrate a lipid Laurdan film at room temperature for 30 min in a phosphate buffer pre-equilibrated to room temperature (20 mM final lipid concentration). For this aim, vortex the vial vigorously for ~5–10 min to solubilize the lipid film. Repeat additionally three to five times short (10–15 s) shaking of the suspension during the hydration step. As a result, a turbid suspension of multilamellar vesicles (MLV) will be formed (*see* **Note 29**).
2. Dilute the obtained lipid suspension with equal volume of buffer to obtain a 10 mM lipid stock (vortex well). Subject the stock to three cycles of freeze-thaw using dry ice and 40 °C water bath, with intensive vortexing of the thawed suspension. Depending on the number of samples in the experiment, part of the 10 mM lipid stock can be sealed with argon/nitrogen, frozen, and stored at −20 °C for replicate experiments (*see* **Note 30**).

3. To obtain an antimicrobial compound-free sample, dilute the 10 mM lipid stock to 1 mM with buffer. Use mini-extruder to prepare large unilamellar vesicles (LUVs). For this, fill one of two 1 mL gastight syringes with MLV suspension and connect to a mini-extruder equipped with two stacked polycarbonate filters with 100 nm pore size. Force the MLV suspension through the filter; a minimum of 21 extrusion cycles was found to be required for optimal LUV preparation (*see* **Notes 31** and **32**). Collect LUVs in a small flat-bottomed glass vial or a microcentrifuge tube.
4. Prepare several dilutions of the antimicrobial compound (0.5–1 mL each) and mix with equal volume of 2 mM lipid stock (diluted from 10 mM) in small flat-bottomed glass vials, shake well. This step provides samples with 1 mM lipid and different lipid-to-peptide (L/P) molar ratios (*see* **Note 33**).
5. If vesicles aggregate due to antibiotic adsorption, use sonication (ultrasonic bath) to dissolve the aggregates. Subject aggregated, highly turbid peptide-lipid samples to one to two cycles of sonication (5 min/cycle) in the bath in order to obtain uniformly opalescent samples.
6. At last, to obtain uniform LUVs, subject the sonicated vesicles to extrusion as described for the antimicrobial compound-free sample (*see* **Step 3**) (*see* **Note 34**).

3.2.3 Fluorescent Spectroscopy Parameters

Two data types can be obtained from Laurdan-labeled vesicles as a characteristic for a lipid membrane state: dye emission spectra and fluorescence intensities at fixed wavelengths.

1. To obtain the emission spectra, choose the emission scan mode of the fluorescent spectrometer (the emission spectrum is scanned, while the excitation wavelength is held constant). Set the excitation wavelength to 350 nm, which roughly corresponds to the adsorption maximum of Laurdan [9]. Set the emission wavelength to be scanned from 370 to 600 nm. Choose appropriate values for the slit widths of both excitation and emission monochromators. Pre-equilibrate the device at the temperature of choice (*see* Figs. 1 and 5 for examples of Laurdan spectra in vesicles).
2. To obtain fluorescence intensities at fixed wavelengths, choose fixed wavelength measurement mode (use dual wavelength mode when possible). Set the excitation wavelength to 350 nm and the emission wavelengths to 435 and/or 500 nm. When dual wavelength mode is not available, the emission wavelength needs to be changed manually in separate measurements. Choose appropriate values for the slit widths of both excitation and emission monochromators. Pre-equilibrate the device at the temperature of choice.

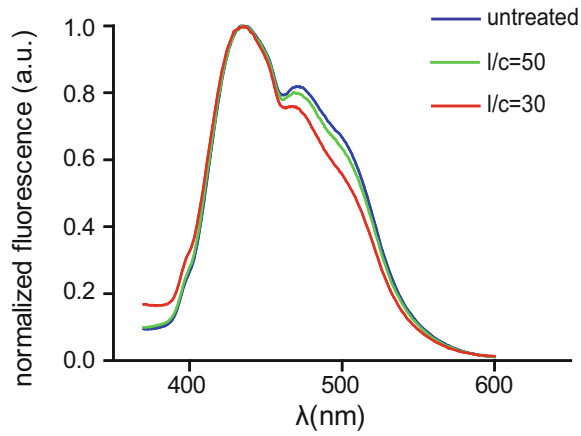

Fig. 5 Normalised fluorescence emission spectrum of Laurdan incorporated in large unilamellar vesicles (LUV's) formed of *E. coli* polar lipid extract. Note the reduced intensity of the higher wavelength shoulder of the spectrum in the presence of cWFW (indicating reduced membrane fluidity). l/c values represent lipid to compound molar ratios. (Figure reprinted from Ref. [8])

3.2.4 Data Acquisition

1. Prepare the samples by diluting 1 mM LUVs stocks with buffer (in 2 mL in disposable fluorescent cuvettes). Usually, 0.25–0.3 mM lipid is enough to obtain good fluorescence intensity signals. Equip the sample cuvette with a magnetic stir bar.
2. Place the sample in the sample compartment of the fluorescence spectrometer and equilibrate the temperature for at least 5 min (in-cell temperature sensor is recommended for accurate temperature control, *see* **Note 35**). Measure the sample containing only vesicles without additive (control) first. As Laurdan is sensitive to photobleaching, reduce the sample's exposure time to the light source by closing the shutters whenever no data are being collected.
3. Record fluorescence emission spectrum/fluorescence intensities at fixed wavelength with the settings specified above (*see* Subheading 3.2.3). If necessary, adjust the sensitivity of the photodetector (gain) to obtain a reasonable signal intensity and good signal-to-noise ratio, and repeat the measurement. Use identical settings for all parallel samples.
4. Repeat fluorescence recording for all parallel samples.
5. When different temperatures are scanned, start at low temperature (*see* **Note 36**). We found that it was more convenient from the practical point of view to scan all samples at one desired temperature and then repeat the procedure for the next temperature points.

3.2.5 Data Analysis

1. Data of fluorescence emission spectra can be easily represented and analyzed in a commonly used spreadsheet program, such as Microsoft Office Excel, SigmaPlot, or Origin. Normalization of the spectra to fluorescence intensity maximum gives more clear information about additive-induced changes in Laurdan fluorescence (*see* Fig. 5 for an example).
2. Fixed wavelength Laurdan fluorescence intensities are used to calculate Laurdan generalized polarization parameter, GP, which is given by following equation [10]:

$$\mathrm{GP} = \frac{I_{435} - I_{500}}{I_{435} + I_{500}}$$

This type of measurement is an in vitro equivalent of the in vivo measurement shown in Fig. 3.

3.3 Laurdan Fluorescence Microscopy

3.3.1 Sample Preparation

1. Grow cells to an OD_{600} of ~0.5 in a suitable growth medium supplemented with 0.1% glucose at the desired growth temperature (*see* **Note 19**).
2. Transfer 100 μL of the culture to a 2 mL (round bottom) microcentrifuge tube. Add Laurdan from a 10 mM stock solution (in 100% DMF) to a final concentration of 100 μM Laurdan and 1% DMF (*see* **Notes 20** and **37**).
3. Incubate the cell suspension for 5 min at the desired growth temperature under vigorous shaking (*see* **Note 38**) in the dark.
4. Remove unbound Laurdan by adding 1.9 mL pre-warmed PBS/glucose followed by centrifugation for 1 min (at max speed on a tabletop centrifuge), removal of the supernatant, and resuspension in 100 μL pre-warmed PBS/glucose (*see* **Note 39**).
5. Incubate the stained cell suspension with the compound of interest for a chosen time period under vigorous shaking. Alternatively, pre-incubate cells with the compound of choice before staining (*see* **Step 2**).
6. Immobilize 0.5 μL of stained cell suspension on a microscopy slide prepared with 1.2% agarose in H_2O (*see* **Notes 40** and **41**).

3.3.2 Microscope Calibration

In principle, the microscopy can be carried out with any widefield fluorescence microscope, but we strongly recommend the use of a microscope setup with an adjustable temperature chamber set to the growth temperature of the analyzed bacteria. It is paramount to use a high-quality microscope objective with a high level of correction for chromatic aberration. Even so, the residual difference in exact focal plane and magnification between the imaged wavelengths (450 and 520 nm) requires pre-calibration of the microscope setup (*see* **Note 42**).

1. Prepare a slide with 1.2% agarose in H_2O and add an appropriate dilution of a suspension of 0.1 μm diameter TetraSpeck™ microspheres.
2. Select a field of view with some fluorescent beads located close to both the left and right edge of the image field.
3. Carry out optical sectioning (200 nm step size, 5 μm depth) with both wavelengths (450 and 520 nm).
4. Measure the distance of two pixels located on the left and right edge of the image field using both wavelengths (due to the wavelength-dependency of magnification, the distance in pixels is slightly larger for the image captured at 450 nm).
5. Note the difference in pixel distance along the x-axis of the image between the chosen bead-pair. This will be used to correct for the wavelength-dependent difference in magnification upon image analysis.
6. Determine the difference in exact focal plane at the different wavelengths (450 and 520 nm) using the captured optical sections.
7. Use the difference in focal planes (z-offset) to correct for the residual difference in chromatic aberration. Most image capture software allows for the use of predefined z-offset values for different wavelengths.

3.3.3 Image Capture

1. Allow the microscope to reach a stable temperature by turning on the microscope body, and the heating unit at least 2 h in advance.
2. Pre-program the microscope for capture of a fluorescence image using a 350 nm excitation filter and a 520 nm emission filter, followed by a second image using a 350 nm excitation filter and a 450 nm emission filter. Define the z-offset value to correct for the different focus.
3. Rapidly capture images on both wavelengths for a required number of cells/fields (*see* **Notes 43** and **44**) and save them in a raw 16-bit uncompressed TIFF format.

3.3.4 Image Analysis

1. Increase the size of the higher wavelength image (520 nm) in order to correct for the wavelength-dependent difference in magnification. For this aim, use the conversion value obtained from the measurement of fluorescent beads upon microscope calibration.
2. Carefully correct the exact position of the cells (x/y-drift) manually in order to ensure a perfect image overlay (*see* Fig. 6) and crop the images to contain only the selected cells.

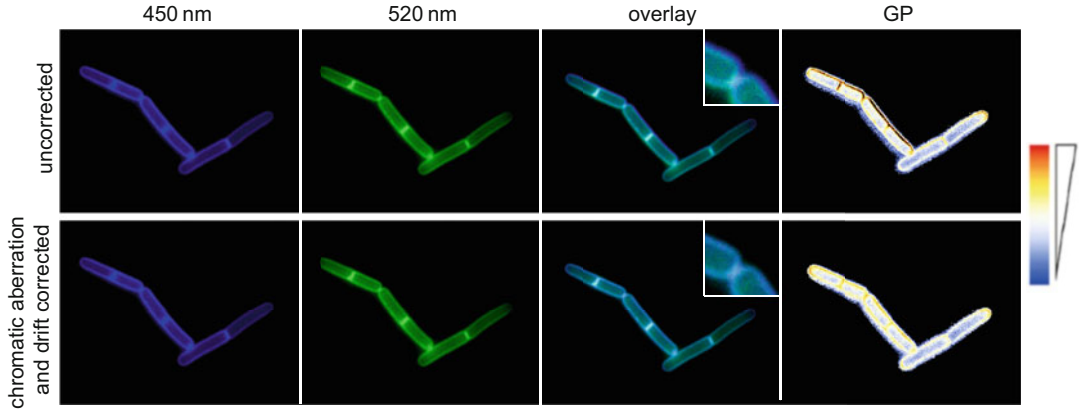

Fig. 6 Fluorescence microscopy of Laurdan-stained untreated *B. subtilis* cells at two different wavelengths (450 and 520 nm, 1st and 2nd panel, respectively). The 3rd panel depicts an overlay of the two micrographs, and the 4th panel pixel-by pixel calculated Laurdan GP values (red colour representing high and blue low membrane fluidity, respectively). Upper images depict the consequence of a poor correction for chromatic aberration and x/y-drift. The lower panels depict the same cells with proper corrections applied. (Figure reprinted from Ref. [8])

3. Convert the images into 32-bit format. This allows the use of decimal places in pixel intensity values, which is necessary for the representation of GP values.
4. With images prepared as above, the pixel-by-pixel calculation of Laurdan GP can now be performed using the equation:

$$GP = \frac{I_{450} - I_{520}}{I_{450} + I_{520}}$$

The specific details of the calculation depend on the program of choice. The corresponding software manual should provide sufficient guidance to perform the calculations. We routinely use Wolfram Mathematica for this step, but any software capable for image arithmetic can be used (*see* **Note 45**).

5. Due to the ratiometric nature of GP calculation, pixels with low fluorescence intensity (such as pixels outside of the cell) will also be assigned a GP-value. For visualization purposes, we find it useful to define an intensity cutoff below, which the GP-values are set to zero (and assigned the color black). An optimal cutoff value depends on the signal-to-background ratio, but 10% is a good starting value. The pixel-GP values associated with the cell (commonly in a positive range between 0.1 and 0.4) are best represented with a blue-red color scale, with blue representing low and red high membrane fluidity (*see* Figs. 6 and 7 for examples).

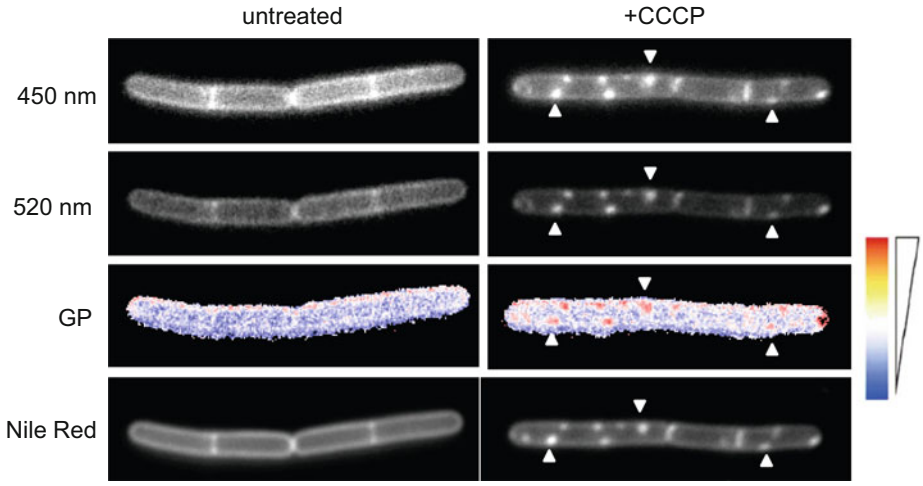

Fig. 7 Comparison of fluorescence microscopy of Laurdan- and Nile Red-stained untreated and CCCP treated (100 μM) *B. subtilis* cells. Laurdan fluorescence was measured at two different wavelengths (450 and 520 nm, 1st and 2nd panel, respectively). The 3rd panel depicts pixel-by pixel calculated Laurdan GP values (red representing high and blue low membrane fluidity, respectively). Nile Red fluorescence image was captured at 542 nm. Examples of CCCP-induced fluid membrane microdomains are indicated by arrows

3.4 Nile Red Fluorescence Microscopy

1. Grow cells to an OD_{600} of maximally 0.5 in a suitable growth medium at the desired growth temperature.
2. Transfer 100 μL of the culture to a 2 mL (round bottom) microcentrifuge tube (*see* **Note 37**). Incubate the cell suspension with the compound of interest for a chosen time period under vigorous shaking (*see* **Note 38**).
3. Add Nile Red from a 50 μg/mL stock solution (in 100% DMSO) to a final concentration of 0.5 μg/mL Nile Red and 1% DMSO, incubate with shaking for 5 min.
4. Immobilize 0.5 μL of stained cell suspension on a microscopy slide prepared with 1.2% agarose in H_2O (*see* **Note 40**).
5. Rapidly capture phase contrast and fluorescence images using suitable light source and filters and save them in a raw 16-bit uncompressed format (*see* **Note 43** and **46**).
6. Post-acquisition analysis of Nile Red fluorescence microscopy can be carried out with standard image analysis techniques (Fig. 7, *see* **Notes 47–49**).

3.5 $DiIC_{12}$ Fluorescence Microscopy

1. Grow overnight cultures (16 h) in medium of choice at the desired temperature (*see* **Note 5**).
2. Dilute the overnight cultures 1:200 using the same medium.
3. Add $DiIC_{12}$ to a final concentration of 1 μg/mL from a 100 μg/mL stock in DMSO (1% final concentration of DMSO, *see* **Notes 7** and **8**)

4. Grow cultures at the desired temperature until the desired cell density, typically exponential growth phase, in which microdomains are clearly visible (*see* **Note 5**).
5. Collect cells by centrifugation using pre-warmed 2 mL microcentrifuge tubes in a pre-warmed microcentrifuge (16,000× *g*, 30 s).
6. Wash the cell pellet four times with pre-warmed growth medium supplemented with 1% DMSO (*see* **Notes 7, 8**, and **50**). During all pipetting steps, keep the tubes at constant temperature using an appropriate thermomixer. It is recommended to resuspend cells by vortexing rather than pipetting to avoid shearing forces (*see* **Note 51**).
7. Resuspend washed cell pellets in the same medium supplemented with 1% DMSO and adjust the cell density to the desired final OD_{600}, typically 0.3–0.5 (*see* **Note 5**).
8. Transfer 200 μL aliquots of resuspended cell culture to pre-warmed 2 mL microcentrifuge tubes in an appropriate thermomixer. Keep samples at constant temperature and shake at all times (see **Notes 9** and **51**).
9. Add antibiotics of choice and incubate for the desired treatment time (*see* **Note 52**). Leave one sample untreated as the negative control, 150 μM CCCP [11] or other antibiotics with a known effect on membrane microdomains [5, 7, 15–17] can be used as the positive control, if desired (*see* **Note 53**).
10. If necessary, wash once more before taking samples for microscopy (*see* **Note 52**).
11. Spot 0.5 μL of the sample on a glass slide covered with a thin layer of 1.2% agarose and let excess liquid evaporate (*see* **Note 40** for preparation of slides).
12. Use phase contrast or bright field to locate a suitable field of view with a sufficient number of cells.
13. Acquire images in phase contrast and Cy3 fluorescence channels. Alternatively, $DiIC_{12}$ fluorescence can be imaged with a standard RFF filter (*see* Fig. 8 and **Notes 14** and **15**).

3.6 B. subtilis *Lipid-Modified Strains for the Analysis of Lipid Specificity of Antimicrobial Compounds*

3.6.1 B. subtilis *Strains with Tunable Phospholipid Composition*

B. subtilis strains with altered phospholipid composition have been successfully generated by us and others. Deletion of the genes required to make specific head groups has given strains lacking in each: cardiolipin, phosphatidylethanolamine, phosphatidylserine (also lacking phosphatidylethanolamine), lysyl-phosphatidylglycerol, and glycolipids (*see* Fig. 9a and Table 1). The use of these strains, when combined with minimum inhibitory concentration (MIC) and comparable susceptibility assays, or with the assays described in this chapter, provides straightforward methods to test if a given membrane-active compound exhibits lipid specificity in vivo and whether the specificity translates to altered susceptibility.

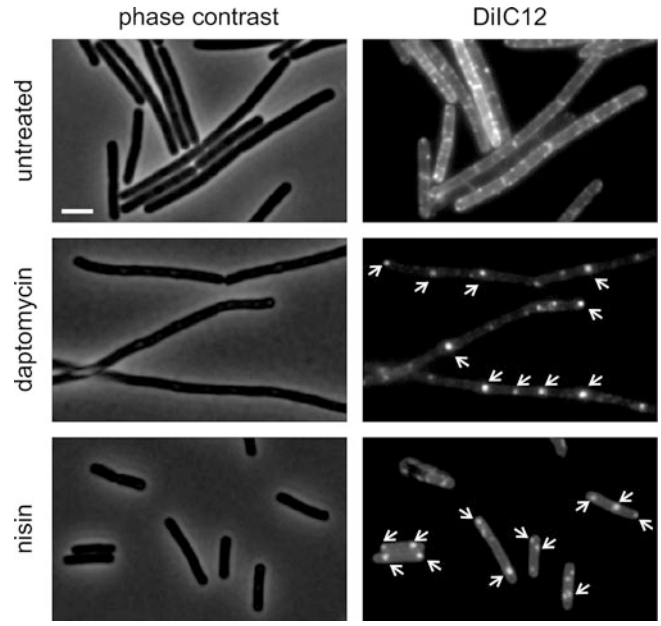

Fig. 8 Effects of antibiotics on RIFs. *B. subtilis* 168 was grown at 37 °C until an OD_{600} of 0.4 and subsequently treated with 2 μg/mL daptomycin (medium supplemented with 1.25 mM $CaCl_2$) for 60 min and 0.75 μg/mL nisin for 10 min, respectively. $DilC_{12}$ clusters are indicated by arrows. Scale bar 2 μm

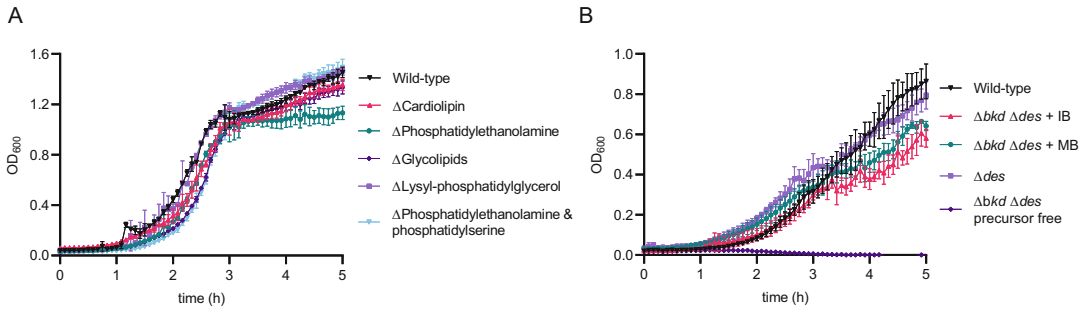

Fig. 9 (**a**) Growth curves of *B. subtilis* lipid head group modified strains grown in LB. Note the remarkable ability of all head group modified strains to grow similar to the wild-type cells. (**b**) Growth curves of *B. subtilis* tuneable fatty acid composition strains grown in fortified SMM media. Note the ability of Δ*bkd* Δ*des* to grow with a similar ability to wild-type cells when supplemented with isobutyric/methylbutyric acid, and the lack of growth in the absence of precursors

3.6.2 B. subtilis *Strains with Tunable Fatty Acid Composition and Fluidity*

We have recently developed a strain in which membrane fluidity can be modified through the deletion of the branched chain keto-dehydrogenase operon (*bkd*) and the desaturase *des* gene. This strain lacks the ability to synthesize branched chain fatty acids (BCFAs) or unsaturated fatty acids, making it dependent on the presence of exogenous fatty acid precursors. This auxotrophy can be exploited to control the BCFA content of the membrane,

Table 1
***B. subtilis* strains with tuneable lipid composition developed by us and others, and their growth requirement**

B. subtilis strain name	Genotypes	Lipid alteration	Growth requirements	Reference
ARK3	*clsA::tet, ywjE::spc, ywiE::kan*	Cardiolipin deficient	–	[20, 21]
KS119	*psd::MLS*	Phosphatidylethanolamine deficient	–	[21]
AK0117B	*ugtP::MLS*	Glycolipid deficient	–	[21]
AK0118B	*mprF::kan*	Lysyl-phoshatidylglycerol deficient	–	[21]
AK0119B	*pssA::spc*	Phosphatidylserine and phosphatidylethanolamine deficient	–	[21]
HS527 or HS550	*bkd::ery, des::spc* or *bkd::ery, des::kan*	Branched chain fatty acid modified	100 μM isobutyric acid for iso-fatty acids/methylbutyric acid for anteiso-fatty acids	[3, 22]
KS20 or KS50	*des::spc* or *des::kan*	Desaturase deficient	–	[3, 22]

through the feeding of specific precursors (see Fig. 9b and Table 1) [3]. Comparable to the lipid head group modified strains, this strain allows the analysis of membrane-fluidity dependency of an antimicrobial compound directly in vivo.

3.6.3 Preparation of Precursors for Tunable Fatty Acid Composition Strain

The tunable fatty acid composition strain, Δ*bkd* Δ*des*, requires supplementation with BCFA precursors. By supplementing with specific precursors, it is possible to tune the BCFA composition and, thus, the membrane fluidity of the strain [3]. Here, anteiso-BCFAs are synthesized when the medium is supplemented with 2-methylbutyric acid and iso-BCFAs when supplemented with isobutyric acid. 2-Methylbutyric acid and isobutyric acid can both be obtained from Sigma-Aldrich. The acids should be diluted with water to stock solution of 100 mM and added to the culture to support growth in a 1/1000 dilution to achieve 100 μM. To prevent the presence of other FA precursors, this strain should be grown in a minimal media, such as fortified Spizizen Minimal Media [3].

4 Notes

1. Some hydrophobic substances strongly adsorb to plastic and/or glass surfaces. This problem can be fixed by using siliconized tubes and pipette tips for all steps handling such a substance [23].
2. Lipid vesicle size defines the scattering intensity of a solution. Light scattering can noticeably influence the signal intensities when performing fluorescence-spectroscopic experiments. Wherever possible, smaller vesicle size is preferable for the studies. Alternatively, to extrusion, small lipid vesicles can be obtained by sonication [19]. Scattering effects can also be taken into account by performing control experiments where fluorescence intensities are measured in dye-free system and then subtracted from the values obtained for the dye.
3. Commonly available filter sets used to image DAPI, FITC, and GFP can be used to carry out Laurdan GP microscopy. In a microscopy setup in which excitation and emission filters and the dichroic mirrors can be chosen independently, the combination of DAPI excitation (commonly ~350 nm), DAPI dichroic mirror (~410 nm), and either DAPI emission (~450 nm) or FITC/GFP emission (500–530 nm) are well suited. In a filter cube-based system, two separate cubes (one containing a regular DAPI filter set, and another combining DAPI excitation, DAPI dichroic mirror and GFP emission) are required.
4. This protocol has been optimized for *B. subtilis* but has been proven to work well for other gram-positive species, including *S. aureus* and *Streptococcus pneumoniae* [7, 19]. $DiIC_{12}$ has been successfully used in *E. coli* as well [15], although this requires weakening of the outer membrane. In mycobacteria, $DiIC_{12}$ stains the mycolic acid layer. $DiIC_{12}$ is compatible with super-resolution structured illumination microscopy, both in bacterial cells and liposomes, and has also been used to stain human erythrocytes [7].
5. The spotty $DiIC_{12}$ staining pattern manifests in exponential growth phase and depends on growth speed [17, 19]. It is a common problem that cells appear less spotty or even completely smooth when not growing under optimal conditions. We have identified a number of factors that promote manifestation of the typical spotty pattern described in [12]:
   (a) Inoculating overnight cultures from glycerol stocks prepared in the same growth medium. We observed that inoculating glycerol stocks, which were prepared in full medium, into minimal medium resulted in varying $DiIC_{12}$ staining patterns. Using glycerol stocks prepared in the

same minimal medium solved this problem and gave reliably spotty stains.

(b) Preparing overnight cultures so they are still in exponential growth phase when diluted in the morning. For *B. subtilis* grown in full media like LB and Muller Hinton broth, we observed that samples inoculated from overnight cultures above an OD_{600} of 4 displayed longer lag phases and smoother $DiIC_{12}$ stains.

(c) Diluting overnight cultures not less than 1:100 and not more than 1:200. Too high starting ODs result in longer time spans to establish RIFs, resulting in samples taken at the typically desired OD_{600} of 0.3–0.5 to still be smooth. Too high dilutions result in longer lag phase, which in our hands correlates with less microdomains and smoother $DiIC_{12}$ stains.

(d) Diluting cells so they are kept in exponential phase. It is possible to dilute cells during exponential phase without affecting microdomain distribution, for example, to repeat an experiment several times with the same culture. However, only exponentially growing cultures should be diluted, and cultures should not be diluted below an OD corresponding to onset of exponential phase. For *B. subtilis* grown in full media like LB and Muller Hinton broth, we observed that cultures grown over an OD_{600} of 2 as well as cultures diluted below an OD_{600} of 0.2 show less RIFs when diluted. In contrast, diluting exponentially growing cells down to an OD_{600} of 0.2 did not affect microdomain distribution.

6. Inoculating from a plate instead of glycerol stocks is possible, yet older cultures display the same issues as overgrown overnight cultures. Thus, only freshly streaked cultures should be used.
7. Maintaining a DMSO concentration of 1% during washing and final resuspension of cells helps keep the dye soluble. If omitted, $DiIC_{12}$ is prone to precipitation, resulting in clearly visible stains on the microscopy slides that are typically much brighter than the signals from cells. If other supplements are used in the medium, for example, inducers, we recommend adding them to the washing medium as well to maintain constant conditions for the cells.
8. Higher DMSO concentrations are not recommended as it might lead to a bacterial stress response, which can affect the bacterial membrane.
9. All plasticware and media should be pre-warmed before coming into contact with cells to avoid temperature shifts. Cultures should be handled inside the water bath or on the thermomixer

at all times possible. Similarly, the centrifuge should be pre-warmed. Cultures should never be stopped from shaking.

10. Similar observations were also made for *S. aureus*.
11. Glassware should not be used as $DiIC_{12}$ strongly adsorbs to and near-irreversibly stains glass surfaces. Furthermore, using glassware can affect membrane fluidity if residual detergent from cleansing solutions is present. It is thus recommended to use disposable plastic ware to avoid chemical contamination.
12. For nonpathogenic organisms, punching a hole into the tube lid with a standard injection needle can improve oxygen supply.
13. Dry incubators are less effective in keeping stable temperature, especially when opened repeatedly, and linear motion shaking incubators provide inferior aeration for *B. subtilis*.
14. $DiIC_{12}$ can be visualized with standard RFP filters (around 570 nm excitation and 645nm emission), yet optimal signal-to-background ratio is obtained with Cy3 filters (535 nm excitation, 590 nm emission).
15. $DiIC_{12}$ is compatible with co-localization with standard DAPI, GFP, CFP, and Cy5, but not with RFP fluorophores. When using $DiIC_{12}$ together with GFP, bleed-through controls should be included. This is most relevant for weakly fluorescent GFP-protein fusions as $DiIC_{12}$ signals are typically strong and require five to ten times lower exposure times than most GFP fusions, which facilitates the bleed-through of $DiIC_{12}$ fluorescence into the GFP channel.
16. Temperature control is advantageous, since temperature shifts impact membrane domain distribution.
17. The described protocol is optimized for *B. subtilis* but provides a good starting point for measurements also in other gram-positive bacteria. With gram-negative species such as *E. coli*, Laurdan staining requires permeabilization of the outer membrane with 30 μg/mL polymyxin B nonapeptide (PMBN) for 1 h prior to staining.
18. Membrane fluidity values are very sensitive to changes in temperature. Furthermore, cells rapidly adapt to changes in temperature by adapting the fatty acid composition of the membrane. As a consequence, all materials including microcentrifuge tubes, buffers, microtiter plates, plate reader, etc. should be pre-warmed to the initial growth temperature.
19. We routinely measure effects of an antibiotic on membrane fluidity for *B. subtilis* grown in LB medium supplemented with glucose. This allows the cells to pre-adapt to utilization of glucose and thus provides the means to keep cells energized upon wash and resuspension in PBS/glucose. As an alternative, initial growth in LB/glucose buffered with 25 mM Tris pH

7.0, followed by staining and resuspension in buffer composed of 25 mM Tris, 10 g/L NaCl, and 0.1% glucose pH 7.0 is possible. If minimal medium is preferred, cells can be stained and washed directly in the same medium.

20. A final concentration of 1% DMF was found to enhance the solubility of Laurdan resulting in stronger staining of *B. subtilis*. Hence, dilution of Laurdan stock solutions should not exceed 1:100. 1% DMF does not affect the viability of *B. subtilis*.
21. The signal-to-background ratio of Laurdan stained cells is best at cell densities of OD_{600} >0.5 (for *B. subtilis*). Reliable measurement can be achieved with lower cell densities, but we do not recommend values lower than OD_{600} of 0.3.
22. Laurdan staining and subsequent washing steps should be carried out in a speedy manner. In this context, it was found appropriate to limit the overall number of samples per run to three 2 mL microcentrifuge tubes (6 mL, sufficient for 12 samples measured in technical triplicate)
23. If changes in fluidity are followed over time, measure the Laurdan fluorescence for 5–10 min under shaking in order to obtain a stable baseline. Pause measurement and quickly add antimicrobial compound at the desired concentration. Make sure the additional volume does not exceed 2 μL per well in order to minimize dilution effects.
24. Benzyl alcohol is a chemical membrane fluidizer, which provides a positive control for the ability of the assay to detect changes in membrane fluidity. In order to achieve the full extent of fluidization, a 5-min incubation is required.
25. Take care not to change the weight afterward by making new labels or writing on the tubes.
26. The molar mass of *E. coli* polar lipid extract was taken as 700 g/mol [24].
27. Do not use too strong gas flow and avoid spattering of the lipid-containing solution out from the tube.
28. We notice a 10–15% intensity decrease comparable to freshly prepared samples for frozen lipid films after 3 months at −20 °C. Thus, a longer storage is not recommended.
29. For lipid hydration and vesicle formation, the temperature of the solution should be maintained above the gel-to-liquid-crystalline phase transition temperature of the lipid. Prolonged vigorous shaking (>30 min) may be required for complete lipid hydration in some cases.

30. MLV suspensions can be stored under argon or nitrogen at −20 °C for months. With Laurdan-containing vesicles, we usually do not exceed 2 months storage period (*see* also **Note 28**).
31. The number of extrusion cycles is always odd. The LUV suspension is always collected in the syringe opposite to the one which initially carried the suspension.
32. It is recommended to check the size and polydispersity (particle size distribution) of the resulting LUVs by dynamic light scattering (DLS). Zetasizer Nano device (Malvern Instruments, UK) is used routinely in many laboratories for this control.
33. Here, glass vials are necessary for the following sample bath sonication. Using plastic tubes is not recommended due to a much lower transparency for soft ultrasound waves of bath sonication.
34. Not all peptides or other additives cause vesicle aggregation. If this is the case, bath sonication step can be omitted. Nevertheless, to reach homogeneous additive redistribution between outer and inner bilayer leaflets in vesicles, the MLV-additive suspension should be intensively mixed (shaking on vortex) and subjected to extrusion. Here, extrusion is preferred over bath sonication as it gives many more vesicles of uniform size.
35. The temperature of the sample must be controlled very accurately. Even a 0.5 °C temperature difference can have a measurable effect on Laurdan-generalized polarization parameter.
36. The fluorescent properties of Laurdan are sensitive to the physical state of the lipid bilayer. The Laurdan signal intensity and shape of the emission spectrum change with temperature. At low temperatures (in a more ordered bilayer), Laurdan fluorescence is high with a maximum at ~440 nm. With increasing temperature, membrane order decreases, and the signal intensity is reduced, while the fluorescence maximum displays a red shift to 490 nm.
37. Incubation in a round bottom 2 mL microcentrifuge tubes (in contrast to conical 1.5 mL tubes) ensures better aeration upon shaking, and therefore minimizes effects caused by de-energization [12, 23].
38. We use Eppendorf ThermoMixer at 850 rpm.
39. A less stringent wash to remove unbound dye is required for the microscopic assay than for the fluorimetric assay.
40. Regular agarose/H_2O microscopy slides are prepared by boiling 1.2% (w/v) in H_2O until agarose is fully dissolved, followed by cooling down to approximately 65 °C. The warm agarose solution (500 μL) is quickly spread on a microscopy slide, covered with another identical slide, and allowed to solidify at least for 10 min at room temperature. Immediately before use,

the upper slide is removed, 0.5 μL of the stained cell suspension applied, gently dried until the liquid drop has evaporated, and covered with a microscopy coverslip. Prepared slides (without cells) can be stored for maximum 3 h in the fridge in a container with wet tissue paper. Too dry agarose slides result in artifacts in membrane stains.

41. The cell suspension in PBS/glucose is applied on an agarose bed, which contains some un-polymerized sugar, which contributes toward osmolarity. During the process of sample embedding, the salts form the cell suspension increase the local osmolarity. If too high volume (more than 0.5 μL) is used, or agarose in undiluted buffer instead of H_2O is used, the resulting high local osmolarity results in visible plasmolysis. For these reasons, the use of H_2O/agarose and 0.5 μL sample volume is strongly recommended.
42. Once defined for a given microscope setup, the values for both scaling the images and for the z-offset can be used in later microscopy without need for re-calibration. Re-calibration is only necessary in case of a different objective, or a different fluorescent filter set.
43. Under the coverslip, the cells are not provided with an adequate supply of O_2. Aerobic microorganisms such as *B. subtilis* cells start to lose energization after approximately 10 min. For these reasons, image acquisition should be carried out in a speedy manner.
44. Laurdan fluorescence bleaches rapidly. For this reason, the illuminated sample area should be kept at minimum necessary to achieve an even illumination across the captured field. Capture of images of cells close to each other should be avoided.
45. A Wolfram Mathematica or ImageJ scripts for calculation of image-based Laurdan-GP can be obtained from the authors upon request.
46. Phase contrast is not essential but aids the automated detection of cells for post-acquisition analysis of the images.
47. We recommend using the freely available open-source image analysis software FIJI.
48. Similar to Laurdan, Nile Red can also be used to visualize fluid membrane microdomains. A comparison of the two dyes used for this purpose is shown in Fig. 7. While less used and established than Laurdan, Nile Red microscopy does not require specialized filters and is exceptionally well suited for colocalization analyses with GFP-tagged proteins. However, care should be taken to control fluorescence bleed-through to the green channel if combined with Laurdan, since Laurdan GP is very sensitive to such an effect.

49. When interpreting Nile Red fluorescent stains, please note that bacterial division septa consist of two adjacent membrane planes, which result in higher local fluorescent signals. This should not be interpreted as higher local fluidity. Also, care is needed when interpreting Nile Red membrane foci if the antibiotic used can trigger membrane invaginations. Such structures also exhibit brighter staining due to local membrane folds.
50. $DiIC_{12}$ has the tendency to form large aggregates generating a strong background noise. Thorough washing of the cells is recommended to reduce this background to a minimum level.
51. Physical stress, for example, shearing forces and temperature shock, or chemical stress, such as residual chemicals in glassware, can affect membrane fluidity and microdomains distribution, affecting $DiIC_{12}$ staining patterns.
52. We have observed that cell samples that appeared "clean" after washing can again display a strong background of precipitated $DiIC_{12}$ dye when imaged after prolonged incubation. We speculate that cells have a mechanism to expel the dye from their membrane over time. This background can be avoided by adding an additional washing step after antibiotic treatment and is recommended after incubation times exceeding 1 h.
53. Several antibiotics have been reported to affect membrane microdomain distribution including CCCP, daptomycin, nisin, rhodomyrtone, tetracycline, anhydrotetracycline, gramicidin D and S, tyrocidine A and C, and thrombocidin-derived peptides (*see* Fig. 8) [5, 7, 12, 16–18]. CCCP was the first compound observed to have this effect. It depolarizes the cell membrane, leading to delocalization of the membrane potential-sensitive peripheral membrane protein MreB, which is involved in organizing RIF distribution [12, 25]. CCCP treatment leads to accumulation of RIFs in larger clusters [12]. Due to its commercial availability, broad-spectrum activity, fast effects, and simple handling, we recommend CCCP as positive control.

Acknowledgments

This work was supported by Newcastle University, Barbour Foundation, and the Swedish Research Council for Sustainable Development (Formas), grant number 2020-00956.

References

1. Yeaman MR, Yount NY (2003) Mechanisms of antimicrobial peptide action and resistance. Pharmacol Rev 55:27–55
2. Zhang Y-M, Rock CO (2008) Membrane lipid homeostasis in bacteria. Nat Rev Microbiol 6: 222–233
3. Gohrbandt M, Lipski A, Grimshaw JW, Buttress JA, Baig Z, Herkenhoff B, Walter S, Kurre R, Deckers-Hebestreit G, Strahl H (2022) Low membrane fluidity triggers lipid phase separation and protein segregation in living bacteria. EMBO J:e109800
4. Epand RM, Epand RF (2009) Domains in bacterial membranes and the action of antimicrobial agents. Mol Biol Syst 5:580–587
5. Mueller A, Wenzel M, Strahl H, Grein F, Saaki T, Kohl B, Siersma T, Bandow J, Sahl H, Schneider T, Hamoen L (2016) Daptomycin inhibits bacterial cell envelope synthesis by interfering with fluid membrane microdomains. Proc Natl Acad Sci U S A 113: E7077–E7086
6. Scheinpflug K, Wenzel M, Krylova O, Bandow JE, Dathe M, Strahl H (2017) Antimicrobial peptide cWFW kills by combining lipid phase separation with autolysis. Sci Rep 7:44332
7. Saeloh D, Tipmanee V, Jim KK, Dekker MP, Bitter W, Voravuthikunchai SP, Wenzel M, Hamoen LW (2018) The novel antibiotic rhodomyrtone traps membrane proteins in vesicles with increased fluidity. PLoS Pathog 14: e1006876
8. Scheinpflug K, Krylova O, Strahl H (2017) Measurement of cell membrane fluidity by Laurdan GP: fluorescence spectroscopy and microscopy. Methods Mol Biol 1520:159–174. Humana Press, New York
9. Parasassi T, De Stasio G, d'Ubaldo A, Gratton E (1990) Phase fluctuation in phospholipid membranes revealed by Laurdan fluorescence. Biophys J 57:1179–1186
10. Parasassi T, De Stasio G, Ravagnan G, Rusch RM, Gratton E (1991) Quantitation of lipid phases in phospholipid vesicles by the generalized polarization of Laurdan fluorescence. Biophys J 60:179–189
11. Wheeler G, Tyler KM (2011) Widefield microscopy for live imaging of lipid domains and membrane dynamics. Biochim Biophys Acta 1808:634–641
12. Strahl H, Burmann F, Hamoen LW (2014) The actin homologue MreB organizes the bacterial cell membrane. Nat Comm 5:3442
13. Bach JN, Bramkamp M (2013) Flotillins functionally organize the bacterial membrane. Mol Microbiol 88:1205–1217
14. Kucherak OA, Oncul S, Darwich Z, Yushchenko DA, Arntz Y, Didier P, Mély Y, Klymchenko AS (2010) Switchable Nile Red-based probe for cholesterol and lipid order at the outer leaflet of biomembranes. J Am Chem Soc 132:4907–4916
15. Oswald F, Varadarajan A, Lill H, Peterman EJG, Bollen YJM (2016) MreB-dependent organization of the *E. coli* cytoplasmic membrane controls membrane protein diffusion. Biophys J 110:1139–1149
16. Omardien S, Drijfhout JW, Vaz FM, Wenzel M, Hamoen LW, Zaat SAJ, Brul S (2018) Bactericidal activity of amphipathic cationic antimicrobial peptides involves altering the membrane fluidity when interacting with the phospholipid bilayer. Biochim Biophys Acta 1860:2404–2415
17. Wenzel M, Rautenbach M, Vosloo JA, Siersma T, Aisenbrey CHM, Zaitseva E, Laubscher WE, van Rensburg W, Behrends J, Bechinger B, Hamoen LW (2018) The multifaceted antibacterial mechanisms of the pioneering peptide antibiotics tyrocidine and gramicidin S. MBio 9:e00802–e00818
18. Wenzel M, Dekker MP, Wang B, Burggraaf MJ, Bitter W, van Weering JRT, Hamoen LW (2021) A flat embedding method for transmission electron microscopy reveals an unknown mechanism of tetracycline. Commun Biol 4: 306
19. Wenzel M, Vischer NOE, Strahl H, Hamoen LW (2018) Assessing membrane fluidity and visualizing fluid membrane domains in bacteria using fluorescent membrane dyes. Bio-protocol 8:e3063
20. Kawai F, Shoda M, Harashima R, Sadaie Y, Hara H, Matsumoto K (2004) Cardiolipin domains in *Bacillus subtilis* Marburg membranes. J Bacteriol 186:1475–1483
21. Salzberg LI, Helmann JD (2008) Phenotypic and transcriptomic characterization of *Bacillus subtilis* mutants with grossly altered membrane composition. J Bacteriol 190:7797–7807
22. Mercier R, Domínguez-Cuevas P, Errington J (2012) Crucial role for membrane fluidity in proliferation of primitive cells. Cell Rep 1:417–423
23. Chico DE, Given RL, Miller BT (2003) Binding of cationic cell-permeable peptides to plastic and glass. Peptides 24:3–9
24. New RRC (1990) Liposomes: a practical approach. IRL Press, Oxford
25. Strahl H, Hamoen LW (2010) Membrane potential is important for bacterial cell division. Proc Natl Acad Sci U S A 107:12281–12286

Chapter 12

Quantitative Analysis of Microscopy Data to Evaluate Bacterial Responses to Antibiotic Treatment

Dominik Brajtenbach, Jan-Samuel Puls, Cruz L. Matos de Opitz, Peter Sass, Ulrich Kubitscheck, and Fabian Grein

Abstract

Microscopy is a powerful method to evaluate the direct effects of antibiotic action on the single cell level. As with other methodologies, microscopy data is obtained through sufficient biological and technical replicate experiments, where evaluation of the sample is generally followed over time. Even if a single antibiotic is tested for a defined time, the most certain outcome is large amounts of raw data that requires systematic analysis. Although microscopy is a helpful qualitative method, the recorded information is stored as defined quantifiable units, the pixels. When this information is transferred to diverse bioinformatic tools, it is possible to analyze the microscopy data while avoiding the inherent bias associated to manual quantification. Here, we briefly describe methods for the analysis of microscopy images using open-source programs, with a special focus on bacteria exposed to antibiotics.

Key words Fluorescence microscopy, Time-lapse microscopy, *Staphylococcus aureus*, *Bacillus subtilis*, Antimicrobials, Microscopy data analysis and quantification, Convolved Average Projections (CAP)

1 Introduction

In vivo fluorescence wide-field microscopy allows understanding the interactions between proteins and antibiotic compounds and their localization, in relation to each other, or delocalization resolved in time. Typical methods of fluorescence localization analysis are often time-consuming and/or include only subsets of cells, for example, only those with a septum aligned with the viewing axis in the case of septal/peripheral ratio analysis [1]. Detailed analysis of phenotype subpopulations is regularly time-intensive and requires a precise parameter design to not fail at the phenotypic

The authors Dominik Brajtenbach, Jan-Samuel Puls and Cruz L. Matos de Opitz have equally contributed to this chapter.

Peter Sass, Ulrich Kubitscheck and Fabian Grein share senior authorship.

Peter Sass (ed.), *Antibiotics: Methods and Protocols*,
Methods in Molecular Biology, vol. 2601, https://doi.org/10.1007/978-1-0716-2855-3_12,

variety of cells. Simple solutions for high-throughput analysis of time-resolved image data are rare and usually linked to time-consuming and labor-intensive processes [2]. Implementation of existing solutions for experiments with open outcomes may be very elaborate. Precise fluorescence localization analysis often requires a preceding hypothesis of the impact toward the signal of interest and a high level of methodical care to avoid selection bias, for example, by missing unknown factors or more moderate effects. This is especially relevant for understanding antibiotic action, as compounds often exert multiple effects on cells and a variety of outcomes due to quantitative differences between individual cells [3]. Furthermore, due to concentration dependencies of antibiotic effects, a high sample size is often required to map the antibiotic impact accurately, making quantitative fluorescence analysis on the single-cell level even more time-consuming [3–5]. The important opportunistic pathogen and model organism *Staphylococcus aureus*, a cocci-shaped bacterium, poses a special problem for automated image analysis. Rod-shape bacteria, such as *Bacillus subtilis*, display some form of geometrical asymmetry in three dimensions, allowing to deduce the cell orientation from the viewing axis in a 2D microscopy image, in contrast, *S. aureus* spherical cell morphology, with only slight elongation during the cell cycle, makes it very difficult to derive the orientation of a cell from a 2D image [6]. Consequently, an existing septum can be tilted in multiple directions—complicating subpopulation analysis—or even in a 90-degree angle orthogonal to the viewing axis, making it problematic to even differentiate between a cell without septum and unspecific membrane signal and a cell with a specific septal signal, where the septum is orthogonal to the viewing axis. Additionally, the minute elongation during the cell cycle implies only minor differences in length between the medial axis and other profiles through the cell. This further complicates automated recognition of the medial plane. These various difficulties in image analysis create a need for a very elaborate method to avoid bias, for example, by misinterpreting the cell cycle phase due to the orientation of the septum, or incorrect analysis of septal specificity of a signal due to false medial plane recognition.

In this chapter, we address these problems and provide detailed protocols for (time-resolved) fluorescence microscopy experiments to investigate dynamic changes in the localization pattern of bacterial proteins, for example, to evaluate respective antibiotic effects qualitatively and quantitatively in *S. aureus* and *B. subtilis*. Here, the described methods further include image deconvolution, subsequent image stabilization, and presentation in averaged projected kymographs, as well as the use of open-source image software to extract and map statistically relevant data such as length, width, shape, and others from microscopic experiments. In addition, we describe convolved average projections (CAPs), a fully

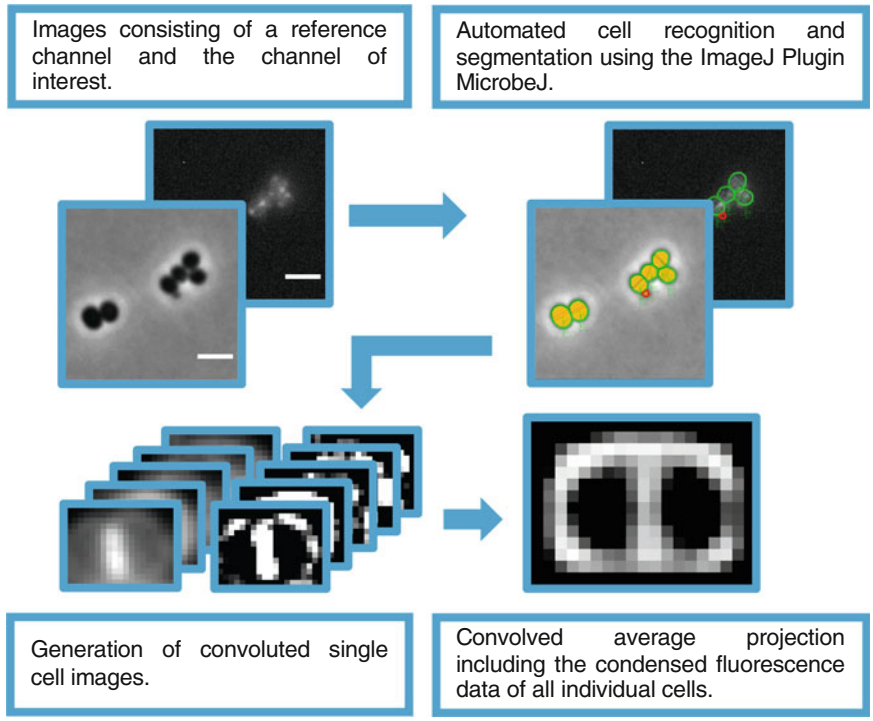

Fig. 1 Workflow of generating convolved average projections

automated method that was developed to combine all individual cell images into a comprehensive single projection (*see* Fig. 1). This enables a fast and unbiased compression of the raw data into a single "cell-like" image that visualizes changes over the total sample population (*see* Fig. 2). As all individual cells are included in a CAP, the additional difficulty of separating the multitude of orientations and morphologies of cocci-shaped bacteria like *S. aureus* is avoided. The results can be quantitatively assessed with methods already established for individual cell analysis and is a suitable basis for a directed and detailed analysis of changes in the signal of interest on the individual cell level.

2 Materials

All solutions should be prepared in ultrapure or double-distilled water (ddH2O).

2.1 Growth Media, Reagents, and Bacterial Strains for (Time-Resolved) Fluorescence Microscopy

1. Double-distilled water (ddH_2O).
2. Mueller Hinton broth (MH): 2 g beef infusion solids, 17.5 g casein hydrolysate, 1.5 g cornstarch, pH 7.4. Add 900 mL water, adjust pH with 1 M NaOH. Complete to 1 L with water. Autoclave, then store at room temperature or 4 °C.

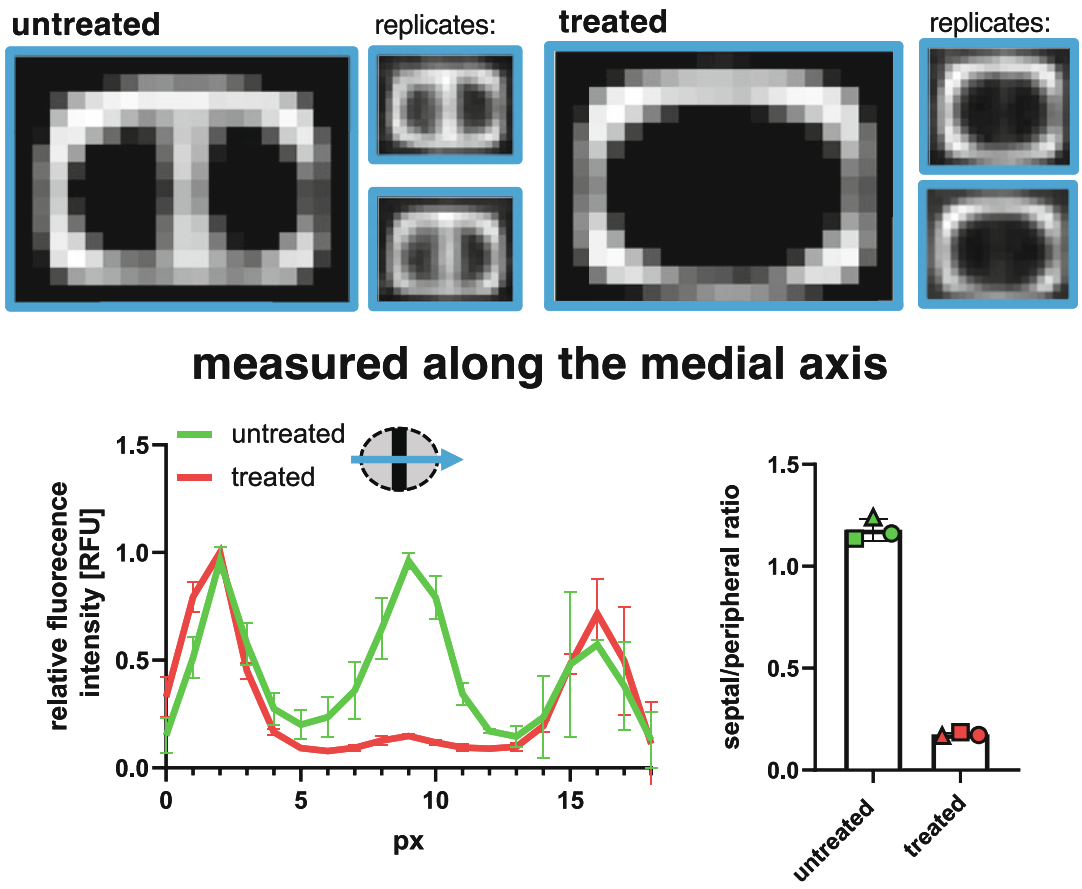

Fig. 2 Comparison of CAPs generated from cells with or without antibiotic treatment, three independent biological replicates per condition (left). CAP demonstrate excellent reproducibility and can be quantitatively analyzed with methods already established for individual cells, for example, profile plotting or septal/peripheral ratio analysis (right)

3. Lysogeny broth (LB): 10 g peptone, 5 g yeast extract, 10 g NaCl, pH 7.3. Add 900 mL water, adjust pH with 1 M NaOH. Complete to 1 L with water. Autoclave, then store at room temperature or 4 °C.
4. Isopropyl-β-D-thiogalactopyranosid (IPTG).
5. Phosphate-buffered saline (1× PBS): 136.89 mM NaCl, 10 mM $Na_2HPO_4{\cdot}2H_2O$, 1.98 mM KH_2PO_4, 2.68 mM KCl.
6. 3% bovine serum albumin (BSA), dissolved in 1× PBS.
7. Human BD Fc Block™ (BD Pharmingen, 0.5 mg/mL stock, *see* **Note 1**).
8. 70% ethanol (EtOH) in water.

9. Antibiotics of choice for treatment or plasmid selection (e.g., erythromycin) (*see* **Note 2**).
10. Bacterial strains of interest, for example, *Staphylococcus aureus* or *Bacillus subtilis* expressing a fluorescent fusion protein such as FtsZ-mCherry [7, 8].

2.2 Hardware, Image Acquisition, and Analysis

1. Computer hardware (*see* **Note 3**) and inverted motorized microscope (*see* **Note 4**) with scientific camera (CCD or sCMOS).
2. Focus stabilization, for example, Perfect Focus System (Nikon), and motorized stage (x, y, z).
3. Hardware controllable bright field illumination (ideally a LED illumination).
4. High magnification objective with temperature correction for 37 °C and high numerical aperture (NA) for total internal reflection fluorescence (TIRF), for example, 100×, oil immersion, NA 1.49, TIRF.
5. Phase contrast (*see* **Note 5**).
6. Highly inclined and laminated optical (HiLo, [9]) illumination system.
7. For time-lapse: Low fluorescence immersion oil corrected for use at 37 °C.
8. For time-lapse: Objective lens heater.
9. For time-lapse: Laser box or laser with emission at 561 nm (*see* **Note 6**) and large illumination field (diameter 110 μm).
10. For time-lapse: Stage-top incubator.
11. For time-lapse: Software to automatically control the microscope (time series, z-stack, focus stabilization, trigger for laser and bright field illumination, and positions).
12. For time-lapse: Sample chamber with in- and outlet to exchange culture media (sample volume ca. 100–150 μL), which fits a 24 × 24 mm coverslip (Fig. 3).
13. For time-lapse: Syringe pump (manual or automatic, 1 mL syringes) with connections to inlet/outlet of sample chamber via a silicon tube with 0.5 mm inner diameter and syringe needles.
14. Coverslip (specified H1.5, 170 μm thickness).
15. Incubator Shaker.
16. Centrifuge (1.5 mL tubes).

2.3 Analysis Software and Plugins

1. Fiji [10] or ImageJ [11] (*see* **Note 7**).
2. Image analysis software, such as Oufti (http://www.oufti.org/) [12], MicrobeJ (https://www.microbej.com/) [13] (*see*

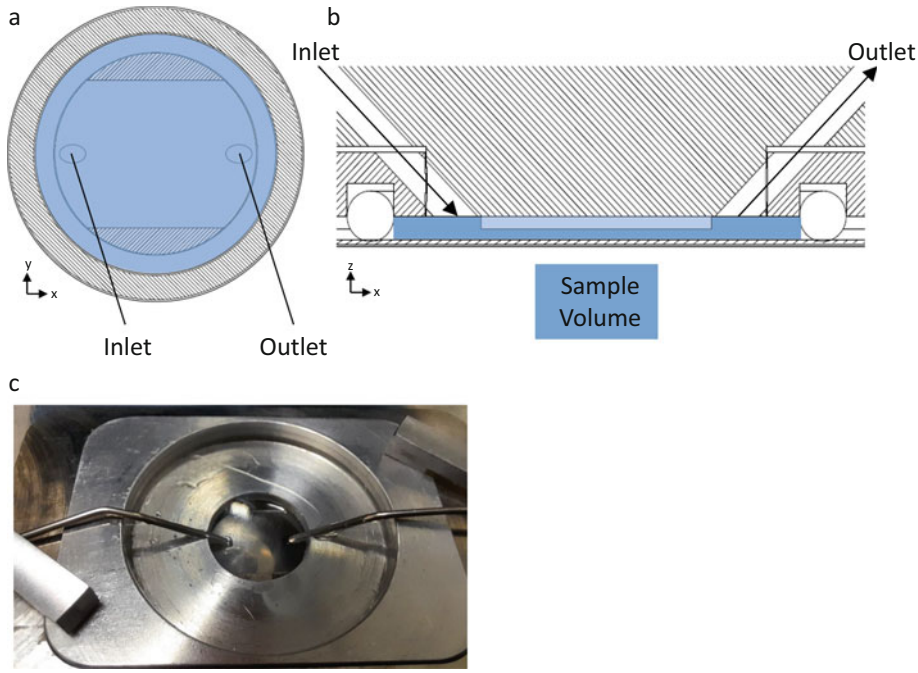

Fig. 3 Sample chamber. (**a**) Schematic top view, (**b**) schematic side view, (**c**) photograph

Note 8), Morphometrics [14] (https://simtk.org/projects/morphometrics), or equivalent.

3. For time-lapse: PSF Generator [15, 16] (Plugin for Fiji or ImageJ).
4. For time-lapse: DeconvolutionLab2 [17] (Plugin for Fiji or ImageJ).
5. For time-lapse: StackReg [18, 19] (Plugin for Fiji or ImageJ).
6. For time-lapse: KymographBuilder [20] (Plugin for ImageJ, included in Fiji).

3 Methods

3.1 Preparation of S. aureus *or* B. subtilis *Cultures*

1. Prepare a preculture of the intended strain under the desired conditions, for example, in Mueller Hinton broth with 10 μg/mL erythromycin.
2. Incubate over night at 37 °C under shaking conditions.
3. Prepare a 2 mL main culture under desired conditions, for example, in Mueller Hinton Broth with 10 μg/mL erythromycin and 100 μM IPTG, and inoculate 1%.
4. Incubate to OD_{600} of 0.4 at 37 °C under shaking conditions.

3.2 Sample Preparation for Time-Lapse Experiments with S. aureus

1. Centrifuge 1 mL of culture at 20,000 × *g* for 1 min.
2. Resuspend bacterial pellet in 500 μL 1× PBS (*see* **Note 9**).
3. Centrifuge at 20,000 *g* for 1 min.
4. Resuspend bacterial pellet in 500 μL 1× PBS and mix thoroughly with a pipette (*see* **Note 10**).
5. Dilute human BD Fc Block stock solution 1:50 in 1× PBS to a total volume of 60 μL.
6. Place a cover slip into the insert for the stage-top incubator.
7. Add 60 μL of diluted human BD Fc Block to the center of the coverslip and wait 5 min (*see* **Note 11**).
8. Remove supernatant from coverslip and wash with 60 μL of 1× PBS.
9. Add 60 μL of bacteria in 1× PBS to the coverslip surface and incubate for 5 min at room temperature.
10. Remove supernatant from coverslip and wash with 60 μL of 1× PBS.
11. Add 60 μL of 3% BSA solution to the coverslip and incubate for 5 min at room temperature (*see* **Note 12**).
12. Remove supernatant from coverslip and place insert with coverslip into the stage-top incubator on the microscope.

3.3 Preparation of the Microscope for Time-Lapse Experiments

1. One hour prior to the experiment: Turn on stage-top incubator and objective heater; also turn on and set-up the camera, light sources, microscope, controls, and computer. Place the immersion oil already on the warmed objective.
2. Attach one empty syringe and one syringe filled with 1 mL of culture media, for example, MH broth with 10 μg/mL erythromycin and 100 μM IPTG, to the syringe pump and connect them to the silicon tubing.
3. Fill the silicon tubing and connectors before connecting the system to the sample chamber to avoid introduction of air (*see* **Note 13**).
4. Connect the syringes to the sample chamber. Raise the objective until the immersion oil touches the coverslip (*see* **Note 14**).
5. Fill the sample chamber slowly and purge the sample chamber with the remaining volume to remove floating bacteria (*see* **Note 15**).
6. Replace both 1 mL syringes for an empty one and one filled with 1 mL of culture media. The filled syringe may contain MH broth with 10 μg/mL erythromycin and 100 μM IPTG (negative control) or the desired antibiotic concentration (treated sample).

3.4 Microscopy of S. aureus in Time-Lapse Experiments

1. Place the condenser above the sample and set the experimental values (*see* **Note 16**).
2. Define measurement positions (*see* **Note 17**).
3. Define time interval and number of intervals, for example, for a 90 min experiment choose nine 10 min intervals.
4. Z-stack settings: To image *S. aureus* in sufficient detail acquire images in an axial range from −0.5 μm to 0.5 μm in 0.25 μm steps (*see* **Note 18**).
5. Channels and exposure times, for example, 200 ms fluorescent excitation using the 561 nm laser, 100 ms for the phase contrast image (*see* **Note 19**).
6. Laser power, for example, 100 mW/cm^2 (in HiLo mode) (*see* **Note 19**).
7. Start data acquisition and observe the first images to make sure the z-range is set appropriately (*see* **Note 20**).
8. Following 20 min of acquisition (after imaging the third time point) exchange the culture media or replace with antibiotic containing culture media using the syringe pump (*see* **Note 13**).
9. After data acquisition, save the data in a Hyperstack (z, position, time; Tiff format) for each position.
10. Immediately after use, flush the sample chamber, all connectors and silicon tubes with 70% EtOH. Sonicate the material for 10 min (*see* **Note 21**).

3.5 Deconvolution

Deconvolution is used to increase contrast and spatial resolution of the imaged data [21, 22]. The effects of deconvolution are depicted in Fig. 4. A point spread function (PSF) is needed for deconvolution and can be obtained experimentally or created synthetically.

1. A synthetic PSF is created with PSF Generator for Fiji or ImageJ for the maximum emission wavelength of the used dye (here, 610 nm for mCherry). The "optical model" used is the "Born & Wolf 3D Optical Model", [23, 24] "accuracy computation" is set to "better". The PSF is created for a volume of 256 × 256 × 65 pixels (XYZ) with linear display, in 16-bits and lookup table "gray". Further settings depend on the used setup; here pixel size is 65 × 65 nm with a Z-step of 250 nm. Save the created image stack in TIFF format.
2. For deconvolution, the hyperstack must be separated into single z-stacks. Follow the steps below or write a macro for ImageJ for faster processing (*see* **Note 22**):
   (a) Duplicate the first channel (mCherry) with t = 0 min and z = 1 to z = 5 to a predetermined folder for the mCherry channel and close the stack. Repeat the same step for the

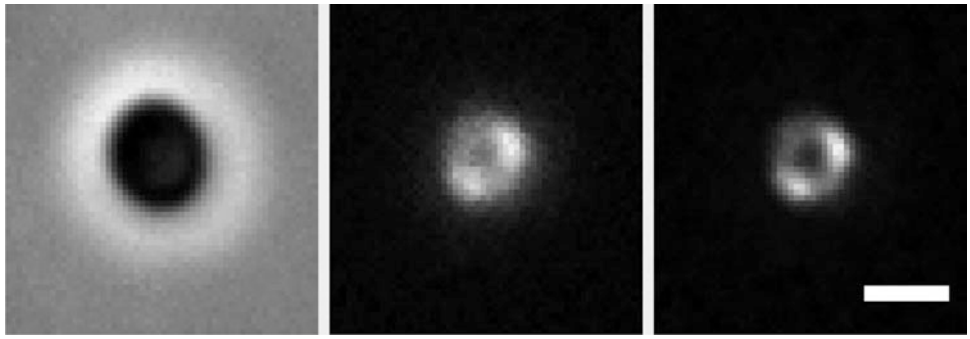

Fig. 4 Effect of deconvolution. Phase contrast image of a *S. aureus* cell (left), raw (middle) and deconvoluted (right) fluorescence micrograph of FtsZ-mCherry fusion protein expressed in *S. aureus*. Scale bar, 1 μm

following time points, that is, duplicate first channel (mCherry) with t = 90 min and z = 1 to z = 5 to a predetermined folder for the mCherry channel and close the stack.

(b) Perform similar steps for the second channel (phase contrast), considering in this instance a predetermined folder for the phase contrast channel and close the stack.

3. Deconvolution is performed with DeconvolutionLab2 for ImageJ. Deconvolute each stack in ten iterations using the Richardson-Lucy algorithm [25, 26]. The plugin works by drag and drop. Drop the experimental and PSF files into the corresponding positions, set the algorithm and number of iterations and run the plugin (*see* **Note 23**).

3.6 Kymograph Analysis of S. aureus

The acquired raw and deconvoluted data can be used for a number of different types of image analyses like relative intensity changes and redistribution of the labeled compound, as a function of time and concentration of applied antibiotics. In this section, we describe a qualitative analysis using kymographs. They describe changes in signal intensity in a condensed representation. Here, we examine changes of the intensity profile perpendicular to the septal plane of single cells in *S. aureus* cells treated with an antibiotic and compare it to a negative control.

In order to produce meaningful kymographs, it may become necessary to sort the single cells into different classes representing, for example, different states of the cell division cycle (*see* **Note 24**).

1. A negative control is used to check if bacteria are growing properly in the sample chamber during the observation and to provide reference kymographs. The single steps of image analysis are condensed in Fig. 5.

(a) Open and concatenate the deconvoluted stacks for one position with ImageJ to form a Hyperstack (z, t). The

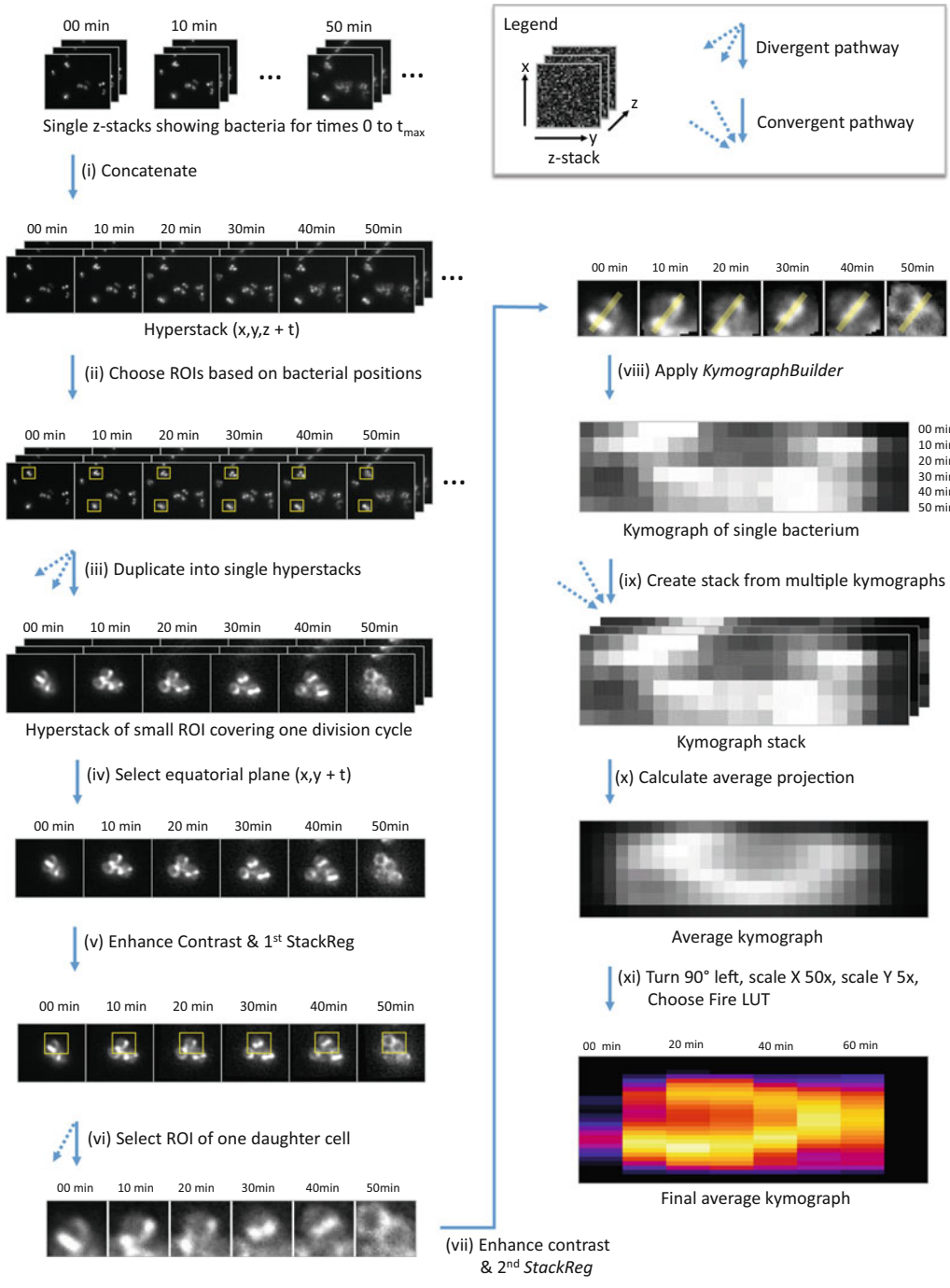

Fig. 5 Flowchart showing an exemplary iteration of the described image processing for the negative control (*see* Subheading 3.6, **step 1**). Corresponding steps: (i) step 1, (ii) steps 3 and 4, (iii) step 4, (iv) step 5, (v) steps 6 and 7, (vi) step 8, (vii) steps 9 and 10, (viii) steps 12 and 13, (ix) step 14, (x) step 15, (xi) step 16. Execution of "3.6.2 Treated Sample" differs only in (iii) where a hyperstack is created over the complete experimental timespan

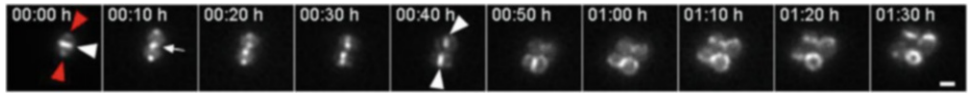

Fig. 6 Exemplary time-lapse images of untreated *S. aureus* on the coverslip. Scale bar, 1 μm. For the meaning of arrows and arrowheads, see text

necessary function can be found under "Image – Stacks – Tools – Concatenate…". It is necessary to tick the box for "Open as 4D image" (*see* **Note 25**).

(b) When observing a number of time-lapse images of a single bacterium (Fig. 6), we perceive a repeating pattern in the intensity distribution of the protein due to the replication cycle. For example, in Fig. 6, at t = 0 min, a line (marked by an arrowhead) corresponding to the septal plane and two foci (marked by red arrowheads) is visible. In the following 10 min, the bacterium divides along the septum. Each new cell exhibits two foci with one overlapping (arrow). The foci of each cell approach each other in the following 30 min until they collapse into two new septa (t = 00:40 h, see white arrowheads). Sometimes, also new foci become visible. Thus, after about 40 min, a new division cycle begins. To capture this periodic behavior in an average kymograph, we need to classify the cells according to distinct and recognizable points of the division cycles. In the given example, they correspond to t = 0 min and t = 40 min.

(c) Choose bacteria in the same cell cycle state from random time frames to make sure the signal distribution and its changes are not related to the duration of the experiment.

(d) Now extract a certain number of individual time-lapse image stacks from three replicate experiments, for example, 30 in total. The time-lapse image stacks of bacteria are created by selecting rectangular regions of interest (ROIs, *Rectangle*) around the bacteria. Each ROI is duplicated ("Image – Duplicate…" or right click "Duplicate…") from the hyperstack (z = 5) for the time interval of one cell cycle. Save the stacks in a respective folder (*see* **Note 26**).

(e) Open the single time-lapses of between 40 and 60 min, select, and duplicate one slice with focus in the middle of the cells body over the whole time span of interest (*see* **Note 27**).

(f) Enhance the contrast of the stack with the "Enhance Contrast" function. "Saturated pixels" is set to 0.1%, "Normalize" and "Process all n slices" (*see* **Note 28**).

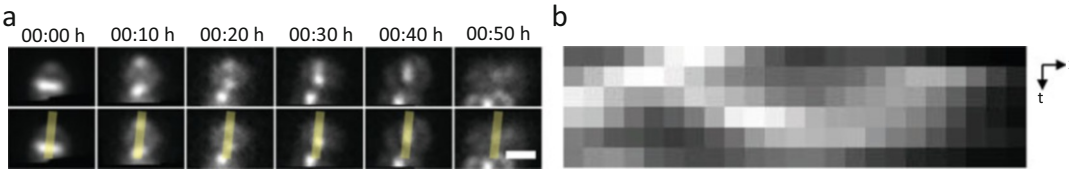

Fig. 7 Creation of a kymograph. (**a**) Aligned time-lapse images of a dividing bacterium (top) and the same image sequence with the lines, along which the profile was measured (bottom). Scale bar, 1 μm. (**b**) Kymograph created from the intensity profiles shown in (**a**). Horizontal pixel size, 65 nm, vertical pixel size, 10 min

(g) Correct any lateral motion of the stage using StackReg for ImageJ with "Transformation" set to "Rigid Body" (*see* **Note 29**).

(h) Draw a new, smaller region around the individual cell of interest to reduce the amount of signal coming from other cells and duplicate (*see* **Note 30**).

(i) Enhance contrast again, as described before (f).

(j) If the alignment is not good enough, a second alignment can be performed with StackReg (*see* **Note 31**).

(k) If the alignment is still not sufficient, small corrections can be made with the "Image – Transform" tool. A time-lapse will look like Fig. 7a when stabilized.

(l) Set the width of lines to 5 pixels and draw a profile to cover all foci needed for the evaluation with some extension beyond the foci (*see* **Note 32**).

(m) Inspect the whole stack and create a kymograph with KymographBuilder for ImageJ. An exemplary single cell kymograph is shown in Fig. 7b (*see* **Note 33**).

(n) After creating all single kymographs, open all of them in ImageJ and create a stack from images ("Image – Stacks – Images to Stack") with the Method set to "copy (center)". Scrolling through the created kymograph stack will reveal if all kymographs were well centered.

(o) Create an average projection of the kymographs ("Images – Stacks – Z-Project…" with projection "Average Intensity").

(p) Finally, the average kymograph is rotated 90° to the left ("Image – Transform – Rotate 90 Degrees Left") in order to associate the abscissa with the time axis. Next, resize 50-fold in x-direction and 5-fold in y-direction ("Image – Scale…" with "X Scale: 50", "Y Scale: 5", "Z Scale", "Interpolation: None"). The lookup table is changed to "Fire LUT" ("Image – Lookup Tables – Fire") and contrast-corrected for extreme values. Figure 8 shows the raw and the modified kymographs (*see* **Note 34**).

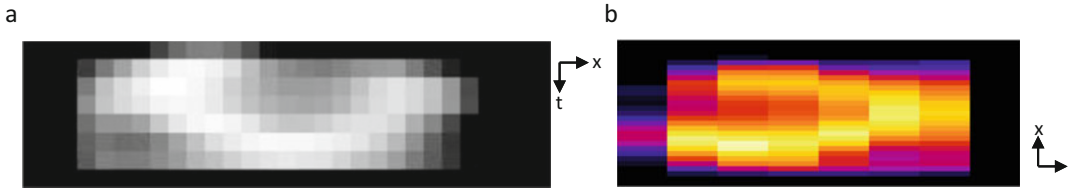

Fig. 8 Kymograph presentation. (**a**) Raw averaged kymograph and (**b**) rotated, scaled and LUT-modified kymograph

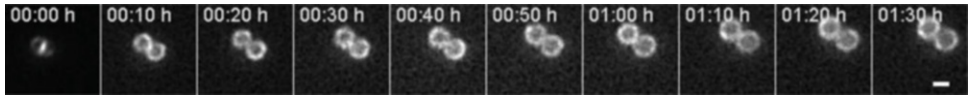

Fig. 9 Exemplary time-lapse images of *S. aureus*. The antibiotic that is tested is added after t = 20 min (immediately after acquisition of the data for the third time point). Scale bar, 1 μm

2. In the *treated sample*, we analyze the effect of the tested antibiotic on the localization of the FtsZ-mCherry fusion protein as an example application. Often, the application of antibiotics results in a growth arrest. Details of this effect are evaluated and quantified by the given approach.
   (a) Open and concatenate the deconvoluted stacks for one position with ImageJ to form a Hyperstack (z, t). The necessary function can be found under "Image – Stacks – Tools – Concatenate. . .". It is necessary to tick the box for "Open as 4D image" (*see* **Note 25**).
   (b) First, we examine time-lapse images to find a possibly needed, meaningful classification for the single cell images. A typical cell is shown in Fig. 9. It can be noted that the bacteria do not exhibit the periodic behavior seen in the control, but rather show a moderate stationary intensity distribution. A size classification in the third frame/time-point is selected due to compound addition. Rescale the pixel size to the true pixel size defined by the hardware of your microscope (*see* **Note 35**). Create a profile with a linewidth of five covering the ring-shaped signal for determination of their diameters. For *S. aureus*, three groups of ring diameters (390–520 nm, 650–715 nm, and 845–910 nm) are appropriate. These groups are chosen to distinguish bacteria with small, medium, and large FtsZ ring size (*see* **Note 36**).
   (c) The following steps are only described for bacteria classified with a ring size of 845–910 nm. The procedure for other size classes is identical.

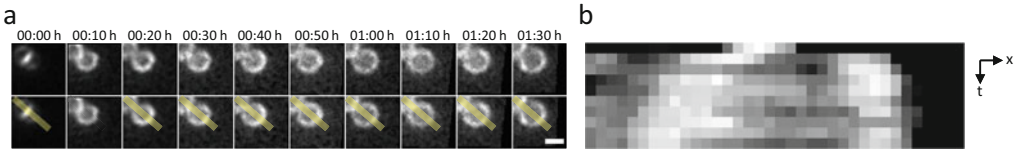

Fig. 10 (**a**) Aligned time-lapse images of antibiotic treated bacteria (top) and the same image sequence with the lines, along which the profile was measured (bottom). Scale bar, 1 μm. (**b**) Kymograph created from the intensity profiles shown in (**a**). Horizontal pixel size, 65 nm, vertical pixel size, 10 min

Fig. 11 Kymograph presentation of a treated cell. (**a**) Raw averaged kymograph and (**b**) rotated, scaled and LUT-modified kymograph

(d) Create 30 different time-lapse image stacks of bacteria with ring diameters in the range of 845–910 nm from the three replicates of the experiment by creating a box selection (*Rectangle*) around the bacteria and duplicating ("Image – Duplicate…" or right click "Duplicate…") the ROI over the hyperstack (z = 5, t = 10). Save the stacks in a respective folder (*see* **Note 26**).

(e) Open the single time-lapse image stacks and select one slice with focus in the axial center of the cell body and duplicate it ("Image – Duplicate…" with z = only single digit, t = 1–10).

(f) Enhance the contrast of the stack with the "Enhance Contrast" function. "Saturated pixels" is set to 0.1%, "Normalize" and "Process all n slices" (*see* **Note 28**).

(g) Repeat steps *g–p* as described in the "1. The Negative Control". The alignment of treated cells is shown in Fig. 10, whereas Fig. 11 depicts the raw and the modified kymographs of antibiotic treated *S. aureus* cells.

3.7 Interpretation of Averaged Kymographs of S. aureus

Due to the size classification performed before the averaging, it is implied that bacteria in the same state of the division cycle will react similarly if not exactly the same to the compound. If intensity distributions in the kymographs of single cells differ from each other, a more diffuse intensity distribution will show up in the averaged kymograph. Similar distributions of the foci will result in higher intensity values. The average kymograph of the control and the treated sample are compared in Fig. 12.

The bacterial cell cycle leads to an initially growing and then shrinking distance of the two intensity foci (Fig. 12a). It is clearly

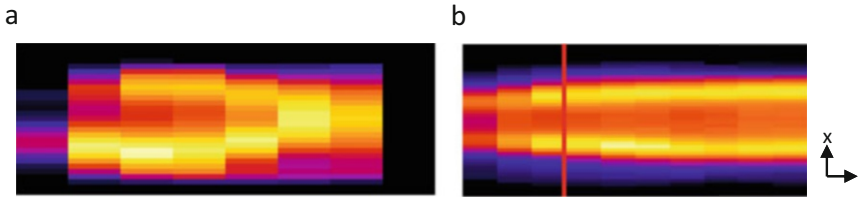

Fig. 12 Averaged kymograph from (**a**) control with cell cycle progression and (**b**) treated sample with cell cycle arrest. The red line indicates the moment of addition of antibiotic

visible that the normal dynamics of FtsZ-mCherry were altered by the compound added in (b) so the larger ring structures between 845 nm and 910 nm did not contract anymore. This is effectively a cell cycle arrest (*see* **Note 37**). The treated sample reveals besides the cell cycle arrest a certain expansion after addition of the antibiotic.

3.8 Analysis of S. aureus *Cells Using Convolved Average Projections (CAP)*

3.8.1 Extraction of Individual Cell Images with MicrobeJ

1. After installing the MicrobeJ plugin, start ImageJ and open MicrobeJ by clicking Plugins – MicrobeJ – MicrobeJ (*see* **Note 38**).
2. Open your raw images within either ImageJ or MicrobeJ (*see* **Note 39**).
3. Select the image to analyze in the MicrobeJ Images tab (*see* Fig. 13).
4. Switch to the MicrobeJ Bacteria tab (*see* Fig. 13). The plugin uses a binary mask created from your reference channel (see Materials) to perform cell recognition and segmentation. Select your reference channel in the first box on the upper left (*see* Fig. 13).
5. Select the background type of your reference channel in the second box and the algorithm for binary mask calculation in the fourth box (*see* **Note 40**). The binary mask defines which regions of your image will be used for cell recognition and segmentation.
6. To visualize the binary mask, click on the rod-shaped bacteria icon on the right side (*see* Fig. 13). A yellow overlay will appear on your reference channel of the selected image. To achieve optimal cell recognition and segmentation, adjust the slider left from the rod-shaped bacteria icon until the yellow overlay resembles the cell morphology as best as possible without introducing too many artifacts in the background (*see* **Note 41**).
7. Adjust your segmentation parameters on the left side of the tab (*see* **Note 42**).

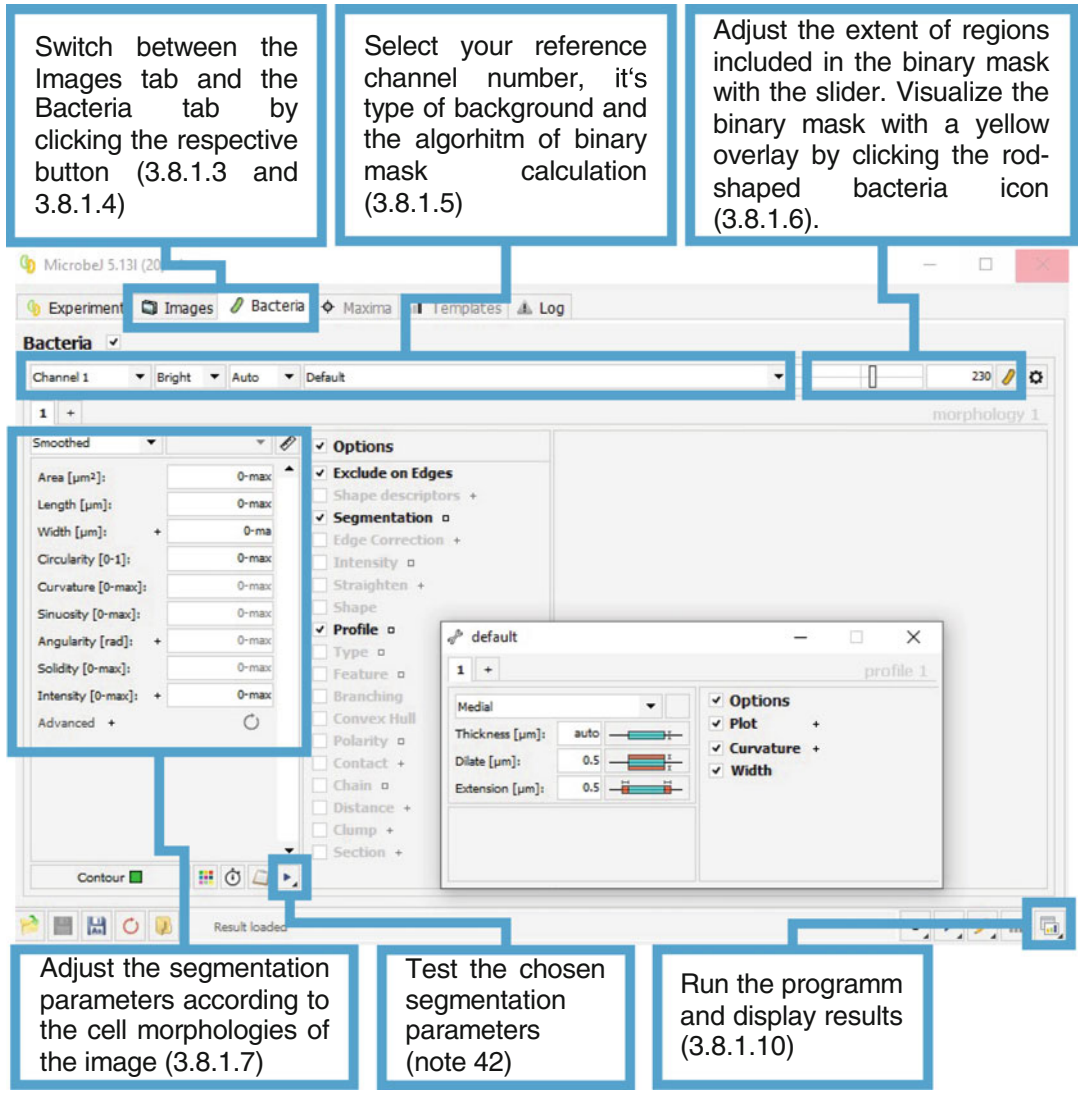

Fig. 13 Graphic user interface of the MicrobeJ window [11]

8. Check the Options menu in the middle of the tab. Check the Segmentation option and the Profile option for the plugin to extract the information necessary to create single cell images.
9. Click on the square right to Profile to open the details of the option. Choose Medial in the box (*see* **Note 43**).
10. Click on the button furthest to the lower right to perform cell recognition and segmentation. A new window named "ResultJ" will open automatically (*see* Fig. 14).
11. Click on Bacteria on the upper left side. Then click on the seventh icon visible in the upper middle section of the window (*see* Fig. 14).

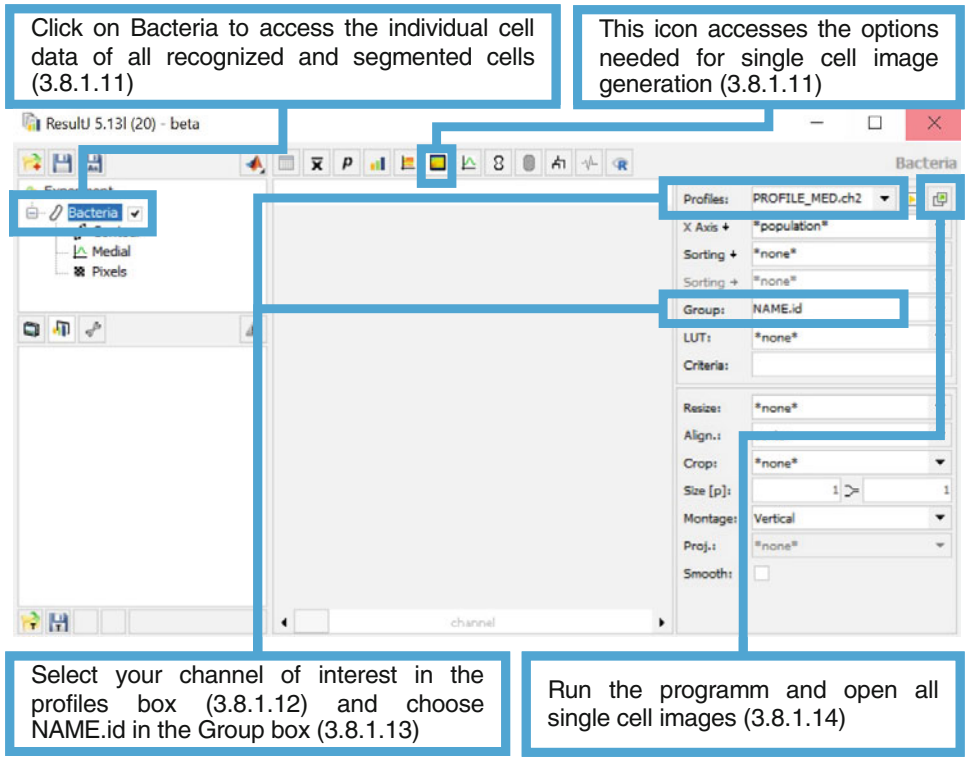

Fig. 14 Graphic user interface of the ResultJ window [11]

12. Select the channel containing your signal of interest in the Profiles box (*see* Fig. 14). The option will be named "PROFILE_MED.chX", where X is the number of your channel of interest.
13. Choose "NAME.id" in the Group box.
14. Click on the second icon right to the profiles box to open individual images of all cells recognized and segmented by MicrobeJ (*see* **Notes 44** and **45**).

3.8.2 Combine Images into a Convolved Average Projection

1. Combine the open images of all individual cells into a stack by clicking Image – Stacks – Images to stack in the ImageJ menu (*see* **Note 46**). Choose Scale (smallest) in the Method box and check the Bicubic Interpolation option. After clicking OK, a new window containing all individual images in a stack will open, while all individual images will close.
2. To convolve all images in the stack, click on Process – Filters – Convolve. Click OK after inserting the correct Convolution Kernel in the text field (*see* **Note 47**) and apply to all images.
3. To condense the convolved data into the final convolved average projection, click on image – stack – Z project. Choose average intensity as projection type and make sure all images are included. Start slice should be number 1, and stop slice should be the total number of individual cells in your stack.

3.9 Analysis of Cell Length, Width, and Cell Count of Rod-Shaped *B. subtilis*, and Generation of Histograms Using Oufti Software

1. Download Oufti [12] (https://oufti.org/download.html). You may select from the stand-alone version or the MATLAB-based program and follow the instructions given by the developers (*see* **Note 48**).
2. Select the images to analyze from your experiment of interest. Here is described the necessary steps to analyze cell parameters in rod-shaped bacteria, for example, *B. subtilis*. The images should be in TIFF format (*see* **Note 49**).
3. Guiding steps for image analysis are shown in Fig. 15. First, start the program and click the button "Load phase" (Fig. 15, **step 1**), to load image(s) for analysis.
4. On the first box on the right, under "Detection & analysis", select the option "Independent frames" (Fig. 15, **step 2**).
5. On the second box on the right, click on "Load parameters" (Fig. 15, **step 3**), here is specified values for the algorithms embedded in the program to recognize the cells and perform segmentation (*see* **Note 50**).
6. On the first box of the right, select "File" (Fig. 15, **step 4**), and give a name and location of where you would like to save your data analysis.
7. Now in the "Parameter test mode" box, click on "Segmentation" (Fig. 15, **step 5**). Here, a new window will pop up, and we can see if the selected parameters are sufficient to recognize the cells, if not you may vary the values to optimize cell recognition (*see* **Note 51**).
8. Now under "Detection & analysis", click the button "This frame" (Fig. 15, **step 6**). The algorithm will calculate the cell mesh, which is necessary to measure other parameters later. The time necessary for calculations will depend greatly on the algorithm you select for analysis (*see* **Note 52**).
9. In the menu bar, follow the path "Tools (Fig. 15, **step 7**) – cell statistics – cellstat", and this will provide a summarized information including the total number of cells and the mean and standard deviation values of the following parameters (in pixels): total number of spots (if applies), cell length, cell width, cell area, and cell volume.
10. The results can be exported as histograms following the desired path "Tools – cell statistics – curvature hist, length hist or mean width hist". A window will appear, and from here, the graph can be exported in several formats suitable for presentation or publication (*see* Fig. 15).
11. Export the data in CSV format to analyze individual cells. To do so, select the menu "Tools – export cellList to csv". The generated file is compatible to Excel, and it contains the

individual values tabulated (in pixels). To visualize and correlate the cell ID number, select in the menu "show mesh as", the option "numbers". The generated data can be used for creating further graph analysis as depicted in Fig. 16.

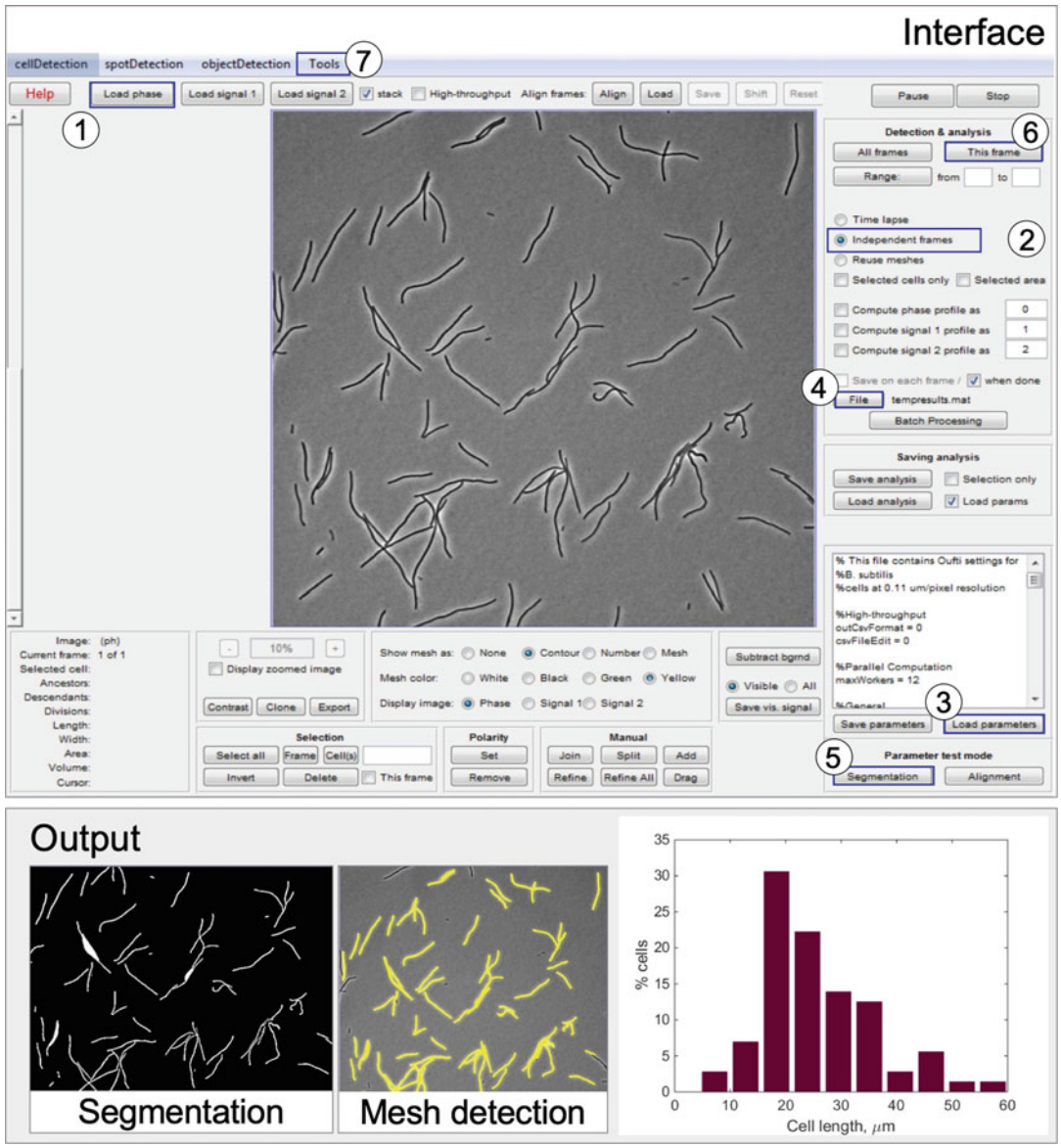

Fig. 15 Graphic user interface of Oufti [12], depicting the steps for the quantification of cell morphology parameters, the typical output for the segmentation, cell detection algorithms, and a generated histogram

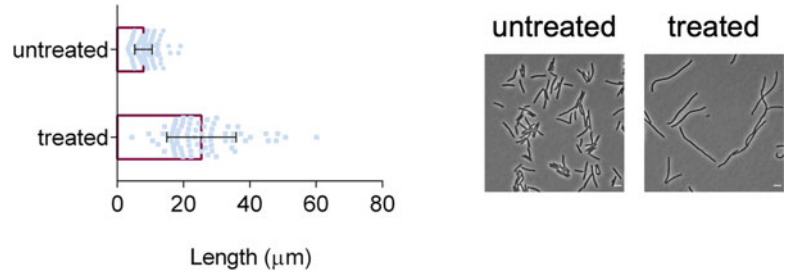

Fig. 16 Analysis of the cell length of *B. subtilis* upon antibiotic treatment, displaying individual cell length values calculated using Oufti [12]

4 Notes

1. Other human or rabbit antibodies work as well. No distinct molar concentration can be given. The manufacturer does not provide information about working concentration.
2. When possible, always work with fresh antibiotic stocks, preparing small aliquots to use once per experiment significantly improves reproducibility and avoids antibiotic degradation related to cycles of freezing and thawing.
3. Minimal configuration for Prime BSI (sCMOS) camera (Teledyne Photometrics, United States): Windows 7 or higher 64-bit operating system, 2.0 GHz or faster Intel processor, 8+ GB RAM, 250+ GB serial ATA (SATA) HDD and/or (better) 512+ GB solid state drive (SSD), open PCI-Express 4× (4 lane) interface slot or higher for use with an interface card (for high speed imaging) or USB 3.0 port for camera and 3+ USB ports (2.0 or higher) for other peripheral hardware (motorized microscope, laserbox/lasers, additional controllers, etc.).
4. We used a Nikon Eclipse Ti automated microscope equipped with a Perfect Focus system (Nikon Instruments Europe BV, Netherlands), an Orca Flash 4.0 camera (Hamamatsu, Photonics, Japan) or Prime BSI camera (Teledyne Photometrics, United States), and CFI Plan-Apo DM 100×/1.45 Oil Ph3 objective (Nikon) or CFI Apo TIRF 100×/1.49 Oil objective (Nikon) with the external Phase Contrast (Nikon; Phaseplate PH3). For measurements with GFP fusion proteins, a highly inclined and laminated (HiLo) [9] illumination system should be used to minimize the fluorescent background of the medium.
5. In addition to the fluorescence channel of interest, sample images have to contain a reference channel for unbiased cell recognition and segmentation. The reference channel needs to contain all relevant cell morphology information, most

importantly the cell contours and area. If possible, use phase contrast images; otherwise, a membrane stain is the recommended alternative.

6. The use of lasers is preferred due to the higher coherence of the emitted light and thus the better suitability in combination with HiLo illumination. We used a C-Flex laser combiner (Hübner Photonics, Germany) with 4 Cobold laser heads (Hübner Photonics, Germany): 405 nm (MLD-Laser), 488 nm (MLD-Laser), 561 nm (DPL-Laser), and 638 nm (MLD-Laser) for time-resolved experiments.
7. The open-source program ImageJ (http://imagej.nih.gov/ij/) [11] in the Fiji package distribution (https://imagej.net/software/fiji/) [10] is used to open images, to run the cell segmentation plugin MicrobeJ (https://www.microbej.com/) [13], and to perform the CAP. Also, ImageJ contains multiple tools to analyze CAPs.
8. The ImageJ plugin MicrobeJ is needed to identify individual cells in a raw image and extract individual cell images.
9. Bacteria need to be washed because autofluorescent components of MH media attach to the cover slip surface creating a fluorescent background. BSA is later applied to further reduce any nonspecific binding of residual fluorescent components.
10. The mixing is performed to separate large groups of cells, which are not suited for analysis.
11. The Fc Block has two functions: It passivates the glass surface and attaches bacteria via the cell wall anchored protein A in their cell wall to the glass.
12. BSA is used to passivate the surface further.
13. Avoiding air bubbles in the sample chamber is crucial. Trapped air is hard to remove due to surface tension of the culture media, which dictates the movement of trapped air and disturbs micrographic experiments. Also, if larger amounts of air get moved through the sample chamber, surface tension of the solution can rip off bacteria from the surface.
14. Contact with the objective respectively the immersion oil leads to transfer of heat between objective and sample. The objective heater is therefore more important than the stage top incubator for the initial temperature of the sample. Conduction of heat through 170 μm glass will be much faster than 5 mm of solution especially when convection is reduced to a minimum.
15. The syringe should not be emptied completely. Usually, a small volume of air is trapped inside. This can be avoided by removing the air before installation. Otherwise, a small volume of 50 μL of air can be left inside the syringe.

16. These values need to be adjusted for each experiment individually.
17. Select adequate positions. Usually, a collection of single cells per field of view is advantageous.
18. This is appropriate to acquire a z-stack to image bacteria with a thickness of about 1 μm. This provides sufficient data for a later deconvolution.
19. Extensive controls are necessary to make sure that the bacteria survive the illumination with the chosen wavelength, power, and exposure time, and these have to be defined accordingly.
20. Slice 2, 3, or 4 should perfectly be in focus.
21. For some compounds, this additional sonication is not needed; nevertheless, cleaning should be done thoroughly.
22. These simple actions can be performed by hand for each frame and channel, but automation is strongly advised, and writing a macro here saves a lot of time if large datasets are analyzed.
23. Deconvolution works best for three-dimensional image data. Deconvolution with DeconvolutionLab2 is easily applicable with a normal computer with 16 GB of RAM and a simple CPU. It is running on a single core. DeconvolutionLab2 is bad in relocating memory; therefore, every 30–40 runs, the garbage collector should be run ("call("java.lang.System.gc");") or the program (ImageJ) should be closed and opened again to free the cache again. A single deconvolution of an image with 2048 × 2048 × 5 pixels uses about 4 MB of RAM and about 6–8 min for ten iterations. Again, a macro is helpful. Information about the implementation of DeconvolutionLab2 can be found online [27]. Higher numbers of iterations might introduce artifacts, so the number of iterations has to be set carefully. The number of iterations must be chosen depending on the initial signal, contrast, and possible image noise.
24. The classification of the single cell images of the time-lapse images is necessary here for the subsequent analysis. Averaging cells in different states will lead to diffuse, unstructured signal profiles in an averaged kymograph.
25. It is useful to name the stacks with numbers in the folder where they are from, select all of them at once and drag the first stack into ImageJ. They will open in order, and they will also fill the positions for the "Concatenate. . ." function in the same order they are opened. Also, no other stack should be opened at that time because these will be included in the order and will need to be shifted. This is usually a lengthy process and can be easily avoided.

26. The region of interest should be drawn large enough to account for the microscopy stages' random movement in lateral direction.
27. It is possible that focus stabilization might introduce slight defocusing. This behavior is usually found once every single or second time lapse and is averaged over in the averaging process later on.
28. Due to bleaching, the enhance contrast function can help with the alignment of the stack. It also enables comparison of localization in different positions in the field of view.
29. "Rigid Body" is chosen such that rotation, but no stretching is performed.
30. Make sure that no black regions at the edges of the images are visible from the correction for lateral movement. Otherwise, the contrast enhancement will be performed, and the lowest gray values will come from this region.
31. If there are signals from neighbored cells present in the time lapse, this might interfere with the function of "StackReg". So, restricting the ROI to the signal of interest simplifies the alignment. If a correct alignment is not possible due to close neighbors, a different cell should be chosen.
32. The line width can be chosen by double clicking the "line tool" (*Straight*). It is easier to cover one of the images with the largest distance between the foci to find the right length for the profile. The surplus length is necessary to cover the complete signal's profile. Profiles across different cells do not have to be of the same length. A larger line width is used to capture the maximum with certainty. With a greater line width than one, ImageJ will take the maximum projection perpendicular to the propagation direction of the line profile.
33. It is essential to place the selected line well centered over the cell body.
34. The kymographs can be used the way they are created, but the observer usually associates the x-axis with the time axis.
35. *DeconvolutionLab2* resets the images pixel size to one pixel in each direction. Consider this if further measurements are done.
36. Classification is necessary because the cells exhibit a range of sizes. Without sorting them into size classes, a very diffuse intensity distribution along the profile would be produced when averaging the kymographs. Classification needs to consider resolution limits and pixel sizes.
37. The kymographs in Fig. 12 have to be read from left to right. Movement along the septal plane is expressed by up and down movement of the foci.

38. The versions (Fiji Is Just) ImageJ 2.0.0.-rc-69/1.52p running with Java 1.8.0_182 [64-bit] and the Plugin MicrobeJ 5.13 L (20) beta were used for preparation of this chapter.
39. If multiple images of the same sample are available, opening the images all at once within MicrobeJ can be advantageous. Select all images in the Explorer and open them using drag-and-drop on the furthest icon on the lower left in MicrobeJ. If the metadata and channel arrangement in the images are correct, MicrobeJ will automatically combine the images and their channels into an optimized hyperstack. This allows the subsequent analysis for all the images at once.
40. For the phase contrast reference channel, the default mode is recommended. For a membrane stain as the reference channel, Huang mode is recommended. However, depending on the individual images, other modes might be preferable.
41. The binary mask yellow overlay should resemble the cell area as best as possible. Errors in the analysis can occur, if not enough of the cell area is covered or the binary mask exceeds the cell borders. Note that MicrobeJ performs an automated algorithmic analysis that will most likely not be able to recognize and segment all individual cells of an image in the correct way. Optimizing the binary mask to reduce false-positive cell recognition is therefore recommended.
42. It is possible to test the chosen parameters by clicking the play icon on the lower right of the segmentation parameter field (*see* Fig. 13). If the icon is clicked, MicrobeJ will perform cell recognition and segmentation according to the configured binary mask and parameters. After completion, an overlay will appear on the analyzed image, contouring all cells recognized. If a recognized shape is rejected based on the chosen segmentation parameters, the contour will appear red. Additionally, the reason for rejection will appear next to the recognized shape in red font. Furthermore, all checked segmentation parameters will be shown in green font for all recognized shapes. This enables fine-tuning of the segmentation parameters if needed.
43. It is possible to extend the area depicted in the individual cell images further from the edge of the recognized cell border by the amount of μm entered in the boxes Dilate (y-Axis) and Extension (x-Axis). Leaving thickness on auto is recommended.
44. Depending on the number of cells recognized, a large number of images may open automatically. This can lead to performance issues, depending on the used computer hardware.

45. It is possible to safe the ResultJ data and the MicrobeJ recognition parameters by clicking on the floppy disc icon in the respective window.
46. Make sure, that all sample images and no other images are opened, as all images opened will be combined into a stack. Combine only cells with a similar cell morphology into a stack. If your sample contains cells with different morphologies (e.g., significant differences in cell length), sorting the cells into groups of approximately similar morphology prior to stack generation is recommended. This can be done manually or by defining respective parameters in 3.8.1.7. In this case, take care not to introduce a bias into the analysis, for example, by neglecting cells in a certain range of length.
47. Using the standard Kernel [-1 -1 -1 -1 -1; -1 -1 -1 -1 -1; -1 -1 24 -1 -1; -1 -1 -1 -1 -1; -1 -1 -1 -1 -1] is recommended. Depending on the specific method and question, other convolution kernels may be useful.
48. Oufti is useful for the detection of several parameters including cell length, width, volume, area, etc. in phase contrast micrographs. The program is also useful for fluorescence channel images and is best suitable for spots, representative of cytoplasmic proteins, and even chromosome staining, but it is not able to properly identify cell contours, for example, when the cell membrane is stained. In these instances, we recommend using other open source software, for example, MicrobeJ.
49. Images obtained using a 60× objective were also suitable for quantification of cells in the phase contrast channel.
50. Oufti download package comes with a preset of parameters suitable for different bacteria including *Escherichia coli* and *Caulobacter crescentus*. Here, you can modify and fine-tune values according to your imaging, especially the resolution (μm/pixel), so the software can better detect your cells. It is important to use the exact image resolution from the raw images, because this is mandatory for accurate calculations using the program.
51. For image analysis, minimal hardware settings should be an Intel Core i3 processor, a memory (RAM) of 8.00 GB and an operating system of Windows 10 (64 bit). Here, for a single image, the analysis time is approximately 90 s. In the tutorial section of the application, the developers suggest using pixel instead of subpixel algorithms to reduce the analysis time, however, sensitivity can be lost significantly [28].
52. In the "Segmentation" pop-up window, the outcome is a binary mask of the original phase contrast image. Here, you should select values that allow a better recognition of the bacterial cells, which should be observed as white rods in a

black background. Depending on the quality of your image, you can adapt the values for the different algorithms, thus creating the most optimal binary mask for your image. In our example, we selected for the "EdgeMode", the option "LOG"; "Dilate", value 1; "openNum", value 1; "InvertImage", value 0; "ThreshFactorM", value 0.98508; "EdgeSigmaL", value 1.1902; "ValleyThresh1", value 0.03; and "LogThresh", value 0.24857. In the Oufti Tutorial section, further information regarding these options are available [28].

Acknowledgments

The authors appreciate funding by the Deutsche Forschungsgemeinschaft (DFG, German Research Foundation): Project-ID 398967434 -TRR261 (projects A02, A11 and Z02).

References

1. Hardt P, Engels I, Rausch M, Gajdiss M, Ulm H, Sass P, Ohlsen K, Sahl H-G, Bierbaum G, Schneider T, Grein F (2017) The cell wall precursor lipid II acts as a molecular signal for the Ser/Thr kinase PknB of *Staphylococcus aureus*. Int J Med Microbiol 307(1):1–10. https://doi.org/10.1016/j.ijmm.2016.12.001
2. Zahir T, Camacho R, Vitale R, Ruckebusch C, Hofkens J, Fauvart M, Michiels J (2019) High-throughput time-resolved morphology screening in bacteria reveals phenotypic responses to antibiotics. Commun Biol 2(1):269. https://doi.org/10.1038/s42003-019-0480-9
3. Grein F, Müller A, Scherer KM, Liu X, Ludwig KC, Klöckner A, Strach M, Sahl H-G, Kubitscheck U, Schneider T (2020) Ca2+-Daptomycin targets cell wall biosynthesis by forming a tripartite complex with undecaprenyl-coupled intermediates and membrane lipids. Nat Commun 11(1):1455. https://doi.org/10.1038/s41467-020-15257-1
4. Salamaga B, Kong L, Pasquina-Lemonche L, Lafage L, von und zur Muhlen M, Gibson JF, Grybchuk D, Tooke AK, Panchal V, Culp EJ, Tatham E, O'Kane ME, Catley TE, Renshaw SA, Wright GD, Plevka P, Bullough PA, Han A, Hobbs JK, Foster SJ (2021) Demonstration of the role of cell wall homeostasis in *Staphylococcus aureus* growth and the action of bactericidal antibiotics. Proc Natl Acad Sci 118(44): e2106022118. https://doi.org/10.1073/pnas.2106022118
5. Silber N, Mayer C, Matos de Opitz CL, Sass P (2021) Progression of the late-stage divisome is unaffected by the depletion of the cytoplasmic FtsZ pool. Commun Biol 4(1):270. https://doi.org/10.1038/s42003-021-01789-9
6. Monteiro JM, Fernandes PB, Vaz F, Pereira AR, Tavares AC, Ferreira MT, Pereira PM, Veiga H, Kuru E, VanNieuwenhze MS, Brun YV, Filipe SR, Pinho MG (2015) Cell shape dynamics during the staphylococcal cell cycle. Nat Commun 6(1):8055. https://doi.org/10.1038/ncomms9055
7. Mayer C, Sass P, Brötz-Oesterhelt H (2019) Consequences of dosing and timing on the antibacterial effects of ADEP antibiotics. Int J Med Microbiol 309(7):151329. https://doi.org/10.1016/j.ijmm.2019.151329
8. Silber N, Matos de Opitz CL, Mayer C, Sass P (2020) Cell division protein FtsZ: from structure and mechanism to antibiotic target. Future Microbiol 15:801–831. https://doi.org/10.2217/fmb-2019-0348
9. Tokunaga M, Imamoto N, Sakata-Sogawa K (2008) Highly inclined thin illumination enables clear single-molecule imaging in cells. Nat Methods 5(2):159–161. https://doi.org/10.1038/nmeth1171
10. Schindelin J, Arganda-Carreras I, Frise E, Kaynig V, Longair M, Pietzsch T, Preibisch S, Rueden C, Saalfeld S, Schmid B, Tinevez J-Y, White DJ, Hartenstein V, Eliceiri K, Tomancak P, Cardona A (2012) Fiji: an open-source platform for biological-image analysis.

Nat Methods 9(7):676–682. https://doi.org/10.1038/nmeth.2019

11. Schneider CA, Rasband WS, Eliceiri KW (2012) NIH image to ImageJ: 25 years of image analysis. Nat Methods 9(7):671–675. https://doi.org/10.1038/nmeth.2089
12. Paintdakhi A, Parry B, Campos M, Irnov I, Elf J, Surovtsev I, Jacobs-Wagner C (2016) Oufti: an integrated software package for high-accuracy, high-throughput quantitative microscopy analysis. Mol Microbiol 99(4): 767–777. https://doi.org/10.1111/mmi.13264
13. Ducret A, Quardokus EM, Brun YV (2016) MicrobeJ, a tool for high throughput bacterial cell detection and quantitative analysis. Nat Microbiol 1(7):16077. https://doi.org/10.1038/nmicrobiol.2016.77
14. Ursell T, Lee TK, Shiomi D, Shi H, Tropini C, Monds RD, Colavin A, Billings G, Bhaya-Grossman I, Broxton M, Huang BE, Niki H, Huang KC (2017) Rapid, precise quantification of bacterial cellular dimensions across a genomic-scale knockout library. BMC Biol 15(1):17. https://doi.org/10.1186/s12915-017-0348-8
15. Kirshner H, Aguet F, Sage D, Unser M (2013) 3-D PSF fitting for fluorescence microscopy: implementation and localization application. J Microsc 249(1):13–25. https://doi.org/10.1111/j.1365-2818.2012.03675.x
16. Kirshner H, Sage D PSF Generator – A Java software package to generate realistic 3D microscope Point-Spread Function (PSF). http://bigwww.epfl.ch/algorithms/psfgenerator/
17. Sage D, Donati L, Soulez F, Fortun D, Schmit G, Seitz A, Guiet R, Vonesch C, Unser M (2017) DeconvolutionLab2: an open-source software for deconvolution microscopy. Methods 115:28–41. https://doi.org/10.1016/j.ymeth.2016.12.015
18. Thévenaz P StackReg – An ImageJ plugin for the recursive alignment of a stack of images. http://bigwww.epfl.ch/thevenaz/stackreg/. Accessed 14 Jan 2022
19. Thévenaz P, Ruttimann UE, Unser M (1998) A pyramid approach to subpixel registration based on intensity. IEEE Trans Image Process 7(1):27–41. https://doi.org/10.1109/83.650848
20. Mary H, Rueden C, Ferreira T Kymograph-Builder: Release 1.2.4. Accessed 14 Jan 2022
21. Jansson PA, Hunt RH, Plyler EK (1970) Resolution enhancement of spectra. J Opt Soc Am 60(5):596–599. https://doi.org/10.1364/JOSA.60.000596
22. Agard DA, Sedat JW (1983) Three-dimensional architecture of a polytene nucleus. Nature 302(5910):676–681. https://doi.org/10.1038/302676a0
23. Aguet F, Van De Ville V, Unser M (2008) Model-based 2.5-D deconvolution for extended depth of field in brightfield microscopy. IEEE Trans Image Process 17(7): 1144–1153. https://doi.org/10.1109/TIP.2008.924393
24. Born M, Wolf E (2003) Principles of optics. In: Fraunhofer diffraction at apertures of various forms, 7th edn. Cambridge University Press, Cambridge/London
25. Richardson WH (1972) Bayesian-based iterative method of image restoration. J Opt Soc Am 62(1):55–59. https://doi.org/10.1364/JOSA.62.000055
26. Lucy LB (1974) An iterative technique for the rectification of observed distributions. Astron J 79:745. https://doi.org/10.1086/111605
27. DeconvolutionLab2. http://bigwww.epfl.ch/deconvolution/deconvolutionlab2/. Accessed 24 Jan 2022
28. Oufti Application. http://www.oufti.org/. Accessed 7 Apr 2022

Chapter 13

Application of a *Bacillus subtilis* Whole-Cell Biosensor (P_{liaI}-*lux*) for the Identification of Cell Wall Active Antibacterial Compounds

Carolin Martina Kobras, Sali May Morris, Thorsten Mascher, and Susanne Gebhard

Abstract

Whole-cell biosensors, based on the visualization of a reporter strain's response to a particular stimulus, are a robust and cost-effective means to monitor defined environmental conditions or the presence of chemical compounds. One specific field in which such biosensors are frequently applied is drug discovery, that is, the screening of large numbers of bacterial or fungal strains for the production of antimicrobial compounds. Here, we describe the application of a luminescence-based *Bacillus subtilis* biosensor for the discovery of cell wall active substances; this article is an update to our previous chapter published in 2017. The system is based on the well-characterized promoter P_{liaI}, which is induced in response to a wide range of conditions that cause cell envelope stress, particularly antibiotics that interfere with the membrane-anchored steps of cell wall biosynthesis. A simple "spot-on-lawn" assay, where colonies of potential producer strains are grown directly on a lawn of the reporter strain, allows for quantitative and time-resolved detection of antimicrobial compounds. Due to the very low technical demands of this procedure, we expect it to be easily applicable to a large variety of candidate producer strains and growth conditions.

Key words Bioassay, Reporter gene, Cell envelope stress, Cell wall, Antibiotic, Antimicrobial peptide, Stress response, Luminescence, Lipid II cycle

1 Introduction

Biosensors are "devices that use specific biochemical reactions mediated by isolated enzymes, immunosystems, tissues, organelles or whole cells to detect chemical compounds, usually by electrical, thermal or optical signals," according to the IUPAC definition [1]. In recent years, whole-cell biosensors in particular have gained increasing attention in different fields of application, such as on-site monitoring of environmental samples, for example, for pollutants such as heavy metal ions or xenobiotics, but also drug discovery and mode-of-action studies [2]. Compared to enzymes or the other

Peter Sass (ed.), *Antibiotics: Methods and Protocols*,
Methods in Molecular Biology, vol. 2601, https://doi.org/10.1007/978-1-0716-2855-3_13,

biosensor platforms mentioned above, they offer the advantage of low costs, high stability, and ease of use [3]. Normally, whole-cell biosensors are genetically modified microorganisms that use the stimulus specificity of signal-transducing regulatory systems to connect an input (compound or condition to be detected) with a measurable output. The latter is usually provided by a reporter gene under control of a promoter that is regulated by the signaling system.

Three different types of microbial reporter systems are most commonly employed. The β-galactosidase (encoded by *lacZ*) is the classical reporter gene and was already established in the early 1970s as a quantitative and highly reproducible measure for differential promoter activity, using the chromogenic substrate ONPG (*o*-nitrophenyl-*β*-D-galactopyranoside) [4]. Despite the disadvantage of having to collect cells and perform a biochemical assay for a quantitative readout, it is still widespread, since it only requires a standard photometer for colorimetric detection of the enzymatic reaction product at a wavelength of 420 nm. Moreover, *lacZ*-based whole-cell biosensors offer the convenience of a low-cost, simple, and fast semiquantitative readout, if X-Gal (5-bromo-4-chloro-3-indoyl- *β*-D-galactopyranoside) is used as a chromogenic substrate in plate-based whole-cell biosensor assays, which are suitable even for field work in the absence of any technical equipment [5].

More recently, two additional reporter systems have found widespread use in biosensors, namely, fluorescent proteins, such as GFP, and bioluminescent reporters, derived either from bacterial or firefly luciferase. While both require more advanced documentation systems for quantitative measurements, their advantage over the β-galactosidase reporter is the possibility for a quantitative online monitoring of promoter activity in viable cells (e.g., growing liquid cultures in microtiter plates) without the need of harvesting cells and performing an assay. While GFP and its many derivatives have found widespread use in numerous biological applications, including whole-cell biosensors [6], the autofluorescence of the cells or media components often limit the dynamic range and hence sensitivity of fluorescence-based biosensors. In contrast, bioluminescence offers a virtually background-free reporter system, thereby enabling biosensors with a high dynamic range and hence sensitivity. Firefly luciferase requires the addition of luciferin as a substrate, which in the presence of ATP and oxygen leads to visible light emission. Bacterial luciferase, encoded by the *luxCDABE* operon of *Photorhabdus luminescens*, catalyzes the oxidation of reduced flavin mononucleotide ($FMNH_2$) and fatty aldehydes to FMN and fatty acids, respectively, in the presence of molecular oxygen, resulting in blue-green light emission [3]. The substrates of this reaction are regenerated by the normal cellular metabolism, and no addition of an external substrate is required, making bacterial luciferase the more convenient and cost-efficient alternative.

This chapter describes the use of a luminescence-based biosensor for the detection of antimicrobial substances that interfere with the membrane-anchored steps of cell wall biosynthesis and provides an update on the previously published methodology [7]. The biosensor is derived from the *liaI* promoter (P_{liaI}) of the Gram-positive model organism *Bacillus subtilis*, which is strictly controlled by the cell-envelope stress-responsive LiaFSR three-component system [8, 9]. It was first reported to strongly respond to the cell wall antibiotics vancomycin and bacitracin [10, 11]. Subsequently, P_{liaI} was thoroughly characterized and developed into a β-galactosidase-based biosensor (P_{liaI}-*lacZ*) for the identification and characterization of lipid-II interfering antibiotics (hence the name "*lia*") [5, 12, 13]. P_{liaI} possesses a very low basal promoter activity and a highly dynamic response (over 100-fold induction) to its specific inducers, making it ideally suited for screening purposes [14]. More recently, a new P_{liaI}-based whole-cell biosensor has been established by employing the bacterial luciferase system from *P. luminescence* [15]. The *luxABCDE* operon used in the resulting P_{liaI}-*lux* biosensor has been optimized for expression in *B. subtilis* [16]. In addition to its convenience and high sensitivity, its short half-life of only 5–10 min allows an almost direct monitoring of not only the induction but also the shut-off of promoter activities, thereby providing another advantage over alternative reporter systems [15].

This chapter provides a detailed protocol of how to apply the P_{liaI}-*lux* whole-cell biosensor for a quantitative bioluminescence detection of antimicrobial compounds interfering with cell wall biosynthesis. This "spot-on-lawn" assay is based on growing a lawn of the reporter strain on solid media and applying spots of potential antibiotic producer strains to this lawn. Production of cell wall active compounds will then induce the activity of P_{liaI}, resulting in a ring-shaped luminescence signal around the producer colony that can be visualized and quantified using basic chemiluminescence detection equipment. For details on applying this biosensor strain for quantitative antibiotic induction experiments in liquid cultures, the readers are referred to the previously published procedure [15]. An alternative qualitative assay based on a P_{liaI}-*lacZ* reporter is described in the "Notes" section (*see* **Note 1**), as well as a modification of the "spot-on-lawn" technique for situations where the producer and reporter organisms do not share the same growth requirements (*see* **Note 2**).

2 Materials

Prepare all media and solutions using deionized waster (dH_2O). All reagents can be prepared and stored at room temperature, except for agar plates (4 °C), or where stated otherwise.

All waste containing bacterial cultures should be disposed of according to local regulations. The reporter strain is a class I genetically modified organism, and all handling and disposal should follow good microbiological practice procedures.

This chapter describes standard growth conditions and media for *Bacillus subtilis*. Depending on special growth conditions that may be required by bacterial strains to be tested for antibiotic production, different media and conditions can be used, provided preliminary tests show that the *B. subtilis* reporter strain is able to grow under such conditions.

2.1 Media and Reagents

1. Lysogeny Broth (LB): 10 g tryptone, 5 g yeast extract, 10 g sodium chloride. Add dH_2O to a volume of 1 l and autoclave.
2. LB agar: add 15 gL^{-1} of agar (1.5% (w/v)) to LB medium prior to autoclaving. Cool down agar to ~50 °C before adding antibiotics. Pour ca. 25 mL of agar per plate into 90 mm sterile petri dishes and let solidify.
3. LB soft agar: add 7.5 gL^{-1} of agar (0.75%) to LB medium prior to autoclaving. For immediate use, split into aliquots after autoclaving. For this, transfer 4 mL of molten soft agar into sterile tubes and keep at 50 °C until further use. For later use, let solidify and store at room temperature until needed.
4. Chloramphenicol stock solution: dissolve 5 mg mL^{-1} in 70% ethanol. Store at −20 °C.

2.2 Bacterial Strains

1. Reporter strain: *B. subtilis* W168 *sacA*::P_{liaI}-*luxABCDE* (strain TMB1858). This strain contains the promoter P_{liaI} fused to the *luxABCDE* luciferase reporter operon [15]. P_{liaI} is activated by lipid II cycle interfering antibiotics, such as bacitracin, nisin, ramoplanin, and vancomycin [5]. Upon promotor induction, a chemiluminescence signal is emitted (*see* **Notes 1** and **3**). Growth media should contain 5 μg mL^{-1} chloramphenicol.
2. Positive control: *B. subtilis* ATCC 6633. This strain is known as a producer of the cell envelope-active antibiotic subtilin and strongly induces the promoter P_{liaI} present in the reporter strain [12].
3. Negative control: *B. subtilis* W168. This strain does not produce any compounds that induce the P_{liaI}-*luxABCDE* reporter strain.
4. Strains to be tested for production of cell envelope-active compounds.

2.3 Special Equipment

1. For development of this assay, a FUSION-SL™ 16-bit chemiluminescence imaging system with the analysis software FUSION-CAPT™ was used (PEQLAB). Settings described in the methods section refer to this imaging system and

software and may vary for other products. Other imaging systems with comparable sensitivity can be used, but exposure times may have to be optimized.

2. Chemiluminescence is quantified using the freely available software ImageJ (http://imagej.nih.gov/ij/). Further calculations can be carried out using Microsoft Excel® (Microsoft Corporation, Redmond, WA, USA) or any other suitable software.

3 Methods

3.1 "Spot-on-Lawn" Reporter Screen

1. Preparation of overnight cultures. Set up overnight cultures of the reporter strain and all bacterial strains to be tested, including the positive and negative controls. Employ sterile technique to avoid contamination. Transfer 3 mL of LB medium into a sterile 20–50 mL test tube or universal. Add antibiotics as required, for example, chloramphenicol from stock (5 mg mL^{-1}) to a final concentration of 5 μg mL^{-1} for the reporter strain. Inoculate with a single colony of the respective strain from a fresh agar plate. Grow cultures at 37 °C overnight (~16 h) with shaking at 180–220 rpm.
2. Preparation of plates. Warm agar plates in an incubator to 20–30 °C for at least 20 min, or leave at room temperature overnight (*see* **Note 4**). Melt soft agar, transfer 4 mL of soft agar to a sterile screw-cap container and allow it to cool down to ~50 °C to prevent killing of the cells. Add 120 μL of the reporter strain overnight culture to the soft agar and mix carefully. Pour the entire mixture onto an agar plate and swirl gently. The agar plate should be evenly covered before the soft agar solidifies (*see* Fig. 1a). Avoid air bubbles. Dry plate for ~20 min or until all condensation has disappeared in order to avoid merging of culture drops in **step 3**.
3. Carefully spot 5 μL drops of the overnight cultures of the strains to be tested, including the controls, onto the soft agar (*see* **Note 5**; Fig. 1a–c). When drops are dry, incubate at 37 °C for 1–7 days (*see* **Note 6**).

3.2 Luminescence Detection

1. Adjust settings of the FUSION-CAPT™ software by selecting "chemiluminescence" and choosing "full resolution" mode. Open the camera's iris to maximal aperture.
2. At each time point to be monitored during incubation, place the agar plate with the spot-on-lawn culture in the imaging system (*see* **Note 7**). Remove the lid of the plate.
3. With epi-white illumination switched on, bring the plate into focus of the camera using preview mode (*see* **Note 8**; Fig. 1d).

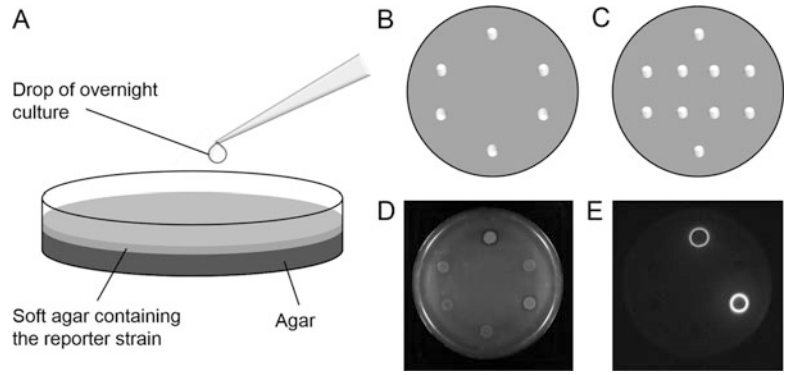

Fig. 1 Preparation of plates. (**a**) The agar plate is covered by a layer of soft agar containing the reporter strain (light gray). Culture drops of potential antimicrobial peptide producers are spotted carefully onto the thoroughly dried plate. (**b**, **c**): Recommended distribution patterns of culture drops. (**d**) Epi-white light image of a plate with spots of potential producer strains growing on the reporter strain lawn. (**e**) Luminescence image of the same plate shown in panel D. Production of cell wall-active compounds (spots) induces the P_{lial} promotor of the reporter strain (lawn). Induction results in a ring-shaped luminescence signal of the reporter strain surrounding the producer colony. (Figure reprinted from [7])

4. Switch off the epi-white light and start the chemiluminescence exposure (10 min). Do not open the door or switch on light during exposure.
5. Save the image (*see* Fig. 1e), place the lid on the plate and return to the incubator until the next measurement is due. Repeat **steps 1–4**, if more than one plate is used for the assay (*see* **Note 9**).

3.3 Luminescence Quantification

1. After starting the ImageJ software, choose your analysis settings ("*Analyze*" → "*Set Measurements...*"). Tick the box "*Min & max gray value*."
2. Open the image of the first time point ("*File*" → "*Open...*" or type *O* using the keyboard). Identify the precise location of each colony using the epi-white image of the same plate as a reference (*see* **Note 10**).
3. Click on the measurement tool depicting a straight line (**straight**, *see* Fig. 2). Set a line across the ring-shaped luminescence signal around a colony and select "Measure" ("*Analyze*" → "*Measure*" or type *M* using the keyboard; *see* Fig. 2, orange line). The measurement result will be automatically added to the "*Results*" window.
4. Repeat **step 3** until 20 independent lines have been measured (*see* **Note 11**). Ensure these lines are arranged randomly to measure the different sections of the luminescence circle. Right click on "*Summarize*" in order to receive the mean

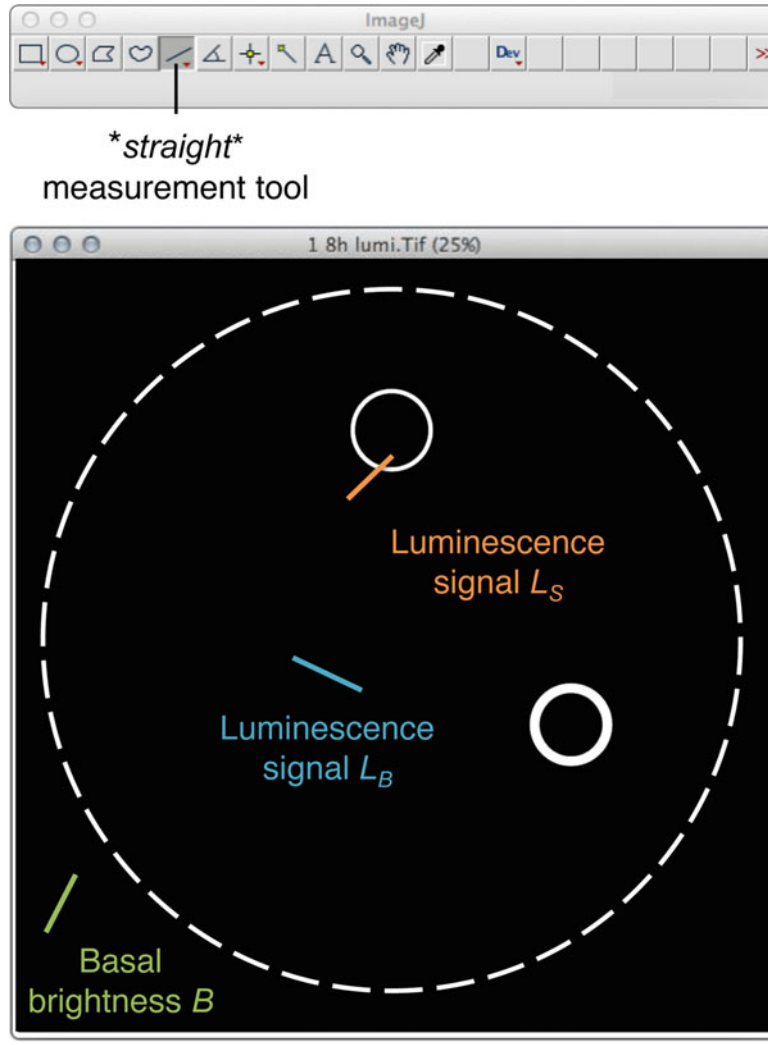

Fig. 2 Luminescence quantification using ImageJ. For determination of the luminescence signal L_S of the reporter strain around the colonies, linear measurements are taken across the luminescent ring (orange line). The background luminescence signal L_B, caused by autoinduction of the reporter strain [18], is determined by linear measurements in an area containing no producer colony (blue line). For determination of the basal image brightness B, linear measurements are taken on areas that are in the image but not on the plate (green line). The edge of the agar plate is indicated by a dashed white circle, and luminescence around producer colonies is indicated by solid white circles. Measurements are automatically summarized by the software in the "*Results*" window. (Figure reprinted from [7])

maximum value L_S and the standard deviation ΔL_S. Repeat measurements for all other colonies on the plate. Transfer all data to Microsoft Excel® or equivalent software for further calculations.

5. To determine the brightness of luminescence intrinsically produced by the reporter strain, follow the same procedure as in **step 4** to set 20 straight lines onto an area of the agar plate image where no colonies are located. These measurements will yield the mean maximum value L_B and the standard deviation ΔL_B needed to correct the signal determined for the producer colonies (*see* **Note 12**; Fig. 2, blue line).
6. Similarly, determine the mean maximum value and the standard deviation of the basal brightness B of the image by analyzing areas that are still in the image but not on the plate (*see* Fig. 2, green line).
7. To calculate the luminescence signal S over the basal brightness B of the image, subtract the mean maximum value of the basal brightness B of the image from the mean maximum value of the measured luminescence L_S or the plate background L_B.

$$S = L - B$$

8. The error propagation of several error-prone values is determined according to the following formula, simplified for two error-prone values in a subtraction.

$$\Delta S = \Delta L + \Delta B$$

S: Signal over basal brightness.

L: Mean maximum value of luminescence (L_S or L_B).

B: Mean of basal brightness.

Δ: Standard deviation of each parameter.

ΔS: Uncertainty of S

9. Analysis of the same plate and colonies at multiple time points allows quantification of the signal over time and thus displays the time course of production of cell wall-active compounds (*see* Fig. 3).

4 Notes

1. Should no sufficiently sensitive equipment for luminescence detection be available, the assays can be performed in a qualitative manner using a reporter strain carrying a P_{liaI}-*lacZ* construct [5]. In this case, both the base agar and soft agar overlay should be supplemented with 100 μg mL^{-1} X-Gal, added after autoclaving from a stock solution of 50 mg mL^{-1} X-Gal dissolved in dimethylformamide. Induction of the reporter will result in the formation of a blue ring surrounding the producer colony. In theory, the intensity of the blue coloration can be quantified with an image analysis software such as ImageJ. However, in contrast to luminescence, which is a transient

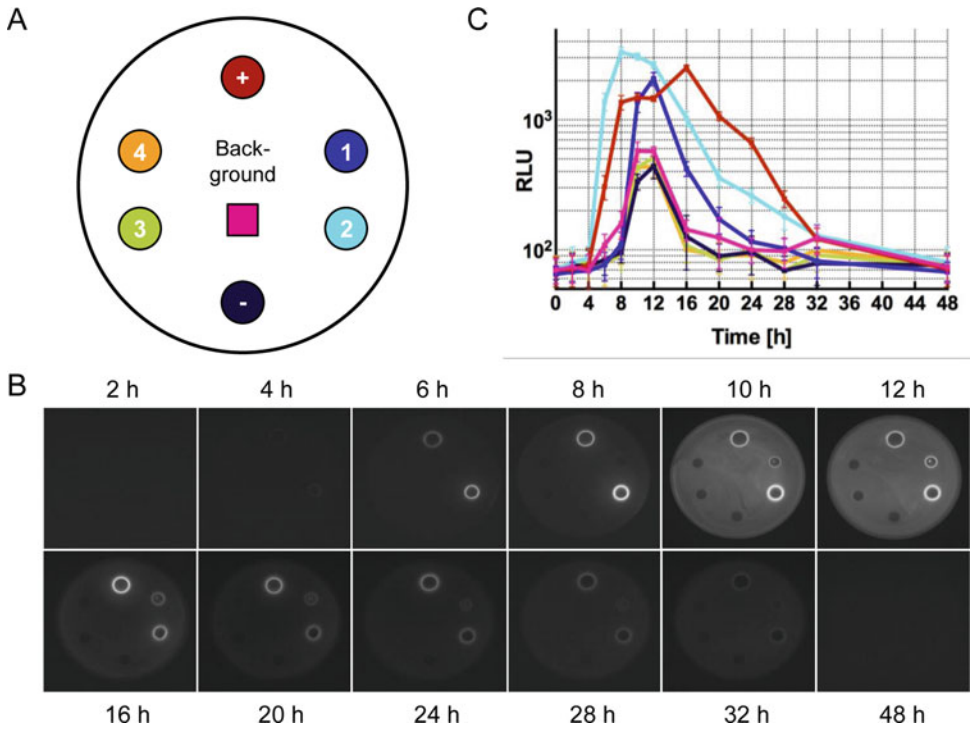

Fig. 3 Time-resolved quantification of antibiotic production. (**a**) Legend detailing the distribution of spots and identity of tested strains for the plates shown in panel B. Colors match those used in panel C. (**b**) Chemiluminescence images of a time course of antimicrobial production for example candidate strains 1–4, as well as positive and negative control strains. Spots of the producer strains are grown on a *B. subtilis* P_{liaI}-*luxABCDE* reporter lawn. (**c**) Quantified luminescence of potential producer strains 1–4, the controls and the autoluminescence of the reporter strain ("Background") caused by stationary phase induction of the reporter strain [18]. Note that tested strains 1 and 2 produce similar levels of luminescence as the positive control strain (i.e., production of a cell wall active compound), while strains 3 and 4 fail to produce a signal above the negative control or reporter strain background level of luminescence (i.e., no production of a cell wall active compound). (Figure reprinted from [7])

emission of photons and where the reporter protein has a very short half-life [15], the β-galactosidase produced by induction of the *lacZ*-reporter is stable, and the blue product of X-Gal cleavage will accumulate over time. It is therefore not possible to perform time resolved analyses as described for the luciferase reporter in Fig. 3.

2. Should the growth rates between the reporter and putative producer strains be too dissimilar to allow simultaneous growth of both, or in case the two strains cannot grow on the same media, a qualitative deferred assay can be carried out by adapting an existing protocol normally used to test growth inhibition by deferred antagonism [17]. This deferred test can also be used if there is a desire to let potential antimicrobials made by the producer accumulate over a longer time period.

For this test, the base layer should be composed of the preferential medium for the producer strain, and the soft agar should be made as described above. If a medium is known that supports growth of both organisms, this medium can be used for the base and soft agar layers. If using the *lacZ*-reporter, both the base and soft agar should be supplemented with 100 μg mL^{-1} X-Gal as described in **Note 1**.

After preparing the base agar, 5 μL of the producer strain should be spotted into the center of the plate and incubated at the strain's optimal growth temperature until visible growth appears. If desired, the plate can then be placed at room temperature (20–25 °C) for an additional 3–5 days to allow accumulation of antimicrobial products, before addition of the overlay with the reporter.

After inoculating the soft agar with the reporter strain, this should be poured onto the plate with the grown producer strain, as described for the standard procedure above, and left to dry. Once dry, the plate should be incubated at room temperature overnight to prevent overgrowth of the producer. If the reporter has not grown sufficiently after 12 h, further incubation can occur at 37 °C for 2–4 h. Quantification of luciferase activity can then be carried out as described above. If the *lacZ*-reporter was used, the readout can be assessed as explained in **Note 1**.

3. The P_{liaI}-reporter will respond to cell envelope stress and is therefore a nonspecific reporter for production of substances that interfere with cell envelope integrity, including but not restricted to lipid II cycle interfering antibiotics. If a more specific screen is desired, two alternative reporters can be used. The target promoter of the BceRS-BceAB resistance system of *B. subtilis*, P_{bceA}, is known to respond to bacitracin, the lantibiotics mersacidin, and actagardine and the fungal defensin plectasin [12]. The target promoter of the paralogues PsdRS-PsdAB system, P_{psdA}, responds to a broad range of cell wall active antimicrobial peptides, such as nisin, subtilin, actagardine, gallidermin, and enduracidin [12]. It is assumed that these lists of inducing substances are not exhaustive and new substrates may be identified from further screens. Fusions of these promoters to the *luxABCDE* reporter may be used, following the same procedures as described here, instead of the P_{liaI} reporter to provide some further information on the nature of the substance produced by the strains under investigation.
4. If the agar plate is too cold, the soft agar will solidify before it is evenly spread onto the plate.
5. Culture spots should be distributed equally over the plate (*see* Fig. 1b), as their location on the plate and their proximity to

each other could affect the luminescence signal. For an initial screening of producer strains, a higher number of cultures can be tested on a single plate (*see* Fig. 1c). To avoid bacterial aerosols and splashes, gently push the drop halfway out of the pipette tip before placing the drop carefully on the soft agar.

6. Plates may dry out when using a small incubator or longer incubation times. Therefore, it is helpful to wrap the plates in foil.
7. Time points depend on the growth rate of the tested strains and the desired time-lapse resolution of antibiotic production and therefore may vary from 2-h intervals to daily measurements over 1–7 days. An initial screening helps to choose the optimal time points and overall duration of experiments.
8. Saving an image of the plate with the light switched on will help to remember the orientation of the plate in case of no or only low luminescence.
9. It might be necessary to enhance the brightness of the image to be able to see the luminescence on screen.
10. Do not adjust the image brightness before or during the analysis. This is essential to allow comparison of the signal strength between the time points.
11. The lines should be distributed around the luminescent ring, as the luminescence signal can be uneven around a colony. The precise length of the measurement lines is not of importance, because only the maximum value will be used for further analysis. Information of angle and length is displayed in the status bar or can be checked in the "*Results*" table.
12. The P_{liaI} promoter was found to be autoinduced during transition of *B. subtilis* to stationary phase [18], which results in a transiently increased luciferase activity of the reporter strain in this assay. It is necessary to consider the effect of autoinduction to avoid false-positive signals during luminescence quantification. Determination of the background luminescence signal, L_B, allows appropriate correction of the actual reporter signal, L_S, obtained for producers of cell wall-active compounds.

References

1. Nic M, Jirat J, Kostata B (2014) IUPAC compendium of chemical terminology – the gold book. http://goldbook.iupac.org. Accessed 01 Apr 2022
2. Wex KW, Saur JS, Handel F, Ortlieb N, Mokeev V, Kulik A, Niedermeyer THJ, Mast Y, Grond S, Berscheid A, Brötz-Oesterhelt H (2021) Bioreporters for direct mode of action-informed screening of antibiotic producer strains. Cell Chem Biol 28:1242–1252.e4
3. Park M, Tsai SL, Chen W (2013) Microbial biosensors: engineered microorganisms as the sensing machinery. Sensors 13:5777–5795
4. Miller JH (1972) Experiments in molecular genetics. Cold Spring Harbor Laboratory Press, Cold Spring Harbor

5. Mascher T, Zimmer SL, Smith TA, Helmann JD (2004) Antibiotic-inducible promoter regulated by the cell envelope stress-sensing two-component system LiaRS of *Bacillus subtilis*. Antimicrob Agents Chemother 48:2888–2896
6. Kremers G-J, Gilbert SG, Cranfill PJ, Davidson MW, Piston DW (2011) Fluorescent proteins at a glance. J Cell Sci 124:157–160
7. Kobras CM, Mascher T, Gebhard S (2017) Application of a *Bacillus subtilis* whole-cell biosensor (P_{liaI}-*lux*) for the identification of cell wall active antibacterial compounds. In: Sass P (ed) Antibiotics. Methods in molecular biology. Humana Press, New York, pp 121–131
8. Jordan S, Junker A, Helmann JD, Mascher T (2006) Regulation of LiaRS-dependent gene expression in *Bacillus subtilis*: identification of inhibitor proteins, regulator binding sites, and target genes of a conserved cell envelope stress-sensing two-component system. J Bacteriol 188:5153–5166
9. Schrecke K, Jordan S, Mascher T (2013) Stoichiometry and perturbation studies of the LiaFSR system of *Bacillus subtilis*. Mol Microbiol 87:769–788
10. Cao M, Wang T, Ye R, Helmann JD (2002) Antibiotics that inhibit cell wall biosynthesis induce expression of the *Bacillus subtilis* σ^W and σ^M regulons. Mol Microbiol 45:1267–1276
11. Mascher T, Margulis NG, Wang T, Ye RW, Helmann JD (2003) Cell wall stress responses in *Bacillus subtilis*: the regulatory network of the bacitracin stimulon. Mol Microbiol 50: 1591–1604
12. Staron A, Finkeisen DE, Mascher T (2011) Peptide antibiotic sensing and detoxification modules of *Bacillus subtilis*. Antimicrob Agents Chemother 55:515–525
13. Helmann JD, Mascher T (2005) Compositions and methods for screening of antibacterial compounds. US Patent 7309484
14. Wolf D, Mascher T (2016) The applied side of antimicrobial peptide-inducible promoters from Firmicutes bacteria: expression systems and whole-cell biosensors. Appl Microbiol Biotechnol 100:4817–4829
15. Radeck J, Kraft K, Bartels J, Cikovic T, Dürr F, Emenegger J, Kelterborn S, Sauer C, Fritz G, Gebhard S, Mascher T (2013) The *Bacillus* BioBrick Box: generation and evaluation of essential genetic building blocks for standardized work with *Bacillus subtilis*. J Biol Eng 7: 29
16. Schmalisch M, Maiques E, Nikolov L, Camp AH, Chevreux B, Muffler A, Rodriguez S, Perkins J, Losick R (2010) Small genes under sporulation control in the *Bacillus subtilis* genome. J Bacteriol 192:5402–5412
17. Lee K, Walker AR, Chakraborty B, Kaspar JR, Nascimento MM, Burne RA, Björkroth J (2019) Novel probiotic mechanisms of the oral bacterium *Streptococcus* sp. A12 as explored with functional genomics. Appl Environ Microbiol 85:e01335-19
18. Jordan S, Rietkotter E, Strauch MA, Kalamorz F, Butcher BG, Helmann JD, Mascher T (2007) LiaRS-dependent gene expression is embedded in transition state regulation in *Bacillus subtilis*. Microbiology 153: 2530–2540

Chapter 14

Determination of Bacterial Membrane Impairment by Antimicrobial Agents

Miriam Fuerst-Wilmes and Hans-Georg Sahl

Abstract

The bacterial cytoplasmic membrane separates the cell from its environment and acts as a selective permeability barrier. In addition, it functions in energy conservation, transport, signaling, and biosynthesis processes. Antimicrobial agents disrupting these functions may lead to pleiotropic effects, including leakage of low molecular weight compounds such as ions, amino acids, and ATP and subsequent membrane depolarization. This updated chapter describes two techniques to assess antibiotic-induced membrane impairment in vivo.

Key words Membrane permeabilization, Membrane potential, Depolarization, Tetraphenyl phosphonium bromide, Potassium efflux

1 Introduction

Many antimicrobial peptides (AMPs) display their activity by impairing the membrane barrier function via pore formation or unspecific membrane permeabilization. For example, the lantibiotic nisin uses lipid-linked cell envelope precursors such as lipid II as docking molecule to form pores in the membrane of susceptible strains [1, 2]. Pore formation results in rapid efflux of small molecules from the cells and subsequently dissipation of the membrane potential [3].

In case of the lantibiotic Pep5 and mammalian θ-defensins, the degree of membrane impairment strongly depends on the level of the membrane potential across the bacterial membrane [4, 5].

In this chapter, which is an update of [6], we describe two methods for measuring the impact of antimicrobial substances on the bacterial membrane integrity in vivo: (1) determination of the bacterial membrane potential ($\Delta\psi$) using [^{3}H]tetraphenylphosphonium bromide and (2) potassium release from whole cells by means of a potassium-sensitive electrode.

Peter Sass (ed.), *Antibiotics: Methods and Protocols*,
Methods in Molecular Biology, vol. 2601, https://doi.org/10.1007/978-1-0716-2855-3_14,

Lipophilic cations such as tetraphenylphosphonium bromide (TPP^+) can easily pass through phospholipid bilayers in response to a trans-negative membrane potential ($\Delta\psi$) and were first used to investigate the mitochondrial oxidative phosphorylation [7–9]. Since then, these molecules have also been exploited to measure the membrane potential in bacteria [10, 11] and the influence of antimicrobials such as bacteriocins on $\Delta\psi$ [4, 12, 13]. For this, growing bacteria are incubated with radiolabeled TPP^+, and the distribution of the cation inside and outside the cells is determined. The intracellular TPP^+ concentration is calculated by the use of the internal cell volume (V_i) and by taking into account unspecific membrane binding. Intra- and extracellular TPP^+ concentrations are then inserted into the Nernst equation for $\Delta\psi$ determination. To evaluate the effect of an antimicrobial agent on the membrane potential, the protonophore CCCP (carbonyl cyanide m-chlorophenylhydrazone) can be used as a positive control. CCCP uncouples the proton gradient across the cytoplasmic membrane leading to fast membrane depolarization and rapid TPP^+ release from cells.

Alternatively, ion-selective electrodes can be used to evaluate the membrane impairment by antimicrobials. Potassium is the major intracellular cation in bacteria, for example, with a concentration of 180–200 mM in *Escherichia coli* [14] and up to 1 M in *Staphylococcus aureus* [15]. Hence, efflux of K^+ from bacterial cells in the presence of an antibiotic indicates a membranolytic effect. Extracellular K^+ concentrations can be calculated from the measured voltage according to Orlov et al. [16] and expressed relative to the total amount of potassium present in the cells. This method has the advantage that it is simple and broadly applicable. Moreover, it does not rely on radiolabeled substances, and the measurement can be performed in real time.

2 Material

Sterilize the culture media and buffer before use. Use sterile glassware and pipette tips.

2.1 Determination of Bacterial Membrane Potential Using [^{3}H] tetraphenyl phosphonium Bromide (TPP^+)

2.1.1 Growth Medium, Bacterial Strains, and Antimicrobial Substances

1. Test strain, for example, *Staphylococcus simulans* 22 or *S. aureus* (*see* **Note 1**).
2. Mueller Hinton (MH) broth: 300 g beef infusion, 17.5 g casein hydrolysate, 1.5 g starch, pH 7.3 (*see* **Note 2**).
3. Antibiotic or antimicrobial peptide of interest.
4. 10 mM Carbonyl cyanide 3-chlorophenylhydrazone (CCCP) stock solution in ethanol, store at −20 °C.

2.1.2 Bacterial Membrane Potential Determination

1. [^{3}H]tetraphenylphosphonium bromide (TPP^+).
2. Cellulose acetate filters with a pore size of 0.2 μm.
3. 50 mM potassium phosphate buffer, pH 7: mix 50 mM K_2HPO_4 (dibasic solution) and 50 mM KH_2PO_4 (monobasic component) until the desired pH is reached.
4. n-Butanol.
5. Glass vacuum filtration apparatus.
6. Spectrophotometer at 600 nm.
7. Shaking water bath.
8. Scintillation fluid.
9. Liquid scintillation counter.

2.1.3 Protein Determination of Whole Cells

1. Bacterial protein extraction reagent (B-PER™).
2. BCA Protein Assay Kit.
3. Benchtop centrifuge.

2.2 Measurement of Potassium Release from Whole Cells

2.2.1 Growth Medium, Bacterial Strains, and Antimicrobial Substances

1. Test strain, for example, *Staphylococcus simulans* 22 or *Lactococcus lactis*.
2. Tryptic soy broth (TSB): 17 g pancreatic digest of casein, 3 g pancreatic digest of soy bean, 5 g NaCl, 2.5 g K_2HPO_4, 2.5 g glucose, pH 7.3.
3. Antibiotic or antimicrobial peptide of interest.
4. Membrane-active antimicrobial as positive control, for example, nisin.

2.2.2 Potassium Efflux Measurement

1. Potassium electrode (stored in 0.1 M KCl) (MI-442, Microelectrodes Inc., Bedford, USA).
2. Reference electrode (filled with 3 M KCl saturated with AgCl) (MI-409F, Microelectrodes Inc, Bedford, USA).
3. Microprocessor pH meter (HANNA® Instruments; Kehl am Rhein, Germany).
4. Choline buffer: 300 mM choline chloride, 30 mM 2-*(N-morpholino)*ethanesulfonic acid, 20 mM Tris base, pH 6.5.
5. Potassium standard solutions: 0.01, 0.1, and 1 mM KCl dissolved in choline buffer.
6. Centrifuge.
7. Magnetic stirrer.
8. 0.7% octylglucoside.

3 Method

3.1 Determination of Bacterial Membrane Potential Using [^{3}H] tetraphenyl-phosphonium Bromide (TPP^+)

3.1.1 Measurement of TPP^+ Uptake and Distribution

1. Inoculate a culture of your test strain in MH broth—using a 2% inoculum (v/v) from an overnight culture–and grow it to an optical density at 600 nm (OD_{600}) of 0.5–0.6 in a water bath with constant shaking.
2. To monitor the membrane potential, add 1 μCi/mL of [^{3}H] TPP^+ to the culture and incubate it for 30 s (*see* **Note 2**).
3. Transfer two samples of 100 μL directly to liquid scintillation vials for determining the total amount of radioactivity.
4. Filter a 100 μL sample through a cellulose acetate filter and wash the filter twice with 5 mL potassium phosphate buffer (*see* **Note 3**). Transfer the filter to a liquid scintillation vial and let it dry.
5. Split the culture into three aliquots. Treat one aliquot (i) with n-butanol for measuring the unspecific binding of [^{3}H]TPP^+ to the cells, treat the second aliquot (ii) with the antibiotic of interest, and run the third aliquot (iii) as a control (Fig. 1).
6. For aliquot (i), add n-butanol to the cells (10% final concentration) and mix it well by repeatedly sucking the sample into a 1 mL pipette. Take four 100 μL samples and filter them as described above (*see* **step 4**).
7. For aliquot (ii), add the antimicrobial of interest at a given concentration (e.g., at 5× or 10× MIC, minimal inhibitory concentration) and immediately take 100 μL of the culture and filter it as described above (*see* **Note 4**). Take further samples at certain time points, for example, 1, 2, 4, 5, 10, 15, and 20 min after antibiotic addition (*see* **Note 5**). Additionally, measure the OD_{600} of the culture periodically (Fig. 1).
8. For aliquot (iii), filter 100 μL samples as described above (*see* **step 4**) and measure the OD_{600}, for example, at time points 3, 8, 13, 18, and 23 min (Fig. 1).

   Optional: At the end of the experiment, add 10 μM CCCP as a positive control to aliquot (iii), take 100 μL samples at certain time points (e.g., 1, 2, and 5 min after addition of CCCP) and filter them as described above (see **step 4**). $\Delta\psi$ is dissipated by CCCP, and the intracellular TPP^+ concentration will decrease rapidly.
9. Add 5 mL scintillation fluid into all liquid scintillation vials.
10. Measure the radioactivity in the samples with a liquid scintillation counter for 5 min per filter.

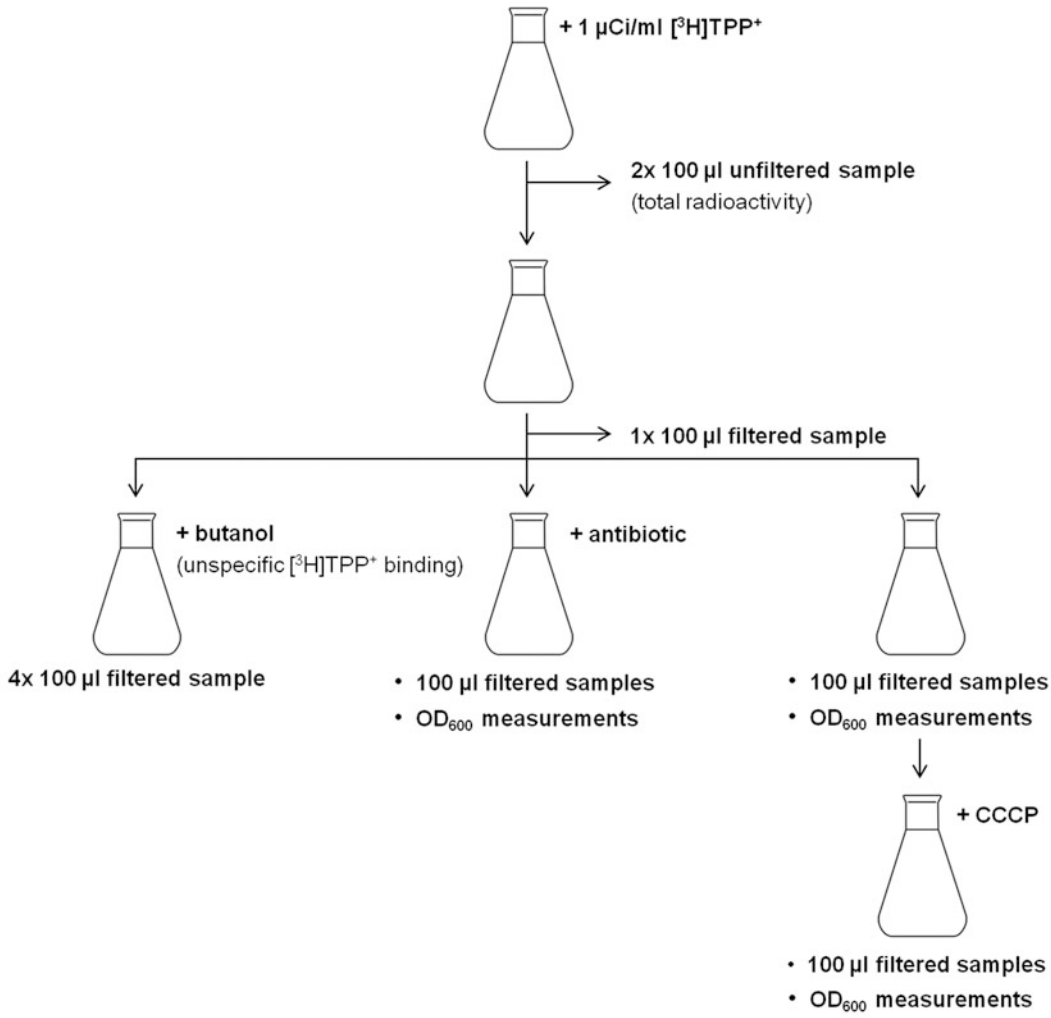

Fig. 1 Experimental scheme. [^{3}H]TPP$^+$ is added to an exponentially growing culture. After taking two samples for determining the total radioactivity, the culture is split into three aliquots. The first aliquot is treated with butanol to measure the unspecific binding of TPP$^+$ to the cells, the second aliquot is treated with the antibiotic of interest and the third aliquot is run as a control. At given time points, 100 µL samples are filtered, and the OD_{600} is measured. CCCP can be used as a positive control. (Figure reprinted from [6])

3.1.2 Protein Determination of Whole Cells

1. Grow a culture of your test strain to an OD_{600} of 1.
2. Centrifuge 2× 1 mL of the culture (9200 g, 5 min).
3. Wash the pellets with potassium phosphate buffer and centrifuge again.
4. Resuspend each pellet in 100 µL B-PER™ and incubate it for 10–15 min at room temperature. Optional: Freeze the cells before extraction to enhance cell lysis.
5. Determine the total protein concentration in the lysate by using the BCA Protein Assay.

3.1.3 Calculation of Bacterial Membrane Potential

1. Calculate the internal and external [^{3}H]TPP$^+$ concentration for each time point using the formulas described below.
2. Correct the counts for unspecific binding of [^{3}H]TPP$^+$ by subtracting the radioactivity of the butanol-treated aliquots.
3. Calculate V_i (μL/mL cells) by taking into account the determined protein concentration (*see* Subheading 3.1.2) and the measured OD_{600} values (*see* Subheading 3.1.1). For example, for *S. simulans* 22, the inner volume was found to be 3.4 μL/mg cell protein [4]. Thus, V_i is 0.2 μL/mL when the determined protein concentration is 0.1 mg/mL and the measured OD_{600} is 0.6.

$$TPP^+_{in} = \frac{\left(cpm_{sample} - cpm_{BuOH}\right) \times M_{TPP+} x\ 1000}{\left(cmp_{total} - cpm_{BuOH}\right) \times V_i}\ [\mu M]$$

$$TPP^+_{out} = \frac{\left[\left(cpm_{total} - cpm_{BuOH}\right) - \left(cpm_{sample} - cpm_{BuOH}\right)\right] \times M_{TPP+}}{\left(cmp_{total} - cpm_{BuOH}\right)}\ [\mu M]$$

TPP^+_{in}: intracellular TPP$^+$ concentration.

TPP^+_{out}: extracellular TPP$^+$ concentration.

cmp_{BuOH}: counts per minute in the butanol control (aliquot i; mean value).

cpm_{sample}: counts per minute in the filtered sample (aliquot ii or aliquot iii).

cpm_{total}: counts per minute in the unfiltered sample (mean value).

M_{TPP+}: molarity of TPP$^+$ (μM).

V_i: internal volume of 1 mL cells (μL/mL)

4. Insert the calculated values for the intra- and extracellular TTP$^+$ concentration into the Nernst equation to determine Δψ.

$$\Delta_\psi = \frac{-2.3 \times R \times T}{F} \times \log \frac{TPP^+_{in}}{TPP^+_{out}}\ [mV]$$

R: universal gas constant ($8.314\ \frac{J}{mol \times K}$).

T: absolute temperature (K).

F: Faraday constant ($96{,}485\ \frac{C}{mol}$)

5. Plot the values of the calculated membrane potential (mV) against time (min).

   Two examples of a typical experiment are shown in Fig. 2.

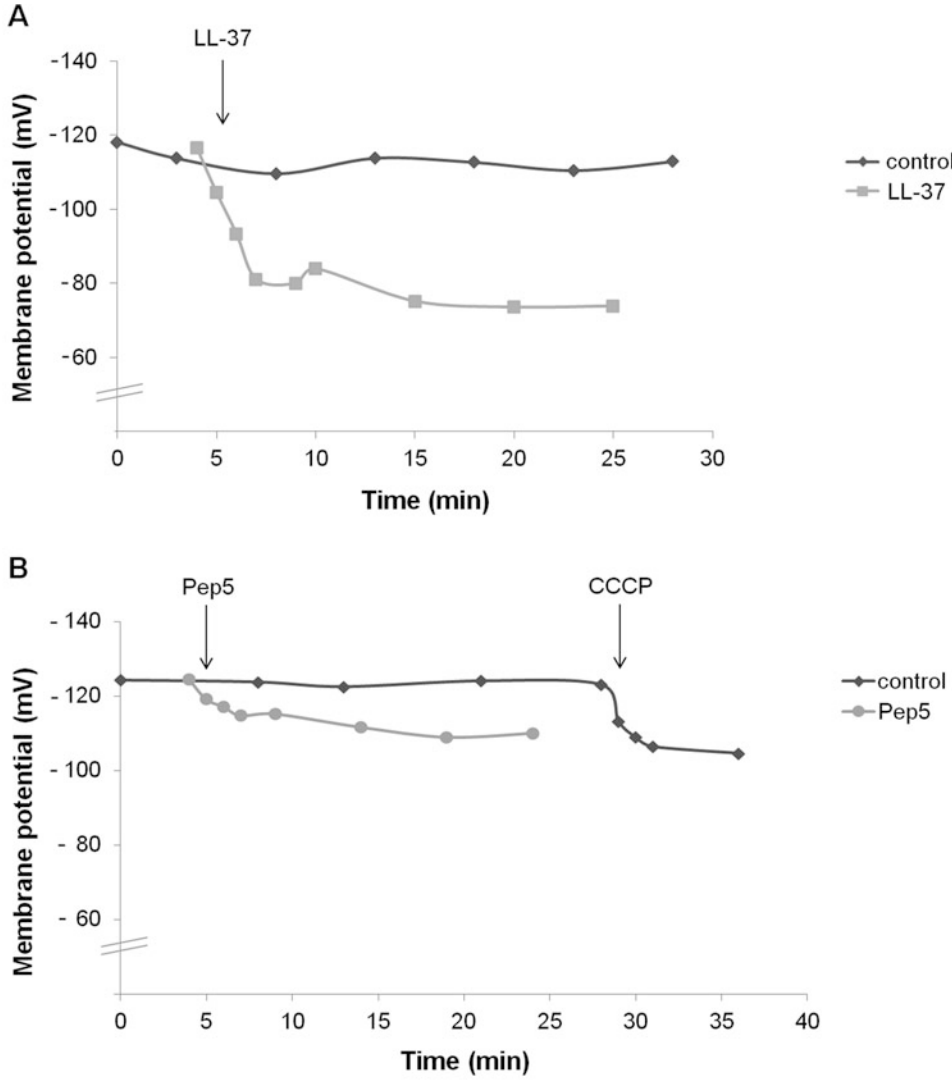

Fig. 2 Representative examples of a membrane potential measurement in the presence of an AMP. (**a**) Membrane potential of *S. aureus* SG511-Berlin in half-concentrated MH broth. The human host defense peptide LL-37 was added at 5× MIC. Immediately, a rapid decrease of the membrane potential was detected. In contrast, no significant changes of the membrane potential were observed in the untreated control cells. (**b**) Membrane potential of *S. aureus* SA113 in half-concentrated MH broth supplemented with 10 mM glucose. Bacteria were exposed to 10× MIC of the lantibiotic Pep5. CCCP (10 μM) was used as positive control. Both compounds induced some depolarization of the bacterial membrane. (Figure reprinted from [6])

3.2 Measurement of Potassium Release from Whole Cells

3.2.1 Measurement of Potassium Efflux

1. Inoculate a 50 mL culture of your test strain in TSB—using a 2% inoculum (v/v) from an overnight culture—and grow it to an OD_{600} of 1–1.5 (*see* **Note 6**).
2. Harvest the bacteria by centrifugation (2300 g, 3 min, 4 °C).

3. Wash the cells with 25 mL prechilled choline buffer and centrifuge again (see **step 2**).
4. Resuspend the cells in choline buffer to a final OD_{600} of 30 and keep them on ice until further use (*see* **Note 7**). For each measurement, dilute 200 µL cells in 1.8 mL choline buffer (final OD_{600} of 3) and gently agitate the culture by using a magnetic stirrer.
5. Calibrate the electrodes (*see* **Note 8**) with the potassium standard solutions starting with the lowest concentration. Measure 5–10 values for each concentration.
6. Rinse both electrodes with distilled water and place them into the stirring culture. Monitor the potassium release for 5 min at room temperature. Collect voltage data every 10 s. Start with the untreated control to determine the K^+ concentration in the buffer ($K^+_{initial}$).
7. Start another measurement (as described in **step 6**) and induce complete potassium release (K^+_{total}) by treatment with a highly membrane-active antibiotic, for example, 1 µM nisin (*see* **Note 9**).
8. Measure the membranolytic effect of your antibiotic of interest, for example, by adding it at 5× or 10× MIC to the cells (*see* **step 6**).
9. At the end of the experiment, wash the electrodes with distilled water and a detergent (e.g., 0.7% octylglucoside).

3.2.2 Calculation of Released Potassium Concentration

1. Generate a linear standard curve of the calibration data (mean value for each concentration) to determine the slope "m" and the y-intercept "z" of the following formula, which relates the measured electrode voltage (V_{meas}) to the extracellular K^+ concentration (Fig. 3a).

$$V_{\text{meas}} = m \log_{10}[K^+] + z$$

2. Calculate the initial K^+ concentration (K^+_{initial}) in the buffer (from your data of the untreated control) and the total K^+ concentration (K^+_{total}), for example, after nisin treatment, from the measured voltages.

$$K^+ = 10^{\frac{\text{Vmeas} - z}{m}}$$

3. Finally, convert the obtained data (K^+_{sample}) to percent potassium release and plot the % potassium release against time (s).

$$\%\text{release} = \frac{K^+_{\text{sample}} - K^+_{\text{initial}}}{K^+_{\text{total}} - K^+_{\text{initial}}} \times 100$$

An example of a typical experiment is shown in Fig. 3b.

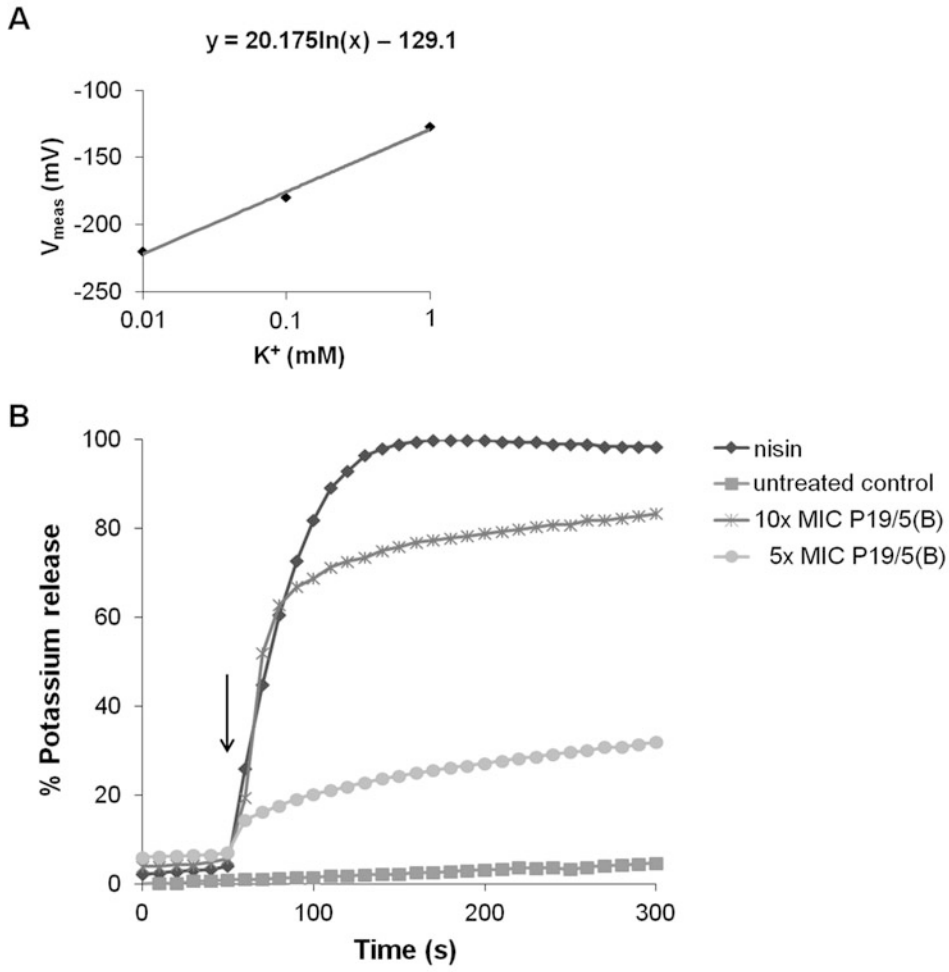

Fig. 3 Measurement of antibiotic-induced potassium efflux. (**a**) Example of a typical electrode calibration curve (m = 20.175, z = −129.1). (**b**) Effect of the antimicrobial peptide P19/5(**b**) on K^+ release of *S. simulans* 22. Ion leakage was expressed relative to the amount of potassium released after addition of 1 μM of the pore-forming lantibotic nisin (100% efflux). The arrow indicates the moment of peptide addition. (Figure reprinted from [6])

4 Notes

1. The membrane potential measurement using TPP^+ was established for some Gram-positive bacteria such as *Lactococcus lactis* [17], *Bacillus subtilis* [18], and *S. simulans* [4] but may also work with other species. However, determination of the membrane potential requires estimates of the inner aqueous volume of the cells (*see* Subheading 3.1.3), which has to be defined for the particular strain. Additionally, in Gram-negative bacteria the permeability to TPP^+ is greatly reduced due to the presence

of the outer membrane. Thus, cells have to be pretreated with EDTA [10, 13, 19], or lipophilic cation-permeable mutants have to be used as test strain [20].

2. Since $\Delta\psi$ and ΔpH are two independent components of the proton motive force ($\Delta p = \Delta\psi - 59\Delta\text{pH}$), it is recommended to perform the measurement at neutral pH to keep the pH difference between the cytoplasm and the exterior of the cells low. $\Delta\psi$ may be transiently increased by addition of a suitable carbon source, for example, 10 mM glucose. This is relevant when membrane action of a compound is dependent on a certain magnitude of $\Delta\psi$ as it has been described for AMPs such as Pep5 [4] and θ-defensins [5].
3. It is recommended to add the sample and 5 mL potassium phosphate buffer simultaneously into the filtration apparatus. After the buffer/sample is flown through the filter, wash it again with 5 mL potassium phosphate buffer.
4. Optional: Take another 100 μL sample before addition of the antibiotic.
5. The membrane potential decreases rapidly in presence of a membrane-active compound (Fig. 2). Thus, it is recommended to take several samples in the first 5 min after antibiotic addition.
6. A 50 mL culture will be sufficient for measuring six to eight samples in one experiment.
7. The bacteria dissolved in choline buffer may start lysing after a while. It is recommended to perform the experiment within 30–60 min. In addition, it may be necessary to energize the cells by addition of a suitable carbon source, for example, 10 mM glucose.
8. It is recommended to store both electrodes in choline buffer for at least 1 h before starting the experiment.
9. Alternatively, the bacteria can be disrupted by prolonged sonication to determine the total K^+ concentration [16].

References

1. Wiedemann I, Breukink E, van Kraaij C, Kuipers OP, Bierbaum G, de Kruijff B, Sahl HG (2001) Specific binding of nisin to the peptidoglycan precursor lipid II combines pore formation and inhibition of cell wall biosynthesis for potent antibiotic activity. J Biol Chem 276: 1772–1779
2. Müller A, Ulm H, Reder-Christ K, Sahl HG, Schneider T (2012) Interaction of type A lantibiotics with undecaprenol-bound cell envelope precursors. Microb Drug Resist 18: 261–270
3. Ruhr E, Sahl HG (1985) Mode of action of the peptide antibiotic nisin and influence on the membrane potential of whole cells and on cytoplasmic and artificial membrane vesicles. Antimicrob Agents Chemother 27:841–845
4. Sahl HG (1985) Influence of the staphylococcin-like peptide Pep 5 on membrane potential of bacterial cells and

cytoplasmic membrane vesicles. J Bacteriol 162:833–836

5. Wilmes M, Stockem M, Bierbaum G, Schlag M, Götz F, Tran DQ, Schaal JB, Ouellette AJ, Selsted ME, Sahl HG (2014) Killing of staphylococci by theta-defensins involves membrane impairment and activation of autolytic enzymes. Antibiotics (Basel) 3:617–631
6. Wilmes M, Sahl HG (2017) Determination of bacterial membrane impairment by antimicrobial agents. Methods Mol Biol 1520:133–143
7. Liberman EA, Topaly VP, Tsofina LM, Jasaitis AA, Skulachev VP (1969) Mechanism of coupling of oxidative phosphorylation and the membrane potential of mitochondria. Nature 222:1076–1078
8. Grinius LL, Jasaitis AA, Kadziauskas YP, Liberman EA, Skulachev VP, Topali VP, Tsofina LM, Vladimirova MA (1970) Conversion of biomembrane-produced energy into electric form. I. Submitochondrial particles. Biochim Biophys Acta 216:1–12
9. Bakeeva LE, Grinius LL, Jasaitis AA, Kuliene VV, Levitsky DO, Liberman EA, Severina II, Skulachev VP (1970) Conversion of biomembrane-produced energy into electric form. II. Intact mitochondria. Biochim Biophys Acta 216:13–21
10. Schuldiner S, Kaback HR (1975) Membrane potential and active transport in membrane vesicles from *Escherichia coli*. Biochemistry 14:5451–5461
11. Szmelcman S, Adler J (1976) Change in membrane potential during bacterial chemotaxis. Proc Natl Acad Sci U S A 73:4387–4391
12. Tokuda H, Konisky J (1978) Mode of action of colicin Ia: effect of colicin on the *Escherichia coli* proton electrochemical gradient. Proc Natl Acad Sci U S A 75:2579–2583
13. Weiss MJ, Luria SE (1978) Reduction of membrane potential, an immediate effect of colicin K. Proc Natl Acad Sci U S A 75:2483–2487
14. Shabala L, Bowman J, Brown J, Ross T, McMeekin T, Shabala S (2009) Ion transport and osmotic adjustment in *Escherichia coli* in response to ionic and non-ionic osmotica. Environ Microbiol 11:137–148
15. Baba T, Takeuchi F, Kuroda M, Ito T, Yuzawa H, Hiramatsu K (2004) The *Staphylococcus aureus* genome. In: Aldeen DA, Hiramatsu K (eds) *Staphylococcus aureus*: molecular and clinical aspects. Horwood Publishing, Chichester, pp 66–145
16. Orlov DS, Nguyen T, Lehrer RI (2002) Potassium release, a useful tool for studying antimicrobial peptides. J Microbiol Methods 49:325–328
17. Kashket ER, Blanchard AG, Metzger WC (1980) Proton motive force during growth of *Streptococcus lactis* cells. J Bacteriol 143:128–134
18. Miller JB, Koshland DE Jr (1977) Sensory electrophysiology of bacteria: relationship of the membrane potential to motility and chemotaxis in *Bacillus subtilis*. Proc Natl Acad Sci U S A 74:4752–4756
19. Griniuviene B, Chmieliauskaite V, Grinius L (1974) Energy-linked transport of permeant ions in *Escherichia coli* cells: evidence for membrane potential generation by proton-pump. Biochem Biophys Res Commun 56:206–213
20. Hirota N, Matsuura S, Mochizuki N, Mutoh N, Imae Y (1981) Use of lipophilic cation-permeable mutants for measurement of transmembrane electrical potential in metabolizing cells of *Escherichia coli*. J Bacteriol 148: 399–405

Chapter 15

A Colorimetric Assay to Identify and Characterize Bacterial Primase Inhibitors

Allan H. Pang and Oleg V. Tsodikov

Abstract

Bacterial DNA primase DnaG is an attractive target for antibiotic discovery since it plays an essential role in DNA replication. Over the last 10 years, we have developed and optimized a robust colorimetric assay that enabled us to identify and validate inhibitors of bacterial primases. Here, we provide a detailed protocol for this colorimetric assay for DnaG from three different pathogenic bacteria (*Mycobacterium tuberculosis*, *Bacillus anthracis*, and *Staphylococcus aureus*), which can be performed in high throughput. We also describe secondary assays to characterize hits from this high-throughput screening assay. These assays are designed to identify inhibitors of the coupled enzyme inorganic pyrophosphatase, DNA binding agents, and elucidate the mode of inhibition of primase inhibitors.

Key words Drug discovery, High-throughput assay, DNA replication, Inorganic pyrophosphatase, DNA intercalation, Mode of inhibition

1 Introduction

Bacterial DNA primase, also known as DnaG, plays an essential role in DNA replication. Targeting DNA replication by small molecule inhibitors has been a classical approach in cancer and antibacterial therapies, with cisplatin and fluoroquinolones as prominent respective examples. Methods to discover inhibitors of DNA replication enzymes have evolved over time, with recent efforts focusing on the target-based approaches [1], which would minimize toxic off-target effects. Due to structurally distinct features of bacterial primase as compared to its eukaryotic counterpart, DnaG is an attractive target for discovery of its inhibitors and their development as novel antibacterial agents [2, 3]. Traditionally, functional studies of primases are carried out by monitoring radioactively labeled primer products on denaturing gels or by high-performance liquid chromatography. Although these techniques are quantitative, they have safety limitations, and they cannot be readily

Peter Sass (ed.), *Antibiotics: Methods and Protocols*,
Methods in Molecular Biology, vol. 2601, https://doi.org/10.1007/978-1-0716-2855-3_15,

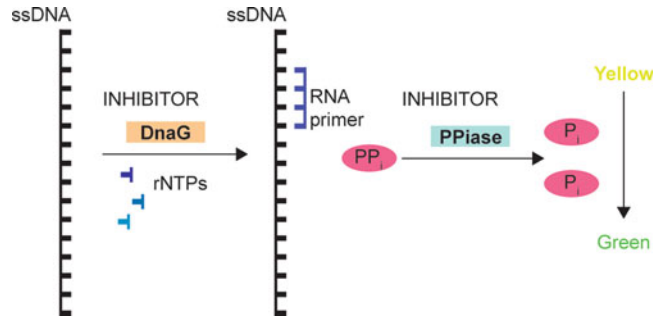

Fig. 1 A schematic of the coupled DnaG-PPiase colorimetric assay. Inhibitors of either DnaG reaction, or the PPiase can be detected at appropriately chosen conditions

employed in a high-throughput fashion. To circumvent these issues in development of a facile technique that could be used in high throughput in an academic setting, we devised and optimized a nonradioactive primase activity assay (Fig. 1) that is both quantitative and amenable to high-throughput applications, such as DnaG inhibitor discovery by chemical library screening [4]. DnaG binds single-stranded DNA (ssDNA) template and catalyzes formation of short RNA primers. A transfer of a nucleoside monophosphate from the respective triphosphate substrate into the elongated RNA primer releases inorganic pyrophosphate (PP_i). In our assay, this reaction is coupled to a hydrolytic cleavage of PP_i by an inorganic pyrophosphatase (PPiase), to yield two phosphate (P_i) molecules. This final P_i product is then detected by the malachite green reagent, a cheap and widely used colorimetric method that changes color from golden yellow to green in the presence of P_i, but not PP_i. This color change is monitored by measuring absorbance at 620 nm. Over the past decade, we successfully optimized and employed this coupled biochemical assay in high throughput to identify inhibitors of bacterial primases. This assay was initially developed for DnaG from *Mycobacterium tuberculosis* (*Mt*) [4]. This colorimetric assay, as applicable to *Mt* DnaG, was described in a prior edition of this book [1]. In this chapter, we expanded this protocol to include two other pathogenic microorganisms: *Bacillus anthracis* (*Ba*) [5] and *Staphylococcus aureus* (*Sa*) [6]. We also described several secondary biochemical assays to characterize the mechanism of action of the inhibitors. This includes the assay to identify PPiase inhibitors to sort them out from DnaG inhibitors and a DNA intercalation assay, to determine which compounds inhibit DnaG by binding DNA. Because multiple homologs of DnaG and PPiase were described, the assays also would allow one to test inhibitor selectivity by testing the inhibitors of DnaG for their activity against *Mt*, *Sa*, and *Ba* primases and inhibitors of PPiase for their activity against *Mt*, *Sa*, and *Escherichia coli* (*Ec*) PPiases. A flow chart for the high-throughput assay and the follow-up assays described here is shown in Fig. 2.

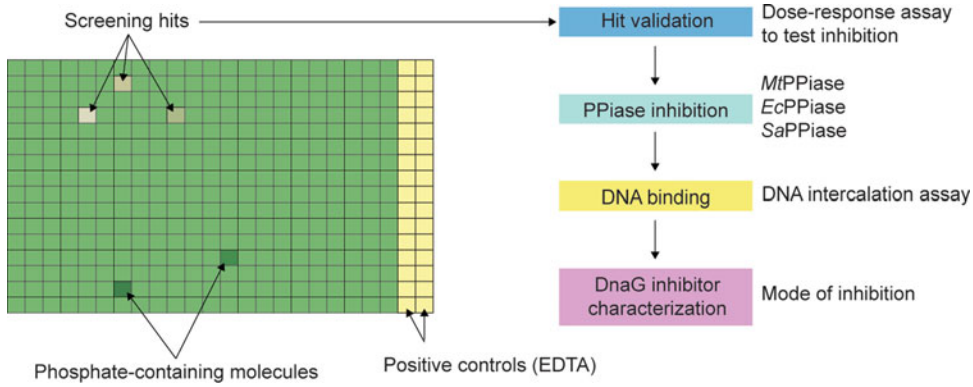

Fig. 2 The experimental workflow for identification and characterization of inhibitors of DnaG and PPiase

2 Materials

All solvents and buffers are prepared using only ultrapure double-distilled water.

2.1 Materials for Production and Purification of Enzymes

1. Plasmids. pET19b-*Mt*DnaG, pET19b-*Ba*DnaG, pET28a-*Sa*DnaG, pJexpress411-*Mt*PPiase, pET22b-*Sa*PPiase, and pET19b-*Ec*PPiase (*see* **Note 1**).
2. *Escherichia coli* BL21(DE3) chemically competent cells.
3. Lysogeny broth (LB) and LB agar. Prepare as specified by manufacturer and autoclave before use.
4. Antibiotic stocks. Stocks of antibiotics are stored in small aliquots (~1 mL) at 20 °C.
   (a) 100 mg/mL ampicillin stock. Dissolve 1 *g* of ampicillin in 10 mL of water.
   (b) 50 mg/mL kanamycin stock. Dissolve 0.5 *g* of kanamycin in 10 mL of water.
5. 1 M IPTG. Dissolve 2.4 g of IPTG in 10 mL of water. Aliquot in small volume (~1 mL) and store at −20 °C.

2.2 Equipment

1. An orbital shaker with temperature control capability (37 °C and 18 °C).
2. A Sorvall RC-6 Plus high-speed centrifuge (or a comparable centrifuge).
3. A sonicator, a French press or a cell homogenizer for cell disruption.
4. 5 mL HiTrap IMAC FF columns.
5. An S-200 size exclusion column.
6. A fast protein liquid chromatography (FPLC) machine.

7. Amicon Ultra-15 centrifugal filters (10,000 Da M_w cutoff).
8. A gel electrophoresis system (SDS-PAGE).
9. 96- or 384-well flat bottom polystyrene plates with a nonbinding surface suitable for absorbance measurements.
10. A Biomek automated workstation or a similar liquid-handling instrument.
11. A PHERAstar plate reader, SpectraMax M5 plate reader, or a similar instrument.
12. A multichannel pipette capable of dispensing 1–20 μL.
13. A vibrating platform shaker for shaking microtiter plates.

2.3 Chemicals, Protease, and Buffer for Purification of Enzymes

1. 1 M Tris-HCl, pH 8.0. Dissolve 121.1 g of Tris base (Trizma) in 800 mL of water. Slowly and carefully add concentrated HCl to adjust the pH to 8.0 while stirring at room temperature. Add water to the final volume of 1 L.
2. TEA Buffer: 200 mM triethanolamine (TEA), pH 7.8. Dissolve 29.8 g of TEA in 800 mL of water. Adjust pH to 7.8 by adding HCl. Add water to the final volume of 1 L.
3. 4 M NaCl. Dissolve 234 g of NaCl in 1 L water.
4. 2 M imidazole. Dissolve 136.2 g of imidazole in water to a final volume of 1 L.
5. 100 mM ATP Mg^{2+} salt. Dissolve 0.51 g of ATP Mg^{2+} salt to a final volume of 10 mL. Split the solution into 1 mL aliquots and store at −20 °C.
6. 1 M $MnCl_2$. Dissolve 9.9 g of $MnCl_2$ tetrahydrate in 50 mL water. Store at −20 °C.
7. 0.5 M EDTA solution. Dissolve 18.6 g of EDTA in 80 mL of water. Adjust the pH to 8.0 by adding NaOH. Add water to the final volume of 100 mL.
8. 100 mM phenylmethylsulfonyl fluoride (PMSF) in ethanol. Dissolve 174 mg of PMSF in 10 mL of ethanol. Mix and store well sealed at −20 °C.
9. β-mercaptoethanol. This chemical is purchased as a solution, at a concentration of 14.3 M. This chemical is not stable in buffers for a long period of time, and, when required, β-mercaptoethanol is added immediately prior to use.
10. PreScission protease. GST-tagged 3C PreScission protease can be purchased from VWR.
11. Buffers for *Mt*DnaG and *Ba*DnaG.
    (a) Basic Buffer: 40 mM Tris-HCl pH 8.0, 600 mM NaCl, 10% glycerol, 2 mM $MgCl_2$. Mix 40 mL of 1 M Tris-HCl pH 8.0, 150 mL of 4 M NaCl, 100 mL of glycerol, and 2 mL of 1 M $MgCl_2$. Add water to make up to 1 L final volume. Degas the solution and store it at 4 °C.

(b) Lysis Buffer: 40 mM Tris-HCl pH 8.0, 600 mM NaCl, 10% glycerol, 2 mM $MgCl_2$, 1 mM PMSF, 0.5 mM ATP (Mg^{2+} salt), 2 mM β-mercaptoethanol, protease inhibitor (*see* **Note 1**). In 100 mL of chilled Basic Buffer, add 500 μL of 100 mM ATP, 1 mL of 100 mM PMSF, 14 μL of β-mercaptoethanol, and two tablets of complete ethylenediaminetetraacetic acid (EDTA)-free protease inhibitor cocktail (Roche Applied Science).

(c) Wash Buffer: 40 mM Tris-HCl pH 8.0, 600 mM NaCl, 10% glycerol, 2 mM $MgCl_2$, 0.5 mM ATP, 2 mM β-mercaptoethanol, and 50 mM imidazole. Add 2.5 mL of 2 M imidazole to 97.5 mL of lysis buffer (without PMSF and protease inhibitors).

(d) Elution Buffer: 40 mM Tris-HCl pH 8.0, 600 mM NaCl, 10% glycerol, 2 mM $MgCl_2$, 0.5 mM ATP, 2 mM β-mercaptoethanol, and 500 mM imidazole. Add 12.5 mL of 2 M imidazole to 37.5 mL of lysis buffer (without PMSF and protease inhibitor).

(e) Size-exclusion column (SEC) Buffer: 40 mM Tris-HCl pH 8.0, 600 mM NaCl, 10% glycerol, 2 mM $MgCl_2$, 0.25 mM ATP, and 2 mM β-mercaptoethanol. To 1 L of Basic Buffer, add 140 μL of β-mercaptoethanol and 2.5 mL of 100 mM ATP.

12. Buffers for *Sa*DnaG.

(a) Lysis Buffer: 40 mM Tris pH 8.0, 400 mM NaCl, 10% glycerol, and 2 mM β-mercaptoethanol. Combine 40 mL of 1 M Tris-HCl pH 8.0, 100 mL of 4 M NaCl, and 100 mL of glycerol and add water to a 1 L final volume. Add 140 μL of β-mercaptoethanol prior to use.

(b) Wash Buffer 1: 40 mM Tris pH 8.0, 400 mM NaCl, 10% glycerol, 2 mM β-mercaptoethanol, and 10 mM imidazole. Add 300 μL of 2 M imidazole to 59.7 mL of lysis buffer.

(c) Wash Buffer 2: 40 mM Tris pH 8.0, 400 mM NaCl, 10% glycerol, 2 mM β-mercaptoethanol, and 20 mM imidazole. Add 200 μL of 2 M imidazole to 19.8 mL of lysis buffer.

(d) Wash Buffer 3: 40 mM Tris pH 8.0, 400 mM NaCl, 10% glycerol, 2 mM β-mercaptoethanol, and 50 mM imidazole. Add 500 μL of 2 M imidazole to 19.5 mL of lysis buffer.

(e) Elution Buffer: 40 mM Tris pH 8.0, 400 mM NaCl, 10% glycerol, 2 mM β-mercaptoethanol, and 250 mM imidazole. Add 2.5 mL of 2 M imidazole to 17.5 mL of lysis buffer.

(f) SEC Buffer: 40 mM Tris pH 8.0, 200 mM NaCl, and 2 mM β-mercaptoethanol. Mix 40 mL of 1 M Tris-HCl pH 8.0 and 50 mL of 4 M NaCl, then add water to a 1 L final volume. Degas the solution, add 140 μL of β-mercaptoethanol prior to use.

13. Buffers for *Mt*PPiase.
    (a) Lysis Buffer: 20 mM triethanolamine (TEA) pH 7.8. For a 100 mL, dilute 10 mL of 200 mM TEA buffer by adding 90 mL of water.
    (b) Wash Buffer: 20 mM TEA buffer, 300 mM NaCl, and 50 mM imidazole. Combine 30 mL of 200 mM TEA buffer, 22.5 mL of 4 M NaCl, and 7.5 mL of 2 M imidazole. Mix and add water to the final volume of 300 mL.
    (c) Elution Buffer: 20 mM TEA pH 7.8, 300 mM NaCl, and 500 mM imidazole. Combine 10 mL of 200 mM TEA buffer, 7.5 mL of 4 M NaCl, and 2.5 mL of 2 M imidazole. Mix and add water to the final volume of 100 mL.
    (d) SEC Buffer: 40 mM Tris-HCl pH 8.0, 100 mM NaCl. Add water to 40 mL of 1 M Tris-HCl pH 8.0 and 25 mL of 4 M NaCl to the final volume of 1 L. Degas this buffer and store it at 4 °C.
14. Buffers for *Sa*PPiase.
    (a) Lysis Buffer: 40 mM Tris-HCl pH 8.0, 300 mM NaCl, and 2 mM β-mercaptoethanol. Mix 40 mL of 1 M Tris-HCl pH 8.0 and 75 mL of 4 M NaCl, and add water to 1 L final volume. Add 140 μL of β-mercaptoethanol prior to use.
    (b) Wash Buffer: 40 mM Tris-HCl pH 8.0, 300 mM NaCl, 50 mM imidazole, and 2 mM β-mercaptoethanol. Add 2.5 mL of 2 M imidazole to 97.5 mL of Lysis Buffer.
    (c) Elution Buffer: 40 mM Tris-HCl pH 8.0, 300 mM NaCl, 500 mM imidazole, 2 mM $MnCl_2$, and 2 mM β-mercaptoethanol. Add 5 mL of 2 M imidazole and 40 μL of 1 M $MnCl_2$ to 14.96 mL Lysis Buffer.
    (d) SEC Buffer: 40 mM Tris-HCl pH 8.0, 100 mM NaCl, 2 mM $MnCl_2$, and 2 mM β-mercaptoethanol. Combine 40 mL of 1-M Tris HCl pH 8.0, 25 mL of 4 M NaCl and 2 mL of 1 M $MnCl_2$ and add water to the final volume of 1 L. Degas this buffer and store it at 4 °C. Add 140 μL of β-mercaptoethanol prior to use.
15. Buffers for *Ec*PPiase.
    (a) Lysis Buffer: 40 mM Tris-HCl pH 8.0, 300 mM NaCl, 10% glycerol, and 2 mM β-mercaptoethanol. Mix 40 mL of 1 M Tris-HCl pH 8.0, 75 mL of 4 M NaCl, 100 mL

glycerol and add water to 1 L final volume. Add 140 μL of β-mercaptoethanol prior to use.

(b) Wash Buffer: 40 mM Tris-HCl pH 8.0, 300 mM NaCl, 10% glycerol, 50 mM imidazole, and 2 mM β-mercaptoethanol. Add 2.5 mL of 2 M imidazole to 97.5 mL of lysis buffer.

(c) Elution Buffer: 40 mM Tris-HCl pH 8.0, 300 mM NaCl, 10% glycerol, 500 mM imidazole, and 2 mM β-mercaptoethanol. Add 5 mL of 2 M imidazole to 15 mL lysis buffer.

(d) SEC Buffer 1: 20 mM Tris-HCl pH 8.0, 100 mM NaCl, 0.5 mM EDTA, and 5 mM β-mercaptoethanol. Mix 20 mL of 1 M Tris-HCl pH 8.0, 25 mL of 4 M NaCl, and 1 mL of 0.5 M EDTA and add water to make up to 1 L final volume. Degas this buffer and store it at 4 °C. Add 350 μL of β-mercaptoethanol prior to use.

(e) SEC Buffer 2: 40 mM Tris-HCl pH 8.0, 100 mM NaCl, and 2 mM β-mercaptoethanol. Mix 40 mL of 1 M Tris-HCl pH 8.0 and 25 mL of 4 M NaCl, then add water to make up to 1 L final volume. Degas this buffer and store it at 4 °C. Add 140 μL of β-mercaptoethanol prior to use.

2.4 Malachite Green Reagent Components

1. 0.0812% *w/v* malachite green (*see* **Note 3**). Dissolve 0.0812 g of malachite green in a 100 mL water. Wrap the tube with aluminum foil to protect the solution from light.
2. 5.72% *w/v* ammonium molybdate. Prepare 100 mL 6 M HCl by adding concentrated HCl (12 M) into 50 mL water (in that order) to a volume of 100 mL. Dissolve 5.72 g ammonium molybdate in this solution.
3. 2.32% *w/v* polyvinyl alcohol. Dissolve 2.32 g of polyvinyl alcohol in a 100 mL water. While stirring, slowly heat up the mixture on a stir plate to 80–90 °C, ensuring that the mixture does not boil. This step should take about 2 h to fully dissolve polyvinyl alcohol. Protect the solution with aluminum foil and store at 4 °C. The solution is usable for up to 2 months and should be warmed up to room temperature before use. Formation of filamentous aggregates is a sign that the solution has become unusable.
4. 10% sodium citrate. Dissolve 1 g of sodium citrate in 100 mL water.

2.5 Stock Solutions, Buffers, and Solvents for Activity Assay

1. 1 M *N*-cyclohexyl-3-aminopropanesulfonic acid (CAPS) pH 8.8. Dissolve 11 g of CAPS in 35 mL of water. Adjust the pH to 8.8 by adding NaOH. Add water to the final volume of 50 mL.

2. 1 M $MnCl_2$. Dissolve 9.9 g of $MnCl_2$ tetrahydrate in 50 mL water. Store at −20 °C.
3. 1 M $MgCl_2$. Dissolve 20.3 g of $MgCl_2$ hexahydrate in 100 mL water.
4. 4 M NaCl. Dissolve 234 g of NaCl in 1 L water.
5. 600 mM potassium glutamate. Dissolve 6 g of L-glutamic acid potassium salt monohydrate (KGlu) in 50 mL water.
6. 1 M 2-morpholinoethanesulfonic acid (MES) pH 6.0. Dissolve 9.8 g of MES in 35 mL of water, then adjust pH to 6.0. Add water to the final volume of 50 mL.

2.6 Activity Assay Reagents for Identification of DnaG Inhibitors

1. Purchase synthetic single-stranded (ss) DNA 32-mer 5′-GAAG CACCAGACGTTTAGCATACATTCACAGA -3′ (a 1 μmol scale). Centrifuge the powdered synthesized DNA at 5000× *g* for 30 s and then dissolve in water at the concentration of 2 mM and store at −20 °C. The amount of water to be added depends on the amount of synthesized DNA obtained from the company.
2. 100 mM of ribonucleotide triphosphates (rCTP, rGTP, and rUTP) from Promega. This company provides rNTPs that are consistently free from phosphate contamination.
3. 3× DNA-enzyme mixture A, to be used for enzymes *Mt*DnaG, *Ba*DnaG, and *Mt*PPiase. 60 mM CAPS pH 8.8, 6 mM $MnCl_2$, 3 mM $MgCl_2$, 150 mM NaCl, 450 mM KGlu, 2.1 μM *Mt*DnaG or 12 μM *Ba*DnaG, and 150 nM *Mt*PPiase. Add 1.8 mL of 1 M CAPS pH 8.8, 180 μL of 1 M $MnCl_2$, 90 μL of 1 M $MgCl_2$, 1.125 mL of 4 M NaCl and 22.5 mL of 600 mM KGlu in a conical tube. Mix the solution well before adding 56 μL of 2 mM ssDNA, 6 μL of *Mt*PPiase (750 μM) and 875 μL of *Mt*DnaG (72 μM), or 2.4 mL of *Ba*DnaG (150 μM). The volumes of enzyme samples will vary depending on the final concentration obtained from the production and purification protocol. Add water to the final volume of 30 mL.
4. DNA-enzyme mixture B, to be used for enzymes *Sa*DnaG/*Sa*PPiase: 30 mM MES pH 6.0, 3 mM $MnCl_2$, 1.5 mM $MgCl_2$, 75 mM NaCl, 225 mM KGlu, 5.5 μM *Sa*DnaG, and 75 nM *Sa*PPiase. In a 50 mL conical tube, combine 0.9 mL of 1 M MES pH 6.0, 90 μL of 1 M $MnCl_2$, 90 μL of 1 M $MgCl_2$, 0.56 mL of 4 M NaCl, and 11.25 mL of 600 mM KGlu. Mix the solution well then add 28 μL of 2 mM ssDNA, 3 μL of *Sa*PPiase (750 μM), and 2.25 mL of *Sa*DnaG (140 μM). Enzyme sample volumes with vary depending on the final concentration obtained from the production and purification protocol. Add water to the final volume of 30 mL.

5. 3× NTP mixture: 330 μM of CTP, GTP, and UTP. In a 29.7 mL of water, add 100 μL of each of the three 100 mM NTPs (CTP, GTP, and UTP) stock.
6. 2 mM suramin. Dissolve 1.43 g of suramin in 500 mL of water.
7. 0.5 M EDTA solution. Dissolve 18.6 g of EDTA in 80 mL of water. Adjust the pH to 8.0 by adding NaOH. Add water to the final volume of 100 mL.
8. Feasibility test plate. Place 2 mM suramin in first two columns, 0.5 M EDTA in the last two columns and 100% DMSO for the rest of the columns. The feasibility test plate contains 50–100 μL of suramin, EDTA, and DMSO. Store the plate at −20 °C.
9. Small molecule compounds to be screened or tested for inhibition. 2 mM of these test compounds are placed in a 96- or 384-well plate, with an exeption of last two columns, which contain 0.5 M EDTA. The compounds containing inorganic phosphate may produce false-positive results. The screening plates contain 50–100 μL of compounds and EDTA. Store the plate at −20 °C.

2.7 Materials for Activity Assay for Confirmation of PPiase Inhibitors

1. 10 mM tetrasodium pyrophosphate ($Na_4P_2O_7$). Dissolve 133 mg of $Na_4P_2O_7$ in 50 mL water.
2. 2× Reaction mixture: 40 mM Tris-HCl pH 7.5, 2 mM $MnCl_2$ (for *Sa*PPiase) or 2 mM $MgCl_2$ (for other non-*Sa* PPiases), and 200 μM tetrasodium pyrophosphate $Na_4P_2O_7$. Combine 2 mL of 1 M Tris-HCl pH 7.5, 0.1 mL of 1 M $MnCl_2$ or 0.1 mL of 1 M $MgCl_2$, and 1 mL of 10 mM $Na_4P_2O_7$. Add water to final volume of 50 mL.
3. Hit compounds. Order or synthesize compounds as powder form and dissolve in DMSO. Solubility varies depending on the compounds. Generally, a compound stock concentration is 10–50 mM. Aliquot in small volumes and store at −20 °C.

2.8 Materials for DNA Intercalation Assay

1. Ethidium bromide stock solution, 5 mM. EtBr can be purchased either as solution (10 mg/ml) or as powder. For the solution form, dilute 2 mL with 8 mL of water. For the powder form, dissolve 19.7 mg with 10 mL of water. Prepare a diluted EtBr stock of 0.05 mM by diluting 10 μL stock concentration with 990 μL of water.
2. Order 25-mer ssDNA, 5′- CACTCGGAAGTGACG CATCCTGTCT -3′ (~1 μmol). Centrifuge the powdered synthesized DNA at 5000× *g* for 30 s then dissolve in 10 mM Tris-HCl, pH 8.0, 50 mM NaCl at the concentration of 1 mM and store at −20 °C. The amount of buffer to be added depends on the amount of synthesized DNA obtained from the company. For dsDNA, anneal with complimentary DNA.

As with EtBr, prepare a lower stock concentration of 0.03 mM by diluting 1.5 mL of DNA with 48.5 μL of buffer.

3. Hit compounds. Synthesize or purchase commercially as powder and dissolve in DMSO. Prepare the following dilutions: 1.5 mM, 1.2 mM, 0.9 mM, 0.6 mM, 0.5 mM, 0.3 mM, 0.15 mM.

3 Methods

3.1 Overexpression of Protein in Escherichia coli (Ec) BL21 (DE3) Cells

1. Prepare LB agar plates by adding antibiotic stock (0.5 mL) to an autoclaved molten 500 mL agar (at ~40 °C) and pour the agar mixture into sterile petri dishes.
2. Transform the plasmid into chemically competent BL21(DE3) cells and plate bacteria on an LB agar plate with appropriate antibiotic. Note that the *Mt*DnaG, *Ba*DnaG, *Sa*PPiase, and *Ec*PPiase encoding plasmids bear an ampicillin resistance gene, while the *Sa*DnaG and *Mt*PPiase plasmids bear a kanamycin resistance gene.
3. Leave plates in a 37 °C incubator overnight.
4. Inoculate five colonies from the agar plate into 4 mL of LB broth supplemented with an appropriate antibiotic.
5. Place the starter culture in a 37 °C incubator, shake at 200 rpm for 3–4 h.
6. Inoculate 1 mL of bacterial culture to 1 L of LB broth. For DnaG, four 1 L of LB broth are used, while for PPiase, two 1 L of cultures are enough. Incubate the LB cultures at 37 °C, shaking at 200 rpm for ~3 h, until reaching the optical density (OD_{600nm}) of 0.3.
7. Move the cultures to an 18 °C incubator shaker. Incubate the culture for 1.5 h with shaking at 200 rpm.
8. Add 0.5 mL of 1 M IPTG to each 1 L of LB culture.
9. Leave the cultures shaking for additional 16 h before harvesting cells.
10. Centrifuge the bacterial cultures at 5000× *g* at 4 °C for 10 min in a Sorvall RC-6 Plus centrifuge.
11. Collect the cell paste and proceed to protein purification or store at −80 °C.

3.2 Cell Lysis and Protein Purification

1. Resuspend the cell paste in 100 mL of lysis buffer.
2. Disrupt the cells on ice by intermittent sonication (or by an equivalent method, such as cell disruption by a French press or a cell homogenizer).

3. Clarify the lysate by centrifugation at 38,000 g for 30–60 min at 4 °C in a Sorvall RC-6 Plus centrifuge.
4. Filter the supernatant through 0.45 μm PVDF filters. Multiple filters may be required.
5. Load the filtrate onto a 5 mL IMAC Ni^{2+} column (washed and charged with Ni^{2+} as recommended by the manufacturer) equilibrated in a respective lysis buffer.

3.2.1 Mt*DnaG and* Ba*DnaG*

1. Wash the column with 100 mL of wash buffer.
2. Elute the protein with 12 mL of elution buffer, discarding the first 2 mL of the eluate.
3. Adjust the NaCl concentration of the 10 mL eluted protein to 200 mM by adding gradually with gentle mixing 20 mL of basic buffer prepared without NaCl.
4. Cleave the His tag overnight at 4 °C with PreScission protease.
5. Concentrate the protein using an Amicon Ultra-15 centrifugal filter device to about 5 mL.
6. Inject the protein sample to an S-200 size exclusion column equilibrated in SEC Buffer and run the column in that buffer at 2 mL/min, collecting 5 mL fractions.
7. Combine the fractions containing DnaG, as determined by SDS-PAGE, and then concentrate the protein to 72 μM (*Mt*DnaG) and 150 μM (*Ba*DnaG).
8. Store DnaG preparations on ice and use the enzyme within 2 weeks after obtaining concentrated purified protein (*see* **Note 2**). This protocol should yield highly pure DnaG (>95% purity), as assessed using 15% SDS-PAGE gel.

3.2.2 Sa*DnaG*

1. Wash the column with 60 mL of *Sa*DnaG wash buffer 1, followed by 20 mL of *Sa*DnaG wash buffer 2 and 20 mL of *Sa*DnaG wash buffer 3.
2. Elute the protein with 12 mL of *Sa*DnaG elution buffer, discarding the first 2 mL of the eluate.
3. Concentrate the remaining 10 mL protein by using an Amicon Ultra-15 centrifugal filter device to approximately 5 mL.
4. Inject the protein sample into an S-200 size exclusion column equilibrated in SEC Buffer and run the column in this buffer, as described in Subheading 3.2.1.
5. Combine the fractions containing *Sa*DnaG and concentrate the protein to 140 μM.
6. Store *Sa*DnaG preparations on ice and use in the assay within 2 weeks of concentrating the purified protein.

3.2.3 Mt*PPiase and* Sa*PPiase*

1. Pass 40 column volumes of wash buffer (200 mL) through the column.
2. Elution the protein with 12 mL of *Sa*DnaG Elution Buffer; discarding the first 2 mL of the eluate.
3. Concentrate the protein in the eluate by using an Amicon Ultra-15 centrifugal filter device to the volume of ~5 mL.
4. Purify the protein further on an S-200 size exclusion column equilibrated and run in SEC Buffer, as described in Subheading 3.2.1.
5. Combine the fractions containing PPiase and concentrate the protein to 750 μM (in monomers).
6. Store the protein preparations at 4 °C. The enzyme should stay active for up to 1 month.

3.2.4 Ec*PPiase*

1. Similar purification step as *Mt*PPiase and *Sa*PPiase.
2. After the gel filtration step using SEC Buffer 1, pool the protein containing fractions and concentrate to ~5 mL, as described in Subheading 3.2.1.
3. PreScission protease is added to the protein solution and left overnight at 4 °C.
4. Carry out a second gel filtration step by re-equilibrating the column in SEC Buffer 2 and running the sample in this buffer.
5. Pool the fractions containing the protein sample and concentrate to 360 μM (in monomers).
6. Store protein preparations in 4 °C, where they should stay active for up to 1 month.

3.3 Activity Assay

3.3.1 Preparation of the Malachite Green Reagent

1. Mix malachite green, polyvinyl alcohol, ammonium molybdate, and water in a 2:1:1:2 ratio. For instance, mix well 10 mL 0.0812% *w/v* malachite green, 5 mL 2.32% *w/v* polyvinyl alcohol, 5 mL 5.72% *w/v* ammonium molybdate, and 10 mL water.
2. Ensure that the tube is fully wrapped in aluminum foil. The malachite green reagent should change its color to golden-yellow after 30 min at room temperature. If after 30 min the malachite green reagent still has a hint of green color, discard this solution and remake the reagent. The presence of green color indicates phosphate contamination. Ensure the stocks water and glassware used are not contaminated with phosphate.
3. The malachite green reagent should be stored wrapped in foil at 4 °C and can be used for about 1 month.

Table 1
Reaction buffers for the DnaG-PPiase assays

Primase	PPiase	Assay conditions	References
*Mt*DnaG	*Mt*PPiase	20 mM CAPS pH 8.8, 2 mM $MnCl_2$, 1 mM $MgCl_2$, 50 mM NaCl, 150 mM KGlu	Biswas et al. [4]
*Ba*DnaG	*Mt*PPiase	20 mM CAPS pH 8.8, 2 mM $MnCl_2$, 1 mM $MgCl_2$, 50 mM NaCl, 150 mM KGlu	Biswas et al. [5]
*Sa*DnaG	*Sa*PPiase	20 mM MES pH 6.0, 2 mM $MnCl_2$, 1 mM $MgCl_2$, 50 mM NaCl, 150 mM KGlu	Green et al. [6]

3.3.2 Testing of Assay Feasibility and Robustness

Perform a test assay first to ensure that the assay is working prior to compound screening. Suramin and EDTA are used as positive controls (*see* **Note 4**). Suramin is a DnaG inhibitor [4, 5], while EDTA is a chelator of a catalytic divalent metal ion needed for primase activity.

1. Transfer 600 nL of suramin, 1.8 μL of 0.5 M EDTA, and 200 nL of DMSO from the feasibility test plate to a 384-well (or a 96-well) plate using a Biomek liquid handling robot.
2. In each well, add 20 μL of the 3× NTP mixture, followed by 10 μL of the 3× DNA-enzyme mixture (*see* **Note 5**), both by using a multichannel pipette. The 3× DNA-enzyme mixture A and B have been optimized for testing *Mt*DnaG or *Ba*DnaG/*Mt*PPiase [4, 5] and *Sa*DnaG/*Sa*PPiase [6], respectively. The final compositions of the reaction buffers for different enzymes are given in Table 1.
3. After a 30 min incubation at room temperature, add 30 μL of malachite green reagent to each well of the reaction plate, then 10 μL of 10% sodium citrate to stabilize the color. Shake the reaction plate for 20–30 s on a vibrating plate shaker then read absorbance at 620 nm on a PHERAstar plate reader in 30 min, after color development.

By doing this test assay, one can identify if the color change is due to DnaG/PPiase activity and not from any phosphate contamination. To measure the assay robustness and feasibility for multiple runs, calculate the Z' score using the formula [7]:

$$Z' = 1 - 3\frac{SD(\text{pos}) + SD(\text{neg})}{|Av(\text{pos}) - Av(\text{neg})|} \quad (1)$$

where SD(pos) and SD(neg) are the standard deviations of the absorbance readouts from the EDTA treated and DMSO containing wells, respectively, while the Av(pos) and Av(neg) are the average values of the absorbance readouts from the EDTA and DMSO containing wells, respectively. A Z' value of >0.5 indicates

that the HTS assay can be used for compound screening. However, a very high Z' value (0.9–1) indicates the reaction may not be in a steady-state regime. To remedy this, perform the assay with a longer reaction time (1 h) to see if the absorbance readout increases twofold. If, however, the signal remains the same, a kinetic experiment needs to be performed using a higher concentration of NTPs or ssDNA or a lower concentration of primase in order to identify the steady-state conditions.

3.3.3 The High-Throughput Screening Assay (384-Well Plate)

1. In a 384-well plate, transfer 200 nL of small molecules from the 2 mM stock plate using a Biomek FX robot. For the last two columns (EDTA), transfer 1.8 μL from the plate; these are positive control wells. The rest of the columns would have a final concentration of 13 μM of small molecules to be tested for inhibition. This is a stringent condition. For detection of weak inhibitors, the concentration of the inhibitors needs to be higher. While a 384-well plate is appropriate for screening a larger number of test compounds, the screening assay can be scaled to a 96-well plate.
2. To start the reaction, add 20 μL of the 3 NTP mixture, followed by 10 μL of the 3× DNA-enzyme mixture. Note that the reaction condition may need to be change, to satisfy the Z' value of 0.5–0.9.
3. After 40-min incubation at room temperature, add 30 μL of malachite green reagent to each well, and then 10 μL of 10% sodium citrate to stabilize the color.
4. Shake the reaction plate for 20–30 s on a vibrating plate shaker before taking an absorbance reading at 620 nm on a PHERAstar plate reader.

3.3.4 Medium-Throughput Screening Assay (96-Well Plate)

The inhibitor screening assay can be carried out in 96-well plates. In this setup, compounds are first dispensed as 10 mM stocks into a 96-well polypropylene U-bottom plate. The compounds are then diluted to 600 μM with DMSO and placed in respective wells of a 96-well flat bottom plate. As above, the last column contains 100% DMSO, serving as a positive control.

1. In a 96-well reaction plate, pipette 1 μL of 600 μM stock compound to each well, 1.8 μL of DMSO control to last column, and mix with 19 μL of DNA-enzyme mixture, followed by 10 μL of the 3× NTP mixture. The test concentration of compounds for this assay is 20 μM.
2. After 40-min incubation at room temperature, add 30 μL of malachite green reagent to each well, and then 10 μL of 10% sodium citrate to stabilize the color.
3. Shake the reaction plate for 20–30 s on a vibrating plate shaker before taking an absorbance reading at 620 nm on a SpectraMax M5 plate reader.

3.3.5 Assessment of Results

Create a scatterplot, with wells containing EDTA as full 100% inhibition, while compounds do not exhibit inhibitory properties serve as negative control. Those compounds that exhibit greater than a 3σ level of inhibition (where σ refers to the standard deviation of the negative control) are considered hits and worth pursuing for confirmation. It is highly plausible to obtain results that display higher than normal absorbance readings, especially if the test compounds are obtained from a commercial library. Inspect whether the compounds are phosphate salts, which could affect the assay. This can be readily tested by titrating the compounds into the malachite green reagent to inspect the color change or absorbance at 620 nm.

3.4 Bacterial PPiase Inhibition

Because the colorimetric assay requires two enzymes, the inhibition may be due to inactivation of inorganic pyrophosphatase and not primase. Therefore, it is important to test the hit compounds as PPiase inhibitors. Identifying novel compounds that inhibit bacterial PPiase can be equally important to finding DnaG inhibitors. PPiase is an essential enzyme that plays an important role in driving key metabolic processes like nucleic acid and protein biosynthesis. More importantly, accumulation of PP_i, which is a product of many enzymatic reactions, can cause cell damage [8]. PPiases can be classified to two nonhomologous and structurally distinct families. Bacterial PPiases from the family I are single-domain, hexameric enzymes, while those from family II are two-domain, dimeric enzymes. *Mt*PPiase [9–11] and *Ec*PPiase [12] belong to family I, whereas *Sa*PPiase belongs to family II [13, 14].

1. First, test the activity of PPiase by adding the enzyme (final concentration of 2 nM PPiase) to the mixture of 15 μL of 2× reaction mixture and water (such that the final reaction volume is 30 μL).
2. In parallel, a negative control should also be set up with no PPiase added to the reaction mixture. This is to ensure that there is no phosphate contamination that can influence the experimental setup.
3. Leave the reaction mixture at room temperature for 8 min.
4. Add 150 μL of malachite green reagent, followed by 15 μL of 10% sodium citrate.
5. After 30 min, measure absorbance at 620 nm using a SpectraMax M5 plate reader.
6. To test the hit compound activity, mix the compounds with 15 μL of 2× reaction mixture, followed by water (to reach the final reaction volume of 30 μL) and then PPiase to initiate the reaction. The hit compound concentration should match that in the original coupled assay.

7. Also, set up a control in the absence of the compound, using only DMSO. EDTA in place of a hit compound is used as a positive inhibition control, as in the coupled assay. Ensure the same amount of DMSO in all the test reactions.
8. It is recommended to use serial dilutions for ease and reproducibility.
9. Once the reaction mixture is added and well mixed with the compound (or DMSO alone), the PPiase is added to initiate the reaction. Then repeat the procedure detailed in the test reaction above. It is recommended to run reactions in triplicate.

3.5 The Dose-Response Assay and Inhibitor Selectivity

A good initial evaluation of hits from the screening assay is a dose-response assay. The assay can be performed analogously to the primary screening assay in the 96-well plates, with varying concentrations of the hit compounds. This assay is used to determine the IC_{50} of the hit compound.

1. The concentrations of the primases are as follows: *Mt*DnaG: 0.5 μM, *Ba*DnaG: 4 μM, *Sa*DnaG: 3.5 μM. These concentrations were established experimentally ensuring the steady-state regime of the enzyme. Note that because enzyme activity may vary somewhat for different enzyme preparations, these concentrations should be used as a guide.
2. The hit compounds should be serially diluted from 100 μM. DMSO without the compound is used as a control. To ensure the constant concentration of DMSO in the reaction mixture, the volume of the compound/DMSO mixture used for each reaction should be the same.
3. Add 3× DNA-enzyme mixture.
4. To initiate the reaction, add 3× NTP mixture, followed by water to the final volume of 30 μL. The reactions are performed in triplicate.
5. Incubate the reaction at room temperature for 30 min.
6. Add 100 μL of Malachite Green Reagent, followed by 10 μL of 10% sodium citrate. Color develops and stabilizes within 30 min.
7. Read the absorbance at 620 nm of 96-well plate containing reaction mixture using a SpectraMax M5 plate reader.
8. Analyze the activity (a; scaled to obtain 100% in the absence of inhibitor) as a function of inhibitor concentration ($[I]$) to obtain IC_{50} and Hill coefficient (h) values using the following equation:

$$a = 100 - \frac{100 - r}{1 + \left(\frac{IC_{50}}{[I]}\right)^h} \tag{2}$$

Here, r is a residual activity extrapolated to infinite inhibitor concentration, which could be fixed at 0, as concluded from the examination of the data, or obtained from the best-fit values and their standard errors.

Once the hits from the HTS are validated by this dose-response assay and tested for their inhibition of PPiase, their selectivity can be determined by using DnaG and PPiase enzymes from other bacteria. In this chapter, in addition to *Mt*DnaG, *Sa*DnaG, *Ba*DnaG, *Mt*PPiase, and *Sa*PPiase, we included the protocol for purification of *Ec*PPiase, which can be included in the selectivity testing of PPiase inhibitors.

3.6 Mode of Inhibition

The mode of inhibition of primase can be determined by performing a steady-state kinetic experiment with different inhibitor concentration (as in above) with (1) fixed concentration of DNA (1.25 μM) at different concentration of NTP (31.25, 62.5, 125, 250, and 500 μM) and (2) fixed concentration of NTP (110 μM) with varying concentrations of DNA (0.19, 0.38. 0.75, and 1.5 μM). The mode of inhibition can be presented either as a direct plot of steady-state reaction rates as a function of varying substrate concentration (Michaelis-Menten plot) or as a double-reciprocal plot (Lineweaver-Burk plot) in Microsoft Excel or SigmaPlot. However, the nonlinear regression fitting should be performed only with reaction rates as a function of substrate and inhibitor concentrations, prior to any variable conversion, because the converted data are generally no longer normally distributed among replicates. The mode of inhibition with respect to either NTP or DNA can be determined by finding the best model that fits all the data. The Lineweaver-Burk plot is used to visualize the mode of inhibition by examining the relationships between the slopes and the intercepts. The Michaelis constants (K_m) and V_{max} can be obtained by nonlinear regression using SigmaPlot (Systat), as we described previously [4].

3.7 Identification of DNA Binding Compounds by DNA Intercalation Assay

DnaG inhibition can be caused by compounds binding DnaG, DnaG-DNA complex, or DNA alone. Therefore, DNA binding compounds may emerge as hits in this coupled colorimetric DnaG-PPiase assay. Because DnaG is bound to ssDNA or to a DNA-RNA hybrid in initiating or elongating a primer, respectively. Generally, ss or ds DNA intercalating compounds have a potential to inhibit DnaG [6, 15]. To detect binding of such compounds to DNA, we developed a facile assay where fluorescence of DNA intercalator ethidium bromide (EtBr) is monitored as a function of compound concentration. Fluorescence of EtBr is enhanced upon DNA intercalation. This fluorescence signal can be monitored in the presence of compound. Decrease of this fluorescence signal indicates that the compound intercalates into DNA and competes with EtBr.

1. Carefully mix 1.8 μL of 0.05 mM EtBr with 1.5 μL of 0.03 mM DNA (ssDNA or dsDNA), followed by 24.7 μL of water.
2. Add 2.0 μL of different concentration of compounds (1.5, 1.2, 0.9, 0.6, 0.3, and 0.15 mM for 100, 80, 60, 40, 20, and 10 μM, respectively) to each reaction mixture. Set up a control sample with EtBr/DNA with equivalent amount of DMSO (2.0 μL). Perform triplicate reactions in a 96-well flat bottom clear plate. Set the fluorescence emission wavelength at 600 nm and excitation wavelength at 520 nm on a SpectraMax M5 plate reader. Measure the fluorescence after incubating the reaction plate for 30 min at room temperature. The data can be plotted and analyzed using SigmaPlot software. Plot the graph with fluorescence intensity (f) against different concentrations of compound ([I]). The IC_{50} and Hill coefficient (h) can be obtained nonlinear regression using Eq. (2) described above for data fitting.

4 Notes

1. The construction of these plasmids is described in detail in our respective publications.
2. *Mt*DnaG and *Ba*DnaG are prone to aggregation and proteolytic degradation. To maximize the protein stability, the protein preparations should be kept and stored at high salt concentration (>300 mM NaCl).
3. Handle malachite green powder with care, as a small amount of this chemical can stain clothing, equipment, etc.
4. DnaG is not very efficient or processive. An excellent control assay can be performed by using an inactive point mutant of a Glu residue in the active site (Glu268Gln in *Mt*DnaG [4]). The mutant can be purified analogously to the wild-type protein.
5. Because DnaG is prone to aggregation at low salt concentrations, DnaG should be added to the reaction buffer (at lower salt concentration than in the storage buffer) after DNA.

References

1. Pang AH, Garneau-Tsodikova S, Tsodikov OV (2017) In vitro assays to identify antibiotics targeting DNA metabolism. Methods Mol Biol 1520:175–200
2. Robinson A, Causer RJ, Dixon NE (2012) Architecture and conservation of the bacterial DNA replication machinery, an underexploited drug target. Curr Drug Targets 13:352–372
3. Ilic S, Cohen S, Singh M et al (2018) DnaG primase-a target for the development of novel antibacterial agents. Antibiotics 7:72
4. Biswas T, Resto-Roldan E, Sawyer SK et al (2013) A novel non-radioactive primase-pyrophosphatase activity assay and its application to the discovery of inhibitors of *Mycobacterium tuberculosis* primase DnaG. Nucleic Acids Res 41:e56

5. Biswas T, Green KD, Garneau-Tsodikova S et al (2013) Discovery of inhibitors of *Bacillus anthracis* primase DnaG. Biochemistry 52: 6905–6910
6. Green KD, Punetha A, Chandrika NT et al (2021) Development of single-stranded DNA bisintercalating inhibitors of primase DnaG as antibiotics. ChemMedChem 16:1986–1995
7. Zhang JH, Chung TD, Oldenburg KR (1999) A simple statistical parameter for use in evaluation and validation of high throughput screening assays. J Biomol Screen 4:67–73
8. Chen J, Brevet A, Fromant M et al (1990) Pyrophosphatase is essential for growth of *Escherichia coli*. J Bacteriol 172:5686–5689
9. Pratt AC, Dewage SW, Pang AH et al (2015) Structural and computational dissection of the catalytic mechanism of the inorganic pyrophosphatase from *Mycobacterium tuberculosis*. J Struct Biol 192:76–87
10. Benini S, Wilson K (2011) Structure of the *Mycobacterium tuberculosis* soluble inorganic pyrophosphatase Rv3628 at pH 7.0. Acta Cryst Sect F 67:866–870
11. Pang AH, Garzan A, Larsen MJ et al (2016) Discovery of allosteric and selective inhibitors of inorganic pyrophosphatase from *Mycobacterium tuberculosis*. ACS Chem Biol 11:3084–3092
12. Harutyunyan EH, Oganessyan VY, Oganessyan NN et al (1997) Crystal structure of holo inorganic pyrophosphatase from *Escherichia coli* at 1.9 Å resolution. Mech Hydrolysis Biochem 36:7754–7760
13. Baykov AA, Anashkin VA, Salminen A et al (2017) Inorganic pyrophosphatases of Family II-two decades after their discovery. FEBS Lett 591:3225–3234
14. Gajadeera CS, Zhang X, Wei Y et al (2015) Structure of inorganic pyrophosphatase from *Staphylococcus aureus* reveals conformational flexibility of the active site. J Struct Biol 189: 81–86
15. Gajadeera C, Willby MJ, Green KD et al (2015) Antimycobacterial activity of DNA intercalator inhibitors of *Mycobacterium tuberculosis* primase DnaG. J Antibiot 68:153–157

Chapter 16

Cell-Based Fluorescent Screen Amenable to HTS to Identify Inhibitors of Bacterial Translation Initiation

Matteo Raneri, Emilio Alvarez-Ruiz, Danuta Mossakovska, and Federica Briani

Abstract

A strategy that can be applied to the research of new molecules with antibacterial activity is to look for inhibitors of essential bacterial processes within large collections of chemically heterogeneous compounds. The implementation of this approach requires the development of assays aimed at the identification of molecules interfering with specific cell pathways that can also be used in high-throughput analysis of large chemical libraries. Here, we describe a fluorescence-based whole-cell assay in *Escherichia coli* devised to find inhibitors of the translation initiation pathway. Translation is a complex and essential mechanism. It involves numerous sub-steps performed by factors that are in many cases sufficiently dissimilar in bacterial and eukaryotic cells to be targetable with domain-specific drugs. As a matter of fact, translation has been proven as one of the few bacterial mechanisms pharmacologically tractable with specific antibiotics. The assay described in this updated chapter is tailored to the identification of molecules affecting the first stage of translation initiation, which is the most dissimilar step in bacteria versus mammals. The effect of the compounds under analysis is measured in living cells, thus allowing evaluation of their in vivo performance as inhibitors of translation initiation. Compared with other assays for antibacterials, the major advantages of this screen are its simplicity, high mechanism specificity, and amenability to scaling up to high-throughput analyses.

Key words Translation initiation, Whole-cell assay, Gram-negative bacteria, Leaderless mRNA, S1 ribosomal protein, Ribosome, Antibacterial compounds

1 Introduction

Protein synthesis is initiated by the assembly on the mRNA of a translation-competent multi-subunit complex constituted by the ribosome, the translation initiation factors, and the initiator tRNA. This process occurs through very different multistep pathways in bacteria versus eukarya [1, 2]. In bacteria the first step is the binding of the 30S small ribosomal subunit to the mRNA transla-

Peter Sass (ed.), *Antibiotics: Methods and Protocols*,
Methods in Molecular Biology, vol. 2601, https://doi.org/10.1007/978-1-0716-2855-3_16,

tion initiation region (TIR), a site within the 5′-untranslated region (5′-UTR) including the Shine-Dalgarno (SD) sequence and the AUG start codon. 30S binding is mediated by the interaction between the mRNA TIR and two main ribosomal elements: the anti-SD, that is, a sequence at the 16S rRNA 3′-end complementary to the SD, and the ribosomal protein S1. S1 has a prominent role in the translation mechanism of Gram-negative and high GC-content Gram-positive bacteria [3–5]; it has been shown that in *Escherichia coli*, S1 is essential for the translation of most mRNAs [6], with the exclusion of a peculiar class of transcripts that are devoid of the 5′-UTR (i.e., leaderless mRNAs) [7–9]. Leaderless mRNAs are translated through a noncanonical, S1-independent pathway that occurs through the loading of a preassembled 70S ribosome on the mRNA 5′-end AUG [8, 10, 11]. Leaderless transcripts are very rare in *E. coli*. One of the few examples is represented by bacteriophage λ *cI* mRNA, which lacks a 5′-UTR when transcribed from the P_{RM} promoter.

S1 and the S1-dependent translation step appear as very good targets for new antibiotics. In fact, S1 is widely conserved among bacteria [4] and is encoded by essential genes in evolutionarily distant bacteria as *E. coli* and *Mycobacterium tuberculosis* [12, 13; Tubercolist database]. On the other hand, in mammals, an S1 orthologue is absent from both the 40S ribosomal subunit and the mitochondrial ribosomes. No inhibitors of the essential S1 activity in translation have been identified so far.

We devised a simple whole-cell fluorescent assay aimed at identifying molecules interfering with the S1-dependent pathway of translation initiation [14, 15]. The assay exploits the differences between leadered and leaderless translation to specifically target the S1 mechanism. In the first step, compounds of interest are screened for their effect on the expression of a reporter gene with a 5′-UTR (leadered reporter) cloned in *E. coli*. In the second step, inhibitors of the leadered reporter are analyzed for their effect on the expression of a leaderless variant of the same reporter (Fig. 1).

Molecules inhibiting the S1-dependent mechanism should not affect the leaderless reporter expression, whose translation does not require S1. This prediction was verified by exploiting the aminoglycoside antibiotic kasugamycin, which specifically inhibits leadered mRNA translation through a complex mechanism that involves the generation of minimal ribosomes lacking several ribosomal proteins, among which is S1 [14, 16, 17]. The results of the analysis with kasugamycin demonstrated that, in principle, compounds that selectively target the canonical pathway of bacterial translation initiation can be identified through the assay [14]. The reporter constructs are carried by the AS19 *E. coli* strain, which has enhanced permeability [14], thus increasing the chance of finding compounds with the required activity in screening campaigns.

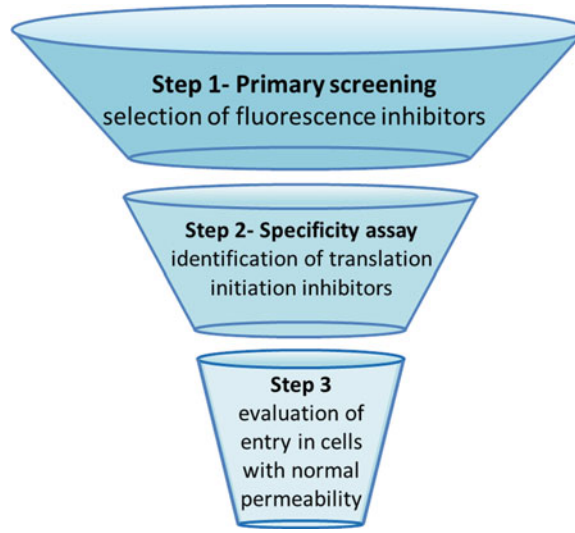

Fig. 1 Outline of the multistep assay and HTS cascade. In Step 1, the compounds of interest are screened with the permeable strain AS19/pGM991. Compounds inhibiting the fluorescence of this strain are then screened with strain AS19/pGM999 (Step 2). Molecules specifically targeting the canonical pathway of translation initiation should not affect AS19/pGM999 fluorescence. In Step 3, the entry of candidate compounds into cells with normal permeability is evaluated by assaying inhibition of DH10B/pGM991 fluorescence. (Figure reprinted and modified from Ref. [15])

This chapter updates our previous chapter [15] and further describes the application of the assay to a high-throughput screening (HTS) campaign of a 1.8 million compound collection of GlaxoSmithKline (GSK). The HTS cascade is outlined in Fig. 2.

One hundred one hits, namely, compounds inhibiting more the expression of the leadered construct than that of the leaderless one, were identified, showing that the assay described in this chapter is amenable to high-throughput analyses. Unfortunately, successive analyses to assess cytotoxicity and activity in bacterial strains with normal permeability showed that no compounds had specificity and potency high enough to be interesting for pharmacological development and the project was concluded. Despite the unlucky outcome, the assay per se showed amenability to high-throughput screening. In fact, the assay specificity is a relevant asset for high-throughput screenings of large collections of compounds as it allows to identify and discard molecules generically toxic to the cells. Moreover, it would also expedite the identification of the molecular target(s) of the hits by restricting their research among cellular factors specifically involved in translation initiation, which is the mechanism targeted by the assay.

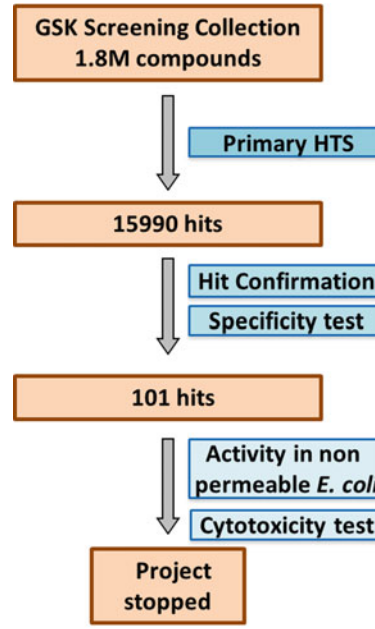

Fig. 2 Outline of the HTS cascade. In Step 1 (Primary Screening), 1.8 M compounds (final concentration, 10 μM) of the GSK collection were screened with the permeable strain AS19/pGM991. Cutoff was set at 2.4 SD. A total of 15,990 compounds inhibiting the fluorescence of this strain were then re-tested with AS19/pGM991 (Hit confirmation) and assayed with strain AS19/pGM999 (Specificity test). A total of 101 molecules were deemed as specific because they had IC_{50} for leadered eGFP expressed by AS19/pGM991 $<$ 10 μM and IC_{50} for leaderless eGFP expressed by AS19/pGM999 $>$ 100 μM. Unfortunately, none of the 101 hits passed the successive tests (Activity in non-permeable *E. coli* and cytotoxicity test), mostly because of their low potency toward an *E. coli* strain with normal membrane permeability (i.e., DH10b/pGM991; data not shown)

2 Materials

2.1 Bacterial Strains

The *E. coli* strains AS19/pGM991, AS19/pGM999, and DH10B/pGM991 are exploited in different screening steps [14, 18, 19]. AS19 is an *E. coli* B derivative with increased permeability due to an unmapped mutation altering the outer membrane [18]. This defect facilitates the entry of compounds into the cells. DH10B is an *E. coli* K-12 laboratory strain with no reported permeability defects [19]. The strains carry either pGM991 or pGM999 plasmid, which are both derivatives of pGM963 [20], a multicopy shuttle vector conferring ampicillin resistance. The vector carries the *araC* gene and *araBp* promoter of the *E. coli* arabinose operon [21] inserted upstream of the eGFP open reading frame (ORF) devoid of the Shine-Dalgarno sequence and ATG

start codon. In pGM991 and pGM999, DNA fragments encompassing either the 5′-UTR and first nine codons of *E. coli recA* or the first 189 bp of phage λ *cI* ORF, respectively, are inserted in frame with the eGFP ORF. Transcription of pGM991 and pGM999 from *araBp* gives either a leadered *recA*-eGFP (pGM991) or a leaderless *cI*-eGFP mRNA (pGM999).

2.2 Culture Media

Prepare all media and solutions with analytical grade water (hereafter indicated as aH_2O) and reagents. Prepare and store all solutions and media at room temperature, if not differently stated.

1. LD broth: dissolve in 1 L of aH_2O 10 g of Bacto tryptone, 5 g of yeast extract and 5 g of NaCl. Sterilize by autoclaving.
2. LD agar: dissolve 10 g of agar in 700 mL of LD. Sterilize by autoclaving.
3. M9 minimal medium: in 1 L of aH_2O, dissolve 2 g NH_4Cl, 32 g $Na_2HPO_4{\cdot}12H_2O$, 6 g KH_2PO_4, and 10 g NaCl. Sterilize by autoclaving. To 250 mL of the above sterile solution, add in the stated order the following sterile components: 250 mL of aH_2O, 0.09 mL 0.5 M $CaCl_2$, 0.54 mL 1 M $MgSO_4$, and 0.05 mL trace elements mix prepared by dissolving in 1 L of aH_2O 3.2 g $FeCl_3{\cdot}6H_2O$, 0.06 g $CaCl_2{\cdot}6H_2O$, 0.17 g Zn $(Acetate)_2{\cdot}2H_2O$, 0.14 g $MnSO_4{\cdot}H_2O$ and 0.05 g $CuSO_4{\cdot}5H_2O$.

2.3 Chemicals and Equipment

1. DMSO, molecular biology grade.
2. D(+)-Glucose. Dissolve 40 g in 100 mL of aH_2O. Sterilize by autoclaving.
3. Glycerol, molecular biology grade. Aliquot in glass bottles and sterilize by autoclaving.
4. L(+)-Arabinose, ≥99% quality grade. Dissolve 10 g in 50 mL of aH_2O and sterilize by filtration through 0.22 μm cellulose acetate membrane. Store at 4 °C.
5. Dissolve ampicillin (Amp) in aH_2O to 50 g/L final concentration and sterilize by filtration through a 0.45 μm cellulose acetate membrane. Store at −20 °C.
6. 50 mL conical centrifuge tubes.
7. Black polystyrene 96-well microplates.
8. Bench centrifuge accommodating 50 mL conical centrifuge tubes.
9. Fluorescence microplate reader and/or fluorescence imaging system.

3 Methods

3.1 Outline of the Assay Cascade

The screening cascade is outlined in Fig. 1. In Step 1, the compounds of interest are assayed for their effect on the fluorescence of the permeable strain AS19/pGM991, which produces a leadered eGFP mRNA (Fig. 3), and fluorescence inhibitors are selected.

All compounds that interfere with fluorescence expression, irrespective of their molecular target(s), and generically toxic molecules will be positively selected at this stage. However, since molecules that affect transcription and translation seem to be preferentially picked by the assay [14], they may be enriched among compounds passing Step 1. The panel of inhibitors identified in Step 1 is then assayed with the permeable strain AS19/pGM999, which expresses the leaderless eGFP mRNA variant (Fig. 3). It should be noted that the difference between the bacterial strains used in these stages of the screen cascade is limited to the translation initiation region of the reporter eGFP mRNAs. Thus, most molecules selected in Step 1 will inhibit fluorescence also in Step 2. Conversely, inhibitors of the S1-dependent step of translation initiation (canonical initiation inhibitors, CIIs) should not affect the synthesis of the CI-eGFP reporter protein and, in turn, strain fluorescence (Table 1). Thus, Step 2 confers high mechanism specificity on the screen. Lastly, in Step, 3 the compounds of interest are assayed for their effect on the fluorescence of strain DH10B/pGM991 to assess their penetration in *E. coli* cells endowed with normal permeability.

Fig. 3 Structure of reporter constructs. The structure of the cassettes expressing either the leadered (pGM991) or the leaderless (pGM999) mRNA is shown on the left. Arrows, *araBp* promoter; line, *recA* 5′-UTR; boxes, chimeric *recA*-eGFP and *cI*-eGFP ORFs. The shadowed parts represent the portions of the two constructs encompassing *recA* and *cI* open reading frames. (Figure reprinted and modified from Ref. [15])

Table 1
Expected performance of translation initiation inhibitors in the assay steps

Step	strain	eGFP mRNA	CII effect on fluorescence[a]
1	AS19/pGM991	leadered	<
2	AS19/pGM999	leaderless	none
3	DH10B/pGM991	leadered	<

[a]*CII* canonical initiation inhibitors, < fluorescence decrease

3.2 Fluorescent Assay Protocol

1. Streak AS19/pGM991 from the glycerol stock stored at −80 °C on LD-Agar plates with 100 mg/L Amp. Incubate 16–20 h at 37 °C.
2. Transfer bacteria from the streak plate to a glass tube containing 5 mL of LD supplemented with 100 mg/L Amp by touching three to four colonies with a sterile loop and inoculating them into the broth. Incubate at 37 °C in a rotatory device for 16–20 h (*see* **Note 1**).
3. Dilute the stationary cultures to $OD_{600} = 0.1–0.12$ in 50 mL of M9 supplemented with 100 mg/l Amp and 0.4% glucose in a 250 mL flask. Incubate the flask at 37 °C with agitation at 120 rpm in a rotatory shaker for about 3 h (*see* **Note 2**).
4. Pour the culture in a 50 mL conical centrifuge tube and centrifuge at 2260 × *g* for 15 min at room temperature in a bench centrifuge. After carefully discarding the supernatant, resuspend the bacterial pellet in M9 to final OD_{600} between 0.8 and 1.
5. Dispense 110 μL aliquots of the cell resuspension into the wells of a black polystyrene 96-well microplate. Add 3 μL of DMSO in the first column wells (control samples) and the compounds to be tested diluted in DMSO in the other wells of the screening microplate. Incubate the microplate at 37 °C 15 min (*see* **Note 3).**
6. Add 10 μL of M9 supplemented with either 2.4% glycerol in four control wells (not induced samples) or 2.4% arabinose, which induces transcription of the reporter gene, in all the others. Incubate the plate 3 h at 37 °C in the dark with slow agitation (*see* **Note 4**).
7. After incubation, measure the fluorescence by means of a microplate reader (*see* **Note 5**) and/or acquire the microplate image with an imaging system (*see* **Note 6**). An example of a screening microplate image is shown in Fig. 4.
8. Compounds that affect the sample fluorescence (Table 1; *see* **Note** 7) enter Step 2.
9. Screen the compounds selected in Step 1 with strain AS19/pGM999 according to the experimental procedure described above (from Subheading 3.2, **steps 1**–7; *see* **Note 8**).
10. At the end of the procedure, identify compounds that do not affect sample fluorescence (Table 1). Such compounds, which should target translation initiation, can be then tested for their effect on the fluorescence of strain DH10B/pGM991 (once again, according to the experimental procedure described above from Subheading 3.2, **steps 1**–7) to assess whether they can enter a strain with a normal permeability (Step 3 in Fig. 1; Table 1).

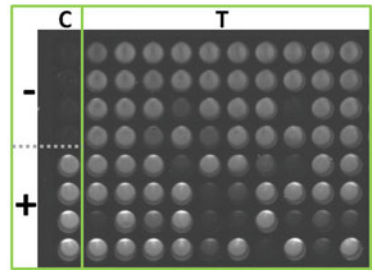

Fig. 4 Fluorescent whole cell assay: an example of a screening microplate. Cultures of AS19/pGM991 were grown and aliquoted in a 96-well microplate as described in the Methods section. 3 μL of 80 heterogeneous compounds in DMSO solution were transferred into the test wells of the screening plate (T) and mixed with the cell resuspension. In the control column (C), 3 μL of DMSO were added to the cell samples. After 3 h at 37 °C, the plate image was acquired with a VersaDoc Imaging system 4000MP (Bio-Rad). C^- wells, cells resuspended in M9 + 0.2% glycerol, transcription of the *recA-eGFP* reporter off; C^+ and T wells, cells in M9 + 0.2% arabinose, transcription of the reporter induced. (Figure reprinted and modified from Ref. [15])

4 Notes

1. In these conditions, cultures of AS19 and DH10B strains carrying either pGM991 or pGM999 usually reach an OD_{600} between 2.5 and 3.5 after the overnight incubation.
2. The AS19 derivatives exhibit a long lag phase and their OD_{600} less than double in this time span. Cultures exhibiting optical density decrease should be discarded as this could be due to cell lysis, an event that we have sporadically observed upon dilution in M9 of these strains.
3. In the HTS campaign, 8 μL of cell resuspension prepared as described were aliquoted in 1536-well plates, and the compounds (1 μL of a 100 μM solution in DMSO) were added. Induction was performed by adding 1 μL of M9 supplemented with 1.8% arabinose.
4. We usually place the microplate on an orbital shaker set at 50 rpm in the dark. No significant growth of the cultures occurs in these conditions. This may explain why the assay seems to be more sensitive to inhibitors of gene expression than to compounds that affect the growth by interfering with other processes [14].
5. A microplate reader for fluorescence detection equipped with 485/530 nm excitation/emission filters can be used.
6. We select Alexa 488 (530BP Blue Led) as the Fluorophore and 500–600 s as exposure time in our imaging system.

7. We consider as inhibitors compounds that reduce fluorescence to the 30% or less of that of the positive controls (induced samples without any added compound).
8. Induced control cultures of AS19/pGM999 show threefold to fourfold lower fluorescence than AS19/pGM991 ones [14].

Acknowledgments

We thank lab members and the GSK staff involved in the screening campaign, and in particular Stephane Huet, for helpful discussions. The development of the assay was supported by the Italian Cystic Fibrosis Research Foundation (grant FFC#8/2013 sponsored by the FFC Delegation of Montebelluna "La bottega delle donne"). The HTS campaign was performed in the frame of 2014 GSK Discovery Fast Track Challenge Initiative.

References

1. Myasnikov AG, Simonetti A, Marzi S, Klaholz BP (2009) Structure-function insights into prokaryotic and eukaryotic translation initiation. Curr Opin Struct Biol 19:300–309
2. Benelli D, Londei P (2009) Begin at the beginning: evolution of translational initiation. Res Microbiol 160:493–501
3. Subramanian AR (1983) Structure and functions of ribosomal protein S1. Prog Nucleic Acid Res Mol Biol 28:101–142
4. Salah P, Bisaglia M, Aliprandi P et al (2009) Probing the relationship between gram-negative and gram-positive S1 proteins by sequence analysis. Nucleic Acids Res 37: 5578–5588
5. Roberts MW, Rabinowitz JC (1989) The effect of *Escherichia coli* ribosomal protein S1 on the translational specificity of bacterial ribosomes. J Biol Chem 264:2228–2235
6. Sørensen MA, Fricke J, Pedersen S (1998) Ribosomal protein S1 is required for translation of most, it not all, natural mRNAs in *Escherichia coli* in vivo. J Mol Biol 280:561–569
7. Tedin K, Resch A, Bläsi U (1997) Requirements for ribosomal protein S1 for translation initiation of mRNAs with and without a 5′ leader sequence. Mol Microbiol 25:189–199
8. Moll I, Grill S, Gualerzi CO, Bläsi U (2002) Leaderless mRNAs in bacteria: surprises in ribosomal recruitment and translational control. Mol Microbiol 43:239–246
9. Delvillani F, Papiani G, Dehó G, Briani F (2011) S1 ribosomal protein and the interplay between translation and mRNA decay. Nucleic Acids Res 39:7702–7715
10. Moll I, Hirokawa G, Kiel MC et al (2004) Translation initiation with 70S ribosomes: an alternative pathway for leaderless mRNAs. Nucleic Acids Res 32:3354–3363
11. Udagawa T, Shimizu Y, Ueda T (2004) Evidence for the translation initiation of leaderless mRNAs by the intact 70 S ribosome without its dissociation into subunits in eubacteria. J Biol Chem 279:8539–8546
12. Briani F, Curti S, Rossi F et al (2008) Polynucleotide phosphorylase hinders mRNA degradation upon ribosomal protein S1 overexpression in *Escherichia coli*. RNA 14: 2417–2429
13. Kitakawa M, Isono K (1982) An amber mutation in the gene *rpsA* for ribosomal protein S1 in *Escherichia coli*. Mol Gen Genet 185:445–447
14. Raneri M, Sciandrone B, Briani F (2015) A whole-cell assay for specific inhibitors of translation initiation in bacteria. J Biomol Screen 20:627–633
15. Briani F (2017) Cell-based fluorescent screen to identify inhibitors of bacterial translation initiation. In: Sass P (ed) Antibiotics. Methods in molecular biology, vol 1520. Humana Press, New York, pp 237–245
16. Schluenzen F, Takemoto C, Wilson DN et al (2006) The antibiotic kasugamycin mimics mRNA nucleotides to destabilize tRNA binding and inhibit canonical translation initiation. Nat Struct Mol Biol 13:871–878

17. Kaberdina AC, Szaflarski W, Nierhaus KH, Moll I (2009) An unexpected type of ribosomes induced by Kasugamycin: a look into ancestral times of protein synthesis? Mol Cell 33:227–236
18. Sekiguchi M, Iida S (1967) Mutants of *Escherichia coli* permeable to actinomycin. Proc Natl Acad Sci U S A 58:2315–2320
19. Grant SGNN, Jessee J, Bloom FR, Hanahan D (1990) Differential plasmid rescue from transgenic mouse DNAs into *Escherichia coli* methylation-restriction mutants. Proc Natl Acad Sci U S A 87:4645–4649
20. Delvillani F, Sciandrone B, Peano C et al (2014) Tet-Trap, a genetic approach to the identification of bacterial RNA thermometers: application to *Pseudomonas aeruginosa*. RNA 20:1963–1976
21. Schleif R (2000) Regulation of the L-arabinose operon of *Escherichia coli*. Trends Genet 16: 559–565

Chapter 17

Bacterial Two Component Systems: Overexpression and Purification: In Vitro and In Vivo Inhibitor Screens

Alina Dietrich, Mike Gajdiss, Michael Türck, Ian Monk, and Gabriele Bierbaum

Abstract

Bacterial histidine kinases are promising targets for new antimicrobial agents. In antibacterial therapy, such agents could inhibit bacterial growth by targeting essential two-component regulatory systems or resensitize bacteria to known antibiotics by blocking stress responses upon cell wall or cell membrane damage. However, (i) activity assays using truncated kinase proteins, that is, the cytoplasmic domains containing the conserved histidine residue for phosphorylation, have been shown to produce artifacts, and (ii) the purification of the full-length histidine kinases is complicated. Here, we describe a standard protocol for the recombinant expression and purification of functional full-length histidine kinases and other membrane proteins from Gram-positive bacteria that do not harbor more than two trans-membrane domains in an *Escherichia coli* host. This guide also presents in vitro and in vivo phosphorylation assays to screen for new antimicrobial compounds that target bacterial histidine kinases, either using a traditional radioactively labeled ATP assay to quantify histidine kinase phosphorylation or Phos-tag acrylamide gel electrophoresis to examine histidine kinase phosphorylation through mobility shift in the polyacrylamide gel. In addition, we describe the use of Phos-tag combined with a western blot approach to visualize the phosphorylation of a response regulator in vivo.

Key words Two-component regulatory system, Histidine kinase, Purification, Response regulator, Kinase inhibitor, Antimicrobial compound, Phosphorylation, Phos-tag, Western blot, FLAG-tag

1 Introduction

Recent research into sensory perception by bacteria has yielded a wider understanding for the role of two-component regulatory systems (TCS) [1, 2]. Bacteria adapt and respond to environmental stimuli, with the relay of external messages being conducted by TCS that act as stimulus-response coupling mechanisms. In their simplest form, TCS are composed of two proteins: a membrane-bound histidine kinase and a cognate cytoplasmic response regulator. The response regulator elicits changes in gene expression through interaction with specific DNA binding sites. Several studies

Peter Sass (ed.), *Antibiotics: Methods and Protocols*,
Methods in Molecular Biology, vol. 2601, https://doi.org/10.1007/978-1-0716-2855-3_17,

have proposed that essential two-component systems could be novel targets for antimicrobial compounds [3–5]. In addition, the inhibition of a nonessential TCS can impair the ability of a pathogen to respond to antimicrobial stress, thereby resensitizing it to established antibiotics. For example, methicillin resistance in *Staphylococcus aureus*, which causes still one of the most frequent nosocomial infections, is abolished after inactivation of the VraSR TCS [6]. Inhibition of one or more histidine kinases in combination with existing antibiotics could offer new treatment options. The identification of new histidine kinase inhibitors requires the production of the full-length protein either in the native context within the bacterium or through the incorporation of the histidine kinase in detergent solubilized micelles [7, 8].

The following guide describes a standard protocol for the recombinant expression and purification of functional full-length histidine kinases and other membrane proteins from Gram-positive bacteria that do not harbor more than two trans-membrane domains, using a detergent and ultracentrifugation to separate membrane-bound proteins from cytosolic proteins.

Phosphorylation assays can be performed using labeled ATP molecules that contain the isotopes ^{32}P or ^{33}P at the γ-position, followed by a sodium dodecyl sulfate polyacrylamide gel-electrophoresis (SDS-PAGE) and exposure of the gel to autoradiography with a conventional x-ray film or a more sensitive phosphorus imaging plate. Phosphorylation of a histidine kinase can also be detected using Phos-tag acrylamide as an additive to SDS-PAGE gels [9]. This compound complexes phosphorylated proteins using manganese ions, leading to a mobility shift of phosphorylated proteins. The bands are detected with conventional staining methods, and the amount of phosphorylated protein can be directly compared to the amount of non-phosphorylated protein (Fig. 1). Both methods also enable observation of the phosphotransfer to a response regulator to detect compounds that inhibit the phosphotransfer reaction.

We also present a standard protocol to visualize the phosphorylation status of a response regulator in vivo. A gene fusion of the response regulator of interest with the FLAG-tag coding region is constructed with phosphorylation followed by Phos-tag SDS PAGE and subsequent western blotting with a specific anti-FLAG antibody [10]. This method takes advantage of the high sensitivity of western blotting. It allows the visualization of potential kinase inhibitor activity on a specific response regulator in vivo, under non-altered expression conditions and in the presence of all known and unknown regulatory factors for the TCS of interest. Here, we used the essential WalR response regulator from *S. aureus* as a model protein for the description of in vivo phosphorylation. This text is an updated and extended version of Chapter 15 in the first edition of this book [11].

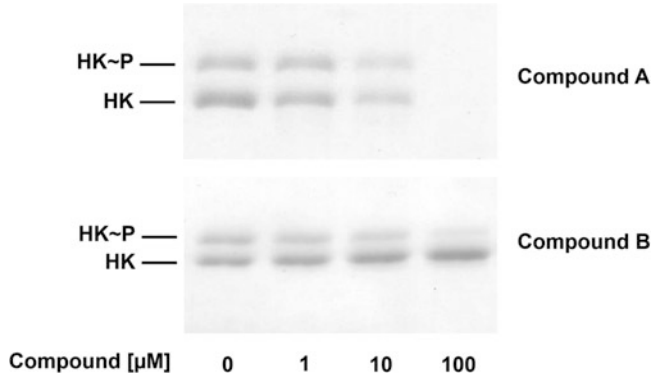

Fig. 1 Phos-tag PAGE of the truncated cytoplasmic variant of a histidine kinase with increasing concentrations of putative inhibitory compounds. Assay was performed as described in Subheading 3.3 and was stained with Coomassie Brilliant Blue R250. The decreasing band intensity of both, the phosphorylated (HK~P) and the non-phosphorylated (HK) histidine kinase, results from an aggregation of the proteins caused by compound A, preventing migration in the acrylamide gel. The ratio of phosphorylated to non-phosphorylated protein does not change significantly, which indicates that the tested compound is not a specific kinase inhibitor that prevents autophosphorylation. To test this side effect, a truncated cytoplasmic variant of the kinase must be used that does not need detergent micelles to autophosphorylate. The addition of Triton X-100 would lead to a separation of the proteins and an aggregation would remain unrevealed. Compound B decreases the ratio of phosphorylated to non-phosphorylated protein but allows the kinase to migrate through the gel even at high concentrations. An inhibition of the autophosphorylation without the formation of protein aggregates occurs. (Figure reprinted from Ref. [11])

2 Materials

2.1 Expression and Purification of a Recombinant Full-Length Histidine Kinase in Escherichia coli

Prepare all solutions in deionized water unless indicated otherwise.

1. Lysogeny broth (LB): 10 g/L tryptone, 5 g/L yeast extract, 10 g/L NaCl, pH 7.5. Autoclave (*see* **Note 1**).
2. 1 M isopropyl-β-D-thiogalactoside (IPTG): Sterilize by filtration before adding to the culture.
3. 2 M Imidazole: Store at 4 °C.
4. 250 mM DDM (n-Dodecyl β-D-maltoside): Store at 4 °C (*see* **Note 2**).
5. Lysis buffer 1: 50 mM NaH_2PO_4, 300 mM NaCl, 10 mM imidazole, 2 mM β-mercaptoethanol, 30% (v/v) glycerol, pH 8. Dissolve NaH_2PO_4 and NaCl in 30% glycerol and add the appropriate amount of imidazole solution. Cool down to 4 °C, add β-mercaptoethanol prior to use and adjust to pH 8. Sterilize by filtration (*see* **Note 3**).

6. Lysis buffer 2: 50 mM NaH_2PO_4, 300 mM NaCl, 20 mM imidazole, 40 mM DDM, 2 mM β-mercaptoethanol, 30% (v/v) glycerol, pH 8. Dissolve NaH_2PO_4 and NaCl in 30% glycerol and add the appropriate amount of the imidazole and DDM solutions. Cool down to 4 °C, add β-mercaptoethanol prior to use and adjust to pH 8. Sterilize by filtration.
7. Wash buffer 1: 50 mM NaH_2PO_4, 300 mM NaCl, 20 mM imidazole, 4 mM DDM, 2 mM β-mercaptoethanol, 30% (v/v) glycerol, pH 8. Prepare as for lysis buffer 2.
8. Wash buffer 2: 50 mM NaH_2PO_4, 300 mM NaCl, 40 mM imidazole, 4 mM DDM, 2 mM β-mercaptoethanol, 30% (v/v) glycerol, pH 8. Prepare as for lysis buffer 2.
9. Elution buffer: 50 mM NaH_2PO_4, 300 mM NaCl, 300 mM imidazole, 4 mM DDM, 2 mM β-mercaptoethanol, 30% (v/v) glycerol, pH 8. Prepare as for lysis buffer 2.
10. Lysozyme: 100 mg/mL. Store at −20 °C.
11. Benzonase (*see* **Note 4**).
12. Ni-NTA affinity resin.
13. Polypropylene column, 1mL.
14. Dialysis buffer: 50 mM HEPES (N-2-Hydroxyethylpiperazine-N'-2-ethanesulfonic acid), 200 mM KCl, 50% (v/v) glycerol, pH 8. Autoclave.
15. Slide-A-Lyzer™ Dialysis Cassettes, 10K MWCO, 0.5 mL.
16. Syringe with needle: 1 mL syringe with 0.9 × 70 mm needle.
17. Reagent using the Bradford method to determine the protein concentration.

2.2 Phosphorylation Assay Using Radioactively Labeled ATP

1. 85 mM Triton X-100.
2. 1 M DTT (Dithiothreitol): Create small aliquots and store at −20 °C.
3. 5× Phosphorylation buffer: 250 mM HEPES, 2.5 M KCl, 25 mM $MgCl_2$, 2.5 mM DTT, 17.5% (v/v) glycerol, pH 8. Add DTT solution to an aliquot of buffer prior to use and discard the buffer afterward. Sterilize by filtration (*see* **Note 5**).
4. ^{33}P-ATP ([γ-^{33}P]Adenosine 5′-triphosphate), Specific activity: >111TBq (3000Ci)/mmol
5. 2× Laemmli Sample Buffer. Add 1:20 β-mercaptoethanol prior to use.
6. Quality precast 10% Bis-Tris gels, 1.0 mm, 10–15 well (*see* **Note 6**).
7. 20× MOPS SDS Running Buffer: 1 M MOPS, 1 M Tris base, 2% SDS, 20 mM EDTA.
8. Prestained protein ladder.

9. Storage Phosphor Screen and exposure cassette or conventional X-ray films.
10. Phosphor imager.
11. Coomassie staining solution: 45% (v/v) methanol, 10% (v/v) acetic acid, 0.25% (w/v) Coomassie Brilliant Blue R250. Mix vigorously after adding Coomassie Brilliant Blue and before every staining procedure.
12. Destaining solution: 45% (v/v) methanol, 10% (v/v) acetic acid.

2.3 Phosphorylation Assay Using Phos-tag Acrylamide

1. 40% acrylamide/bisacrylamide (37.5:1).
2. Resolving gel solution: 3 M Tris base, pH 8.5. Store at 4 °C.
3. 10 mM $MnCl_2$: Dissolve in MilliQ water. Store at 4 °C.
4. 5 mM Phos-tag acrylamide (Wako Pure Chemical Industries) in 3% methanol: Dissolve in methanol first by vortexing vigorously. Add ultrapure water, vortex and store at 4 °C (*see* **Note 7**).
5. Ammonium persulfate: 21 mg/mL in ultrapure water. Create solution prior to use.
6. TEMED (N,N,N′,N′-Tetramethylethylendiamine).
7. 2-propanol.
8. Stacking gel solution: 1 M Tris base, 0.8% SDS (sodium dodecyl sulfate). Store at 4 °C.
9. 10 mM ATP (Adenosine 5′-triphosphate): Dissolve in MilliQ water. Store at −20 °C.
10. 20% SDS. Store at room temperature (*see* **Note 8**).
11. SDS-PAGE running buffer: 25 mM Tris base, 192 mM glycine, 0.1% (w/v) SDS. Create a stock solution without SDS and store at 4 °C. Add 0.1% SDS (final concentration) to the 1× solution.
12. Coomassie staining solution: 45% (v/v) methanol, 10% (v/v) acetic acid, 0.25% (w/v) Coomassie Brilliant Blue R250. Mix vigorously after adding Coomassie (*see* **Note 9**).
13. Destaining solution: 45% (v/v) methanol, 10% (v/v) acetic acid.

2.4 Construction of WalR-FLAG Tagged Strains

1. *E. coli* strain IMxxB (specific for the target *S. aureus* clonal complex).
2. Plasmid pIMAYZ with tag construct inserted. Temperature-sensitive plasmid for allelic exchange.
3. BHI (Brain Heart Infusion) broth: 37 g/L, Oxoid or BBL. Autoclave.
4. BHIS: BHI broth (autoclaved) with 500 mM sucrose added, filter sterilized through 0.2 μM filter.

5. MilliQ water, autoclaved.
6. 10% glycerol (w/v) in MilliQ water, filter sterilized through 0.2 μM filter. Store at 4 °C.
7. 10% glycerol (w/v) with 500 mM sucrose added, filter sterilized through 0.2 μM filter.
8. BHIA: BHI agar: 37 g/L BHI, 15 g/L agar; BHIA-X: BHIA with 100 μg/mL X-gal; BHIA-CX: BHIA with 10 μg/mL chloramphenicol and 100 μg/mL X-gal. Autoclave.
9. 100 mg/mL X-gal (5-Bromo-4-Chloro-3-Indolyl β-D-Galactopyranoside): dissolve in dimethylformamide, store at −20 °C.
10. 10 mg/mL chloramphenicol dissolved in ethanol, stored at −20 °C.
11. Phosphate buffered saline (PBS): 137 mM NaCl, 2.7 mM KCl, 10 mM Na_2HPO_4, 1.8 mM KH_2PO_4. Autoclave.
12. 1 mm electroporation cuvettes.
13. Gene Pulser Xcell Microbial Electroporation System or BTX630.
14. Hot Start DNA polymerase.
15. Oligonucleotides to amplify the *walR/walK* region from NRS384 (USA300 isolate) up and downstream of the FLAG tag.

    IM13 5′-TGACGCGTAGAGGCGTTGGATATTTCC-3′;

    IM181 5′-TTTTTCAAGGTTATTTGTAAAATATAACCC-3′.
16. 10 mg/mL Lysostaphin: Dissolved in sterile water (*see* **Note 10**). Freeze at −20 °C.
17. Genomic DNA purification kit.

2.5 In Vivo Phosphorylation Assay Using Phos-tag Acrylamide and Western Blotting

Prepare all solutions in double deionized water (ddH_2O/MilliQ water) unless indicated otherwise.

1. TSB (Tryptic soy broth), autoclaved.
2. 1:1 ethanol/acetone, ice cold.
3. Sterile double-distilled water.
4. Tris-buffered saline (TBS): 50 mM Tris base, 150 mM NaCl, pH 7.5.
5. Precellys24 Tubes and glass beads (0.1 mm).
6. Reagent using the Bradford method to determine the protein concentration.
7. Transfer buffer: 25 mM Tris base, 192 mM glycine, 20% MeOH, pH 8.3 (*see* **Note 11**).
8. Transfer buffer with EDTA: Transfer buffer, 10 mM EDTA.
9. TBS-T: TBS, 0.05% Tween 20.

10. Immun-Blot® PVDF membrane for protein blotting (*see* **Note 12**).
11. Blotting papers (7.5 × 10 cm, extra thick blot paper).
12. Ethanol.
13. Blocking buffer: TBST, 5% Easy Blocker (*see* **Note 13**).
14. Anti-FLAG M2-HRP (Sigma, A8592).
15. ECL substrate solution, for example, Western Sure® PREMIUM Chemiluminescent Substrate (LI-COR (*see* **Note 14**).

3 Methods

3.1 Recombinant Expression and Purification of a Full-Length Histidine Kinase in Escherichia coli *(see Note 15)*

1. In a 5 L Erlenmeyer flask, inoculate 1 L of LB containing the appropriate antibiotic(s) with 10 mL of an overnight culture of the expression strain and incubate in a water bath at 37 °C and constant shaking at 100 rpm. Observe the growth by measuring the absorbance at 600 nm with a spectrophotometer (*see* **Note 16**).
2. When the culture has reached an OD_{600} of 0.5, induce the expression of the protein by the addition of 1 M IPTG solution (final concentration: 1 mM).
3. Adjust the temperature in your water bath to 30 °C and incubate the culture for another 16–20 h.
4. Cool down the centrifuge to 4 °C.
5. Harvest the cells by centrifuging the culture at 7000 × *g* for 10 min. Decant the supernatant.

   Perform all the following steps on ice or in the cold room.

6. Resuspend the pelleted cells in 20 mL lysis buffer 1 and transfer the solution to a sterile 50 mL conical centrifuge tube (*see* **Note 17**). The volume should now be around 25 mL. At this point, the lysate can be stored at −20 °C if desired.
7. Add 250 μL of a 100 mg/mL lysozyme solution (final concentration: 1 mg/mL) and vortex.
8. Add Benzonase to a final concentration of 25 U/mL and vortex.
9. Incubate the lysate for 30 min on ice.
10. Lyse the cells by ultrasonication on ice or with the cooling module (if available) to avoid heating of the lysate. Conduct 10–15 pulses of 10 s with 30 s of breaks between the pulses. Pulse number and duration are dependent on the strength of the sonicator. Stop the sonication immediately when the lysate starts to foam.

11. Add more benzonase at this point if the lysate is too viscous. If added, an additional 30-min incubation is required.
12. Centrifuge the lysate at 15,000 × *g* for 10 min at 4 °C. Set the brake of the centrifuge to a low value to prevent detaching of the pellet from the wall of the tube.
13. Transfer the supernatant to a fresh 50 mL conical centrifuge tube and repeat the centrifugation step twice to remove as much of the cell debris as possible (*see* **Note 18**).
14. Transfer the supernatant to ultracentrifugation tubes (*see* **Note 19**).
15. Ultracentrifuge at 218,000 × *g* at 4 °C for 60 min and decant the supernatant.
16. Pipette 4 mL of lysis buffer 2 to the pellet and gently release the pellet from the centrifuge tube wall using a clean glass rod or spatula. Transfer the released pellet by decanting it with the buffer into a fresh 50 mL conical centrifuge tube.
17. Resuspend the pellet with a small stir bar for 30–60 min (*see* **Note 20**) and transfer to a clean ultracentrifugation tube.
18. Ultracentrifuge the lysate for 30 min at 218,000 × *g* at 4 °C and transfer the supernatant to a fresh 50 mL conical centrifuge tube. At this point, the lysate can be stored at –20 °C if desired.
19. Add 1 mL Ni-NTA affinity resin to the lysate and let it stir gently for 2 h at 4 °C.
20. Equilibrate a polypropylene column with 1–2 mL lysis buffer 2, avoiding formation of bubbles (*see* **Note 21**).
21. Load 5 mL of the lysate/resin mixture onto the polypropylene column containing lysis buffer 2. Open the lower cap of the column and let the buffer run out until the formation of a resin column is visible. Add the rest of the mixture and collect the flow-through (*see* **Note 22**).
22. Let the entire lysate run through, but do not let the column run dry.
23. Wash the column with 5 mL of wash buffer 1 and then with 5 mL of wash buffer 2. Collect both fractions separately.
24. Elute the protein with 6× 200 µL aliquots of elution buffer and collect each fraction.
25. Immediately add 80 µL of glycerol to each eluted fraction (final percentage: 40%), mix and freeze the samples at −20 °C.
26. Perform an SDS-PAGE with 10 µL of each fraction collected. The protocol for casting the Phos-tag acrylamide gel described in Subheading 3.3 can be used for a conventional SDS-PAGE, but omit the addition of the Phos-tag acrylamide and the $MnCl_2$.

27. When the dye front has reached the end of the gel, stop the electrophoresis and take the gel out of the cassette.
28. Wash the gel in deionized water for 5 min and incubate it for 30 min in the staining solution with gentle agitation.
29. Wash the stained gel in deionized water for 5 min and destain for 2 h in destaining solution. Leaving the gel overnight in deionized water with gentle agitation will help to reduce the background.
30. Choose the fractions with the highest yields of your protein for dialysis (*see* **Note 23**).
31. Pipette one or two eluted fractions into a dialysis cassette (Slide-A-Lyzer™ Dialysis Cassettes, 10K MWCO, 0.5 mL) with a syringe. Attach the cassette to a float buoy and incubate in 400 mL of dialysis buffer for 2 h at 4 °C with constant gentle stirring.
32. Discard the dialysis buffer and repeat the dialysis step with fresh buffer for another 2 h.
33. Change the dialysis buffer again and incubate for 16 h.
34. Use a syringe to recover the protein from the dialysis cassette and store the dialyzed protein at –20 °C.
35. Determine the concentration of the dialyzed protein using the Bradford protein assay.

3.2 Phosphorylation Assay Using Radioactively Labeled ATP

The following protocol is an example for a radioactive phosphorylation assay with a sample volume of 10 µL to test an inhibiting compound at different concentrations (*see* **Note 24**).

1. Pipette ultrapure water, 1 µg of the histidine kinase, 1 µL 85 mM Triton X-100 (final concentration: 8.5 mM) and 2 µL 5× phosphorylation buffer to each reaction tube (*see* **Note 25**).
2. Add 1 µL of different dilutions of the compound (histidine kinase inhibitor) to each reaction and incubate for 10 min at 15 °C (*see* **Note 26**).
3. Add the desired volume of ^{33}P-ATP to each reaction and incubate for 30 min at 15 °C (*see* **Note 27**).
4. Stop the reaction with 10 µL 2× Laemmli SDS sample buffer with 1:20 β-mercaptoethanol (*see* **Note 28**).
5. Load the samples and 2 µL of prestained protein ladder to a Bis-Tris precast gel, and add the according MOPS SDS running buffer. Run at a constant voltage of 180 V for approximately 1 h until the dye front reached the end of the gel.
6. Disassemble the gel cassette and cut approximately 1 cm from the upper and the lower end. Use the pre-stained bands of the protein marker as a guide to ensure that the region where you expect the protein bands remains intact (*see* **Note 29**).

7. Heat seal the gel into a translucent small autoclave bag.
8. Expose the gel to a storage phosphor screen or x-ray film. Phosphor imaging plates are much more sensitive, an exposure time of 30–90 min should be sufficient. An overnight exposure is recommended for x-ray films (*see* **Note 30**).
9. Scan the phosphor imaging plate using a phosphor imager or develop the x-ray film.
10. After autoradiography, wash the gel in deionized water for 5 min and incubate it for 30 min in the staining solution with gentle agitation (*see* **Note 31**).
11. Wash the gel in deionized water for 5 min and destain for 2 h in destaining solution. Leaving the gel overnight in deionized water with gentle agitation will help to reduce background.
12. Heat seal the gel in a translucent plastic bag and scan to obtain a high-quality digital image.
13. For a more precise analysis, use the software provided with the storage phosphor screen or any other quantification software to identify the intensity of the bands. The phosphorylation activity can be defined as the intensity of the radioactive band per protein band. Use the control sample without the inhibitor as a reference to analyze any reduction of autophosphorylation activity (*see* **Note 32**).

3.3 Phosphorylation Assay Using Phos-tag Acrylamide

Casting of a resolving (7%) gel containing 50 μM Phos-tag acrylamide and 100 μM $MnCl_2$ with a total gel volume of 8 mL (or 7.5 mL for the 8% resolving gel) and a 4% stacking gel with a volume of 4 mL (*see* **Notes 33** and **34**). Cast an 8% resolving gel with a total gel volume of 7.5 mL for western blotting, containing the Phos-tag acrylamide $MnCl_2$-concentrations above (*see* values in brackets and **Note 34**).

1. Mix 5.11 mL (4.53 mL) ultrapure water, 1.4 mL (1.5 mL) of 40% (w/v) acrylamide/bisacrylamide (37.5:1), 1.33 mL (1.25 mL) of the resolving gel solution, 80 μL (75 μL) of 10 mM $MnCl_2$ and 80 μL (75 μL) of 5 mM Phos-tag acrylamide in a 50 mL conical centrifuge tube and vortex. Adjust the volumes when you have a different resolving gel volume (*see* **Note 35**).
2. Ensure you have the gel casting apparatus prepared under a fume hood before continuing with the next steps (*see* **Note 36**).
3. Add 104 μL (97.5 μL) of 21 mg/mL APS and 5.36 μL (5.03 μL) of TEMED to the resolving gel and vortex (*see* **Note 37**).
4. Pipette the mixture quickly between the glass plates, while avoiding formation of bubbles.

5. Overlay the gel with 1 mL 2-propanol and leave it to polymerize for 30 min.
6. Decant the 2-propanol from the casting apparatus and allow it to evaporate for a few minutes.
7. Mix 3.12 mL ultrapure water, 0.4 mL of 40% (w/v) acrylamide/bisacrylamide (37.5:1) and 0.48 mL of the stacking gel solution in a 50 mL conical centrifuge tube and vortex.
8. Add 128 μL of 21 mg/mL APS and 3.2 μL of TEMED and vortex.
9. Pipette the mixture onto the resolving gel and fill up the gel cassette. Insert the well comb immediately and let the stacking gel polymerize for 30 min.
10. Transfer the Phos-tag gel from the casting apparatus into the electrophoresis cell. Fill the inner and the outer tank with SDS-PAGE running buffer and remove the well comb carefully from the gel.
11. Perform the phosphorylation assay of the kinase as described in Subheading 3.2 for the radioactive assay but use non-radioactive ATP.
12. Add 1 μL of the 10 mM ATP solution to start the phosphorylation reaction (*see* **Note 38**).
13. Load the samples into the wells and run the gel at a constant current of 30 mA. Phos-tag gels run more slowly than a conventional acrylamide gel, and it takes about 2 h for a run to complete. The voltage will increase continuously (*see* **Note 39**).
14. When the dye front reaches the end of the gel, stop the electrophoresis and take the gel out of the cassette.
15. Perform the staining and destaining as described above in Subheading 3.1 for the SDS PAGE (*see* **Note 40**). For western blotting, leave the gel unstained and continue with **step 13** in Subheading 3.5.

3.4 Construction of the WalR-FLAG Strain

1. In a 250 mL Erlenmeyer flask, inoculate 50 mL of BHI broth to an OD_{600} of 0.5 with an overnight culture of the target *S. aureus* strain, incubate in a water bath at 37 °C with constant shaking at 200 rpm and grow to an OD_{600} of 1 (~40 min).
2. Centrifuge at 7000 × *g* at 4 °C for 5 min to pellet the cells. Wash the pellet twice with 50 mL of ice cold MilliQ water and once with 10 mL of ice cold 10% glycerol. Finally, resuspend the pellet by pipetting with 1 mL of 10% glycerol and then make up to 10 mL. Centrifuge and resuspend the pellet in 10% glycerol and dispense in five equal aliquots. Freeze the electrocompetent cells at −70 °C.

3. Thaw electro-competent cells on ice (~5 min), centrifuge at 5000 × *g* for 3 min at room temperature and pipette off the supernatant. Resuspend the cells in 80 μL of room temperature 10% glycerol with 500 mM sucrose by pipetting.
4. Add 1–5 μg of the purified pIMAYZ allelic exchange construct (up to 10 μL) (*see* **Note 41**) isolated from the correct IMxxB *E. coli* strain (*see* **Note 42**) to obtain the maximal transformation efficiency. Transfer the cells to a 1 mm electroporation cuvette at room temperature and pulse at 2.1 kV/cm, 100 Ω, and 25 μF. Immediately add 1 mL of BHIS, pipette up and down three times, transfer to a sterile tube and incubate at 28–30 °C with shaking at 200 rpm for 1 h.
5. Spread plate 100 μL of the regenerated cells onto BHIA-CX and incubate at 30 °C for 24–48 h. Centrifuge (7000 × *g* for 5 min) the remaining ~900 μL, resuspend the pellet in 100 μL of BHIS and spread plate onto BHIA-CX and incubate at 37 °C for 18–24 h.
6. In some strains of *S. aureus*, for example, Newman or JE2, "direct" integration of pIMAYZ can be selected on the 37 °C plate as larger blue colonies in a lawn of yellow/white colonies. Single colony purify (SCP) the blue colonies on BHIA-CX and incubate overnight at 37 °C. If "direct" integration is not possible (called the "slow" protocol), homogenize a colony from the 30 °C plate in 200 μL of PBS and serially dilute to 10^{-4}. Spread plate 100 μL of the undiluted and spot plate 10 μL of the dilutions on separate BHIA-CX plates. Incubate at 37 °C overnight. SCP six blue colonies on BHIA-CX and incubate at 37 °C overnight.
7. From the SCP integration plates (either "direct" or from the "slow" protocol), pick two colonies, inoculate into separate 10 mL BHI broths and grow overnight at 30 °C with shaking at 200 rpm. Serially dilute the overnight broths in PBS to 10^{-6}, plate 50 μL of the 10^{-5} and 10^{-6} dilution onto BHIA-X and incubate at 37 C overnight.
8. Preform colony PCR on white colonies (*see* **Note 43**), SCP onto BHIA-X and incubate overnight at 37 °C. Run the PCR on a 2% agarose gel with the wild-type product at 174 bp and the WalR-FLAG clones exhibiting a shift to 245 bp.
9. From positive WalR-FLAG containing clones, inoculate 10 mL BHI broths, incubate overnight at 37 °C with shaking at 200 rpm. Isolate genomic DNA with a Genomic DNA purification kit, including 10 μg/mL lysostaphin (in the lysis step). Repeat PCR on genomic DNA, stock correct clones at −70 °C and whole genome sequence (e.g., Illumina, Nanopore or PacBio) (*see* **Note 44**).

3.5 In Vivo Phosphorylation Assay Using Phos-tag Acrylamide and Western Blotting

1. In a 3 L Erlenmeyer flask, inoculate 1 L of TSB with 1 mL of an overnight culture of the test strain that produces the WalR-Flag fusion and incubate in a water bath at 37 °C and with constant shaking (60 rpm). Observe the growth by measuring the absorbance at 600 nm with a spectrophotometer every 30 min. If the phosphorylation status of two or more strains is compared, the OD_{600} of the pre-culture should be measured to adjust the starting-OD_{600} to the same value.
2. Set the centrifuge temperature to 4°C.

   Perform all following steps on ice or in the cold room.
3. Take samples of the cultures at 120, 150, 180, 210, 240, 300, and 360 min after inoculation, which should comprise samples from exponential to the early stationary phase of growth (*see* **Note 45**). The harvested volume depends on the OD_{600} reached at this specific time point in the growth curve (see table 1) (*see* **Note 46**).
4. Immediately mix the sample volume 1:1 in ice-cold ethanol/acetone. This prevents further modulation of the phosphorylation status of the observed response regulator.
5. Harvest the cells by centrifuging the culture at 7300 × *g* for 5 min at 4 °C. Decant the supernatant.
6. Resuspend the pellet in 20 mL MilliQ water, transfer the solution to a sterile 50 mL conical centrifuge tube. Centrifuge at 14,580 × *g* for 5 min at 4 °C and decant the supernatant. At this point, the pellet can be stored at −20 °C (*see* **Note 17**).
7. Prepare Precellys24 tubes with 0.1 mm glass beads. The ratio of cell suspension to glass beads should be 1:3 (v/v). Resuspend the cell pellets in 250 μL TBS and transfer the cell suspension into the Precellys24 tubes.

Table 1
Assignment of measured OD_{600} of the main culture and harvested culture volume

OD_{600}	Culture volume harvested [mL]
0.125	150
0.25	100
0.5	50
0.8	25
1.2	20
2	10
2.5	10

8. Disrupt the cells by bead beating (3 × 30 s at 5000 rpm, with pauses of 120 s).
9. Centrifuge the cell lysate at 7380 × *g* for 5 min at 4 °C and transfer 100 µL into a sterile 1.5 mL reaction tube. Repeat the centrifugation step to remove as much of the cell debris/glass beads as possible and transfer 80 µL of the supernatant into a fresh 1.5 mL reaction tube.
10. Determine the protein concentration of the lysate using the Bradford protein assay.
11. Use 10 µg protein per sample, make up to 10 µL with TBS and add 10 µL 2× Laemmli SDS sample buffer with 1:20 β-mercaptoethanol (*see* **Note 28**). Freeze the samples or run the Phos-tag gel immediately.
12. Cast and run a Phos-tag gel as described in Subheading 3.3, then continue as described below.
13. Wash the gel twice in transfer buffer containing EDTA and once in transfer buffer without EDTA for 20 min each, with gentle agitation (*see* **Note 47**).
14. Meanwhile soak two blot papers in transfer buffer. Wash the PVDF membrane in ethanol for 30 s and then in water 2 min, and incubate the PVDF membrane for at least 10 min in transfer buffer (*see* **Note 48**). All washing steps should be carried out with gentle agitation.
15. Arrange the transfer sandwich as follows for the semidry western-blot:

    Anode – Blot paper – PVDF membrane – Gel – blot paper – Cathode (*see* **Note 49**).
16. Remove air with a blot roller or an empty glass tube and blot the gel onto the PVDF membrane with 25 V at 1 A for 60 min.
17. Block the membrane with blocking buffer (0.5 g Easy blocker in 10 mL TBS-T) in a rotating conical centrifuge tube overnight.
18. The Anti-FLAG M2-Horseradish peroxidase (HRP) (Sigma, A8592) is used for detection of the FLAG-tagged WalR, including the phosphorylated and the non-phosphorylated protein, which should have been separated by the Phos-tag SDS PAGE. Add 10 µL of the Anti-FLAG M2-HRP to 10 mL blocking buffer (1:1,000), pour over the PVDF membrane and incubate for 1 h at room temperature with gentle agitation (*see* **Note 50**).
19. Wash the membrane three times for 5 min with 20 mL TBS-T with agitation to remove unbound antibody (*see* **Note 51**).
20. The antibody is visualized by the HRP-activity. Place the membrane in a clean tray, pipette the chemiluminescent substrate

(we used the Western Sure® Premium Chemiluminescent Substrate (LI-COR) with a volume of 4 mL) directly on the membrane, incubate for 5 min, and scan the membrane with high sensitivity (*see* **Note 52**).

21. Image the membrane with a chemiluminescent imaging system. Determine the relative intensity of the phosphorylated and non-phosphorylated protein bands and calculate the ratio (*see* **Note 32**).
22. Optimize your sample concentration. The concentration of your protein of interest might vary throughout the different growth phases, so the signal intensity of some of your samples in the western blot might need optimization. Therefore, optimize the sample volumes in two steps:
    (a) Calculate the modification factor: Calculate the sum of the relative intensities of the phosphorylated and non-phosphorylated band in each lane. Choose the lane with the optimal signal intensity; here, the sample volume will be maintained, so the modification factor is 1. For the residual samples, divide the sum of relative intensities of the samples by optimal signal intensity. Multiply the originally used sample volume with this factor.
    (b) Limit your sample volume: Divide the sample volume (we used 10 μL) by the largest sample volume you calculated in the previous step. Multiply the calculated sample volumes with this factor. As before, fill up the sample volume with TBS to a total of 10 μL. Then, repeat the Phos-tag PAGE and western blot.

4 Notes

1. LB is a standard medium and works fine for most applications. However, when facing good purity but low yield of the purified protein, different media can be tested to increase the final cell weight. Try "terrific broth": Dissolve 12 g tryptone, 24 g yeast extract, and 5 g glycerol in 900 mL deionized water. In another flask, dissolve 2.31 g KH_2PO_4 (170 mM) and 12.54 g K_2HPO_4 (720 mM) in 100 mL deionized water. Autoclave separately and after cooling mix the components prior to use. Note that a high cell density does not necessarily result in a higher protein purity.
2. Other detergents are also suitable and other groups use Triton X-100. If you are not sure, perform a small-scale screening to check which detergent works best for your protein.
3. β-Mercaptoethanol decomposes within hours and impacts the pH, as well as temperature. Let the buffer cool down, add

β-mercaptoethanol, and adjust the pH prior to use. There are several guides like this one that describe a purification method. You need to know the function of every component in your purification buffer and adjust it to your personal purification strategy. The method described here however worked well for all full-length histidine kinases from Gram-positive bacteria we have tested so far.

4. You can also use DNaseI and RNaseA instead of benzonase according to the manufacturer's instructions.
5. Similar to β-mercaptoethanol, DTT decomposes within hours. Prepare the 5× phosphorylation buffer without DTT and add DTT to a 1 mL aliquot prior to use and discard the buffer afterward. You can also create a phosphorylation buffer without KCl and add different concentrations of KCl to the reactions to check which concentration works best.
6. Precast gels are easier to handle when using radioactive material.
7. Add methanol directly to the tube containing Phos-tag acrylamide. It is sticky and must be fully dissolved before use.
8. Without heating it will not dissolve. Use an incubator (~60 °C).
9. This staining method worked best for the gels we created so far. There are also other staining methods, like silver staining or Colloidal Blue Staining that uses the more sensitive Coomassie G250 instead of R250.
10. For us, lysostaphin from Ambi worked best (www.lysostaphin.com).
11. Transfer buffers without SDS are better. Prepare the buffer the day before blotting and give it time to cool down to overcome the heat generated during the transfer of proteins from the gel to the membrane.
12. The most commonly used membranes are polyvinylidene fluoride (PVDF) and nitrocellulose. PVDF is resilient and stable and better for protein retention.
13. The addition of a mild detergent in wash and blocking buffers is helpful to avoid nonspecific bands in the western blots. Give your blocking buffer time to dissolve. Particulates can be removed by filtering.
14. Enhanced chemiluminescence (ECL) allows the detection of pico and femto grams of target protein.
15. The protein should be encoded on a vector with an inducible promoter (e.g., with IPTG). Novagen's pET expression systems always worked well for our requirements and offer a broad range of different affinity tags and purification strategies. A C-terminal 6x His-tag without a leader peptide worked well

for the histidine kinases we have tested so far. We also use a plasmid-encoded chaperone in some of our expression strains to prevent the formation of inclusion bodies. The so-called "Walker strains" *E. coli* C41(DE3) and C43(DE3) are recommended as expression hosts [12]. The cloning strategy is described in the literature [13].

16. There is no ideal protocol for protein expression/purification, and it has to be optimized for each protein. The expression can alter with incubation duration and temperature. Even other growth conditions like shaking frequency, flask shape or the apparatus used for incubation can change the expression. It is recommended to search for the best expression conditions by performing a small-scale screening. In our case, a large Erlenmeyer flask with a proportionate low culture volume incubated in a traditional water bath and a moderate shaking frequency gave the best results. Observe the growth of your culture after induction of the expression. When the culture stops growing after a short time, your protein seems to inhibit growth of the expression strain. Nevertheless, the expression can still work, but formation of inclusion bodies can occur.
17. A good trick to overcome the problematic resuspension of big and sticky cell pellets is to shake two sterile glass marbles carefully in the centrifuge tube.
18. Removing as much of the cell debris as possible is crucial to increase the flow rate of the gravity-flow columns. Three centrifugation steps help reduce the contamination with cell debris.
19. Split the lysate in several small centrifugation tubes if necessary and combine them afterward.
20. Any remaining cell debris visible as dark residue that cannot be resuspended will be pelleted in the next ultracentrifugation step.
21. Any air inclusions around the membrane inside the polypropylene column slow down the gravity-flow column.
22. Gravity-flow columns can take some time to run through. Do not use pressure or the resin becomes more compressed, which will additionally slow down the flow rate.
23. Check for co-purified contaminating proteins. Sometimes fractions that are more pure rather than having the most protein are the better option to choose.
24. The sample volume is limited to the well size of the SDS-PAGE gel used and can be increased if needed. A time series measurement of the autophosphorylation activity can be performed using a bigger volume, taking small samples at different time points. To test different conditions like temperature or

concentration of inhibitory substances, small-scale single reactions in small reaction tubes are recommended.

25. Decide how much of the histidine kinase you want to use. A 1 μg aliquot is a good amount to start with, making it easily detectable by Coomassie stain.
26. Dilute the tested compound to obtain a wide range of concentrations in the assay starting with 10 μg/mL and going up to 10 mg/mL. Because many compounds require a special solvent for solubility, use the solvent for dilution and create a control sample only using the solvent. For many hydrophobic compounds, DMSO is used, which does not interfere with this assay in our experience.
27. The signal strength can be adjusted by altering the assay conditions. You can use more radioactive material but note that this will also increase the background signal. It is recommended to first screen for a suitable signal strength using different temperatures and incubation times. We have encountered different properties of each histidine kinase and how they react to assay conditions and buffer components like alkali salts. Follow the manufacturer's instructions to calculate the volume of labeled ATP needed and create a master mix with ultrapure water to simplify the pipetting. Try 1 μCi of ^{33}P-ATP for 1 μg of the kinase and adjust the concentration when the signal appears too low or too high. For very low activity, ^{32}P-ATP is an option.
28. We experienced that using 2× Lämmli SDS sample buffer with 1:20 β-mercaptoethanol works best to denature the histidine kinase to an extent that allows it run mostly as a monomer in the polyacrylamide gel. Often a weak signal of the histidine kinase dimer remains visible. Do not boil the samples since this will lead to dephosphorylation of the kinase.
29. Cutting of the gel is recommended to reduce the background signal that is present in the wells and the lower end of the gel, where the unbound ATP remains.
30. Increase the exposure time using the same gel when the signal appears to be too weak but note that the background will also increase.
31. It is important to analyze the gel using a conventional acrylamide gel staining like Coomassie Brilliant Blue R250 to ensure that the amount of the histidine kinase does not differ in any of the samples.
32. ImageQuant TL is the software provided with the phosphor imaging system from GE Healthcare. GelAnalyzer 2010a is an alternative software free of charge.

33. Cast the gels just prior to use. According to the manufacturer's instructions Phos-tag acrylamide decomposes within hours.
34. To minimize your background signal, always wear non-powdered gloves, clean all plates and combs with either 1% SDS or 70% ethanol followed by distilled water then wipe them dry. Make sure all other equipment like forceps are also clean.
35. Assemble your gel casting apparatus and check for the exact volume of the resolving gel using water. This will save some of the expensive Phos-tag acrylamide.
36. Using adhesive tape at the lower end of the glass plates helps it to seal properly.
37. The concentration of APS can be increased when facing problems with polymerization. Use a fume hood when pipetting TEMED.
38. A screen with different ATP concentrations is recommended to optimize the assay for each histidine kinase. A high ATP concentration will let the histidine kinase work at full capacity.
39. Use a power supply that is able to run a constant current independently of the voltage. Nevertheless, we always limit the voltage to a maximum of 160 V to avoid heating of the gel.
40. When the separation of the bands is not satisfactory, increase the concentration of Phos-tag acrylamide or/and decrease the total acrylamide/bisacrylamide concentration in the resolving gel. For very low density gels, the addition of agarose is required.
41. The allelic exchange construct can either be assembled by SOE-PCR or synthesized as a gBlock from IDT. For either approach, a region encompassing the entire *walR* gene from the start codon, a 3x-FLAG tag preceding the stop codon and the downstream 500 bp of homology to *walK* is synthesized or amplified. The product is tailed with the regions complementary to either side of the multiple cloning site of pIMAYZ (Tail A: 5′-CCTCACTAAAGGGAACAAAAGCTGGGTACC and Tail D: 5′- CGACTCACTATAGGGCGAATTGGAGCTC). The assembled or synthesized insert can be cloned into pIMAYZ by SLiCE cloning. Finally, high-quality plasmid DNA, free of salts is required for *S. aureus* transformation. Detailed instructions for the entire process can be found here [14].
42. The majority of *S. aureus* strains produce a strong restriction modification barrier comprising type I and type IV components. *E. coli* strains have been constructed to bypass type IV (recognizes cytosine methylation at 5′-S^{5m}CNGS-3′) through the deletion of the *dcm* gene and the addition of *S. aureus*

clonal complex (CC) specific type I adenine methylation (*hsdMS* genes) yielding IM01B (CC1), IM08B (CC8, ST239 and partial CC5), IM30B (CC30), and IM93B (ST93) [15]. It is important to choose the correct IMxxB for the *S. aureus* target strain.

43. Colony PCR. Touch a very small amount of a colony to the side of a PCR tube, add 50 μL of the PCR master mix (0.5 U Phire Hot Start II DNA polymerase and 200 nM of each primer) and conduct a 35 cycle PCR. The only change to the manufacturer's instructions was extending the initial 98 °C denaturation from 30 s to 3 min. We normally screen eight white colonies from each broth plated.
44. Whole genome sequencing is important to rule out additional mutations, especially mutations in regulatory proteins.
45. It is not advisable to take samples in the lag phase or in early exponential phase, because the cell density is too low to yield a good signal in the western blot. Pay attention to the growth-phase dependent expression of your protein of interest and possibly adapt the time points of sampling.
46. For reliable OD-measurements, dilute your samples 1:10 in medium when the culture reaches an OD_{600} above 0.3.
47. Equilibration of the gel in transfer buffer prevents changes in the size during transfer.
48. PVDF membranes will not wet from just being placed into transfer buffer, because they are hydrophobic. Do not let the membrane dry during the blotting process.
49. When adding the buffer soaked PDVF membrane to the gel, keep off excess liquid. The membrane should be in between the gel and the positive electrode (anode, red side).
50. Avoid temperature changes to protect the antibody, for example, carry them in a mini-cooler. Test a series of different concentrations of your antibodies and work out which one gives you the best/cleanest band on your blot. The correct speed of the shaker will determine if the antibody binds uniformly to the membrane.
51. Adjust the buffer volume to the size of your blot. Increase the number of washing steps (to 5 or 6) or sightly increase the concentration of detergent during the washing steps, if the background signal is very strong. But avoid excessive washing, as it reduces your signal.
52. Use multiple exposure lengths to identify the most optimal exposure time.

References

1. Fritz G, Mascher T (2014) A balancing act times two: sensing and regulating cell envelope homeostasis in *Bacillus subtilis*. Mol Microbiol 94:1201–1207
2. Villanueva M, García B, Valle J et al (2018) Sensory deprivation in *Staphylococcus aureus*. Nat Commun 9:523
3. Gotoh Y, Eguchi Y, Watanabe T et al (2010) Two-component signal transduction as potential drug targets in pathogenic bacteria. Curr Opin Microbiol 13:232–239
4. Matsushita M, Janda KD (2002) Histidine kinases as targets for new antimicrobial agents. Bioorg Med Chem 10:855–867
5. Schreiber M, Res I, Matter A (2009) Protein kinases as antibacterial targets. Curr Opin Cell Biol 21:325–330
6. Boyle-Vavra S, Yin S, Daum RS (2006) The VraS/VraR two-component regulatory system required for oxacillin resistance in community-acquired methicillin-resistant *Staphylococcus aureus*. FEMS Microbiol Lett 262:163–171
7. Francis S, Wilke KE, Brown DE et al (2013) Mechanistic insight into inhibition of two-component system signaling. Med Chem Comm 4:269–277
8. Stephenson K, Yamaguchi Y, Hoch JA (2000) The mechanism of action of inhibitors of bacterial two-component signal transduction systems. J Biol Chem 275:38900–38904
9. Kinoshita E, Kinoshita-Kikuta E, Takiyama K et al (2006) Phosphate-binding tag, a new tool to visualize phosphorylated proteins. Mol Cell Proteomics 5:749–757
10. Monk IR, Shaikh N, Begg SL et al (2019) Zinc-binding to the cytoplasmic PAS domain regulates the essential WalK histidine kinase of *Staphylococcus aureus*. Nat Commun 10:3067
11. Gajdiss M, Türck M, Bierbaum G (2017) Bacterial histidine kinases: overexpression, purification, and inhibitor screen. Methods Mol Biol 1520:247–259
12. Miroux B, Walker JE (1996) Over-production of proteins in *Escherichia coli*: mutant hosts that allow synthesis of some membrane proteins and globular proteins at high levels. J Mol Biol 260:289–298
13. Türck M, Bierbaum G (2012) Purification and activity testing of the full-length YycFGHI proteins of *Staphylococcus aureus*. PLoS One 7: e30403
14. Monk IR, Stinear TP (2021) From cloning to mutant in 5 days: rapid allelic exchange in *Staphylococcus aureus*. Access Microbiol 3:193
15. Monk IR, Tree JJ, Howden BP et al (2015) Complete bypass of restriction systems for major *Staphylococcus aureus* lineages. MBio 6: e00308–e00315

Chapter 18

Sample Preparation for Mass Spectrometry-Based Absolute Quantification of Bacterial Proteins in Antibiotic Stress Research

Sandra Maaß, Minia Antelo-Varela, Florian Bonn, and Dörte Becher

Abstract

Absolute protein quantification is an essential tool for system biology approaches and elucidation of stoichiometry of multi-protein complexes. In this updated chapter, a universal protocol for gel-free absolute protein quantification in bacterial systems is described, which provides adapted methods for cytosolic and membrane proteins. This protocol can be used for sample preparation prior to miscellaneous mass spectrometry-based quantification workflows like AQUA, Hi3, and emPAI. In addition, a focus has been set to the specific challenges in antibiotic stress research.

Key words Gel free proteomics, Sample preparation, Absolute protein quantification, Cytosol, Membrane, In-solution digest, S-trap, Mass spectrometry, Antibiotic stress response

1 Introduction

Antibiotics trigger stress responses in bacteria, when the cells try to adapt their metabolism and cell envelope to the treatment. As metabolism and the structure of the cell surface are driven by enzymes, necessary adaptations to antibiotic stress or resistance development are connected to changes in the cellular and membrane proteome. Proteomics is a valuable tool to understand antibiotic action and bacterial resistance mechanisms in multiple ways. For example, 2D gel-based signature libraries can help to elucidate the mode of action of new, antibacterial compounds. As the focus of this chapter is gel-free proteomics, an excellent review from the group of Julia Bandow is recommended for readers, who are interested in 2D gel-based proteomics in antibiotic research [1].

Besides the development on new drugs, the elucidation of bacterial resistance mechanism is a main issue in antibiotic research. Proteomic studies can help to understand the physiological adapta-

Peter Sass (ed.), *Antibiotics: Methods and Protocols*,
Methods in Molecular Biology, vol. 2601, https://doi.org/10.1007/978-1-0716-2855-3_18,

tions in resistant strains [2]. Another option to study antibiotic action and bacterial adaptation is the treatment of nonresistant bacteria with antibiotics in stress experiments. For elucidation of changes in the proteome of resistant strains compared to sensitive strains or the analysis of the antibiotic stress response, all kinds of quantitative proteomic techniques can be applied. An overview about the technical possibilities in quantitative microbial proteomics can be found in a review by Otto et al. [3].

Mass spectrometry (MS)-based proteomics is in principle only suitable for relative quantification, which allows for the comparison of protein abundances between different samples. However, relative quantification does not compare the concentration of different proteins within one sample. This objective can be achieved by determination of absolute protein amounts in a single sample or even in a single cell. Several strategies for absolute protein quantification have been established, which enable estimations on protein copy numbers per cell. This data can be used for determination of stoichiometry within physiological or functional protein complexes or for kinetic calculations of biochemical reactions. Global absolute proteome studies are therefore extremely helpful for the examination of complex metabolic adaptations like in antibiotic-resistant bacterial isolates or in antibiotic stress experiments.

Absolute protein quantification in prokaryotic systems has been reviewed extensively [4]; therefore, in this chapter, only a brief overview is provided. For absolute protein quantification by MS, the addition of reference peptides or proteins of known amount is crucial. One commonly used approach to achieve highest accuracy is based on reference peptides, which were derived from the target protein, labeled with stable isotopes (^{2}D, ^{13}C, ^{15}N), and spiked into the digested cell extract. By comparison with the spiked heavy isotope of known amount, the natural homologues of the isotopically labeled peptides can be quantified [5, 6]. However, due to the requirement of isotopically labeled peptides of the target proteins, these approaches are limited to a rather small number of proteins. Calibrating 2D gels with reference proteins brought absolute quantification to a nearly global scale [7]. As 2D gel-based analyses are time-consuming and incompatible with membrane proteins, gel-free approaches are nowadays preferred by most research groups. Gel-free absolute quantification of a large number of proteins in one sample can be achieved via the combined (and eventually corrected) intensities or spectral counts of detected peptides [8–11], which are then compared to unlabeled reference proteins of known amounts to determine absolute intensities. All approaches have advantages and drawbacks, but in most cases, the choice will be made on the availability of the necessary instrumentation and the scale of the experiment to be performed. Absolute protein quantification of membrane proteins imposes additional challenges due to the characteristics of this specific subset of

proteins, namely, their low abundance and their highly hydrophobic nature. Hence, membrane proteins need to be enriched from whole cell lysates, and their complete digestion requires adapted protocols. One of the digestion protocols compatible with the high concentrations of sodium dodecyl sulfate (SDS) used during enrichment of membrane proteins is based on suspension trapping (S-Trap) [12]. In this method, a fine protein particulate suspension is created, trapped in a stack of filtration material, and residual SDS is washed away. Proteins are digested in the filter before analysis via MS. In order to still be able to determine absolute protein amounts of membrane proteins from mass spectrometric data, enrichment and correction factors need to be considered, for example, which could be obtained from targeted MS of selected native membrane proteins and the corresponding isotopically labeled peptides [13].

As the protocols for sample preparation prior to absolute quantification of microbial proteins are dependent on the analyzed organisms, subproteomic fraction, and selected quantification approach, a general suggestion of a suitable workflow is not possible. However, sample preparation requirements are very similar for all gel-free workflows. Complete extraction and unbiased determination of protein concentration is crucial for absolute quantification, whereas digestion of the target proteins needs to be adapted toward the specific class of proteins. To determine copy numbers per cell and protein concentration in the cell exact determination of cell number and cellular volume in a given sample is essential.

In this chapter, we update our previously described workflow for complete extraction, digestion, and sample purification for gel-free proteomic analyses and absolute quantification of cytosolic proteins [14]. We now also provide protocols for subcellular fractions and preparation of membrane proteins, which are compatible with absolute proteins quantification approaches. Although the protocols have been initially developed for gram-positive bacteria, especially *Bacillus subtilis* and *Staphylococcus aureus*, they can be applied to other microorganisms. However, in these cases especially the cell lysis efficiency should be monitored carefully.

Furthermore, a focus is set on the specific challenges in the elucidation of antibiotic stress responses, which take effect especially in the first steps of the workflow. Antibiotics can induce morphological changes, which influence the number of cells per mL and OD unit. In addition, the composition and thickness of the cell wall and membrane can be influenced by antibiotics, which could lead to a decrease in cell disruption efficiency. For a calculation of proteins per cells, the number of harvested cells as well as the disruption efficiency are crucial information, as it is absolutely essential to know the number of cells, which were disrupted in the experiment. In this protocol, mechanical cell disruption by glass beat beating is suggested, which is an excellent choice for many gram-positive and gram-negative species. In some cases,

other cell-disruption methods may be favorable. It is recommended to test different cell lysis strategies and choose the most effective in terms of cell disruption efficiency and protein yield.

2 Materials

Prepare all solutions in MilliQ quality water and use MilliQ quality water for all dilutions. Prepare and store all reagents at ambient conditions if not indicated elsewise.

2.1 Cell Counting

1. A Neubauer cell counting chamber or an alternative device, which allows for effective cell counting with your organism of choice.
2. Physiological saline: Solve 900 mg NaCl in water. Autoclave or sterile filter the solution.

2.2 Cell Harvest and Lysis

1. TE buffer: 20 mM Tris−HCl, 10 mM EDTA, pH 7.5. Dissolve 2.4 g Tris base and 2.92 g EDTA in 0.9 L water. Adjust the pH to 7.5 with hydrochloric acid and add water to a final volume of 1 L.
3. A ribolyzer.
4. Glass beads with a diameter of approximately 0.1 mm.
5. Low binding reaction tubes.

2.3 Determination of Protein Concentration

1. 10 mg/mL BSA (bovine serum albumin) stock solution: Solve 10 mg BSA in 1 mL of water and store in a low binding reaction tube. Otherwise, dilute higher concentrated BSA solutions (*see* **Note 1**).
2. BSA solutions: Prepare solutions with the following BSA concentrations by diluting the BSA stock solution in TE buffer: 0.25 μg/μL, 0.5 μg/μL, 1.0 μg/μL, 1.5 μg/μL, 2.0 μg/μL, 4.0 μg/μL, 6.0 μg/μL, 8.0 μg/μL, 10.0 μg/μL.
3. Concentrated hydrochloric acid (37%)
4. Stannous chloride solution: Dissolve 1 g $SnCl_2$ in 10 mL ethylene glycol (*see* **Note 2**).
5. Sodium acetate buffer: Solve 54.4 g sodium acetate in 20 mL acetic acid and fill up to 95 mL with water. Adjust pH to 5.5 with NaOH solution and fill up to 100 mL with water.
6. Ninhydrin solution: Solve 1 g ninhydrin in 37.5 mL ethylene glycol and 12.5 mL sodium acetate buffer. Mix carefully in the dark until all ninhydrin is dissolved (at least 1 h). This solution should be stored only for few hours. Directly before adding the ninhydrin solution to the sample, add 1.25 mL stannous chloride solution to the ninhydrin reagent (*see* **Note 2**).
7. Lightproof reaction tubes (e.g., brown reaction tubes).

2.4 Enrichment of Membrane Proteins

1. TE buffer: 20 mM Tris–HCl, 10 mM EDTA, pH 7.5. Dissolve 2.4 g Tris base and 2.92 g EDTA in 0.9 L water. Adjust the pH to 7.5 with hydrochloric acid and add water to a final volume of 1 L.
2. High-salt buffer: 20 mM Tris–HCl, 10 mM EDTA, 1 M NaCl, pH 7.5. Dissolve 58.44 g NaCl in 0.9 L TE buffer. Add TE buffer to a final volume of 1 L.
3. Alkaline carbonate buffer: 10 mM EDTA, 100 mM Na_2CO_3, 100 mM NaCl, pH 11. Dissolve 5.3 g Na_2CO_3, 1.46 g EDTA, and 2.92 g NaCl in 400 mL water. Adjust the pH to 11 with NaOH. Fill up to 500 mL with water.
4. 50 mM TEAB: Dilute 0.5 mL of a 1 M TEAB (triethyl ammonium bicarbonate) stock solution with 9.5 mL of water (*see* **Note 3**).
5. 1× SDS (sodium dodecyl sulfate) solubilization buffer: 5% SDS, 50 mM TEAB, pH 7.55. Dilute 5 g SDS in 90 mL 50 mM TEAB. Add 50 mM TEAB to a final volume of 100 mL.
6. An ultracentrifuge.
7. A 360° rotating shaker.

2.5 In-Solution Digest of Cytosolic Proteins and Sample Purification

1. 50 mM TEAB: Dilute 0.5 mL of a 1 M TEAB (triethyl ammonium bicarbonate) stock solution with 9.5 mL of water (*see* **Note 3**).
2. 0.5% RapiGest: Solve RapiGest (Waters) in 50 mM TEAB to a final concentration of 0.5% (w/v).
3. 500 mM TCEP: Dissolve 10 mg TCEP (Tris(2-carboxyethyl) phosphine) in 70 µL 50 mM TEAB. Prepare this solution freshly.
4. 500 mM IAA: Dissolve 10 mg iodoacetamide in 108 µL 50 mM TEAB. Prepare this solution freshly and store in the dark.
5. Trypsin solution: Solve 20 µg of sequencing grade modified trypsin in 100 µL trypsin resuspension buffer (e.g., Promega, delivered together with the trypsin). Prepare shortly before use or prepare aliquots in low-binding reaction tubes and store at −20 °C.
6. Activated trypsin: Incubate trypsin solution at 30–37 °C with vigorous shaking for 10–15 min. Prepare directly before use.
7. Trifluoroacetic acid.
8. Weighted LC-MS sample vials.

For the purification of the generated peptide samples before MS-analysis, the following materials are needed:

9. Methanol.
10. Bulk C18 chromatographic material with a particle size of 5 µm or less
11. Buffer A: Add 10 µL acetic acid (LC-MS quality) to 9.99 mL water.
12. Buffer B: Add 10 µL acetic acid (LC-MS quality) to 9.99 mL acetonitrile (LC-MS quality).
13. Elution solution: Mix 700 µL Buffer B with 300 µL Buffer A (*see* **Note 4**).
14. StageTips (Thermo) (*see* **Note 5**).
15. Gelloader pipette tips (*see* **Note 6**).

2.6 S-Trap Digest of Membrane Proteins and Sample Purification

1. 50 mM TEAB: Dilute 0.5 mL of a 1 M TEAB (triethyl ammonium bicarbonate) stock solution with 9.5 mL of water (*see* **Note 3**).
2. 100 mM TEAB: Dilute 1 mL of a 1 M TEAB stock solution with 9 mL of water (*see* **Note 3**).
3. 2× SDS (sodium dodecyl sulfate) solubilization buffer: 10% SDS, 100 mM TEAB, pH 7.55. Dilute 10 g SDS in 90 mL 100 mM TEAB. Add 100 mM TEAB to a final volume of 100 mL.
4. 200 mM DTT: Dissolve 10 mg dithiothreitol in 324.3 µL 1 M TEAB. Prepare this solution freshly.
5. 200 mM IAA: Dissolve 10 mg iodoacetamide in 270 µL water. Prepare this solution freshly and store in the dark.
6. S-Trap Buffer: Mix 9 mL methanol and 1 mL 1 M TEAB.
7. 12% (w/v) phosphoric acid: Add 210 µL 85% (w/v) phosphoric acid to 1390 µL water.
8. Trypsin solution: Solve 20 µg of sequencing grade modified trypsin in 100 µL trypsin resuspension buffer (e.g., Promega, delivered together with the trypsin). Prepare shortly before use or prepare aliquots in low-binding reaction tubes and store at −20 °C.
9. Activated trypsin: Incubate trypsin solution at 30–37 °C with vigorous shaking for 10–15 min. Prepare directly before use.
10. Elution Solution 2: Dilute 0.1 mL acetic acid with 99.9 mL water.
11. Elution Solution 3: Mix 0.1 mL acetic acid, 60 mL acetonitrile, and 39.9 mL water.
12. S-Trap micro columns (ProtiFi) for every sample.

3 Methods

Handle cells and protein extracts at 4 °C or on ice whenever it is possible.

3.1 Cell Counting

1. Choose an antibiotic concentration for the experiments. We recommend to use a concentration, which will decrease the growth rate by approximately 50% in the exponential growth phase (*see* **Note 7**).
2. Determine the ratio between optical density and cell count. Do this separately for stressed and unstressed or resistant and susceptible strain, respectively. Dilute an aliquot of the culture with physiological saline until you can count individual cells in the Neubauer chamber. It is recommended to count cells at least in four fields with 20–100 cells each in two replicates for every sample (*see* **Note 8**).
3. Calculate the number of cells per mL and OD unit for all samples.

3.2 Cell Harvest and Lysis

1. Take an aliquot of the culture to determine the optical density at the time point of cell harvest.
2. Fill the culture in centrifuge tubes and determine the exact volume either with a measuring cylinder or preferentially by weighing the tubes before and after filling (*see* **Note 9**).
3. Harvest the cells by centrifugation at 4 °C and 8000 × *g*. Choose a centrifugation duration that is sufficient to achieve a stable cell pellet. The duration depends on organism, optical density, and media but is usually between 3 and 10 min.
4. Wash the cells two times with TE buffer. For each washing step, use approximately 0.1 mL TE per mL and OD unit of the original culture. Be careful not to lose any cells during washing.
5. Resuspend the cells in approximately 0.02 mL TE buffer per mL and OD unit of the original culture. Determine the number of cells per mL.
6. Transfer the cell suspension to tubes, which can be used in your ribolyzer and are prefilled with glass beads in a ratio of 1:2. Determine the weight of all tubes without and with cell suspension to determine the exact volume of the suspension.
7. Lyse the cells by beat beating. Three 30 s cycles at 5000 rpm are in most cases sufficient to lyse at least 95% of all cells. Between the cycles cool the cells for 5 min on ice. Determine the number of intact cells per mL by cell counting (see Subheading 3.1).
8. Calculate the cell lysis efficiency (*see* **Note 10**).

9. Pellet cell debris and glass beads by centrifugation at 4 °C and 8000 × *g* for 2 min. Transfer the supernatant to a low binding reaction tube.
10. Pellet the remaining cell debris by centrifugation at 4 °C and 15,000 × *g* for 15 min. Transfer the supernatant to a new low binding reaction tube. Determine the weight of all tubes before and after adding the protein extract to determine the exact volume.
11. Calculate the sample loss during the cell lysis process.
12. Calculate the number of cells which proteins are in your final sample on the base of the number of harvested cells, the cell lysis efficiency, and the sample volume lost during the cell lysis process.

3.3 Determination of Protein Concentration

1. Prepare reaction tubes for all concentrations and add 20 µL BSA solution to each tube. Prepare an additional tube for the blank and add 20 µL TE buffer.
2. Prepare for each sample three reaction tubes with 20 µL protein extract each.
3. Add 20 µL concentrated HCl to all samples (including BSA solutions and blank) and seal the reaction tubes (*see* **Note 11**).
4. Incubate all samples for 24 h at 100 °C to achieve quantitative hydrolysis of all proteins.
5. Cool the samples to room temperature on ice. Be careful as the samples are pressurized and corrosive!
6. Centrifuge all samples for 30 s at 5000 × *g* to remove all liquids from the lid of the tubes.
7. Dilute 10 µL of every hydrolyzed sample with 90 µL water. Further dilute 50 µL of these solutions with 450 µL water to create 1:100 dilutions of the samples (*see* **Note 12**).
8. Transfer 200 µL of each 1:100 dilutions to a lightproof reaction tube.
9. Mix thoroughly with 200 µL water and 600 µL fresh ninhydrin solution (*see* **Note 13**).
10. Incubate for 10 min at 100 °C.
11. Cool the samples shortly on ice. Be careful as the samples are pressurized.
12. Transfer the samples to micro cuvettes and measure absorbance at 575 nm against the blank.
13. Use the BSA samples to create a calibration curve. Calculate the protein concentration of the other samples on the base of this curve.

3.4 Enrichment of Membrane Proteins

1. Use an aliquot of the protein extract with a protein content of 2.5 mg as starting material for membrane preparation
2. Adjust the aliquot volume up to 1.5 mL with TE buffer and subject the sample to ultracentrifugation (1 h, 100,000 × *g* at 4 °C).
3. The supernatant contains soluble proteins, most of them predicted to locate in the cytosol. Hence, this fraction represents the cytosolic proteome sample (*see* **Note 14**).
4. Detach the pellet from the bottom of the centrifugation tube by adding 0.75 mL of high-salt buffer and solubilize the pellet (*see* **Note 15**).
5. Rinse the tip with 0.75 mL high-salt buffer thereby adding the buffer to the sample.
6. Seal the ultracentrifuge tube with parafilm. Incubate in a 360° rotating shaker with 8 rpm at 4 °C for 30 min.
7. Centrifuge at 100,000 × *g* and 4 °C for 1 h. Discard the supernatant.
8. Resuspend the pellet in 1.5 mL alkaline carbonate buffer (*see* **Note 15**).
9. Centrifuge at 100,000 × *g* and 4 °C for 1 h. Discard the supernatant. If necessary, the pellet can be stored at −20 °C until further processing.
10. Resuspend the pellet in 1.5 mL 50 mM TEAB (*see* **Note 15**).
11. Resuspend the pellet in 50 µL 1× SDS solubilization buffer (*see* **Note 15**).
12. The sample is now enriched for membrane proteins.

3.5 In-Solution Digest of Cytosolic Proteins and Sample Purification

1. Transfer samples with a total protein amount of 100 µg per samples to low binding reaction tubes. Fill up to 77 µL with 50 mM TEAB (*see* **Note 16**).
2. Add 20 µL 0.5% RapiGest.
3. If necessary, add undigested reference protein for absolute protein quantification.
4. To reduce disulfide bridges, add 1 µL 500 mM TCEP and incubate the samples for 30–45 min at 60 °C (*see* **Note 16**).
5. Cool the samples shortly on ice and spin down all samples.
6. Add 2 µL 500 mM IAA and incubate for 15 min in the dark at ambient temperature (*see* **Note 16**).
7. Add 2.5 µL activated trypsin and incubate for 5–6 h at 37 °C and shaking (900 rpm) (*see* **Note 16**).
8. To stop the tryptic digest, add 0.5–1 µL trifluoroacetic acid. Check the pH, which needs to be below 3 (*see* **Note 17**).

9. Incubate for 30 min at 37 °C without shaking to precipitate the RapiGest. Mix the samples every 5–10 min by inverting the tubes.
10. Spin down the RapiGest by centrifugation at 20,000 × *g* for 12 min. Transfer the supernatant to a new low binding tube and repeat this step twice.
11. Store the supernatant at −20 °C or proceed with the desalting.
12. For sample purification create a mount for every sample by puncturing a hole of 1.5–2.5 mm diameter in the lid of a 2 mL reaction tube. Cut the StageTip approximately 2 mm below the original C18 and place it in the mount.
13. Resuspend 10 μL chromatographic material per sample in twice the amount of methanol.
14. Add 15 μL of the C18 suspension to every StageTip and sediment it by centrifugation (2000–5000 × *g*, 10–20 s). Add more C18 material until the lower tampered part over the original chromatographic material is filled with C18 material (*see* **Notes 18** and **19**).
15. Wash the C18 material twice with 100 μL Buffer A. Fill the buffer without air bubbles into the tip and squeeze it though by centrifugal forces (8000 × *g*, 1–2 min) (*see* **Note 20**).
16. Wash the chromatographic material twice with Buffer B (*see* **Note 21**).
17. Equilibrate the C18 material with 100 μL Buffer A. Squeeze the buffer until only 1–2 mm of the tip above the custom C18 are filled with liquid. Do not let the C18 material run dry in the following steps (*see* **Note 22**).
18. Fill the samples into the tips, place it directly over the C18 without an air bubble in between.
19. Load the peptides onto the C18 material by squeezing the sample through by centrifugation (8000 × *g*, 1–2 min).
20. Wash the peptide loaded C18 with 100 μL Buffer A. Repeat this step once.
21. Squeeze the rest of the buffer through the C18 with a syringe (syringes are supplied with the StageTips) until the upper layer of the buffer is directly over the C18.
22. Prepare one LC-MS vial for every sample and determine the weight of each vial.
23. Elute the sample with 30 μL elution solution. Use a syringe to squeeze the eluate directly into the prepared vials (*see* **Note 23**).
24. Add 10 μL Buffer A to every sample.

25. Reduce the sample volume to 3–10 µL in a vacuum centrifuge (*see* **Note 24**).
26. Add peptide references for absolute quantification if necessary.
27. Determine the exact sample volume by weight and fill up with Buffer A to a final volume of 100 µL.
28. Prepare aliquots for LC-MS analysis and analyze directly or store at −70 °C.

3.6 S-Trap Digest of Membrane Proteins and Sample Purification

1. Use 10 µg of enriched membrane proteins (*see* **Note 25**). In cases where absolute protein quantification is performed, UPS2 standards should be added to the sample in a 1:4 ratio according to sample amount (e.g., for 10 µg of sample, 2.5 µg of UPS2 standards) (*see* **Note 26**).
2. Fill your sample up to 25 µL with 1× SDS solubilization buffer.
3. Add 0.5 µL of 200 mM DTT and incubate for 10 min at 95 °C.
4. Add 1 µL of 200 mM IAA and incubate for 30 min at room temperature in the dark.
5. Add 2.5 µL 12% phosphoric acid and vortex thoroughly.
6. Add 165 µL S-trap Buffer and vortex thoroughly.
7. Place the S-Trap micro column in a 2 mL reaction tube.
8. Load the sample onto the column by centrifuging at 4000 × *g* until the sample has flowed through (1–2 min) (*see* **Note 27**).
9. Add 150 µL S-trap Buffer for washing and centrifuge at 4000 × *g* until the buffer has flowed through (1–2 min).
10. Repeat the washing from **step 9** three times. Discard the flow-through before the liquid reaches the sample tip.
11. Transfer the S-trap column to a new 1.7 mL reaction tube.
12. Activate an aliquot of trypsin (see Materials).
13. Mix 8 µL 50 mM TEAB with 2 µL activated trypsin per sample to generate the protease solution.
14. Add 10 µL of the protease solution (resulting in a 1:25 ratio amount of trypsin:protein amount) and incubate for 1 h at 47 °C (*see* **Note 28**).
15. Add 40 µL 50 mM TEAB to elute hydrophilic peptides. Centrifuge at 4000 × *g* for 1 min and keep the flow-through.
16. Add 40 µL of Elution Solution 2 to elute intermediate peptides. Centrifuge at 4000 × *g* for 1 min and add the flow-through to the latter one.
17. Add 35 µL of Elution Solution 3 to elute hydrophobic peptides. Centrifuge at 4000 × *g* for 1 min and add the flow-through to the latter ones.

18. Dry the pooled eluted peptides in a vacuum centrifuge. Store the supernatant at −20 °C or proceed with sample purification.
19. For sample purification resuspend the sample in 0.1% acetic acid (*see* **Note 29**).

4 Notes

1. BSA is not easy to resolve completely, and it is recommended to use a commercially available BSA solution with known amount.
2. Ethylene glycol is very viscous, cut the top of the pipette tips before use and pipette very slowly and cautiously.
3. 1 M stock solution is commercially available. Store dilution at 4 °C for a maximum of 2 weeks.
4. Because acetonitrile evaporates faster than water, this solution should not be stored for more than a few hours and the tube should be kept close.
5. Commercially available C18-based solid phase extraction kits for peptide desalting with a binding capacity of at least 100 μg can be used alternatively according to the manufacturer's instructions.
6. The low-cost products normally have a rather wide capillary and are therefore better suited for this protocol.
7. Do not limit yourself to subinhibitory concentrations. If antibiotic stress is induced in the exponential growth phase or later, higher doses of antibiotics can be necessary to induce considerable effects on proteome level.
8. Antibiotics can change the cellular shape dramatically. This also changes the ratio between cell numbers per mL and optical density. The ratio between OD and cell number can be determined in preliminary tests.
9. With standard media a mass density of 1 g per mL can be assumed.
10. If the cell lysis efficiency is below 95%, you should optimize the cell lysis process and eventually test other protocols.
11. There are special clamps available for sealing reaction tubes (e.g., MCP LidLocks, Sorenson), as an alternative you can put a glass plate with some weights on top of the tubes if you boil them in a heating block.
12. Do not forget to vortex the sample before every pipetting step to have it mixed well.
13. The ninhydrin solution is viscous and needs to be pipetted slowly and cautiously.

14. If you aim to only work with the cytosolic proteins, you can omit this centrifugation step and can start the in-solution digest directly with the sample obtained after cell harvest and lysis.
15. Use a small scoop to remove the pellet from the bottom of the tube. The solubilization of the pellet can be supported by pipetting the suspension up and down until the pellet was homogenized and by incubating in an ultrasonic bath for 5 min at room temperature. Take care that the sample does not get too warm during this treatment. Solubilization of the pellet is complete, when it is not visible anymore.
16. The protocol can be scaled down easily to an initial protein amount of 20 μg per sample by linearly adapting the amounts of all reagents. Also, upscaling is possible, but the maximum load of each StageTip should not exceed 150 μg.
17. The pH should not be below 1.5, to avoid acidic hydrolysis. An optimum is a pH between 2 and 3.
18. If C18 material is sticking at the side of the StageTip, you can use either methanol or acetonitrile to flush it.
19. In order to add a comparable amount of C18 material to the single Stage Tips, it is recommended to vortex the slurry thoroughly before every pipetting step.
20. It is preferable to use GELoader Tips for loading as they allow to apply the solvent directly to the column without extended air bubbles.
21. Because of the lower back pressure of acetonitrile, the centrifugation times for squeezing Buffer B are shorter than for Buffer A.
22. Ensure that there is always solvent remaining on top of the column. To do so, the durations for centrifuging have to be adapted. If necessary, the speed of centrifuging can be reduced.
23. Especially if you have a high number of samples, you can put some tissue on top of the forcer of the syringe to protect your finger.
24. Quantitative solvation of peptides without detergents or chaotropes is complicated; therefore, the samples should not run dry!
25. This is the lower limit for the protocol we have tested. Upscaling can be done until 50 μg.
26. UPS2 is the Proteomics Dynamic Range Standard Set, produced from a mixture of 48 individual human source or human sequence recombinant proteins. The protein standard is formulated from six mixtures of eight proteins to present a dynamic range of five orders of magnitude, ranging from

50 pmoles to 500 amoles. This standard can be purchased from Sigma-Aldrich. However, you may add any other proteins standard suitable for absolute proteins quantification.

27. Do not exceed the maximum filling height of 165 µL. Higher sample volumes need to be loaded by centrifuging several times.
28. Make sure you do not leave any bubbles between buffer and tip.
29. Although there is usually no need for subsequent sample purification and desalting, an additional purification step should be considered.

References

1. Wenzel M, Bandow JE (2011) Proteomic signatures in antibiotic research. Proteomics 11: 3256–3268
2. Tsakou F, Jersie-Christensen R, Jenssen H, Mojsoska B (2020) The role of proteomics in bacterial response to antibiotics. Pharmaceuticals 13:214
3. Otto A, Becher D, Schmidt F (2014) Quantitative proteomics in the field of microbiology. Proteomics 14:547–565
4. Maaß S, Becher D (2016) Methods and applications of absolute protein quantification in microbial systems. J Proteome 136:222–233
5. Gerber SA, Rush J, Stemman O et al (2003) Absolute quantification of proteins and phosphoproteins from cell lysates by tandem MS. Proc Natl Acad Sci U S A 100:6940
6. Pratt JM, Simpson DM, Doherty MK et al (2006) Multiplexed absolute quantification for proteomics using concatenated signature peptides encoded by QconCAT genes. Nat Protoc 1:1029–1043
7. Maass S, Sievers S, Zühlke D et al (2011) Efficient, global-scale quantification of absolute protein amounts by integration of targeted mass spectrometry and two-dimensional gel--based proteomics. Anal Chem 83:2677–2684
8. Ishihama Y, Oda Y, Tabata T et al (2005) Exponentially modified protein abundance index (emPAI) for estimation of absolute protein amount in proteomics by the number of sequenced peptides per protein. Mol Cell Proteomics 4:1265–1272
9. Lu P, Vogel C, Wang R et al (2007) Absolute protein expression profiling estimates the relative contributions of transcriptional and translational regulation. Nat Biotechnol 25:117–124
10. Schwanhäusser B, Busse D, Li N et al (2011) Global quantification of mammalian gene expression control. Nature 473:337–342
11. Silva JC, Gorenstein MV, Li G-Z et al (2006) Absolute quantification of proteins by LCMS^{E}: a virtue of parallel MS acquisition. Mol Cell Proteomics 5:144–156
12. Zougman A, Selby PJ, Banks RE (2014) Suspension trapping (STrap) sample preparation method for bottom-up proteomics analysis. Proteomics 14:1006–1000
13. Antelo-Varela M, Bartel J, Quesada-Ganuza A et al (2019) Ariadne's thread in the analytical labyrinth of membrane proteins: integration of targeted and shotgun proteomics for global absolute quantification of membrane proteins. Anal Chem 91:11972–11980
14. Bonn F, Maaß S, Becher D (2017) Sample preparation for mass-spectrometry based absolute protein quantification in antibiotic stress research. In: Sass P (ed) Antibiotics. Springer, New York, pp 281–289

Chapter 19

Elemental Analysis for the Characterization of Antimicrobial Effects

Christoph H. R. Senges and Julia E. Bandow

Abstract

To address the mounting resistance challenge, novel antibiotics and unprecedented mechanisms of action are urgently needed. In this context, metals have attracted attention in two distinct ways: First, the bacterial metal ion homeostasis is essential for many cellular processes, making it a putatively lucrative antibiotic target. Metal ions are, for example, cofactors for enzymes, and they contribute to signaling and transport processes or to energy metabolism. Possible antibacterial strategies include, for example, depletion of accessible essential metals by sequestration or disruption of metal ion homeostasis by ionophores that transport ions across membranes. Second, organometallic antibiotics that contain metals as integral structural elements can provide unique chemistry with unique modes of action. Since many metal-containing structures used in synthetic chemistry are unprecedented in nature, such antibiotics could circumvent existing mechanisms of resistance. Here, we present a method for quantification of cellular metal/metalloid levels and outline the procedures necessary for antibiotic treatment of *Bacillus subtilis*, subsequent sample preparation, elemental analysis, and data evaluation. This approach allows to investigate disturbances of the cellular metal ion homeostasis, as well as the localization and quantitation of antibiotics that contain metals rarely found in biological systems, overall aiding in the elucidation of antibiotic mechanisms of action.

Key words Elemental analysis, Ionophore, Metal ions, Transport, Tracer groups, Organometallic antibiotic

1 Introduction

The maintenance of a stable intracellular metal ion homeostasis is integral to most cellular processes [1]. Many metal ions are essential micronutrients like sodium (Na), potassium (K), magnesium (Mg), calcium (Ca), manganese (Mn), iron (Fe), nickel (Ni), copper (Cu), or zinc (Zn). They are not only cofactors of enzymes or provide force by means of concentration gradients, but they also create a milieu generally conducive to enzyme stability. For most metal ions, bacteria have to regulate intracellular levels closely: While a sufficient supply of essential metal ions is necessary, excessive amounts

Peter Sass (ed.), *Antibiotics: Methods and Protocols*,
Methods in Molecular Biology, vol. 2601, https://doi.org/10.1007/978-1-0716-2855-3_19,

may be detrimental [1]. This is particularly true for redox-active metals like iron or copper that can generate reactive oxygen species through Fenton or Haber-Weiss chemistry [2, 3]. Since regulation of the homeostasis of different metals is closely connected, also the stoichiometries between metal ions are important. For example, in the soil organism *Bacillus subtilis*, the regulation of iron and manganese levels and responses to oxidative stress are interlinked [4].

The importance of metal ion homeostasis for cellular survival and the toxicity of certain metals offer interesting perspectives for antibiotic development [5]. Excess copper, for example, is so toxic for bacteria that free intracellular copper is kept at attomolar levels and enzymes carrying a copper cofactor are compartmentalized to the membrane [6, 7]. The antibiotic potential of metals can be harnessed (I) by disturbing the cellular ion homeostasis for example with ionophores, (II) by chelating cellular ions causing the inactivation of metal-dependent enzymes, (III) by limiting access to essential ions by extracellular chelation, or (IV) by employing metal-containing antibiotics.

Ionophores are molecules that transport ions across biological membranes. Two groups of ionophores can be distinguished based on their mode of transport: channel ionophores and carrier ionophores. Channel ionophores like gramicidin A (Fig. 1a) form hydrophilic, ion-selective pores. One gramicidin A dimer forms a channel that allows the diffusion of monovalent cations like K^+ and Na^+ over membranes [8, 9]. Following concentration gradients between the extracellular medium and the cytosol, a one- or bidirectional ion-flux can be observed. Another channel ionophore is nystatin (Fig. 1b), which binds to ergosterol in fungal membranes and causes K^+ leakage [10, 11]. Carrier ionophores form complexes with metal ions and usually transport only a single ion per membrane passage [12]. Since the membrane passage in either direction typically requires an ion to be bound, their net transport is considered electroneutral [12]. A carrier ionophore employed in research is the polyether calcimycin (A23187) (Fig. 1c), which, in a complex of two molecules of calcimycin with one divalent metal cation, can transport cations across membranes [12–14]. It is used to increase intracellular calcium concentrations in eukaryotic cells to study signaling processes [15]. The in vitro transport preferences of calcimycin in model membrane vesicles are $Zn^{2+} > Mn^{2+} > Ca^{2+} > Co^{2+} > Ni^{2+} > Sr^{2+}$ [12–14]. Interestingly, when *B. subtilis* was treated with calcimycin in chemically defined medium, an influx of calcium and an efflux of iron and manganese were observed [16]. This illustrates that transport information obtained in experiments with model membrane vesicles is difficult to transfer to living cells. The reasons are manifold. The biologically relevant ions may not have been tested in vitro resulting in knowledge gaps, as was the case for the in vitro iron transport of calcimycin [12–14, 16]. Even if the in vitro data were complete, chemical factors, such as pH and

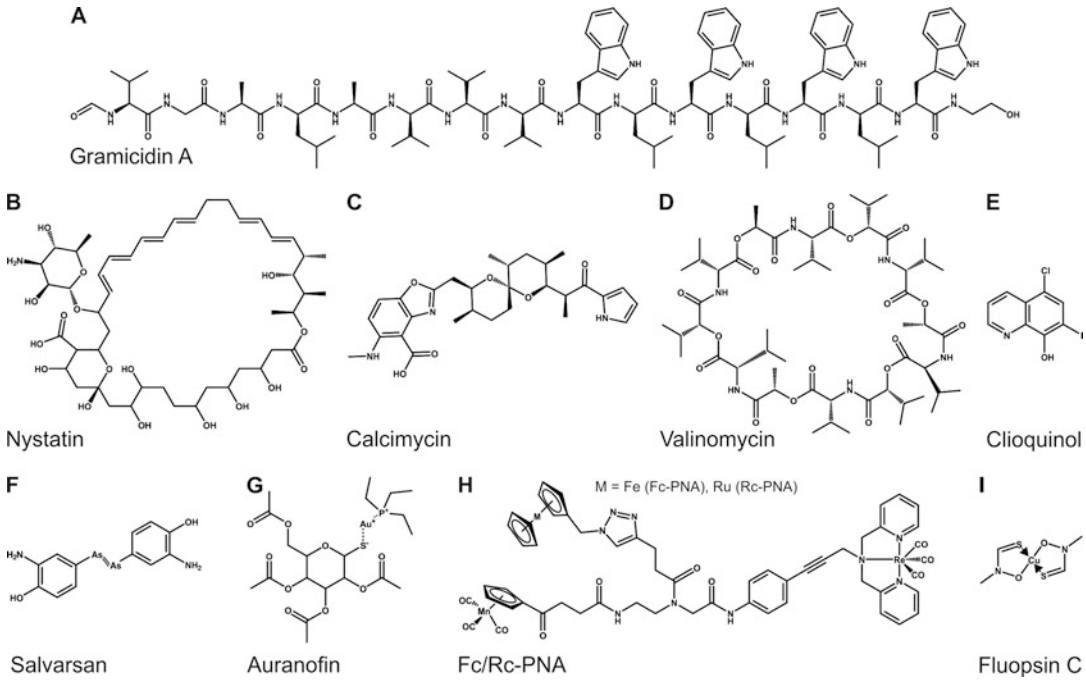

Fig. 1 Exemplary antibiotics. Examples of channel ionophores (gramicidin A, nystatin), carrier ionophores (calcimycin, valinomycin), a chelator (clioquinol), as well as metal and metalloid-containing antibiotics (salvarsan, auranofin, Fc-PNA, Rc-PNA, fluopsin C)

concentration gradients of individual ion species, and biological factors, such as ion binding proteins and active compensatory transport, influence the overall effect on cellular homeostasis [12–14, 16]. Another example of a carrier ionophore is valinomycin (Fig. 1d), a depsipeptide that transports K^+ with excellent affinity [17, 18].

Limiting access to essential metal ions, both intracellularly and extracellularly, is also a promising antibacterial strategy. Clioquinol, which is used for topical antifungal treatment (Fig. 1e), can sequester metal ions intracellularly and thereby cause cytosolic metal depletion [19–21]. Some probiotic bacteria limit the growth of pathogenic bacteria by competition for nutrients like extracellular metal ions. *Escherichia coli* strain Nissle 1917, for example, reduces intestinal colonization by the pathogenic *Salmonella* Typhimurium by limiting iron availability [22, 23]. A strategy that could be exploited using synthetic chelators.

Metal or metalloid-containing antibiotics can either provide a framework for toxic metals/metalloids to cross bacterial membranes more easily, or they can provide unique chemistry and mechanisms of action. Salvarsan (arsphenamine) (Fig. 1f), once used to treat syphilis, is based on the metalloid arsenic [24]. Its mechanism of action was shown to be similar to that of plain arsenic

(III) oxide, but it was more efficient at lower concentrations [25]. The antirheumatic agent auranofin (Fig. 1g), which today is being considered for repurposing as an antibiotic, contains one gold(I), through which it readily interacts with thiol groups, for example, of the thioredoxin reductase, thereby disturbing bacterial redox homeostasis [26, 27]. The metals in organometallic antibiotics are often essential for the antibiotic activity, and exchanging the metal alters activity. In Rc-PNA and Fc-PNA (Fig. 1h), which both impair the integrity of the bacterial cell envelope, exchanging the incorporated metal from the redox-inactive ruthenium to the redox-active iron resulted in oxidative stress as an additional mechanism of action [28]. An example for a metal-containing antibiotic that recently attracted attention is the cupric fluopsin C (Fig. 1i), which seems to cause permeabilization of the cytoplasmic membrane [29, 30]. Notably, for antibiotics that contain elements like ruthenium, gold, or arsenic that are either not found in natural biological systems or found only in trace amounts, methods like elemental analysis and transmission electron microscopy allow element-based compound quantitation and subcellular localization [28, 31].

The protocol described here focuses on the investigation of changes in intracellular ion concentrations in the gram-positive model organism *B. subtilis* after treatment with ionophores using inductively coupled plasma optical emission spectroscopy (ICP-OES) for quantification of trace metals (Fig. 2) [16]. Yet, the approach is transferable to other organisms and means of detection. It can be combined with the fractionation of subcellular compartments for localization of metals or metal-containing antibiotics. Swapping *B. subtilis* for another bacterial species likely requires adaptation of growth and treatment conditions, particularly to find a suitable medium, as well as adaptation of metal and antibiotic concentrations. Here, we use ICP-OES for detection and quantification, but other approaches like atomic absorption spectroscopy (AAS) or ICP-coupled mass spectrometry (ICP-MS) may also be suitable methods, which may require modifications of sample preparation.

2 Materials

2.1 Cultivation of B. subtilis *in Belitzky Minimal Medium (See Notes 1 and 2)*

Work sterile and protect all samples from metal contaminations by avoiding contact to metal surfaces.

1. Shaking water bath (*see* **Note 3**).
2. Sterile Erlenmeyer glass flasks (100 mL, 300 mL, and 1 L) with cotton plugs (*see* **Notes 4** and **5**).
3. Photometer.

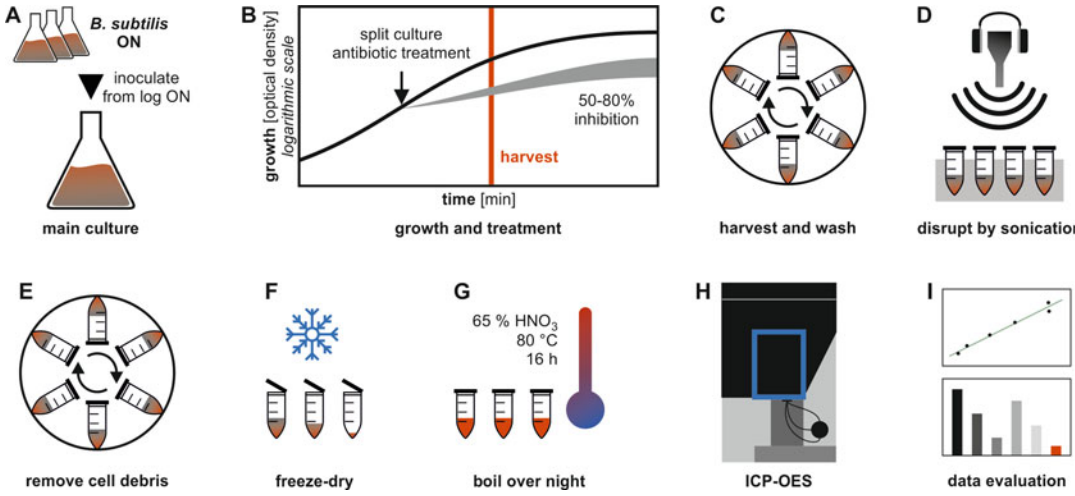

Fig. 2 Method overview. The method described here covers the analysis of changes in intracellular metal ion concentrations from the cultivation of *B. subtilis* starting with (**a**) a logarithmically growing overnight culture (log ON), (**b**) to treatment with antibiotics, (**c**) sample harvest, (**d**) disruption, and (**e**) removal of cell debris, (**f**) to final sample preparation with freeze drying and (**g**) boiling in nitric acid. Samples are (**h**) measured in an ICP-OES machine and (**i**) the data is evaluated by translating emissions into concentrations using calibration curves and by comparing metal ion concentrations of treated and untreated samples

4. Centrifuge for conical centrifuge tubes (50 mL).
5. Belitzky base medium: 27 mM KCl, 15 mM $(NH_4)_2SO_4$, 8 mM $MgSO_4$, 7 mM $Na_3C_6H_5O_7$, 50 mM Tris–HCl, pH 7.5 (*see* **Notes 6** and **7**).
6. 1 M $CaCl_2$, autoclaved, stored at room temperature.
7. 500 mM L-glutamic acid, filter-sterilized, stored at 4 °C.
8. 200 mM KH_2PO_4, autoclaved, stored at room temperature.
9. 30 mM L-tryptophan, filter-sterilized, stored at 4 °C.
10. 25 mM $MnSO_4$, filter-sterilized, stored at room temperature.
11. 1 mM $FeSO_4$, filter-sterilized, stored at room temperature.
12. 20% (w/v) D-glucose, filter-sterilized, stored at 4 °C.
13. Supplemented Belitzky Minimal Medium (BMM): Belitzky base medium supplemented with 4.5 mM L-glutamic acid, 2 mM $CaCl_2$, 780 μM L-tryptophan, 600 μM KH_2PO_4, 10 μM $MnSO_4$, 2 μM $FeSO_4$, and 0.2% glucose.
14. Glycerol stocks of *B. subtilis* 168 in BMM for inoculation (*see* **Note 8**).
15. Antibiotic stock solutions (*see* **Notes 9** and **10**).
16. Conical centrifuge tubes (50 mL).
17. Washing buffer: 100 mM Tris–HCl, 10 mM EDTA pH 7.5 (*see* **Note 11**).

18. Lysis buffer: 10 mM Tris–HCl pH 7.5 (*see* **Note 11**).
19. Centrifuge for 2 mL reaction tubes.
20. Reaction tubes (2 mL).

2.2 Sample Preparation

1. Lysis buffer: 10 mM Tris–HCl, pH 7.5 (*see* **Note 11**).
2. VialTweeter sonicator for cell disruption (*see* **Note 12**).
3. Centrifuge for 2 mL reaction tubes.
4. Conical centrifuge tubes (15 mL) (*see* **Note 13**).
5. Freezer (−80 °C).
6. Freeze dryer (*see* **Note 14**).
7. Ultrapure water (*see* **Note 15**).
8. 65% nitric acid (*see* **Note 16**).
9. Heating water bath at 80 °C.

2.3 Sample Measurement and Data Evaluation

1. Metal standard solutions (here: Ca, Cu, Fe, K, Mg, Mn, Mo, Na, Ni, and Zn) (*see* **Note 17**).
2. Ultrapure water (*see* **Note 15**).
3. ICP-OES (*see* **Note 18**).
4. Microsoft Excel software.

3 Methods

3.1 Cultivation of B. subtilis

Be sure to work sterile while preparing media and handling cultures. To prevent metal contaminations, avoid contact of samples to metal surfaces. Grow cultures of *B. subtilis* at 37 °C in a water bath under constant agitation at 200 rpm in Erlenmeyer flasks.

1. Prepare an overnight culture by using 10 µL of a glycerol stock of *B. subtilis* 168 to inoculate 20 mL of BMM in a 100 mL Erlenmeyer flask. Prepare two to five decadic dilutions, each with 20 mL BMM in a 100 mL Erlenmeyer flask and incubate overnight at 37 °C in a shaking water bath at 200 rpm. Store the remaining BMM at 4 °C for the next day (Fig. 2a).
2. After overnight cultivation, measure the optical density at 500 nm (OD_{500}) against BMM as blank. Choose an exponential overnight culture (OD_{500} 0.25–0.8) to inoculate the main culture to an OD_{500} of 0.05 in 200 mL of pre-warmed (37 °C) BMM in a 1 L Erlenmeyer flask. Incubate culture at 37 °C and 200 rpm and determine growth photometrically at OD_{500} in regular intervals (Fig. 2a, b) (*see* **Note 19**).
3. At $OD_{500} = 0.30$ split the culture by transferring 60 mL of aliquots into pre-warmed 300 mL Erlenmeyer flasks. Incubate subcultures at 37 °C and 200 rpm (*see* **Note 20**) (Fig. 2b).

4. At OD_{500} = 0.35 leave one of the subcultures as untreated control and treat the remaining subcultures with the physiologically effective concentration of the antibiotic (50–80% reduction of growth) (*see* **Notes 20** and **21**) (Fig. 2b).
5. After 15 min of treatment measure the OD_{500} of all subcultures and harvest 50 mL of each culture in 50 mL conical centrifuge tubes by centrifugation (2 min, 37 °C, 3000 x g, soft break settings) (*see* **Note 22**) (Fig. 2b, c).
6. Resuspend pellets in 1 mL pre-warmed (37 °C) washing buffer and transfer to 2 mL reaction tubes. Wash again once with 1 mL washing buffer and once with 1 mL lysis buffer (2 min, 37 °C, 16,000 × *g*, soft break settings) (*see* **Note 22**) (Fig. 2c).
7. Store dry pellet at −80 °C until further use.

3.2 Sample Preparation (See Note 23)

1. Thaw pellet and resuspend in 500 µL of lysis buffer.
2. Disrupt cells in 2 mL reaction tubes using a VialTweeter sonicator (place sonotrode on ice, 8 × 1 min of sonication with 1 min pauses; settings: amplitude 90%, 0.5 s cycle) (*see* **Note 12**) (Fig. 2d).
3. Remove cell debris by centrifugation (20 min, 4 °C, 16,000 × *g*) (Fig. 2e).
4. Transfer supernatant to 15 mL conical centrifuge tubes (*see* **Note 13**).
5. Freeze conical centrifuge tubes at −80 °C overnight (*see* **Note 14**) (Fig. 2f).
6. Evaporate samples to dryness in the freeze dryer (*see* **Note 14**) (Fig. 2f).
7. Dissolve the resulting pellet in 2.5 mL of 65% nitric acid and boil in the closed conical centrifuge tube at 80 °C for 16 h (*see* **Notes 13** and **24**) (Fig. 2g).
8. Dilute samples by adding 7.5 mL of water to each sample (*see* **Note 15**).

3.3 Sample Measurement and Data Evaluation

1. Prepare separate 15 mL conical centrifuge tubes with 10 mL of each metal standard dilution series. Dilute standards from 1 g/L with 10% nitric acid to 10 mg/L, 1 mg/L, 0.1 mg/L, and 0.01 mg/L. Add a further tube with 10 mL of water as 0 mg/mL (*see* **Note 15**).
2. Measure samples by ICP-OES. Take three measurements of every sample and calculate the average of the three technical replicates (*see* **Note 25**) (Fig. 2h).
3. Fit calibration curves and calculate metal ion levels in µg/L. Modern software of ICP-OES devices can often fit calibration

curves and provide values in μg/L for the measured samples automatically, if a method with defined standards is used (*see* **Note 26**) (Fig. 2i).

4. To determine relative changes in metal concentrations in treated and untreated cells, correct for differences in cell number using the OD_{500} measurements taken at harvest (*see* Subheading 3.1, **step 5**) and calculate ratios between normalized μg/L values of treated and untreated samples (*see* **Notes 27** and **28**) (Fig. 2i).
5. The absolute amount of each metal per colony forming unit (CFU) (*see* **Note 29**) can be estimated with the following formula, ICP-OES output *(x)* in μg/L, the volume of the sample (10 mL), the molecular weight *(m)* of the corresponding metal in g/mol, the OD_{500} (*see* Subheading 3.1, **step 5**), and the assumption that an $OD_{500} = 1$ equals a cell density of 6 x 10^7 CFU/mL. Expected amounts of different elements in untreated exponentially growing *B. subtilis* are shown in Table 1.

$$n = (x * 10\ \text{mL}) * m^{-1} * \left(\text{OD} * 6 * \frac{10^7 \text{cells}}{\text{mL}} * 50\ \text{mL}\right)^{-1}$$

Table 1
Cytosolic metal ion amounts of untreated *B. subtilis*. Shown are the averages of 12 biological replicates with standard deviations

Element	amol per colony forming unit ± SD	
Potassium (K)	743.708	± 187.516
Magnesium (Mg)	381.406	± 117.564
Sodium (Na)	181.739	± 106.551
Calcium (Ca)	34.302	± 16.359
Iron (Fe)	6.091	± 1.973
Zinc (Zn)	2.071	± 0.991
Nickel (Ni)	0.349	± 0.320
Copper (Cu)	0.340	± 0.083
Molybdenum (Mo)	0.020	± 0.015

4 Notes

1. This protocol describes the cultivation of *B. subtilis* in a chemically defined medium, which allows control over the medium composition. However, this is not critical for the successful application of the following steps and bacterial cultures can be grown in complex media.
2. Beware of the quality of used media components. Most salts are contaminated with trace metals to a certain degree and trace metal contaminations can vary from batch to batch. Use salts and water of sufficient purity.
3. Orbital shakers give the best results when cultivating *B. subtilis* in Erlenmeyer flasks.
4. Rinse glassware with 1 M hydrochloric acid and incubate in distilled water (*A. dest.*) overnight prior to sterilization.
5. Sterilize glassware by dry heat sterilization to prevent trace metal contaminations from autoclave steam.
6. Weigh in the components for 1 L of base medium und dissolve in 800 mL *A. dest.*, adjust pH to 7.5 with HCl, fill up to 1 L with *A. dest.*, autoclave, and store at room temperature.
7. Standard Belitzky base medium contains citrate, which can facilitate iron uptake as 2-citrate-1-iron complex. If iron uptake is to be investigated, consider replacing 7 mM $Na_3C_6H_5O_7$ with 21 mM NaCl.
8. To prepare glycerol stocks let *B. subtilis* 168 grow to exponential phase in BMM at 37 °C and 200 rpm, dilute 1:1 with sterile 100% glycerol and store as 50 µL aliquots at −80 °C.
9. Antibiotic stocks are typically prepared as 10 mg/mL solutions in DMSO.
10. Beware that antibiotic stocks can be contaminated with metals, especially when the compound in question binds metals or when metals are used during chemical synthesis. This can be accounted for by analyzing the elemental composition of the antibiotic stock.
11. Use water suited for elemental analysis and components of the highest available purity to prepare buffers.
12. The VialTweeter sonicator (Hielscher, Teltow, Germany) allows to disrupt cells in closed 2 mL reaction tubes (no contact to metal surfaces), minimizing trace metal contaminations. Avoid cell disruption by French press or sonication with a submersed metal sonotrode that is in direct contact with the sample.

13. Some 15 mL conical centrifuge tubes will leak after boiling overnight with nitric acid. From our experience, BD *Falcon tubes* (blue lid, Becton Dickinson, Franklin Lakes, USA) will leak but comparable tubes from, for example, Sarstedt (red lid, Sarstedt, Nümbrecht, Germany) are suitable.
14. Any method of drying is suitable in which none of the dry material is lost.
15. Use water suited for elemental analysis.
16. Use nitric acid of the highest available quality, suited for elemental analysis.
17. Use standards suited for elemental analysis.
18. In this example an iCAP 6500 Duo View ICP Spectrometer is used (Thermo Fisher Scientific, Waltham, USA).
19. *B. subtilis* is particularly sensitive to temperature changes. If exposed to cold media, flasks, or even pipettes, it may take several hours before *B. subtilis* returns to normal growth. Pre-warm all media and flasks before adding *B. subtilis*. Also, pre-warm larger pipettes (>1 mL), conical centrifuge tubes, or measuring cylinders if they are used to aliquot a growing *B. subtilis* cultures. Pipette tips for 100 μL and 1 mL usually suffice at room temperature.
20. In addition to an untreated control subculture, one flask is needed per tested antibiotic.
21. The physiologically effective concentration of the tested antibiotics is a concentration that causes a 50–80% reduction of growth but does not cause lysis of the bacteria. This concentration has to be determined in growth experiments prior to the experiment described here. It is not sufficient to infer this concentration from a microdilution experiment.
22. Some bacterial species, including *B. subtilis*, will secrete compatible solutes and metal ions into the medium if centrifuged for prolonged times in hypotonic buffers and/or at cold temperatures.
23. In some settings, precipitation of iron can hamper analysis via ICP-OES. Precipitated iron can be observed during ICP-OES analysis as sporadic spikes in emission intensity in contrast to an otherwise stable signal, as larger iron particles in the sample are analyzed at irregular intervals. A dye-based approach can be used as an alternative for iron quantification. If not stated otherwise, the alternative approach described here follows the procedures mentioned under Subheadings 3.1 and 3.2. For dye-based quantification of iron, use 25 mL of *B. subtilis* culture per sample. After harvesting and washing, resuspend the pellet in 500 μL of 10% nitric acid and disrupt bacteria using the VialTweeter (*see* **Note 12**). Incubate the lysate at 100 °C

and 800 rpm for 30 min in a thermomixer and remove the cell debris by centrifugation. Mix 50 μL of the remaining sample with 950 μL of reaction solution (0.2 mM chrome azurol S (CAS), 0.07 mM cetyltrimethylammonium bromide (CTAB), 200 mM acetate, pH 4.75). Mix well and let equilibrate for 20 min. Afterward, measure the absorption at 630 nm and determine iron levels using a calibration curve prepared from a standard [16].

24. If the sample is turbid after 16 h or precipitation is observed, centrifuge (20 min, room temperature, 16,000 × *g*) and transfer to a fresh tube. Some material will be lost, which can hamper the quantification, but particles are detrimental to the measurement. Especially large quantities of iron under oxygenic conditions and alkaline pH are prone to precipitate (*see* **Note 23**).
25. Beware of emission at overlapping wavelengths. Depending on the resolution of the used ICP-OES device the emission of several elements can be overlapping (e.g., As 228.812 nm and Cd 228.802 nm). Choose an appropriate set of wavelengths for elements that emit at several wavelengths to allow analysis of all elements of interest in the expected sample matrix. This can be a tradeoff between specificity and sensitivity, but finding the best setup is often simplified as modern ICP-OES devices can record several wavelengths for several elements simultaneously, and the accompanying software is often equipped with wavelength libraries as well as optimization tools. The wavelengths used here are K: 769.896 nm, Mg: 279.079 nm, Na: 818.326 nm Ca: 318.128 nm, Fe: 238.204 nm, Zn: 213.856 nm, Ni: 231.604 nm, Cu: 324.754 nm, and Mo: 202.030 nm.
26. Most modern analysis software allows for automatic quantitation by using defined, method-specific calibration standards.
27. Correction for differences in cell number is necessary to account for the reduced growth of subcultures treated with antibiotics.
28. Changes in intracellular ion amounts are well expressed by determining the ratio of the untreated control to the treated culture.
29. When calculating absolute intracellular concentrations, beware of differences in cell volume. The volume of bacteria changes depending on media, cultivation conditions, and growth phases. Best results are obtained, when cell volumes are determined, for example, from microscopic images under conditions used for the elemental analysis.

Acknowledgments

We thank Ute Krämer, Plant Physiology, Ruhr University Bochum, for providing access to OES and Petra Düchting for technical support. JEB acknowledges funding from NRW and the European Union, European Regional Development Fund, Investing in your future (Research Infrastructure "Center for System-based Antibiotic Research (CESAR)").

References

1. Chandrangsu P, Rensing C, Helmann JD (2017) Metal homeostasis and resistance in bacteria. Nat Rev Microbiol 15:338–350
2. Py B, Barras F (2010) Building Fe-S proteins: bacterial strategies. Nat Rev Microbiol 8:436–446
3. Macomber L, Rensing C, Imlay JA (2007) Intracellular copper does not catalyze the formation of oxidative DNA damage in *Escherichia coli*. J Bacteriol 189:1616–1626
4. Helmann JD (2014) Specificity of metal sensing: iron and manganese homeostasis in *Bacillus subtilis*. J Biol Chem 289:28112–28120
5. Argüello JM, Raimunda D, Padilla-Benavides T (2013) Mechanisms of copper homeostasis in bacteria. Front Cell Infect Microbiol 3:73
6. Andrei A, Öztürk Y, Khalfaoui-Hassani B et al (2020) Cu homeostasis in bacteria: the ins and outs. Membranes 10:242
7. Wiebelhaus N, Zaengle-Barone JM et al (2021) Protein folding stability changes across the proteome reveal targets of cu toxicity in *E. coli*. ACS Chem Biol 16:214–224
8. David JM, Rasajsekaran AK (2015) Gramicidin A: A new mission for an old antibiotic. J Kidney Cancer VHL 2:14–24
9. Gordon AH, Martin AJ, Synge RL (1943) The amino-acid composition of gramicidin. Biochem J 37:86–92
10. Cohen R, Webb PA (1952) Nystatin, a coccidoidocidal antibiotic. Arch Pediatr 69:414–416
11. Hammond SM (1977) Biological activity of polyene antibiotics. Prog Med Chem 14:105–179
12. Erdahl WL, Chapman CJ, Taylor RW, Pfeiffer DR (1994) Ca^{2+} transport properties of ionophores A23187, ionomycin, and 4-BrA23187 in a well defined model system. Biophys J 66: 1678–1693
13. Erdahl WL, Chapman CJ, Wang E, Taylor RW, Pfeiffer DR (1996) Ionophore 4-BrA23187 transports Zn^{2+} and Mn^{2+} with high selectivity over Ca^{2+}. Biochemistry 35:13817–13825
14. Erdahl WL, Chapman CJ, Taylor RW, Pfeiffer DR (1995) Effects of pH conditions on Ca^{2+} transport catalyzed by ionophres A23187, 4-BrA23187, and ionomycin suggest problems with common applications of these compounds in biological systems. Biophys J 69:2350–2363
15. Bailey JL, Buhr MM (1993) Ca^{2+} regulation by cryopreserved bull spermatozoa in response to A23187. Cryobiology 30:470–481
16. Raatschen N, Wenzel M, Leichert LIO et al (2013) Extractin iron and manganese from bacteria with ionophores – a mechanism against competitors characterized by increased potency in environments low in micronutrients. Proteomics 13:1358–1370
17. MacDonald JC (1960) Biosynthesis of valinomycin. Can J Microbiol 6:27–34
18. Cammann K (1985) Ion-selective bulk membranes as models for biomembranes. Top Curr Chem 128:219–258
19. Li C, Wang J, Zhou B (2010) The metal chelating and chaperoning effects of clioquinol: insights from yeast studies. J Alzheimers Dis 21:1249–1262
20. Chan DCK, Guo I, Burrows LL (2020) Forging new antibiotic combinations under iron-limiting conditions. Antimicrob Agents Chemother 64:e01909–e01919
21. Green MW (1946) Acetarsone, carbazone, iodochlorohydroxyquinoline. J Am Pharm Assoc (Baltim) 7:150–152
22. Deriu E, Liu JZ, Pezeshki M, Edwards RA et al (2013) Probiotic bacteria reduce salmonella typhimurium intestinal colonization by competing for iron. Cell Host Microbe 14:26–37
23. Valdebenito CAL, Winkelmann G, Hantke K (2006) Environmental factors influence the production of enterobactin, salmochelin, aerobactin, and yersiniabactin in *Escherichia coli* strain Nissle 1917. Int J Med Microbiol 296: 513–520

24. Arora N, Schuenemann VJ, Jäger G (2017) Origin of modern syphilis and emergence of a pandemic *Treponema pallidum* cluster. Nat Microbiol 2:16245
25. Senges CHR, Stepanek JJ, Wenzel M et al (2021) Comparison of proteomic responses as global approach to antibiotic mechanism of action elucidation. Antimicrob Agents Chemother 65:e01373–e01320
26. Finkelstein AE, Walz DT, Batista V et al (1976) Auranofin. New oral gold compound for treatment of rheumatoid arthritis. Ann Rheum Dis 35:251–257
27. Harbut MB, Vilchèze C, Luo X et al (2015) Auranofin exerts broad-spectrum bactericidal activities by targeting thiol-redox homeostasis. Proc Natl Acad Sci U S A 112:4453–4458
28. Wenzel M, Patra M, Senges CHR (2013) Analysis of the mechanism of action of potent antibacterial hetero-tri-organometallic compounds: a structurally new class of antibiotics. ACS Chem Biol 8:1442–1450
29. Del Rio LA, Gorgé JL, Olivares J, Mayor F (1972) Antibiotics from *Pseudomonas reptilivora* II. Isolation, purification, and properties. Antimicrob Agents Chemother 2:189–194
30. Pérez Navarro MO, Dilarri G, Simionato AS et al (2020) Determining the targets of fluopsin C action on gram-negative and gram-positive bacteria. Front Microbiol 11:1076
31. Wenzel M, Chiriac AI, Otto A et al (2014) Small cationic antimicrobial peptides delocalize peripheral membrane proteins. Proc Natl Acad Sci U S A 111:E1409–E1418

Chapter 20

Label-Free Quantitation of Ribosomal Proteins from *Bacillus subtilis* for Antibiotic Research

Sina Schäkermann, Pascal Dietze, and Julia E. Bandow

Abstract

Current research is focusing on ribosome heterogeneity as a response to changing environmental conditions and stresses. Altered stoichiometry and composition of ribosomal proteins as well as association of additional protein factors are mechanisms for shaping the protein expression profile or hibernating ribosomes. In this updated chapter, we present a method for the isolation of ribosomes to analyze antibiotic-induced changes in the composition of ribosomes in *Bacillus subtilis* or other bacteria. Ribosomes and associated proteins are isolated by ultracentrifugation, and proteins are identified and quantified using label-free mass spectrometry.

Key words Mass spectrometry, Ribosome heterogeneity, Stress, Proteomics

1 Introduction

Ribosomes are remarkable ribonucleoprotein complexes and essential for translation in all living cells. Due to their key role in cellular physiology, ribosomes are targeted by many clinically used antibiotics [1, 2]. To allow for protein synthesis, more than 50 ribosomal proteins and three ribosomal RNAs assemble into the bacterial 70S ribosome. Yet, the ribosome is not a fixed entity but is adapted to changing environmental conditions and stresses, resulting in ribosome heterogeneity. As previously reviewed [4–9], ribosome heterogeneity is, for example, achieved by altered stoichiometry and composition of ribosomal proteins, the modification status of ribosomal proteins or rRNA, and interaction with additional proteins. For instance, the stoichiometry of ribosomal proteins in *Escherichia coli* was found to change depending on the growth rate [10–12]. During transition to stationary phase, changes in proteins associating with ribosomes are observed, and ribosomal core proteins L31A and L36A are replaced by their respective

Peter Sass (ed.), *Antibiotics: Methods and Protocols*,
Methods in Molecular Biology, vol. 2601, https://doi.org/10.1007/978-1-0716-2855-3_20,

paralogs [13, 14]. Similarly, upon zinc-limiting conditions in *Bacillus subtilis*, ribosomal proteins L31 and S14 containing zinc-binding motifs are replaced by non-zinc-binding homologues [15, 16]. In *Mycobacterium smegmatis*, alternative ribosomes containing paralogous ribosomal proteins lacking cysteine-rich motifs exhibit a distinct translational profile and play a role in iron homeostasis [17]. During cold shock, bulk protein translation is repressed as *E. coli* ribosomes are inactivated by binding of protein Y (pY), which is rapidly released when growth conditions improve [18]. Yet, to allow for selective translation of cold shock proteins while bulk protein production is repressed, increased levels of translation initiation factors IF1 and IF3 are necessary [19, 20]. Ribosome hibernation due to dimerization into 100S particles is mediated by associating proteins and is a common response to environmental stress conditions in bacteria [21–23]. Ribosome hibernation is also important for tolerance toward aminoglycosides in stationary phase [24]. In response to the antibiotic kasugamycin, *E. coli* ribosomes lacking some ribosomal proteins of the small subunit like S1 occur. Although these ribosomes are unable to translate canonical mRNAs, translation of leaderless mRNAs (lmRNAs) was confirmed in vivo and in vitro [25]. Ribosomes lacking S1 are also present upon normal growth conditions, and lmRNA translation might be relevant under stress conditions [26, 27]. The role of ribosomes as regulatory elements shaping the protein expression profile by ribosomal heterogeneity is discussed as the ribosome filter hypothesis [28, 29].

This chapter is an updated version of a chapter previously published in the first edition of this book [30]. The method described here is suitable for label-free quantitation of ribosomal proteins from *B. subtilis* and other bacteria for studying ribosome heterogeneity upon antibiotic treatment or other stress conditions. Studying ribosome heterogeneity can be helpful for understanding changes in protein expression counteracting antibiotic-induced stress or to analyze adaption strategies in response to ribosome-targeting antibiotics. Using this method, we quantified 380 proteins of untreated *B. subtilis* ribosome isolations. Among those, 27 of 35 and 18 of 22 ribosomal proteins were quantified, which according to Ref. [31] can be part of the large and small ribosomal subunit, respectively (Table 1). In *B. subtilis*, 35 ribosomal proteins are thought to be essential, as gene disruption was not possible [31]. All but one of these essential proteins were identified using the described method (Table 1). Furthermore, proteins typically associated with the ribosome were found like initiation factors InfB and InfC; elongation factors TufA, FusA, Tsf, and Efp; trigger factor Tig; ribosome recycling factor Frr; and the GTPases involved in ribosome assembly YsxC and YqeH.

Table 1
Quantification of ribosomal proteins after ribosome isolation from untreated *B. subtilis*

Ribosomal protein[a]		fmol replicate 1	2	3	mean	SD	% SD[b]
RplA	L1	86.5	78.6	92.1	85.7	5.5	6.5
RplB	**L2**	124.1	145.6	181.3	150.3	23.6	15.7
RplC	**L3**	87.8	84.5	79.6	83.9	3.4	4.0
RplD	**L4**	117.4	106.5	118.8	114.2	5.5	4.8
RplE	**L5**	130.7	113.1	126.8	123.5	7.5	6.1
RplF	**L6**	104.1	100.5	106.2	103.6	2.4	2.3
RplI	L9	7.7	8.1	9.0	8.3	0.5	6.2
RplJ	**L10**	43.1	40.1	38.0	40.4	2.1	5.2
RplK	L11	81.6	70.9	69.2	73.9	5.5	7.5
RplL	**L7/L12**	239.3	214.8	210.3	221.5	12.8	5.8
RplM	**L13**	119.4	100.4	126.2	115.3	10.9	9.5
RplN	**L14**	53.8	46.9	48.5	49.7	3.0	6.0
RplO	L15	90.6	77.3	86.5	84.8	5.6	6.6
RplP	**L16**	64.9	63.1	65.6	64.5	1.0	1.6
RplQ	**L17**	98.7	91.2	91.7	93.9	3.4	3.7
RplR	**L18**	76.3	60.0	53.8	63.4	9.5	14.9
RplS	**L19**	118.8	105.4	100.9	108.3	7.6	7.0
RplT	**L20**	65.8	72.3	77.1	71.7	4.6	6.4
RplU	**L21**	77.7	73.9	92.6	81.4	8.1	9.9
RplV	L22	107.2	95.0	100.2	100.8	5.0	4.9
RplW	L23	44.5	39.7	44.8	43.0	2.3	5.5
RplX	**L24**	NF[c]	63.1	86.9	75.0	11.9	15.8
Ctc	L25 homologue	ND[d]					
RpmA	**L27**	61.8	59.6	40.6	54.0	9.5	17.6
RpmB	L28	ND					
RpmC	L29	94.3	78.6	85.9	86.2	6.4	7.4
RpmD	**L30**	49.6	45.1	54.8	49.8	3.9	7.9
RpmEA	L31A	6.8	7.6	15.5	10.0	3.9	**39.2**
RpmEB	L31B	ND					
RpmF	L32	ND					

(continued)

Table 1
(continued)

Ribosomal protein[a]		fmol replicate 1	2	3	mean	SD	% SD[b]
RpmGA	L33.1	ND					
RpmGB	L33.2	ND					
RpmH	L34	ND					
RpmI	L35	NF	9.0	31.1	20.0	11.1	**55.3**
RpmJ	L36	ND					
YpfD	S1	2.3	2.1	1.0	1.8	0.6	31.5
RpsB	**S2**	52.5	51.0	76.6	60.0	11.7	19.5
RpsC	**S3**	61.1	53.3	70.8	61.7	7.2	11.6
RpsD	**S4**	103.8	87.4	142.1	111.1	22.9	20.6
RpsE	**S5**	124.0	121.7	181.2	142.3	27.5	19.3
RpsF	S6	73.3	60.2	82.0	71.8	9.0	12.5
RpsG	**S7**	108.0	92.1	129.9	110.0	15.5	14.1
RpsH	**S8**	85.1	74.1	98.1	85.8	9.8	11.5
RpsI	**S9**	44.1	40.7	58.6	47.8	7.7	16.2
RpsJ	**S10**	61.0	56.4	92.9	70.1	16.2	23.2
RpsK	**S11**	59.9	57.7	79.9	65.8	10.0	15.1
RpsL	**S12**	29.0	34.4	66.9	43.5	16.7	**38.4**
RpsM	**S13**	62.4	53.4	77.6	64.5	10.0	15.4
RpsN	**S14**	ND					
YhzA	S14 homologue	ND					
RpsO	**S15**	48.7	40.9	69.6	53.1	12.1	22.8
RpsP	**S16**	48.5	43.5	66.7	52.9	10.0	18.8
RpsQ	**S17**	36.6	35.8	43.6	38.7	3.5	9.0
RpsR	**S18**	21.7	17.9	25.4	21.6	3.0	14.1
RpsS	**S19**	51.1	46.9	80.8	59.6	15.1	25.3
RpsT	S20	ND					
RpsU	S21	ND					

For ribosomal proteins identified in at least two of three replicates, the normalized amount is shown as fmol on column. Arithmetic means (mean) and standard deviations (SD) are given

[a]Proteins that according to Ref. [31] are thought to be essential in *B. subtilis* are marked in bold

[b]Values ≥39% are marked in bold (*see* **Note 37**)

[c]Protein not found in this replicate

[d]Protein not detected in at least two of three replicates

2 Materials

Unless noted otherwise, prepare stock solutions in distilled water (A. dest.). Use UPLC/MS grade solvents, formic acid (FA), and trifluoroacetic acid (TFA) for mass spectrometry. Make sure to follow regional waste disposal regulations.

2.1 *Cultivation of* B. subtilis *in Belitzky Minimal Medium (BMM) (See Note 1)*

1. Water bath shaker.
2. Sterile Erlenmeyer glass flasks (100 mL, 500 mL) with cotton plugs.
3. Photometer.
4. Centrifuge for conical tubes.
5. Belitzky base medium: 15 mM $(NH_4)_2SO_4$, 8 mM $MgSO_4$, 27 mM KCl, 7 mM $Na_3C_6H_5O_7$, 50 mM Tris-HCl, pH 7.5. Weigh in all components for 1 L of basal medium and dissolve in 800 mL *A. dest.* Adjust pH to 7.5 using HCl, fill up to 1000 mL with *A. dest.*, prepare 250 mL aliquots, autoclave, and store at room temperature (RT).
6. Supplemented BMM: 600 μM KH_2PO_4, 2 mM $CaCl_2$, 2 μM $FeSO_4$, 10 μM $MnSO_4$, 0.2% glucose, 4.5 mM L-glutamic acid, 780 μM L-tryptophan in base medium. Stock solutions prepared in A. dest. Are: 200 mM KH_2PO_4, 1 M $CaCl_2$, 1 mM $FeSO_4$, 25 mM $MnSO_4$, 20% (w/v) D-glucose, 500 mM L-glutamic acid, 39 mM L-tryptophan.
7. Glycerol stocks of *B. subtilis* 168 for inoculation (*see* **Note 2**).

2.2 *Ribosome Isolation by Ultracentrifugation*

To protect samples from RNase activity, only use autoclaved water for buffer preparation. This method was modified from Ref. [32, 33].

1. French Press cell disruption system (*see* **Note 3**).
2. Ultracentrifuge equipped with fixed angle and swing-out rotors.
3. Appropriate ultracentrifugation tubes.
4. Magnetic stirrer.
5. Magnetic stir bars (≤ 0.6 cm).
6. Glass beaker.
7. 10% H_2O_2 in a squirt bottle.
8. 1.1 M sucrose, filter sterilized, stored at 4 °C.
9. 0.1 M DTT (*see* **Note 4**).
10. 10 mg/mL DNase I, stored as 100 μL aliquots at −20 °C.
11. Buffer A: 10 mM Tris-HCl, pH 7.5, 10 mM MgAc, 60 mM NH_4Cl, 0.5 mM EDTA, 3 mM β-mercaptoethanol (*see* **Note**

5). Prepare fresh from the following stock solutions: 1 M Tris-HCl, pH 7.5, 1 M magnesium acetate (MgAc), 2 M NH_4Cl, 0.5 M EDTA. For the EDTA stock solution, adjust pH to 8 with NaOH, otherwise EDTA will not dissolve.

12. Buffer B: 20 mM Tris-HCl, pH 7.5, 10.5 mM MgAc, 0.5 mM NH_4Cl, 0.5 mM EDTA, 3 mM β-mercaptoethanol (*see* **Note 6**). Prepare fresh from stock solutions as listed for buffer A.
13. Protease inhibitor cocktail of choice.

2.3 Tryptic Digest of Isolated Ribosomes

Use MS grade water and solvents for preparation of stock solutions. To avoid contaminations with keratin, wear protective gloves and clean lab coats, and clean the working bench thoroughly (*see* **Note 6**).

1. Refrigerated table-top centrifuge.
2. Thermomixer adjustable to 60 °C and 37 °C (*see* **Note 7**).
3. 1% (w/v) stock solution of RapiGest (Waters, Milford, USA), 100 μL aliquots stored at −20 °C.
4. 250 mM Tris-(2-carboxyethyl)phosphine hydrochloride (TCEP), 25 μL aliquots stored at −20 °C.
5. 500 mM iodoacetamide (*see* **Note 8**).
6. 0.5 μg/μL trypsin (*see* **Note 9**).
7. TFA.

2.4 UPLC-MS^E Analysis

1. Synapt G2-S HDMS ToF mass spectrometer equipped with an ESI nanoLockSpray source coupled online to a nanoAcquity UPLC system and operated with MassLynx software (e.g., version V4.1 SCN932; Waters, *see* **Note 10**).
2. NanoACQUITY UPLC Symmetry C18 Trap Column (pore size, 100 Å; particle diameter, 5 μm; inner diameter, 180 μm; length, 20 mm; Waters).
3. NanoACQUITY UPLC peptide CSH C18 Column (pore size, 130 Å; particle diameter, 1.7 μm; inner diameter, 75 μm; length, 150 mm; Waters).
4. Ultrasonic bath.
5. Glass vials for mass spectrometry.
6. Hi3 quantitation standard (Hi3 PhosB standard, Waters; *see* **Note 11**), stored as 10 μL aliquots of 10 pmol/μL in 3% acetonitrile/0.5% TFA at −80 °C.
7. 0.1% FA in MS-grade *A. dest*. For dilution of tryptic digests.
8. Solvent A: 0.1% FA in MS-grade *A. dest*., degassed in an ultrasonic bath for 10 min.

9. Solvent B: 0.1% FA in acetonitrile, degassed in an ultrasonic bath for 10 min.
10. Lock mass, 0.25 μg/mL leucine enkephalin (*see* **Note 12**) in 50% acetonitrile containing 0.1% FA, degassed in an ultrasonic bath for 10 min.

2.5 Label-Free Quantitation of MS^E Data

1. ProteinLynx Global Server (PLGS, version 2.5.2, Waters).
2. Microsoft Excel (e.g., version 2010) or comparable software.

3 Methods

3.1 Cultivation of* B. subtilis *for Ribosome Isolation (*See *Note 13)

Be sure to work sterilely while preparing media and handling cultures. Grow all cultures of *B. subtilis* at 37 °C in a shaking water bath under steady agitation at 200 rpm in sterile Erlenmeyer flasks with cotton plugs. The ribosome isolation and label-free quantitation method of course is not restricted to *B. subtilis*, but this organism is chosen here as example for the experimental procedure. The method described here can also be combined with in vivo cross-linking techniques to stabilize transient protein interactions if necessary.

1. Use 10 μL of a glycerol stock of *B. subtilis* 168 to inoculate 20 mL of BMM in a 100 mL Erlenmeyer flask (*see* **Note 14**). Prepare three to ten serial 1:10 dilutions of the same volume in Erlenmeyer flasks and incubate overnight at 37 °C in a shaking water bath (*see* **Note 15**). Store the remaining supplemented BMM at 4 °C for short-term usage.
2. After overnight incubation, measure the OD_{500} against BMM. Choose one of the cultures, which is still in exponential phase (*see* **Note 16**; OD_{500} 0.25–0.8) to inoculate the main culture to an OD_{500} of 0.05. Use 100 mL (*see* **Note 17**) of BMM pre-warmed to 37 °C in a 500 mL Erlenmeyer flask for the main culture.
3. Let the culture grow to OD_{500} 0.15 (*see* **Note 18**), split the volume and transfer to new pre-warmed Erlenmeyer flasks (*see* **Note 19**). Leave one of the cultures untreated as control and add your antibiotic of choice in appropriate concentrations to the second flask (*see* **Note 20**). Incubate in the water bath for 1 h to allow adaptation of the proteome to the antibiotic stress.
4. Transfer each culture to 50 mL falcon tubes and harvest the cells by centrifugation for 10 min at 4 °C and 3000× *g*. From now on, keep the samples cool at all times. Discard the supernatant and wash the cells by suspending in 25 mL buffer A. Centrifuge again (10 min, 4 °C, 3000× *g*), discard the supernatant, and store at −80 °C until further use.

3.2 Cell Disruption and Ribosome Isolation (See Note 21)

To protect your samples from RNases, use 10% H_2O_2 to clean the working bench and ultracentrifugation tubes. Make sure to exactly balance all samples for ultracentrifugation using a scale (*see* **Note 22**).

1. Resuspend each pellet in 5 mL buffer B and protease inhibitor of choice, DNase (15 μL of stock), and DTT (25 μL of stock).
2. Disrupt cells by French Press using eight to ten passages (*see* **Note 23**).
3. Transfer the suspensions to appropriate ultracentrifugation tubes and remove cell debris in three ultracentrifugation steps in a fixed-angle rotor at 4 °C (*see* **Note 24**). Centrifuge at 16,000× *g* for 8 min, discard the pellet and subject the supernatant to a second centrifugation at 22,000× *g* for 8 min. Again, discard the pellet and centrifuge the supernatant at 43,000× *g* for 25 min.
4. Slowly load the supernatant onto 5 mL of sucrose in appropriate ultracentrifugation tubes and fill up completely with buffer B. Make sure that the weight of all tubes is exactly balanced before proceeding to ultracentrifugation in a swing-out rotor at 4 °C for 20 h at 80,000× *g*.
5. Slowly decant the supernatant and rinse the ribosome pellet with buffer B (*see* **Note 25**). Add a magnetic stir bar (0.6 cm) and resolve the pellet on ice for ~2 h in 500 μL buffer B (*see* **Note 26**).
6. Determine the protein concentration, for example, by using Bradford or Ninhydrin assays following manufacturer's instructions or standard lab protocols and store as 0.25 μg/μL aliquots with a volume of 50 μL in 1.5 mL tubes (*see* **Note 27**) at −80 °C until further use.
7. To confirm that ribosome isolation was successful, use 10 μg of the samples for sodium dodecyl sulfate polyacrylamide gel electrophoresis (SDS PAGE) and Coomassie staining using standard protocols. In addition, 16S and 23S rRNA can be extracted and analyzed by 3-(N-morpholino)propanesulfonic acid (MOPS) agarose gels using standard protocols. As a reference, Fig. 1 shows a Coomassie-stained SDS gel of a typical isolation of ribosomal proteins from *B. subtilis* (A) and a corresponding RNA gel for extracted 16S and 23S rRNA from the same sample (B).

3.3 Tryptic Digest (See Note 28)

1. Add 0.1% RapiGest and 2.5 mM TCEP to each sample and incubate at 60 °C for 45 min.
2. Add 5 mM freshly prepared iodoacetamide and incubate at RT for 25 °C in the dark (*see* **Note 29**).

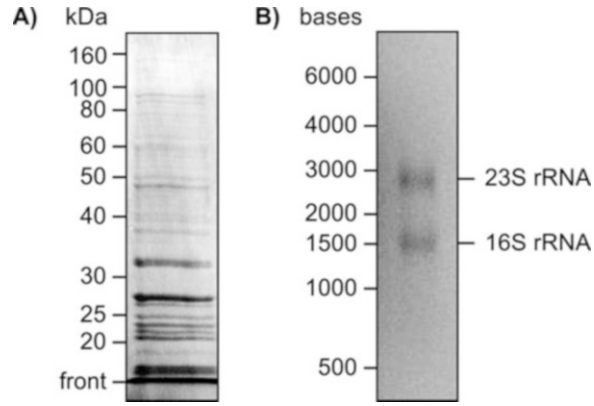

Fig. 1 Visualization of ribosomal proteins (**a**) and ribosomal RNA (**b**) after ribosome isolation from *B. subtilis*. Ribosomal proteins after SDS-PAGE and Coomassie staining are shown in (**a**). rRNA was extracted from isolated ribosomes, separated by MOPS agarose electrophoresis and visualized by ethidium bromide (**b**). (Figure reprinted from [30])

3. Add 0.25 μL trypsin to reach an enzyme to protein ratio of 1: 100 and mildly shake samples incubating at 37 °C (*see* **Note 10**) for 5 h.
4. Add 2 μL TFA sample to precipitate RapiGest and to terminate the digestion. Remove RapiGest by centrifugation at 16,000 × *g* for 10 min at 4 °C. Transfer the supernatant to a fresh tube and repeat until RapiGest is removed completely (*see* **Note 30**).
5. Store tryptic digest at −80 °C until further use.

3.4 Mass Spectrometry

1. Tryptic digests are diluted 1:10 in 0.1% FA containing 12.5 fmol/μL Hi3 quantitation standard and 10–20 μL are transferred into glass vials. For analysis, 4 μL are loaded onto the trap column (*see* **Note 31**). Samples are desalted with a flow of 10 μL/min 0.5% solvent B for 3 min.
2. Peptides are eluted with a linear gradient from 0.5 to 60% B in 150 min. The column is subsequently washed and re-equilibrated with the following steps: linear gradient to 99.5% B in 5 min, hold at 99.5% B for 10 min, linear gradient to 0.5% B in 5 min, hold at 99.5% for 10 min.
3. In parallel, leucine-enkephalin is pumped with a flow rate of 0.5 μL/min as lock mass.
4. Mass spectra in MS^E mode are recorded with MassLynx software using the following settings:
   4.1 Acquisition times: start time, 0 min; end time, 180 min.
   4.2 Acquisition mode: polarity, positive; analyzer mode, resolution.

4.3 MS^E mass range: low mass, 50 Da; high mass, 1200 Da; scan time, 1 s.

4.4 Collision energy: in function 2 (high energy) ramp trap collision energy from 14 to 45 V.

4.5 LockSpray properties: acquire LockSpray, do not apply correction; scan time, 1 s; interval, 60 s; scans to average, 3; mass window, ± 0.3 Da.

3.5 Label-Free Quantitation of Proteins

1. Load MS^E raw data into PLGS for processing.
2. Use the following Apex3D settings as processing parameters to generate mass spectra for database analysis:
   (a) Chromatographic peak width, automatic.
   (b) MS ToF resolution, automatic.
   (c) Lock mass, 556.2771 Da/e; lock mass window, 0.25 Da.
   (d) Low energy threshold, 50 counts; elevated energy threshold, 15 counts, intensity threshold, 500 counts.
3. For database analysis, use a nonredundant database containing protein sequences of *B. subtilis* 168 (e.g., NCBI Reference Sequence: NC_000964.3) as well as the sequences for the Hi3 quantitation standard (refer to manufacturer's instructions), trypsin and keratin. The following parameters are suitable for the database search:
   (a) Peptide and fragment tolerance, automatic.
   (b) Minimal fragment ion matches per peptide, 2; minimal fragment ion matches per protein, 6; minimal peptide matches per protein, 3.
   (c) Maximum protein mass, 250,000 Da.
   (d) Primary digest reagent, trypsin; secondary digest reagent, none; missed cleavages, 1.
   (e) Fixed modifications, carbamidomethyl C; variable modifications: deamidation N, deamidation Q, oxidation M.
   (f) False positive rate, 4%.
   (g) Calibration protein, PhosB; calibration protein concentration, 50 fmol.
4. Activate the automation setup option for IdentityE (Ion accounting output) for automated export of peptide and protein lists for each sample to manually analyze the proteomics data as described below or use the automated Expression Analysis provided by PLGS following manufacturer's instructions.

3.6 Manual Analysis of Regulated Proteins (See *Note 32*)

1. Open all protein lists (typically three biologically independent replicates per condition are investigated) in Excel.

2. Using the filter function in Excel, reject proteins with <95% probability (proteins with "green OK" symbol in PLGS or "Green" written in excel sheet in column "protein.AutoCurate" are of at least 95% probability), proteins found in the random reverse database (protein.dataBaseType random) and proteins that could not be quantified (no entry in protein. fmolOnColumn).
3. To compensate for possible variations in sample load, apply the following normalization. For each sample, calculate the sum for protein.fmolOnColumn (absolute protein amount) of all proteins, then normalize the value for each protein in the sample against this sum (*see* **Note 33**).
4. Combine the protein amount data of all samples in one spreadsheet. For further analysis, for each condition include only proteins for which data exists from at least two out of three biological replicates.
5. Calculate arithmetic means and standard deviations (SD) for each condition (*see* **Note 34,** Table 1). To select upregulated and downregulated proteins, calculate the $\log_2$ ratio of the arithmetic means of control and antibiotic-treated conditions for each protein.
6. Select for upregulated or downregulated proteins using a confidence interval of 95% ($\text{mean}_{\text{log2ratio}} \pm 1.963 \times \text{SD}_{\text{log2ratio}}$), p-values below 0.05 and appropriate SD values (*see* **Note 34**). Proteins found in all three replicates representing one condition but in none of the replicates representing the other condition can be considered as "unique" for this condition if the SD value is appropriate (*see* **Note 34**).

4 Notes

1. This protocol describes cell cultivation in chemically defined medium, which allows full control over medium composition. However, this is not critical for the successful application of the following steps of the protocol, and bacterial cultures can be grown in complex media.
2. Let *B. subtilis* 168 grow to exponential phase in BMM at 37 °C and 200 rpm, dilute 1:1 with 100% glycerol and store as 50 μL aliquots at −80 °C.
3. French Press is comparably gentle for cell disruption, yet other methods like bead beating or sonication might work as well for this protocol.
4. Store aliquots at −20 °C. DTT in solution is not suitable for long-term storage. Discard thawed aliquots and prepare fresh if aliquots lost the typical odor of DTT. Do not refreeze thawed aliquots.

5. β-Mercaptoethanol solutions of 99% purity have a concentration of 14.3 M.
6. Keratin contaminations will interfere with ionization of your samples during mass spectrometry. Use lint-free precision wipes for all cleaning purposes. If you refill pipette tips manually, wear clean gloves and wash out tip boxes with MS grade ethanol or methanol regularly. Do not autoclave tips for tryptic digest or mass spectrometry to minimize contaminations derived from the autoclaving process.
7. Use a thermomixer with ~100 rpm at 37 °C and without shaking at 60 °C, respectively. Alternatively, tape a tube rack onto an orbital shaker in a 37 °C climate chamber and use a standard heating block for 60 °C.
8. Prepare fresh, use on the same day only and store at 4 °C in the dark until needed.
9. Use sequencing grade trypsin. Prepare stock solutions in the buffer recommended by the manufacturer and store as 10 μL aliquots at −80 °C. Thaw and refreeze for a maximum of three times.
10. In principle, ribosomes can of course be analyzed by alternative quantitation strategies and other types of instruments. As we use label-free quantitation based on the Hi3 technology of MS^E data with a Synapt setup, this protocol will only cover this approach.
11. This standard is suitable for bacterial proteomics, as these peptide sequences are not encoded in bacterial genomes.
12. Store 400 μg/mL stocks in 0.1% FA at −80 °C. Alternatively, use 500 fmol/μL [Glu1]-fibrinopeptide B (250 pmol/μL stocks in 0.1% FA) as lock mass, yet this compound is drastically less stable.
13. For quantitative analysis of antibiotic-induced changes of the ribosome composition, cultures are grown as biologically independent triplicates. All following steps including cell disruption, ribosome isolation, and tryptic digest should be performed simultaneously and mass spectrometrical analysis should be performed en bloc to minimize technical variation.
14. Use a minimal ratio of medium to flask volume of 1:5 to allow aerobic growth of the cultures.
15. This is done to yield exponentially growing cultures for inoculation of the main culture. The number of dilutions needed may vary and depends on the used glycerol cultures and incubation times.
16. This is important to avoid a lag phase when starting the main culture, which will happen if stationary phase cells are used or if cells are cold-shocked by inoculating cold BMM.

17. The protocol works fine for a minimum volume of ~50 mL per sample for successful ribosome isolation from *B. subtilis*.
18. This cell density is suitable for monitoring proteome changes after 60 min of antibiotic stress with control cultures still in exponential phase at the time of harvest. This is critical, as the composition of the ribosome is altered upon entry into stationary phase.
19. Use pre-warmed and sterile falcons, pipettes, or measuring cylinders for this purpose.
20. The amount of antibiotic used should reduce growth rates to 50–70% but should not kill the cells. This makes sure that the cells can adapt their proteome to the stress caused by the antibiotic.
21. The method described here does not separate the 30S from the 50S subunits. To do so, a subsequent sucrose gradient centrifugation is needed.
22. Wipe the outside of the ultracentifugation tubes to remove water stemming from keeping the samples on ice and place tubes on a scale in a glass beaker. To balance tubes against each other, remove the cap, place it on the scale next to the glass beaker, and use a pipette to add the appropriate amount of buffer B.
23. The number of passages needed for successful cell disruption has to be adjusted to the bacterial strain investigated and the volume of the pressure cell. Use as many passages as needed to reach a clear suspension. Make sure the pressure cell is cooled down prior to use (on ice or in a cooling chamber) to avoid heating of the sample. If necessary, interrupt the disruption process to cool the pressure cell on ice.
24. Please refer to the manual of your ultracentrifuge for detailed information on handling centrifugation tubes, as operating errors can be extremely dangerous and procedures may vary between centrifuges and rotors.
25. Gently rinse pellet with buffer B, but do not resuspend the pellet.
26. Place the ultracentrifugation tube in a glass beaker filled with ice and put it onto a magnetic stirrer in a cool room (4 °C).
27. We recommend to use low-bind tubes for storage and handling of proteinaceous samples.
28. It is highly recommended to use pipettes suitable for accurately transferring very small volumes (0.1–2.5 μL pipettes and 10 μL pipettes, respectively).
29. Put the tubes into a lightproof box or wrap in aluminum foil.

30. Make sure that no precipitated RapiGest remains in the solution—this may take additional one to two centrifugation steps. If RapiGest is not pelleted properly (solution is opaque or particles are visible in the solution), add few more μL of TFA, incubate at 37 °C and repeat the centrifugation steps.
31. The volume of sample loaded may depend on the sample loop. For this example, a 5 μL loop was used and an injection volume of 4 μL contains tryptic peptides of 100 ng isolated protein plus 50 fmol of Hi3 quantitation standard.
32. In Excel, conditional formatting and the "vlookup" command are useful for manual handling of proteomics data.
33. Standard techniques like Bradford or Ninhydrin assays for whole protein quantitation in the samples prior to tryptic digests are not very reliable when determining rather low protein concentrations. The total protein amount loaded onto the column as detected by MS is calculated as a quality check for all samples and serves as reference for the normalization. If the average deviation between samples is high (e.g., more than 30%), you should consider repeating the MS analysis or preparing additional replicates for quantitation.
34. For technical replicates, the standard deviation using the MS^E-based Hi3 Method was shown to be less than 15% [3]. For quality control, calculate the mean standard deviation across the three biological samples representing each condition. For example, we found that the mean standard deviation for protein amounts of ribosome isolations (representing the combined biological and technical variability) to be ~21% ±18%. As an example, results for ribosomal proteins isolated from untreated *B. subtilis* are given in Table 1.

Acknowledgments

We thank Birgit Klinkert and Johanna Roßmanith for the practical introduction into ribosome isolation and for technical support. Furthermore, we would like to thank Dörte Becher and Knut Büttner for sharing mass spectrometry protocols. Funding from the German Federal State of North Rhine Westphalia (NRW) is acknowledged for the mass spectrometer ("Forschungsgroßgeräte der Länder") used in this protocol. JEB acknowledges funding from NRW from the grant "Translation of innovative antibiotics from NRW" for performing the original work and preparing the original chapter and from NRW and the European Union, European Regional Development Fund, Investing in your future (Research Infrastructure "Center for System-based Antibiotic Research (CESAR)") for updating the chapter.

References

1. McCoy LS, Xie Y, Tor Y (2011) Antibiotics that target protein synthesis. Wiley Interdiscip Rev RNA 2:209–232
2. Wilson DN (2014) Ribosome-targeting antibiotics and mechanisms of bacterial resistance. Nat Rev Microbiol 12:35–48
3. Silva JC, Gorenstein MV, Li G-Z et al (2006) Absolute quantification of proteins by LCMSE: a virtue of parallel MS acquisition. Mol Cell Proteomics 5:144–156
4. Byrgazov K, Vesper O, Moll I (2013) Ribosome heterogeneity: another level of complexity in bacterial translation regulation. Curr Opin Microbiol 16:133–139
5. Starosta AL, Lassak J, Jung K et al (2014) The bacterial translation stress response. FEMS Microbiol Rev 38:1172–1201
6. Sauert M, Temmel H, Moll I (2015) Heterogeneity of the translational machinery: variations on a common theme. Biochimie 114: 39–47
7. Xue S, Barna M (2012) Specialized ribosomes: a new frontier in gene regulation and organismal biology. Nat Rev Mol Cell Biol 13:355–369
8. Petibon C, Malik Ghulam M, Catala M et al (2021) Regulation of ribosomal protein genes: an ordered anarchy. Wiley Interdiscip Rev RNA 12:e1632
9. Gay DM, Lund AH, Jansson MD (2022) Translational control through ribosome heterogeneity and functional specialization. Trends Biochem Sci 47:66–81
10. Deusser E, Wittmann HG (1972) Ribosomal proteins: variation of the protein composition in *Escherichia coli* ribosomes as function of growth rate. Nature 238:269–270
11. van Duin J, Kurland CG (1970) Functional heterogeneity of the 30S ribosomal subunit of *E. coli*. Mol Gen Genet 109:169–176
12. Kurland CG, Voynow P, Hardy SJ et al (1969) Physical and functional heterogeneity of *E. coli* ribosomes. Cold Spring Harb Symp Quant Biol 34:17–24
13. Lilleorg S, Reier K, Pulk A et al (2019) Bacterial ribosome heterogeneity: changes in ribosomal protein composition during transition into stationary growth phase. Biochimie 156: 169–180
14. Lilleorg S, Reier K, Volõnkin P et al (2020) Phenotypic effects of paralogous ribosomal proteins bL31A and bL31B in *E. coli*. Sci Rep 10:11682
15. Nanamiya H, Akanuma G, Natori Y et al (2004) Zinc is a key factor in controlling alternation of two types of L31 protein in the *Bacillus subtilis* ribosome. Mol Microbiol 52:273–283
16. Natori Y, Nanamiya H, Akanuma G et al (2007) A fail-safe system for the ribosome under zinc-limiting conditions in *Bacillus subtilis*. Mol Microbiol 63:294–307
17. Chen Y-X, Xu Z-Y, Ge X et al (2020) Selective translation by alternative bacterial ribosomes. Proc Natl Acad Sci U S A 117:19487–19496
18. Agafonov DE, Kolb VA, Spirin AS (2001) Ribosome-associated protein that inhibits translation at the aminoacyl-tRNA binding stage. EMBO Rep 2:399–402
19. Giangrossi M, Brandi A, Giuliodori AM et al (2007) Cold-shock-induced de novo transcription and translation of *infA* and role of IF1 during cold adaptation. Mol Microbiol 64: 807–821
20. Giuliodori AM, Brandi A, Giangrossi M et al (2007) Cold-stress-induced de novo expression of *infC* and role of IF3 in cold-shock translational bias. RNA 13:1355–1365
21. Wada A, Yamazaki Y, Fujita N et al (1990) Structure and probable genetic location of a "ribosome modulation factor" associated with 100S ribosomes in stationary-phase *Escherichia coli* cells. Proc Natl Acad Sci U S A 87:2657–2661
22. Ueta M, Yoshida H, Wada C et al (2005) Ribosome binding proteins YhbH and YfiA have opposite functions during 100S formation in the stationary phase of *Escherichia coli*. Genes Cells 10:1103–1112
23. Tagami K, Nanamiya H, Kazo Y et al (2012) Expression of a small (p)ppGpp synthetase, YwaC, in the (p)ppGpp(0) mutant of *Bacillus subtilis* triggers YvyD-dependent dimerization of ribosome. Microbiology 1:115–134
24. McKay SL, Portnoy DA (2015) Ribosome hibernation facilitates tolerance of stationary-phase bacteria to aminoglycosides. Antimicrob Agents Chemother 59:6992–6999
25. Kaberdina AC, Szaflarski W, Nierhaus KH et al (2009) An unexpected type of ribosomes induced by kasugamycin: a look into ancestral times of protein synthesis? Mol Cell 33:227–236
26. Delvillani F, Papiani G, Dehò G et al (2011) S1 ribosomal protein and the interplay between translation and mRNA decay. Nucleic Acids Res 39:7702–7715

27. Vesper O, Amitai S, Belitsky M et al (2011) Selective translation of leaderless mRNAs by specialized ribosomes generated by MazF in *Escherichia coli*. Cell 147:147–157
28. Mauro VP, Matsuda D (2016) Translation regulation by ribosomes: increased complexity and expanded scope. RNA Biol 13:748–755
29. Mauro VP, Edelman GM (2002) The ribosome filter hypothesis. Proc Natl Acad Sci U S A 99: 12031–12036
30. Schäkermann S, Prochnow P, Bandow JE (2017) Label-free quantitation of ribosomal proteins from *Bacillus subtilis* for antibiotic research. Methods Mol Biol 1520:291–306
31. Akanuma G, Nanamiya H, Natori Y et al (2012) Inactivation of ribosomal protein genes in *Bacillus subtilis* reveals importance of each ribosomal protein for cell proliferation and cell differentiation. J Bacteriol 194:6282–6291
32. Spedding G (1990) Isolation and analysis of ribosomes from prokaryotes, eukaryotes, and organelles. In: Spedding (ed) Ribosomes and protein synthesis. A practical approach. IRL Press, Oxford
33. Blaha G, Stelzl U, Spahn CM et al (2000) Preparation of functional ribosomal complexes and effect of buffer conditions on tRNA positions observed by cryoelectron microscopy. Methods Enzymol 317:292–309

Chapter 21

Functional Metagenomics to Study Antibiotic Resistance

Bejan Mahmud, Manish Boolchandani, Sanket Patel, and Gautam Dantas

Abstract

The construction and screening of metagenomic expression libraries have a great potential to identify novel genes with desired functions. Here, we describe metagenomic library preparation from fecal DNA, screening of libraries for antibiotic resistance genes (ARGs), massively parallel DNA sequencing of the enriched DNA fragments, and a computational pipeline for high-throughput assembly and annotation of functionally selected DNA.

Key words Functional metagenomics, Antibiotic resistance genes, Resistome, Functional selections, Massively parallel DNA sequencing, High-throughput assembly, Profile HMM-based annotation, PARFuMS, Resfams

1 Introduction

The continued evolution and global spread of antibiotic resistance genes (ARGs) in pathogens has become a major clinical and public health problem [1]. The increase in number, diversity, and range of multidrug-resistant organisms limits therapeutic options to resolve infections. To effectively mitigate or counter the antibiotic resistance problem, identification and characterization of ARGs, as well as their modes of transmission and mechanisms of action, is crucial.

The extensive use of antibiotics has unarguably led to a widespread increase in diversity and spread of ARGs in environmental reservoirs and pathogenic bacteria [2]. However, antibiotic resistance is ancient, existing long prior to the first discovery of natural product antibiotics by Fleming [3]. Bacteria from diverse habitats carry extensive reservoirs of ARGs, collectively termed the "resistome," which have the potential for facile transmission to pathogens [2, 4–6].

Authors Bejan Mahmud, Manish Boolchandani, Sanket Patel have contributed equally to this chapter.

Peter Sass (ed.), *Antibiotics: Methods and Protocols*,
Methods in Molecular Biology, vol. 2601, https://doi.org/10.1007/978-1-0716-2855-3_21,

Two conventional approaches, culture-based [7] and targeted PCR-based [8], have been frequently applied to study ARGs in complex microbial communities. While cultivation in the lab is the "gold standard" for identifying bacteria with antibiotic resistance, a large proportion (70–80%) of bacteria are difficult to culture in the laboratory [9]. This leads to a vast under-sampling of microorganisms belonging to diverse habitats, and, as such, their ARGs remain unanalyzed [10]. Targeted PCR-based approaches are generally used to identify and quantify ARGs with known sequences, bypassing the need for culture. However, these methods are only able to detect previously described genes and often require cloning into expression vectors and subsequent experimentation to verify function. Furthermore, homology-based identification and characterization of ARGs in shotgun sequences of microbial communities is inherently limited to the low number of genes with high sequence similarity to previously identified genes. In addition, such in silico analyses are unable to confirm the function encoded in putative ARGs and therefore require additional experimentation.

A much more efficient and powerful technique for characterizing resistomes is functional metagenomics (Fig. 1a) [3, 11–14], wherein total community DNA is cloned into an expression vector and transformed into a susceptible (and easily cultured) indicator strain. The resulting transformant library is assayed for antibiotic resistance by plating on selective media, and selected ARGs are sequenced and annotated. This allows the analysis of 10^9–10^{10} bp of DNA in a single experiment while exploiting three key advantages over culture- or PCR-based studies [12]: (i) no need to culture recalcitrant microorganisms, (ii) no prior knowledge required about ARG sequences, and (iii) direct association of resistance phenotypes with cloned and sequenced ARGs. Recent developments in high-throughput functional metagenomics [12] allow researchers to multiplex up to 400 functional metagenomic selections on a single Illumina sequencing lane. With the custom-built tool PARFuMS (Parallel Annotation and Reassembly of Functional Metagenomic Selections, Fig. 1b) [2], researchers can now perform demultiplexing, quality-filtering, trimming, assembly of the reads into full-length metagenomic fragments, and annotation in a single automated step, substantially reducing experimental cost.

Functional metagenomics has proven to be the most efficient and powerful method to date for sequence-agnostic investigation of antibiotic resistance mechanisms and their associated genes across a wide variety of habitats. Our lab actively uses the following protocol and pipeline to identify and characterize ARGs derived from samples collected from different environmental and human-associated microbial communities (*see* **Note 1**).

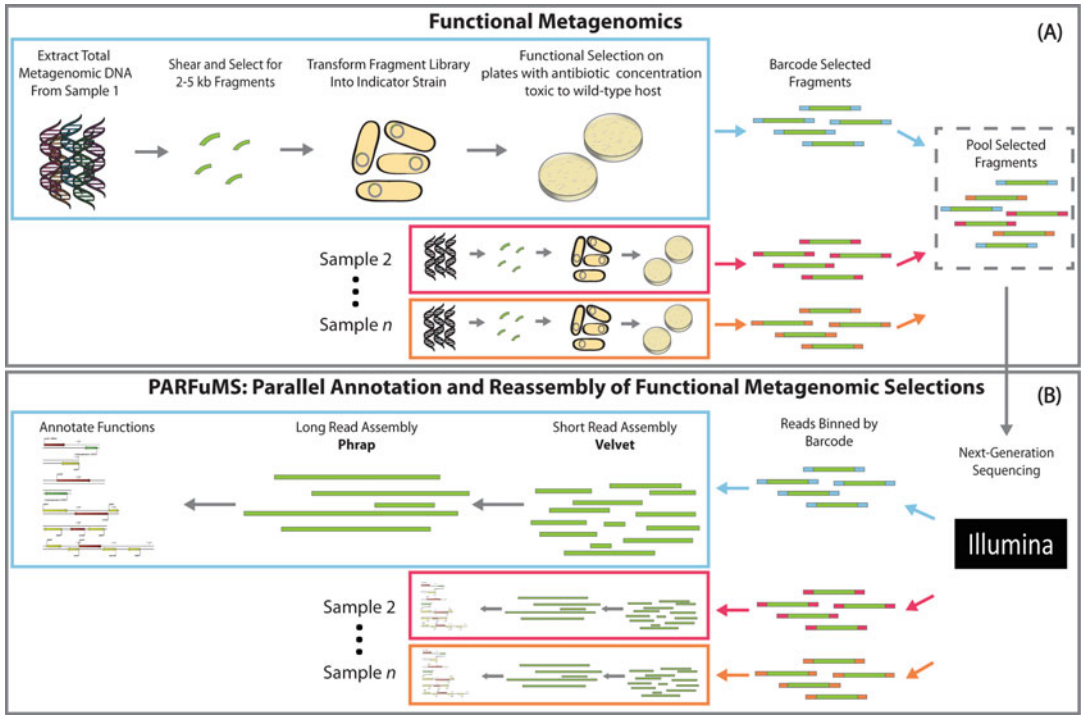

Fig. 1 Schematic representation of high-throughput functional metagenomic selection and resistome characterization. (**a**) DNA is extracted from the microbial community (e.g., feces), and 2–5-kb fragments are cloned into an expression system in an indicator strain (e.g., *Escherichia coli*). Transformants harboring resistance genes are selected using antibiotics at concentrations inhibitory to the isogenic, vector-only control strain. Plasmids from colonies containing DNA fragments conferring resistance to corresponding antibiotics are isolated, tagmented, indexed with unique dual sequences, and pooled in sets of up to 400 selections for next-generation sequencing. (**b**) Short sequencing reads from the Illumina platform are computationally binned by indices and assembled with computational pipeline PARFuMS, in which intermediate-length contigs from multiple rounds of assembly with the short-read assembler Velvet are assembled into full-length contigs using the long-read assembler Phrap. Contigs are annotated using BLAST (CARD, ResFinder, and NCBI AMRFinder-Plus) and profile HMM (Resfam, Pfam, and TIGRFam) databases. (Figure reprinted from [36])

2 Materials

Prepare all reagents and buffers in ultrapure water. Use nuclease-free water to set up all reactions that involve DNA. Prepare and store all reagents at room temperature unless indicated otherwise. Thoroughly follow all applicable waste disposal regulations when disposing of biological and chemical waste.

2.1 DNA Extraction

1. DNA extraction buffer: 100 mM NaCl, 100 mM Tris, 10 mM EDTA in ultrapure water. Add 0.6 g of NaCl to 80 mL of water and add 0.5 mL of 0.5 M EDTA (pH 8.0), as well as 10 mL of 1 M Tris–HCl (pH 7.5). Add ultrapure water to 100 mL.
2. 20% Sodium dodecyl sulfate (SDS).

3. 0.1 mm zirconium beads.
4. 3 M sodium acetate, pH 5.5.
5. Phenol:chloroform:isoamyl alcohol (25:24:1), pH 8.0 (*see* **Note 2**).
6. Mini-Bead beater (BioSpec Products, Bartlesville, OK, USA).
7. 5Prime Phase-lock gel tube (PLG) (Quantabio, Beverly, MA, USA).
8. Molecular biology grade Isopropyl alcohol (Isopropanol).
9. Ethyl alcohol (ethanol).
10. Tris-EDTA (TE) buffer: 10 mM Tris-HCl, pH 8.0, 1 mM EDTA, pH 8.0.
11. 100 mg/mL RNase A.
12. PCR Purification Kit.
13. Qubit® dsDNA BR Assay Kit (ThermoFisher Scientific, Waltham, MA, USA).
14. Qubit® dsDNA HS Assay Kit (ThermoFisher Scientific, Waltham, MA, USA).
15. Qubit® 2.0 Fluorometer (ThermoFisher Scientific, Waltham, MA, USA).
16. Quant-iT™ PicoGreen™ dsDNA Assay Kits and dsDNA Reagents (ThermoFisher Scientific, Waltham, MA, USA).

2.2 Construction of Metagenomic Library

1. 1% low-melting point agarose gel in 0.5X Tris-Borate-EDTA (TBE) buffer with SYBR green I DNA binding dye.
2. 6X gel loading dye.
3. pZE21 MCS-1 expression vector [15] (*see* **Note 3**).
4. High-fidelity (HF) DNA Polymerase Kit (*see* **Note 4**).
5. Quick calf intestinal alkaline phosphatase (CIP) and corresponding 10X rCutSmart™ Buffer (New England Biolabs, Ipswich, MA, USA).
6. EB buffer (Qiagen, Hilden, Germany).
7. QIAquick Gel Extraction Kit (Qiagen, Hilden, Germany).
8. MinElute PCR Purification Kit (Qiagen, Hilden, Germany).
9. MinElute Gel Extraction Kit (Qiagen, Hilden, Germany).
10. End-It™ DNA End-Repair Kit (Epicentre, Madison, WI, USA).
11. Fast-Link™ DNA Ligation Kit (Epicentre, Madison, WI, USA).
12. 0.025 μm cellulose membrane.
13. 0.1-cm–gap Gene Pulser®/MicroPulser™ Electroporation Cuvettes (Bio-Rad, Hercules, CA, USA).

14. High efficiency ($\geq 4 \times 10^{10}$ cfu/μg) electrocompetent *E. coli* cells (*see* **Note 5**).
15. *Taq* DNA polymerase with corresponding 10X reaction buffer.
16. 10 mM deoxynucleotide (dNTP) solution mix.
17. 0.75% agarose pre-cast agarose gel cassettes for DNA size selection (Saga Science, Beverly, MA, USA) (*see* **Note 6**)
18. PowerSoil® DNA Isolation Kit (Qiagen, Hilden, Germany).

2.3 Nextera Library Preparation and Sequencing

1. Tagment DNA enzyme (TDE1) and buffer (TD) (Illumina, San Diego, CA, USA).
2. KAPA HiFi HotStart Library Amplification Kit (Roche Molecular Systems Inc, Branchburg, NJ, USA).
3. 5 μM Illumina indexing primers (*see* **Note 7**).
4. AMPure XP PCR purification and cleanup kit (Beckman Coulter, Brea, CA, USA)

2.4 Antibiotics and Media

1. Antibiotics: Purchase antibiotics in dry powdered form and prepare stock solutions as detailed in the manufacturer's MSDS. Detailed information on antibiotics is listed in Table 1 (*see* **Note 8**).
2. Lysogeny Broth (LB) agar medium: Add 5 g yeast extract, 10 g NaCl, 10 g tryptone, and 15 g agar in 900 mL of dH_2O. Mix well to dissolve and adjust pH to 7.5 using 1 N NaOH. Add dH_2O to 1 L. Autoclave on liquid cycle for 20 min or according to your autoclave's specification (*see* **Notes 9** and **10**).
3. Lysogeny Broth (LB): Add 5 g yeast extract, 10 g NaCl, and 10 g tryptone in 900 mL of dH_2O. Mix well to dissolve and adjust pH to 7.5 using 1 N NaOH. Add dH_2O to 1 L. Autoclave on liquid cycle for 20 min or according to your autoclave's specifications (*see* **Notes 9** and **10**).
4. Lysogeny Broth (LB) with 15% glycerol and 50 μg/mL kanamycin: Mix 15 mL glycerol and 85 mL autoclaved LB in a clean sterile flask. Mix well and filter sterilize. Add kanamycin to the final concentration of 50 μg/mL.
5. Mueller–Hinton (MH) agar: Add 2 g beef infusion solids, 1.5 g starch, 17 g agar, and 17.5 g casein hydrolysate to 900 mL of dH_2O. Mix well to dissolve and adjust pH to 7.4 using 1 N NaOH. Add dH_2O to 1 L. Autoclave on liquid cycle for 20 min or according to your autoclave's specifications (*see* **Notes 9** and **10**).

2.5 Instruments and Glassware

1. Thermocycler
2. Centrifuges for 1.5 mL and 50 mL tubes
3. Heat block

Table 1
Commonly used antibiotics and their MICs are listed

Antibiotics	Code	Selection concentration (μg/mL)	Antibiotic class	Antibiotic type
Aztreonam	AZ	8	β-Lactam	Synthetic
Chloramphenicol	CH	8	Amphenicol	Natural
Ciprofloxacin	CI	0.5	Fluoroquinolone	Synthetic
Colistin	CL	8	Polymyxin	Natural
Cefepime	CP	8	β-Lactam	Synthetic
Cefotaxime	CT	8	β-Lactam	Semisynthetic
Cefoxitin	CX	64	β-Lactam	Semisynthetic
D-Cycloserine	CY	32	Amino acid derivative	Natural
Ceftazidime	CZ	16	β-Lactam	Semisynthetic
Gentamicin	GE	16	Aminoglycoside	Natural
Meropenem	ME	16	β-Lactam	Semisynthetic
Penicillin	PE	128	β-Lactam	Natural
Piperacillin	PI	16	β-Lactam	Semisynthetic
Piperacillin-Tazobactam	PI-TZ	16-PI/4-TZ	β-Lactam	Semisynthetic
Tetracycline	TE	8	Tetracycline	Natural
Tigecycline	TG	2	Tetracycline	Semisynthetic
Trimethoprim	TR	8	Folate synthesis inhibitor	Synthetic
Trimethoprim-Sulfamethoxazole	TR-SX	2-TR/38-SX	Folate synthesis inhibitor	Synthetic

4. Sonicator
5. Electroporator
6. Electrophoresis unit
7. Gel trays and tank
8. Gel imager and conversion screen
9. Petri dish
10. Cryotubes
11. BluePippin DNA size selection system (Saga Science, Beverly, MA, USA) (*see* **Note 6**)

2.6 Primers

1. pZE21 linearizing forward primer (5′ GACGGTATCGATAAG CTTGAT 3′).
2. pZE21 linearizing reverse primer (5′ GACCTCGA GGGGGGG 3′).
3. Colony PCR forward primer (5′ GATACTGAGCACATCAG CAGGA 3′).
4. Colony PCR reverse primer (5′ CCTGATTCTGTGGAT AACCGTA 3′).

3 Methods

Carry out all procedures at room temperature unless otherwise specified. Procedures involving bacterial culture, media preparation, and transformation should be performed in a clean, sterile environment. Phenol:chloroform:isoamyl alcohol should be handled in the chemical hood. A PCR hood should be used to set up PCR reactions to avoid cross-contamination. Instruction may vary for reagents and kits from different manufacturers; make necessary adjustments to the protocol accordingly.

3.1 Metagenomic DNA Extraction (see Note 11)

1. On dry ice, aliquot 50–100 mg of fecal material into a 2 mL sterile polypropylene tube (*see* **Note 12**).
2. Prepare samples for bead-beating by adding 250 μL 0.1 mm zirconium beads, 210 μL 20% SDS, 500 μL DNA extraction buffer, and 500 μL phenol:chloroform:isoamyl alcohol (25:24:1; pH 8.0) to the tube containing the fecal material. Keep samples on ice for about 5 min to cool down (*see* **Note 13**).
3. Lyse microbial cells by bead-beating using the Mini-Bead beater on the "homogenize" setting for a total of 4 min (bead-beating for 2 min, followed by cooling the samples on ice for 2 min, and bead-beating again for additional 2 min) (*see* **Note 14**).
4. Centrifuge samples at 6081 × g for 5 min at 4 °C.
5. Immediately prior to use, pellet Phase Lock Gel (PLG) tube at maximum speed (~16,058 × g) in a microcentrifuge for 20–30 s.
6. Taking care to avoid the pellet, transfer the top aqueous phase using a micropipette to a clean phase-lock gel tube, and add 600 μL of phenol:chloroform:isoamyl alcohol (25:24:1; pH 8.0) to the tube. Gently mix by inversion ten times. Do not vortex the tubes (*see* **Note 15**).
7. Centrifuge samples at ~16,058 × *g* at room temperature for 5 min.

8. Transfer top aqueous phase from the phase-lock gel tube (~600 µL) into a clean 1.5 mL reaction tube.
9. Add 1/10 volume of 3 M sodium acetate (pH 5.5) (~60 µL) and 1 volume (~600 µL) of −20 °C isopropanol to the tube containing the aqueous phase from the previous step. Mix thoroughly by inversion.
10. Store at −20 °C for at least 2 h or overnight. DNA precipitate should be visible immediately or after incubation (PAUSE POINT: The samples can be stored overnight at −20 °C).
11. After incubation, centrifuge the tube containing DNA at ~16,058 × g at 4 °C for 20 min. Carefully discard supernatant without disturbing the DNA pellet.
12. Wash the pellet with 1 mL of 4 °C 100% ethanol. Vortex to loosen the DNA pellet from the tube. Centrifuge for 5 min at ~16,058 × g at 4 °C. Remove ethanol without disturbing the pellet.
13. Evaporate residual ethanol by placing sample tube on a 55 °C heat block (*see* **Notes 16** and **17**).
14. Add 150 µL of TE (pH 8.0) buffer and incubate at 55 °C until DNA is completely dissolved. Gently vortex sample if needed.
15. Add 10 µL of RNase A (100 mg/mL) to the DNA sample and incubate for 5 min at room temperature.
16. Purify DNA using the PCR Purification kit using the manufacturer's protocol.
17. Quantify purified DNA using the Qubit dsDNA BR or HS Assay Kit and the Qubit 2.0 Fluorometer using the manufacturer's protocols (*see* **Note 18**).

3.2 Metagenomic Library Preparation

3.2.1 Plasmid Preparation

1. Prepare the pZE21 MCS-1 expression vector for ligation by linearizing at the *Hinc*II target site via inverse PCR using a blunt-end HF DNA polymerase. Set up the 50 µL reaction as follows (*see* **Notes 3**, **4**, and **19**):

   10.0 µL 10X Polymerase reaction buffer

   1.5 µL 10 mM dNTP mix

   1.0 µL 50 mM $MgSO_4$

   5.0 µL Polymerase enhancer solution

   1.0 µL 100 pg/µL circular pZE21 DNA

   0.75 µL 10 µM pZE21 linearizing forward primer

   0.75 µL 10 µM pZE21 linearizing reverse primer

   0.4 µL HF DNA polymerase

   29.6 µL Nuclease-free H_2O to a final volume of 50 µL

2. Run PCR with the following settings: 95 °C for 5 min, then 35 cycles of [95 °C for 45 s, 55 °C for 45 s, 72 °C for 2.5 min], then 72 °C for 5 min.
3. Prepare 1% agarose gel by adding 1 g of agarose to 100 mL of 0.5X Tris-Borate-EDTA (TBE) buffer (10X stock concentration). Heat the mixture until agarose is completely dissolved. Let it cool to about 65 °C by placing at room temperature and occasionally swirl the flask to let it cool evenly. Add SYBR green I DNA binding dye (10,000X in water) to a final concentration of 1X (10 μL). Prepare a gel-casting tray with a comb for sample loading and pour the liquid agarose solution into the casting tray. Allow to solidify. Place the gel in electrophoresis chamber, add enough 0.5X TBE buffer to cover the surface of the gel, and remove the comb (*see* **Note 20**).
4. Add 6X gel loading dye to the PCR-amplified DNA in a 1:5 ratio by volume. Load the sample on the gel and run at 70 V for 120 min.
5. Excise a gel slice containing the ~2,200-bp fragment and transfer to a clean tube. Purify the DNA using the gel extraction kit. Elute the DNA in 50 μL of nuclease-free, molecular biology grade water (*see* **Notes 21** and **22**).
6. Dephosphorylate the linearized plasmid using Quick CIP:

   For a 50 μL reaction, add 40 μL of the gel-purified DNA, 5 μL of Quick CIP (5 U/μL), and 5 μL of the 10X rCutSmart™ Buffer. Incubate the reaction mixture at 37 °C overnight, and heat-inactivate the reaction by incubating for 15 min at 70 °C (*see* **Note 23**).
7. Purify plasmid using the PCR purification kit as per manufacturer's protocol.
8. Quantify purified plasmid using Qubit dsDNA HS Assay Kit and the Qubit 2.0 Fluorometer. Store the sample at −20 °C. Avoid multiple freeze-thaw cycles (*see* **Notes 18** and **24**).

3.2.2 Insert Preparation

1. Dilute up to 20 μg metagenomic DNA in EB buffer to a final volume of 200 μL. Shear the DNA to approximately 3 kb using a sonicator with manufacturer's recommended settings (*see* **Note 25**).
2. Add 6X gel loading dye to sheared DNA to final concentration of 1X. Run sample through 1% low-melting point agarose gel with SYBR green I DNA binding dye as described above (70 V for 120 min). Excise a gel slice corresponding to 2–5-kb fragment size using a clean disposable knife (*see* **Notes 6**, **20**, **22**, and **26**).
3. Extract metagenomic DNA from the excised gel slice using the gel extraction kit, eluting in 34 μL of nuclease-free water.

4. Following the purification, use the END-It™ DNA End Repair kit to end-repair the DNA. To 34 μL of size-selected metagenomic DNA add the following:

   5 μL dNTP mix (2.5 mM)

   5 μL ATP (10 mM)

   5 μL 10X End-Repair Buffer

   1 μL End-Repair Enzyme

   Mix gently and incubate at room temperature for 45 min. Heat-inactivate the reaction at 70 °C for 15 min.

5. Purify DNA using PCR purification kit. Elute the DNA with 30 μL of nuclease-free water.

6. Quantify purified DNA using the Qubit dsDNA HS Assay Kit and the Qubit 2.0 Fluorometer. Concentrate DNA using a heat block at 55 °C to a final volume of 8–10 μL (*see* **Notes 17**, **18**, and **27**).

3.2.3 Ligation and Dialysis

1. Perform ligation reaction of the end-repaired metagenomic DNA and the linearized vector using the Fast-Link DNA Ligation Kit. Maintain a 5:1 insert:vector mass ratio for ligation. Set up the ligation reaction as follows:

   1.5 μL 10X Fast-Link buffer

   0.75 μL 10 mM ATP

   1 μL Fast-Link DNA ligase (2 U/μL)

   Metagenomic DNA

   Linearized vector

   Nuclease-free H_2O to a final reaction volume of 15 μL.

   Along with each set of ligations, prepare a negative control ligation reaction without any insert (i.e., metagenomic DNA) (*see* **Notes 27**–**29**).

2. Incubate reaction at room temperature overnight.

3. Heat-inactivate reaction by incubating for 15 min at 70 °C.

4. After heat inactivation, dialyze ligation reactions as follows:

   Fill clean petri dish with 20 mL of nuclease-free water. Place a 0.025 μm cellulose membrane on top of the water so that it floats. Carefully transfer entire volume of the reaction mixture to the membrane and close the lid. Incubate for 45–60 min, and carefully collect the sample in a clean 1.5 mL tube. Use the full reaction volume for transformation (*see* **Note 30**).

3.2.4 Electroporation, Metagenomic Library Amplification, and Quantification

1. Place a 0.1-cm-gap sterile electroporation cuvette, microcentrifuge tube, and ligated DNA on ice.

2. Thaw electrocompetent cells on ice. Mix by tapping gently (*see* **Note 5**).

3. Aliquot 25 μL of electrocompetent cells to pre-chilled micro-centrifuge tube on ice.
4. Add the entire volume of the ligated product (~15 μL) to the aliquoted electrocompetent cells and stir briefly with a pipet tip (*see* **Note 31**).
5. Perform electroporation using a 0.1-cm cuvette with the following settings on the electroporator: 10 μF, 600 Ω, and 1800 V (*see* **Note 5**).
6. After pulsing for 10 s, add 975 μL of recovery medium to the cuvette and gently pipet up and down to resuspend the cells. Transfer the cells and to a clean tube.
7. Place the tube in a shaking incubator for 1 h at 37 °C and 250 rpm.
8. Repeat steps 4–7 for the negative control ligation reaction.
9. After 1 h incubation, prepare 10^{-2}, 10^{-4}, and 10^{-6} dilutions of metagenomic sample libraries and the negative control in LB with 50 μg/mL kanamycin. Also include a 10^{-1} dilution for the negative control.
10. Plate 100 μL of each dilution onto separate LB agar plates containing 50 μg/mL kanamycin. Incubate plates overnight at 37 °C. The following day, count and record the number of colonies for each plate (*see* **Note 32**).
11. Inoculate the rest of the recovered cells into 50 mL of LB containing 50 μg/mL kanamycin and grow overnight with shaking at 26 °C.
12. Harvest the cells when the optical density at 600 nm (OD_{600}) of the culture is within the 0.6–1.0 range. Centrifuge the overnight culture at 855 × g for 8 min to pellet the cells. Discard the supernatant and resuspend the pellet in 15 mL of LB containing 15% glycerol and 50 μg/mL kanamycin. Aliquot the metagenomic library into 2 mL cryotubes and store at −80 °C for subsequent screening.
13. Pick 36 random colonies from the titer plates and resuspend each in 50 μL of nuclease-free water. Use these suspensions as templates for PCR reactions to estimate the average insert size. Set up each PCR reaction as follows:

    2.5 μL cellular suspension

    2.5 μL 10X reaction buffer

    1.0 μL 10 mM dNTP mix

    1.0 μL 10 μM Colony PCR forward primer

    1.0 μL 10 μM Colony PCR reverse primer

    0.5 μL *Taq* DNA polymerase (5 U/μL)

    16.5 μL nuclease-free water to bring the final volume to 25 μL.

Use the following thermo-cycler settings to amplify DNA:

94 °C for 10 min, 25 cycles of [94 °C for 45 s, 55 °C for 45 s, 72 °C for 5 min], and 72 °C for 10 min.

14. Run PCR amplified fragments on 1% low melting point agarose as described above. Visualize DNA fragments using a gel imager and record the size of each fragment. Calculate the average insert size and estimate the total library size using the following equation (*see* **Note 33**):

$$\text{Library Size (GB)} = \frac{\left\{\text{TC} \times \left(\frac{\text{TR} - (\text{FR}+\text{NI}+\text{LS})}{\text{TR} - \text{FR}}\right) \times \text{AI}\right\}}{10^9}$$

where TC = total clones (cfu/mL of the library determined from the titer plates), TR = total number of PCR reactions, FR = number of failed reactions, NI = number of colonies with no inserts, resulting in ~300-bp bands, LS = number of reactions that yield inserts smaller than 500 bp (estimated by subtracting 300 bp from the resulting band size), AI = average insert size after subtracting 300 bp from the band size.

3.3 Screening for Antibiotic Resistance and Amplification of Antibiotic Resistance-Conferring DNA Fragments

1. Determine the minimum inhibitory concentration (MIC) of each antibiotic by plating the negative control electrocompetent cells transformed with unmodified pZE21 on MH agar with 50 μg/mL of kanamycin and the antibiotic of choice. Each batch of antibiotics should be tested in this manner before library screening. Commonly used antibiotics and related MICs are listed in Table 1.
2. Calculate the amount of library stock needed for screening. Adjust the concentration of the frozen metagenomic library with LB-Kan such that each 100 μL aliquot contains at least ten times the number of unique clones in the library.
3. To calculate the titer of the frozen metagenomic library stock, thaw one frozen aliquot on ice, prepare 10^{-2}, 10^{-4}, and 10^{-5} dilutions, and plate on LB agar plates containing 50 μg/mL kanamycin. Incubate plates overnight at 37 °C. Count and record the number of colonies on each plate.
4. Calculate the amount of the library stock needed for screening using the following equation (*see* **Note 34**):

$$\text{Amount required} = \frac{\text{Library titer post electroporation}\left(\frac{\text{cfu}}{\text{mL}}\right) \times 10{,}000}{\text{Frozen metagenomic library stock titer}\left(\frac{\text{cfu}}{\text{mL}}\right)}$$

5. Make enough diluted library stock to screen all antibiotic plates for each library. Prepare at least 100 μL extra to set up titer plates and account for pipetting error.
6. Plate 100 μL of diluted library on MH agar with 50 μg/mL of kanamycin and the antibiotic of choice at the MIC determined earlier. Additionally, plate negative control electrocompetent cells transformed with unmodified pZE21 to ensure that the concentration of antibiotic used entirely inhibits the growth of vector-only cells.
7. Incubate plates for 24 h at 37 °C.
8. After incubation, inspect plates for colonies.
9. Collect all colonies by adding 750 μL of the LB-Kan broth with 15% glycerol to the plates and gently scraping the colonies with a sterile L-shaped cell-spreader. If required, repeat this step to collect any leftover colonies.
10. Collect the slurries of functionally selected clones in 2 mL cryotubes and store at −80 °C.
11. To isolate the plasmid containing antibiotic-resistant metagenomic inserts, thaw the stock of antibiotic-resistant slurries from the above step on ice and transfer 300 μL of cells into 5 mL LB medium containing 50 μg/mL of kanamycin and incubate for 12–16 h at 37 °C with vigorous shaking (*see* **Note 35**).
12. Harvest the bacterial cells by centrifugation at >6800 × g in a conventional table-top microcentrifuge for 3 min at room temperature.
13. Perform plasmid purification using the QIAprep Miniprep kit and quantify purified product using the Qubit dsDNA HS assay kit. Follow manufacturers' protocol for detailed instructions.

3.4 Illumina Library Preparation and Sequencing

1. Dilute the purified plasmid from each selection to 0.5 ng/μL just before use.
2. Thaw TD buffer and TDE1 enzyme and index on ice. Preheat thermo cycler to 55 °C.
3. Prepare tagmentation master mix. For each reaction, the following components are mixed together:

   1.25 μL of TD buffer

   0.125 μL nuclease-free H_2O

   0.125 μL TDE1 enzyme
4. Transfer 1.5 μL of tagmentation master mix to each well of 96-well PCR plate and add 1 μL of diluted DNA (0.5 ng/μL). Seal plate and spin briefly.

5. Immediately transfer plate on thermo cycler and incubate for 15 min at 55 °C.
6. At the end of incubation, transfer plate on ice.
7. Add 11.2 μL of KAPA HiFi PCR master mix into each well.
8. Add 8.8 μL (5 μM) of a unique Illumina indexing primer into each well and mix my pipetting. Seal the plate and spin (*see* **Note** 7).
9. Amplify DNA at 72 °C for 3 min, 98 °C for 5 min, followed by 14 cycles of [98 °C for 10 s, 63 °C for 30 s, and 72 °C for 30 s] with a final extension of 5 min at 72 °C.
10. Purify PCR amplified DNA using AMpure XP beads. Add 22.5 μL of beads to each well and mix by pipetting.
11. Incubate at room temperature for 5 min. At and of incubation, place plate on magnetic stand separate beads for 2 min.
12. Remove clear supernatant without disturbing beads.
13. Wash beads three times using 80% ethyl alcohol.
14. After final wash, allow the plate to air dry for 15–20 min.
15. Remove the plate from magnetic stand and add 60 μL of resuspension buffer (10 mM Tris-Cl, 1 mM EDTA, 0.05% Tween 20, pH 8.0)
16. Pipette up and down 15–20 times to mix. Avoid introducing air bubbles during mixing. Incubate the plate at room temperature for at least 5 min.
17. Place the plate on a magnetic stand and allow the liquid to clarify for at least 2 min. Transfer 57 μL of purified DNA sample into clean PCR plate.
18. Quantify DNA sample using Qubit HS DNA quantification kit or PicoGreen DNA quantification kit.
19. Dilute each sample to 10 nM and combine an equal volume of each 10-nM sample in one tube for sequencing (*see* **Note 36**).

3.5 Assembly and Annotation of ARGs

In order to carry out functional characterization of the metagenomic insert library, quality-filtered short read sequences need to be assembled into longer contiguous sequences, commonly referred to as contigs. Several assembly programs have been specifically developed to carry out this task, such as Meta-IDBA [16], Meta-Velvet [17], and InteMap [18]. We have developed a computational pipeline, PARFuMS, as previously described in [2], for high-throughput assembly of resistance-conferring DNA fragments obtained from many independent functional selections. Below, we have described a general workflow of the pipeline. It is important to note that the steps mentioned below include modifications that were made after the publication.

3.5.1 Demultiplexing and Preprocessing of Sequencing Reads

After sequencing, Illumina paired-end sequencing reads are demultiplexed based on index sequences, generating several sample-specific sequencing files and allowing for assembly and annotation for each sample to be performed in parallel. This is typically done by the sequencing core where the sequencing of samples takes place; please check with your sequencing services provider to ensure that the demultiplexing of sequencing reads has taken place. Subsequently, reads are quality filtered using Trimmomatic [19], and the reads corresponding to the expression vector (pZE21) are removed before proceeding to assembly (*see* **Note 37**).

3.5.2 De Novo Assembly of Short-Read Sequences Using PARFuMS

First, short reads are assembled into intermediate length contigs using three iterations of the short-read assembler Velvet [20]. Following each round of assembly, redundant contigs are collapsed to one sequence using CD-HIT [21], and chimeric sequences are removed by mapping raw reads against assembled contigs using FR-HIT [22]. The first iteration of Velvet takes all reads as an input, while in the second and third rounds, the reads not mapped to previously assembled contigs are utilized. The velvet-assembled, nonredundant contig set is then passed to the long-read assembler Phrap [23] for two iterations. The first iteration assembles the Velvet output into more complete contigs, which are subsequently linked together if two contigs are bridged by sufficient number of raw paired-end reads. The final iteration of Phrap uses these linked contigs as input and provides a more complete assembly of linked contigs, which are subsequently annotated for resistance determinants by searching protein coding genes against BLAST- and HMM-based antibiotic resistance reference databases.

3.5.3 Annotation of Contigs with Antibiotic Resistance Functions

1. First, the selections, in which the number of assembled contigs is higher than 10X the number of colonies generated during screening, are excluded.
2. Identification of open reading frames in assembled contigs can be achieved by using gene prediction tools such as MGC [24], Metagenemark [25], MetaGenAnnotator [26], GLIMMER-MG [27], and Prodigal [28] (*see* **Note 38**).
3. Annotation of protein coding regions is done following a hierarchical approach where the sequences are first searched against BLAST-based ARG reference databases (e.g., CARD [29], ResFinder [30], AMRFinder-Prot [31]) with strict criteria (≥95% identity and ≥95% coverage), and then the remaining sequences are searched using HMM-based ARG databases (e.g., Resfams [32], NCBI AMRFinderPlus [31], Pfam [33], TIGRFam [34]) (*see* **Note 39**, **40**). Using this approach, we have implemented a pipeline, *resAnnotator* [35], which is available on GitHub (*see* **Note 41**).

4 Notes

1. This chapter is an updated version of the one published in the first edition of the book [36].
2. Check the pH of the packaged product before use. Some products are packaged at pH 6.7 and come with separate alkaline buffers. Add sufficient volume of alkaline buffer to phenol:chloroform:isoamyl alcohol (25:24:1) (pH 6.7) to achieve pH 8.0. Store at 4 °C.
3. Other expression plasmids may be used to construct the library. While selecting another plasmid consider compatibility, copy number, and selective marker. Selecting different plasmid will also require redesigning of primers (for plasmid linearization, colony PCR, sequencing library preparation, etc.), and re-establishment of minimum inhibitory concentration for each antibiotic for *E. coli* with the new empty plasmid.
4. It is critical to use a high-fidelity polymerase for efficient amplification of DNA fragments with a low error rate. The given reaction volumes and conditions for PCR in this protocol are optimized for Platinum™ SuperFi™ DNA Polymerase and may differ for other high-fidelity polymerases. For a different polymerase, adjust PCR reaction conditions as per the manufacturer's recommendation.
5. Electroporation settings and minimum inhibitory concentration (Table 1) are optimized for *E. coli* E. cloni 10G SUPREME cells ($\geq 4 \times 10^{10}$ cfu/μg transformation efficiency) (Lucigen Corporation, Middleton, WI, USA). If using different electrocompetent cells, follow manufacturer instructions for optimal electroporation condition. Reestablish MIC against each antibiotic with electrocompetent cells transformed with empty plasmid.
6. Alternatively, insert size selection can be performed using the BluePippin size selection system. Concentrate sonicated DNA using Qiagen PCR purification kit, elute in 35 μL of TE buffer, and check DNA concentration using Qubit DNA quantification kit. To create protocol on BluePippin software, select protocol editor tab and select cassette type by clicking 0.75% agarose dye-free/0.75% DF 2–6KB Marker S1. Select "Range" mode and enter 1Kb-6Kb. Assign marker position and apply reference to all lanes and save protocol. Calibrate instrument, perform continuity test and inspect gel cassette as per manufacture protocol and adjust if needed. Remove 40 μL of buffer from sample well and load 30 μL (5 μg in 30 μL) of the purified and sonicated DNA sample to the sample well and the marker to the assigned well as per the protocol.

7. We use unique dual indexes (UDI) for sequencing library preparations. Each UDI consists of a pair of indexing primers with binding sites corresponding to the Nextera tagmentation adapters. The primers also consist of unique 10-bp oligonucleotide sequences (indexes), facilitating the de-multiplexing of the dually indexed reads on a sequencing run to enable separate assembly of contigs corresponding to each sample. Forward and reverse sequencing adapters are annealed by heating the 5 μM mixture to 95 °C followed by slow cooling (0.1 °C per second) to a final holding temperature of 4 °C. Store pre-annealed barcoded adapters at −20 °C.
8. Carefully read the MSDS for each antibiotic and store antibiotics accordingly. Antibiotic stock solutions prepared in ultrapure water need to be filter sterilized. Antibiotic solutions prepared in organic solvents do not need filter sterilization. It is advisable to prepare stock solutions just before use and, if necessary, to store at −20 °C.
9. Pre-warm the water bath to 55 °C. After removing the medium from the autoclave, allow it to cool to 55 °C by placing in a pre-warmed water bath. Add the appropriate amount of the desired antibiotic to this medium and pour 20 mL of liquid medium per 10 cm sterile petri dish. When pouring plates, keep your bench area sterile and clean.
10. For premixed powders, use the amounts suggested by the manufacturers.
11. Metagenomic DNA from fecal samples can alternatively be extracted using the DNeasy PowerSoil Pro Kit (Qiagen, Hilden, Germany).
12. Although 10–20 μg of starting DNA is required for one metagenomic library preparation, it is recommended to extract DNA sufficient for at least three metagenomic library preparations (50–60 μg). Insert yield may vary from sample to sample, and lower yields may hinder the process of library preparation. Thus, it is advisable to begin the library preparation with 10–20 μg of DNA, and if insert yield is insufficient, the insert preparation step can be repeated to achieve the requisite amount. It is not recommended to perform the complete DNA extraction process again for a subset of samples as that may introduce extraction-specific biases into the study. Conversely, DNA preparations from too much fecal sample may have inhibitors that will interfere with downstream steps.
13. Close the tube cap tightly to avoid any leakage during bead beating.
14. Continuous bead beating for 4 min may overheat samples. Cooling samples before and during bead beating helps prevent heat-induced DNA damage.

15. Use of phase lock gel tubes helps eliminate interphase protein contamination during phenol extraction. The organic phase and the interphase materials are effectively trapped in or below the gel, thus allowing easy removal of the top aqueous phase containing DNA by pipetting or decanting.
16. Do not over dry DNA pellet; dried DNA is sometimes difficult to dissolve.
17. Alternatively, the residual ethanol can be removed more rapidly by using a vacuum concentrator. A vacuum concentrator can also be used as a more rapid alternative to heating to concentrate DNA samples.
18. DNA quantification using spectrometric methods may overestimate DNA concentration due to the presence of other compounds in solution. Measurement of DNA concentration using a fluorimeter may thus give a more accurate concentration.
19. Do not use high amounts of the template plasmid. Carryover circular plasmid (template) may result in high levels of transformants carrying plasmids without inserts during metagenomic library preparation.
20. Use a separate gel box for each sample and clean the gel box before use with 10% bleach for 10 min. Wash gel boxes at least three times with dH_2O between each run to avoid cross-contamination.
21. Gel purification and size selection are preferred over a simple PCR cleanup to remove any primer dimers and other forms of the plasmid. During gel extraction, try to avoid bands differing from 2,200 bp in size. Elute DNA with nuclease-free water instead of the purification kit-provided elution buffer; elution buffer contains salts that may interfere with the following steps of plasmid preparation. *Optional:* further purify the plasmid DNA using a PCR purification kit to concentrate the DNA sample. This step may reduce the amount of CIP needed for the dephosphorylation step.
22. Use conversion screen and filter while acquiring images of DNA electrophoresis samples in order to avoid exposing samples or users to harmful UV radiation. Use face and eye protection while working under UV lights.
23. Dephosphorylation removes the terminal 5′-phosphate group from DNA and suppresses self-ligation and circularization of linearized plasmid DNA. This is a crucial step for high-efficiency plasmid preparation. Maintain a proper buffer ratio for optimal results.
24. Prepare enough plasmid for one project. Different batches of pZE21 prepared in this way have different ligation efficiencies, even when the same protocol has been followed for all. Quality

control of each batch is required before using any new batch of plasmid. The easiest way to do this is by preparing an insert library from salmon sperm DNA and ligating it into your new vector. Once you confirm the ligation efficiency (ideally >70% of transformants should contain insert), you may start with the real ligation.

25. If using Covaris E210, we recommend the following settings: duty cycle: 20%, intensity: 0.1, cycles per burst: 1000, treatment time: 900 s.
26. Some commercially available molecular DNA markers (ladders) consist of various DNA fragments and may contain ARGs. Make sure that the molecular marker used during gel purification does not contain any ARGs. You can also prepare a custom molecular DNA marker by amplifying specific sizes of nonbacterial DNA.
27. 200 ng or more insert is required for ligation. If a sufficient amount of the insert is not obtained, repeat the insert preparation step (*see* **Note 12**). It is also advisable to set up two separate ligation reactions if the total amount of insert is more than 1 μg.
28. When setting up multiple ligation reactions, it is preferable to make a master mix of ligation reagents to avoid pipetting errors.
29. The average insert and the vector are of similar sizes (~2 kb); thus, the mass ratio approximates the molar ratio.
30. Dialysis of samples removes salt traces. Higher salt concentrations in the DNA sample may cause arcing during electroporation. Make sure that no part of the cellulose membrane sinks into the water. If multiple samples are applied on same membrane, keep at least 2 cm space between each sample to avoid contamination.
31. Do not vortex or pipet up and down to mix the sample. This can introduce air bubbles and warm the cells. Air bubbles in sample may cause arcing during electroporation.
32. The pZE21 expression vector has the kanamycin resistance cassette.
33. Colony PCR primers are designed such that they will amplify insert at the cloning site and approximately 150 bp of plasmid on each side. Thus, when no insert is present, these primers will yield a band of 321 bp in size. This serves as a colony PCR control. Do not count PCR reactions in any calculation that failed to amplify the 321-bp fragment. While calculating fragment size, deduct 321 bp from the size on the gel. For example, if a 1,500-bp band is observed on the gel, the actual

fragment size is 1,179 bp. Repeat colony PCR if more than 20% of reactions failed to amplify.

34. If the concentration of the frozen library stock is higher than desired, dilute library with LB with 50 μg/mL kanamycin; if it is lower than the desired concentration, pellet cells by gentle centrifugation at 855 × g and reconstitute in an appropriate volume of LB-Kan. Dilute the libraries in LB with 50 μg/mL kanamycin so that 100 μL of plating solution contains about ten copies of each clone. For example, if colony count following electroporation indicates that the metagenomic library contains 500,000 clones, prepare 100 μL of plating solution which contains (10 × 500,000) clones. To avoid underestimation of amount of library stock you need to plate, use the highest estimated colony count following electroporation and the lowest estimated titer of your library stock in the formula.
35. Growth for more than 16 h is not recommended to prevent cells from lysing, which reduces the DNA yield. Use a tube or flask with a volume of at least four times the volume of the culture.
36. We submit the samples for 2 × 150 bp paired-end sequencing on the Illumina NextSeq or NovaSeq platforms with a target sequencing depth of five million reads per sample.
37. We use cross_match from the Phrap package with the following options to remove vector sequences:

    -gap1_only –minmatch 6 –minscore 10 –gap_init -3
38. We use prodigal with default parameters to identify open reading frames.
39. Resfams is a curated database of protein families and their associated profile HMMs that are confirmed for antibiotic resistance function using experimental methods and are organized in ontology [32]. It is extensively used for high-throughput annotation of sequence-novel ARGs. There are two variants of the Resfams database: *Resfam-core.hmm* and *Resfam-full.hmm*. The core database of Resfams profile HMMs was trained using curated antibiotic resistance protein sequences from the Comprehensive Antibiotic Resistance Database (CARD) database, the Lactamase Engineering Database (LacED), and Jacoby and Bush's collection of curated beta-lactamase proteins. The core database of Resfams profile HMMs are supplemented with additional profile HMMs from the Pfam and TIGRFam databases to generate the full Resfams profile HMM database. The core Resfams database should be used with *resAnnotator* pipeline. The latest version of the Resfams database and supporting datafiles are available at http://dantaslab.wustl.edu/resfams.

40. The Pfam and TIGRFam annotation outputs should only be used when there is previous functional evidence of antibiotic resistance activity, such as in functional metagenomic selections.
41. The *resAnnotator* pipeline and configuration files are available at https://github.com/dantaslab/resAnnotator. A brief description of the workflow of the *resAnnotator* pipeline is provided as an example on GitHub, but the nature and order of the databases can be modified in accordance with the experimental needs.

Acknowledgments

The original implementation of functional metagenomics selections for interrogating resistance genes was described by J. Handelsman and colleagues in 1998. We thank A. Moore and B. Wang for protocol optimization of high-throughput versions of this method presented in this manuscript, A. Reyes and K. Forsberg for computational implementation of PARFuMS, M. Gibson for development of the Resfams database, and members of the Dantas lab for helpful general discussions and for comments on the manuscript.

This work was supported in part by the NIH Director's New Innovator Award (http://commonfund.nih.gov/newinnovator/), the National Institute of Diabetes and Digestive and Kidney Diseases (NIDDK: http://www.niddk.nih.gov/), and the National Institute of General Medical Sciences (NIGMS: http://www.nigms.nih.gov/), of the National Institutes of Health (NIH) under award numbers DP2DK098089 and R01GM099538 to G.D. The content is solely the responsibility of the authors and does not necessarily represent the official views of the funding agencies.

References

1. Levy SB, Marshall B (2004) Antibacterial resistance worldwide: causes, challenges and responses. Nat Med 10:S122
2. Forsberg KJ, Reyes A, Wang B, Selleck EM, Sommer MO, Dantas G (2012) The shared antibiotic resistome of soil bacteria and human pathogens. Science 337(6098): 1107–1111
3. Perron GG, Whyte L, Turnbaugh PJ, Goordial J, Hanage WP, Dantas G, Desai MM (2015) Functional characterization of bacteria isolated from ancient Arctic soil exposes diverse resistance mechanisms to modern antibiotics. PLoS One 10(3):e0069533
4. Allen HK, Donato J, Wang HH, Cloud-Hansen KA, Davies J, Handelsman J (2010) Call of the wild: antibiotic resistance genes in natural environments. Nat Rev Microbiol 8(4): 251–259
5. Sommer MOA, Church GM, Dantas G (2010) The human microbiome harbors a diverse reservoir of antibiotic resistance genes. Virulence 1(4):299–303. https://doi.org/10.4161/viru.1.4.12010
6. Monier J-M, Demanèche S, Delmont TO, Mathieu A, Vogel TM, Simonet P (2011) Metagenomic exploration of antibiotic resistance in soil. Curr Opin Microbiol 14(3): 229–235

7. D'Costa VM, McGrann KM, Hughes DW, Wright GD (2006) Sampling the antibiotic resistome. Science 311(5759):374–377
8. Pérez-Pérez FJ, Hanson ND (2002) Detection of plasmid-mediated AmpC β-lactamase genes in clinical isolates by using multiplex PCR. J Clin Microbiol 40(6):2153–2162
9. Eckburg PB, Bik EM, Bernstein CN, Purdom E, Dethlefsen L, Sargent M, Gill SR, Nelson KE, Relman DA (2005) Diversity of the human intestinal microbial flora. Science 308(5728):1635–1638
10. Daniel R (2005) The metagenomics of soil. Nat Rev Microbiol 3(6):470–478
11. Handelsman J, Rondon MR, Brady SF, Clardy J, Goodman RM (1998) Molecular biological access to the chemistry of unknown soil microbes: a new frontier for natural products. Chem Biol 5(10):R245–R249
12. Pehrsson EC, Forsberg KJ, Gibson MK, Ahmadi S, Dantas G (2013) Novel resistance functions uncovered using functional metagenomic investigations of resistance reservoirs. Front Microbiol 4:145
13. Riesenfeld CS, Department of Plant Pathology, Microbiology Doctoral Training Program a, Goodman RM, Department of Plant Pathology, Microbiology Doctoral Training Program a, Gaylord Nelson Institute for Environmental Studies UoWM, Madison, WI 53706, USA., Handelsman J, Department of Plant Pathology, Microbiology Doctoral Training Program a (2015) Uncultured soil bacteria are a reservoir of new antibiotic resistance genes. Environ Microbiol 6(9):981–989
14. Boolchandani M, D'Souza AW, Dantas G (2019) Sequencing-based methods and resources to study antimicrobial resistance. Nat Rev Genet 20(6):356–370
15. Lutz R, Bujard H (1997) Independent and tight regulation of transcriptional units in Escherichia coli via the LacR/O, the TetR/O and AraC/I1-I2 regulatory elements. Nucleic Acids Res 25(6):1203–1210
16. Peng Y, Leung HC, Yiu SM, Chin FY (2011) Meta-IDBA: a de Novo assembler for metagenomic data. Bioinformatics 27 (13):i94-i101
17. Namiki T, Hachiya T, Tanaka H, Sakakibara Y (2012) MetaVelvet: an extension of Velvet assembler to de novo metagenome assembly from short sequence reads. Nucleic Acids Res 40(20):e155
18. Lai B, Wang F, Wang X, Duan L, Zhu H (2015) InteMAP: integrated metagenomic assembly pipeline for NGS short reads. BMC Bioinformatics 16:244
19. Bolger AM, Lohse M, Usadel B (2014) Trimmomatic: a flexible trimmer for Illumina sequence data. Bioinformatics 30(15): 2114–2120
20. Zerbino DR (2010) Using the Velvet de novo assembler for short-read sequencing technologies. Current protocols in bioinformatics/editoral board, Andreas D Baxevanis [et al] CHAPTER:Unit-11.15
21. Fu L, Niu B, Zhu Z, Wu S, Li W (2012) CD-HIT: accelerated for clustering the next-generation sequencing data. Bioinformatics 28(23):3150–3152
22. Niu B, Zhu Z, Fu L, Wu S, Li W (2011) FR-HIT, a very fast program to recruit metagenomic reads to homologous reference genomes. Bioinformatics 27(12):1704–1705
23. de la Bastide M, McCombie WR (2007) Assembling genomic DNA sequences with PHRAP. Curr Protoc Bioinformatics Chapter 11(Unit11):14
24. El Allali A, Rose JR (2013) MGC: a metagenomic gene caller. BMC Bioinformatics 14 (Suppl 9):S6–S6
25. Zhu W, Lomsadze A, Borodovsky M (2010) Ab initio gene identification in metagenomic sequences. Nucleic Acids Res 38(12):e132
26. Noguchi H, Taniguchi T, Itoh T (2008) MetaGeneAnnotator: detecting species-specific patterns of ribosomal binding site for precise gene prediction in anonymous prokaryotic and phage genomes. DNA Res Int J Rapid Publ Rep Genes Genomes 15(6):387–396
27. Kelley DR, Liu B, Delcher AL, Pop M, Salzberg SL (2012) Gene prediction with Glimmer for metagenomic sequences augmented by classification and clustering. Nucleic Acids Res 40(1):e9
28. Hyatt D, Chen GL, Locascio PF, Land ML, Larimer FW, Hauser LJ (2010) Prodigal: prokaryotic gene recognition and translation initiation site identification. BMC Bioinformatics 11:119
29. Alcock BP, Raphenya AR, Lau TTY, Tsang KK, Bouchard M, Edalatmand A, Huynh W, Nguyen AV, Cheng AA, Liu S, Min SY, Miroshnichenko A, Tran HK, Werfalli RE, Nasir JA, Oloni M, Speicher DJ, Florescu A, Singh B, Faltyn M, Hernandez-Koutoucheva A, Sharma AN, Bordeleau E, Pawlowski AC, Zubyk HL, Dooley D, Griffiths E, Maguire F, Winsor GL, Beiko RG, Brinkman FSL, Hsiao WWL, Domselaar GV, McArthur AG (2020) CARD 2020: antibiotic resistome surveillance with the comprehensive antibiotic resistance database. Nucleic Acids Res 48(D1):D517–D525

30. Zankari E, Hasman H, Cosentino S, Vestergaard M, Rasmussen S, Lund O, Aarestrup FM, Larsen MV (2012) Identification of acquired antimicrobial resistance genes. J Antimicrob Chemother 67(11):2640–2644
31. Feldgarden M, Brover V, Haft DH, Prasad AB, Slotta DJ, Tolstoy I, Tyson GH, Zhao S, Hsu CH, McDermott PF, Tadesse DA, Morales C, Simmons M, Tillman G, Wasilenko J, Folster JP, Klimke W (2019) Validating the AMRFinder tool and resistance gene database by using antimicrobial resistance genotype-phenotype correlations in a collection of isolates. Antimicrob Agents Chemother 63(11):e00483-19
32. Gibson MK, Forsberg KJ, Dantas G (2015) Improved annotation of antibiotic resistance determinants reveals microbial resistomes cluster by ecology. The ISME J 9(1):207–216
33. Mistry J, Chuguransky S, Williams L, Qureshi M, Salazar GA, Sonnhammer ELL, Tosatto SCE, Paladin L, Raj S, Richardson LJ, Finn RD, Bateman A (2021) Pfam: the protein families database in 2021. Nucleic Acids Res 49 (D1):D412–D419
34. Haft DH, Selengut JD, White O (2003) The TIGRFAMs database of protein families. Nucleic Acids Res 31(1):371–373
35. D'Souza AW, Boolchandani M, Patel S, Galazzo G, van Hattem JM, Arcilla MS, Melles DC, de Jong MD, Schultsz C, Consortium C, Dantas G, Penders J (2021) Destination shapes antibiotic resistance gene acquisitions, abundance increases, and diversity changes in Dutch travelers. Genome Med 13(1):79
36. Boolchandani M, Patel S, Dantas G (2017) Functional metagenomics to study antibiotic resistance. Methods Mol Biol 1520:307–329

INDEX

Peter Sass (ed.), *Antibiotics: Methods and Protocols*, Methods in Molecular Biology, vol. 2601,
https://doi.org/10.1007/978-1-0716-2855-3,

F

G

H

I

K

L

M

N

O

P

R

S

T

W